UNIVERSAL
LIBRARY

OU_158867

UNIVERSAL
LIBRARY

OSMANIA UNIVERSITY LIBRARY

Call No. 539·7/W74P Accession No. 43834

Author Wilson, J. G., ed.

Title Progress in cosmic ray physics. v.3. 1956.

This book should be returned on or before the date last marked below.

SERIES IN PHYSICS

General Editors:

J. DE BOER, H. BRINKMAN and H. B. G. CASIMIR

L. ROSENFELD, Nuclear Forces

E. A. GUGGENHEIM, Thermodynamics

BØRGE BAK, Elementary Introduction to Molecular Spectra

L. ROSENFELD, Theory of Electrons

W. ELENBAAS, The High Pressure Mercury Vapour Discharge

S. R. DE GROOT, Thermodynamics of Irreversible Processes

E. A. GUGGENHEIM and J. E. PRUE, Physicochemical Calculations

E. A. GUGGENHEIM, Boltzmann's Distribution Law

J. L. SYNGE, Relativity: the Special Theory

H. C. BRINKMAN, Applications of Spinor Invariants in Atomic Physics

H. UMEZAWA, Quantum Field Theory

J. BOUMAN (editor), Selected Topics in X-Ray Crystallography

J. G. WILSON (editor), Progress in Cosmic Ray Physics Volume I, II, III

C. J. GORTER (editor), Progress in Low Temperature Physics I, II

J. M. BURGERS and H. C. VAN DE HULST (editors), Gas Dynamics of Cosmic Clouds. A Symposium

KAI SIEGBAHN (editor), Beta- and Gamma-Ray Spectroscopy

Z. KOPAL (editor), Astronomical Optics and Related Subjects

PREFACE

This volume is written mainly from the standpoint of early 1955, although some reference to later work will be found.

It includes two reviews concerning problems of the unstable nuclear particles in which the emphasis is predominantly upon observations in the cosmic radiation. The rapid progress of experimental techniques associated with the study of artificially produced particles makes it certain that the emphasis of subsequent reviews in this field will be very different. The present reviews accordingly provide a record of the extent to which the problems set by the heavy mesons and hyperons were resolved in the phase during which the work depended almost exclusively upon natural sources.

J. G. WILSON

Leeds, May 1956

CONTENTS

CHAPTER I

THE EXTENSIVE AIR SHOWERS

by K. GREISEN

INTRODUCTION 3

1. LONGITUDINAL DEVELOPMENT OF ELECTRON CASCADES 9

1. 1 The analytical approximations. 10
1. 2 Analytical solutions 12
1. 3 Approximate expressions 17
1. 4 Fluctuations in the longitudinal development 18

2. ANGULAR AND LATERAL DISTRIBUTIONS IN ELECTRON CASCADES 19

2. 1 Approximations in the calculations. 20
2. 2 Solutions for all electrons above zero energy. 22
2. 3 Behaviour of the distribution near the axis 25
2. 4 Approximate formulae for the lateral distribution of all electrons 26
2. 5 Effect of single scattering 27
2. 6 Lateral and angular distributions as functions of energy. . . 28
2. 7 Effect of atmospheric density variation 34
2. 8 Magnetic deflections 35
2. 9 Summary 36

3. EXPERIMENTS ON THE LATERAL DISTRIBUTION OF ELECTRONS 37

3. 1 Medium distances $0.03 < r/r_1 < 2$ 37
3. 2 Large distances $0.4 < r/r_1 < 5$. 42
3. 3 Small distances from the axis 44
3. 4 Interpretation of observations near the shower axis 46
3. 5 Multiple shower cores 48
3. 6 Theoretical implications 49

4. DENSITY AND NUMBER SPECTRA OF EAS. 53

4. 1 Determination of the density spectrum 54
4. 2 Variation of the index 'γ' 57
4. 3 Total number of electrons in EAS 61
4. 4 Density spectrum at high altitudes. 62

4. 5 Evaluation of the number spectrum of EAS in the lower atmosphere 65

5. VARIATION OF INTENSITY WITH ALTITUDE, BAROMETRIC PRESSURE AND ZENITH ANGLE 70

5. 1 Altitude variation 70
5. 2 Barometric effect 72
5. 3 Zenith angle effect 74
5. 4 Analysis of the variation of the vertical intensity with altitude 81
5. 5 Interpretation of the rate of absorption 83
5. 6 Energy transfer to electronic cascades in the lower atmosphere 89

6. MESON AND NUCLEON COMPONENTS OF THE EAS . . . 93

6. 1 Methods of detection 94
6. 2 Proportion of penetrating particles *vs.* distance from the axis 96
6. 3 Proportion of penetrating particles *vs.* size of the showers . . 100
6. 4 Relative intensity of the nuclear-active component 102
6. 5 The energy spectrum of the nuclear-active component . . . 104
6. 6 Influence of shower size on the composition 106
6. 7 Lateral distribution of the nuclear-active component 107
6. 8 Relative numbers of neutral and charged particles 108
6. 9 Variation of the N-component of EAS with altitude 109
6. 10 Range spectrum of the μ-mesons 113
6. 11 Calculations of the nuclear cascade 117

7. TIME VARIATIONS OF THE EAS 117

7. 1 Galactic magnetic fields 118
7. 2 Origin of directional asymmetry 119
7. 3 Experimental observations on sidereal variations 122
7. 4 Significance of sidereal variations 122
7. 5 Solar and atmospheric effects 123
7. 6 Comparative virtues of various experimental arrangements . 127

8. THE PRIMARY ENERGY SPECTRUM 129

8. 1 The track-length integral 130
8. 2 Exponent of the primary energy spectrum 132
8. 3 Form of the primary spectrum 134
8. 4 Maximum energy of primaries of observed showers 135

REFERENCES 137

CHAPTER II

EXPERIMENTAL RESULTS ON CHARGED K-MESONS AND HYPERONS

by H. S. BRIDGE

INTRODUCTION 145

1. THE TAU-MESON 149
1. 1 Mode of production 149
1. 2 Decay scheme, mass and Q-value of the τ-meson 150
1. 3 Alternative modes of decay 151
1. 4 Charge of the τ-meson 152
1. 5 Spin and parity 153
1. 6 Lifetime of the τ-meson 155
2, 3, 4 DECAY EVENTS PRODUCED BY K-MESONS AND CHARACTERIZED BY THE EMISSION OF A SINGLE CHARGED SECONDARY PARTICLE
2. RESULTS CONCERNING S-EVENTS: OBSERVATIONS WITH PHOTOEMULSIONS 156
2. 1 The alternate mode of decay of the τ-meson 156
2. 2 The ϰ-meson 158
2. 3 The mass of the ϰ-meson 166
2. 4 Evidence concerning the χ-meson 168
2. 5 The pβ distribution of the secondary particles 172
2. 6 The electron secondaries 177
3. RESULTS CONCERNING S-EVENTS: OBSERVATIONS WITH CLOUD CHAMBERS 179
3. 1 The experimental results 182
3. 2 The range distribution of the secondary particles 184
EVIDENCE CONCERNING THE K_μ-MESON
3. 3 Discussion of experimental results 193
3. 4 Direct measurement of the primary mass 195
3. 5 The long range group of secondary particles 196
3. 6 The decay scheme of the K_μ-meson 198
3. 7 The mass of the K_μ-meson 199
EVIDENCE CONCERNING THE χ-MESON
3. 8 The occurrence of photons among the decay products . . . 202
3. 9 Discussion of the cloud chamber results 203
3. 10 The decay scheme of the χ-meson: Discussion of the cloud chamber and emulsion results 205
3. 11 Other results concerning the χ-meson 205
THE CHARGE ASYMMETRY OF S-PARTICLES OBSERVED IN CLOUD CHAMBERS
3. 12 Results of the EP group 207
4. RESULTS CONCERNING CHARGED V-PARTICLES OBTAINED WITH CLOUD CHAMBERS USING A MAGNETIC FIELD 207
4. 1 Introduction 207
4. 2 Dynamical analysis of V-events 209
4. 3 Discussion of the experimental data: events with low values of p* 212
4. 4 Nature of the secondary particles associated with high p* events 218
4. 5 The charge asymmetry 219

4. 6 Lifetime estimates 221
4. 7 Discussion of results 225
4. 8 Delayed coincidence experiments on S-events 226
4. 9 Comparison with the charged V-particle data 227

5. THE CHARGED HYPERONS 228
5. 1 The decay process $\Sigma^+ \rightarrow p + \pi^\circ$ 228
5. 2 Decay events in which the charged product is an L-meson . 234
5. 3 Experimental evidence for the decay processes $\Sigma^+ \rightarrow \pi^+ + n$ and $\Sigma^- \rightarrow \pi^- + n$. 235
5. 4 Other modes of decay 237

6. NUCLEAR ABSORPTION OF HEAVY MESONS AND HYPERONS 237
6. 1 Possible absorption processes of K-mesons 237
6. 2 Observations with photoemulsions 238
6. 3 Observations with cloud chambers 244
6. 4 Interpretation 245
6. 5 The absorption of negative hyperons 246

ACKNOWLEDGEMENTS 248

REFERENCES 249

CHAPTER III

DECAY PROCESSES OF HEAVY UNSTABLE NEUTRAL PARTICLES

by R. W. THOMPSON

INTRODUCTION 255

1. EARLY WORK ON V°-PARTICLES 256
1. 1 Discovery of V°-particles 256
1. 2 Early evidence for the complexity of V°-particles 258

2. EXPERIMENTAL AND ANALYTICAL TECHNIQUES 259
2. 1 Experimental techniques 259
2. 2 Analysis and representation of V°-particle data 266

3. THE Λ°-PARTICLE 280
3. 1 The nature of the charged fragments 280
3. 2 Two-body decay 282
3. 3 The abnormal $Q(p,\pi)$-values 289
3. 4 Lifetime of the Λ°-particle 289
3. 5 The emulsion work 290
3. 6 The cascade decay 293

4. THE θ-PARTICLE 297
4. 1 The Q-surface representation of the data 298
4. 2 Identification of the fragments 301
4. 3 The $Q(\pi,\pi)$-values 304
4. 4 Emulsion work on the θ^0-meson 306
4. 5 Lifetime of the θ^0-particle 309
4. 6 Relationship of the θ^0-meson to the K-particles 309
5. THE ANOMALOUS V°-DECAYS 310
5. 1 The basic data 310
5. 2 The Q-surface representation of the data 311
5. 3 The $Q(\pi,\pi)$-values, and discussion 316
5. 4 The Cowan photograph 319
6. THE PRODUCTION OF V°-PARTICLES 321
6. 1 The production of V°-particles at cosmic ray energies 322
6. 2 The production of V°-particles at low energies 324
7. SUMMARY 331
ACKNOWLEDGEMENTS 333
REFERENCES 334

CHAPTER IV

THE ENERGY BALANCE OF COSMIC RADIATION

by G. PUPPI

INTRODUCTION 341
1. THE MESONIC COMPONENT 345
1. 1 The μ-spectrum at sea level 345
1. 2 Construction of the generation function of muons in the atmosphere 350
1. 3 Development of the mesonic component in the atmosphere . 355
1. 4 Angular corrections on the vertical beam 359
1. 5 The positive excess for the vertical muon beam 365
2. THE ELECTRON-PHOTON COMPONENT 369
2. 1 Origin of the electron-photon component 369
2. 2 Division of the integral electron track length 370
2. 3 Spectra of electrons and photons 371
2. 4 The total contribution arising from neutral and charged pions 375
2. 5 Comments on secondary generation processes 376
3. THE NUCLEONIC COMPONENT 378
3. 1 Collision losses at star formation 378

3. 2 Slow neutron data 381
3. 3 Comparison between the stars and neutron captures 383
4. CONCLUSIONS 385
ACKNOWLEDGEMENTS 386
REFERENCES 387
AUTHOR INDEX 389
SUBJECT INDEX 416

CHAPTER I

THE EXTENSIVE AIR SHOWERS

BY

K. GREISEN
Department of Physics, Cornell University

INTRODUCTION 3

1. LONGITUDINAL DEVELOPMENT OF ELECTRONIC CASCADES 9

2. ANGULAR AND LATERAL DISTRIBUTIONS IN ELECTRONIC CASCADES 19

3. EXPERIMENTS ON THE LATERAL DISTRIBUTION OF ELECTRONS 37

4. DENSITY AND NUMBER SPECTRA OF EAS . . . 53

5. VARIATION OF INTENSITY WITH ALTITUDE, BAROMETRIC PRESSURE AND ZENITH ANGLE 70

6. MESON AND NUCLEON COMPONENTS 93

7. TIME VARIATIONS OF THE EAS 117

8. THE PRIMARY ENERGY SPECTRUM 129

REFERENCES 137

INTRODUCTION

In 1937 Schmeiser and Bothe pointed out that measurements of the Rossi transition curve (the frequency of coherent groups of particles *vs.* thickness of solid matter placed above the detector) always yield a positive intercept at zero thickness, and that this implies the occurrence of showers in the free air (Bothe *et al.* [1937]). Schmeiser & Bothe [1938] demonstrated that particles in the showers had separations up to at least 40 cm; but within a short time, Auger, Maze & Grivet-Meyer [1938] and Kolhörster, Matthes & Weber [1938] had measured coincidences between counters several tens of meters apart. The phenomena responsible for such coincidences have come to be known as extensive air showers, abbreviated as EAS.

By 1939 much of our present experimental information about the EAS had already been accumulated, largely by the efforts of the Paris group working with Auger. The decoherence curve (coincidences between counters as a function of their horizontal separation) had been measured out to 300 m (Auger, Maze & Robley [1939]). The EAS has been observed in a cloud chamber containing a lead plate, in which the multiplication of particles established their predominantly electronic nature (Janossy & Lovell [1938]). Slow proton tracks had also been seen, from which the presence of a nuclear active component consisting of protons and neutrons was inferred (Auger, Maze, Ehrenfest & Freon [1939]; Auger, Ehrenfest *et al.* [1939]). Transition effects and absorption curves measured with counters had demonstrated the predominant abundance of electrons and photons in EAS as well as the presence of a small penetrating component capable of traversing more than 20 cm of lead (Auger, Maze *et al.* [1939]; Auger, Ehrenfest *et al.* [1939]). The strong altitude variation and barometric coefficient had been measured. The frequency of EAS as a function of the density of particles had been described qualitatively (Janossy & Lovell [1938]; Auger, Maze *et al.* [1939]), and many estimates had been made of the total number of particles in the EAS and of the primary energies.

It was already clear at this time that some of the showers

represented effects of primary cosmic rays having extraordinarily high energy. More recent investigations have verified that the frequency as a function of shower size is sufficient to permit practical measurements on events with primary energy up to at least 10^{17} eV. This fact accounts for the two principal motives for continued study of the EAS: to gather information related to the origin of the primary cosmic rays, and to investigate the nature of the interactions of extremely energetic particles.

The origin of the primary particles, the nature of any subsequent acceleration that they may experience, and the properties of the space in which they travel before reaching the earth determine several features of the local intensity that may be observable: the charge spectrum of the primaries; the shape of the energy spectrum; fluctuations of the intensity that may be correlated with disturbances on the sun or elsewhere outside the earth; and a possible asymmetry of the directional distribution in space, appearing as a periodic variation of the local intensity with solar or sidereal time owing to the rotation of the earth. In all of these respects, the primary rays that have extremely high energy, exceeding 10^{15} eV, may be expected to differ from the much more abundant particles of comparatively low energy; and observation of the differences may shed light not only on the problem of the origin of cosmic rays but on various related astrophysical matters.

At low primary energies, the incident spectrum and the directional distribution are distorted by the magnetic field of the earth and by magnetic or electrical disturbances occurring in its immediate vicinity. These would have no appreciable effect on the primaries of the EAS.

Secondly, the energy density and isotropy of the bulk of the primary cosmic rays apparently cannot be accounted for without the existence of a trapping mechanism, generally believed to be a magnetic field, that prevents escape of the particles to regions of low stellar density. Storage of the particles in the neighborhood of their sources both enriches the density, permitting the sources to be weaker than otherwise, and also randomizes the directions. But if the trapping mechanism is so effective as to contain within the galaxy the primaries of the biggest air showers, it appears likely that the more ordinary primaries would be constrained to exist in small regions near their places of origin. The average primaries may therefore reflect chiefly the production of cosmic

rays at the sun and other local stars, while the high energy primaries may be expected to come from more distant regions, and to retain certain asymmetries that can give information about gradients of the cosmic ray density in the galaxy and the mechanisms of the retention and acceleration of the particles.

The retention must be expected to break down ultimately, when the energy is so high that the particles can no longer be effectively trapped. This will occur when the radius of curvature of the particles is of the same order as the dimensions of the scattering elements. Hence an upper limit of the energy spectrum must be foreseen, depending not only on the magnetic field strengths, but on the size of the magnetic clouds and the degree of order in their orientation.

Furthermore, leakage from a magnetic field depends on the magnetic rigidity rather than the total energy of the particles; therefore the cut-off would occur at a higher energy for heavy nuclei than for protons, and it is conceivable on this account that the most energetic primaries may all be heavy. On the other hand, if the energy is acquired through a gradual process of acceleration, the most energetic particles will be those that have the longest lifetimes within the galaxy, and the heavy nuclei may be expected to have shorter mean lives than the protons, owing to the greater probability of suffering collisions with interstellar atoms.

Little information is available as yet on these matters, but it can be seen that many interesting questions remain to be answered by future explorations of the frequency, the time variations and the charge of the particles which initiate the largest of the air showers.

For several years it was thought that the EAS, as distinguished from other cosmic ray phenomena, represented the effects of primary electrons or photons of very high energy. The small numbers of mesons and nucleons in the EAS were considered to be secondary to the more numerous photons and electrons. However, in the last decade both theory and experiments have indicated that there are practically no electrons or photons of high energy in the primary radiation. Although they are the most numerous elements of EAS at maximum development, it has become evident that the photons and electrons are themselves a secondary component, while the EAS are initiated and dominated

in their development by the nuclear-active particles. Besides, it is now recognized that the EAS are not a distinct type of cosmic ray phenomenon, but represent the common chain of events following the incidence of any high energy proton or heavy nucleus on the atmosphere. The only distinguishing feature of the EAS is the magnitude of the primary energy: when this is great enough, the cascade of nucleons, mesons, photons and electrons proceeds without exhaustion until a considerable density of particles is developed, sufficient to make the simultaneous detection of more than one particle in a small volume of the atmosphere a probable occurrence. Thus, in enquiring about the events near the origin of the EAS, it is now evident that one is investigating interactions involving nuclear forces rather than electromagnetic processes.

The feasibility of constructing laboratory machines that accelerate particles up to energies on the order of 10^{10} eV has made accelerators by far the most efficient and precise means of studying nuclear interactions up to such energies. In the range 10^{10} to 10^{14} eV, it has been demonstrated that stacks of emulsions flown near the top of the atmosphere can provide much better information than can any indirect experiments performed lower in the atmosphere on the secondary effects of the primaries. But at higher energies the emulsion technique is defeated by the low primary intensity. For instance, the total intensity above 10^{16} eV, according to the spectrum derived later in this chapter, is $5 \cdot 10^{-8}$ $m^{-2}sec^{-1}sterad^{-1}$. An emulsion stack usually constitutes about 10^{-2} m^2 area, remains aloft about $3 \cdot 10^4$ sec, and has a sensitive angle of about 3 steradians. Therefore one may only expect to see a primary of 10^{16} eV about once in 20,000 emulsion stack experiments, each of which involves considerable expense both for the balloon flight and for the scanning of the emulsions. In contrast, single air shower experiments have succeeded in detecting secondary effects of primaries of 10^{16} eV with a frequency exceeding one per hour.

The sole reason for this efficiency is that the EAS contain very many secondary particles dispersed over a large area. Consider for example an event of primary energy 10^{16} eV. At 3200 m elevation the electron shower is not far from its maximum development and contains about $6 \cdot 10^6$ electrons. Out to a distance of 120 m from the axis, the density of the electrons exceeds 20 per

square meter, enough to be measured easily with a set of counters. Thus the shower can be detected if its axis falls anywhere within an area on the order of $5 \cdot 10^4$ m^2 around the counter set, and the rate of such events is about 10 per hour.

If one considers still higher energies, the reduced frequency of the primaries is somewhat compensated for by an increase of the radius within which the density is measurable. Therefore EAS exceeding 10^{17} eV can be detected about once every two hours, and, barring the occurrence of a cutoff in the primary spectrum, one might expect to record EAS of more than 10^{18} eV several times per week.

Returning now to the motives for continued study of EAS, one can see that if the purpose is to investigate the frequency of primary cosmic rays as a function of energy and of direction in space, it may be sufficient to detect only the secondary electrons which are scattered far from the axes of the showers. In this case the efficiencies estimated above are realizable. By sampling the density of the electrons at several places in each shower one can estimate the total number of electrons and thereby the primary energy; while by observing the average direction of the electrons and knowing the time of the occurrence, one can determine the direction of motion of the primary with respect to the stars.

However, if the purpose is to study the nature of nuclear interactions and meson production at very high energies, one is in much greater difficulty. The very existence of an EAS implies that many successive interactions of the particles have occurred. The multitude of electrons and photons and even the less numerous mesons and nucleons that are distributed over wide regions of space have originated in interactions of comparatively low energy, suffered by shower particles many generations removed from the primary of the EAS. The energy distribution and the angular and lateral distributions of this multitude of secondaries are determined mainly by the laws governing low energy interactions and coulomb scattering. Such particles and processes can be duplicated in the laboratory with accelerating machines, and are more efficiently studied that way than by measurements of EAS. The only property of the primary which is directly and sensitively felt by the low energy secondaries is the total energy, which is reflected in the total number of secondaries at a given depth in the atmosphere.

The inherent difficulty of the situation is well illustrated by the fact that the gross features of EAS have been accounted for in theories based on the assumption of primary electrons, completely ignoring the nuclear-active component.

To gain information about ultra-energetic nuclear interactions, therefore, just detecting the showers and observing their gross features is not enough. One cannot be content with first approximation experiments, nor with qualitative agreement between a theory and a limited amount of experimental data. The showers must be studied in as much detail as possible, and a theory must agree with all the features of the showers before it is considered acceptable.

Some of the most critical experimental information pertains to a small region in the EAS very near the central axes, and pertains to the high energy mesons and nucleons that are only a minute proportion of all the particles. When such information is sought, the efficiency of detecting the showers is much less than has been estimated above. A practical upper limit of the primary energies of events that can be studied in such detail is 10^{15} to 10^{16} eV rather than 10^{17} or 10^{18} eV, because of the limited frequency with which shower axes occur very close to a complex piece of detecting equipment.

Even more serious than the handicap of low frequencies is the usual necessity of using methods of indirect inference in proceeding from experimental observations of EAS towards conclusions of a fundamental nature. Such methods can never be as satisfying as the well-defined, direct interpretations of experiments that are possible at lower energy. But the lack of simple clarity in the analysis of EAS cannot justify abandonment of the effort to comprehend them. In the foreseeable future, there is probably no other way to reach an understanding of the ultra-energetic particles or to confirm theories of their behaviour.

In spite of the difficulties, some progress in this direction has been made. The lateral distribution of the particles near the central axis, for instance, has been related to the angular distribution of the secondary mesons and nucleons emerging from the most energetic nuclear interactions occurring in the shower. The propagation of the showers in the lower atmosphere has been shown to be dependent on the nuclear processes, being influenced by the rate of degradation of the energy of the most energetic

particles that are responsible for the propagation of the nuclear cascade. The abundance of mesons and nucleons in the showers, compared with the electrons, reflects the distribution of energy between the various kinds of secondaries produced in the early nuclear encounters. Showers of μ-mesons detected far underground are strongly affected by the multiplicities of particle production, the nature of the produced particles and the division of energy among them, occurring in the early stages of EAS development.

In reaching satisfactory explanations of these phenomena, only rough beginnings have been made; and the account given in the present chapter must of necessity be vague and incomplete in many respects. Little emphasis will be given to the existing theoretical calculations related to the nuclear cascade, because the bases of these calculations are not yet well established, and some of the approximations in the treatments can be misleading. A summary will be given of the results of the electron cascade theory, since it rests on a sound foundation and is basic to the interpretation of all the experiments. Otherwise, chief emphasis will be placed on an assembly and comparison of experimental observations of the EAS. Where it is possible, brief discussions will be given of the connections between these observations and the more fundamental problems that provide the current motivation of the experiments.

1. Longitudinal Development of Electronic Cascades

The EAS are detected and studied mainly by means of the electron component, not because the behaviour of the electrons is of particular interest, but because these are by far the most numerous particles near the axis of a large air shower, and are therefore the easiest particles to detect. Thus, although the chief concern may be about the nucleonic cascade of which the electron cascade is an outgrowth, it is necessary first to understand the development of the electronic component, in order to be able to make use of the experimental measurements.

Following the customary subdivision of the problem, the solutions for the longitudinal development and for the lateral and angular distribution of the particles will be summarized separately.

1. 1 The analytical approximations

At the outset, it merits emphasis that the theoretical expressions for all the elementary processes occurring in electronic cascades (with the possible exception of pair production by electrons) [1] have been confirmed by experiments, and in every case the basis of the theory has been established as sound. The only difficulty in the shower problem has been one of combining the formulae for the elementary processes in a way that could be treated analytically with simple mathematical expressions. This has led to the adoption of various simplifications of the problem.

In "Approximation A", all processes are neglected except bremsstrahlung and pair formation, and these are described with the asymptotic formulae valid under complete screening of the atomic nuclei. For air showers, the most important omission is the ionization loss of the electrons. On this account, the results are accurate only for particles of energy $E \gg \varepsilon_0$, where ε_0 is the "critical energy".

Pair production by photons and bremsstrahlung by electrons in the electric field of atomic electrons are taken into account by replacing Z^2 in the radiative collision formulae with $Z(Z + 1)$. Thus one obtains 37.7 g. cm^{-2} for the radiation length in air, and 84.2 MeV for the critical energy (Rossi [1952]).

The solutions of the shower problem that are useful in analysis of EAS are derived from diffusion equations by the use of Laplace and Mellin transforms. The methods of inversion of the transforms limit the solutions to being accurate only for thicknesses t large compared with one radiation length, and for secondary particles of energy E much less than the primary energy W_0.

"Approximation B" is the same as Approximation A, except that the ionization loss of electrons is taken into account, under

[1] Some recent observations of tridents in high energy cascades (Freier & Naugle [1953], Naugle & Freier [1953], Koshiba & Kaplon [1955]) cast doubt on the theory, suggesting that the trident process is much more important than the theory indicates. Other observations, however (Camac [1952], Hooper *et al.* [1952], Block *et al.* [1954]), have been consistent with the theory; and the fundamental similarity between trident formation and the processes of bremsstrahlung and pair formation, together with the success of electromagnetic theory in accounting for the latter processes, encourages one to maintain confidence in the theory—at least until the present evidence of a contradiction is extended and improved.

the assumption that it is continuous and equal to a constant amount, ε_0, per radiation length. Processes which are still neglected include trident production by the electrons, Compton effect and nuclear interactions of the photons, and the production of secondary electrons by knock-on collisions.

Some of the above simplifications are quite harmless. The cross-section for nuclear interaction of high energy photons with air nuclei, for instance, is only a few millibarns, while the pair production cross-section is about 200 times greater. In regard to the trident process, electromagnetic theory predicts that the direct production of pairs by electrons is about 100 times less important than the indirect creation of pairs by bremsstrahlung and subsequent conversion of the photons (BHABHA [1935], RACAH [1937], RAVENHALL [1950]) [1]. Similarly, the energy transfer from high energy electrons to secondary electrons by knock-on collisions is so small, in comparison with the radiative energy transfer to photons, that the production of electrons by the knock-on process is always of very minor importance. This has been confirmed even in the low energy region by the calculations of RICHARDS and NORDHEIM [1948]. The use of a constant for the ionization loss introduces very little error, because the ionization loss varies slowly with electron energy, and because accuracy in this term is only important at energies near the critical energy.

Bernstein has investigated the error due to the use of asymptotic formulae for the radiation and pair creation processes (BERNSTEIN [1950]). Insertion of the correct probabilities as a function of energy was found to reduce the number of electrons at the cascade maximum by a small amount (of the order of 10% at moderately high energy, the correction decreasing with increasing primary energy), and to increase the number of electrons at thicknesses far beyond the maximum. Practically the entire modification resulted from taking into account the decrease of the pair formation cross section at low energies. This correction attributes to the photons longer ranges before conversion into electrons, and hence "stretches" the showers. Bernstein neglected the Compton effect. In air, the sum of the Compton and pair cross-sections is nearly constant down to an energy of about $0.1\ \varepsilon_0$. Hence, consideration of the Compton effect would compensate for the variation of the pair cross-section. We therefore infer that the un-

[1] See footnote p. 10.

corrected results under Approximation B are more accurate than the modified treatment by Bernstein, and that the error due to the use of inaccurate cross-sections is negligible.

The reason for the insignificance of the variation of the bremsstrahlung cross-section with energy is that the ionization loss of electrons is dominant over the radiation process at all energies where the asymptotic radiation formula is inaccurate.

All of the solutions under Approximation B have the property that the total track length of all the electrons (i.e., the number of electrons integrated over the length of the shower) is equal to W_0/ε_0, which is correct within the accuracy involved in the assumption of a constant for the ionization loss. One may conclude from this and from the arguments given above that the average behavior of electronic showers in air, calculated under Approximation B, can be trusted within about 10% in regard to the total number of electrons and in regard to the energy spectrum at energies exceeding the critical energy. The shape of the energy spectrum might be expected to be inaccurate for energies less than ε_0 because of the neglect of the Compton effect and the use of inaccurate cross-sections for bremsstrahlung and pair formation. More detailed calculations to be discussed below, however, show that even in this energy range the errors are small.

It needs emphasis that this high degree of accuracy can only be attributed to the shower theory in light elements. It cannot be extended, for instance, to showers in lead, where the critical energy is so low that the errors in the asymptotic radiation and pair formation cross-sections are very serious. Such accuracy also cannot be inferred, even for showers in air, very near the origin of the showers or far out in the tail. Fortunately, in applying the results of the shower problem one is primarily concerned with the intermediate region where the number of particles is large.

1. 2 Analytic solutions

Analytic solutions for the average behavior of showers under Approximation B have been given by Snyder [1938, 1949]), Serber [1938], Tamm & Belenky [1946] (also Belenky [1941, 1944]), and Bhabha & Chakrabarty[1948]. These and the solutions under Approximation A have been thoroughly discussed by Rossi (Rossi & Greisen [1941], Rossi [1952]). The solutions

given by Bhabha and Chakrabarty and by Snyder [1949] are equivalent but different in form, the former being more convenient for the calculation of the number of electrons above a finite energy, and the latter being more convenient for the calculation of the total number of electrons. For the convenience of the reader, the total number of electrons as a function of depth and primary energy, in air showers initiated by single photons, has been computed from the Snyder formulae and is displayed graphically in Fig. 1, 2 and 3.

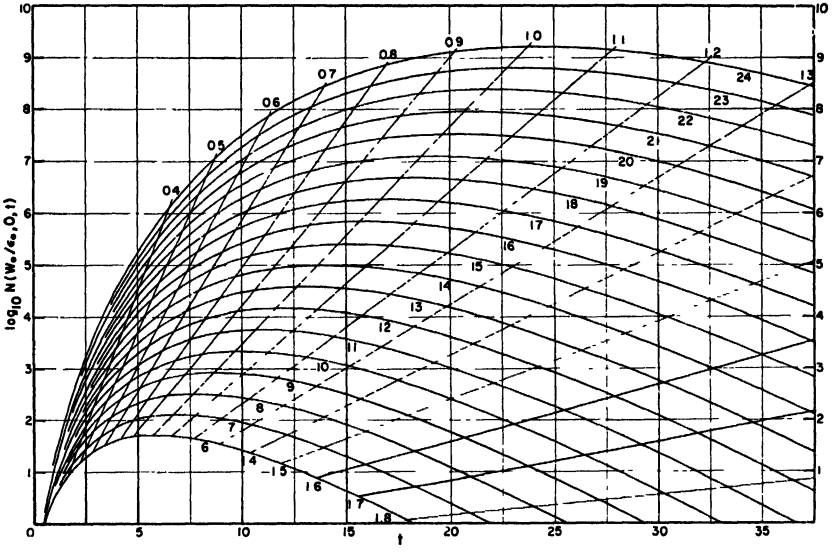

Fig. 1 – Total number of electrons as a function of the thickness of air in radiation units (37.7 g.cm^{-2}) for showers initiated by single photons of various energies, according to SNYDER [1949]. The numerical energy parameter attached to each curve is the natural logarithm of the ratio of the primary energy to the critical energy (84.2 MeV). The radial lines indicate values of the age parameter, s.

The solution of the shower problem under Approximation A is simply related to the equation for the total number of electrons, derived under Approximation B; therefore Fig. 1 to 3 can also be used to obtain the number of electrons above an arbitrary energy E as a function of atmospheric thickness, provided $W_0 \gg E \gg \varepsilon_0$. One need only substitute E for ε_0 and divide the numbers of electrons indicated in the figures by the function

$K(s, -s)$, which is defined in the references on the shower theory (e.g., Rossi & Greisen [1941]). This function is given to an adequate approximation by $2.29\,[1 + 0.4\,(s-1)]$. Appropriate values of the age parameter, s, can be obtained by interpolation between the values indicated by the radial lines drawn in Fig. 1.

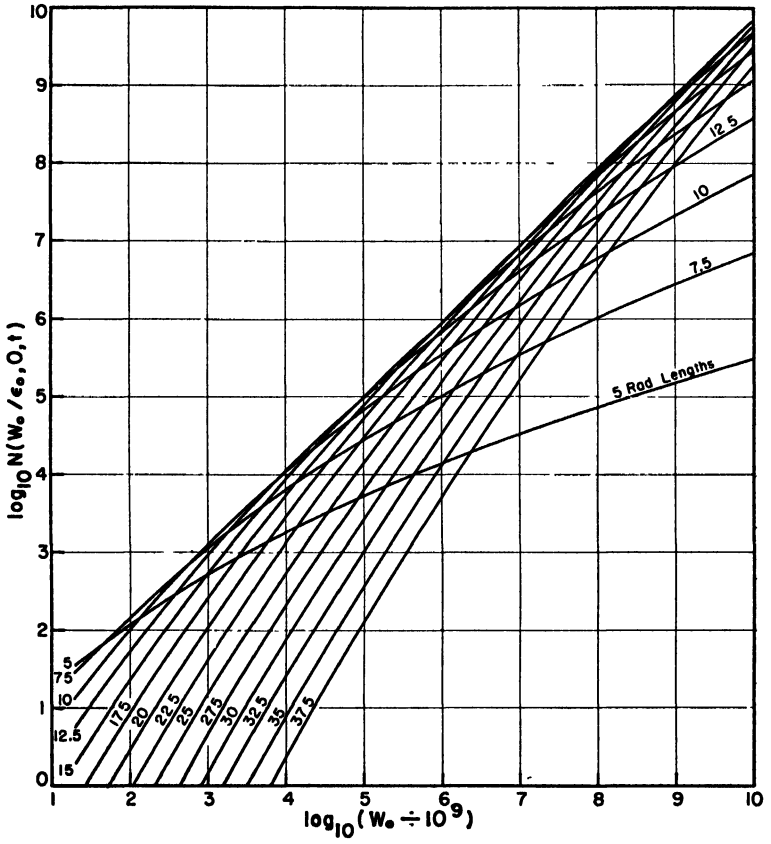

Fig. 2 – Total number of electrons as a function of primary photon energy after various thicknesses of air, according to Snyder [1949].

In principle, numerical calculations or methods of successive approximations are required in order to compute accurately the shape of the energy spectrum in the low energy region. Richards & Nordheim [1948] have carried out such calculations of the track length distribution, which is equivalent to the energy spectrum at the shower maximum. Since the shape of the low energy part of the spectrum does not vary strongly with position near the

maximum of a shower, the results can be applied without serious error throughout the region that is of importance in EAS experiments. Accurate cross-sections were employed for pair formation and bremsstrahlung, and the Compton effect and generation of electrons by knock-on collisions were taken into account as well as the ionization loss. Fig. 4 represents the integral spectra of electrons and photons, normalized to one electron of $E > 0$.

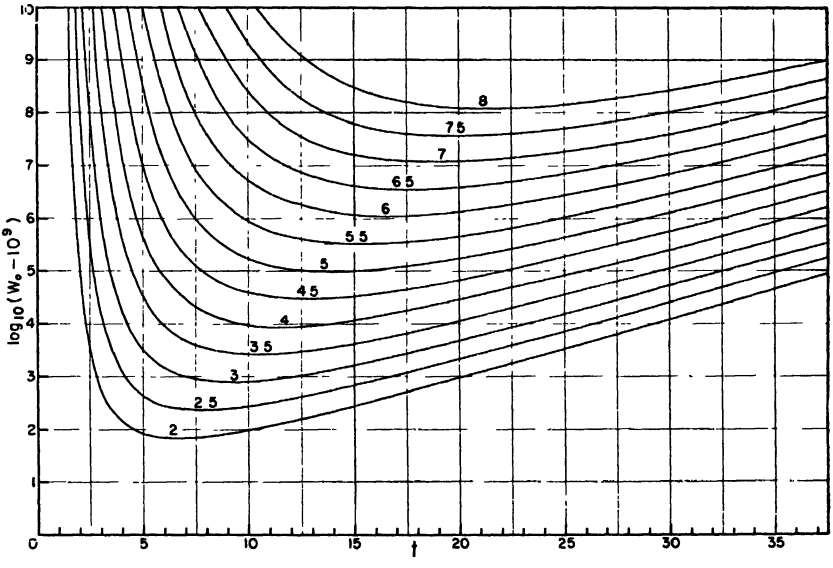

Fig. 3 – Primary photon energy required to produce showers having various total numbers of electrons, as a function of the thickness of air through which the showers have developed, according to SNYDER [1949]. The number attached to each curve is the logarithm to the base 10 of the total number of electrons.

The remarkable fact brought out by these calculations is the large fraction of the particles that are of low energy. Indeed, the photon spectrum diverges as $E \to 0$, because of the shape of the bremsstrahlung spectrum, while about 3/4 of the electrons have energy less than ε_0.

The energy spectrum has also been calculated, with a different mathematical approach, by the Padua group, (DALLAPORTA & CLEMENTEL [1946], DALLAPORTA & POIANI [1947], CLEMENTEL & FABRICHESI [1948, 1949]). For secondary particles of low energy, the Compton effect, ionization loss, and the decrease of the pair

production cross-section were taken into account. The solution has the advantage of representing the shower as a function of depth, rather than only at the maximum or averaged over the total length. Averaged over the length in air, their electron spectrum and that of Richards and Nordheim are in excellent agreement,

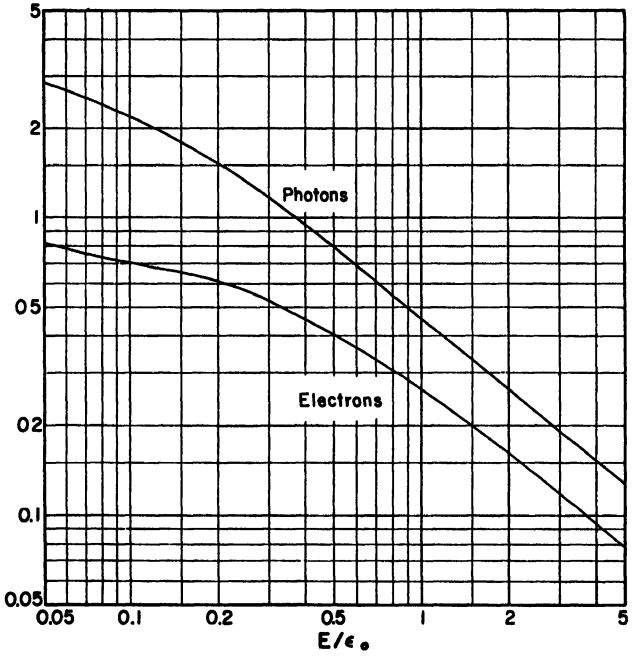

Fig. 4 – Integral energy spectra of electrons and photons, integrated over the length of the shower or at the shower maximum, according to RICHARDS and NORDHEIM [1948]. The ordinates give the number of particles with energy exceeding E, per electron in the shower.

while the photon spectra, although not identical, are in reasonable accord.

Because the Compton effect and the decrease of the pair cross-section somewhat compensate for each other in air (as contrasted with lead), the results of the Padua group for air showers do not differ greatly from those of BHABHA & CHAKRABARTY [1948] (derived under Approximation B), which are more easily accessible for calculations because of the tables and graphs that have been presented.

1. 3 Approximate Expressions

Attention is called to the shower age, s, a parameter that enters into the solutions of the diffusion equations representing the showers. Fig. 1 shows how s varies throughout the growth and decay of showers. At the origin of an event initiated by a single particle, $s = 0$; at the maximum, $s = 1$; and when s has reached 2.0 the number of particles has again been reduced to less than one.

The curves drawn in Fig. 1 are well represented, in the region where the number of particles is large, by

$$N(W_0, 0, t) \backsimeq \frac{0.31}{\beta_0^{1/2}} \exp\left[t(1 - \tfrac{3}{2} \ln s)\right]$$
$$\text{with } s \backsimeq \frac{3t}{t + 2\beta_0} \text{ and } \beta_0 = \ln(W_0/\varepsilon_0). \tag{1}$$

One may compute the approximate number of particles having an energy exceeding E, provided $W_0 \gg E \gg \varepsilon_0$, from Eq. 1 by replacing the coefficient 0.31 with 0.135 and substituting for β_0 the quantity $\beta = \ln(W_0/E)$.

The gradual increase of s describes the progressive softening of the energy spectrum of the particles, the number with energy exceeding E being proportional to $(W_0/E)^s$ over limited intervals of E. The variation in number of particles as a function of depth is also given in first approximation by a simple relation involving s:

$$\frac{\partial \ln N}{\partial t} \backsimeq \lambda_1(s) \backsimeq \tfrac{1}{2}(s - 1 - 3 \ln s). \tag{2}$$

An analytic expression for the integral energy spectrum and the number of electrons at the maximum of a shower has been given by Tamm and Belenky (Belenky [1941], Tamm & Belenky [1946]):

$$N_{\max}(W_0, E) = \frac{0.31\, W_0/\varepsilon_0}{[\ln(W_0/\varepsilon_0)]^{1/2}} \phi(\varepsilon), \tag{3}$$

where $\phi(\varepsilon) = 1 - \varepsilon e^{\varepsilon}[-\mathrm{Ei}(-\varepsilon)]$, $\varepsilon = 2.3\, E/\varepsilon_0$, and $-\mathrm{Ei}(-\varepsilon) = \int_{\varepsilon}^{\infty} dx\, e^{-x}/x$ is the well-known exponential integral. By using asymptotic expressions for $-\mathrm{Ei}(-\varepsilon)$, Eq. 3 may be expanded:

$$\phi(\varepsilon) \backsimeq \begin{cases} 1 - \varepsilon e^{\varepsilon}\left[\ln \dfrac{1}{\gamma\varepsilon} + \varepsilon - \dfrac{\varepsilon^2}{2 \cdot 2!} + \ldots\right], & \varepsilon < 1 \\ \dfrac{1}{\varepsilon}\left(1 - \dfrac{2}{\varepsilon} + \ldots\right), & \varepsilon \gg 1. \end{cases} \tag{4}$$

In Eq. 4, γ is the Euler constant, 1.7811; $\ln \gamma = 0.5772$.

The Tamm-Belenky function $\phi(\varepsilon)$ happens to agree well with the spectrum calculated numerically with accurate cross-sections by Richards and Nordheim (Fig. 4).

1. 4 Fluctuations in the longitudinal development

Once a large shower is well under way, further fluctuations in the development are small because of the great number of particles that interact independently of each other. The place where the fluctuations are most serious is near the origin, where chance variations in the behavior of one or a few particles may retard or accelerate the entire subsequent shower development. For instance, a primary photon having an energy of 10^{14} eV gives rise on the average to 550 electrons in the first 3 radiation lengths; but since this thickness is only 2.3 pair conversion lengths, 10% of the showers will still have no electrons at all.

After the first pair creation there are two electrons, each of which radiates many photons in a radiation length. Therefore to a first approximation the fluctuations of large showers initiated by single photons may be ascribed solely to variations in the depth at which the first pair creation occurs.

In this crude model, the root mean square variation of the effective thickness through which the shower has propagated is 1.3 radiation lengths, the reciprocal of the pair formation probability per unit length. Over small intervals, the number of particles can be considered to vary exponentially with thickness, according to Eq. 2, with s treated as a constant. The root mean square variation of $\ln N$ is therefore given roughly by $< \partial \ln N > \cong 0.7\,(s - 1 - 3 \ln s)$. At shower maxima, $s = 1$ and the fluctuations are negligible; but in other regions the effect is by no means small. Many of the EAS studied near sea level, for instance, have $s \cong 1.4$; for these, $< \partial \ln N >$ is about 0.4, which corresponds to a factor of 1.5 in the number of electrons. This is a minimal estimate of the fluctuations, since only the variations in behavior of the primary photon have been considered.

An elegant solution of the fluctuation problem under Approximation A has been given by Janossy & Messel [1950]. At the shower maximum, they found the fluctuations to be a minimum, and to be consistent with the Poisson formula. Fractional deviations of this order $(1/\sqrt{N})$ are negligible in large showers. Before

and beyond the maximum, the deviations were found to be larger, leading Janossy and Messel to propose the concept of fluctuations in the effective depth of initiation of the showers, which has been applied above in a very simplified form.

Bhabha and Ramakrishnan have independently derived a solution of the fluctuation problem under the same assumptions as those of Janossy and Messel, but with very different results: $\{\overline{N^2}-(\overline{N})^2\}^{\frac{1}{2}}$ was found to be on the order of $\overline{N}$ rather than $(\overline{N})^{\frac{1}{2}}$ (BHABHA & RAMAKRISHNAN [1950], RAMAKRISHNAN & MATHEWS [1953]). These results seem unreasonable by qualitative arguments; and Wilson's Monte Carlo calculations for small showers agree much better with the results of Janossy and Messel (WILSON [1952]).

The evidence available up to the present points to multiple production of mesons at the origin of EAS, with the decay $\pi^\circ \to 2\gamma$ being responsible for initiation of the electronic component of the showers. At high primary energy, the multiplicity of photons at the origin of a shower probably reduces to a great extent the importance of the fluctuations in the development of the purely electronic cascades. On the other hand, additional sources of variation in size of showers having a given primary energy must be considered: fluctuations in the depth at which the first nuclear interaction occurs, statistical variations in the types of secondaries produced and in the distribution of energy among them, and chance variations in the behaviour of the first generation of high energy secondaries. Since the nuclear interaction length is about two radiation lengths, the first of these sources of deviation alone overshadows the effect of fluctuations in the purely electronic cascade development.

2. Angular and Lateral Distributions in Electronic Cascades

Coulomb scattering of electrons is the only mechanism of lateral and angular spreading that has been taken into account in the existing calculations of the distributions. The dominant process is called multiple scattering, which is the cumulative effect of many random scatterings through small angles; although single large-angle scatterings, occurring with low probability, are the principal source of unusually large deflections in small thicknesses of matter.

2. 1 Approximations in the calculations

Many qualitative properties of the distributions are understandable on the basis of the mean square multiple scattering of relativistic electrons of energy E in a small thickness δt:

$$< \delta\theta^2 > = \left(\frac{E_s}{E}\right)^2 \delta t , \tag{5}$$

where t is measured in radiation lengths and E_s is a constant equal to $mc^2(4\pi \cdot 137)^{\frac{1}{2}} = 21.2$ MeV (Rossi & Greisen [1941]). Quantitative computations of the distributions, however, must take into account simultaneously the scattering, the energy losses, and the creation and absorption of particles.

The published calculations are of two types: calculations of the even moments of the distributions, $< r^2 >, < r^4 >, \ldots, < \theta^2 >, < \theta^4 >, \ldots$ (Euler & Wergeland [1940], Landau [1940], Belenky [1944], Moliere [1942, 1946, 1953], Roberg & Nordheim [1949], Poiani & Villi [1952b], Borsellino [1950], Janossy [1948, 1950], Nishimura & Kamata [1950], Eyges & Fernbach [1951], Fernbach [1951], Green & Messel [1952]), and calculations of the distribution functions themselves (Moliere [1942, 1946, 1953], Nishimura & Kamata [1950, 1951, 1952], Eyges & Fernbach [1951] Eyges [1948], Fernbach [1951], Poiani & Villi [1952a]). The starting point in either case has almost universally been the diffusion equations set up by Landau [1940], which may be written as follows under Approximation B of the cascade theory:

$$\left.\begin{aligned} \frac{\partial \pi}{\partial t} &= -A'\pi + B'\gamma + \frac{E_s^2}{4E^2}\left(\frac{\partial^2}{\partial\theta_x^2} + \frac{\partial^2}{\partial\theta_y^2}\right)\pi - \left(\theta_x \frac{\partial}{\partial x} + \theta_y \frac{\partial}{\partial y}\right)\pi + \varepsilon_0 \frac{\partial \pi}{\partial E} \\ \frac{\partial \gamma}{\partial t} &= C'\pi - \sigma_0\gamma - \left(\theta_x \frac{\partial}{\partial x} + \theta_y \frac{\partial}{\partial y}\right)\gamma . \end{aligned}\right\} \tag{6}$$

In these equations, A', B', C' and σ_0 are the operators of the longitudinal cascade theory representing loss and gain of particles by bremsstrahlung and pair formation, $\pi(E, x, y, \theta_x, \theta_y, t)$ is the differential spectrum of electrons, while γ is the analogous function for photons; ε_0 is the critical energy, and $\varepsilon_0\, \partial\pi/\partial E$ represents the ionization loss under Approximation B.

The terms in Eq. 6 involving $(\theta_x \partial/\partial x + \theta_y \partial/\partial y)$ describe the change of the distributions as a result of displacements occurring in dt, owing to scattering angles θ_x and θ_y acquired prior to the depth t. The term involving $(\partial^2/\partial\theta_x^2 + \partial^2/\theta_y^2)\pi$ describes the effect

of the change of direction of the electrons owing to coulomb scattering in the thickness dt. This term should include an integral over all values of θ'_x, θ'_y, of the function $\pi(E, x, y, \theta'_x, \theta'_y)$ times the probability of suffering a scattering in dt that changes the angular coordinates from θ'_x, θ'_y to θ_x, θ_y. By expanding the function π in a power series about the coordinates θ_x, θ_y, and dropping terms beyond the second order, one obtains the expression contained in the Landau equations.

It has been pointed out by GREEN & MESSEL [1952] that although the omission of the higher order scattering terms does not influence the second moments derived from the Landau equations, it directly affects all the higher even moments, the error growing worse with increasing order.

MOLIÈRE [1954] has remarked, however, that the Landau equations include the full effect of multiple small angle scattering, and that the omitted higher order terms are concerned primarily with the effects of single large angle scattering. The single scattering and the higher moments which are affected by it are of significance only for a very small proportion of the particles: computation of the fourth and higher order moments of the distributions weights the functions with a factor that vanishes rapidly for small r and θ, where most of the particles are to be found, and grows enormous in regions of large r and θ, where there are practically no particles and accuracy in the distribution functions is not very important.

Furthermore, even the second order term in the Landau equations would diverge logarithmically, if there were not a cut-off of the scattering probability at large angles (because of the radius of the nuclear charge distribution); but the higher order terms are extremely sensitive to the exact form of the cut-off, which is not well known.

Molière's approach to the problem has been to calculate the major part of the distribution from the Landau equations, and to consider the effect of single scattering separately. Another approach is to admit that the higher order moments derived from Eq. 6 have errors increasing with the order, but to insist that a distribution function derived directly from Eq. 6, or reconstructed from the moments based on these equations, will not contain appreciable errors except in the region of large r and θ, where the number of particles is inconsequential.

The Landau equations contain another error, insofar as they are applied to air showers, owing to the implicit approximation of constant density of the scattering medium (GREEN & MESSEL [1952]). This error does not influence the angular distribution, but has a significant effect, to be discussed later, on the lateral distribution.

2. 2 SOLUTIONS FOR ALL ELECTRONS ABOVE ZERO ENERGY

Lateral and angular distributions of all electrons at the maximum of a shower have been calculated by MOLIÈRE [1942, 1946, 1953]. His method was accurate in principle for the high energy particles; but he treated the shower down to the critical energy under Approximation A, and took into account the particles of lower energy with the ARLEY [1938] approximation, which is admittedly inexact. Thus, the number of particles with energy near ε_0 is overestimated and the number with lower energy underestimated. These errors are partially compensating, leading to good agreement of the Molière results with later, more exact treatments of the problem.

NISHIMURA & KAMATA [1950, 1951, 1952] have more recently obtained a solution of the Landau equations for the total number of particles at any depth in the shower, without neglecting or approximating the effect of the ionization loss term. They have given graphs of numerical results for the lateral distribution at depths represented by $s = 1$ (the shower maximum) and $s = 1.4$ (rather old showers). These results are reproduced in Fig. 5.

The natural unit of length in scattering calculations at high energy is E_s/E radiation lengths, and the natural unit of angular measure is E_s/E radians. In these units, particles of all high energies ($E \gg \varepsilon_0$) scatter similarly. However, in discussing the distributions of all particles irrespective of energy, the natural units are $r_1 = E_s/\varepsilon_0$ radiation lengths $= 9.5$ g. cm^{-2} for air, and $\theta_1 = E_s/\varepsilon_0 = 1/4$ radian. These are called the "scattering units" or "Molière units" of length and angle. Lengths measured in scattering units will be designated by the symbol x.

The ordinate in Fig. 5 is the quantity $xf(x)$, so normalized that $\int_0^\infty 2\pi x f(x)\, dx = 1$. The function f is related to the electron

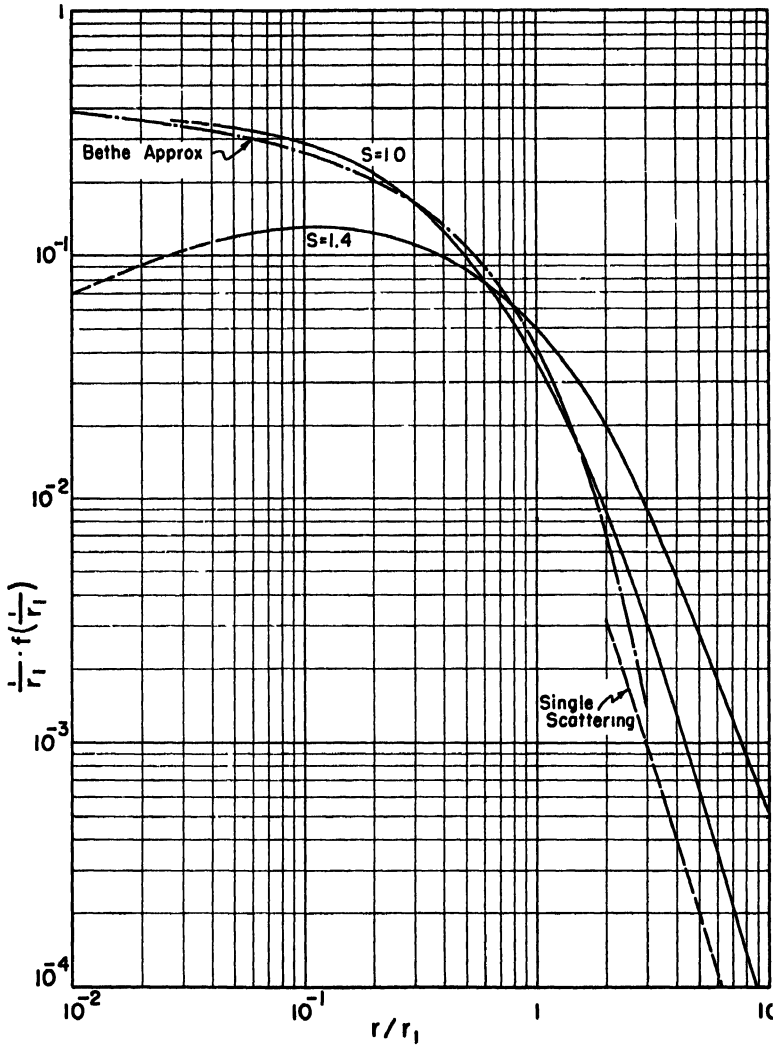

Fig. 5 – Lateral distribution of all electrons in showers at their maxima ($s = 1$) and in showers of age $s = 1.4$. The solid curves represent the calculations of NISHIMURA and KAMATA [1951], made under Approximation B; these curves are well reproduced by Eq. 11. The dot-dash curve is a much-used analytic approximation (Eq. 10) to the Molière distribution ($s = 1$) for small values of r/r_1. The dashed line is the contribution of single scattering, integrated over the shower or at the maximum, as calculated by EYGES [1948]. Normalization is such that $\int_0^\infty 2\pi x f(x)\, dx = 1$.

density Δ by $\Delta = Nf(x)/r_1^2$, N being the total number of electrons in the shower.

NISHIMURA & KAMATA [1952] have verified that their theory yields the same total number of electrons as the one-dimensional calculation of SNYDER [1949]. A comparison of the lateral distribution for $s = 1$ with that of Molière reveals good agreement for $x < 2$ and fair agreement out to $x = 6$ (NISHIMURA & KAMATA [1951]). Beyond $x = 6$, the Nishimura-Kamata distribution is higher than that of Molière, despite the neglect of single scattering by Nishimura and Kamata. The discrepancy is probably due to Molière's approximate treatment of the low energy particles.

A slight ambiguity, important in the interpretation of recent experiments, must be recognized in the graphs of the Nishimura-Kamata results. Their evaluation proceeds by way of a saddle-point integration, in the course of which the following definition of the parameter s is evolved (NISHIMURA & KAMATA [1950]):

$$\lambda_1'(s)t + \ln(E_0/\varepsilon_0) + \ln x \backsimeq 0. \tag{7}$$

Except at $r = r_1$, this differs from the usual definition encountered in the one-dimensional calculation of the total number of electrons: namely, $\lambda_1'(s)t + \ln(E_0/\varepsilon_0) \backsimeq 0$. The function $\lambda_1'(s)$, which is tabulated in references on cascade shower theory (JANOSSY [1948], ROSSI & GREISEN [1941], SNYDER [1949]), is represented approximately by $\lambda_1'(s) \backsimeq \frac{1}{2}(1 - 3/s)$; hence s is given, according to Nishimura and Kamata, by

$$s \backsimeq \frac{3t}{t + 2\ln(E_0/\varepsilon_0) + 2\ln x}. \tag{8}$$

Thus, for a fixed primary E_0 and thickness t, s is not a constant, but increases with decreasing r. This corresponds physically to the fact that the maximum of a shower is reached earlier for the high energy particles near the axis than for the low energy particles far from the axis.

Eq. 7 and 8 are closely related to the expression found in the longitudinal cascade theory for the age of a shower as a function of the energy, E, of the particles under consideration: $\lambda_1'(s)t + \ln(E_0/E) \backsimeq 0$ for particles such that $E \gg \varepsilon_0$. If one combines this relation with the expression for the characteristic radius as a function of E; namely, $r(E) = E_s/E$ radiation lengths $= r_1\,\varepsilon_0/E$, the relation becomes identical with Eq. 7.

In principle, therefore, the lateral distribution of a single shower should not be calculated with a fixed s, as was done by Nishimura and Kamata for the graphs reproduced in Fig. 5. This would only be justified if $\ln(E_0/\varepsilon_0) \gg \ln(r_{max}/r_{min})$, where E_0 is the primary energy and r_{max}, r_{min} limit the range of r over which the theory is applied. In a realistic case of a common EAS, say $\ln(E_0/\varepsilon_0) = 15$ at $t = 15$ (i.e., near the maximum of a shower with primary energy $3 \cdot 10^{14}$ eV), the distribution should have a shape corresponding to $s = 1.26$ near $x = 0.01$, 1.11 near $x = 0.1$, 1.0 near $x = 1.0$ and 0.91 near $x = 10$. This would produce a distribution appreciably less steep near the shower axis than that calculated for $s = 1$ throughout the shower, and one that falls off more steeply at large distances.

2. 3 Behaviour of the distribution near the axis

According to Nishimura & Kamata [1950], the behavior of the density distribution of all electrons near $r = 0$ is given by $f(x) \propto x^{s-2}$. This asymptotic form agrees with that derived earlier by Pomeranchuk [1944] and by Migdal [1945], except that as defined by Pomeranchuk and Migdal, s was independent of r, whereas in the Nishimura-Kamata theory s increases slowly with decreasing r, reducing the divergence of f as $r \to 0$.

When s becomes equal to or greater than 2, the density distribution becomes flat. This condition defines a region in which the position of the axis of a shower is indeterminate, owing to Coulomb scattering of the few particles of highest energy which remain in the narrow core region. One can calculate the "radius of the core", r_c, from Eq. 7. At $s = 2$, $\lambda_1' = -1/4$; therefore

$$r_c/r_1 = (\varepsilon_0/E_0)\, e^{t/4}\,. \tag{9}$$

For instance, if $\ln(E_0/\varepsilon_0) = 15$ and $t = 28$ (near sea level), one finds $r_c \cong 3$ cm. This is quite small, but for radii out to one meter, $s > 1.7$, which is so close to 2.0 that the distribution may be experimentally indistinguishable from flat.

Many experiments have sought and failed to find clear evidence of multiple cores in EAS. The above considerations suggest that the negative results may be due to the diffuseness of the single cores, rather than to an absence of multiple cores or to a very close superposition of them.

The lateral and angular distribution of electrons having a given energy are much less strongly divergent at the axis than are the distributions of all electrons: e.g., according to Molière, for $s = 1$ the density of monoenergetic electrons goes as $r^{-1/3}$ near the axis, while that of all electrons goes as r^{-1}. The difference is even more striking in the case of the angular distribution, which is finite for monoenergetic electrons, but diverges as θ^{-1} for all electrons. The divergence of the total radial and angular densities is due to the integration over energy: since the area and aperture containing the particles of energy E are inversely proportional to E^2, the energy spectrum $E^{-(s+1)}\,dE$ leads directly to the forms r^{s-2} and θ^{s-2} for the density variation near $r = 0$ or $\theta = 0$ (with s defined by Eq. 7 in agreement with Nishimura and Kamata). Thus, the high density near the axis is accounted for by the most energetic particles in the shower.

Caution must be exercised in applications of the asymptotic expression $f(r) \propto r^{s-2}$, partly because the high energy particles pass the maximum in their shower development very early (i.e., s varies rather rapidly with r near $r = 0$, never being as small as 1 at $r = 0$), and partly because the dependence of the density on r departs rapidly from the asymptotic expression as r increases. $f(r)$ is already appreciably steeper than r^{s-2} at $r/r_1 = 0.02$.

2. 4 Approximate formulae for the lateral distribution of all electrons

Bethe (quoted in Williams [1948]) has suggested the following analytic expression, which approximates the Molière distribution for small values of the argument x:

$$x f(x) = 0.45\,(1 + 4x)\exp(-4\,x^{2/3})\,. \tag{10}$$

The dot-dash curve in Fig. 5 represents this approximation.

The following empirical formula fits the Nishimura-Kamata distributions well, both for $s = 1$ and for $s = 1.4$, over the entire range of r/r_1 shown in Fig. 5:

$$x f(x) = c(s)\,x^{s-1}\,(x + 1)^{s-4.5}\,. \tag{11}$$

This expression also has the correct dependence on r near $r = 0$ for all s. Since the correct function must vary smoothly with s, it is likely that Eq. 11 can be used without great error for values

of s intermediate between 1 and 1.4, and slightly outside this range as well—say, $0.8 \leqq s \leqq 1.6$, which covers the region of principal significance in experiments on EAS.

Some values of the normalization constant $c(s)$ are given in Table 1. They are approximated for $s < 1.6$ by $0.443\, s^2(1.90 - s)$, or for $s < 1.8$ by $0.366\, s^2(2.07 - s)^{5/4}$. They were derived under the approximation of s being independent of r; hence they are only highly accurate for very large values of E_0/ε_0.

TABLE 1

Normalization constant $c(s)$ in the approximate expression of the lateral distribution, Eq. 11.

s	$c(s)$
0.50	$16/(10\,\pi^2)$
0.75	$231/(256\,\pi)$
1.00	$5/(4\,\pi)$
1.25	$45/(32\,\pi)$
1.50	$4/\pi^2$
1.75	$7/(8\,\pi)$
2.00	$3/(8\,\pi)$

2. 5 Effect of single scattering

The lateral distribution arising from single scattering has been computed for the shower maximum by Molière, using the Arley approximation for the number of low energy particles. The integral of the single scattering contribution over the length of the shower, which is nearly the same as the contribution at the maximum, has been computed by Eyges [1948], using the Belenky formula, Eq. 3, for the low energy spectrum. A similar calculation has been made by Poiani & Villi [1952a], using the longitudinal theory of the Padua group (Clementel & Fabbrichesi [1949]). In all of the calculations the form of the distribution was found to be $xf(x) = \text{const.}\ x^{-3}$ for $x \gg 1$. Molière's treatment, which underestimated the number of low energy electrons, yielded 0.015 for the value of the constant, while Eyges obtained 0.026, and Poiani and Villi obtained the value 0.024. The Eyges results are shown by the dashed line in Fig. 5.

Apparently, single scattering is not the dominant factor determining the density of electrons until very large distances from the

shower axis are reached. When the effect is predominant it is mainly due to low energy photons, which after emission by singly scattered electrons travel a long distance from the axis before releasing Compton electrons.

EYGES ([1948], p. 1806) has pointed out a source of error in these calculations, which if corrected would ultimately make the distribution fall off in approximately exponential fashion, allowing all the moments to converge. The correction is not easily evaluated, and without it, as has been mentioned, the second moment and all higher moments diverge.

2. 6 LATERAL AND ANGULAR DISTRIBUTIONS AS FUNCTIONS OF ENERGY

Molière has given for the shower maximum, and Nishimura and Kamata as a function of the shower age s, expressions for the angular and lateral distributions of particles having an energy E such that Approximation A of the shower theory is valid: i.e., $\varepsilon_0 \ll E \ll E_0$. The Nishimura-Kamata equations have not yet been evaluated numerically.

EYGES & FERNBACH [1951] and FERNBACH [1951] have derived the moments of the distribution functions from the Landau equations, under Approximation A and under Approximation B, obtaining in the latter case semi-convergent series that can be used for energies down to about $2\,\varepsilon_0$. Their calculations under Approximation B apply to the average of the distribution functions over the length of the shower; the results are therefore applicable also at the shower maximum (i.e., the depth where the number of particles of the energy under consideration is a maximum—not the depth of the maximum in the total number of particles). The calculations under Approximation A have been made not only in the average over the shower, but also for $s = 0.6$ and $s = 1.5$, corresponding respectively to rather young and old showers (see Fig. 1).

Eyges and Fernbach have found that the lateral and angular distributions can be reconstructed from their first few even moments if the shape of the functions near the origin (i.e., the order of the singularity) is known by some other means. For $s = 1$ and $E \gg \varepsilon_0$, the solutions given by Molière were assumed to be accurate near the origin. For other values of s and for low energy

particles, the assumed behavior at the origin was essentially a guess.

The distributions derived by Eyges and Fernbach corresponding to $s = 1$ are shown in Fig. 6 and 7. The normalization, which differs by a factor of 2π from the original publications, is such that

$$\int_0^\infty P(x)\, 2\pi x\, dx = 1 \text{ and } \int_0^\infty P(y)\, 2\pi y\, dy = 1,$$

where $x = rE/E_s = (r/r_1)\,(E/\varepsilon_0)$ and $y = 0\,E/E_s = (\theta/\theta_1)\,(E/\varepsilon_0)$. Thus, for instance, the relation between $P(x)$ and the density of electrons having energy between E and $E + dE$ is:

$$\Delta\,(E, r)\, dE = \left(\frac{E}{r_1\, \varepsilon_0}\right)^2 P\,[x(r)]\, \pi\,(E)\, dE\,,$$

where $\pi\,(E)\, dE$ is the total number of electrons with energy in (E, dE).

The roots of the moments calculated by Eyges and Fernbach for $s = 0.6$, $s = 1.0$ and $s = 1.5$ appear to be simply related: that is, the ratio $< r^n(s_1) >^{1/n} \div < r^n(s_2) >^{1/n}$ is practically the same for all the values of n. This implies that under Approximation A, within the accuracy of the Eyges-Fernbach calculations, the variation of s produces only a scale change of the radial coordinate. This inference has been verified graphically with the distributions tabulated by Fernbach. It is reasonable to conclude that the inference applies not only to $s = 0.6$, 1.0 and 1.5, but to other values of s as well, at least to intermediate ones. The variation of the shower geometry with age (for particles of a given high energy) [1] can thereupon be treated in an elementary fashion as a simple stretching of the scale; and the scale factor can be derived from knowledge of only the second moment of the distribution, which has been extensively and accurately calculated (see Fig. 8 and 9).

BORSELLINO [1950] has independently derived, from the Landau equations under Approximation A, expressions identical to those used by Eyges and Fernbach for all the radial and angular moments of the distributions as functions of the age parameter. His tabulated values of the second moments are the ones repre-

[1] The lateral distribution of *all* the electrons changes with shower age in a more complicated way than the distribution of particles having a given energy, because of the change of the shape of the energy spectrum with age of the shower.

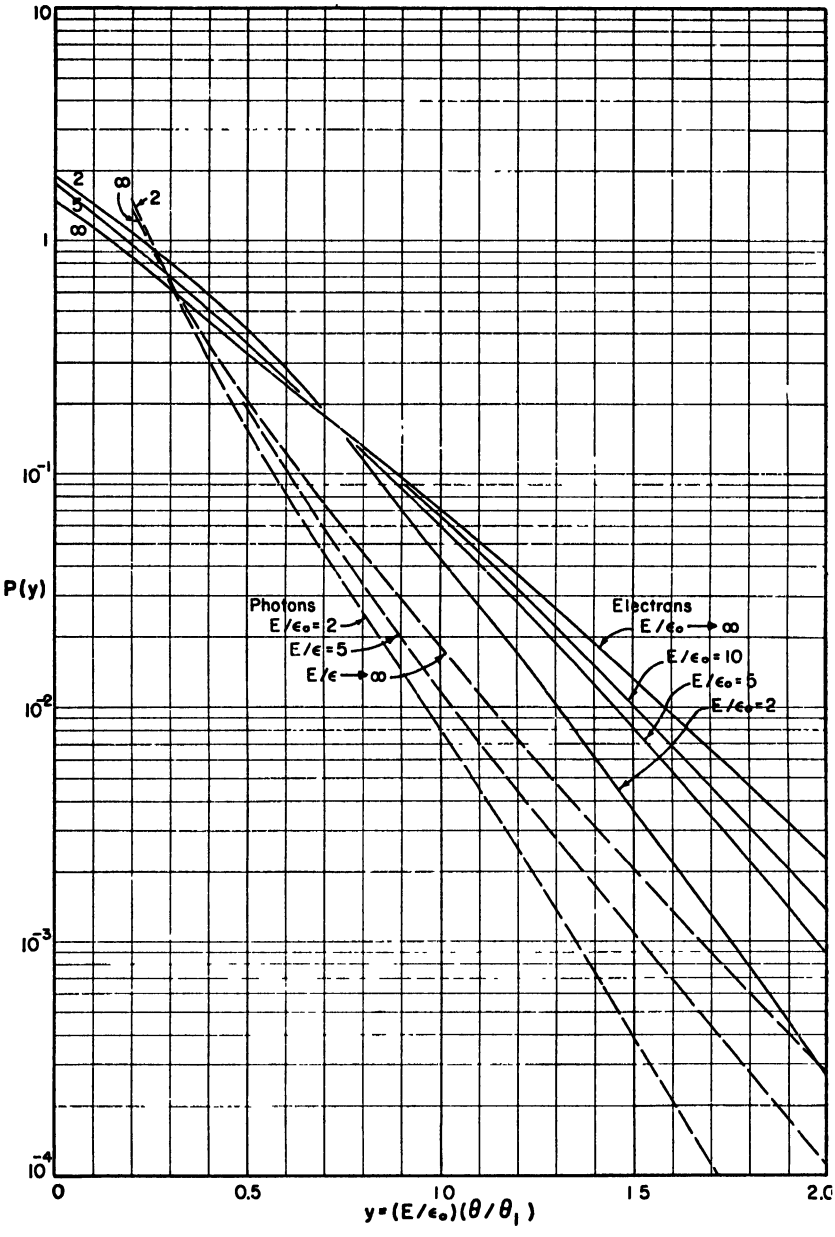

Fig. 6 – Angular distributions of photons and electrons of various energies, derived by Eyges and Fernbach from the moments of the distributions averaged over the length of the shower, under Approximation B.

$$\int P(y)\, 2\pi y\, dy = 1 .$$

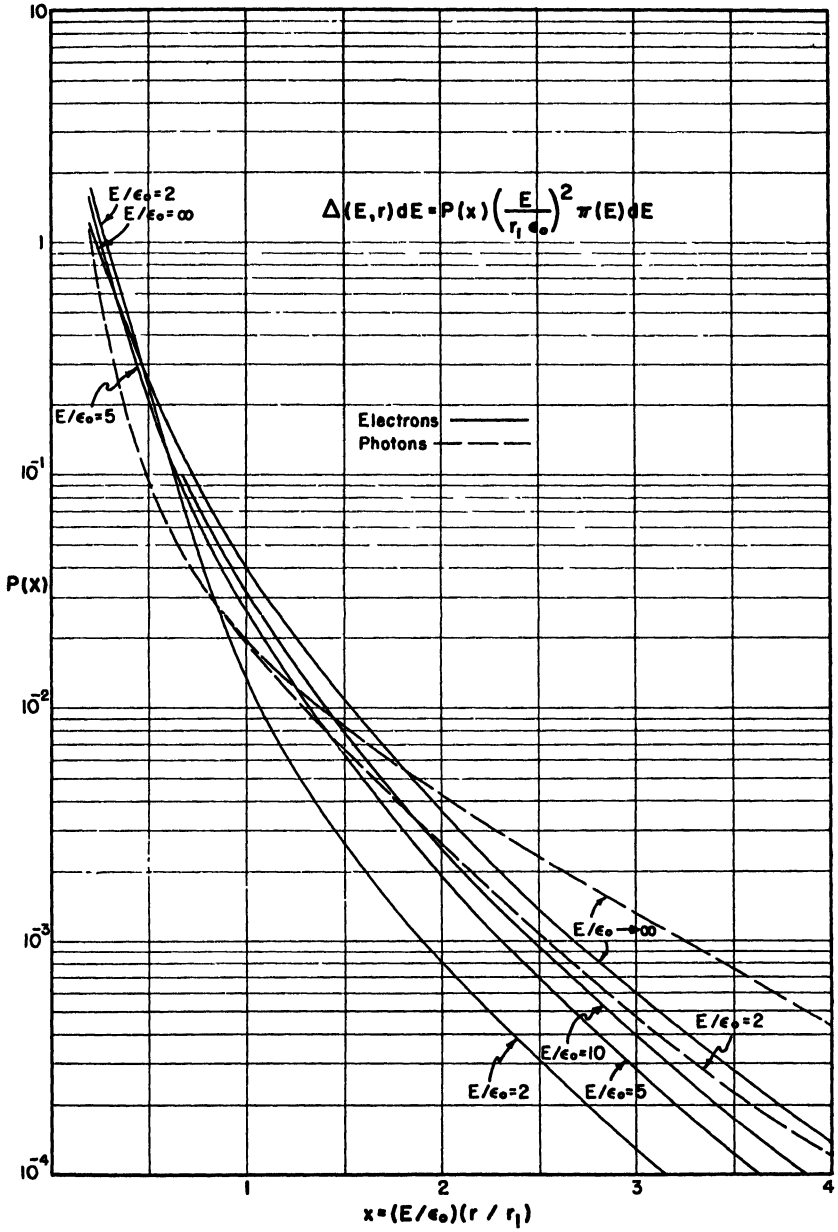

Fig 7 – Lateral distributions of photons and electrons of various energies, derived by Eyges and Fernbach from the moments of the distributions averaged over the length of the shower, under Approximation B.

$$\int P(x)\, 2\pi x\, dx = 1 .$$

sented in Fig. 8. The same expressions for the second moments have also been obtained independently by JANOSSY [1950a].

It is interesting to note (Fig. 6, 7, 8) that the photons of a shower travel at smaller angles to the axis than the electrons, and yet are more abundant than the electrons at large distances from the axis. The reason for the smaller angles is that photons of a given energy retain rather accurately the direction of their

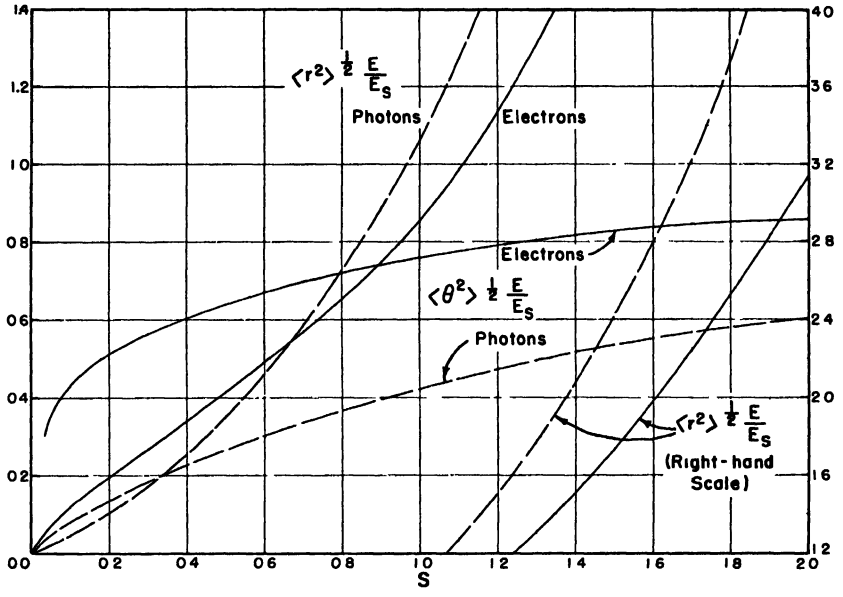

Fig. 8 – Root-mean-square radial and angular displacements of particles of energy E as functions of the shower age, calculated for pure electronic showers in a medium of constant density, from the Landau equations under Approximation A (BORSELLINO [1950]). Single scattering has been neglected.

parent electrons, which had higher energy. The reason for the comparatively large distances of some of the photons from the axis is the possibility of a photon travelling a long way without energy loss. This effect becomes most pronounced at low energy (10^7—10^8 eV), where the photon absorption cross-section is a minimum while the electrons have very short range on account of the ionization loss.

No lateral and angular distributions as functions of energy are available at this time for particles between zero energy and twice the critical energy. This is the interval in which even Approximation B is not accurate. However, Roberg and Nordheim have

calculated the second moments averaged over the shower length, without neglecting any of the important interaction processes, and without the approximation of asymptotic cross-sections, but ignoring single scattering and the variation of atmospheric density (ROBERG & NORDHEIM [1949]). Some of their results are graphed in Fig. 9. Analogous calculations leading to similar

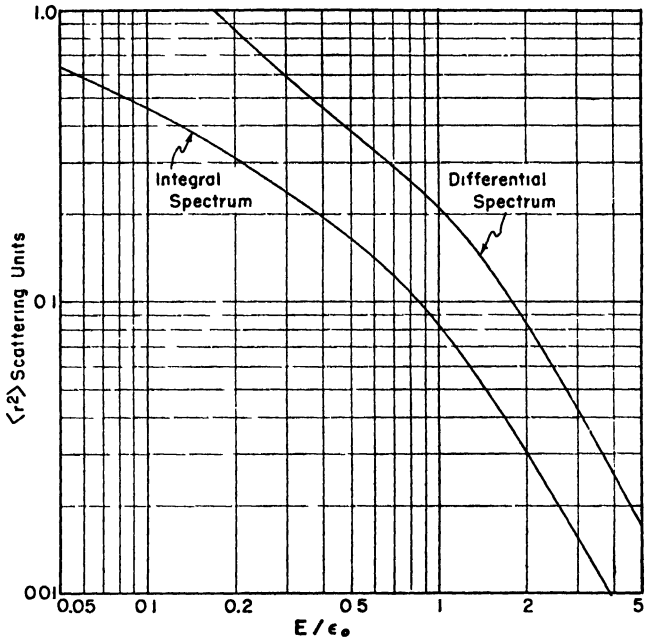

Fig. 9 – Mean square radial displacement of electrons as a function of the energy, averaged over the length of a shower; from the numerical calculations of ROBERG and NORDHEIM [1949]. Single scattering and the variation of the density of the air have been neglected.

results have also been carried out by POIANI & VILLI [1952b] on the basis of the longitudinal theory developed by the Padua group (CLEMENTEL & FABBRICHESI [1949]).

According to Roberg and Nordheim, electrons of energy less than 4 MeV have $< \theta^2 > \geqq 1$, meaning that these electrons diffuse in random directions instead of following the axis of the shower. Cloud chamber pictures of EAS show these scattered electrons very commonly. According to the spectrum of Richards and Nordheim, they comprise about 1/6 of all the electrons in the showers.

2. 7 Effect of atmospheric density variation

The variation of the density of the atmosphere along the path of a shower affects the radial distribution of the particles in a way that can be discussed with reference to Fig. 10. The various symbols t, t', . ., used in describing the development of the number of particles in the shower, represent atmospheric thicknesses in mass units (radiation lengths).

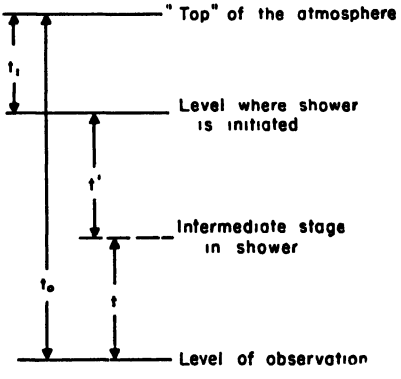

Fig. 10 – Illustration of symbols representing atmospheric thicknesses involved in the discussion of shower development in an atmosphere of varying density.

In all of the calculations described above, the radial displacements of particles at t_0 have been computed essentially by multiplying the angular scattering of their parents, occurring at intermediate levels of the shower, by the lever arm t, and integrating over all the intermediate levels between t_1 and t_0.

Let the unit of radial displacement be the geometrical radiation length computed with the density of air at t_0. Then for an isothermal atmosphere the correct lever arm is not t, but Δz, where

$$\Delta z = t_0 \ln \frac{t_0}{t_0 - t} = t\left[1 + \tfrac{1}{2}\frac{t}{t_0} + \tfrac{1}{3}\left(\frac{t_0}{t}\right)^2 + \ldots\right].$$

The computed radii are therefore too small by a factor equal to the quantity in brackets averaged over the above-mentioned integral. An accurate solution should also take into account the fact that the atmosphere is not isothermal: the decrease of temperature with elevation reduces the correction factor.

Green & Messel [1952] have indicated a formal approach to the solution of the problem for an isothermal atmosphere, but have only carried through the solution for the case of an assumed power law spectrum of electrons incident on the top of the atmosphere (and neglecting ionization losses). This solution has little resemblance to showers initiated within the atmosphere by single photons.

An estimate of the correction factor can be made by reviewing the calculation of the mean square radial displacement of electrons,

averaged over showers in all stages of development. Physically, the averaging corresponds to weighting with equal probabilities showers that begin at all possible levels t_1 (see Fig. 10); hence the results only have meaning for large values of t_0. The integrand occurring in the solution of this problem (for an atmosphere of constant density) has been calculated and shown graphically by JANOSSY ([1948], p. 322). By numerical averaging of the correction factor to $< r^2 >$; i.e., $(\Delta z/t)^2$, over the integral with respect to t, one finds that the average value of the correction factor is very nearly equal to $(1 - 4/t_0)^{-1}$ for all large t_0. Within the limitations of Approximation A of the shower theory, this result is independent of the primary energy of the shower and the energy of the secondary particles under consideration.

For showers detected in the lower part of the atmosphere, the indicated modification of the lateral distribution can be effected by merely evaluating the geometrical radiation length with the air density two radiation lengths back along the shower axis from the point at which the showers are observed. It is obvious, however, that a correction such as this is not precise, and can only be used reliably where the correction is small and precision in it is not required, namely at low altitudes.

2. 8 MAGNETIC DEFLECTIONS

It has been remarked by COCCONI [1954b] that deflections of the secondary electrons by the earth's magnetic field produce a lateral dispersion which is not very small compared with that due to Coulomb scattering. The magnetic deflection bends the positons towards the east and the negatons towards the west. Thus the lateral distribution loses its azimuthal symmetry and the showers are stretched from a circular shape into one that is roughly elliptical.

The calculated factor by which the east-west axis of a vertical shower is stretched by the horizontal component of the earth's field is $[1 + 0.05\,(\cos \lambda/P)^2]^{\frac{1}{2}}$ for particles of all energies (λ is the geomagnetic latitude and P the pressure in atmospheres). This is a very small correction near sea level, even if the rough calculation should be considerably in error. But at airplane altitudes the factor $1/P^2$ may be in the range 10—20; and at these altitudes showers frequently arrive with large inclinations, in which case the vertical component of the field, as well as the horizontal

component, contributes to the magnetic deflections. Thus, at 240 g. cm^{-2} pressure and 45° latitude, for showers coming from the north at 45° relative to the zenith, the magnetic effect exceeds the coulomb scattering, making the east-west stretching factor about $\sqrt{3}$. The distribution function at this altitude will not only by highly asymmetrical, but will differ strongly for inclined showers arriving at different azimuths.

CHALOUPKA [1954] has sought to detect the magnetic effect at 2634 m elevation, by recording EAS with two parallel, unshielded counter telescopes, inclined at 45° relative to the zenith. As expected, the coincidence rate was found to vary with the azimuthal angle, being 10% greater than the average when the telescopes pointed to the east or west and 10% smaller than the average when they pointed to the north or south. Although the observations cannot easily be submitted to a quantitative comparison with the theory, they suggest that even at low elevations the magnetic deflections are not entirely negligible.

2. 9 SUMMARY

In review, it appears that the shower theory of Nishimura and Kamata, supplemented by the energy and age dependence of the distributions calculated by Eyges and Fernbach, Roberg and Nordheim, Poiani and Villi, and Borsellino, gives a reasonably adequate description of the lateral distribution in pure electronic showers, provided that the following restrictions are maintained: (1) the theory should only be used for showers observed in the lower half of the atmosphere, because it does not properly account for the variation of atmospheric density or the deflections due to the earth's magnetic field; (2) a first-order correction for the density variation should be made by evaluating the radiation length at an elevation 2 cos θ radiation lengths above the level of observation (thus, for vertical showers the scattering unit of length, $X_0 E_s/\varepsilon_0$, should be taken as 79 m at sea level and 120 m at 3250 m elevation, assuming at both elevations a temperature of 0 °C. two radiation lengths above ground level); and (3) the theory should not be applied for $(r/r_1)(E/\varepsilon_0) \gtrsim 1$, nor should the higher moments of the distributions be relied on for accuracy, because of possible errors at large values of r where single scattering is important.

3. Experiments on the Lateral Distribution of Electrons

Numerous measurements have provided information on the lateral distribution in overlapping intervals of the distance from the shower axis. We omit extensive discussion of the simple decoherence curves of counters or ion chambers—the frequency of coincidences as a function of separation—because the interpretation depends on too many other factors besides the lateral distribution, and is not very sensitive to the distribution itself. The directly indicative experiments, summarized below, are those in which the density of particles was measured either at known distances from the axis or at more than one point in each recorded shower.

3. 1 Medium distances, $0.03 < r/r_1 < 2$

Cocconi, Tongiorgi & Greisen [1949b] used a combination of an unshielded counter and four counters under 9 cm of lead as a "core selector"—henceforth abbreviated C.S.—at 3260 m elevation. It is not obvious whether nuclear-active particles or high energy photons and electrons contributed most to the triggering of a C.S., but the results of the experiment and the rapid decrease of the coincidence rate of two C.S. with increasing separation show that each C.S. discriminated strongly in favor of showers whose central axes fell within a small number of meters of the C.S. At two different distances from the C.S., groups of unshielded counters were disposed by which the electron density could be measured within a factor of about two as long as the density lay between 2 and 500 particles per square meter.

Fig. 11 shows the frequency with which different relative densities were measured at the various pairs of distances investigated in the experiment. The widths of the distributions can be accounted for, except for a few isolated events, by the expected errors in density measurement without assuming any errors in the location of the shower axes (although the average value of the smallest radial distance, taken as 4 m, must nevertheless be somewhat in doubt). This consistency not only confirms, as mentioned above, that the C.S. fulfilled their intended function, but also shows that the density decreases smoothly with distance from the axis, without large fluctuations due to local concentrations of particles.

The latter conclusion is of importance to the methods of estimating the magnitude and the primary energy of EAS. It follows that if one measures the density at a known distance from the axis of an EAS, or if the density is determined at several positions, so that the location of the axis can be deduced from the

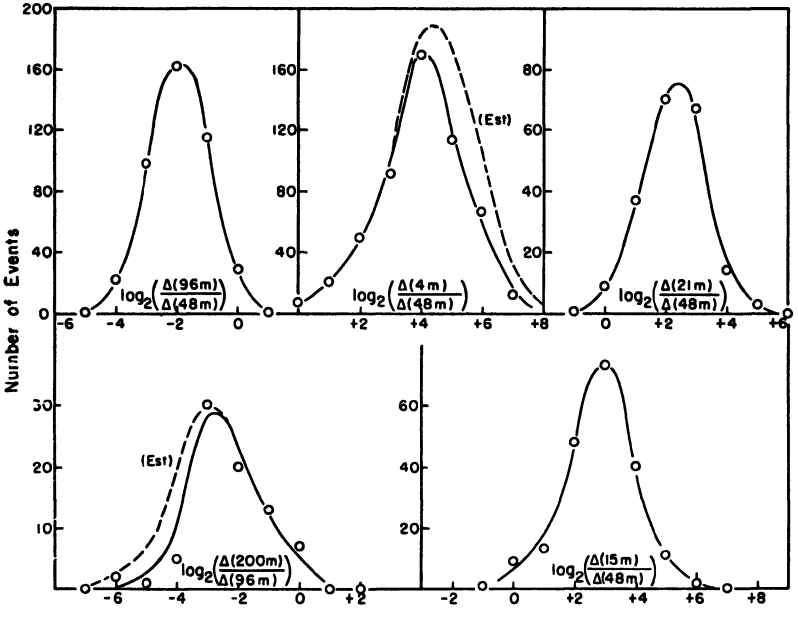

Fig. 11 – Frequency with which various relative densities were measured at different pairs of distances from the axes of EAS at 3260 m elevation; from the data of Cocconi, Tongiorgi and Greisen [1949b]. Fluctuations in the measurements cause a slight bias, associated with cases where the density at the greater distance is too small for measurement or the density at the smaller distance is too great for measurement. Estimates of the corrections in the two situations where the bias is greatest are shown by the dashed curves.

relative densities, one can safely infer the total number of electrons in the shower. From this, one can presumably compute an approximate value of the primary energy.

The average relative densities obtained by Cocconi *et al.* are plotted as a function of r in Fig. 12, where they are compared with the theory of Nishimura and Kamata for several values of the age parameter. The experimental uncertainty at the extremes of the radial distance range is estimated to be a factor 1.5, as

shown on the graph. The results are observed to be in excellent agreement with the theory for either $s = 1.0$ or $s = 1.2$.

The smallest of the showers included in these measurements

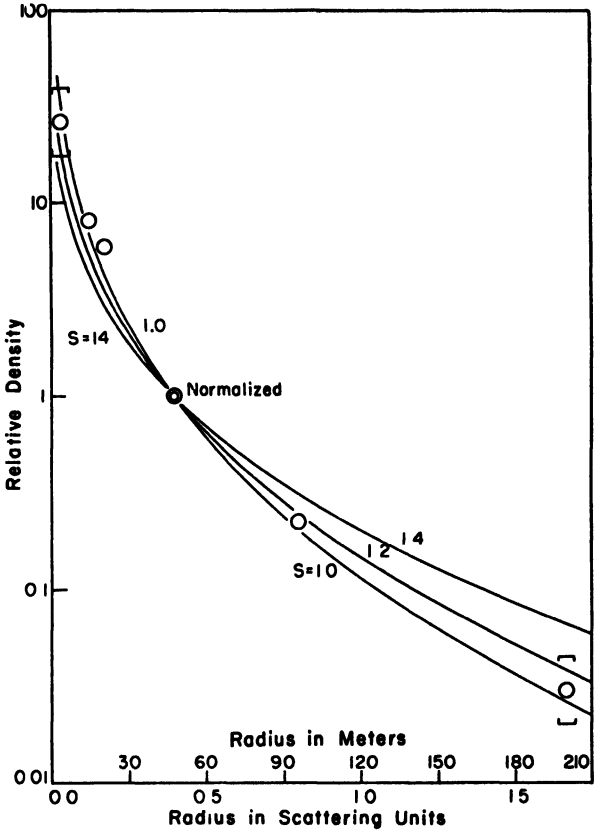

Fig. 12 – Relative density of particles in showers of 10^5–10^8 electrons as a function of distance from the central axis, at 3260 m above sea level. The points are taken from the data of Cocconi, Tongiorgi and Greisen [1949b]. The curves are drawn according to the theory of Nishimura and Kamata, under the assumption that each shower has but a single axis and that the lateral displacements are entirely due to Coulomb scattering of the electrons.

had the minimum measurable density, 2 m^{-2}, at 48 m, corresponding to a shower of 10^5 electrons. The largest showers, of which very few were recorded, had densities of 500 m^{-2} at 96 m, corresponding to a total of 10^8 electrons. If one assumes that all the showers were initiated at the same pressure level, about 100 g. cm^{-2}, one finds from Eq. 8 that the variation in both r and E_0

should have caused s to change from about 0.9, for the largest showers at the biggest distance from the axis, to about 1.5 for the smallest of the events at the shorter distances. [1] Each point on the graph represents an average over shower sizes, however, making the expected variation of the apparent age with r smaller, about 1.1 to 1.4. While the data are not accurate enough to preclude this, they agree better with still less variation of s, say from 1.2 to 1.0, or with no variation. This observation appears to be related to the nuclear origin and propagation of the showers, and will be discussed later, after the assembly of more information bearing on the subject.

On the other hand, if each shower represented a superposition of numerous cascades having axes distributed uniformly over a radius as large as 5 m, the density distribution for small values of r should have been considerably flatter than was observed. Also, the decoherence curve of the C.S. should have levelled off at small spacings, whereas, on the contrary, it remained steep down to one or two meters. One must conclude that if showers of $\sim 10^6$ electrons are inherently multiple at the origin, the axes are concentrated within a radius of a few meters.

At sea level, an experiment very similar to that of Cocconi *et al.*, using the same kind of core selectors, has been reported by FUJIOKA [1953]. Relative densities were determined at distances from the C.S. ranging from 5 to 47 m, in showers containing 10^5—10^7 electrons. The results are shown graphically in Fig. 13. As suggested in the figure, one should make allowance for a slight underestimate of the smallest distance from the axes of the EAS, owing to lack of precision in the core selection.

Measurements of the lateral distribution at sea level have also been made by HADDARA & JAKEMAN [1953], with results that are shown together with those of Fujioka in Fig. 13. Haddara and Jakeman employed a core selection device that in principle is superior to the one of Cocconi and of Fujioka: cores were identified by the occurrence of cascades of at least 9 particles, entering a cloud chamber from a 5-cm lead shield. Such events require the presence of a high energy photon or electron, which presumably implies proximity of the central axis of the shower.

[1] In making this calculation, an estimated multiplicity of photons was assumed at the origin of the shower. The results are not very sensitive to the accuracy of this estimate.

Unfortunately, the counting rate was very low (one every two days), so that the results had to be inferred by a statistical analysis of only 36 events. Each point is represented doubly in Fig. 13, in keeping with the reported estimate of the maximum

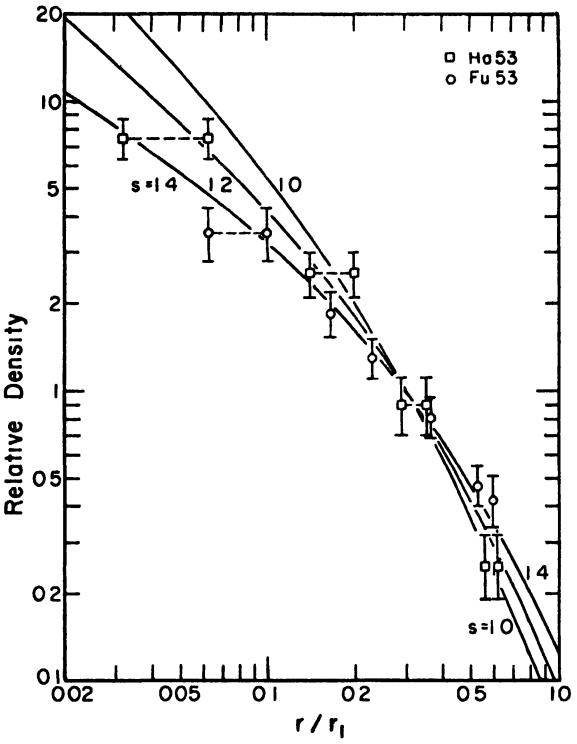

Fig. 13 – Relative density *vs.* distance from the axis of showers at sea level. The points represent measurements by FUJIOKA [1953] and by HADDARA and JAKEMAN [1953], while the curves are drawn according to the theory of Nishimura and Kamata. Normalization was made at $r/r_1 = 0.3$ ($r = 24$ m). Most of the recorded showers contained 10^5–10^6 electrons.

systematic error (certainly an overcorrection) in the location of the shower axes.

The smooth curves in Fig. 13 represent the theory of Nishimura and Kamata. The results of Fujioka agree well with $s = 1.4$ or 1.5, while the points of Haddara and Jakeman agree better with $s = 1.2$; but both sets of points are quite consistent with a smooth curve corresponding to $s = 1.3$. Even if the showers were initiated by primary electrons, this would be a very reasonable

value for the age parameter of showers of $\sim 10^6$ particles at sea level in the radius interval 0.03 to 0.5 r_1; and there is no indication, even at distances as small as 3 m from the axis, of an excessive flattening of the lateral distribution, such as might be expected to result from a multiplicity of shower cores.

3. 2 Large distances, $0.4 < r/r_1 < 5$

Barrett, Bollinger, Cocconi, Eisenberg & Greisen [1952] located the axes of air showers at sea level by observing with a hodoscope the directions of μ-mesons detected at 1600 m water equivalent underground. To penetrate that far underground the mesons had to be created with an average energy near 10^{12} eV. It was shown that the trajectories of the mesons were accurately parallel to the axes of the EAS, by observing that showers of mesons detected undergrond were very narrow. By projecting the track of a meson to the surface, the distance could be computed between the axis of the associated EAS and four trays of unshielded counters located on the surface of the ground above the meson detector.

Invariably, it was observed that the counter tray nearest to the projected axis of the shower was the one in which the most counters were discharged. This confirms other indications that there are no distinct, widely separated multiple cores in the EAS, but that the density decreases smoothly (except for statistical fluctuations) with distance from the axis.

The frequency with which the unshielded counters were discharged, as a function of the distance of the counters from the axis, depended on both the lateral distribution and the size distribution (i.e., distribution with respect to number of electrons) of the showers in which mesons were detected undergrond. The shape of the size distribution could be deduced separately from the records of the relative frequency, averaged over all distances from the shower axes, with which various numbers of counters in the trays were discharged. Thereafter, with an assumed lateral distribution function, and with the known angular resolution function of the underground telescopes, it was possible to compute numerically the expected number of coincidences as a function of the apparent distance from the axis. Computations made with the Nishimura-Kamata theory corresponding to an age $s = 1.4$ agreed well with the observations throughout the range 30 to

300 m from the axis. Similar computations made with the Molière function or the Nishimura-Kamata theory for $s = 1$ disagreed with the data, but any value of s in the range 1.4 ± 0.15 would probably have been satisfactory.

The size distribution in the above experiment was rather flat because of the bias introduced by requiring a meson far underground. Thus the inferred age represents an average over a very wide range of shower size, about 10^3 to 10^7 particles. Except for the presence of the high energy mesons, the experimental results could be consistent with the hypothesis of primary electrons originating the EAS.

In Russia, at 3860 m elevation, ZATSEPIN and his collaborators [1953] made use of multiple counter trays in hodoscope arrangement for the simultaneous measurement of density at widely distributed points in individual showers. Density measuring sets were placed at the corners and center of a diamond-shaped area with diagonals of 600 and 1000 m. The relative densities made possible the locating of the central shower axes and thus the determination of density as a function of distance from the axis.

Between 200 and 600 m from the axis (i.e., $1.5 \leq r/r_1 \leq 4.6$), the density of charged particles was found to vary as r^{-n} with $2.7 < n < 3.1$. The proportion of the particles that are mesons was also determined, and was found to increase linearly with r, attaining the value 0.25 at $r = 600$ m (see Fig. 28). By subtracting the mesons, the electron density is found to vary approximately as $r^{-n'}$ with $2.9 < n' < 3.3$. This variation is slower than that expected of showers at their maximum development, but agrees with that expected of showers having an age parameter of 1.25 ± 0.12.

The showers with measurable density at such large distances are great in size ($\gtrsim 10^7$ particles); hence the question arises as to whether it is reasonable for such large showers to be beyond their maximum development at mountain elevations. Partial justification is provided by the expectation that the very big showers should have axes inclined at large zenith angles, on the average, and the mean thickness of the atmosphere through which the showers have developed should be greater than the vertical depth. A more important factor probably arises from the fact that the showers are not caused by single high energy photons or electrons, but by a succession of groups of lower energy photons,

created both in the initial collision of the primary and in the succeeding chain of nuclear interactions.

3. 3 Small distances from the axis

Numerous investigations have been made of the density distribution near the central axis, in an effort to obtain information about the multiplicity and angular distribution of the secondaries emerging from the primary interaction. The experimental results have, in general, been compared with predictions calculated from the Molière theory. Within a few meters of the axis, significant discrepancies have been noted: the electron density has not been found to diverge as r^{-1}, but to have a somewhat smaller gradient. Beyond a few meters from the shower axis, the discrepancies with the Molière theory have generally not been discernible.

The experiments may be summarized briefly as follows:

(1) *Cloud Chamber Observations*

From pictures of EAS taken with a large cloud chamber at 3000 m elevation, Hazen [1952] selected and analyzed those which most nearly resembled the expected appearance of showers in the neigborhood of their central axes. The cases exhibiting the biggest density gradients probably represented small showers (10^4—10^5 electrons) with axes inside or within 1/2 meter of the chamber. The density gradients, however, were found to be much smaller than those predicted by the Molière theory.

On the other hand, Relf [1955] observed EAS at sea level with a very large diffusion chamber (two square meters of horizontal sensitive area), and obtained a few events in which the axes appeared to be near the chamber and the density gradients seemed large enough to be consistent with the Molière theory.

(2) *The Burst Ratio Distribution*

Campbell & Prescott [1952] have shown that the frequency with which two nearby ionization chambers register simultaneous bursts having a size ratio exceeding λ, as a function of λ, is sensitively dependent on the lateral distribution function, $f(x)$. Under the approximation $f(x) \propto x^{s-2}$, their measurements, made at sea level, indicate $s = 1.23 \pm 0.09$. If this result is corrected for the error in the approximation $f(x) \propto x^{s-2}$ at finite values of x, the value of s is increased to 1.38 ± 0.10.

(3) *The Ionization Chamber Decoherence Curve*

The frequence of coincident bursts in two ionization chambers as a function of their separation has been measured by WILLIAMS [1948] at 3050 m elevation and by CAMPBELL and PRESCOTT [1952] at sea level. Williams' data have been analyzed by BLATT [1949], and the same analysis was followed by Campbell and Prescott. In both cases the decoherence curve calculated with the Molière distribution was found to be too steep in the region of small chamber separations (less than 5 m).

The contributions to the rise of the curve in this region are expected to be made by rather small showers, which should normally be old. Blatt has shown that if $f(x) \propto x^{s-2}$ near $x = 0$ and if γ is the exponent of the number distribution, the curve should be horizontal at zero separation provided $s \geqq 2 - \gamma^{-1} \approx 1.33$.

(4) *Frequency vs. Density near the Shower Axis*

KASNITZ & SITTE [1954] used counters in coincidence and anti-coincidence, at 3260 m elevation, to select showers with axes striking close to a cloud chamber and a counter hodoscope, with which the shower density could be determined. The relative frequency as a function of density was found to correspond to an age $s = 1.24$ for small showers of 10^4—10^5 electrons, $s = 1.20$ for showers of 10^5—10^6 electrons, and $s = 1.15$ for large showers of 10^6 -10^7 electrons. The remarkable feature of these results is the smallness of the variation of age with size of the shower, a feature that also appeared in the lateral distribution at larger radii according to the data of Cocconi *et al.* and of Zatsepin *et al.*

(5) *Hodoscope Measurement of $f(x)$.*

With five trays of unshielded counters connected to a hodoscope, SITTE, STIERWALT & KOFSKY [1954] selected showers whose axes struck close to the central tray, and determined the relative electron densities at distances of approximately 2 m, 4 m and 8 m from the axes. With the aid of further trays of lightly shielded counters, the showers were classified into different age groups on the basis of the apparent energy spectra of the electrons and photons. The youngest showers, which presumably had an age less than 0.8, had distributions in agreement with the Molière function ($s = 1.0$). The other age groups, regardless of the ap-

parent age, were found to have almost identical lateral distributions corresponding to $s \approx 1.2$. (It is possible that the apparent variation of age, deduced from the energy spectrum, was in part spurious, being influenced by small variations of the distance between the shielded trays and the shower axes).

(6) *Multiple Ionization Chambers*

With the aid of an assumed lateral distribution function, the coincident pulse heights registered by three ion chambers can determine the locations of the axes of individual showers and the sizes of the showers. If more than three chambers are used, the results are overdetermined, and the consistency is a test (although not a very sensitive one) of the correctness of the assumed distribution. The method is only applicable to the showers whose axes fall near or within the array of ion chambers.

With this method, WILLIAMS [1948] analyzed 28 showers detected at 3050 m elevation, and found them all to be consistent with the assumed Molière distribution function. The chambers were at the vertices and center of an equilateral triangle 12.2 m on a side, and the usable events were rather large showers, 10^6 — 10^8 electrons.

HAZEN, WILLIAMS & RANDALL [1954] later applied the same method to smaller showers with axes at smaller distances from the ion chambers: five chambers were used in this case, four of them at the vertices and center of a triangle 2.2 m on a side, with the fifth chamber 3.6 m from the center. The elevation was 3260 m. The data were observed to be consistent with the Molière distribution in 80% of the events. These corresponded to shower axes between 0.5 and 4 m from the nearest detector. At distances less than $\frac{1}{2}$ m, the results indicated a much flatter distribution.

3. 4 INTERPRETATION OF OBSERVATIONS NEAR THE SHOWER AXIS.

The indications that the lateral distribution near the shower core is flatter than that predicted by Molière have occasionally been discussed as evidence of the multiple production of high energy secondaries at the origin of the EAS. However, a consideration of the Nishimura-Kamata theory, and in particular of the variation of the age parameter with r, indicates that the observations described above can all be accounted for without any

lateral spreading owing to the initial nuclear interaction or the subsequent nuclear cascade.

Consider a typical instance, involving a shower of 10^5 electrons detected 16 radiation lengths below the point of origin. If the shower is imagined to be due to a single high energy photon, $\ln(E_0/\varepsilon_0) \approx 14$ and $s = 1.1$ for the shower as a whole; but at different radii, $s \approx 1.1\,[1 + 0.045 \ln(r/r_1)]^{-1}$. At one meter from the axis, the appropriate value of s would be 1.4, and the expected gradient of the density, owing to Coulomb scattering alone, would be much less than that given by the Molière theory. If the shower is imagined to be due to, say, ten identical, colinear photons at the origin, the expected gradient would be even smaller, since the age would be $1.2\,[1 + 0.05 \ln(r/r_1)]^{-1}$, which is about 1.6 at one meter from the axis.

Indeed, the greatest difficulty in interpreting the experiments described above, in view of the nuclear origin of the showers, lies in explaining why the lateral distributions are as steep near the axis as the experiments have indicated. One must at the same time explain why the small showers, on the average, do not have much flatter distributions than the large showers.

The latter point cannot be accounted for under the old hypothesis of electron primaries, all of which would interact at the top of the atmosphere. Two properties of nuclear initiation help to reduce the difference in apparent age between small and large showers. One is the variation in the depth of initiation of the showers. Since the efficiency of detection is greatest for showers near their maxima, the smaller of the detected showers will have points of initiation lower in the atmosphere, on the average, than the larger showers. The other factor is the nuclear cascade, which can assist in the propagation of the showers and retard the advancement of the age.

To account for the steepness of the distributions near the axis, it is necessary to conclude that at the origin of a shower of 10^5 or more electrons, the most energetic photons and secondary nuclear-active particles are contained in a cone of half-angle not exceeding $2 \cdot 10^{-4}$ radians. It is also necessary to conclude that as the nuclear cascade progresses, the particles that contribute materially to the electronic shower retain a lateral distribution that is strongly peaked within a few meters of the axis.

3. 5 Multiple shower cores

The experiments described above have given no clear indications of the existence of multiple cores in the EAS. The data have been remarkably consistent with a smooth decrease of the density with distance from the axis. The local fluctuations have in most cases been about equal to those expected from a Poisson distribution of independent particles (Relf [1955], Hazen [1952] Heineman & Hazen [1953] Hazen *et al.* [1954] Sitte *et al.* [1954] Williams [1948]).

In a small number of instances, however, the ionization chamber data have indicated a distinctly "lumpy" distribution (Hazen *et al.* [1954]). Unusual examples of this phenomenon have been obtained by Heineman, Hazen and Davis (Heineman & Hazen [1953], Heineman [1954], Davis *et al.* [1954]) with a set of 20 parallel, adjacent ionization chambers. One may seek to explain these few occurrences by heavily ionizing particles released from stars created in the gas or the chamber walls, since it is known that the EAS contain many neutrons and other N-component particles capable of star production. But the presence of so much N component in the EAS, in itself, assures that the electron component should have a complex origin. The ensemble of individual cascade showers in an EAS seems usually to add up to a smooth distribution, especially at distances more than a few meters from the axis. The few observed cases of lumpy distributions may well represent young cascades created locally by the high energy N-component, resulting in apparently distinct axes among the electron showers.

The usual failure to recognize multiple cores in the EAS, even near the central axis, can be accounted for by the fact that at small radii, comparable with the separation of the multiple shower axes, the component electron showers are generally very old and do not have strongly divergent density distributions. El-Mofty [1953] has attempted to overcome this difficulty by recording the decoherence curve of two ionization chambers under water, at depths of 185 and 274 cm (5 and 7.4 radiation lengths); while Barrett *et al.* [1952] have measured the decoherence curve of the showers of mesons that penetrate to 1600 m.w.e. underground.

The underwater experiment, performed at 2765 m elevation, was inconclusive in regard to the existence of multiple cores in the

air. The coincidence rate was observed to decrease strongly as the separation of the chambers was increased from 0.9 to 6.5 m. An analysis made by HAZEN [1954] has shown that the theoretical decoherence curve, calculated for a pure electronic shower with a single axis, is not as steep as was originally supposed, and is not in grave disagreement with the measurements. Furthermore, many of the coincidences were probably not due to high energy photons and electrons incident on the water, but to local showers generated in the water by the N-component that is present in the EAS.

Although multiple cores are not required to explain the data of El-Mofty, the experiment shows that if multiple cores are present (i.e., if there are laterally separated concentrations of high energy photons and electrons), the width of the distribution is no more than a few meters. Moreover, the experiment affirms that the high energy N-component also has a distribution that is strongly peaked in the neighborhood of the central axis.

Barrett *et al.* found that showers of 10^{12}eV mesons have a radius of about 13 m at a depth of 600 m underground. The mesons may originate not only from the primary nuclear interaction, but also from second and third generation processes of the nuclear cascade. The mean energy of the interacting particles that produce the mesons was estimated to be of the order of $4 \cdot 10^{13}$ eV; and the experimental results suggest that the secondaries of such interactions are contained in a cone of half-angle 10^{-3} radians. This conclusion should apply not only to the charged π-mesons that decay into μ-mesons, but equally to the π°-mesons that decay into photons initiating subsidiary cascades in the EAS.

3. 6 THEORETICAL IMPLICATIONS

There is no doubt that the soft component of an EAS is of complex origin, and therefore that the central region should have some structure. The π°-mesons (or any other secondaries that give birth to the soft component) of comparable energies, created at or near the origin of the EAS, must give rise to overlapping electronic showers, the axes of which diverge by angles that are determined by the velocity of the center of mass of the nuclear collisions and the angular distribution in the c.m. system. Whether or not the axes of the overlapping showers are separately distinguishable depends on the number of secondary π°-mesons of comparable energy and on their average spacing, as well as on the

background growing out of later generations of the nuclear cascade. But the shower cannot have one and only one centre of high density gradient. Either there are multiple centres or there is a single diffuse centre in which the particle density is high but the gradient is small.

The composite shower may be less concentrated around the central axis than are the electronic showers that develop from the primary nuclear encounter, but not more concentrated. The slow variation of apparent age with shower size suggests that the contribution of later generations of the nuclear cascade is important even near the central axis. The ensemble of subsidiary showers must be diffuse within a region at least as wide that determined by the angular spread of the nuclear-active secondaries emerging from the initial collision. Therefore the observations of the lateral distribution of particles near the axes of EAS permit one to set limits on the angular divergence of secondaries in the primary nuclear interactions.

If the secondaries were created isotropically in the c.m. system, the angle of half-maximum intensity in the laboratory frame of reference would be $\Phi = 0.64/L$, where $L = (1 - \beta^2)^{-\frac{1}{2}}$, the Lorentz factor of the moving system. Within the cone of half-angle Φ, the energy variation introduced by the coordinate transformation would be only a factor of $\sqrt{2}$; hence Φ would define the cone containing secondaries of approximately equal energy and uniform density. The radius of the base of the cone, R, is estimated by multiplying Φ with 15 km, an approximate average of the distances from the points of initiation of the showers to the levels where they have been studied in detail.

For single nucleon-nucleon encounters at high energy, $L = (E_0/2Mc^2)^{\frac{1}{2}}$. Thus for $E_0 = 10^{15}$ eV, $\Phi \approx 9 \cdot 10^{-4}$ and $R \approx 13$ m, while for $E_0 = = 4 \cdot 10^{13}$ eV, $\Phi \approx 4.4 \cdot 10^{-3}$ and $R \approx 66$ m. These radii are five times too large to fit the observed steepness of electron distributions a couple of meters from the central axes of EAS, and to fit the width of the meson showers measured far underground.

The discrepancy is somewhat worse than these figures suggest, because when a primary nucleon interacts with a nucleus of air, more than one nucleon of the target nucleus is apt to be involved. In view of the strong collimation, the average number of target nucleons participating in the interaction is about $A^{\frac{1}{3}}$, where A

is the atomic weight. The successive collisions within a nucleus occur before the products of the first interaction can leave the interaction volume. Hence the collisions are not distinct as in a cascade process; instead, a single excited volume is probably formed, containing all the nucleons that have been swept into the interaction. Within that concept, $L^{-1} \approx (2Mc^2A^{\frac{1}{4}}/E_0)^{\frac{1}{2}}$. Thus the above estimates of Φ and R should be increased by a factor of about $A^{\frac{1}{4}}$, which for air is 1.56.

If the primary particle is not a single nucleon but a nucleus of atomic weight A_0, the energy per nucleon corresponding to a given total energy E_0 is reduced. Laterally separated nucleons of the incident nucleus suffer independent collisions with transversely separated nucleons of the target nucleus; but the nucleons lying along a line in the direction of the motion will more likely plunge into single interaction volumes. By pursuing this concept, one obtains

$$L^{-1} \approx [2\, A^{\frac{1}{4}}\, A_0^{\frac{1}{4}}\, Mc^2/E_0]^{\frac{1}{2}}\,.$$

Thus for given values of E_0, the estimates of Φ and R are further increased by a factor $A_0^{\frac{1}{4}}$.

FERMI [1951] has pointed out, in connection with his statistical model of nuclear interactions, that in non-central collisions between single nucleons the angular distribution of the secondaries cannot be isotropic in the c.m. system because of the need to conserve angular momentum. Application of this condition reduces the average angular spread of the secondaries in a theoretical model that would otherwise predict isotropy. GOAD [1953] has shown that in the Fermi model the r.m.s. value of Φ for secondary particles having a high energy in the laboratory system is $(1 - \varrho)^{\frac{1}{2}}L^{-1}$, where ϱ is a parameter related to the impact distance. The median value of ϱ for nucleon-nucleon collisions is 0.959; hence $\Phi \approx 0.2\ \mathrm{L}^{-1}$, about 1/3 of the value for isotropic emission.

This factor is not quite large enough to bring about agreement with the observations. Moreover, it applies only to single nucleon-nucleon encounters, which occur principally in glancing collisions of the primaries with air nuclei. When a primary nucleon makes a tunnel through a nucleus, the complex collision is more nearly central, on the average, than are single nucleon-nucleon collisions; consequently the predicted angular distribution is more nearly isotropic in the c.m. system.

Thus there remains a significant disagreement between the experiments and the angular distribution given by the Fermi theory. The thermodynamic concept of nuclear interactions need not be cast aside because of this discrepancy, but some modification of the details of the Fermi picture seems to be called for.

Arguments for such modifications have also been proposed on theoretical grounds. BHABHA [1953], for instance, has suggested that the mass of a nucleon may not be entirely of field origin, but partly contained in a central core. The nucleon-nucleon collision time is too short, at ultra-high energies, for signals to travel from one core to the other when the collision is not head-on; therefore the core of the incident nucleon would usually intereact only with part of the meson field of the struck nucleon, and would emit mesons while moving forwards more rapidly than the center of mass of the two nucleons. The result of such a collision would be two narrow jets in the forwards and backwards directions in the c.m. system, in addition to a spray of mesons emitted at wider angles owing to the mutual interaction of the two meson fields.

HEISENBERG [1953] & LANDAU [1953] have proposed other modifications of the Fermi theory, arising from a consideration of the interactions occurring between the secondaries during the expansion of the interaction volume. The result is an angular distribution strongly dependent on the energy of the emitted mesons; the particles of the highest energy in the c.m. system are expected to emerge in very narrow forwards and backwards cones.

A model bearing some resemblance to that of Bhabha has also been proposed by KRAUSHAAR & MARKS [1954]. This model, too, leads to the prediction of a narrower distribution than that given by the Fermi theory.

The data on the lateral distribution of EAS do not as yet permit a choice among all of these modifications of the Fermi theory, more than one of which probably contain elements of truth; but further guidance may possibly be obtained from other aspects of the EAS, to be discussed below.

The needed alteration of the Fermi angular distribution is greater if the showers are generated by heavy nuclei than if they are produced by protons. On the other hand, studies of high energy showers in emulsions have given evidence that the Fermi

theory is not very far from correct (KAPLON *et al.* [1949), LORD *et al.* [1950], PICKUP & VOYVODIC [1951], LAL *et al.* [1952], KAPLON & RITSON [1952a, b], MARSHAK [1952], COCCONI [1954a]). If one accepts this evidence, the steepness of the electron distribution in EAS and the narrowness of the meson showers far underground suggest that the EAS are initiated by protons, and possibly by alpha particles, but not often by heavy nuclei.

4. Density and Number Spectra of EAS

If individual particles of a shower are sufficiently independent of each other in position and in the probability of occurrence, it is meaningful to define the local density, Δ, of an EAS by $dP = \Delta\, d\sigma$, where dP is the probability that a charged particle should cross an elementary area $d\sigma$ normal to the shower axis, and Δ is related to the number of particles in the shower and to the lateral distribution function by $\Delta = N f(x)/r_1^2$. The validity of the assumption of local independence of the particles is affirmed by the experiments already described on the lateral distribution; further experimental tests will be recounted below. In brief, the assumption is justified in the open air, but not beneath roofs or screens of dense material in which local multiplication of the particles can occur.

The density spectrum of EAS means the frequency of occurrence of showers having a particle density between Δ and $\Delta + d\Delta$ at a particular place, irrespective of the sizes and locations of the axes of the showers. This function will be designated by $h(\Delta)\, d\Delta$, and the corresponding integral spectrum by $H(\Delta)$.

The number spectrum means the frequency of showers containing a total of N to $N + dN$ charged particles and having a central axis that crosses a unit area. The differential number spectrum will be indicated by $k(N)\, dN$, and its integral from N to infinity by $K(N)$.

Most of the showers in the lower atmosphere are nearly vertical. For the moment all showers will be considered to arrive in directions so near the vertical that the cosine of the zenith angle can be approximated as 1.0. With this understanding, the spectra $h(\Delta)$ and $k(N)$ include showers arriving in all directions.

Empirically, the density spectrum has been found to follow rather accurately a power law, represented by

$$H(\Delta) = H_0\, \Delta^{-\gamma}, \tag{12}$$

(Cocconi *et al.* [1948, 1944], Daudin [1943, 1944b]), where γ and H_0 may be taken as constant at a given altitude over a wide range of Δ, and the exponent γ changes very little with altitude. Since γ and H_0 are not strictly constant, it must be noted that γ is defined in analysis of experimental data by $\gamma = -\partial(\ln H)/\partial(\ln \Delta)$, and H_0 is adjusted to give correct values of H, following the determination of γ.

In first approximation, the density spectrum is simply related to the number spectrum. Suppose that the number spectrum is given by a power law,

$$K(N) = K_0 N^{-\gamma'}, \tag{13}$$

and assume that the lateral distribution of showers is independent of N, postponing until later a consideration of the effect of the slight error in this assumption. Then the frequency of showers having a density exceeding Δ is given by

$$\begin{aligned} H(\Delta) &= \int_0^\infty 2\pi r\, dr\, K[r_1^2 \Delta / f(x)] \\ &= 2\pi r_1^{-2(\gamma'-1)} \Delta^{-\gamma'} K_0 \int_0^\infty [f(x)]^{\gamma'} x\, dx. \end{aligned} \tag{14}$$

Thus, at a given altitude $H(\Delta) = (\text{const})\, \Delta^{-\gamma'}$, indicating that Eq. 12 follows from Eq. 13 or *vice versa*, and that the two exponents, γ' and γ, are equal.

4. 1 Determinations of the density spectrum

In determining $H(\Delta)$ experimentally, one must use detectors of finite area and, except in cloud chamber experiments, one must use two or more horizontally separated detectors in order to distinguish EAS from other phenomena. Some of the recorded showers have central axes sufficiently near the apparatus that the variation of Δ from one part of the apparatus to another is quite appreciable. The question arises as to whether the ignoring of the density gradient over the apparatus leads to significant errors in determining the shape of $H(\Delta)$.

Under the assumptions that the shower particles are locally independent and that the shower geometry is independent of N, there are at least two methods of determining the exponent γ that are unaffected by the density gradient.

One method is measurement of the frequency of coincident pulses in a set of ionization chambers, each pulse being required to equal or exceed the size corresponding to n particles crossing a chamber, with $n \gg 1$ so that fluctuations can be ignored. (One can equally well require that the average pulse height exceed that due to n particles). In each event, the smallest of the pulse sizes (or the average size) is equal to the total number of particles in the shower times a factor depending only on the location of the shower axis relative to the apparatus and the geometry of the set of ionization chambers. The frequency of coincidences as a function of n is therefore $n^{-\gamma}$ times a purely geometrical integral, and the logarithmic derivative of the frequency with respect to n yields the exponent γ directly.

In other words, the shape of the spectrum of average or minimum densities over finite areas is the same as that of the hypothetical density spectrum at an infinitesimal area, despite the density gradients.

More frequently, the density spectrum has been determined with GM counters, because this method is applicable to lower particle densities, which occur with greater frequency. If one adds to the assumptions made above the further assumption that the individual counters or counter trays are so small that the variation of Δ over single counting units can be ignored, one can demonstrate that when the areas of all the counters are changed in the same proportion, the coincidence rate of any combination of them will vary with the area according to

$$\frac{\partial \ln C}{\partial \ln S} = \gamma, \tag{15}$$

(Ise & Fretter [1949], Singer [1951]). Verification that the logarithm of the coincidence rate varies linearly with the logarithm of the counter area has been the most accurate method of substantiating the power law form of the density spectrum, Eq. 12.

By ignoring the gradient of the density, not only over single counters but also over the entire array, one may calculate the frequency with which a set i of counters is discharged while a set j fails to be discharged as follows:

$$F_{i,j} = \int_0^\infty d\Delta \; h(\Delta) \prod_i (1 - e^{-s_k \Delta}) \prod_j (e^{-s_k \Delta}) , \tag{16}$$

where the S_k are the areas of the individual counters or counter trays. The relative values of F for different numbers of counters in the sets i and j are sensitive functions of γ alone, from which, by comparison with experiment, γ may be determined.

This method can lead to serious errors for certain geometrical arrangements of the counters, such that the average particle density is appreciably greater at the counters of set i than at the counters of set j (TREAT & GREISEN [1948], ISE & FRETTER [1949], BROADBENT *et al.* [1950]). But such a bias can be avoided by properly locating the counters with respect to each other. For instance, COCCONI & TONGIORGI [1949] determined γ by comparing the 3-fold coincidence rate of counters at the vertices of an equilaterial triangle with the 4-fold coincidence rate between these counters and a fourth located at the center of the triangle. The values of γ thus found were in good agreement with those derived in the same experiment by the method of area variation.

Cloud chamber studies of the density spectrum have been made by triggering a chamber with coincidences of a set of counters spaced around it. The type of counter coincidence can be expected to determine the probability of observing various numbers of tracks in the pictures. For instance, if the trigger represents the discharge of p counters of area S while q counters of the same area are missed, the predicted spectrum of densities striking the chamber is proportional to

$$\Delta^{-(\gamma+1)}\, d\Delta\, (1 - e^{-S\Delta})^p\, e^{-qS\Delta}\,, \tag{17}$$

provided the density gradients of the showers over the apparatus are neglected. If S' is the sensitive area of the cloud chamber, the average probability of observing exactly n tracks under such a trigger should be

$$P(n) = \frac{\int_0^\infty (n!)^{-1}(S'\Delta)^n\, e^{-S'\Delta}\, (1 - e^{-S\Delta})^p\, e^{-qS\Delta}\, \Delta^{-(\gamma+1)}\, d\Delta}{\int_0^\infty (1 - e^{-S\Delta})^p\, e^{-qS\Delta}\, \Delta^{-(\gamma+1)}\, d\Delta}$$

$$= \left(\frac{S'}{S}\right)^n \frac{1}{n!} \frac{(n - \gamma - 1)!}{(-\gamma - 1)!} \frac{\sum_{k=0}^{p} (-1)^k\, C_p^k\, (S'/S + q + k)^{\gamma - n}}{\sum_{k=0}^{p} (-1)^k\, C_p^k\, (q + k)^{\gamma}} \tag{18}$$

where $C_p^k = \dfrac{p!}{k!\,(p-k)!}$ is the binomial coefficient.

Thus, with an assumed value of γ, the relative frequencies have been calculated with which 0, 1, 2, 3, etc. tracks should have been seen in the cloud chambers, and the calculations have been compared with the observations (AUGER & DAUDIN [1945], CHOWDHURI [1948], CRESTI *et al.* [1953]). At sea level and at 2000 m elevation, in the density range 50 to 5000 m^{-2}, satisfactory agreement has been obtained with a single value of γ, equal to 1.5, although the data do not preclude a slow variation of the exponent.

The principal conclusions from the cloud chamber observations are that the coherence which exists among the particles has very little effect on the density distributions, and that expression such as 14 — 18, which treat the particles as if they were independent, give an adequate representation of the fluctuations of the local particle density.

4. 2 VARIATION OF THE INDEX "γ"

Many of the reported measurements of γ, made with counters and ionization chambers at sea level and at mountain elevations, are assembled in Figs. 14 and 15.

The way in which an "average" density was assigned to the individual measurements was as follows. It was considered that the coincidence rate of n identical counters of area S essentially represents the integral density spectrum $H(\Delta_1)$, where Δ_1 is defined by

$$H(\Delta_1) = \int_0^\infty d\Delta\, h(\Delta)\,(1 - e^{-S\Delta})^n\ ;$$

$$(\Delta_1 S)^{-\gamma} = -(-\gamma)!\sum_{k=1}^{n}(-1)^k\, C_n^k\, k^\gamma\ . \qquad (19)$$

For instance, for $n = 3$, Δ_1 is very nearly $1/S$, and for $n = 4$, Δ_1 is about $4S/3$. If the area S is changed or the number of counters in coincidence is varied, one essentially determines the shape of $H(\Delta)$ between the two corresponding values of Δ_1; and the experimental exponent γ is considered to represent most closely the correct value at a density which is the geometric mean of the involved values of Δ_1. For the ionization chamber measurements, the values of Δ_1 are given directly by the chamber calibrations and the minimum pulse heights accepted. In both counter and ion chamber experiments, the values of Δ_1 are less than the linear averages of the densities of the recorded showers.

Figures 14 and 15 show that γ increases slowly with Δ. This trend has been observed frequently, but not universally. Unless the range of densities is extremely wide, the use of a fixed value of γ appropriate to the middle of the interval gives such an accurate representation of the distribution, that discrepancies are difficult to observe. The increase of γ is particularly clear in the data of Cocconi and Tongiorgi and of Zatsepin *et al.*, which extended over a very wide range of density.

It is obvious, *a priori*, that for low densities γ must become less

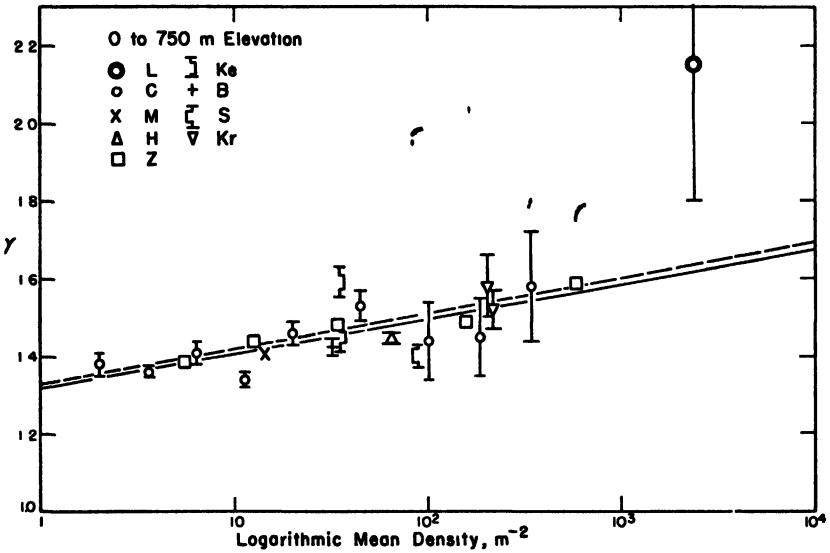

Fig. 14 – Measurements of the exponent γ in the density spectrum of EAS near sea level. L refers to LAPP [1943, 1946], ion chamber measurements. Only bursts of more than 250 particles (by Lapp's calibration) were used in this determination. Associated pulses in G-M counters showed that these bursts were practically all due to EAS. The burst sizes have been corrected with a different specific ionization and for transition effects in the walls. All the other points were determined from counter data. C = COCCONI & TONGIORGI [1949], M = MILONE [1952a]. H = HODSON [1953a]. Ke = KECK & GREISEN [1949]: the lower point corresponds to $\frac{1}{2}$ m counter separation, the upper point to 4 m separation. B = BROADBENT *et al.* [1950]. S = SINGER [1951]. Kr = KRAYBILL [1949]: the lower point is for 2 to 5 m spread of the counters, while the upper point corresponds to a spread of 13 to 16 m. Z refers to approximate readings taken from a graph published in references ZATSEPIN *et al.* [1947] and ZATSEPIN *et al.* [1953]. The solid line is intended to represent the data without correction. The dashed line includes a correction for the errors in the determinations of γ owing to the finite derivative of γ with respect to Δ.

than one; otherwise the integral $\int_0^\infty (1 - e^{-\delta\Delta})h(\Delta)d\Delta$, which is proportional to the counting rate of a single counter, would diverge.

Measurements that have been repeated with detectors at different spacings have yielded higher values of γ, the farther the detectors were separated (LOVERDO & DAUDIN [1948], WILLIAMS [1948], KECK & GREISEN [1949], KRAYBILL [1949]). This variation is associated with the increase of γ with density, since separating the counters or ion chambers eliminates the contribution of small

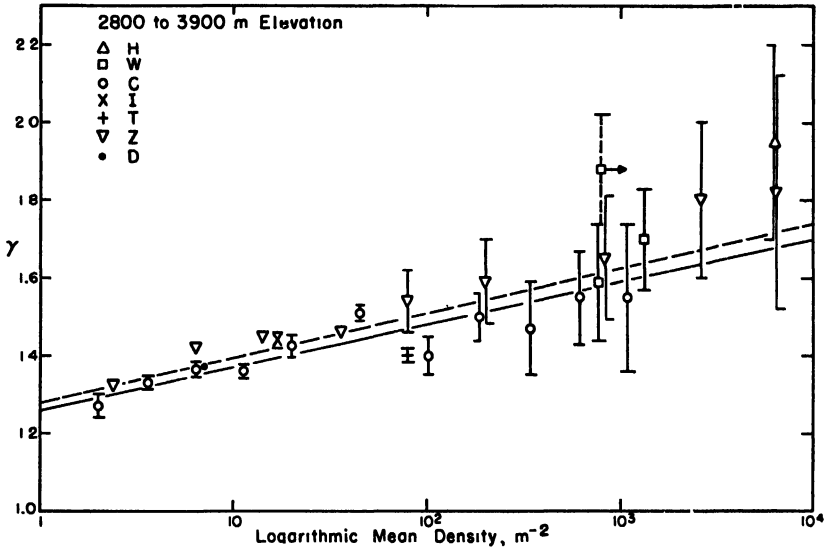

Fig. 15 – Measurements of the exponent γ in the density spectrum of EAS at mountain elevations. H = HUDSON [1950]; three ion chambers (8 cm between centers) measured the density, while three trays of counters identified events as EAS. The apparatus is described in reference HUDSON [1952]. W = WILLIAMS [1948], ion chamber measurements. The point with an arrow attached is the average result with chamber separations of 7 and 12 m; the other points are averages for separations of 0.2 to 1 m and 0.2 to 3 m. The remaining determinations of γ were made with counters. C = COCCONI & TONGIORGI [1949], I = ISE & FRETTER [1949], T = TREAT & GREISEN [1948]. (The plotted points I and T were those determined by the method of area variation, with an upwards correction of 0.02 for the overlapping of counter areas at large zenith angles). D = DAUDIN & DAUDIN [1953]. Z refers to approximate readings from a graph published in references ZATSEPIN *et al.* [1947] and ZATSEPIN *et al.* [1953]. The solid line is intended to represent the data without correction; the dashed line includes the correction owing to the derivative of γ with respect to Δ.

showers to the coincidence rate, and thus increases the average size of the detected showers, like requiring a higher density.

The variation of γ with Δ appears to be less at sea level than at mountain elevations. The equations of the solid lines drawn in Fig. 14 and 15 (in terms of natural logarithms) are:

$$\gamma = -\frac{\partial \ln H}{\partial \ln \Delta} = a + b \ln \Delta, \quad 1 < \Delta < 10^4 \text{ m}^{-2} \cdot \qquad (20)$$

with $a = 1.26$, $b = 0.048$ at the mountain elevations and $a = 1.32$, $b = 0.038$ near sea level.

These coefficients are in need of a small but not quite negligible correction, owing to the fact that the derivative of γ with respect to Δ was neglected in computing the experimental values of γ from the data. The variation of Δ_1 with area of the counters, or with the number of counters required to be discharged in coincidence, is less than the variation calculated for a constant γ; hence the plotted values of γ are too low. The correction has been computed, and is indicated in Fig. 14 and 15 by the dashed lines, which correspond to Eq. 20 with
$a = 1.28$, $b = 0.050$ at 700 ± 50 g. cm^{-2} atmospheric pressure,
$a = 1.33$, $b = 0.039$ at ~ 1000 g. cm^{-2}.

By integrating Eq. 20, one obtains the integral density distribution in second order approximation:

$$H(\Delta) = c\Delta^{-(a + \frac{1}{2}b \ln \Delta)}. \qquad (21)$$

The first order approximation to Eq. 21 in the neighbourhood of Δ_0 is given by Eq. 12 with $H_0 = c\,\Delta_0^{\frac{1}{2}b \ln \Delta_0}$ and $\gamma = a + b \ln \Delta_0$.

The coefficient c can be evaluated from these relations by comparing experimental counting rates with those calculated from Eq. 12. This has been done with the data of Cocconi and Tongiorgi at 3260 m and 260 m elevation. A correction factor of 4/3 was included for the loss of counts owing to the separation of the counters (Cocconi *et al.* [1949a]). Thus for detectors with negligible separation one finds $c = 1.75$ sec^{-1} at 3260 m and $c = 0.210$ at 260 m, with densities expressed in m^{-2}. From the altitude dependence of the shower frequency, one may infer $c = 0.167$ at sea level.

4. 3 Total number of electrons in EAS

By daring to extrapolate Eq. 21 to lower densities than those for which it has been verified, one may calculate the integral of $\Delta h(\Delta)\, d\Delta$ over all densities for which the expression of $h(\Delta)$ is positive, and thus obtain the total intensity of electrons in the EAS. The extrapolation beyond the density where γ becomes less than one and the precise value of the lower limit of the integral are not very critical, since the contributions to the integral diminish with diminishing Δ when γ is less than one.

Neglecting small terms, the result of the integration is

$$I_0 = \sqrt{\frac{2\pi}{b}}\, c\, e^{\frac{(a-1)^2}{2b}} = \begin{cases} 43 \text{ sec}^{-1}\text{m}^{-2} \text{ at } 3260 \text{ m}, \\ 11 \text{ sec}^{-1}\text{m}^{-2} \text{ at } 260 \text{ m}. \end{cases}$$

The integral from $\Delta = 1$ to $\Delta = \infty$ yields only 6.3 $\text{sec}^{-1}\text{m}^{-2}$ at 3260 m and 0.74 $\text{sec}^{-1}\text{m}^{-2}$ at 260 m, showing that most of the electrons are contained in very low density regions of the showers. By inferring the zenith angle dependence from the altitude variation (see the following section of this chapter), the vertical intensities of electrons in the EAS are computed to be 48 $\text{sec}^{-1}\text{m}^{-2}$ sterad^{-1} at 3260 m, and 17 at 260 m.

Palmatier has measured the electron intensities at these elevations, and has succeeded in separating the part that is due to decay and knock-on processes of μ-mesons from the total intensity (Palmatier [1952]). The residual number of electrons having energy greater than 31 MeV was found to be approximately 87 m^{-2} sec^{-1} sterad^{-1} at 3260 m, and 12 at 260 m. With the aid of the Richards-Nordheim energy spectrum (Fig. 4) one may take into account the electrons having less energy than 31 MeV but sufficient to penetrate the counter walls. The results are $I_v \cong 150$ m^{-2} sec^{-1} sterad^{-1} at 3260 m, and 21 at 260 m.

Thus the electrons in the EAS appear to comprise about 30 to 80% of the entire electron intensity, excluding the electrons arising by decay and collisions of μ-mesons. A similar extrapolation of the number spectra, derived below from the density spectra, and calculation of the integrals $\int_1^\infty N\, k(N)\, dN$, yields similar proportions: about 50% at 3260 m and 100% at 260 m. The accuracy of the extrapolations of the density and number spectra is only sufficient to show that these proportions are not small.

However, of all the electrons in the EAS, only $13 \pm 7\%$ are in regions of density greater than one electron per square meter, or in showers containing more than 10^4 electrons.

4. 4 Density spectrum at high altitudes

If the EAS were sustained primarily by the high energy photons and electrons in the cores of the showers the exponent of the density spectrum should increase with altitude. The events of high density are principally caused by large showers, and Fig. 1 shows that for electronic cascades, the larger the shower, the less the variation of its size with depth. As one goes up in the atmosphere, it would be expected that one should detect many more small showers, but not many more large ones; thus, the density spectrum should become steeper.

Nevertheless, Fig. 14 and 15 show no significant increase of γ between sea level and 3860 m elevation; nor is any significant increase apparent in the measurements at 4300 m (Treat & Greisen [1948]). The first measurements at higher altitudes, reached by means of an acroplane, actually indicated a decrease of γ with elevation (Maze & Freon [1949]). Subsequently, the following experiments have been reported:

(1) Kraybill [1949] determined γ by comparing n-fold with $(n + m)$-fold coincidences. The average result at altitude was 1.74 ± 0.02, and no significant variation of γ was seen, either with altitude in the range 9–12 km, or with spacing of the counters in the range 2–15 m overall spread. At sea level, with the same apparatus, γ was found to be 1.52 ± 0.04 for an average counter spread of 4 m, and 1.58 ± 0.08 for a spread of 15 m. These measurements received criticism because of the possible effect of density gradients in this method of determining γ; but the insensitivity of the results at altitude to the counter spread suggests that the error may have been small. The measurement applies to densities centered around 200 m^{-2}.

(2) Biehl & Neher [1951] used eight counter trays with a spread up to 3.2 m, and determined γ both by area variation (using only two different areas) and by comparing n-fold with $(n + m)$-fold coincidences. The results by the two methods were in agreement, yielding $\gamma \cong 1.54 \pm 0.05$ at 6.9 km, 1.48 ± 0.04 at 9.1 km and 1.66 ± 0.05 at 10.7 km. The mean shower density was about 30 m^{-2}.

(3) HODSON [1953a] used the method of area variation, with three counter trays having 2.2 m spread. At sea level γ was found to be 1.445 ± 0.014. Between altitudes of 6.1 and 10.1 km no significant variation of γ was observed, the average value being 1.549 ± 0.018. The mean shower density was 60 m^{-2}.

(4) KRAYBILL [1954] redetermined γ with the method of area variation, using three trays with a spread of 4 m, and varying the area by a factor of 8. The average values of γ were found to be 1.45 at 7.6 km, 1.50 ± 0.05 at 9.1 km, and 1.56 ± 0.03 at 10.1 km, all much less than in the first measurements.

However, at 7.6 km, where the statistical accuracy was best, Kraybill observed that the graph of the logarithm of counting rate *vs.* the logarithm of the area was non-linear. The apparent value of γ was 1.25 for the larger areas (or smaller densities) and 1.65 for the smaller areas (higher densities). The mean density to which the results apply is 46 m^{-2}, 26 m^{-2} for the low-density interval and 75 m^{-2} for the high-density interval.

This non-linearity would not have been observed by Hodson or by Bichl and Neher, because they varied the counter area by a smaller factor and used only two or three different areas.

A suggestion that the variation of γ with Δ increases with altitude has already appeared in comparing the results near sea level and at mountain elevations. It now seems plausible that the variation continues to grow, and becomes quite large at aeroplane altitudes. This inference can explain the high values of γ obtained in KRAYBILL'S earlier experiment [1949] in which the average shower density was higher than in the later measurements.

The high-altitude results described above are plotted in Fig. 16. If the points may be represented by the solid line drawn in the figure, the correction for the errors in the measurements, owing to the derivative of γ with respect to Δ, would shift the results to the dashed line, which is represented by $\gamma = 0.93 + 0.18 \ln \Delta$. However, the assumption of a linear relation between γ and $\ln \Delta$ is rash in this case, and the large derivative, which determines the correction, is very uncertain. Moreover, if the variation of γ with Δ is so rapid, the empirical density spectrum, Eq. 12, no longer represents the density distribution well, and the significance attached to the parameter γ must be revised.

Insofar as the concept of a power law can be used in describing

the density spectrum of EAS, the effective value of the exponent seems to increase with elevation for high-density showers, and to decrease with elevation for low-density showers.

This would imply that the rate of absorption of the particles in EAS does not diminish monotonically with shower size, as is expected of pure electronic cascades. Among small showers, the absorption coefficient seems to increase with the number of particles in the shower. The discrepancy with the expected behavior of electronic cascades has been illustrated by ZATSEPIN *et al.*

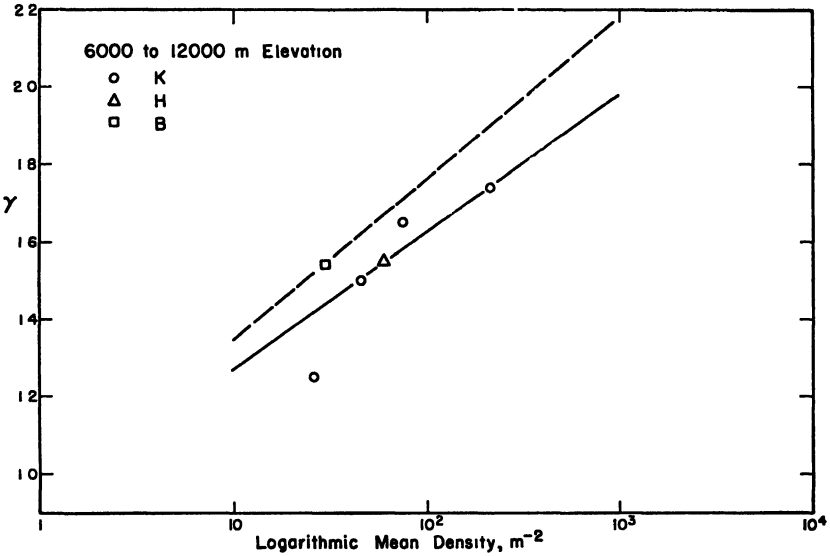

Fig 16 – Measurements of the exponent γ in the density spectrum of EAS at aeroplane altitudes, by KRAYBILL [1949, 1954], BIEHL and NEHER [1951], and HODSON [1953a]. If the solid line were considered to represent the uncorrected measurements, the dashed line would indicate the results corrected for the errors owing to the finite derivative of γ with respect to Δ.

[1947, 1953], by computing the number of showers expected at sea level from the number observed at 3860 m elevation. The disagreement with the observed numbers at sea level was far less for large showers than for the small ones, which are absorbed much less rapidly than electronic showers of the same size would be.

In the limit, this observation would be trivial. Exceedingly small showers have lost their electrons, photons and nuclear-active component, retaining only a small complement of μ-mesons, which are very slowly absorbed. Such low energy showers account

for the bulk of the meson intensity at sea level. But the measurements described above are not concerned with such low energy events. Even in the neighborhood of $\Delta = 1\ m^{-2}$, most of the recorded showers have more than 10^4 particles, and are detected near the shower axes, where the charged particles are predominantly electrons — which are not regenerated appreciably by the μ-mesons. These showers must be sustained primarily by the nuclear-active particles.

The following qualitative picture seems capable of accounting for the observations. In showers near maximum development, the particles may be principally electrons and photons of the cascades arising from the initial nuclear interactions. At first, these particles are absorbed approximately as one expects the soft component to behave. But after the initial electronic cascades have lost their vitality, smaller electronic showers, born in later generations of the nuclear cascade, assume increasing importance. Although they are not of great range, their continual regeneration gives them an apparent rate of attenuation equal to that of the high energy N-component in the EAS. Large EAS are detected mostly in the first, electron-dominated phase, while small EAS are far beyond their maxima and are mostly detected in the second or nuclear-dominated phase. During the transition from one type of domination to the other, the absorption coefficient of the particles can have a maximum.

4. 5 Evaluation of the number spectrum of EAS in the lower atmosphere

There is a slight difference between the exponent γ' of the number spectrum and the exponent γ of the density spectrum, for the following reason. The larger showers, on the average, are "younger" than small showers, and therefore have a more compressed lateral distribution. This makes the large showers contribute more efficiently to the density spectrum than do the smaller, more dispersed showers. As a result, the decrease of $H(\Delta)$ with increasing Δ is less rapid than the diminution of $K(N)$ with increasing N. Thus, γ' is a little bigger than γ.

The magnitude of the difference, γ'—γ, depends on the rate of change of the average age with respect to the number of electrons in the showers, $\partial \bar{s}/\partial \ln N$. The calculation of this derivative, in

turn, depends on the model assumed for the generation and development of the showers.

If one assumes the showers to be generated by high energy electrons incident on the top of the atmosphere, the small showers near sea level must all be very old, and the age must decrease rapidly with ln N, making the correction, $\gamma'-\gamma$, quite appreciable (on the order of 0.1, increasing both with γ and with elevation). However, this model is highly unrealistic. As noted above, it also predicts erroneously that small showers should be attenuated much more rapidly than large ones between mountain elevations and sea level, and hence that γ should be considerably larger at mountain elevations than at sea level.

In a model based on nuclear interactions of primary nuclei as the source of EAS, the derivative $\partial\bar{s}/\partial \ln N$ tends to be smaller for several reasons. Firstly, as s increases, and with it the derivative $-\partial \ln N/\partial t$, showers initiated farther down in the atmosphere assume increasing importance relative to those produced near the top of the atmosphere. Thus, the average depth of initiation increases with diminishing N, reducing the variation of $\bar{s}$ with N. Secondly, multiple production of the particles at the origin of an EAS, if the multiplicity increases with primary energy, reduces the dependence of the age on the shower size. Thirdly, the nucleonic cascade within EAS apparently has a longer attenuation length than the soft component, and sustains the soft component by initiating new electronic cascades. Beyond the shower maximum, this process reduces the apparent age difference between small and large showers.

Measurements of the lateral distribution, described above, have indicated that the variation of $\bar{s}$ with shower size is less than half that which is predicted on the basis of a primary electron spectrum. Analysis of the altitude dependence of the EAS, described in the following section of this chapter, suggests that the variation of $\bar{s}$ in the lower part of the atmosphere is no more than one-fourth of that which is computed for pure electronic showers.

Present knowledge of the details of the nucleonic cascade is not sufficient to permit an accurate computation of $\partial\bar{s}/\partial \ln N$; but the fact that the derivative and the correction depending on it are small reduces the need of accuracy. Our estimates indicate that $\gamma'-\gamma \approx 0.02$ both at sea level and at 3260 m elevation. This is such a small correction as to be almost insignificant.

The number spectrum can therefore be represented by an equation like Eq. 21, which described the density spectrum. At a given elevation,

$$K(N) = k_0 (N/N_0)^{-[a' + \frac{1}{2}b' \ln (N/N_0)]} . \tag{22}$$

The power-law approximation to Eq. 22 in the neighbourhood of N_1 is given by

$$K(N) \approx k_0 \left(\frac{N_1}{N_0}\right)^{\frac{1}{2}b' \ln (N_1/N_0)} \left(\frac{N}{N_0}\right)^{-\gamma'} , \tag{23}$$

$$\text{with } \gamma' = a' + b' \ln (N_1/N_0).$$

In order to evaluate the constants a' and b', γ' must be equated to $\gamma + 0.02$, setting $\ln N_1$ equal to the average of $\ln N$ over the shower sizes contributing to $H(\Delta)$. These are represented by the following integral:

$$H(\Delta) = \pi r_1^{\gamma} \int_0^{\infty} x^2 \, k(N) \, dN , \tag{24}$$

where x is related to N and Δ through the lateral distribution function, $f(x) = r_1^{\gamma} \Delta / N$. Under the power-law approximation for $k(N)$, neglecting the variation of shower age, and with the substitution $z = \ln [f(x)]^{-1} = \ln (N/r_1^{\gamma} \Delta)$, Eq. 24 reduces to

$$H(\Delta) - \text{const.} \; \Delta^{-\gamma'} \int_{-\infty}^{+\infty} x^2(z) \, e^{-\gamma' z} \, dz . \tag{25}$$

The integrand of this equation is illustrated by the curves in Fig. 17, which were drawn for $\gamma' = 1.5$ and three different values of s, by using Eq. 11 to represent the lateral distribution function. It is apparent from the shape of the curves that the average values of $\ln(N/r_1^{\gamma} \Delta)$ are close to the values at the maxima. The corresponding values of $(N/r_1^{\gamma} \Delta)$ are shown as a function of s for several values of γ' in Fig. 18.

The appropriate mean values of s are estimated from the altitude variation of $H(\Delta)$. According to Fig. 24, for $\Delta_1 \approx 50$ m^{-2}, $\bar{s} = 1.17$ at 3260 m elevation and 1.23 at sea level. In the lateral distribution equations, s is a function of the radius x, being somewhat larger than the s of the longitudinal theory for the small values of x that contribute most heavily to $H(\Delta)$. By averaging $\ln x$ over the integral in Eq. 14, one determines $\bar{s} \approx 1.24$ at 3260 m and 1.30 at sea level.

Thus, for $\gamma' \approx 1.50$ and densities in the neighbourhood of 50 m^{-2}, one finds $N_1/r_1^{\gamma} \Delta = 1.31$ at 3260 m and 1.69 at sea level.

Since $r_1 = 120$ m at the higher elevation and 79 m at sea level, the showers with density greater than 50 m^{-2} have on the average $9.4 \cdot 10^5$ charged particles at 3260 m and $5.3 \cdot 10^5$ at sea level. If one sets N_0 equal to 10^6, the coefficients a' and b' in Eqs. 22 and 23 become

$$a' = 1.50, \quad b' = 0.050 \text{ at } 3260 \text{ m},$$
$$a' = 1.53, \quad b' = 0.039 \text{ at sea level.}$$

By evaluating the integral in either Eq. 14 or Eq. 24, the coefficient k_0 of the number spectrum may also be found. The values so obtained are

$$k_0 = \begin{cases} 5.3 \cdot 10^{-7} \text{ m}^{-2} \text{ sec}^{-1} \text{ at } 3260 \text{ m}, \\ 3.5 \cdot 10^{-8} \text{ m}^{-2} \text{ sec}^{-1} \text{ at sea level.} \end{cases}$$

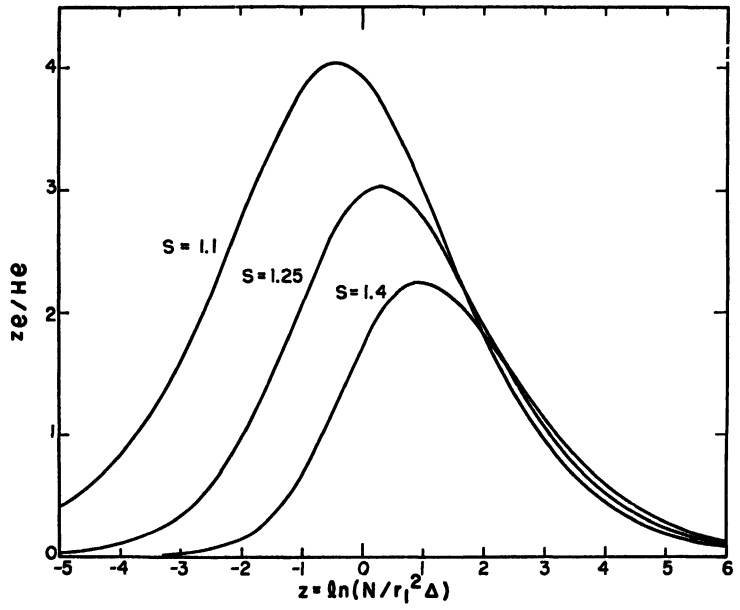

Fig. 17 – Relative contributions of EAS containing various numbers of particles to the showers of density exceeding Δ over an infinitesimal area: i.e., the integrand of Eq. 25 as a function of z, or $\ln(N/r_1^2\Delta)$, for $\gamma' = 1.5$ and three different values of the age parameter s.

In these units the derived number spectra are therefore

$$K(N) = 5.3 \cdot 10^{-7} \left(\frac{N}{10^6}\right)^{-[1.50 + 0.025 \ln (N/10^6)]} \text{ at } 3260 \text{ m},$$
$$K(N) = 3.5 \cdot 10^{-8} \left(\frac{N}{10^6}\right)^{-[1.53 + 0.0195 \ln (N/10^6)]} \text{ at sea level.} \qquad (26)$$

These results should be applicable at least within the range $10^4 < N < 3 \cdot 10^7$. They agree satisfactorily with the absolute frequency of showers of about 10^6 particles, evaluated by BLATT [1949] on the basis of Williams' data, and with the frequency of showers containing about 1000 electrons near sea level, calculated by BARRETT *et al.* [1952].

The most sensitive point in the determination of the number spectra was the choice of the average age parameter, $\bar{s}$. Because

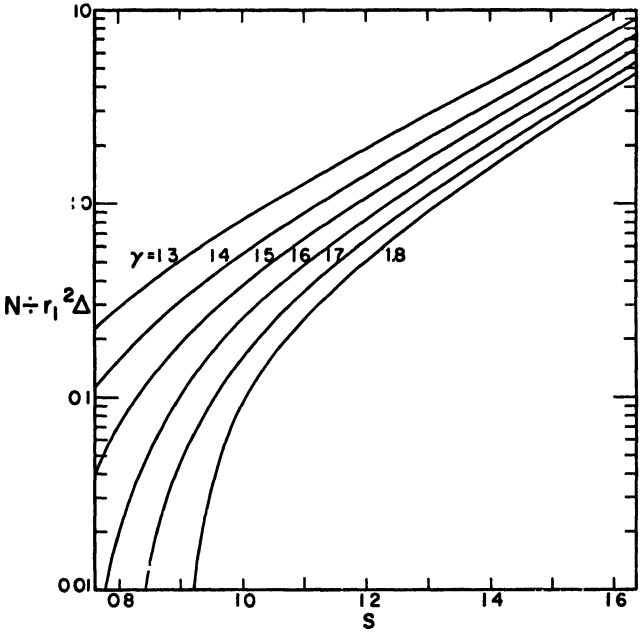

Fig. 18 – The shower size (in units of $r_1^2\Delta$) contributing most heavily to $H(\Delta)$, for various values of the average age, $\bar{s}$, and the exponent of the number spectrum, γ'.

of the variation of the lateral distribution with $\bar{s}$, the coefficient k_0 changes by about 2.7% for a change of 0.01 in $\bar{s}$. Since the showers are not pure electronic cascades, there is no assurance that the values of $\bar{s}$ inferred from the rate of absorption are applicable to the lateral distribution. The Nishimura-Kamata function with these values of $\bar{s}$ is consistent with the measurements of the lateral distribution described in the previous section, but they were not precise enough to dermine $\bar{s}$ accurately. The

coefficients, c, in the density spectra were also sensitive to a rather uncertain extrapolation to zero spacing between the counters. Therefore, the values of k_0 have an estimated uncertainty on the order of 20%.

The spectra determined above refer to showers arriving in all directions, as detected with trays of cylindrical counters spaced far enough apart that the areas did not overlap. From the zenith angle distributions derived below, the number spectra of the showers arriving in the vertical direction may be computed. The parameters a' and b' are not significantly different from their values for showers arriving in all directions, but the coefficients k_0 are found to be

$$k^{0v} = \begin{cases} 6.0 \cdot 10^{-7}\ \mathrm{m^{-2}\ sec^{-1}\ sterad^{-1}} \text{ at 3260 m,} \\ 5.5 \cdot 10^{-8}\ \mathrm{m^{-2}\ sec^{-1}\ sterad^{-1}} \text{ at sea level.} \end{cases}$$

At higher elevations, the experimental data do not permit such a detailed evaluation of the number spectra. The approximate variation with altitude of the coefficients H_0 and K_0 in the first-order density and number spectra are analyzed in the next section.

5. Variation of Intensity with Altitude, Barometric Pressure, and Zenith Angle

The change of shower counting rate with varying altitude, varying barometric pressure at a fixed elevation, and varying zenith angle are closely related, all being due primarily to the growth and decay of the electronic cascades as they traverse increasing amounts of matter. Interest in these phenomena persists nowadays because the development and absorption of the EAS are influenced not only by the properties of pure electronic cascades, but also by the shape of the primary cosmic ray energy spectrum and the nature of the processes by which the primary energy is transferred to the soft component, both at the origin of the EAS and throughout the associated nuclear cascade.

5. 1 Altitude variation

The statistically accurate measurements of the variation of intensity with altitude have been made by recording coincidences of three or four trays of counters, that have usually been held in a fixed geometry as the altitude was varied. The data of Hilberry

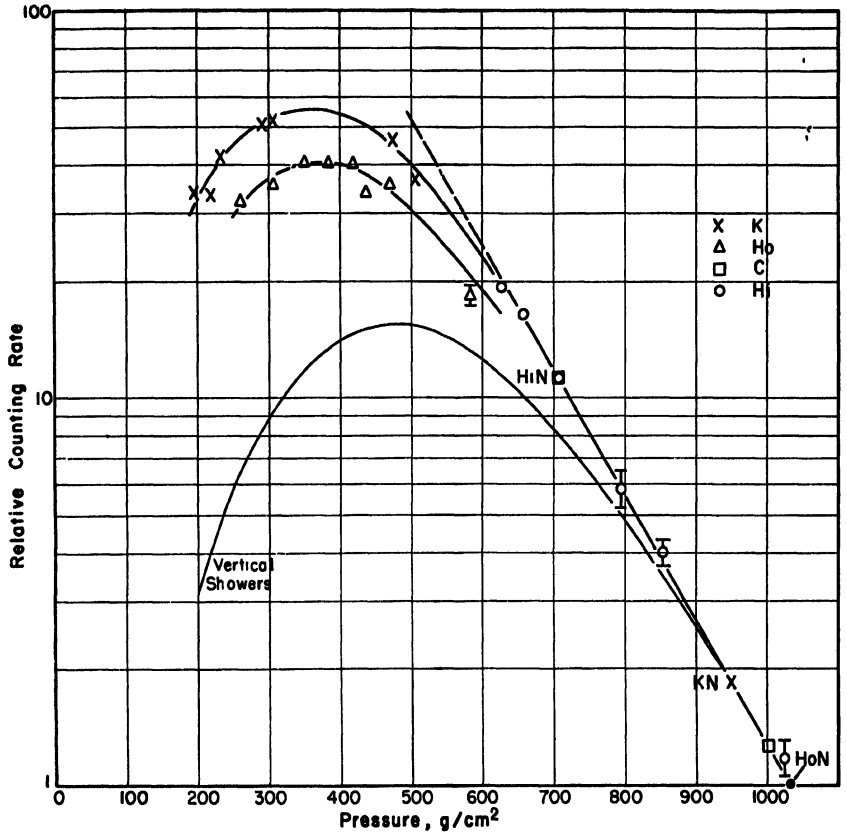

Fig. 19 – Relative counting rate of EAS *vs.* altitude. The data represent coincidence rates either of single G-M counters or of trays in which the sensitive counter areas did not overlap. The recorded EAS were essentially those of density exceeding $\sim 50\ m^{-2}$. Points marked K are the data of KRAYBILL [1949], normalized to the smooth curve at the lowest point (KN). Ho signifies the data of HODSON [1953a], normalized at HoN. The HILBERRY [1941] data are normalized to the measurements of COCCONI and TONGIORGI [1949a] at the point marked HiN. The curve labelled "Vertical Showers" was inferred by means of a Gross transformation from a smooth curve going midway between the points of HODSON and KRAYBILL at high altitudes.

[1941], KRAYBILL [1949], HODSON [1953a], and COCCONI & TONGIORGI [1949] are shown in Fig. 19. All of these data refer to the frequency of showers with density exceeding about $50\ m^{-2}$. The measurements of Cocconi and Tongiorgi were exceptional in that the spacing of the counters was changed with the elevation in proportion to the scattering length r_1.

The discrepancy between the data of Kraybill and those of Hodson has not been explained. In both experiments, the relative sensitivity to showers arriving at different zenith angles should have been the same, since parallel, cylindrical counters were used in both experiments, and counters connected together were spaced far enough apart that the overlapping of sensitive areas should not have been appreciable. In any case, the shower counting rate has a broad maximum in the neighbourhood of 365 g.cm^{-2} pressure, where the rate is roughly 50 times the value at sea level.

In the lowest third of the atmosphere, the data are consistent with an exponential attenuation, the coefficient being $(135\,\text{g.cm}^{-2})^{-1}$ or 0.279 per radiation length. If there is any increase in the slope between 700 g.cm^{-2} and sea level, the change is probably less than from 0.25 to 0.30 per radiation length.

5. 2 Barometric effect

The constancy of the rate of absorption in the lower atmosphere is borne out also by measurements of the barometric effect of the EAS. The barometric coefficient should be equivalent to the attenuation coefficient derived from the altitude variation, except for a very small difference owing to the systematic change of temperature with elevation. (The compression of the showers because of the drop in temperature with elevation makes the altitude effect larger than in an isothermal atmosphere by approximately $0.18/P$, where P is the pressure).

The statistically most accurate of the determinations of the barometric effect are listed in Table II.

It is difficult to assess the accuracy of these measurements; in the original references a variety of methods was used with widely varying answers. In most instances no correction was made for the correlation between local temperature and pressure, which can have an effect on the order of 0.5%/cm Hg. Differences observed by Daudin [1953] and Citron [1952] between measurements over different periods of time show that the fluctuations are neither purely statistical nor completely explainable in terms of the variations of local temperature. In some of the experiments, the barometric coefficient appeared to vary with counter spacing or with the mean density of the selected showers, but these trends were not borne out by other experiments. With these evidences of possible error in mind, the determinations of the barometric

effect are all consistent with the coefficient 0.27 per radiation length, inferred from the slope of Fig. 19 (with a correction of about 0.008 for the temperature variation).

TABLE II

Barometric Coefficients

Altitude	Approx. No. of Counts	Coefficient, %/cm Hg	Coefficient, (rad. lengths)$^{-1}$	Reference
Sea level	35,000	9.0	0.25	Auger & Daudin [1942]
Sea level	16,000	11.1	0.31	Millar [1951]
Sea level	37,000	9.0	0.25	Hodson [1953a]
280 m	70,000	11.8 *	0.33	Citron [1952]
550 m	100,000	9.2	0.26	Daudin & Daudin [1949]
1230 m	340,000	9.0 *	0.25	Citron [1952]
2860 m	70,000	11.0	0.30	Auger & Daudin [1942]
2860 m	640,000	10.2	0.28	Daudin & Daudin [1949]
2860 m	30,000,000	10.0 †	0.28	Daudin & Daudin [1953]
3500 m	130,000	9.8	0.27	Castagnoli *et al.* [1950]

* The coefficient in the table is the average value for all the showers recorded. Different series of measurements yielded coefficients varying from 9.9 ± 0.3 to 12.3 ± 0.2%/cm Hg at 280 m elevation, and from 7.1 ± 0.7 to 12.6 ± 1.8%/cm Hg at 1230 m. An apparent dependence of the coefficient on the mean density of the showers appeared in some of the series but not in others.

† Corrected for local temperature variations. The corrected coefficient varied with the season and frem year to year over the range 8.3 to 10.4%/cm; and the average value varied between 9.4 and 10.5%/cm, depending on whether the temperature correction was omitted, or was obtained from the local temperature, from that of the 300 mb level, or from the height of the 200 mb level. These figures suggest how correlations between temperature and pressure may justify discrepancies among the various measurements listed in the table.

The barometric coefficient appears to be slightly higher at 2860-m altitude than at sea level. A difference in this direction is so unexpected that one may discount it in view of the experimental uncertainties. Nevertheless, it is clear that the attenuation

coefficient does not increase appreciably as one goes from 3500 m elevation to sea level.

This observation, in itself, is enough to rule out the hypothesis that primary electrons originate the EAS. By judicious choice of the exponent of a primary electron spectrum, one can match the sea level absorption coefficient or match the average absorption coefficient between any two elevations (BUDINI [1951]); but one cannot avoid the prediction that the absorption coefficient should decrease rapidly with elevation.

5. 3 ZENITH ANGLE EFFECT

The variation of shower counting rate with altitude is complicated by a change of the zenith-angle distribution of the showers and also by a change in their geometry, owing to variation of the density of the air and variation of the average age of the showers. One of these complicating factors, the zenith-angle distribution, can be eliminated by a generalized Gross transformation, following the method used by KRAYBILL [1954] and by BIEHL and NEHER [1951].

The essential assumption in the application of the transformation is that except for geometrical effects, $R(h, \theta)$ would equal $R(h/\cos\theta, 0)$, where h is the vertical atmospheric depth, θ is the zenith angle, and R is the counting rate of showers with axes in the direction θ, per unit solid angle. The difference between $R(h, \theta)$ and $R(h/\cos 0, 0)$ owing to the variation of the scattering unit r_1 with pressure and temperature of the atmosphere can be approximated by a factor $(\cos\theta)^{1.8(\gamma-1)}$ for an isotropic detector of negligible extension. The change of the sensitive area of the counters with zenith angle contributes a factor $(\cos\theta)^{a\gamma}$, where a would equal zero for isotropic detectors, 1.0 for perfectly flat rectangular counter trays, and 0.5 for separated cylindrical counters of infinite length compared with diameter, were it not for the influence of electron scattering. In view of the scattering and the dimensions of the cylindrical counters that were used to obtain the data in Fig. 19, we approximate $a \approx 0.35$. The further difference between $R(h, \theta)$ and $R(h/\cos 0, 0)$, owing to variation of the separations of the counters normal to the shower axis, we approximate with the factor $(\cos\theta)^{0.2}$. Thus,

$$R(h, \theta) = x^n R(h/x, 0) \tag{27}$$

with $x = \cos\theta$ and $n = 1.8(\gamma - 1) + 0.35\gamma - 0.2$. From this

equation one can deduce the following expression for the counting rate of vertical showers in terms of the measured, integrated counting rates, C:

$$R(h, 0) = \frac{C(h)}{2\pi}\left[n + 1 - h\frac{\partial \ln C}{\partial h}\right]. \tag{28}$$

Eq. 27 and 28 together specify the zenith angle dependence of the recorded showers. By dividing $R(h, \theta)$ with $x^{a\gamma}$, one obtains a more fundamental quantity, the zenith-angle variation that would be recorded by an isotropic detector.

By drawing a smooth curve to represent the data in Fig. 19 and measuring the derivative as a function of h, values of C and $\partial \ln C/\partial h$ have been obtained, with which the rate $R(h, 0)$ has been computed. The results, normalized to 1.0 at sea level, are represented by the lowest curve in Fig. 19.

The derived curve is not sensitive, over most of its length, to small errors in the value of n. The probable error grows with altitude, however, for several reasons: the increasing uncertainty in the value of γ (on which n depends), the possible error in the smooth curve representing the counting rate at high altitudes, the increasing uncertainty of the lateral distribution function with decreasing pressure, and the fact that n represents a larger and larger portion of the bracketed term in Eq. 28 with increasing elevation, particularly beyond the maximum of the curve. Thus, in the lower half of the atmosphere the derived curve is probably accurate; up to 350 or 300 g.cm^{-2} the errors are probably not very serious; but above 300 g.cm^{-2} the curve must be considered only qualitative.

Despite the possible inaccuracy at high altitudes, it is clear that the curve representing vertical showers has a maximum about 100 g.cm^{-2} lower in the atmosphere, and about 3 times less in intensity relative to sea level, than the maximum of the integrated counting rates.

Before analyzing the directional intensity further, it is possible to compare the derived zenith-angle distributions of the showers with experiments.

Relative intensities per unit solid angle (for an isotropic detector), derived from the variation of the vertical counting rate with elevation, are represented by smooth curves in Fig. 20–23. In order to obtain the sea-level curve, $C(h)$ had to be extrapolated

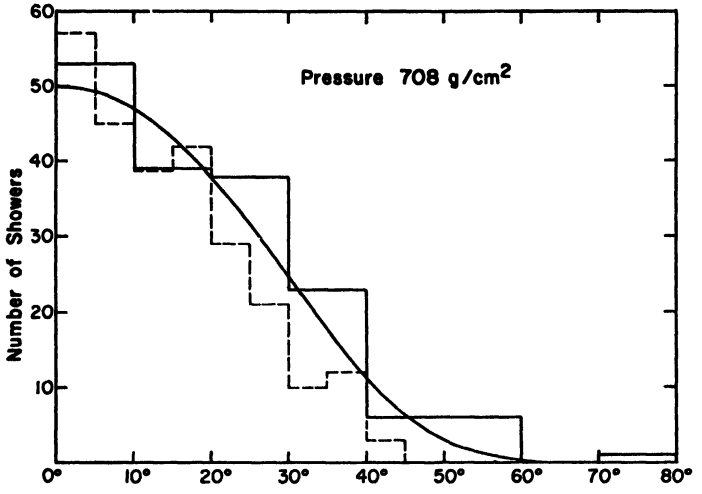

Fig. 20 – Comparison of the experimental zenith angle distribution of EAS with that derived from the altitude variation. The smooth curve is the derived distribution per unit solid angle at 3260 m elevation. The solid histogram represents actual numbers of showers with $\Delta \gtrsim 300$ m^{-2}, observed in 10° intervals of *projected* zenith angle by BROWN and MCKAY [1949]. The total number of EAS in this distribution is 166. The dashed-line histogram represents numbers of showers with $\Delta \gtrsim 200$ m^{-2}, observed in 5° intervals of projected angle by HAZEN, WILLIAMS and RANDALL [1954], the total number being 258.

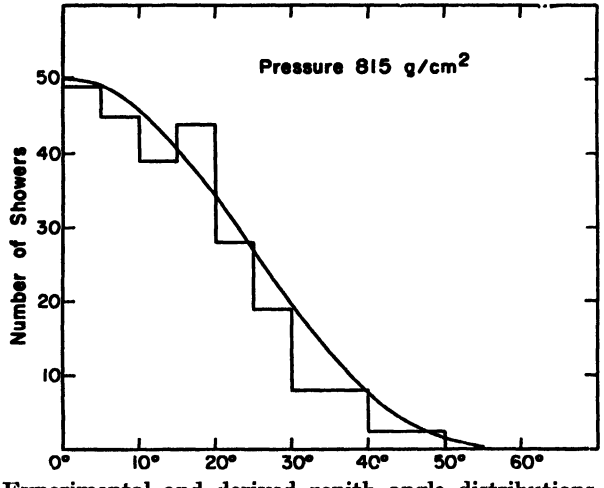

Fig. 21 – Experimental and derived zenith angle distributions at 2000 m elevation. The curve is the spacc-angle distribution for showers of $\Delta \gtrsim 50$ m^{-2}, derived from the altitude variation. The histogram shows the projected zenith angle distribution, based on 191 events with $\Delta \gtrsim 400$ m^{-2}, observed by DAUDIN [1945].

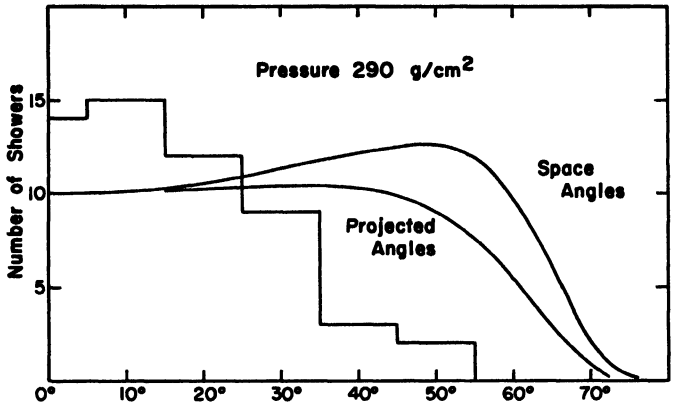

Fig. 22 – The smooth curves are angular distributions derived from the relative number of showers as a function of altitude. The histogram represents the projected zenith angle distribution, based on 48 EAS observed by ADAMS, ANDERSON and COWAN [1949] at 31,000 ft elevation. The curves and the histogram both refer to EAS having $A \gtrsim 50$ m^{-2}.

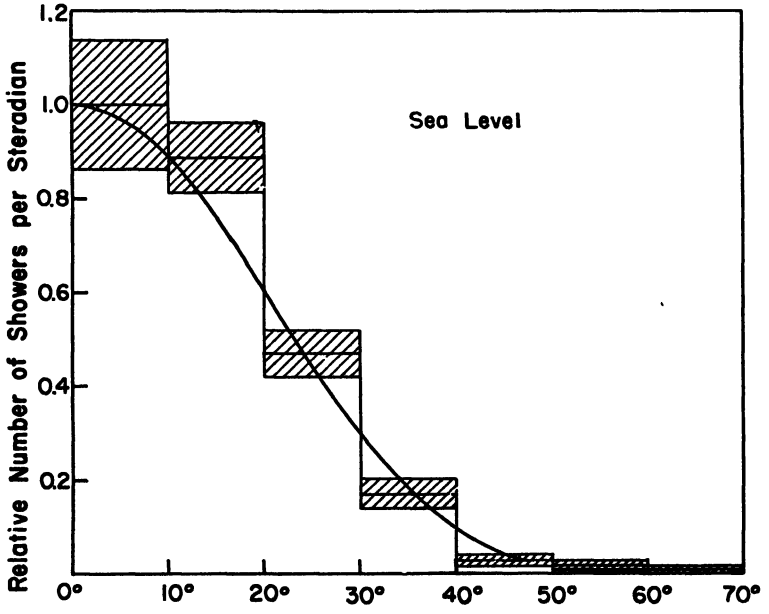

Fig. 23 – The histogram represents the space-angle distribution of EAS having densities exceeding ~ 20 m^{-2} at sea level, based on 350 showers observed by BASSI, CLARK and ROSSI [1953]. The smooth curve is derived from the altitude variation of the number of EAS with density exceeding ~ 50 m^{-2}. The agreement suggests that the extrapolation of the altitude variation beyond sea level with a constant attenuation coefficient of 0.0075 g^{-1}cm^2 is approximately correct.

beyond sea level; this extrapolation was made with a constant derivative, $\partial \ln C/\partial h$, equal to —0.0075 per g.cm^{-2}.

The computed space-angle distributions must be compared in most cases with measurements of the distribution of projected angles. The comparisons are simplified by the fact that if the space-angle distribution is a cosine power law, the projected angle distribution is also a cosine power law with the same exponent. Although the derived distributions do not have exactly this form, they approximate cosine power laws rather well in the lower half of the atmosphere. For instance, at 708 g.cm^{-2} if $R(0)$ is arbitrarily set equal to $R(0)\cos^m\theta$, m is found to vary from 4 at 10° to 6 at 45°, and $R(\theta)$ is well approximated by $\cos^5\theta$; at 815 g.cm^{-2}, m varies from 5.6 at small angles to 7.4 at 45° and can be approximated by 6.5; while at sea level, m varies from 7.4 at 10° to 9.1 at 45° and can be approximated by 8.3. However, at 290 g.cm^{-2} $R(\theta)$ has no resemblance to a cosine power law; therefore at this depth the projected angle distribution was computed from the space-angle distribution by approximate numerical integration.

One method of measuring the zenith-angle distribution has been to compare coincidence rates obtained with counter axes vertical and with the axes horizontal (Kraybill [1954], Bassi *et al.* [1952]). An analogous method is to measure the angles of the tracks of all shower particles seen in a cloud chamber (Cresti *et al.* [1953]). These experiments, however, yield the angular distribution not of the shower axes, but of the shower particles, many of which have been badly scattered. Therefore the results are not useful for the present purposes.

Another method has been to consider only those cloud chamber pictures that showed high energy electrons or several nearly parallel tracks of which the average direction could be well determined (Williams [1948], Daudin [1945], Deutschmann [1947], Brown & McKay [1949], Adams *et al.* [1949], Hazen *et al.* [1954]). The measurements then represent the directional distribution of the shower axes. In most of the experiments, because of the orientation of the triggering counters, the cylindrical shape of the cloud chamber, and the selection on the basis of the number of tracks visible in the chamber, there was no significantly varying bias as a function of projected zenith angle. In the experiment of Daudin, where such a bias existed, corrections have been applied.

The main limitation of the accuracy of the experiments is the statistical errors, since the distributions are in every case based on a small number of observed showers.

A newly developed method of measuring the angular distribution of shower axes is to measure the difference in the time of response of counters that are separated from each other in a horizontal plane. This method, which has been developed by BASSI, CLARK & ROSSI [1953], can yield the space-angle distribution as well as the distribution of projected angles. [1]

Histograms representing the experimental results at various elevations are compared with the derived angular distributions in Fig. 20–23. It apparently does not matter that the average shower densities to which the results apply are variable, because the altitude effect and the zenith-angle distribution are not strongly dependent on the shower size, at least in the lower atmosphere. The measurements at 290 g.cm^{-2} were made with a very large cloud chamber and refer to a mean density about the same as in the measurements of the altitude variation, from which the derived angular distributions were computed.

The agreement between experimental and derived distributions is satisfactory in all cases except the one at 290 g.cm^{-2}. In this case the discrepancy is strong and has not been explained; but the statistical errors are large and the computed distribution is also somewhat uncertain. It was pointed out in Section 3 that the lateral distribution calculated for an isothermal atmosphere could not be applied with accuracy in the upper part of the atmosphere, where the scattering length changes radically in a few radiation lengths. The lack of agreement in Fig. 22 suggests that the first-order correction for the changing density of the atmosphere is seriously inadequate at high elevations.

If the discrepancy in Fig. 22 can be ignored, the remaining agreement between the experimental and computed angular distributions may be considered as evidence in support of the assumption underlying the Gross transformation: that the shower intensity depends only on the amount of matter the showers have traversed. If this is

[1] In this work, independent measurements were reported of the space-angle and projected angle distributions, which were not consistent with each other. A private communication from one of the authors has indicated that the projected angle distribution was in error; hence only the space-angle measurements are shown in Fig. 23.

true, decay processes with long enough lifetimes to be suppressed by nuclear absorption in the upper atmosphere do not play an important role in the initiation or development of the showers.

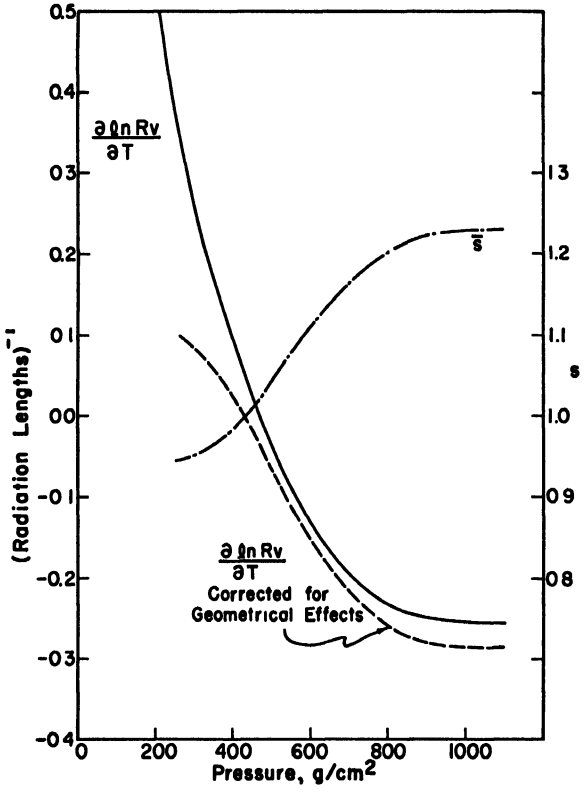

Fig 24 – The attenuation coefficient of EAS. The solid curve is the derivative of the curve labelled "Vertical Showers" in Fig. 19. After applying corrections for the change of shower geometry with altitude, the dashed curve is obtained, which represents as a function of altitude the frequency of showers having a given number of particles (N). By defining $\lambda = \partial \ln N/\partial t$ and identifying λ with the electronic cascade parameter $\lambda_1(s)$, the average age of the showers as a function of depth is found, as shown by the dot-dash curve.

The finite lifetime of π°-mesons should not suppress their decay significantly until their energies are greater than 10^{17} eV. In view of the evidence on multiple meson production, this suppression would only be of importance in showers of primary energy around 10^{19} eV or more, which have not yet been observed.

5. 4 Analysis of the variation of the vertical intensity with altitude

The derivative of the vertical intensity with respect to atmospheric depth in radiation units is shown by the solid curve in Fig. 24. The derivative can be corrected for the variation of the scattering length, r_1, with pressure and temperature of the atmosphere by noting that the counting rate is proportional to $r_1^{-2(\gamma-1)}$, that the effective value of r_1 is the value corresponding to the air density two radiation lengths above the point of observation, and that the temperature of the atmosphere is approximately proportional to the 0.18 power of the pressure between 250 g.cm^{-2} and sea level. Thus, the correction is made by subtracting $2(0.82)\,(\gamma - 1)/(T - 2)$ from $\partial \ln R_v/\partial T$.

A correction should also be made for the variation of the counter separation relative to r_1 as the altitude is changed. The effect is difficult to compute, however, and is compensated for by the fact that the showers are younger at high altitudes than at low ones. Experimentally, the variation of counting rate with counter separation is nearly independent of altitude (Biehl & Neher [1951], Wei & Montgomery [1949], Kraybill [1949]); moreover, the rates plotted in Fig. 19 were measured with counters only a few meters apart. Hence this correction will be ignored.

The corrected variation of R_v with T is due mostly to the growth and decay of the number of electrons in the showers. If the number spectrum is describable by a power law with exponent γ', and one defines $\lambda = (\partial \ln N/\partial T)_{.1v}$, the relation between R_v and T is

$$\frac{\partial \ln R_v}{\partial T} = \gamma' \lambda . \tag{29}$$

By identifying λ with the analogous parameter $\lambda_1(s)$ of the cascade theory, an average shower age, $\bar{s}$, can be obtained as a function of T.

A further correction is needed, even for counters with zero separation, because of the variation of the average shower age with depth: younger showers are more compressed than old ones, and hence are registered more efficiently. A similar correction has already been discussed in deriving the number spectra of the showers.

The counting rate is proportional to the integral $\int_0^\infty [f(x, s)]^{\gamma'} x\, dx$,

as may be seen from Eq. 14. Let s_0 be the average age of the recorded showers. By utilizing Eq. 11, $f(x, s)$ may be expanded about $s = s_0$, and the slowly varying factor may be removed from the integrand, assigning suitable average values to the parameters in this factor.

The counting rate is then found to be proportional to

$$e^{(\bar{s}-s_0)\gamma'[\ln \bar{x}(\bar{x}+1)+c'(s_0)/c(s_0)]} \int_0^\infty [f(x, s_0)]^{\gamma'} x\, dx .$$

The variation of $\bar{s}$ with T contributes to $\partial \ln R_v/\partial T$ an amount

$$\left(\frac{\partial \ln R_v}{\partial T}\right)_s = \gamma'[\ln \bar{x}(\bar{x}+1) + c'(s_0)/c(s_0)]\frac{\partial \bar{s}}{\partial T} . \qquad (30)$$

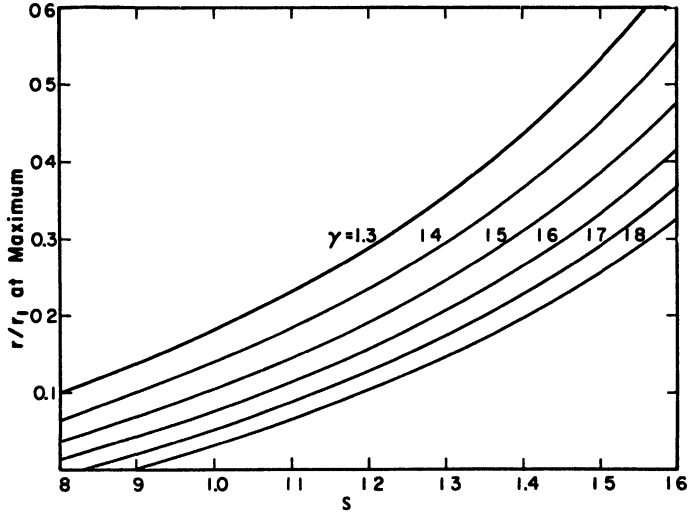

Fig 25 – If the integrand with respect to ln x in Eq. 14 is plotted, a nearly symmetrical curve results, having a strong peak. The value of ln x at this peak represents fairly well the average of ln x over the integral. The corresponding value of x (i.e., of r/r_1) is shown in the present figure as a function of the age of the electronic showers and the exponent of the number spectrum. These values of x may be interpreted as the mean distance to the axes of showers that give rise to a given particle density at an arbitrary point.

Values of $\bar{x}$ as a function of γ' and s_0 are shown in Fig. 25, and values of c' and c can be obtained from Table I. [1] The derivative $\partial \bar{s}/\partial T$ is taken from the first-order analysis of the altitude variation, before the present correction.

[1] In applying Eq. 30, in accordance with the Nishimura-Kamata theory, s_0 must differ from the s of the longitudinal theory by an amount depending on $\bar{x}$. Since $\bar{x} < 1$, s_0 is larger than the s of the longitudinal theory.

After subtracting the correction $(\partial \ln R_v/\partial T)_s$, which is a very small correction in the lower atmosphere, owing to the approximate constancy of $\bar{s}$, the values of $\partial \ln R_v/\partial T$ are obtained which are indicated by the dashed curve in Fig. 24. The corresponding values of $\bar{s}$ are shown by the dot-dash curve in the same figure.

The uncorrected curve $(\partial \ln R_v/\partial T)$ in Fig. 24 and the curve labelled "vertical showers" in Fig. 19 essentially describe the variation with altitude of the number of vertical showers yielding a density greater than $\sim 50\ m^{-2}$. The curve $(\partial \ln R_v/\partial T)$ corrected for geometrical factors describes the variation with elevation of the number of showers having more than N electrons, for $N \approx 10^6$. By integrating the corrected values of $\partial \ln R_v/\partial T$, one obtains an altitude curve for R_v that rises from 1.0 at sea level to 10 at 708 $g.cm^{-2}$, and continues to rise more slowly until a maximum of ~ 25 is reached at a depth of 430 $g.cm^{-2}$; above this level, the curve drops at a rate that soon becomes very uncertain because of the importance of the large geometrical corrections, which could not be made accurately.

5. 5 Interpretation of the rate of absorption

We now wish to discuss further the remarkable constancy of $\bar{s}$, or of $\partial \ln R_v/\partial T$, in the lowest third of the atmosphere.

Independently of how the electronic component is created, each of the electronic cascades within an EAS grows and decays with a continually decreasing value of $\partial \ln N/\partial T$, approaching as $T \to \infty$ the value —0.64, which is the minimum absorption coefficient of photons in air. The corresponding value of $\partial \ln R_v/\partial T$ equals $\gamma'(\partial \ln N/\partial T)$, approximately —1.0. The fact that $-\partial \ln R_v/\partial T$ approaches a smaller plateau value, about 0.3, at the base of the atmosphere is well established by the experimental barometric coefficients and the altitude effect. Therefore, a process involving a longer absorption length than that of electronic cascades must prolong their length.

One effect of this type is the initiation of EAS at varying depths in the atmosphere. If this were the only modification of the simple electronic cascade picture, the plateau value approached by $-\partial \ln R_v/\partial T$ would be σ_p, the cross-section per radiation length for the initiation of showers by the primary cosmic rays.

In light elements, the mean free path for shower production by protons or neutrons of high energy has been found to be

about 80 g.cm^{-2}, which corresponds to $\sigma_p = 0.47$ per radiation length, nearly the geometrical cross-section; and no evidence of any trend towards decreasing cross-section with increasing energy has ever been observed. For primary alpha particles and heavier nuclei the cross-sections are greater. Therefore the variable depth of shower production should lead to a plateau value of $-\partial \ln R_v/\partial T$ greater than or equal to —0.47. Hence, this is not the only effect that prolongs the cascades.

One is thus led inevitably to account for the plateau of the shower absorption rate in terms of the nuclear cascade. Other evidence leading to the same conclusion may be summarized as follows.

(1) *Rate of Absorption as a Function of Shower Size*

In the discussion of the density and number spectra, it was pointed out that the exponent γ does not change appreciably with elevation in the lower part of the atmosphere, and that this implies that large showers are absorbed about as rapidly as small ones, contrary to the behavior of pure electronic showers (Cocconi [1947], Budini [1951]). Similarly, the barometric coefficient has been found either to increase with shower size or to be nearly independent of the size, instead of being smaller for the larger showers (Citron [1952], Daudin [1953]). The measurements of Hazen, Williams & Randall [1954] indicate that the steepness of the zenith angle distribution is nearly independent of shower size; and the comparisons of the zenith angle distribution with the altitude effect in Fig. 20, 21 and 23 suggest the same conclusion.

Hence the showers cannot be propagated entirely by the mechanisms involved in electronic cascades. The large showers must not be as rich in high energy electrons and photons as if the showers derived from single electron primaries, and the small showers must have a means of sustenance other then the energy in the electronic component.

(2) *The Energy Spectrum*

Hazen [1952], Hazen *et al.* [1954] have studied the energy spectra of electrons and photons near the axes of EAS, by observing the multiplication of the particles in lead plates within a cloud chamber. In the more recent of these experiments, the shower sizes and the distances to the axes were determined by pulse heights registered in five ionization chambers. The experi-

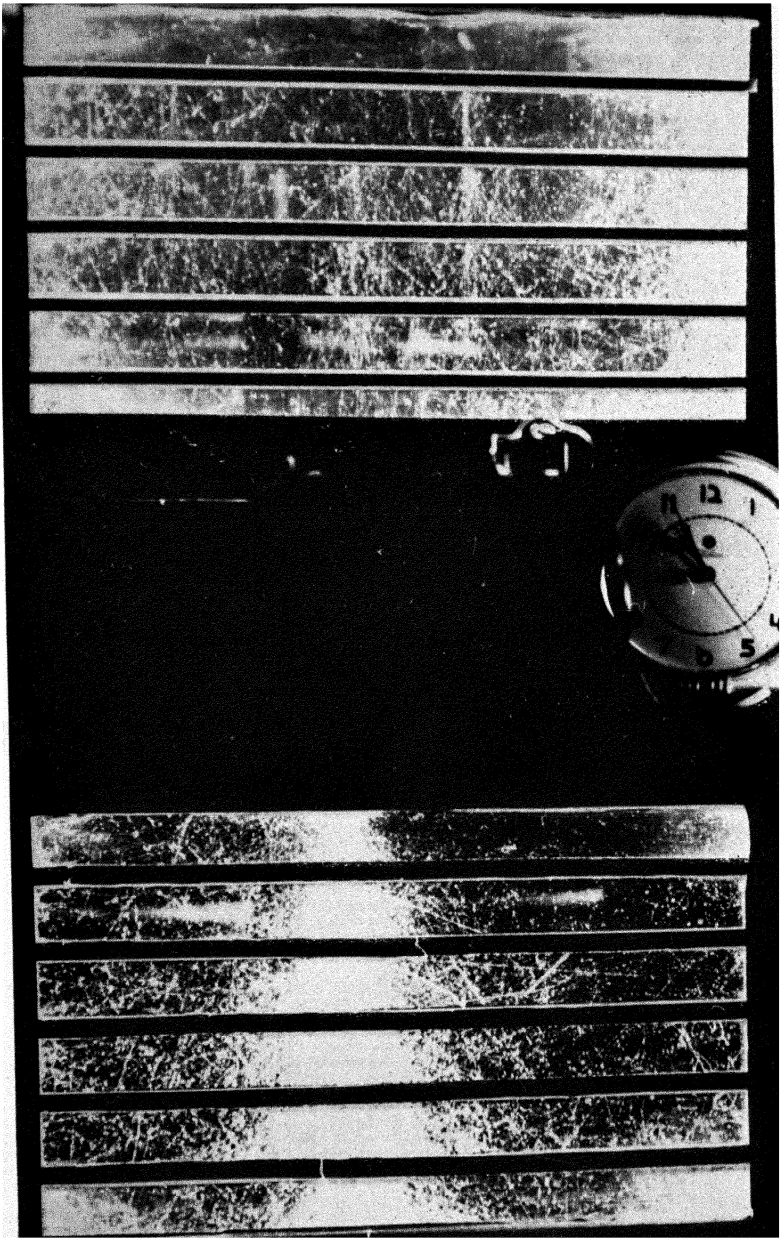

Plate I – Cloud chamber picture taken by G. M. BRANCH [1951] at 3260 m elevation. Neon bulbs indicated the triggering of several horizontally separated counters by an associated EAS. The two chambers were separated by six inches of lead, and the very dense electron shower visible in the lower chamber was initiated in the lead by one of the particles in the air shower. The lead plates in the chambers were $\frac{1}{2}$-in thick.

mental numbers of high energy electrons and photons were compared with predictions calculated on the basis of the longitudinal cascade theory under Approximation A and the lateral distribution functions of Eyges and Fernbach.

At distances up to a few meters from the shower axes, the observed number of high energy electrons and photons was much less than the number predicted for showers of $s = 1$, and varied less rapidly with distance from the shower axis than was predicted. The observations agreed much better with calculations for old showers, having $s = 1.5$. But the absorption of the showers in the atmosphere corresponds to a much smaller age, $s \approx 1.17$; and the lateral distribution at distances exceeding a few meters from the axis was found to be not very different from the Molière function, which is correct only at the maximum of a shower.

Therefore the core of a shower is not rich enough in high energy electrons and photons, on the average, to account for the propagation of the shower in the lower part of the atmosphere, or to account for the lateral distribution of the low energy electrons. There must be in the neighbourhood of the core another source continually feeding energy into the electronic component. One concludes that this source is the N-component cascade.

(3) *Direct Observations*

The release of new electronic cascades within EAS has been demonstrated by the cloud chamber pictures of Brown & McKay [1949], Gottlieb [1951], and Branch [1951]. An extreme example is shown in Plate I. Local electronic showers associated with EAS have also been recorded by ionization chambers; indeed, almost all of the largest bursts and penetrating showers created under thick lead seem to be associated with EAS (Fahy [1951], Stinchcomb [1951], Greisen *et al.* [1950], Greisen *et al.* [1953], Ticho [1952]).

The abundance of the high energy N-component near the axes of the showers has been found to be on the order of 1/200 the number of electrons in the lower part of the atmosphere (McCusker [1950], Sitte [1950], Greisen *et al.* [1950], Sitte [1952], Kasnitz & Sitte [1954]). Since the N-component was identified by penetrating shower production, the average energy of the recognized particles was on the order of tens of GeV, at least 100 times greater than the average energy of the electrons. Hence there is evidence of the existence of as much energy in the nuclear-

active component as in the electronic component of the showers at low elevations. The data presented in section 7 suggest that the N-component is more abundant relative to the electrons at sea level than at mountain elevations.

Pictures like Plate I represent the phenomenon of the creation of new electronic showers in a somewhat distorted way, owing to the rapid development of cascades on a very compressed scale in lead. One would not expect the subsidiary showers to be individually prominent in the air, because of multiple overlapping and because the showers would generally not contain enough high energy electrons and photons to be strongly divergent in density at the individual axes. Since the high energy N-component is concentrated near the central axis (GREISEN *et al.* [1950], COCCONI & TONGIORGI [1950], BROWN & MCKAY [1949], ANISHENKO *et al.* [1952]), it is not contradictory that the experiments on the lateral distribution of the electrons were consistent with the showers having a single origin.

(4) *Growth of the Showers at High Altitudes*

Numerous calculations of the development of the EAS in the atmosphere have been made under the assumption of a primary electron spectrum (MILLS [1948], LEWIS [1948], BUDINI [1951]). A primary energy spectrum selected to suit the number spectrum and the rate of absorption of the EAS near sea level invariably predicts a smaller maximum in the shower curve, occurring at a lower altitude, than is observed experimentally.

Recently, calculations of the development of the EAS have been carried out by GOAD [1953] on a more realistic model, based on the Fermi theory of nuclear interactions, which seems to account for most of the features of high energy events observed in emulsions (KAPLON *et al.* [1949], LORD *et al.* [1950], PICKUP & VOYVODIC [1951], LAL *et al.* [1952], KAPLON & RITSON [1952a, 1952b], MARSHAK [1952], COCCONI [1954a]). Goad took into account the fluctuations in the depth at which showers are initiated, computed as accurately as possible the effects of the change in shower geometry with elevation, and considered the showers produced by primary alpha particles as well as protons. However, he neglected all contributions to the electronic component except those arising from the π^0-mesons produced in the initial nucleon-nucleon collisions. Once again, a smaller maximum of the shower

curve, occurring lower in the atmosphere than in the experiments, was calculated.

A related difficulty also appeared in the theoretical calculation of the exponent γ of the density spectrum: as in the earlier calculations based on a primary electron spectrum, Goad found that γ was expected to increase with elevation more rapidly than it does.

One can shift the computed maximum of the shower curve to a higher value, occurring at a higher elevation, by assuming a steeper primary energy spectrum; but then the predicted rate of absorption of the showers at sea level becomes much too great. Similarly, by departing from a power law for the primary energy spectrum (letting the exponent increase with the energy), one can predict a more constant γ as a function of elevation; but this change makes the discrepancy in the computed altitude variation worse, since one needs a high exponent at comparatively low energies to account for the numerous showers at high elevation. Furthermore, this change results in the prediction that γ should vary with shower size at a given elevation more rapidly than is observed. Thus, it does not seem possible, by adjusting the free parameters of the model, to fit all the data on the electronic component.

At high altitudes, a better fit could be obtained if the theoretical multiplicity with which the π^0-mesons are created could be increased; it would also help if the multiplicity were even more strongly dependent on the primary energy than in Goad's application of the Fermi theory. Raising the multiplicity would accelerate the early development of the showers, and the rapid increase of multiplicity with energy would make showers of different sizes more similar, farther down in the atmosphere, in their rates of absorption, lateral distributions and energy spectra.

Some increase in the multiplicity is justified, within the framework of the Fermi theory, by the fact that primary protons collide with nuclei of nitrogen or oxygen rather than with single nucleons. Cocconi [1954a] has considered the tunnelling through a nucleus at high energy under the reasonable assumption that if n target nucleons are involved, a single interaction volume is formed, n times as large as in a nucleon-nucleon collision. This assumption yields a predicted multiplicity proportional to $n^{\frac{1}{4}}$, plus an additional factor that may be as large as 2, arising because

the n nucleons are not aligned and hence the correction for the conservation of angular momentum is reduced. The calculations were shown to be consistent with the reported observations of high energy stars in emulsions. For air, the increase of the average multiplicity would be a factor between 2 and 4.

The heavy nuclei among the primaries, of course, will generally initiate showers higher in the atmosphere than will primary protons, and with a greater initial multiplicity of secondaries. But one can probably account for the rapid growth of EAS at high elevations without requiring the showers to be initiated by heavy nuclei.

A further effect that operates in the same direction as raising the multiplicity in the primary collision is the production of π^0-mesons in secondary interactions of the successive generations of the nuclear cascade. The energy of the photons thus created decreases from one generation to the next by an average factor v_i, where v_i is about one-half of the total multiplicity of particle creation in collisions of the i^{th} generation. This degradation of energy reduces the distance to the maxima of the electronic showers by $\ln v_i$, which for very high energy collisions is bigger than the average distance (2 radiation lengths) between the nuclear interactions of successive generations. Therefore the electronic cascades of the second and third generations reach their maxima and begin to die out earlier than the showers of the first generation. Thus, the successive generations (until $\ln v_i < 2$) contribute principally to the early part of the shower, shifting the maximum to higher altitudes. Proper consideration of this effect can certainly reduce and may possibly eliminate the discrepancy between the calculations and observations in the high altitude region.

If $v_i = a\, E_{i-1}^{\frac{1}{4}}$ as in the Fermi theory, and if one simplifies the theory by neglecting particles emitted backwards in the c.m. system and assuming that all particles emitted forwards have the same energy in the laboratory system, the degradation of the energy of the nuclear-active particles in k successive collisions is

$$\frac{E_0}{E_k} = \prod_{i=1}^{k} v_i = (a^4 E_0)^{1-(\frac{1}{4})^k} \quad . \tag{31}$$

The degradation over several successive generations is thus a much stronger function of the primary energy than is the multiplicity in the first encounter. This helps to make large and small showers similar in energy spectra and rate of absorption by the time they have passed through the first half of the atmosphere.

5. 6 Energy transfer to electronic cascades in the lower atmosphere

In order to account for the plateau in the shower absorption rate at low elevations, two further conditions must be fulfilled. The attenuation coefficient of the number of vertical showers of a given size levels off at about 0.29 per radiation length, implying that the number of particles in each EAS decays with an absorption length equal to $\gamma'/0.29$ radiation lengths or about 195 g.cm^{-2}. As this is much greater than the limiting absorption length of electronic cascades, it must represent the absorption length of the source of electronic energy, namely the energy in the nuclear cascade. Secondly, since the nuclear-active component must dominate the longitudinal propagation of typical EAS below 600–700 g.cm^{-2}, the proportion of the energy remaining in the nuclear-active component after ~ 8 interaction lengths must be approximately equal to the proportion of the energy dissipated in ionization by the electrons below this level. These conditions allow one to set upper limits on the fraction of the energy given to π°-mesons in energetic nuclear encounters, and to the degradation of energy of the nuclear-active particles from generation to generation.

Let f_i be the fraction of the incident energy retained by non-decaying nuclear-active particles in the i^{th}-generation collisions; let g_i be the energy given to π°-mesons; and let $h_i = 1 - f_i - g_i$ be the energy lost by decay to μ-mesons and neutrinos, or in other forms that do not contribute to the nuclear or electromagnetic cascades. For simplicity, continue to assume, for the present, an equipartition of the incident energy among the v_i secondaries emitted forwards in the c.m. system. It then follows that the energy of all the nuclear-active particles in the k^{th} generation at a depth t in the atmosphere is

$$E_0 \frac{(\sigma t)^k e^{-\sigma t}}{k!} \prod_{i=1}^{k} f_i \, .$$

Assume further that for energies above a particular E_k, $h_i \approx 0$ and $f_i = f =$ constant, while for energies below this value, h_i is large and f_i is very small. The total energy of the nuclear-active particles effective in propagating the cascade thereupon becomes

$$W = E_0 \, e^{-\sigma t} \sum_{p=0}^{k} \frac{(f \sigma t)^p}{p!} \, . \tag{32}$$

The energy E will be on the order of 10^{11} eV, because mesons produced in interactions of particles having less energy than 10^{11} eV mostly decay before interacting, even in the middle of the atmosphere.

By taking the logarithmic derivative of W with respect to t, one obtains the following ratio of the attenuation coefficient, σ', to the interaction coefficient σ:

$$\frac{\sigma'}{\sigma} = 1 - f \frac{\sum_0^{k-1} \frac{(f\sigma t)^p}{p!}}{\sum_0^{k} \frac{(f\sigma t)^p}{p!}} . \tag{33}$$

In the limit as $k \to \infty$, $W \to E_0 \exp[-\sigma t(1-f)]$ and $\sigma'/\sigma \to 1-f$; but for the small values of k with which we are concerned, W is smaller than this and σ' is larger. It follows from Eq. 31 that the number of generations required to reduce the energy from E_0 to E_k is

$$k = \frac{1}{\ln(4/3)} \ln \frac{\ln E_0 + 4 \ln a}{\ln E_k + 4 \ln a} . \tag{34}$$

According to the Fermi theory, if energy is measured in units of $Mc^2 \approx 10^9$ eV, the constant a would be about 0.8 for nucleon-nucleon collisons in which only pions are produced, and more if other particles are also created; but in Cocconi's adaptation of the theory to collisions with complex nuclei the appropriate mean value of a would be at least 2. With $a = 2$, it takes only 3 generations to go from $E_0 = 10^{16}$ to $E_k = 10^{11}$ eV, where f drops to a low value (if $a = 0.8$ the number of generations would be 5). It may be noted that k is very insensitive to the value of E_0 because of the dependence of v_i on the energy.

If only π-mesons are produced in high energy collisions, one might expect $f \approx 2/3$. With $f = 2/3$ and $k = 3$, Eq. 33 yields $\sigma'/\sigma = 0.70$ or 0.78 at $t = 8$ or 12 respectively. These values are much too high in comparison with the ratio 0.41 indicated by the data. Indeed, the calculated ratio does not reach 0.41 until 7 generations of secondaries are taken into account at $\sigma t = 8$, or 10 generations at $\sigma t = 12$. If nucleon-antinucleon pairs are produced as well as pions, with relative statistical weights 8 and 3, f may be as large as 10/11. Even so, it still requires 6 to 9 generations for σ'/σ to reach 0.41 at $\sigma t = 8$ to 12.

In six generations, according to Eq. 31 with $a = 2$, the nuclear-active particles would be degraded from a primary energy of

10^{16} eV down to $E_6 = 3$ GeV. Long before such low energies are reached, the nuclear collisions must become largely dissipative, implying a low value of f and insignificant further contributions to the electronic cascade.

Similar contradictions are met in evaluating the fraction of the total primary energy that must be retained by the nuclear cascade in the lower part of the atmosphere. It has been pointed out that the quantity $\partial \ln R_v/\partial T$ (corrected for changes of shower geometry), which has been plotted in Fig. 24, is equal to $\gamma'\lambda$, where γ' is the exponent of the number spectrum and λ is the average value of $\partial \ln N/\partial T$ for the showers selected by the apparatus. By dividing the dashed curve in Fig. 24 with γ' and integrating, one obtains the average variation of shower size, N, with atmospheric depth. Normalized to 1 at sea level, this curve rises to a broad maximum of about 8.5 in the neighbourhood of 450 g.cm^{-2}, and then falls with increasing rapidity as one approaches the top of the atmosphere. The energy dissipated by the shower is given by the track length integral, $\varepsilon_0 \int_0^\infty N\,dt$, which yields 12 GeV per electron at sea level: 11.5 GeV in the integral over the atmosphere and 0.4—0.5 GeV in the integral over the portion of the curve that is extrapolated below sea level.

In the lower atmosphere the curve is represented by $N/N_{SL} \approx \exp\,[-0.28(t - t_0)/\gamma'] \approx \exp\,[-0.19[t - t_0)]$. The track length integral beyond 700 g.cm^{-2} yields about 2.4 GeV per electron at sea level, indicating that the energy dissipated by the electrons below 700 g.cm^{-2} is 20% of the total. Since this energy must come from the nuclear cascade, the nuclear-active particles must still retain about 1/5 of the primary energy at $\sigma t \approx 8$. [1]

According to Eq. 32, on the contrary, if $f = 2/3$ and $k = 3$, one obtains $W/E_0 = 0.015$ at $\sigma t = 8$, more than an order of magnitude too little energy to account for the further propagation of the electronic showers. One cannot correct the discrepancy

[1] Some of the energy dissipated below 700 g.cm^{-2} is transferred to the electrons above the level 640 g.cm^{-2} implied by $\sigma t = 8$; but on the other hand, the energy still possessed by the nuclear cascade at $\sigma t = 8$ cannot be transferred to the electronic component with perfect efficiency. The compensation of these two effects makes the assumed equality approximately correct, though admittedly not accurate. An error by a factor on the order of two will not alter the conclusions.

by raising either f of k alone. A minimum value of f is about 0.8, while even if f is as large as 0.9, the energy must be summed over six generations of secondaries to be sufficient.

If $f \geqq 0.8$ and if one assumes $a \leqq 0.5$ in the relation $v_t = a E_{t-1}^{\frac{1}{4}}$, both the energy and the absorption coefficient of the nuclear-active component in the lower atmosphere, as computed with Eq. 32 and 33, are consistent with the analysis of EAS data.

The high value of f is open to at least two kinds of interpretation. If only pions are created, the high energy collisions must be partially elastic, about half of the energy being retained by the incident particle and the recoil nucleons. If, instead, the collision is completely inelastic, other particles as well as pions must be produced, all of them except the π^0 having long enough lives and large enough nuclear cross-sections to produce further interactions.

The most likely interpretation of the low value required of the constant a is that the incident energy is very unequally distributed among the secondary particles. It is not likely that the multiplicities of meson production are indeed less than is predicted by the Fermi theory, for that would be contrary to the evidence from high energy stars seen in emulsions, and besides, high multiplicaties were found to be helpful in accounting for the growth of EAS at high altitudes. But if the energy is very unevenly shared, the significant multiplicity, as far as the energy degradation is concerned, is the comparatively small number of secondaries that carry most of the energy. Near the origin of an electronic cascade, on the other hand, the rate of growth is not strongly dependent on the initial energy; hence π^0-mesons produced with moderate energy as well as those produced with the greatest energy can be influential in accelerating the early development of the EAS.

The assumption of uniform sharing of the energy is not faithful to the Fermi theory, which actually predicts a rather broad distribution of the energy among the secondaries in the laboratory system (FERMI [1951], HAZEN *et al.* [1952] GOAD [1953]). No calculation of the nuclear cascade with the Fermi theory has yet taken this into account. But the width of the distribution does not appear to be sufficient to explain the very large attenuation length required by the data.

As mentioned earlier, even on purely theoretical grounds some modification of the Fermi theory seems appropriate. Some of the

proposals which were found helpful in accounting for the steepness of the lateral distribution can also assist, at least qualitatively, in explaining the phenomena under present discussion.

For example, the suggestion by BHABHA [1953] that part of the nucleonic energy may be associated with a core, small in radius compared with the meson field, leads to the prediction of semi-elastic collisions in which a large fraction of the energy may be retained by the incident nucleon. (Partially elastic collisions are also a potential outcome of the theoretical model proposed by KRAUSHAAR & MARKS [1954]. This type of collision would account for both the high value of the fractional energy retained by nuclear-active particles, f, and the low value of the energy degradation per collision.

Another experimental observation related to the present discussion is the ratio of neutral to charged particles among the N-component in EAS. As mentioned in the next section of this chapter, the ratio is rather high, about 0.7, and this is difficult to explain unless the collisions are partly elastic, the energy being retained preferentially by one or more nucleons instead of being given up almost entirely to mesons. Bhabha's theory accounts for this observation also.

The modification of the Fermi theory by LANDAU [1953], taking into account interactions during expansion of the excited volume, leads to a very non-uniform distribution of the energy among the secondaries. Such a distribution can help to account for the apparently small degradation of energy per collision; but it does not, without further assumptions, explain the high value of f or the ratio of neutral to charged particles in the N-component. The proposals of Bhabha and Landau, however, are not competitive but complementary; the one treats of only the influence of the mass distribution on the distribution of excitation in the colliding nucleons, while the other concerns the subsequent emission of particles. The present discussion does not pretend to judge the correctness of the theories, but only suggests that they help in a qualitative way to account for the properties of the EAS.

6. Meson and Nucleon Components of the EAS

The most direct evidence of the nuclear cascade in EAS is the presence of numerous μ-mesons, neutrons of moderate energy, and high energy particles of the N-component. These particles

are too abundant to be accounted for as secondaries of the photons and electrons; moreover, absorption experiments have shown that neutrons and mesons are locally produced in EAS predominantly by the high energy N-component, rather than by the soft component.

An analysis of the meson and nucleon intensities and their variations, like the analysis of the electronic component, does not specify very detailed properties of the high energy nuclear interactions that are reponsible for the particles, but it does reveal some of the qualitative features of the nuclear cascade and provide tests which can be applied to various theories.

6. 1 Methods of detection

The non-electronic components have most often been detected with trays of G-M counters placed under thick lead shields, which are supposed to filter out the electrons and photons that are incident from the air. In practice, this has not always been done adequately. If the showers are selected by coincidences of several trays of unshielded counters, one has to deal principally with the central part of the showers, where the electron and photon densities greatly exceed those of the other particles. The filtering must therefore attenuate the electronic component by a factor of at least 1000. It has been shown experimentally and theoretically that this requires a minimum of 20 cm of lead (Cocconi *et al.* [1949a], Greisen [1949], Brown & McKay [1949], Ise & Fretter [1949]). If one uses only 15 cm of lead, for instance, about 25% of the "penetrating particles" registered at 3250 m elevation are photons and electrons. Some of the measurements to be reported below have been corrected slightly for this reason.

The shield is not without effect on the other particles also. Energetic neutrons may produce charged secondaries in it and thereby be counted. Indeed, because of the lateral spread of local penetrating showers, the neutrons, protons and π-mesons of high energy sometimes are detected with greater efficiency than μ-mesons. Many of the protons and neutrons of insufficient energy to produce penetrating showers are absorbed in the shield, and even the μ-mesons are slightly reduced in number by the ionization loss.

In experiments performed with adequately shielded counter trays, in each of which the counters are all connected in parallel,

one measures indiscriminately what is called the "penetrating component", the counts being due partly to μ-mesons, π-mesons and protons pre-existing in the air, and partly to local secondaries created in the shield.

If the counters in the trays are subdivided electrically or connected individually to a hodoscope, one can verify that the frequency of multiple discharges is greater than can be accounted for by independent μ-mesons arriving from the air, and one can determine the approximate proportions of "interacting" and "non-interacting" particles (COCCONI *et al.* [1949b], SALVINI & TAGLIAFERRI [1949], MCCUSKER [1950], CHOWDHURI [1950], GREISEN *et al.* [1950], SITTE [1950, 1952], FUJIOKA [1953]). With elaborate hodoscopes, one can even trace the paths and count the numbers of the secondary penetrating particles that are locally produced, and thus estimate the energies of the incident N-component particles. With shielded anticoincidence trays, one can also determine the relative proportions of charged and neutral N-component.

If one simply requires a highly multiple coincidence among shielded counters, as in the well-known Janossy [1942] "P-set" — when the uppermost tray of the P-set is shielded by at least 10 cm of lead instead of being left uncovered — it is possible for a single high energy particle of the N-component to discharge the counters by producing a local shower; but a similar coincidence cannot be produced by μ-mesons unless two or more mesons are incident on the apparatus. Therefore the majority of the counts are due to the N-component.

Neutrons of moderate energy (1 — 15 MeV) in EAS have been detected by slowing them down in paraffin and counting them with boron-filled counters, in delayed coincidence with unshielded G-M counters that are discharged by the electrons. This method takes advantage of the long lifetime of slow neutrons in paraffin to distinguish between pulses due to neutrons and those due to dense electron showers (TONGIORGI [1948a, 1948b, 1949]). The detected neutrons consist partly of neutrons pre-existing in the air showers, and partly of neutrons produced locally. These contributions can be distinguished by varying the thickness of the paraffin and by adding other materials in proximity to the neutron counters (TONGIORGI [1949], LEVINGER [1949]). When dense materials such as lead are placed within the paraffin moderator, it is found that the great majority of the detected neutrons are

produced in the lead, mostly in large stars and penetrating showers generated by the N-component with energy exceeding 10^8 eV. Thus a specific detector of the N-component can be set up, which is insensitive to the μ-meson and electronic components.

In addition to the techniques already mentioned, of course, there is the cloud chamber, with which invaluable information on the nature of the penetrating component of EAS has been obtained (FRETTER [1949], ISE & FRETTER [1949], BROWN & MCKAY [1949], BRANCH [1951], CHOWDHURI *et al.* [1952]). In some cases, a cloud chamber has been used together with a hodoscope (KASNITZ & SITTE [1954]). The chambers have usually been equipped with lead plates to permit a distinction between electrons and penetrating particles, and to permit identification of the N-component by virtue of nuclear scattering or shower production.

6. 2 PROPORTION OF PENETRATING PARTICLES VS. DISTANCE FROM THE AXIS

Before reviewing experiments in which an attempt was made to distinguish nuclear-active particles from μ-mesons, some of the properties of the collective penetrating component will be summarized: first, the relative number of penetrating particles in comparison with the total number of charged particles in the showers, R_p, and the dependence of R_p on the distance from the axis; and afterwards, the dependence of R_p on the size of the shower.

Various determinations of R_p *vs.* the radial distance, r, are shown in Fig. 26 and 27: Fig. 26 contains the sea level measurements and Fig. 27 the ones made at mountain elevations. Some of the reported values result from rather direct experiments, and others from more indirect analyses, which will be described below.

The measurements that extend to the largest distances are those of EIDUS *et al.* [1952] at sea level, and of ZATSEPIN and collaborators [1953] at 3860 m elevation. These observations were made with widely separated sets of shielded and unshielded counters connected to a hodoscope. The electron densities, measured with the unshielded counters, permitted an approximate location of the shower axis and an estimation of the size of each shower, while the number of shielded counters that were discharged afforded determinations of the density of penetrating particles. The values of R_p so obtained reportedly refer to showers of $\gtrsim 10^7$ particles.

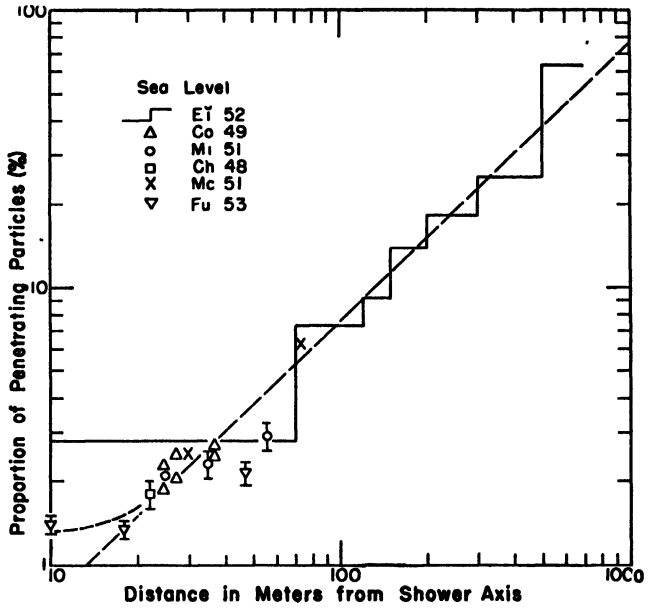

Fig. 26 – Proportion of penetrating particles *vs.* distance from the shower axis at sea level.

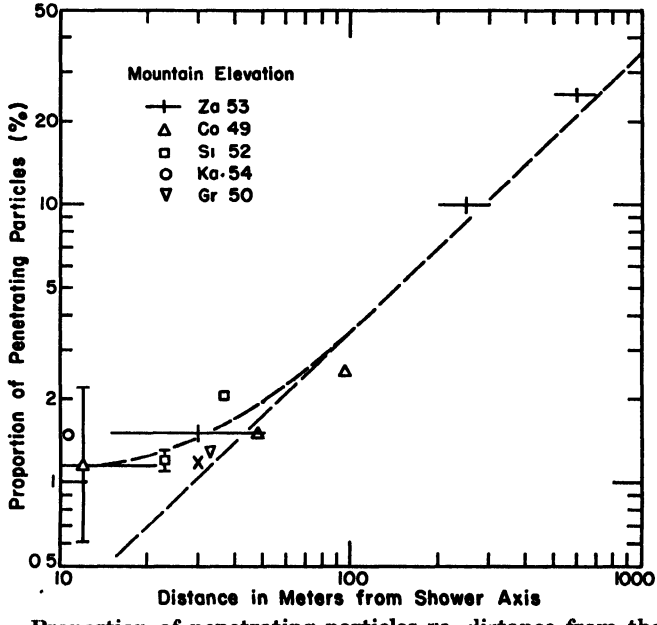

Fig. 27 – Proportion of penetrating particles *vs.* distance from the shower axis at mountain elevations. The point marked "×" is that of SALVINI and TAGLIAFERRI [1949].

At 3260 m above sea level, COCCONI, TONGIORGI & GREISEN [1949b] made use of "core selectors" to locate the axes of the showers, with large trays of unshielded and shielded counters in hodoscope connection to determine the densities of electrons and penetrating particles, and thus R_p, at various distances from the core selectors, Further measurements with apparatus very similar to that of Cocconi *et al.* have been made by FUJIOKA [1953] at sea level.

Values of R_p at sea level have also been derived from the experiments of CHOWDHURI [1948], MCCUSKER & MILLAR [1951], MILONE [1951] and COCCONI *et al.* [1949a]; while further points at mountain elevations have been derived from the measurements of SITTE and KASNITZ [1952, 1954], SALVINI & TAGLIAFERRI [1949] and GREISEN & WALKER [1950]. But in order to place these points in Figs. 26 and 27, it was necessary to compute the average distance from the shower axis to which each measurement applied.

Most of the measurements were made by selecting showers with a few trays of counters distributed around the penetrating particle detector; R_p was computed from the fraction of the showers in which a penetrating particle was observed. Thus, R_p is an average weighted according to the distribution of distances from a group of unshielded counters to the axes of the recorded showers.

If the counters are not too far apart, the n-fold coincidence rate is approximately equal to the following integral:

$$C = 2\pi r_1^2 \iint (1 - e^{-S\Delta})^n \, x \, dx \, k(N) \, dN \,, \qquad (35)$$

where $k(N)$ is the differential number spectrum, which is set equal to $\gamma K_0 N^{-(\gamma+1)}$; Δ is the total particle density; S is the area of each counter; and x is the distance from the centre of the counter array to the axis of the showers, in units of the scattering length r_1. The finite size and separation of the counter trays can be taken into account approximately by noting that if a is the radius of the counter array, the average distance of the shower axis from the counters has a minimum value equal to a. Thus, one may use the following approximate relation between Δ, x and N:

$$N = r_1' \Delta / f(x + a) \,,$$

where $f(x)$ is the lateral distribution function, represented by $c(s) \, x^{s-2} \, (x + 1)^{s-4.5}$.

With this substitution, Eq. 35 becomes:

$$C = 2\pi r_1^{-2(\gamma-1)}\gamma K_0 \int_0^{\infty} (1 - e^{-s\Delta})\, \Delta^{-(\gamma+1)}\, d\Delta$$

$$\int_{\ln x = -\infty}^{\ln x = +\infty} [c(s)]^{\gamma}\, x^2 (x + a)^{\gamma(s-2)} (x + a + 1)^{\gamma(s-4.5)}\, d(\ln x)\,.$$

On the assumption that γ and s are independent of shower size, the two integrals are completely separate. More accurately, the slow variation of γ and s with N may be considered to make the x-distribution weakly dependent on the mean value of Δ, and thereby slightly dependent on n and the counter area S.

The integrand with respect to ln x is reasonably symmetric about a rather sharp maximum, the position of which depends on the values of γ, a, and s. Under the assumption that the ratio R_p does not vary too rapidly with x, the experiments yield the value of $R_p(x)$ at x equal to the position of the maximum of the integrand. [1]

For instance, for the shower selector of MILONE [1951], one may use $\gamma = 1.45$, $a = 0.029$ and $s = 1.30$, which yield $x_m = 0.32$ or $r_m = 25$ m. When the penetrating particle detector and the electron density detector were displaced a distance D from the shower selector, the value of r_m was increased according to $r_m = [(25)^2 + D^2]^{\frac{1}{2}}$. Thus the measurements of Milone, which were made with values of D between 2 and 50 m, refer to values of r_m between 25 and 56 m. [2]

The measurements of MCCUSKER & MILLAR [1951] are particularly interesting in regard to the effect of the method of shower selection. In part of the experiment, showers were selected with three trays of shielded counters in coincidence, and the electron density distribution of these showers was examined with unshielded counters connected to a hodoscope. The results agreed best with $R_p = 6.25\%$. In another part of the experiment, showers were selected with two unshielded trays, and R_p was inferred from the proportion of the showers in which a shielded tray was also

[1] Fig. 25 shows values of x_m as a function of γ and s for the case $a = 0$.

[2] This evaluation differs from that of Milone mainly because he used the Molière lateral distribution function ($s = 1$). The theory of Nishimura and Kamata and the experiments on the lateral distribution of the electrons agree in indicating that the Molière function is too steep, especially at small distances from the shower axis.

discharged. The data indicated $R_p = 2.55 \pm 0.1\%$, $2\frac{1}{2}$ times lower than the first determination. By accepting guidance from the other data in Fig. 26, and assuming that the penetrating particle distribution, $f_M(x)$, is proportional to $x f(x)$, where $f(x)$ is the electron lateral distribution function, one can compute the average distances to the shower axes in the two parts of the experiment. The distances are found to be about 73 and 30 m, approximately in the same ratio as the two values of R_p. The two measurements are plotted at the calculated values of r_m in Fig. 26, and are both found to be consistent with the other data.

Thus, all of the measurements indicate that R_p increases with r. At large distances the relationship is approximately a direct proportion: $R_p \approx 0.06\ (r/r_1)$ at sea level for $0.3 < r/r_1 < 9$; and $R_p \approx 0.04\ (r/r_1)$ at mountain elevations for $0.5 < r/r_1 < 6$. At smaller distances from the axis, especially at mountain elevations, there is an indication that the variation or R_p with r is less rapid, levelling off at $R_p \approx 0.01$ near the axis.

The measurements near the shower axis exhibit considerable variation, particularly at mountain altitudes. This may be due in small part to the differences of the elevations at which the measurements were made. More important factors, however, are the variation of R_p with size of the selected showers and with efficiency of the apparatus for detection of the N component, which constitutes a large fraction of the penetrating particles near the axis.

By integrating over r, one finds that the total number of penetrating particles is about 8% of the number of electrons in the showers at sea level, and about 4% of the number of electrons at mountain elevations. These figures can only be given in first approximation, and apply to rather large showers, $10^6 - 10^8$ electrons.

6. 3 Proportion of penetrating particles vs. size of the showers

At 3260 m elevation, Cocconi *et al.* [1949a] have measured R_p as a function of shower size, selecting the showers with coincidences of unshielded counters having different surface areas. R_p was found to increase with the area of the counters, or to decrease with increasing shower size, according to $R_p \propto S^{0.13}$, suggesting

that the number of penetrating particles is proportional to the 0.87 power of the number of electrons.

Part of the apparent dependence of R_p on shower size is due to a variation of the mean distance of the shower axes from the counters: the exponent γ increases with shower size and the age s decreases, hence the showers selected with small counters have axes slightly nearer to the apparatus than the showers selected with larger counters. Indeed, the smallest area utilized was 9 cm^2. The average size of the showers that discharge three of these counters in a triangle of 6-meter base is computed to be $2.5 \cdot 10^7$ electrons, and the corresponding value of r_m is 32 m. The largest counter area was 1560 cm^2, for which the mean shower size is $2.7 \cdot 10^5$ electrons and the mean distance r_m is 43 m. This variation of r_m, however, can only account for 1/4 of the apparent change of R_p.

MILONE [1952b] has performed a similar experiment at sea level, and obtained analogous results: $R_p \propto \Delta^{-0.11}$. Within the statistical error, the exponent is the same as that found by Cocconi *et al.*

At 3026 m elevation, by measuring the variation of the coincidence rate of shielded counters with their surface area, ISE and FRETTER [1949] have shown that a power law can describe adequately the density spectrum of the penetrating particles, as well as that of the electrons. The value of γ for the penetrating showers was found to be $\gamma_p = 1.65 \pm 0.09$. For electron showers having the same frequency (45 times greater density), the value of γ is 1.54. The difference does not have great statistical significance, but adds a little further evidence that on the average, the density of penetrating particles increases slightly less rapidly with shower size than does the density of electrons.

Qualitative reasons for this observation are easily found. One is the competition between decay and interaction of the parents of the μ-mesons. The higher the primary energy, the larger will be the number of nuclear generations in which interactions will predominate over decays. The nuclear interactions feed energy into the electronic component and prevent the energy going to the μ-mesons. Hence the proportion of the primary energy that is given to the electronic component increases with the energy, while the proportion given to μ-mesons decreases. A second reason is that electrons are absorbed more rapidly than μ-mesons beyond the shower maximum, and in the lower atmosphere small showers are farther beyond their maxima than are larger ones. In showers

of modest primary energy, up to about 10^{13} eV, μ-mesons and their secondaries are practically the only particles remaining at sea level.

6. 4 Relative intensity of the nuclear-active component

The experiments in which the N-component has been distinguished from μ-mesons have mostly provided little or no information about the distance from the shower axis at which the particles were observed, except that the shower selection with unshielded counters emphasizes small distances, $0 < r/r_1 < 0.5$. The information about the efficiency of detection of the N-component as a function of energy is also vague at best; hence the results described below must be considered approximate.

(*a*) *Sea Level*

From the number of multiple discharges in trays of shielded counters, McCusker [1950] has inferred that 2/3 of the penetrating particles in EAS are μ-mesons, while 1/3 consist of charged or neutral N-component. The local showers by which the N-component was recognized were not required to contain more than two particles or to penetrate more than 2.5 cm of lead, but stars and nuclear scatterings without production of a penetrating secondary could not be observed; therefore the recognized N-component represents the number of neutrons and protons having energy greater than several GeV. The selected EAS were restricted to electron densities between about 1 and 50 m^{-2} by the use of an anticoincidence tray; hence the mean shower size was about 10^5 electrons.

In the experiment of Fujioka [1953] on the lateral distribution of the electrons and penetrating particles, the hodoscope records of the penetrating particle detector permitted a rough distinction between μ-mesons and N-component: events with extra counters discharged in at least two counter trays were attributed to nuclear interactions. The proportion of nuclear-active particles among the penetrating component, in showers of $\sim 10^6$ electrons, was thus found to be $0.64\ ^{+0.07}_{-0.14}$ at 5 m from the core selectors, $0.52\ ^{+0.07}_{-0.22}$ at 18 m, and $0.37\ ^{+0.09}_{-0.14}$ at 47 m. The relative density of nuclear-active particles and electrons seemed to be independent of distance from the core selector, while the proportion of μ-mesons was found to increase with the distance.

CHOWDHURI, SAXENA & SUBRAMANIAN [1952] have studied showers of $\Delta \geqq 30$ m^{-2} with a shielded cloud chamber. From the observation of one local shower and 5 scatterings of more than 12° in the lead plates of the chamber, they inferred that about 40% of the singly occurring charged penetrating particles under 6 inches of lead belong to the N-component. The ratio of μ-mesons to electrons was found to be $0.7 \pm 0.2\%$. Low-energy interactions produced by neutral particles were also seen, raising the estimate of the total N-component under the shield to $\sim 90\%$ of the μ-meson intensity. On the basis of a small number of energetic showers entering the chamber from the shield, it was estimated that the highly energetic N-component (both charged and neutral, with $E > 10$ GeV) is about 30% as abundant as μ-mesons.

HODSON [1952, 1953b] has recorded the coincidence rate of a Janossy P-set with an unshielded extension tray both at sea level and at aeroplane elevations (see Fig. 28). By comparing the results with the coincidence rates of unshielded counter trays at the same altitudes, he has inferred that the number of particles capable of being recorded by the P-set, relative to the number of electrons, increases by a factor 6.5 between sea level and 30,000 ft. Hodson has also measured the proportion of penetrating particles, R_p, in the showers at these elevations, with a single shielded counter tray in coincidence with unshielded counters. R_p was found to increase by a factor of only 1.8 ± 0.5. One can calculate an upper limit to the part of R_p that is due to N-component at sea level by assuming that all of R_p at 30,000 ft. is due to nuclear-active particles, and that the P-set is sensitive only to nuclear-active particles at both altitudes. As the assumptions are reasonable ones, the upper limit is probably not far above the correct value. Thus one finds that the charged plus neutral N-component at sea level is less than or equal to $28 \pm 8\%$ of the penetrating component. This estimate is consistent with that of McCusker, but lower than those of Fujioka and of Chowdhuri, Saxena and Subramanian.

V. C. TONGIORGI ([1948a, 1948b, 1949], LEVINGER [1949]) has demonstrated that neutrons of moderate energy (1–20 MeV) are present in the EAS, as well as particles capable of producing such neutrons by local nuclear disintegrations. The neutron producers make rather large stars, often setting off nuclear cascades, in lead and other heavy materials. The average energy seems to be on the

order of one GeV, and it is likely that energetic neutrons comprise a rather large fraction of the incident particles. At sea level and also at altitudes of 3260 and 4300 m, the abundance of the neutron producers near the shower axes has been found to be on the order of two percent of the number of electrons. The number of moderate-energy neutrons present in the air at sea level is on the order of three percent of the number of electrons near the axes of the EAS; but because of the diffusion of the neutrons and the isotropy of their production, their lateral distribution must be much broader than that of the electrons, and the ratio of the total numbers of neutrons and electrons in the showers must be much higher than the measured value, possibly on the order of unity.

(b) *Mountain Elevations*

At elevations between 3000 and 4300 m, observations of the composition of the EAS have been much more numerous than at sea level, and sufficiently varied to give some indication not only of the average division of the penetrating component between μ-mesons and nuclear-active particles, but also about several other questions of interest: the variation of the composition with size of the showers, the variation with distance from the axis, the energy spectrum of the N-component, and the relative number of neutral and charged particles in the N-component. It is not to be implied that the information on these questions is complete: difficulties in the interpretation of the experiments preclude exact definitions of the quantities that have been measured and prevent quantitative accuracy; but the observations nevertheless afford some insight into the nature of EAS.

6. 5 The energy spectrum of the nuclear-active component

In regard to the energy spectrum, it is significant that experiments with widely varying requirements for the recognition of the nuclear-active component have yielded results not differing by orders of magnitude, but reasonably consistent with each other. The lowest determination of the proportion of nuclear-active particles in the penetrating component is about 0.15, a value derived from observations made by Fretter and Ise with an unshielded cloud chamber (Fretter [1949], Ise &Fretter [1949]). Here it must be recognized that some of the nuclear interactions, particularly of the neutral particles, must have been obscured

in the presence of dense electron showers. Furthermore, it has been demonstrated in the absence of air showers that about half of the interactions of particles having $E > 2$ GeV fail to be observed in cloud chambers with $\frac{1}{2}$-inch lead plates, owing to the absorption of the less energetic secondaries in the plates in which they are produced (BROWN & MCKAY [1950], BRANCH &COCCONI [1951], LOVATI *et al.* [1951]). Besides, the showers investigated by Fretter and Ise were of very high mean density (on the order of 200 m^{-2}), in which, according to other measurements that will be mentioned, the comparative abundance of N-particles is smaller than in less dense showers.

The highest determination of the relative number of nuclear-active particles was derived by COCCONI & TONGIORGI [1950] from the observations of the local production of neutrons of moderate energy. These measurements were sensitive to incident particles of low as well as high energy, including neutrons down to ~ 0.1 GeV, which are only capable of producing nuclear evaporations. The abundance near the shower axes was found to be one to two percent of the number of electrons, about equal to the total penetrating component as measured with shielded G-M counters.

Between these extreme determinations fall all the other measurements, made with shielded cloud chambers or with counter hodoscopes. Generally speaking, the total amount of both charged and neutral N-component, capable of producing charged secondaries beneath a thick lead shield, is found to be about 40% of the penetrating component, or roughly 1/200 times the number of electrons. This figure may be considered to represent the relative abundance, near the axes of moderate-sized showers (10^5—10^6 particles), of the nuclear-active particles with energy exceeding about 5 GeV.

The degree of consistency in the measurements of the nuclear-active component suggests that the energy spectrum is not very steep. The same inference emerges from examination of the size distribution of local events in EAS. GREISEN & WALKER [1950, 1953], for instance, have found that penetrating showers which contain large numbers of secondaries or give rise to unusually large bursts of electrons are relatively much more common in EAS than among events not observably associated with EAS. The comparative richness of high energy particles among the N-component in EAS will be further demonstrated below, by showing

that the atmospheric attenuation coefficient is much less than that of the nuclear-active particles not associated with dense air showers.

6.6 Influence of shower size on the composition

The variation of the amount of N-component with size of the EAS has come to light qualitatively in two recent experiments by Sitte and Kasnitz. In one of them Sitte [1952], attempted to select showers of two different mean sizes but equal age by using two different elevations: at 3260 m small unshielded counters were utilized to select showers of a high average density ($\sim 250\ m^{-2}$), while at 4300 m, larger counters were set up to detect showers of a low mean density ($\sim 10\ m^{-2}$). Identical shielded counters in hodoscope connection were used in both places to detect the N-component. In both of the measurements the μ-meson/electron ratio was found to be about 0.75%; but in the large showers at the lower elevation, the N-component was found to constitute $38 \pm 6\%$ of the penetrating particles, while in the small showers at the higher elevation the proportion was $62 \pm 7\%$.

In the second of these experiments (Kasnitz & Sitte [1954]), which was performed entirely at 3260 m elevation, counters of different dimensions and at different locations were connected in coincidence and anticoincidence in such a way as to favor the selection of showers with axes very close to a central station, and to subdivide the recorded showers according to their size. At the central station, a shielded counter hodoscope and a cloud chamber were operated in order to distinguish the penetrating and nuclear-active particles. The two detectors yielded consistent results for the composition of the showers; average values are reproduced in Table III.

The recurring observation that the N-component is relatively more abundant in small showers than in large ones is consistent with the conclusions that have already been drawn from the analysis of the electronic component alone: that the nuclear cascade dominates the propagation of EAS most markedly when they are small or old, and that the N-component ages very slowly in showers beyond their maxima. If the showers are sustained mainly by a continual energy supply from the N-component rather than by the energy contained in the soft component, the relative number of electrons and nuclear-active particles may be expected to reflect the mean energy of the latter (averaged with certain weighting factors over the past history of the showers).

In small showers, the electronic cascades growing out of each nuclear interaction may be expected to be somewhat smaller, in comparison to the number of nuclear-active secondaries that are produced, than in large showers, and hence the number of electrons per nuclear-active particle would be slightly less in small showers than in large ones.

TABLE III

Composition of EAS near the central axes at 3260 m elevation, as measured by KASNITZ & SITTE [1954]

	A showers (small)	B showers (medium)	C showers (large)
Approx. range of size (no. of electrons)	3.10^4— 2.10^5	2.10^5— 10^6	$> 10^6$
Penetrating particles / electrons (%)	1.51 ± 0.12	1.41 ± 0.09	1.17 ± 0.09
μ-mesons / electrons (%)	0.86 ± 0.08	0.85 ± 0.07	0.74 ± 0.07
N-comp. (ch. & neutral) / electrons (%)	0.63 ± 0.08	0.56 ± 0.06	0.43 ± 0.06
N-component / All pen. particles	0.43 ± 0.05	0.40 ± 0.04	0.37 ± 0.05

6. 7 LATERAL DISTRIBUTION OF THE NUCLEAR-ACTIVE COMPONENT

Information about the lateral distribution of the nuclear-active particles, supplementing the sea-level data of Fujioka, has been afforded by the observations of BROWN & MCKAY [1949], COOL & PICCIONI [1951], COCCONI & TONGIORGI [1950], GREISEN & WALKER [1950], and ANISHENKO, ZATSEPIN, ROSENTAL & SARITCHEVA [1952]. While it cannot be claimed that the measurements are very precise, they are remarkably consistent in indicating that the N-component is strongly concentrated near the central axes of the showers. In the range $2 \text{ m} < r < 40 \text{ m}$, the density of nuclear-active particles has been found to diminish with distance from the axis even more rapidly than the electron density—somewhat faster than $1/r$.

In contrast to these results, the total penetrating component has been found to increase in density, relative to the electrons, with distance from the axis. One infers, therefore, that at large distances the penetrating component consists almost entirely of μ-mesons. One may roughly estimate the relative abundance of

μ-mesons as a function of the radius by the straight lines drawn in Figs. 26 and 27. The lines fall below the total intensity of the penetrating component near the axis; the difference may be interpreted tentatively as the intensity of the energetic N-component, which approaches one percent of the number of electrons.

The steepness of the lateral distribution of nuclear-active particles of modest energy requires the existence of an active cascade of extremely energetic N-component, concentrated in a narrow core of the shower, within a couple of meters of the axis. The continual creation of N-particles, feeding outwards from the core, can account for a lateral distribution having the approximate form r^{-1}, without reference to the detailed nature of the nuclear interactions.

The vitality of the nuclear cascade in the shower core implies that at about eight interaction lengths from the top of the atmosphere, the showers are still rich in nuclear-active particles of very high energy. This conclusion is essentially the same as that which was reached previously by examination of the rate of attenuation of the electronic component.

The extremely narrow lateral distribution required of the particles in the core, that are responsible for carrying forwards the energy of the nuclear cascade, reinforces the conclusion drawn from the lateral distribution of the electrons. In neither case can one account for the results with a model of nuclear interactions in which the angular distribution of the secondaries is almost isotropic in the c.m. system. It seems much more likely that the distribution depends strongly on the energies of the secondary particles, and is at least an order of magnitude narrower than an isotropic distribution for the most energetic secondaries.

6. 8 Relative numbers of neutral and charged particles

The ratio of neutral to charged particles in the N-component was found to be 0.7 ± 0.2 in the hodoscope and cloud chamber experiment of Kasnitz and Sitte [1954] at 3260 m elevation. At 4300 m, a hodoscope experiment by Greisen and Walker [1950] yielded a similar ratio, neutral-charged $= 0.7 \pm 0.15$.

The significance of this ratio has been discussed by Greisen & Walker [1953]. The lifetimes of neutral nuclear-active particles other than neutrons are so short that one is forced to identify the neutral component exclusively with neutrons. Since high

energy protons have to be at least as numerous as the neutrons, one must infer that charged π-mesons constitute only $18 \pm 10\%$ of the nuclear-active particles. This must be reconciled with the fact that at a pressure of 600–700 g.cm^{-2}, the probability is rather high that $\pi^{\pm}$-mesons of sufficient energy to generate penetrating showers should escape decay long enough to traverse a mean interaction length.

The reconciliation is difficult unless one assumes that the major part of the available energy, in interactions of particles with $E > 10^{11}$ eV, is retained by nucleons in preference to π-mesons. Yet it is known that $\pi^{\pm}$-mesons are the most numerous charged secondaries (KAPLON & RITSON [1952*b*], KAPLON *et al.* [1954]). One is thus led to the conclusion that the interactions are significantly elastic, in the sense that the incident nucleon is likely to emerge from the collision, not necessarily with the same charge, but with a considerable portion of the initial energy. This could also help to account for the long attenuation length of the nuclear cascade.

6. 9 VARIATION OF THE N-COMPONENT OF THE EAS WITH ALTITUDE

The data described above suggest that the proportion of N-component among the penetrating particles near the shower axis increases from about 30% at sea level to about 40% at 3260 m elevation. Relative to the number of electrons, the N-component appears to *decrease* from about 0.7% at sea level to about 0.5% at the mountain elevations (while the μ-meson component near the axis decreases more strongly, from $\sim$ 1.7% of the electrons at sea level to $\sim$ 0.8% at the mountain elevations). Because of the uncertain efficiencies and variations in the bias introduced by the shower selection, however, it would be safer to infer the altitude variation of the N-component only from measurements taken with identical apparatus at the different elevations.

COOL & PICCIONI [1951, 1953] have measured the N-component/electron ratio with a hodoscope at sea level, at mountain elevations and at aeroplane altitudes. They report that between sea level and 11,000 ft. (700 g.cm^{-2}), the ratio is approximately constant, but that above 11,000 ft. the relative amount of N-component increases with altitude. At 35,000 ft. the penetrating showers associated with EAS were recorded 200 times more frequently than at sea level.

GEORGE & JASON [1950] have measured the coincidence rate of a Janossy P-set with an unshielded extension tray at sea level and 3457 m elevation. The data taken with the P-set covered by 5 to 20 cm of lead are assumed to be due principally to single energetic N-particles striking the P-set, accompanied by electrons striking the extension tray. The increase in the coincidence rate $(P + E)$ with altitude was a factor 9.5 ± 1, as contrasted with a factor 19 ± 1 for the unassociated discharges of the P-set $(P - E)$ and a factor ~ 13.5 for air showers selected by simple coincidences of unshielded counters.

The difference between the altitude effects of the associated and unassociated N-components is even larger than it appears at first glance. The rate $(P - E)$ is directly proportional to the intensity of the unassociated N-component; but the coincidence rate $(P + E)$ varies more rapidly with altitude than the number of particles in the showers, because of the experimental requirement that more than one particle strike the apparatus. According to the analysis of the electron component, the average number of electrons per shower changes by a factor 5.3 between sea level and 3460 m elevation. The data of George and Jason indicate that the relative density in EAS of the particles that can discharge the P-set decreases by a factor $\sim 3/4$; hence these particles increase in number by only a factor ~ 4 between sea level and 680 g.cm^{-2} pressure.

A small correction may be necessary, because some of the $(P + E)$ events at sea level may be due to pairs of independent μ-mesons striking the P-set. However, the data of Chowdhuri and of BROADBENT & JANOSSY [1947] indicate that the majority of the coincidences at sea level are due to single particles incident on the P-set. Therefore the N-component in detectable air showers cannot increase by a factor greater than 6 between the two elevations: i.e., not appreciably faster than the increase of the number of electrons.

FRETTER [1949] has obtained results similar to those of George and Jason by cloud chamber observations of the penetrating showers. Between sea level and 3027 m elevation (728 g.cm^{-2}), the rate of unaccompanied penetrating showers was found to increase by a factor 12 ± 2.4, the rate of electron showers to increase by a factor 10.2 ± 0.4, and the rate of penetrating showers accompanied by observable EAS to increase only by a

factor 7.2 $\pm$ 1.3. In this case no correction such as that discussed above is needed.

HODSON [1952, 1953b] has measured, at aeroplane altitudes and at sea level, the coincidence rate of a Janossy P-set, both accompanied ($P + E$) and not accompanied ($P - E$) by discharges of counters in unshielded extension trays. The data taken with 10 cm of lead above the top tray of the P-set are shown in Fig. 28, together with the data of George and Jason, Fretter, and Piccioni and Cool.

It is interesting that in the lowest third of the atmosphere, where the rate of absorption of the air showers is essentially constant, the number of particles of the N-component increases slightly with increasing depth, relative to the number of electrons. This is consistent with our earlier conclusion that the electron showers are sustained in the lower atmosphere primarily by the energy supplied by the N-component.

An accurate interpretation of the altitude variation of the N-component in EAS must take into account the change of geometry of the showers with elevation. With increasing atmospheric depth the electronic cascades are expected to grow more compressed, while the heavy particle cascade ought to spread outwards. The apparatus employed in these experiments does not indicate the composition of entire showers, but the relative densities in regions selected with a strong experimental bias. Not enough is known at present about the geometry of the electron and N-component cascades at high altitudes to permit an accurate analysis of measurements made under these conditions.

One may note, however, that the nuclear-active particles which are observed to be associated with EAS are absorbed much more slowly in the atmosphere than is the unassociated N-component. The latter is absorbed exponentially with an absorption length of 130 g.cm^{-2}, which implies a factor of about 260 between 30,000 ft. and sea level (after making the Gross transformation), or a factor 15 between 3500 m elevation and sea level. The electrons in large vertical EAS, on the other hand, decrease in number by an average factor $(25)^{1/\gamma} \approx 8.5$ between high aeroplane elevations and sea level or a factor 5.3 between 3500 m and sea level. The N-component in the showers, in view of the changing relative geometry, does not change in abundance much more than the electrons: an upper limit, obtained by ignoring the change of rela-

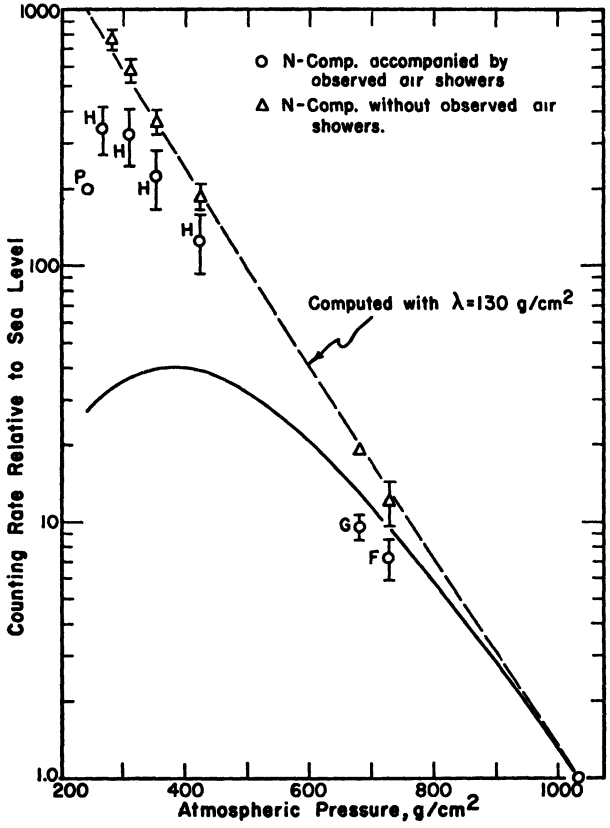

Fig. 28 – Variation with altitude of the counting rates of (a) local penetrating showers not associated with observed air showers, (b) local penetrating showers associated with observed air showers, and (c) air showers, as registered by coincidences of horizontally separated unshielded counters. (The air showers are represented by the lower smooth curve in the figure). H refers to the data of HODSON [1952, 1953b], P to the data of PICCIONI and COOL [1953], G to the data of GEORGE and JASON [1950], and F to the data of FRETTER [1949]. The dashed curve, representing the unassociated N component, was computed by means of a Gross transformation under the assumption of exponential absorption, following the analysis of HODSON [1953b].

tive geometry, would be a factor of about 60 between 30,000 ft. and sea level, or about 5 between 3500 m and sea level. The average absorption length, therefore, probably exceeds 200 g.cm^{-2}.

It may be recalled that in order to account for the plateau in the rate of absorption of the electronic component of EAS in the lower atmosphere, it was necessary to infer that the attenuation

length of the energy retained by the energetic N-component was about $\gamma/0.29$ radiation lengths, or 195 g.cm^{-2}. Since the energy spectrum of the N-particles grows softer with increasing shower age, one must expect that the *number* of nuclear-active particles has an attenuation length greater than 195 g.cm^{-2}, in qualitative agreement with the inference drawn in the present section.

The large value of the average absorption length is related to the high average energy of the N-component in dense air showers—to the existence of a core of extremely energetic particles that are capable of multiplying and thus replacing the lower-energy particles which are lost by nuclear interactions.

6. 10 Range spectrum of the μ-mesons

With a counter hodoscope at 3260 m elevation, Sitte [1950] has measured the range distribution of the non-interacting particles in EAS at an average distance on the order of 30 m from the shower axis. The results are listed in Table IV.

TABLE IV

Range Spectrum of μ-mesons in EAS (Sitte [1950])

Absorber	Relative numbers of non-interacting penetrating particles
280 g/cm^2 Pb	1.0
380	0.92
470	0.83
570	0.72
660	0.65

These measurements (which have standard errors of about 0.05) imply a rather flat energy distribution between 0.35 and 0.8 GeV, with about 40% of the mesons having less than 0.8 GeV of energy.

The absorption measurements of Cocconi, Tongiorgi & Greisen [1949a] indicated a slower rate of attenuation: if all the penetrating particles were μ-mesons, the data would imply that about 25% had energy less than 0.8 GeV.

In both of the above experiments, however, some of the absorption could have been due to nuclear-active particles having insufficient energy to generate penetrating showers. Hence, these measurements may lead one to underestimate the mean energy of the μ-meson component. The experiments on extensive pene-

trating showers far underground do not have this ambiguity, because the thick absorber of earth thoroughly filters out the N-component.

At sea level, the determinations of R_p *vs.* distance from the shower axis have led to the inference that in large showers, about 8% of the particles are penetrating. Most of the penetrating particles are found at big distances from the axis, and can be assumed to be μ-mesons. Thus, in a shower of 10^6 particles there are about $8 \cdot 10^4$ mesons with kinetic energy exceeding 0.3 GeV. If one accepts the experimental indication that the relative number of μ-mesons and electrons is proportional to the distance from the axis, and that the electron distribution in large showers can be described by the Nishimura-Kamata function with an age parameter $s = 1.25$, one may compute that half of the mesons are within 220 m of the shower axis.

At 1574 meters water equivalent underground, BARRETT *et al.* [1952] found that the extensive meson showers were much narrower than at sea level; half of the mesons appeared to fall within 9 m of the axis. The energy required for vertical penetration to this depth is 500–600 GeV. The number-spectrum of the meson showers was determined from the frequencies of single mesons, two-fold meson coincidences and three-fold coincidences, and also from the size distribution of the air showers on the surface of the ground in coincidence with the mesons far underground. All of these observations were consistent with the following differential number spectrum: $F(M) = 2.35 \cdot 10^{-3}\, M^{-3.4}$ (m^2 sec sterad)$^{-1}$ for $1 \leqq M < 1000$, where M is the number of mesons in individual EAS that penetrate 1574 mwe underground.

By equating the integral number spectrum of the meson showers to the number spectrum of EAS at sea level, one finds that M varies with the number of electrons in the EAS at sea level according to

$$M \propto N^{1.5/2.4} \approx N^{0.6},$$

and that in EAS containing 10^6 charged particles at sea level there are about 60 μ-mesons of energy greater than 500–600 GeV.

At an intermediate depth, 60 mwe underground, where the energy limit for μ-meson penetration is 12.5 GeV, GEORGE, MACANUFF & STURGESS [1953] have also observed extensive penetrating showers. The decoherence curve suggests a shower radius of

about 60 m and a differential number spectrum representable by a power law with exponent $\gamma_\mu + 1 = 3.2$. The exponent was not well determined for very small showers, and there is an indication that it may decrease with decreasing shower size; hence one hesitates to normalize the number spectrum at this depth with the vertical intensity of single particles. At both depths underground one may apply a second method of normalization, which is based on the three-fold coincidence rates of shielded detectors at spacings small compared with the spread of the showers.

The rate of such coincidences has been measured at sea level by McCusker & Millar [1951] with the result $T = 0.116 \pm 0.006$ per hour for detectors of area $S = 0.175$ m^2. George *et al.* obtained $T = (1.8 \pm 0.3)\ 10^{-2}$ per hour at 60 mwe, with $S = 0.35$ m^2. Barrett *et al.* found $T = (0.93 \pm 0.24)\ 10^{-3}$ per hour at 1574 mwe with $S = 0.67$ m^2.

The rate T is related to the coefficient of the integral meson number spectrum, K_M, by

$$T \propto \gamma_\mu I_\mu K_M R_0^2 (S/R_0^2)^{\gamma_\mu},$$

where $I = (-\gamma - 1)!\ (-3 + 3 \cdot 2^\gamma - 3^\gamma)$, and R_0 is the characteristic radius of the showers. At sea level, $\gamma_\mu = 1.65$ as measured by Ise & Fretter [1949] or inferred from the electron density spectrum and the ratio of penetrating particles to electrons, measured by Cocconi *et al.* [1949a]; we further assume $R_0 = 220$ m as discussed above. At 60 mwe, $\gamma_\mu = 2.2$ and $R_0 = 60$ m; while at 1574 mwe $\gamma_\mu = 2.4$ and $R_0 = 9$ m. With these constants one may compute that a shower containing $8 \cdot 10^4$ mesons at sea level (i.e., a shower of about 10^6 electrons) would still contain 4300 mesons at 60 mwe and 65 mesons at 1574 mwe.

It is gratifying that the second method of normalization leads to essentially the same number of mesons at 1574 mwe (in showers of 10^6 electrons at sea level) as was obtained by the first method, employed on the previous page. Although a fortuitous cancellation of errors may have occurred, the agreement strengthens the confidence that may be placed in the values of the quantities entering into the analysis.

Within the accuracy of the computation, the proportion of the mesons that penetrate to 60 mwe in large EAS is found to be equal to the proportion of all mesons at sea level that penetrate to 60 mwe; about 8%. But the proportion of mesons in EAS

(of $\sim 10^6$ electrons) that penetrate to 1574 mwe is a factor 20 greater than the proportion of all mesons at sea level that penetrate so far underground.

The few points that have been determined fit an integral energy spectrum of the form $(E + 1.5)^{-1.25}$, with E measured in GeV. This spectrum also agrees within experimental errors with the absorption measurements of Sitte and Cocconi: i.e., it predicts that 26.5% of the mesons with $E > 0.3$ GeV have energy less than 0.8 GeV. Nevertheless, the average energy is rather high: averaged over the mesons with $E > 0.3$ GeV it is 7.5 GeV. If one computes with this spectrum the total energy of the mesons in the showers containing $N \approx 10^6$ electrons at sea level, the result is $\sim 0.6\,N$ GeV, about equal to the energy of the electronic component.

It follows from the increase of the exponent in the number spectrum, γ_μ, with depth underground that the energy spectrum of the μ-mesons is less steep (and thus the average energy is higher) in comparatively small EAS than in large ones. Similarly, the excess of γ_μ over the exponent in the electron number spectrum implies that there are relatively more μ-mesons, compared with the electrons, in small showers than in large ones.

These observations have a straightforward qualitative interpretation. The higher the primary energy of an EAS, the greater is the probability that charged π-mesons created in the first few generations of the nuclear cascade will not decay into μ-mesons, but rather suffer nuclear interactions in the high atmosphere. These interactions transfer to the electronic component energy which might otherwise be given to μ-mesons. Besides, if decay is avoided in the first few interaction lengths, it must occur in a denser part of the atmosphere, where decay becomes increasingly improbable for π-mesons of high energy.

Therefore, μ-mesons of high energy are produced most efficiently by the primary cosmic rays having not much more than the minimum energy that is required. With increasing primary energy beyond this minimum value, the electron component is generated more efficiently and the high energy μ-mesons less efficiently. Thus it occurs that showers of about 500 electrons at sea level contain on the average one μ-meson with energy exceeding 500–600 GeV, while showers of 10^6 electrons contain not 2000 of these mesons, but only about 60.

At low meson energies the competition between decay and nuclear interaction of the π-mesons is less important: practically all of the low energy π-mesons decay before suffering nuclear interaction. Thus it occurs that at sea level the relation between the numbers of mesons and electrons is $M \propto N^{1.5/1.65} \approx N^{0.9}$, whereas at 60 mwe $M \propto N^{1.5/2.2} \approx N^{0.7}$ and at 1574 mwe $M \propto N^{0.6}$.

Although the explanation of this phenomenon is already qualitatively satisfying, the quantitative variation of γ_μ or of M/N with depth far underground depends on the details of the nuclear cascade in the early stages of the EAS—on the nature, the energy spectra and the relative abundance of the various particles produced in very energetic interactions. Hence it is hopeful that in the future, more detailed calculations and experiments along these lines may succeed in revealing some of the features of the high energy interactions.

6.11 Calculations of the nuclear cascade

It is not within the scope of the present review to analyze the calculations of the nuclear cascade in sufficient detail to do justice to the treatments that have been published; but it would be a serious omission not to mention, at least, the papers on this subject by Rosental [1952], Budini & Molière [1953], Messel & Potts [1953, 1954], and Amaldi, Mezzetti & Stoppini [1953].

Any comparison of the calculations with experiments should take into account the consequences of the simplifications adopted in the calculations, the special conditions associated with the experimental measurements—that is, the bias introduced by the methods of shower selection and particle recognition; and above all, the many points in which the calculations can be varied without altering the basic concepts. The task is therefore formidable, and will perhaps be more profitable at a later time, when the theories have been further refined and more precise experimental information is available.

7. Time Variations of the EAS

The average frequency of the EAS varies with time because of changes in atmospheric conditions and probably, in addition, because of asymmetry in the directional distribution of high

energy primary cosmic rays outside the earth. The various conceivable physical causes of such an asymmetry may be expected to produce characteristically different effects. The presence or absence of such effects in the experimental observations may thus reveal information about the origin and acccleration of cosmic rays, and about the nature of the space through which they have travelled before reaching the earth.

For instance, if interstellar spaces were field-free, the cosmic rays would travel in straight lines. The non-uniform distribution of the likely stellar sources would therefore cause a strong anisotropy like that found in starlight or radio noise. The fine structure might be unresolvable, but the smoothed directional intensity would be expected to have a few prominent minima and maxima depending on the stellar density in a small cone centered about the direction of observation.

7.1 Galactic magnetic fields

There are two overpowering arguments against the above hypothesis. One is the energy density of the cosmic rays, which is about equal to that of starlight, and is apparently unexplainable without the aid of a storage mechanism. The other is the extreme isotropy of the primary cosmic rays. The amplitude of the variation of intensity with sidereal time is no more than a few hundredths of one percent for the average primary cosmic rays (Elliot [1952]), nor greater than about one percent, as will be shown below, even for primaries of energy $\sim 10^{15}$ eV.

Biermann [1953a, 1953b] and others have discussed reasons and evidence for the existence of magnetic fields in interstellar space, concluding that fields on the order of 10^{-6} to 10^{-5} gauss would have arisen out of the turbulent motions of ionized gases in the galaxy, even if there had been no field in the beginning. The magnetic fields provide a convenient means of storing cosmic-ray energy in the galaxy, and of randomizing the directional intensity.

In the initial version of Fermi's theory [1949] of the acceleration of cosmic rays and in the extension of the theory by Morrison, Olbert & Rossi [1954], the fields were considered to be oriented at random, stirred up and carried about by the turbulent motion of clouds of ionized gas. In order to account for the charge spectrum of the primaries, the cosmic rays had to be allowed to

leak out of the galaxy in an average time of about 10^6 years. Then to account for the energy spectrum and the nearly perfect isotropy of the cosmic rays, the clouds had to be assumed to have both a high rms velocity ($\sim$ 120 km.sec^{-1}) and a small size (mean separation $\sim$ one light year).

In this theory the residual anisotropy is due to the leakage of the cosmic rays out of the sides of the galactic disc. As long as the mean scattering length is independent of the cosmic-ray energy, the anisotropy remains very small and likewise independent of the energy. At energies so high that the particles can penetrate through the magnetic clouds, the isotropy must cease, but for the same reason the acceleration mechanism must fail and the escape probability must become large, implying a cutoff of the intensity. No appreciable anisotropy is therefore expected to be observable.

Against some features of this theory, too, there are strong arguments. One is the evidence, derived from the EAS, of the existence of primaries having energy up to and exceeding 10^{17} eV, with no sign of a rapidly approaching cutoff. The path of a proton of 10^{17} eV, normal to a magnetic field of 10^{-5} gauss, would have a radius of curvature of 35 light years. Randomly oriented clouds about one light year apart would give rise to an average scattering length of about $(35)^2 \approx 10^3$ light years for such particles, about equal to the distance from the center to the edge of the galactic disc. Therefore the particles would escape quite freely; indeed, the "cutoff energy", at which the spectrum would become very steep, would be near 10^{15} eV per nucleon. Another objection to the theory is the high velocity required of the magnetic clouds, which is hard to reconcile with direct observations. Furthermore, the uniformity of the plane of polarization of starlight suggests that the fields are not random, but coherently orientated, apparently along the arms of the galaxy (Davis [1951], Davis & Greenstein [1951], Hiltner [1951], Stranahan [1954]).

If the turbulent elements of the magnetic fields are dominated by a coherent field having an extension as wide as the galactic arms, there is no difficulty in accounting for the retention within the galaxy of cosmic rays with energy up to about 10^{18} eV.

7. 2 Origin of directional asymmetry

The concept of the superposition of magneto-hydrodynamic waves on a nearly uniform field directed along the galactic arms

has been explored by CHANDRASEKHAR & FERMI [1953]; and FERMI [1954] has pointed out how such a model can result in a more efficient acceleration of the cosmic rays than that produced by purely random turbulent motion. DAVIS [1954] has subsequently described the physical causes of directional asymmetry that may be operative in such a model. His arguments are summarized below.

The cosmic rays are pictured as spiraling along the lines of force in the magnetic field, frequently reversing the component of motion along the field by colliding with a shock front where the field intensity changes rapidly. The orbits drift laterally because of field gradients, and suffer more rapid alteration by interaction with turbulent elements of the field. Very high energies are attained over a long period of time, by a statistical accumulation of small accelerations owing to betatron action and to reflections from the moving shock fronts. In consequence, the direction of arrival of a high energy cosmic ray at the earth has no relation to the direction from its original source; any asymmetry that may be observed is not expected to be related to the spatial distribution of the sources in the galaxy, but rather to the properties of the magnetic field and the process of acceleration.

One of the causes of asymmetry is a net diffusion of the cosmic rays along the field lines towards the nearest point of escape from the galaxy (either the end of an arm or a local bulge where the field is weak). This effect should produce a maximum intensity in one direction, approximately along the arm of the galaxy, and a minimum in the reverse direction. The rotation of the earth would consequently produce a 24-hour periodic intensity variation in sidereal time. Davis has estimated the time of the maximum to be 20h L.S.T.

A second effect is that of density gradients, most easily illustrated by the diagram in Fig. 29, which has been copied from Davis' article. The asymmetry is proportional to the gradient of the cosmic-ray density normal to the magnetic field, and to the radius of curvature of the trajectories. Thus it is an effect that increases strongly with the primary energy. Like the asymmetry due to diffusion, it gives rise to a 24-hour period in the observed intensity, but with a different phase, since the maximum and minimum in the cosmic-ray flux are perpendicular to the magnetic field. Davis has tentatively estimated the time of the maximum to be either 0 or 12h L.S.T.

Further asymmetry may be due to the mechanism of acceleration, and will be significant if the acceleration of cosmic rays by interaction with the magnetic fields is responsible for an important part of the cosmic-ray energy. The pitch of the helix followed by a particle affects the likelihood of acceleration, and is changed in the course of magnetic collisions by addition of momenta parallel or antiparallel to the field. The net effect depends on whether the most important acceleration is by a type of betatron action or by collisions with moving inhomogeneities of the field: in one case, the intensity will be greatest in the plane normal to the field, while in the other case it may be greatest parallel and antiparallel to the field; but in either event a 12-hour periodic variation should arise in addition to a 24-hour period. Davis has shown that the asymmetry arising from the acceleration process should differ from the other types of asymmetry not only in the existence of the second harmonic, but also in that the first harmonic should have its maximum 12 hours later for observations in the Southern hemisphere than for observations in the Northern hemisphere.

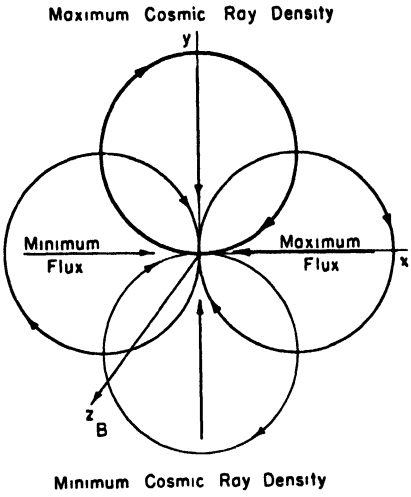

Fig. 29 – Illustration of the origin of a directional asymmetry of high energy cosmic rays, owing to the existence of a magnetic field normal to the plane of the diagram and a gradient of the cosmic ray density in the plane of the diagram (taken from reference DAVIS [1954]).

The expected amplitudes of these effects have not yet been calculated, and even the estimates of phase are somewhat tentative. But one might hope to learn from experiments whether or not the qualitative descriptions of the asymmetry fit the facts and which of the causes of asymmetry is predominant. Unfortunately, the experimental data are not yet sufficiently precise or in sufficiently good agreement to permit such an accomplishment. One can at best gain from the existing experiments some guidance for further, more definitive measurements.

7. 3 Experimental observations on sidereal variations

The available data on the periodic variation of the intensity of high energy primary cosmic rays in sidereal time are summarized in Table V. The energy estimates are based on a rough evaluation of the most probable shower size contributing to the recorded events, and an estimate of the corresponding primary energy by a track length integral over the atmosphere. Although these energies are reliable in order of magnitude, they are not intended to be interpreted as precise.

The phases and amplitudes listed in the table are not entirely consistent with each other. Some of the differences in the amplitudes may possibly be explainable by the differences in the latitudes of the experiments and in the average primary energies of the selected showers, but not all of the discrepancies can be so accounted for; and these considerations do not help to explain how Cranshaw and Galbraith find a maximum at 10h L.S.T. in the Northern hemisphere, while Daudin, Hodson, and Fornaca and Martelli find the maximum to occur about 12 hours later.

The only point of complete agreement is that up to a primary energy of about 10^{16} eV, the sidereal asymmetry, if real at all, is extremely small—not more than about two percent of the average intensity. This in itself is a highly significant conclusion, but it raises great difficulties for the determination of the phase and amplitude of the variation.

7. 4 Significance of Sidereal Variations

The data suggest that the amplitude increases with the primary energy, but it is remarkable how the statistical errors keep pace with the apparent amplitude, so that the latter is never more than four times the standard error.

In searching for a sidereal time effect, it is easy to be misled by chance combinations of statistical fluctuations resembling a systematic intensity variation. In examining even normal data, one always finds that the particular set of deviations can be made to appear more probable by the inference of a systematic trend. The usual method of analysis for the amplitude of a small periodic variation leads to a standard error about equal to $\sqrt{2/N}$, where N is the total number of events included in the analysis; but with data exhibiting only normal random fluctuations, the expectancy

of the most probable amplitude that will appear in such an analysis is $2/\sqrt{N}$, 1.4 times the standard error. Only when the effect is many times the standard error can the latter be assigned its usual significance in terms of confidence limits; and if the indicated amplitude is less than three times the standard error, the data do not constitute impressive evidence for the reality of the periodic variation.

If one has recorded several sets of data, say with counters in different geometries, or if numerous experiments are performed by different persons, the likelihood is increased that at least one of the sets of data will exhibit an improbable fluctuation.

From this point of view, one must admit, in agreement with most of the authors of the work quoted in Table V, that although the measurements are suggestive, they do not as yet establish conclusively the existence of any sidereal time effect, and that even if a real effect is present, the apparent phases and the apparent variation of the effect with energy could be misleading.

7. 5 Solar and atmospheric effects

The experimental difficulty in ascertaining the time variations is not due entirely to the limitations of statistical accuracy, although the importance of this obstacle is not to be minimized. In addition, the frequency of registration of even the largest of the air showers is sensitive to changes of the atmospheric temperature and pressure. These variations are partly erratic, but the influence of the sun on the atmosphere gives rise to certain periodicities. There is a solar diurnal temperature variation, and both a diurnal and a semidiurnal pressure wave; an annual temperature cycle, and also a pronounced annual variation of the diurnal amplitudes. The seasonal modulation of the diurnal waves gives rise to a Fourier component that has one more cycle per year than the solar variation; hence spurious daily intensity variations are present in sidereal time as well as solar time.

Measurements of the barometric coefficient, which is about 10%/cm Hg, have been listed in a previous section. These measurements have exhibited unexplained differences outside the statistical errors, indicating that the effect is complex and precluding perfectly accurate corrections for the influence of observed pressure variations (Citron [1952], Daudin & Daudin [1953].)

The perturbations of the barometric effect are probably associ-

TABLE V

Experiments on the Variation of Intensity with Sidereal Time[a,b]

Reference	Location and Geog. Latitude	Elevation (m)	Approx. Counting Rate (h^{-1})	Approx. No of Counts Registered	Approx. Primary Energy (eV)	First harmonic Amplitude %	First harmonic T_{max} (L.S.T.)	Second harmonic[e] Amplitude (%)	Second harmonic[e] T_{max} (L.S.T.)
Sherman [1953]	Michigan 42°N	Underground 846 mwe	108	$7 \cdot 10^5$	10^{13}	0.2 ± 0.2	—	—	—
Barrett *et al.* [1954]	Ithaca, N.Y. 43°N	Underground 1574 mwe	30	$2.5 \cdot 10^5$	$4 \cdot 10^{13}$	0.1 ± 0.3	16.5 h	—	—
Daudin & Daudin [1953]	Pic du Midi 43°N	2860	1520	$26 \cdot 10^6$	$3 \cdot 10^{14}$	0.05 ± 0.03[c]	20.7 ± 1.1	0.07 ± 0.03[c]	5.5 ± 0.8
			355	$7 \cdot 10^6$	$6 \cdot 10^{14}$	0.15 ± 0.07[c]	19.8 ± 1.9	0.05 ± 0.06[c]	5.8 ± 2.3
			175	$4 \cdot 10^6$	$2 \cdot 10^{15}$	0.23 ± 0.10[c]	22.2 ± 2.0	0.12 ± 0.09[c]	7.0 ± 1.4
			65	$1 \cdot 10^6$	$4 \cdot 10^{15}$	0.18 ± 0.19[c]	22.3 ± 4.0	0.18 ± 0.19[c]	8.2 ± 2.0
Citron [1952]	Schauinsland 48°N	1230	104	$2 \cdot 10^5$	10^{15}	$\sim 0 \pm 0.3$	—	—	—
Farley & Storey [1954]	Auckland 37°S	40	50	$3 \cdot 10^5$	10^{15}	1.10 ± 0.26 / 1.43 ± 0.38[d]	19.8 ± 0.9 / 17.6 ± 1.0	0.41 ± 0.26	2.0 ± 1.2
			18	$1 \cdot 10^5$	$1.4 \cdot 10^{15}$	0.52 ± 0.41	19.7 ± 3.0	—	—
			8	$5 \cdot 10^4$	$2 \cdot 10^{15}$	0.52 ± 0.61	20.7 ± 4.5	—	—
Hodson [1951]	Manchester 53°N	Sea Level	11	$6 \cdot 10^1$	$4 \cdot 10^{15}$	1.15 ± 0.6	23.5 ± 2.0	—	—
Fornaca & Martelli [1953]	Pisa 44°N	Sea Level	1.14	1460	10^{16}	4 ± 4	14	—	—
			0.67	850	$1.5 \cdot 10^{16}$	7 ± 5	12	—	—
			0.38	485	$2 \cdot 10^{16}$	13 ± 7	20.5	—	—
			0.20	260	$3 \cdot 10^{16}$	41 ± 10	21.4	—	—
			0.096	124	$5 \cdot 10^{16}$	50 ± 14	21.6	—	—
Cranshaw & Galbraith [1954]	Harwell 52°N	Sea Level	10	$7 \cdot 10^4$	10^{16}	0.63 ± 0.5	13.3 ± 3.2	1.1 ± 0.5	3.9 ± 0.9
			3.2	$2 \cdot 10^4$	$2 \cdot 10^{16}$	2.05 ± 1.0	9.5 ± 1.8	3.0 ± 1.0	3.7 ± 0.6
			1.3	$8 \cdot 10^3$	$5 \cdot 10^{16}$	4.9 ± 1.5	10.5 ± 1.2	3.5 ± 1.6	4.5 ± 0.9
			0.2	$1.2 \cdot 10^3$	10^{17}	10.1 ± 4.1	4.0 ± 1.6	2.8 ± 4.2	2.9 ± 5.1
Elliot [1953]	Manchester 53°N	Sea Level	—	3000	$2 \cdot 10^{16}$	$\sim 0 \pm 3$	—	—	—
			—	700	10^{17}	$\sim 0 \pm 6$	—	—	—

[a] The errors given are purely statistical standard errors, calculated (as far as could be inferred) in classical fashion; but the probability-of-error distribution does *not* resemble a gaussian error curve unless the probable amplitude is an order of magnitude greater than the standard error, which is not true of any results in this table.

[b] In the experiments of Farley and Storey, Cranshaw and Galbraith, and Fornaca and Martelli, the results listed in successive rows, representing progressively higher energies, are not completely independent, since the low energy shower selection includes the high energy events. This is also partially true in the measurements of Daudin.

[c] Corrected for the residual pressure wave in sidereal time.

[d] Corrected for the inferred sidereal wave owing to the seasonal modulation of the solar wave (due to pressure and temperature effects). The other results of Farley and Storey have not been so corrected.

[e] The absence of an entry in the second harmonic column does not imply that no second harmonic appeared to be present, but only that its probable amplitude and phase were not computed.

ated with the distribution in height of the various atmospheric pressure levels, or to the related temperature distribution. The *semi*-diurnal pressure wave, however, may be expected to be comparatively independent of atmospheric temperature changes. DAUDIN & DAUDIN [1953] have observed a small semi-diurnal variation of the frequency of EAS, agreeing perfectly in phase ($T_{max} = 4.7$h) and in amplitude ($0.21 \pm 0.03\%$) with the observed pressure wave and the coefficient 10%/cm.

The influence of the temperature is believed to be felt only through the change of shower geometry with density of the air. If the lateral distribution is in equilibrium with the atmospheric density ϱ, the counting rates are expected to vary as $\varrho^{(2\gamma-2-\alpha)}$, where γ is the exponent in the density spectrum ($\varrho^{-\alpha}$ expresses the effect of the change of the counter separation relative to the scattering length r_1, $\varrho^{2\gamma}$ the change of counter surface relative to r_1^2, and ϱ^{-2} the change of the area within which the showers can be detected). The temperature coefficient is therefore expected to equal $-(2\gamma - 2 - \alpha)/T$, where T is the absolute temperature. Because of the lack of perfect equilibrium of the lateral distribution with the local temperature, the fluctuations should correspond to a weighted average of the temperature in the atmosphere above the detector, with greatest weight at distances of one to five radiation lengths.

DAUDIN & DAUDIN [1953] point out that one must expect the temperature effect to depend on the size of the showers and the separation of the counters; but to estimate a representative magnitude, one may use $\gamma = 1.4 - 1.45$, $\alpha = 0.1 - 0.2$ and $T = 280$, which yield a temperature coefficient of about $-0.25\%/°C$. This can account for a seasonal wave with amplitude of the order of 3% of the average intensity, superimposed on a diurnal variation with amplitude on the order of one percent, both amplitudes being sensitive to the geographic location.

By measurement of the seasonal intensity variation of the EAS at sea level, HODSON [1951] has found the temperature coefficient to be -0.38 ± 0.11 %/°C. During these measurements (at Manchester), the diurnal temperature variation was very small, the amplitude being 0.7°C. Thus a solar diurnal intensity variation of about 0.2% was expected. A Fourier analysis yielded the amplitude 0.3 ± 0.6 %, which is not significant statistically but is at least consistent with the expected value.

At the Pic du Midi, DAUDIN & DAUDIN [1953] observed a correlation between local temperature and the counting rate of EAS, corresponding to coefficients of -0.10 ± 0.02 and $-0.17 \pm 0.03\%/°C$ for data recorded in different periods of time with the same apparatus (two-fold coincidences between counter trays of 2400 cm^2 area 5 m apart, recorded in winter and summer respectively). Somewhat better correlations were found in the winter period by using the temperature of the 300 mb level instead of the local temperature (although the correlation was poor with levels above 200 mb); the coefficient with respect to the 300 mb level was reported to be -0.135 ± 0.015 %/°C.

At sea level in Auckland, New Zealand, by analysis of data taken over a period of one year, FARLEY & STOREY [1954] obtained an average solar diurnal variation of EAS having an amplitude of $1.45 \pm 0.25\%$ of the average intensity, with the maximum at 2.7 ± 0.6 hours local solar time. The phase agreed with the interpretation of the variation as a temperature effect, while the amplitude corresponded to an apparent temperature coefficient of $-0.51 \pm 0.09\%/°C$.

KRAYBILL [1949] has observed a small latitude effect of EAS, which is consistent in sign and magnitude with an explanation based on the variation of temperature with latitude.

All of these experiments confirm at least qualitatively the predicted variation of shower counting rate with atmospheric temperature; and no reported experiment gives any significant indication of a solar diurnal intensity variation other than that which is due to changes of temperature and pressure.

The absence of a solar diurnal effect in the primary intensity at energies of 10^{13} to 10^{16} eV provides convincing evidence that the sun is not the only source of the cosmic rays that reach the earth; indeed, that it is at most a very minor source as far as the most energetic particles are concerned.

7.6 COMPARATIVE VIRTUES OF VARIOUS EXPERIMENTAL ARRANGEMENTS

It is apparent from the extremely precise measurements of Jean and Alice Daudin that, at least in the Northern hemisphere, the asymmetry at energies below 10^{15} eV is so small that it will always be difficult to separate it from atmospheric effects.

By detecting showers of mesons at great depths underground,

one can select events of primary energy 10^{15} eV or higher (BARRETT *et al.* [1952]), and the observed time variations would be comparatively free of perturbation by atmospheric pressure changes. But the difficulty of obtaining sufficient statistical accuracy in such measurements appears to be insurmountable; and besides, the meson showers are subject to an atmospheric temperature effect that is just as large as that of the air showers.

The data in Table V suggest, however, that at energies above 10^{16} eV, and especially above 10^{17} eV, the sidereal time effect may be large enough that the atmospheric perturbations of the EAS would be comparatively insignificant. Future experiments should therefore be designed to select the largest possible showers. A second purpose of the experiments might be to search for signs of a high energy cutoff of the cosmic-ray energy spectrum.

In general, two methods have been used to select showers of high average primary energy: one is to require a high density at a particular location, and the other is to require sufficient density at large distances from the shower axis to cause the discharge of widely separated counters. The latter method can be shown to have several important advantages, particularly if each of the widely separated counting units requires several particles in coincidence, so as to define a low but finite and fairly sharp density requirement.

In the first place, the energy discrimination is better. Large densities at one location can be created by small showers with axes close by (often showers of very little energy, initiated low in the atmosphere) as well as by big showers, although the latter can be detected over a comparatively large area. In consequence, the primary energy spectrum of the recorded events is very broad (see Fig. 17), and there is no sharp low energy cutoff of the sensitivity. On the other hand, when small but finite particle densities are required over a large area, there is a sharp cutoff of the sensitivity as a function of shower size, and also there is less bias in favor of young showers, initiated low in the atmosphere, over those initiated in the stratosphere.

Secondly, the computation of the primary energy is less dependent on the assumed age and lateral distribution of the showers.

Thirdly, and most importantly, for a given average shower size the counting rate is much higher. The average distance to the

axes of showers detected with closely spaced counters is about 20 m, hence the sensitive area, within which the axes of recorded showers may fall, is of the order of 1000 m^2; but the sensitive area of a widely spaced set is on the order of the square of the radius of the array. Without excessive difficulty, this area can be as large as 100,000 m^2.

Finally, if widely spaced counters are used, it is feasible to measure the differences in the times of the signals. By this means the directional resolution can be improved.

If the EAS were purely electronic cascades, there would be no advantage in seeking high-elevation locations for the detection of very large showers ($E > 10^{17}$ eV). But the available information on the variation of the exponent of the density spectrum with elevation, on the barometric effect of small and large showers, on the altitude effect and on the zenith angle distribution of small and large showers has all indicated that big showers reach their maxima higher in the atmosphere than would pure electronic cascades, and are absorbed in the lower atmosphere much like the small showers. Therefore more efficiency in detecting the high energy events—and hence higher counting rates—can be obtained if the measurements are performed at mountain elevations.

The present information on the time variations of the EAS seems to point to the desirability of organizing a cooperative venture along the lines suggested above, to measure simultaneously, at several different latitudes, the time variations and the frequency of primaries in the energy range 10^{17}—10^{18} eV.

8. The Primary Energy Spectrum

In a previous section, the number spectrum of the showers has been derived from experiments, both at sea level and at a mountain altitude. If the average primary energy of EAS having a given number of charged particles at a particular depth in the atmosphere could be calculated, the number spectra would lead directly to the energy spectrum of the cosmic-ray primaries. But since the EAS do not develop and propagate like purely electronic cascade showers, and since the detailed features of the nuclear cascade are still largely unknown, one cannot with reliability calculate the relation theoretically.

8. 1 The track-length integral

A semi-experimental solution of the problem can be carried out in a manner that has already been suggested in a previous section, utilizing the altitude variation of the shower counting rates and the concept of track lengths. Fig. 24 summarizes the analysis of the altitude variation of the frequency, R_v, of vertical showers containing a given number, N, of charged particles. It has been pointed out that the quantity $\partial \ln R_v/\partial t$, corrected for changes of shower geometry, is equal to $\gamma'\lambda$, where γ' is the exponent in the number spectrum and λ is the average value of $\partial \ln N/\partial t$ for the showers selected by the apparatus. In following the development of showers having a given primary energy, one should in principle utilize values of $\partial \ln R_v/\partial t$ determined for showers of appropriately different size at the different elevations; but the derivative has been shown to be insensitive to the shower size. Therefore by dividing the dashed curve in Fig. 24 with appropriate values of γ' and integrating, one can obtain the average variation of N with atmospheric depth. The track length integral, $\varepsilon_0 \int N dt$, then yields the total energy dissipated in ionization by the charged shower particles. (ε_0 is the critical energy and t is measured in radiation lengths; it is assumed that ε_0 represents accurately the average energy dissipation per radiation length for all the charged particles).

At depths below sea level, R_v can be extrapolated with a constant attenuation length, and thus the ionization energy dissipated in the crust of the earth can be taken into account. This is a very small addition to the energy loss in the atmosphere; hence it is not worth while to debate the accuracy of the extrapolation.

The integrated energy thus obtained includes not only the electron and photon energies, but also most of the energy of the nuclear-active component, since the latter energy is dissipated mainly by the ionization loss of electrons and other charged particles created as a result of the nuclear interactions. Some parts of the primary energy, however, escape inclusion in the above analysis. One part is the energy of the μ-mesons. These particles are distributed so widely that they do not contribute much to the shower counting rates; and their energy is dissipated mainly by ionization deep in the crust of the earth. The relative

number of mesons and electrons in the showers at sea level has been found to be 0.08, and the average meson energy has been estimated from the range spectrum to be 7.5 GeV; thus the total energy of the mesons is about 0.6 GeV per electron at sea level. A correction for the decay of μ-mesons in the atmosphere raises the estimate a little, making it closer to one GeV per electron.

Other parts of the primary energy that escape inclusion in the track length integral are the energy of neutrinos produced in π-μ-decay (about 0.27 of the μ-meson energy), and the energy lost in nuclear excitation and the release of low energy neutrons, heavily ionizing protons, and alpha particles. If the nuclear-active component of all energies, averaged over the shower, is about 3 percent of the number of electrons, if the average disintegration energy is about 200 MeV, and if the mean free path is about two radiation lengths, the energy dissipated in the nuclear disintegrations is about 4 percent of the ionization loss of the electrons.

The major term in the energy accounting is the ionization integral over the atmosphere. The graph of N *vs.* altitude rises from $N = N_1$ at sea level to a broad maximum of about $8.5\,N_1$ in the neighbourhood of 450 g.cm^{-2}, and then falls with increasing rapidity as one approaches the top of the atmosphere. The integral $\varepsilon_0 \int N\,dt$ over the atmosphere yields 11.5 GeV per electron at sea level, with an uncertainty of the order of 25 percent because of possible errors in the data and their interpretation at high altitudes. The integral below sea level yields 0.4—0.5 GeV per electron at sea level. With the addition of 1 GeV per electron for the μ-mesons, 0.3 GeV per electron for neutrinos, and 0.5 Gev per electron for nuclear excitation and low energy nucleons, one obtains a total primary energy of 14 ± 3 GeV per electron in the showers at sea level.

Although the average rate of absorption of the EAS in the lower half of the atmosphere does not depend strongly on the shower size, the energy integral cannot be strictly proportional to N_1; hence one must enquire to what size the above data and calculations refer.

The altitude variation was based on measurements of the frequency of showers with density exceeding $\Delta_1 \approx 50$ m^{-2}. According to the discussion in the section on the density and number

spectra, the major contribution to the measurements at sea level is due to showers having N in the neighborhood of $1.7\, r_1^2\, \Delta_1 \approx 5 \cdot 10^5$. With increasing altitude, the increase of r_1 tends to make the average value of N larger, but this tendency competes with a decrease in the ratio $N/(r_1^2 \Delta_1)$, owing to a reduction of the shower age s and an increase of the exponent γ (see Fig. 18). In the part of the atmosphere contributing most heavily to the track length integral, where the showers are about 8 times bigger (in number of particles) than at sea level, the average size of the recorded showers is found to be a little less than 10^6 particles. Therefore the showers best described by the energy accounting are those that contain 10^5 particles at sea level.

The frequency of vertical showers of this size is obtainable from the section on the number spectra: $K_v(10^5) = (1.7 \pm 0.3)$ 10^{-6} m^{-2} sec^{-1} sterad^{-1}. This, therefore, is the frequency of cosmic ray primaries with total energy exceeding (1.4 ± 0.3) 10^{15} eV.

8. 2 Exponent of the primary energy spectrum

It remains to calculate how the frequency of the primaries varies with changing primary energy. In a qualitative way, it is known that larger showers have their maxima lower in the atmosphere than do smaller showers, and that larger ones dissipate less of their energy in the production of μ-mesons. For both reasons, with increasing shower size the energy accounting must yield gradually less primary energy per electron at sea level. Therefore, the primary energy spectrum will be found to be steeper than the number spectrum of the showers.

For EAS of moderate density (10 to 100 m^{-2}), the very slow variation of γ with elevation indicates that $\partial \ln R_v/\partial t$ is nearly independent of shower size. In the lower part of the atmosphere, this derivative can be approximated by a constant, —0.28 per radiation length. The functional dependence of the track length integral can therefore be represented by the approximate relation

$$E_s = \varepsilon_0 N_{SL} \int_{t_{max}}^{\infty} \exp\left[\frac{0.28}{\gamma}(t_{SL} - t)\right] dt,$$

where E_s is the total energy of the soft component, t_{max} is the atmospheric depth of the shower maximum, and the subscript

SL refers to the sea level values of N and t. The variation of the primary energy, E_0, with N_{SL} can be expressed as the sum of three terms:

$$\frac{\partial \ln N_{SL}}{\partial \ln E_0} = \frac{0.28}{\gamma} \frac{\partial t_{max}}{\partial \ln E_0} + \frac{1}{\gamma} \ln \left(\frac{N_{max}}{N_{SL}}\right) \frac{\partial \gamma}{\partial \ln E_0} + \frac{\partial \ln E_s}{\partial \ln E_0} .$$

The first term on the right-hand side of this equation comes from the variation of the track length integral with the height at which the shower reaches its maximum. If this height is the same as that of the maximum of the electronic cascades of the first generation, and if the multiplicity of production of π°-mesons is proportional to $E_0^{\frac{1}{4}}$ (more precisely, if the energy of the π°-mesons of the first generation is proportional to $E_0^{\frac{1}{4}}$), the value of this term is $0.21/\gamma \approx 0.14_5$.

The second term arises from the variation of the exponent γ with size of the showers. Since $\partial\gamma/\partial \ln N \approx 0.04$, $\partial \ln N/\partial \ln E_0 \approx 5/4$ and $\ln (N_{max}/N_{SL}) \approx 2.1$, this term is equal to about 0.07_5.

The third term describes the competition between the feeding of energy from the nuclear cascade to the soft component through creation of π°-mesons and the loss of energy by the creation of μ-mesons, neutrinos and low energy nucleons. In accordance with a crude model of the nuclear cascade, used previously in discussing the absorption of the electronic component of EAS, one may assume that for k generations, energy is lost from the nuclear cascade only to the soft component, the fractional transfer per generation being $1 - f$; and that after k generations the energy of the nuclear-active particles is dissipated by decay, etc., instead of going to the soft component. The relation between k and E_0 is given by Eq. 34. In this way one obtains

$$\frac{\partial \ln E_s}{\partial \ln E_0} = 1 + \frac{f^k}{1 - f^k} \frac{\ln (1/f)}{\ln v_1} \cdot \frac{1}{4 \ln (4/3)}$$

(where $v_1 = a E_0^{\frac{1}{4}}$ is the average degradation of energy in the first nuclear collision). In order to account for the long absorption length of the nuclear cascade, it was found necessary in the previous discussion to assume rather high values for f and k, and a rather low value for the constant a. With $f = 5/6$, $k = 6$ and $a = 0.5$, one finds $\partial \ln E_s/\partial \ln E_0 \approx 1.03$ in the neighborhood of $E_0 = 10^{15}$ eV.

By summing the three terms, one obtains $\partial \ln N_{SL}/\partial \ln E_0 \approx 1.25$. Accordingly, the exponent, Γ, in the integral primary energy spectrum near $E_0 = 10^{15}$ eV would be 1.25 times the exponent in the number spectrum of EAS at sea level, for shower sizes in the neighbourhood of 10^5 particles. Eq. 26 yields $\gamma'_{SL} = = 1.44$ for $N = 10^5$, hence $\Gamma(10^{15}\text{ eV}) \approx 1.80$.

The most likely source of significant error in the above estimates is in the first term: the correct magnitude of $\partial t_{max}/\partial \ln E_0$ is likely to be less than the assumed value, 3/4, because of the influence of the nuclear cascade in shifting the maxima of large showers towards high altitudes. With this possibility and other sources of error in mind, a revised estimate of $\partial \ln N_{SL}/\partial \ln E_0$ is given as 1.21 ± 0.06, and the exponent of the integral primary energy spectrum near 10^{15} eV is revised to $\Gamma(10^{15}\text{ eV}) = 1.74 \pm \pm 0.09$.

8.3 Form of the primary spectrum

The primary spectrum is not a perfect power law. The variation of the exponent is most rapid, however, in the low energy, latitude sensitive region below 14 GeV, where Γ is about 1.0. Between $1.4 \cdot 10^{10}$ and $1.4 \cdot 10^{15}$ eV, the average value of Γ is 1.64 ± 0.04, almost as large as the value at the upper end of the energy range. Throughout most of this interval, therefore, the variation of the exponent with energy must be very slow.

In the range 10^{14}—10^{17} eV, the variation of Γ with energy may be estimated from the slow variation of γ' with N_{SL} and the partially compensating variation of the factor $\partial \ln N_{SL}/\partial \ln E_0$. The result is:

$$\Gamma = -\partial \ln I/\partial \ln E_0 = (1.74 \pm 0.09) + (0.04 \pm 0.01) \ln (E_0/10^{15}) .$$

Beyond 10^{17} eV the variation of Γ with $\ln E_0$ may be more rapid, indicating the approach of a cutoff, but on this point we have no information.

The conclusions that have been reached about the integral primary energy spectrum responsible for the EAS may be summarized by the equation

$$I = (3 \pm 1)\ 10^{-6} \left(\frac{10^{15}}{E_0}\right)^{(1.74 \pm 0.09) + 0.02 \ln (E_0/10^{15})} \qquad (36)$$

in units of $(\text{m}^2 \text{ sec sterad})^{-1}$, with E_0 measured in eV. Eq. 36 happens to agree, within the reported uncertainties, with the

points and the smooth curve published earlier by BARRETT *et al.* [1952].

8.4 MAXIMUM ENERGY OF PRIMARIES OF OBSERVED SHOWERS

A matter of strong concern in connection with theories of the origin of cosmic rays is the maximum energy per nucleon of the primary particles. In this regard it is interesting that there is as yet no definite experimental evidence for a cutoff of the primary intensity at any energy.

The density spectrum of the EAS has been measured as far as densities of $10^4\ m^{-2}$. Throughout the entire spectrum, the steepness, as indicated by the exponent γ, increases slowly with the density, and there is only a weak indication that the exponent may increase more rapidly near the highest densities (see Fig. 14 and 15). The average size of the showers contributing to the highest recorded densities exceeds 10^7 electrons.

Experiments in which the shower axis was located and the density measured at known distances from the axis have indicated small numbers of showers having as many as 10^8 electrons (WILLIAMS [1948], COCCONI *et al.* [1949b], EIDUS *et al.* [1952], ZATSEPIN *et al.* [1953]). The failure to detect still larger showers can be accounted for with a smooth extrapolation of the number spectrum and a calculation of the number of events expected in the operating time of the experiments.

It is possible to suggest plausible errors in the experiments that may have led to a slight exaggeration of the size of the largest showers. But it seems imprudent to place confidence in any theory of cosmic-ray origins according to which the maximum observable shower size is 10^8 particles or less.

A minimal estimate of the primary energy of showers containing 10^8 electrons is $2 \cdot 10^{17}$ eV. Even if the largest showers are initiated by heavy nuclei, the minimal energy is about 10^{16} eV per nucleon.

As yet, there is little evidence as to the charge or mass of the primaries of EAS; but the heavy elements are so rare in the universe and among the primary cosmic rays of energy up to 10^{13} eV per nucleon, that it seems unreasonable to try to account for the frequency of the large showers entirely with nuclei of $Z > 10$.

Indeed, if the primaries are gradually accelerated by collisions with magnetic clouds, the primaries of highest energy are those

that have survived both escape from the galaxy and nuclear collisions for the longest time. The increase of the collision cross-section with atomic weight discriminates in favor of the light elements, making the steepness of the energy spectrum increase with Z. At moderate energies a tendency in this direction seems to be verified by experiments; and it appears artificial to assume that the trend is strongly reversed at high energy.

Therefore theories of the origin are faced with the need to account for the presence of protons having energy up to at least $2 \cdot 10^{17}$ eV. It seems out of the question to conceive of such particles being confined within any field associated with our solar system. Even the retention of the particles within the galaxy may be considered as indirect evidence for the existence of coherent magnetic fields with extensions on the order of hundreds of light years. Thus the cosmic rays confirm the inferences that have been drawn by astronomers from the parallelism of the planes of polarization of light coming from different stars. It will be interesting in the future, in connection with the structure of the galaxy, to see how far the cosmic-ray spectrum extends beyond the presently explored range.

REFERENCES

ADAMS, R. V., C. D. ANDERSON and E. W. COWAN, 1949, Rev. Mod. Phys., **21**, 72.

AMALDI, E., L. MEZZETTI and G. STOPPINI, 1953, Nuovo Cim., **10**, 803.

ANISHENKO, U. V., G. T. ZATSEPIN, I. L. ROSENTAL and L. I. SARITCHEVA, 1952, J. Exp. Theor. Phys., **22**, 143.

ARLEY, N., 1938, Proc. Roy. Soc., **A168**, 519.

AUGER, P., R. MAZE and T. GRIVET-MEYER, 1938, C. R. Acad. Sci. Paris, **206**, 1721.

AUGER, P. and R. MAZE, 1938, C. R. Acad. Sci. Paris, **207**, 228.

AUGER, P., R. MAZE, P. EHRENFEST and A. FRÉON, 1939, J. Phys. Radium, **10**, 39.

AUGER, P., R. MAZE and J. ROBLEY, 1939, C. R. Acad. Sci. Paris, **208**, 164.

AUGER, P., P. EHRENFEST, R. MAZE, J. DAUDIN, J. ROBLEY and A. FRÉON, 1939, Rev. Mod. Phys., **11**, 288.

AUGER, P. and J. DAUDIN, 1942, Phys. Rev., **61**, 91.

AUGER, P. and J. DAUDIN, 1945, J. Phys. Radium, **6**, 233.

BARRETT, P. H., L. M. BOLLINGER, G. COCCONI, Y. EISENBERG and K. GREISEN, 1952, Rev. Mod. Phys., **24**, 133.

BARRETT, P. H., G. COCCONI, Y. EISENBERG and K. GREISEN, 1954, Phys. Rev., **95**, 1571.

BASSI, P., A. M. BIANCHI, C. CADORIN and C. MANDUCHI, 1952, Nuovo Cim., **9**, 1037.

BASSI, P., G. CLARK and B. ROSSI, 1953, Phys. Rev., **92**, 441.

BELENKY, S. Z., 1941, C. R. Acad. Sci. USSR, **30**, 608.

BELENKY, S. Z., 1944, J. Phys. USSR, **8**, 9.

BERNSTEIN, I. B., 1950, Phys. Rev., **80**, 995.

BHABHA, H. J., 1935, Proc. Roy Soc., **A152**, 559.

BHABHA, H. J. and S. K. CHAKRABARTY, 1948, Phys. Rev., **74**, 1352.

BHABHA, H. J. and A. RAMAKRISHNAN, 1950, Proc. Ind. Acad. Sci., **32**, 141.

BHABHA, H. J., 1953, Proc. Roy. Soc., **A219**, 293.

BIEHL, A. T. and H. V. Neher, 1951, Phys. Rev., **83**, 1169.

BIERMANN, L., 1953(a), Ann. Rev. Nuclear Sci., **2**, 335.

BIERMANN, L., 1953(b), Vorträge über Kosmische Strahlung, (ed. W. HEISENBERG; Springer, Berlin).

BLATT, J. M., 1949, Phys. Rev., **75**, 1584.

BLOCK, M. M., D. T. KING and W. W. WADA, 1954, Phys, Rev., **96**, 1627.

BOTHE, W., W. GENTNER, H. MAIER-LEIBNITZ, W. MAURER, E. WILHELMY and K. SCHMEISER, 1937, Physik. Zeits., **38**, 964.

BORSELLINO, A., 1950, Nuovo Cim., **7**, 323, 638 and 700.

BROADBENT, D. and L. JANOSSY, 1947, Proc. Roy. Soc., **A191**, 517.

BROADBENT, D., E. W. KELLERMANN and M. A. HAKEEM, 1950, Proc. Phys. Soc. **A63**, 864.

BROWN, W. W. and A. S. MCKAY, 1949, Phys. Rev., **76**, 1034.

Brown, W. W. and A. S. McKay, 1950, Phys. Rev., **77**, 342.
Branch, G. M., 1951, Phys. Rev., **84**, 147.
Branch, G. M. and G. Cocconi, 1951, Phys. Rev., **84**, 146.
Budini, P., 1951, Nuovo Cim., **8**, 446.
Budini, P. and G. Molière, 1953, Vorträge über Kosmische Strahlung, (ed. W. Heisenberg; Springer, Berlin).
Camac, M., 1952, Phys. Rev., **88**, 745.
Campbell, I. D. and J. R. Prescott, 1952, Proc. Phys. Soc., **A65**, 258.
Castagnoli, C., A. Gigli and S. Sciuti, 1950, Nuovo Cim., **7**, 307.
Chaloupka, P., 1954, Phys. Rev., **96**, 1709.
Chandrasekhar, S. and E. Fermi, 1953, Astrophys. J., **118**, 113.
Chowdhuri, B., 1948, Nature, Lond., **161**, 680.
Chowdhuri, B., 1950, Proc. Phys. Soc., **A63**, 165.
Chowdhuri, B., R. C. Saxena and A. Subramanian, 1952, Proc. Ind. Acad. Sci., **A36**, 457.
Citron, A., 1952, Z. Naturforsch., **7a**, 712.
Clementel, E. and L. Fabbrichesi, 1948, Nuovo Cim., **5**, 78.
Clementel, E. and L. Fabbrichesi, 1949, Nuovo Cim., **6**, 399.
Cocconi, G., A. Loverdo and V. Tongiorgi, 1943, Nuovo Cim., **1**, 314.
Cocconi, G., A. Loverdo and V. Tongiorgi, 1944, Nuovo Cim., **2**, 14.
Cocconi, G., 1947, Phys. Rev., **72**, 964.
Cocconi, G. and V. C. Tongiorgi, 1949, Phys. Rev., **75**, 1058.
Cocconi, G., V. C. Tongiorgi and K. Greisen, 1949a, Phys. Rev., **75**, 1063.
Cocconi, G., V. C. Tongiorgi and K. Greisen, 1949b, Phys. Rev., **76**, 1020.
Cocconi, G. and V. C. Tongiorgi, 1950, Phys. Rev., **79**, 730.
Cocconi, G., 1954a, Phys. Rev., **93**, 1107.
Cocconi, G., 1954b, Phys. Rev., **93**, 646 and **95**, 1705.
Cool, R. L. and O. Piccioni, 1951, Phys. Rev., **82**, 306.
Cranshaw, T. E. and W. Galbraith, 1954, Phil. Mag., **45**, 1109.
Cresti, M., A. Loria and G. Zago, 1953, Nuovo Cim., **10**, 779.
Daudin, A. and J. Daudin, 1949, J. Phys. Radium, **10**, 394.
Daudin, A. and J. Daudin, 1953, J. Atmos. Terr. Phys., **3**. 245 and J. Phys. Radium, **14**, 169, Bagnères-de-Bigorre Conf.; and Thesis (A. Daudin), Univ. of Paris, 1954. (The thesis contains the most complete and up-to-date account of this work).
Daudin, J., 1943, C. R. Acad. Sci. Paris, **216**, 483.
Daudin, J., 1944a, C. R. Acad. Sci. Paris, **218**, 830.
Daudin. J., 1944b, C. R. Acad. Sci. Paris, **218**, 882.
Daudin, J., 1945, J. Phys. Radium, **6**, 302.
Dallaporta, N. and E. Clementel, 1946, Nuovo Cim., **3**, 235.
Dallaporta, N. and G. Poiani, 1947, Nuovo Cim., **4**, 1.
Davis, L., 1951, Phys. Rev., **81**, 890.
Davis, L. and J. L. Greenstein, 1951, Astrophys. J., **114**, 206.
Davis, L., 1954, Phys. Rev., **96**, 743.
Davis, W. P., W. E. Hazen and R. E. Heineman, 1954, Nuovo Cim., **12**, 233.
Deutschmann, M., 1947, Z. Naturforsch., **2a**, 61.
Eidus, L. K., M. I. Adamovitch, I. A. Ivanovskaya, V. S. Nikolaev and M. S. Tulyankina, 1952, J. Exp. Theor. Phys., **22**, 440.

ELLIOT, H., 1952, Progress in Cosmic Ray Physics (Amsterdam: North-Holland Publishing Co.), Chap. VIII.
ELLIOT, H., 1953, Bagnères-de-Bigorre Conf.
EL-MOFTY, O., 1953, Phys. Rev., **92**, 461.
EULER, H. and H. WERGELAND, 1940, Astrophys. Norwegica, **3**, 165.
EYGES, L., 1948, Phys. Rev., **74**, 1801.
EYGES, L. and S. FERNBACH, 1951, Phys. Rev., **82**, 23 and 287.
FAHY, E. H., 1951, Phys. Rev., **83**, 413.
FARLEY, F. J. M. and J. R. STOREY, 1954, Nature, Lond., **173**, 445 *and* private communication.
FERMI, E., 1949, Phys. Rev., **75**, 1169.
FERMI. E., 1951, Progr. Theor. Phys., **5**, 570, *and* Phys. Rev., **81**, 683.
FERMI, E., 1954, Astrophys. J., **119**, 1.
FERNBACH, S., 1951, Phys. Rev., **82**, 288.
FORNACA, G. and G. MARTELLI, 1953, Bagnères-de-Bigorre Conf.
FREIER, P. and J. NAUGLE, 1953, Proc. Duke Univ. Cosmic Ray Conf.
FRETTER, W. B., 1949, Phys. Rev., **76**, 511.
FUJIOKA, G., 1953, Internat. Conf. Theor. Phys. (Japan).
GEORGE, E. P. and A. C. JASON, 1950, Proc. Phys. Soc., **A63**, 1081.
GEORGE, E. P., J. W. MACANUFF and J. W. STURGESS, 1953, Proc. Phys. Soc., **A66**, 345.
GOAD, W., 1953, Thesis, Duke Univ.
GOTTLIEB, M. B., 1951, Phys. Rev., **82**, 349.
GREEN, H. S. and H. MESSEL, 1952, Phys. Rev., **88**, 331.
GREISEN, K., 1949, Phys. Rev., **75**, 1071.
GREISEN, K., W. D. WALKER and S. P. WALKER, 1950, Phys. Rev., **80**, 535.
GREISEN, K. and W. D. WALKER, 1953, Phys. Rev., **90**, 915.
HADDARA, S. R. and D. JAKEMAN, 1953, Proc. Phys. Soc., **A66**, 540.
HAZEN, W. E., 1952, Phys. Rev., **85**, 455.
HAZEN, W. E., R. E. HEINEMAN and E. S. LENNOX, 1952, Phys. Rev., **86**, 198.
HAZEN, W. E., R. W. WILLIAMS and C. A. RANDALL, Jr., 1954, Phys. Rev., **93**, 578.
HAZEN, W. E., 1954, Nuovo Cim., **11**, 393.
HEINEMAN, R. E. and W. E. HAZEN, 1953, Phys. Rev., **90**, 496.
HEINEMAN, R. E., 1954, Phys. Rev., **96**, 161.
HEISENBERG, W., 1953, Vorträge über Kosmische Strahlung (Springer, Berlin), p. 148.
HILBERRY, N., 1941, Phys. Rev., **60**, 1.
HILTNER, W. A., 1951, Astrophys. J., **114**, 241.
HODSON, A. L., 1951, Proc. Phys. Soc., **A64**, 1061.
HODSON, A. L., 1952, Proc. Phys. Soc., **A65**, 702.
HODSON, A. L., 1953a, Proc. Phys. Soc., **A66**, 49.
HODSON, A. L., 1953b, Proc. Phys. Soc., **A66**, 65.
HOOPER, J. E., D. T. KING and A. H. MORRISH, 1952, Phil. Mag., **43**, 853.
HUDSON, D. E., 1950, Thesis, Cornell Univ.
HUDSON, D. E., 1952, Phys. Rev., **86**, 453.
ISE, J. Jr., and W. B. FRETTER, 1949, Phys. Rev., **76**, 933.
JANOSSY, L. and A. C. B. LOVELL, 1938, Nature, Lond., **142**, 716.

JANOSSY, L., 1942, Proc. Roy. Soc., **A179**, 361.
JANOSSY, L., 1948, Cosmic Rays (Oxford Univ. Press, London).
JANOSSY, L., 1950, Proc. Phys. Soc., **A63**, 1009.
JANOSSY, L. and H. MESSEL, 1950, Proc. Phys. Soc., **A63**, 1101.
KAPLON, M. F., B. PETERS and H. L. BRADT, 1949, Phys. Rev., **76**, 1735, *and* Helv. Phys. Acta, **23**, 24.
KAPLON, M. F. and D. M. RITSON, 1952a, Phys. Rev., **85**, 932.
KAPLON, M. F. and D. M. RITSON, 1952b, Phys. Rev., **88**, 386.
KAPLON, M. F., W. D. WALKER and M. KOSHIBA, 1954, Phys. Rev., **93**, 1424.
KASNITZ, H. L. and K. SITTE, 1954, Phys. Rev., **94**, 977.
KECK, J. C. and K. GREISEN, 1949, Proc. Echo Lake Cosmic Ray Conf.
KOLHÖRSTER, W., I. MATTHES and E. WEBER, 1938, Naturwiss., **26**, 576.
KOSHIBA, M. and M. F. KAPLON, 1955, Phys. Rev., **97**, 193.
KRAUSHAAR, W. L. and L. J. MARKS, 1954, Phys. Rev., **93**, 326.
KRAYBILL, H. L., 1949, Phys. Rev., **76**, 1092.
KRAYBILL, H. L., 1954, Phys. Rev., **93**, 1362.
LANDAU, L., 1940, J. Phys. USSR, **3**, 237.
LANDAU, L., 1953, Izv. Akad. Nauk. SSSR, Ser. Fiz., **17**, n.l.
LAL, D., Y. PAL, B. PETERS and M. S. SWAMI, 1952, Proc. Ind. Acad. Sci. **A36**, 75, *and* Phys. Rev., **87**, 545.
LAPP, R. E., 1943, Phys. Rev., **64**, 129.
LAPP, R. E., 1946, Phys. Rev., **69**, 321.
LEVINGER, J., 1949, Phys. Rev., **75**, 1540.
LEWIS, H. W., 1948, Phys. Rev., **73**, 1341.
LORD, J. J., J. FAINBERG and M. SCHEIN, 1950, Phys. Rev., **80**, 970, *and* Nuovo Cim., **7**, 774.
LOVATI, A., A. MURA, C. SUCCI and G. TAGLIAFERRI, 1951, Nuovo Cim., **8**, 271.
LOVERDO, A. and J. DAUDIN, 1948, J. Phys. Radium, **9**, 134.
MARSHAK, R. A., 1952, Meson Physics (McGraw-Hill Book Co., New York).
MAZE, R. and A. FRÉON, 1949, J. Phys. Radium., **10**, 85.
MCCUSKER, C. B. A., 1950, Proc. Phys. Soc., **A63**, 1240.
MCCUSKER, C. B. A. and D. D. MILLAR, 1951, Proc. Phys. Soc., **A64**, 915.
MESSEL, H. and R. B. POTTS, 1953, Nuovo Cim., **10**, 754.
MESSEL, H., 1954, Progress in Cosmic Ray Physics, Vol II (Amsterdam: North-Holland Publishing Co.), Chap. IV.
MIGDAL, A., 1945, J. Phys. USSR, **9**, 183.
MILLAR, D. D., 1951, Proc. Roy. Irish Acad., **54**, 115.
MILLS, M. M., 1948, Phys. Rev., **74**, 1555, *and* Thesis, Calif. Inst. Tech.
MILONE, C., 1951, Nuovo Cim., **8**, 643.
MILONE, C., 1952a, Nuovo Cim., **9**, 549.
MILONE, C., 1952b, Nuovo Cim., **9**, 637.
MOLIÈRE, G., 1942, Naturwiss., **30**, 87.
MOLIÈRE, G., 1946, Cosmic Radiation, (ed. W. Heisenberg; Dover Publ., New York).
MOLIÈRE, G., 1953, Vorträge über Kosmische Strahlung, (ed. W. Heisenberg; Springer, Berlin), p. 446.
MOLIÈRE, G., 1954, Phys. Rev., **93**, 636.

MORRISON, P., S. OLBERT and B. ROSSI, 1954, Phys. Rev., **94**, 440.
NAUGLE, J. E. and P. S. FREIER, 1953, Phys. Rev., **92**, 1086.
NISHIMURA, J. and K. KAMATA, 1950, Progr. Theor. Phys., **5**, 899.
NISHIMURA, J. and K. KAMATA, 1951, Progr. Theor. Phys., **6**, 628.
NISHIMURA, J. and K. KAMATA, 1952, Progr. Theor. Phys., **7**, 185.
PALMATIER, E. D., 1952, Phys. Rev., **88**, 761.
PICCIONI, O. and R. L. COOL, 1953, Phys. Rev., **91**, 433.
PICKUP, E. and L. VOYVODIC, 1951, Phys. Rev., **84**, 1190.
POIANI, G. and C. VILLI, 1952a, Nuovo Cim., **9**, 825.
POIANI, G. and C. VILLI, 1952b, Nuovo Cim., **9**, 1109.
POMERANCHUK, I., 1944, J. Phys. USSR, **8**, 17.
RACAH, G., 1937, Nuovo Cim., **14**, 93.
RAMAKRISHNAN, A. and P. M. MATHEWS, 1953, Progr. Theor. Phys., **9**, 679.
RAVENHALL, D. G., 1950, Proc. Phys. Soc., **A63**, 1177.
RELF, K. E., 1955, Phys. Rev., **97**, 172.
RICHARDS, J. A., Jr. and L. W. NORDHEIM, 1948, Phys. Rev., **74**, 1106.
ROBERG, J. and L. W. NORDHEIM, 1949, Phys. Rev., **75**, 444.
ROSENTAL, I. L., 1952, J. Exp. Theor. Phys., **23**, 440.
ROSSI, B. and K. GREISEN, 1941, Rev. Mod. Phys., **13**, 240.
ROSSI, B., 1952, High Energy Particles (Prentice-Hall, New York).
SALVINI, G. and G. TAGLIAFERRI, 1949, Nuovo Cim., **6**, 108.
SCHMEISER, K. and W. BOTHE, 1938, Ann. Phys., Lpz., **32**, 161.
SERBER, R., 1938, Phys. Rev., **54**, 317.
SHERMAN, N., 1953, Phys. Rev., **89**, 25.
SINGER, S. F., 1951, Phys. Rev., **81**, 579.
SITTE, K., 1950, Phys. Rev., **78**, 721.
SITTE, K., 1952, Phys. Rev., **87**, 351.
SITTE, K., D. L. STIERWALT and I. L. KOFSKY, 1954, Phys. Rev., **94**, 988.
SNYDER, H. S., 1938, Phys. Rev., **53**, 960.
SNYDER, H. S., 1949, Phys. Rev., **76**, 1563.
STINCHCOMB, T. G., 1951, Phys. Rev., **83**, 422.
STRANAHAN, G., 1954, Astrophys. J., **119**, 465.
TAMM, I. and S. BELENKY, 1946, Phys. Rev., **70**, 660.
TICHO, H. K., 1952, Phys. Rev., **88**, 236.
TONGIORGI, V., 1948a, Phys. Rev., **73**, 923.
TONGIORGI, V., 1948b, Phys. Rev., **74**, 226.
TONGIORGI, V., 1949, Phys. Rev., **75**, 1532.
TREAT, J. E. and K. GREISEN, 1948, Phys. Rev., **74**, 414.
WEI, J. and C. G. MONTGOMERY, 1949, Phys. Rev., **76**, 1488.
WILLIAMS, R. W., 1948, Phys. Rev., **74**, 1689.
WILSON, R. R., 1952, Phys. Rev., **86**, 261.
ZATSEPIN, G. T., V. V. MILLER, I. L. ROSENTAL and L. K. EIDUS, 1947, J. Exp. Theor. Phys., **17**, 1125.
ZATSEPIN, G. T., I. L. ROSENTAL, L. I. SARITCHEVA, G. B. KHRISTIANSEN and L. K. EIDUS, 1953, Izv. Akad. Nauk, SSSR, Ser. Fiz., **17**, 39

*

CHAPTER II

EXPERIMENTAL RESULTS ON CHARGED K-MESONS AND HYPERONS

BY

H. S. BRIDGE

Massachusetts Institute of Technology

INTRODUCTION 145

1. THE TAU-MESON 149

2, 3, 4. DECAY EVENTS PRODUCED BY K-MESONS AND CHARACTERIZED BY THE EMISSION OF A SINGLE CHARGED SECONDARY PARTICLE

2. RESULTS CONCERNING S-EVENTS: OBSERVATIONS WITH PHOTOEMULSIONS 156

3. RESULTS CONCERNING S-EVENTS: OBSERVATIONS WITH CLOUD CHAMBERS 179

4. RESULTS CONCERNING CHARGED V-PARTICLES OBTAINED WITH CLOUD CHAMBERS USING A MAGNETIC FIELD 207

5. THE CHARGED HYPERONS 228

6. NUCLEAR ABSORPTION OF HEAVY MESONS AND HYPERONS 237

ACKNOWLEDGEMENTS 248

REFERENCES 249

INTRODUCTION

The information concerning unstable heavy particles is now so extensive that it has seemed expedient to divide the material arbitrarily into two parts. The present chapter therefore deals with the experimental material concerning charged unstable particles heavier than the π-meson while the following chapter by R. W. Thompson is concerned with the neutral particles.

The chronological development of the subject and the nature of the available experimental data up to 1952 have been considered in the two previous volumes of this series. Consequently the more recent data receives emphasis here and the earlier results will be considered only insofar as they affect the present situation. Experimental results available up to about January 1955 are included in the present chapter.

Only a small fraction of the experimental data concerning charged unstable particles can be uniquely classified in terms of the various decay schemes which have been proposed to explain the observations. This difficulty in classifying the observed events results primarily from the fact that many different decay schemes and probably several parent particles of about the same mass contribute to the observed data. In such a situation the statistical methods of analysis which have been used with such success in the case of the data concerning neutral V-particles have been of little use because the experimental information obtained from *individual* events is not sufficiently precise to distinguish between possible modes of decay.

A great deal of progress in the endeavour to obtain more complete and more accurate information is being made at the present time. Cloud chamber measurements have been improved by the use of better techniques to measure momentum and ionization, and a further important development is the use of combined magnetic and multiplate cloud chambers which afford measurements of momentum and residual range on the same track. However perhaps the most promising method is the use of large emulsion blocks. These experiments are still in a preliminary stage, but the initial results, mostly obtained in the Sardinia expedition of 1954, demonstrate the power of this approach.

Since many decay events can only be classified on a phenomenological basis and since the data obtained using different experimental techniques are frequently very difficult to correlate, a discussion of the experimental results according to the decay schemes alone is not practical. In the following presentation, therefore, we shall group the experimental data phenomenologically according to characteristic features of the event and according to the experimental techniques employed. The experimental methods will not be considered in detail except for those features which directly affect the type of data obtained or its interpretation.

Nomenclature

The nomenclature proposed by Amaldi *et al.* [1954a], is used in this and in the following chapter. According to this scheme particles are classified in three ways:

(*a*) *According to mass* with the division indicated by a capital Latin letter as follows.

(1) L-mesons (Symbol L): π-mesons and all lighter particles.
(2) K-mesons (Symbol K): particles whose mass lies between that of the π-meson and the nucleon mass.
(3) Y-particles, Hyperons (Symbol Y): particles whose mass lies between that of the nucleon and the mass of the deuteron.

(*b*) *By individual name* according to a decay scheme either postulated or established. Small Greek letters identify L-mesons and K-mesons while capital Greek letters distinguish hyperons.

(*c*) *Phenomenologically* according to some characteristic feature.

(1) V-event: an observation which can be interpreted as the decay in flight of a K-meson or hyperon. Subclasses V^0 and $V^{\pm}$.
(2) S-event: an observation which can be interpreted as the decay or nuclear capture of a K-meson or hyperon at rest.

No scheme such as the one above proves adequate for long in a rapidly changing field of research. Some inconsistencies mostly carried over from the original description of the events in question will be obvious.

Resumé of particles and decay schemes

In order to explain the experimental facts a rather large number of particles each with a unique mass and decay scheme has been postulated. The more important particles and their decay schemes are listed in Table I, and much of the interpretation which follows is in terms of the assumptions implied by this classification. It is necessary to keep in mind here, and in what follows, that the word "particle" really means an observed mode of decay. The number of actual "fundamental particles" which produce the observed

TABLE I(a)

Summary of well established particles and decay schemes

The body of the table lists some of the more important physical quantities for each particle. Columns 1 and 2 list the particle and its decay products. Column 3 gives the sign of the electric charge; column 4 the rest energy in MeV; column 5 the mean life in seconds; column 6 lists the spin in units of $\hbar$. Column 7 gives the quantum number, S, which specifies the Gell-Mann, Pais selection rules. In column 6, (0) indicates integer spin, ($\frac{1}{2}$) indicates half-integer spin.

Particle	Decay Products	Sign	Rest Energy MeV	Mean Life sec	Spin $\hbar$	S
			K-Mesons			
τ-meson	$\pi^{\pm} + \pi^{\pm} + \pi^{\mp}$					
	$(\pi^0 + \pi^0 + \pi^{\pm})$	+	493 + 3	$\sim 10^{-8}$	(0)	
χ-meson	$\pi^+ + \pi^0$	+ (-)	480 — 493	10^{-9} — 10^{-8}	(0)	
$\varkappa$-meson	$\mu^{\pm} + \gamma^0 + \gamma^0$	± (—)	~493	$> 10^{-10}$		
K_μ-meson	$\mu^{\pm} + \nu$	± (-)	475 — 493	$\sim 10^{-8}$	(0)	
K_e-meson	$e^{\pm} + \gamma^0 + \gamma^0$	± (-)	493	$> 10^{-10}$		
θ-meson	$\pi^+ + \pi^-$	0	494 ± 5	$\sim 1.5 \times 10^{-10}$	(0)	+ 1
			Hyperons			
Σ-particle	$p + \pi^0$	+ (-)	1189 ± 2	$\sim 10^{-10}$	($\frac{1}{2}$)	— 1
	$(n + \pi^+)$					
	$(n + \pi^-)$					
Ξ-particle	$\Lambda^0 + \pi^-$	—	~1320	$\sim 10^{-10}$	($\frac{1}{2}$)	— 2
Λ-particle	$p + \pi^-$	0	1114 ± 1	$\sim 3.7 \times 10^{-10}$	($\frac{1}{2}$)	— 1
			Particles lighter than L-mesons, L-mesons, and nucleons			
photon	stable	0	0		1	
neutrino	stable	0	(0)		$\frac{1}{2}$	
electron	stable	+ —	.51098		$\frac{1}{2}$	
μ-meson	$e^{\pm} + \nu + \nu$	+ —	105.6	2.2×10^{-6}	$\frac{1}{2}$	
π-meson	$\mu^{\pm} + \nu$	+ —	139.5	$\sim 2.5 \times 10^{-8}$	0	0
	$\gamma + \gamma$	0	135.0	$\sim 5 \times 10^{-15}$	0	0
proton	stable	+	938.23	—	$\frac{1}{2}$	0
neutron	$p + e^- + \nu$	0	939.53	$\sim 1.1 \times 10^3$	$\frac{1}{2}$	0

TABLE I (b)

Some characteristic quantities for various observed and postulated decay modes of K-mesons and Hyperons

The more important quantities which characterize a two-body decay are given in the body of the table. The numerical values have been computed for the decay schemes listed in column 1 using the assumed values for the rest energy of the primary particle also listed in column 1. The rest energies used for the decay products are those given in Table I (a). Column 2 gives values of $\bar{a} = (m_{\pm}{}^2c^4 - m_0{}^2c^4)/M^2c^4$, where $m_{\pm}c^2$, m_0c^2, and Mc^2 are, respectively, the rest energies of the charged decay product, the neutral decay product and the primary particle. $\bar{a}$ is a measure of the assymetry of the decay process; it is discussed in § 4. Column 3 lists the energy release, Q, of the decay in MeV. The remaining columns refer to the charged secondary particle in the rest system of the primary. Column 4 gives the momentum, p^*, in MeV/c and column 5 the total energy, U^*, in MeV. In the last four columns other frequently used derived quantities are tabulated. These are, in order, column 6 the kinetic energy, E, in MeV, column 7 the velocity relative to light, β, column 8, the value of $p\beta$ in MeV/c. Finally, in column 9, values of the secondary range in copper are listed. These were computed from the range tables of ARON, HOFFMANN and WILLIAMS [1949] and are based on a mean ionization potential, I, of 333.5 eV. This value of I is somewhat uncertain, see § 3.7, consequently the above values of range may be slightly in error. For convenience, it may be noted that the ranges for copper are almost identical to those for emulsion (density 3.815) obtained by BARKAS and YOUNG [1954]; an approximate conversion from copper to lead results if the tabulated ranges are multiplied by 4/3.

In addition to the two-body decay processes considered in column 1, data are also given for several three-body decay schemes. In these the various quantities relating to the charged secondary particle are not unique, and the tabulated values are maximum quantities for the decay process in question.

			Charged Secondary Particle					
Rest Energy MeV, Decay Product	$\bar{a}$	Q MeV	p^* MeV/c	U^* MeV	E^* MeV	β^*	$p^*\beta^*$ MeV/c	Range g cm^{-2} Copper
480.0 K →								
$\mu + \nu$	.0484	374.4	228.4	251.6	146.0	.908	207.4	75.3
$\mu + \nu + \nu$			⩽228.4	⩽251.6	⩽146.0	⩽.908	⩽207.4	⩽75.3
$\pi^{\pm} + \pi^0$	.0054	205.5	196.9	241.3	101.8	.816	160.7	41.0
$\pi^{\pm} + \gamma$	.0845	340.5	219.7	260.3	120.8	.844	185.4	52.5
$\pi^{\pm} + \pi^0 + \pi^0$			⩽120.5	⩽184.3	⩽ 44.8	⩽.654	⩽78.8	⩽11.4
493.0 K →								
$\mu + \nu$	.0459	387.4	235.2	257.8	152.2	.912	214.6	79.4
$\mu + \nu + \nu$			⩽235.2	⩽257.8	⩽152.2	⩽.912	⩽214.6	⩽79.4
$\pi^{\pm} + \pi^0$	.0051	218.5	204.7	247.8	108.3	.826	169.1	44.9
$\pi^{\pm} + \gamma$	.0801	353.5	226.8	266.2	126.7	.852	193.2	56.2
$\pi^{\pm} + \pi^0 + \pi^0$			⩽132.4	⩽192.3	⩽ 52.8	⩽.689	⩽91.2	⩽14.9
$\mu^{\pm} + \pi^0 + \nu$			⩽214.8	⩽239.3	⩽133.7	⩽.898	⩽192.8	⩽67.0
$e + \nu + \nu$			⩽246.4	⩽246.5	⩽246.0	⩽1.000	⩽246.4	—
1189.0 Y →								
$p + \pi^0$	.6098	115.8	188.8	957.0	18.77	.1973	37.25	.629
$n + \pi^+$ $n + \pi^-$	−.6106	110.0	184.7	231.5	92.0	.798	147.4	35.3
1320.0 Y →								
$\Lambda^0 + \pi^-$	−.7023	65.5	138.3	196.5	57.0	.704	97.3	16.9

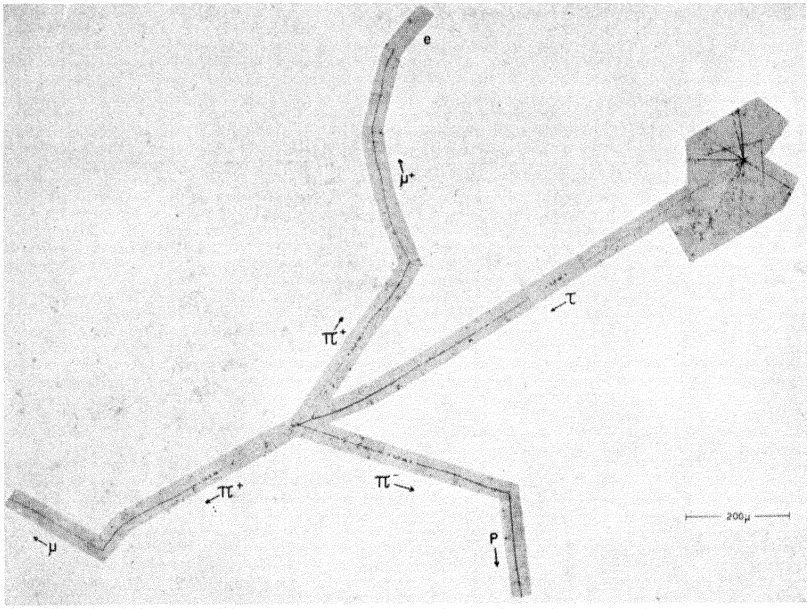

Plate I – Decay of the τ-meson. This is the first example obtained (BELLIBONI *et al.* [1954]) in which all three of the π-mesons produced in the decay of the τ-meson came to rest in the emulsion. Two of the L-meson secondary particles decay to μ-mesons and are thus identified as π^+-mesons. The third secondary particle is captured by a nucleus and produces a small star; thus it must have been a π^--meson. One of the positive secondary particles exhibits a complete $\pi^+ \to \mu^+ \to e^+$ decay.

events is at present one of the major problems under investigation experimentally and theoretically. For example, Table I lists six well established decay modes for K-mesons. However the number of actual particles reponsible for these events, their relationships to one another, and their connection with more familiar particles (protons, π-mesons, etc.) are all unknown.

Some partially successful attempts at relating the various unstable particles have already been made (PAIS [1953], GOLDHABER [1953], GELL-MANN and PAIS [1954]). At present these efforts are in the nature of selection rules whose foundation is not apparent. However their increasing success gives some reason to believe that a theory is at least possible. In the following presentation we will not discuss any of the above attempts to systematize the data; rather we consider the experimental evidence which must be explained by a successful theory.

1. The Tau-Meson

The first τ-meson decay was observed in a photographic emulsion by the Bristol group (BROWN, *et al.* [1949]). Since that time more than 40 similar events in which the τ-meson decayed at rest have been observed in emulsions and $\sim$20 decays in flight have been observed in cloud chambers operated with an associated magnetic field. It is certain that, in agreement with the original interpretation of Brown *et al*, the τ-meson decays into three π-mesons, viz.,

$$\tau^{\pm} \rightarrow \pi^{\pm} + \pi^{\pm} + \pi^{\mp} + Q$$

The energy release, Q, is about 75 MeV so that the energies of the secondary π-mesons are low. However the range of at least one secondary always exceeds 1 cm and in the majority of the events one or more of the secondaries leaves the emulsion before coming to rest. The first complete τ-meson decay is shown in Plate I. (BELLIBONI *et al.* [1954]).

1.1 MODE OF PRODUCTION

Tau-mesons are produced directly in high energy nuclear interactions. In the earlier emulsion work most of the K-mesons which were observed originated outside the plate and it was therefore impossible to determine whether the τ-meson was produced direct-

ly or whether it arose through the decay of some heavier particle. The first example of the production of a τ-meson in a nuclear interaction was obtained in a large emulsion stack by the Padua group (CECCARELLI *et al.* [1954]). Many other examples have been obtained since the use of large blocks of emulsion has become common.

Tau mesons have been produced using 3 GeV protons accelerated in the Cosmotron at the Brookhaven Laboratory (HILL *et al.* [1954]). It is not known whether they are produced singly, in pairs, or in association with another type of unstable particle.

1. 2 DECAY SCHEME, MASS, AND Q-VALUE OF THE τ-MESON

In all but two of the τ-meson decays observed in emulsions the three L-meson secondaries are coplanar to within 1° or 2°. It follows that in the majority of the events, the primary particle decays at rest and that no neutral particles are emitted in the decay.

In many events it has been established that all three of the secondaries are π-mesons and there is no example in which a μ-meson has been identified among the decay products. If in a particular event it is known that some of the secondaries are π-mesons it is then possible to show using the conservation laws that the mass differences between the secondary particles are less than the mass difference between the π- and μ-meson. There are in addition an increasing number of events in which the three π-mesons can be all identified by their behaviour at the end of the range. No μ-mesons have been observed among the decay products in these events in which all three secondary particles can be identified.

The most accurate value of the primary mass is obtained using the assumed decay scheme and the relation

$$M_{\tau^+} = \{2m_{\pi^+}c^2 + m_{\pi^-}c^2\} + Q.$$

For the earlier data on τ-mesons the energies of the secondaries were determined from measurements of scattering and ionization. Most of the recent data have been obtained using large emulsion stacks in which one or more of the secondary particles commonly comes to rest. In these cases the energies of the stopped particles are determined from the ranges.

Because the decay takes place at rest, the Q-value is determined by a measurement of the angles between the three secondary tracks

and the energy of a single secondary particle. Since the energy of more than one secondary particle is usually measured, the value of Q is usually overdetermined. (This fact provides the basis for the demonstration of the equality of the masses of the individual secondary particles mentioned above).

A summary of the available experimental evidence based on data for 39 τ-meson decays observed in emulsions was presented at the Padua conference (AMALDI *et al.* [1954]). The weighted mean value of Q obtained from 25 events observed in stripped emulsions by various groups was: $Q = (74 \pm 0.3)$ MeV. The value obtained from 14 events observed in ordinary plates is in agreement with this value but does not contribute appreciably to the precision of the Q-value. Using $(2m_{\pi^+} + m_{\pi^-}) = (819.3 \pm 0.4)\, m_e$ the authors find $M_\tau = (965.5 \pm 0.7)\, m_e$. As they point out, the error in the Q-value is certainly underestimated because there are known sources of systematic error which have not been taken into account.

The major uncertainty in the primary mass appears to lie in the range energy relation on which the determinations of Q are based, see discussion § 3.7. In the case of the τ-meson the effect is minimized because the energy release is small compared to the total mass of the secondary π-mesons and thus contributes proportionally less to the error in primary mass. Nevertheless it is estimated that the uncertainty in the mass of the τ-meson arising from the lack of knowledge of the range energy relation is $\pm$ 6 m_e (CALDWELL [1955a]).

1. 3 ALTERNATE MODES OF DECAY

In addition to the normal decay into three charged π-mesons the τ-meson is expected to decay into a single charged and two neutral π-mesons. This process is discussed in a following section. We consider here the possibility of anomolous decays which involve three charged secondary particles. A single event of this kind has been reported (R. R. DANIEL and YASH PAL [1954]). Although the decay apparently occurred at rest, the three secondaries were not coplanar. Two of the secondary particles stopped and underwent π-μ-e decay. The negative secondary escaped from the emulsion; its mass from ionization and scattering was $(315 \pm 75)\, m_e$. Under the assumption that the negative particle was a π^--meson the sum of the kinetic energies of the charged secondaries was only (46.1 ± 2.2) MeV. It is impossible to interpret the event as a decay

in flight and the possibility that it represents a K^--capture seems quite unlikely. There remains the hypothesis, that a τ-meson decayed into three charged π-mesons and an additional neutral particle. If this neutral particle were as heavy as a μ-meson, the mass of the parent particle would have to be about 1110 m_e. Since the direct mass measurement on the primary yielded a value of (980 ± 50) m_e it is safe to assume that the rest mass of the neutral particle was zero.

If the parent particle is assumed to be a τ-meson which decays into three π-mesons and a *single* massless neutral particle the Q-value is found to be (78.2 ± 4.9) MeV. If there were additional neutral particles emitted in the decay, the Q-value would be larger than the above value unless the neutral particles were all emitted in the same direction or unless all but one were produced at rest.

Daniel and Pal suggest that the event indeed represents an alternate decay mode of the τ-meson and they assume that the neutral particle is a γ-ray (a neutrino is ruled out as the neutral product from spin considerations):

$$\tau^+ \rightarrow 2\pi^+ + \pi^- + \gamma + Q.$$

The possibility that a photon of such an energy arises from a radiative process during the decay is extremely small, but on the basis of one event cannot be completely ruled out.

1. 4 Charge of the τ-meson

If all τ-mesons were positive and if there were no bias in observing the unlike particle, 2/3 of the stopped π-meson secondaries should be positive and undergo π-μ-e decay; the remaining 1/3 should be negative and should produce σ-stars ($\sim$80%) or no visible interaction ($\sim$20%). In 28 events reported at the Padua conference 54 π-meson secondaries stopped in the emulsion. The ratio of positive π-mesons to the total number of stopped secondaries is 35/54 and the corresponding ratio of negative π-mesons is 19/54. This is consistent with the assumption that all τ-mesons which decay at rest in emulsions are positive.

More detailed statistical arguments applied to groups of events in which the signs of one, two, or three of the secondary particles can be determined reinforce this conclusion and yield the result that probably at least 88% of the 28 τ-mesons considered were positive (Amaldi *et al* [1954]). The secondary particles in the six

completely identified events so far reported fall into the class $(+\,+\,-)$ and no event of the class $(+\,-\,-)$ has been found. Furthermore if a negative τ-meson decays after being captured into a bound orbit by a nucleus, the coplanarity of the decay is in general destroyed (DALITZ [1953a]). No appreciable number of non-coplanar events has been observed. For these reasons one concludes that the majority of the τ-mesons which are observed to decay in emulsions are positive.

On the other hand the *decay in flight* of both positive and negative τ-mesons has been observed in cloud chambers; twelve positive, seven negative, and one case in which the sign could not be determined have been reported. A few of the negative events can be analyzed rather well and the existence of the negative τ-meson is certain.

The absence of τ^--decays in emulsions can then be accounted for in two ways: (a) at low energies the τ^+-meson is produced preferentially, or (b) the τ^--meson undergoes nuclear capture. If (a) is correct, the τ^+-meson is produced predominately at low energies and the production of the negative particle increases with energy. This hypothesis is consistent with the emulsion and cloud chamber evidence. It would account for the relative scarcity of well measurable negative events in the cloud chamber data, and since the emulsion events result from low energy particles they would then be mostly positive. If (b) is correct, there is no way to distinguish cases of τ^--absorption from the absorption of K^--particles in general (see § 6). This hypothesis is also consistent with the experimental results. In either case the actual ratio of positive to negative particles cannot be determined from the present data.

1. 5 SPIN AND PARITY

Some important consequences concerning the possible relations among K-mesons follow from conservation of spin, j, and parity, w. For the normal τ-decay into three charged π-mesons the conservation of angular momentum and parity gives the result that the case of zero spin and even parity, $(0, +)$, is forbidden and that all other possibilities are allowed.* On the other hand a K-meson

* For the application of the conservation laws, including isotopic spin, to processes of spontaneous decay see MICHEL: Proceedings of the Bagnères Conference, pp. 272–279, 1953. Also MICHEL, Ch. 3, Progress in Cosmic Ray Physics, Vol. I, pp. 154, 158, and for the specific case of the τ-meson, DALITZ [1953b] and FABRI [1954].

can decay into two π-mesons only under the condition $w = (-1)^j$. Table II lists allowed and forbidden modes of decay for some assumed values of j and w.

The distribution of energy among the decay products has been calculated for various combinations of j and w (DALITZ [1953b]; FABRI [1954]), and, in principle, a comparison of the experimental data with the predicted distribution can be used to determine the spin and parity of the τ-meson.

TABLE II

Possible modes of decay of charged K-mesons for various combinations of spin and parity

K-meson		Possible Decay Modes	
Spin	Parity	Allowed	Forbidden
0	+	$K^\pm \to \pi^\pm + \pi^0$	$K^\pm \to 2\pi^\pm + \pi^\mp$ $K^\pm \to \pi^\pm + \gamma$
0	−	$K^\pm \to 2\pi^\pm + \pi^\mp$	$K^\pm \to \pi^\pm + \pi^0$ $K^\pm \to \pi^\pm + \gamma$
1	+	$K^\pm \to 2\pi^\pm + \pi^\mp$ $K^\pm \to \pi^\pm + \gamma$	$K^\pm \to \pi^\pm + \pi^0$
1	−	$K^\pm \to 2\pi^\pm + \pi^\mp$ $K^\pm \to \pi^\pm + \gamma$ $K^\pm \to \pi^\pm + \pi^0$	
even > 2 odd > 3	+ −	$K^\pm \to 2\pi^\pm + \pi^\mp$ $K^\pm \to \pi^\pm + \pi^0$ $K^\pm \to \pi^\pm + \gamma$	
even > 2 odd > 3	− +	$K^\pm \to 2\pi^\pm + \pi^\mp$ $K^\pm \to \pi^\pm + \gamma$	$K^\pm \to \pi^\pm + \pi^0$
Any	+ or −	$K^\pm \to \mu^\pm + \nu$ $K^\pm \to \mu^\pm + \nu + \gamma$	

The original procedure of comparing the experimental and theoretical results was suggested by Dalitz and is applicable when the energies of the three π-meson secondaries are known but the charges of individual secondaries are not distinguishable. Because of the small amount of information provided by individual events the method is not very sensitive. Fortunately in the more recent data the unlike particle is usually identified, and, in this case, a direct comparison of the observed energy spectrum with the various theoretical energy distributions provides a sensitive test for j

and w. Additional statistically independent evidence can be obtained from angular correlations between the secondary particles. Dalitz has considered, in addition to the energy distribution of the unlike particle, the expected distribution of the angle between the relative motion of the two like mesons and the motion of the unlike meson.

He concludes (DALITZ [1955]) that the experimental data are consistent with the predicted angular and energy distributions for the cases (0, −), (2, · −), (4, −) and (3, +); (1, +) is less likely and (4, +) very improbable, while (1, −), (2, +) and (3, −) are certainly ruled out. Thus the simplest possibility is that the τ-meson is pseudoscalar, (0, −). Among the first five possibilities mentioned above the decay into two π-mesons is allowed only for (4, +), hence the identity $\chi \equiv \tau$ is not possible unless $j \geqslant 4$.

1. 6 LIFETIME OF THE τ-MESON

The mean life of the τ-meson appears to lie in the region of 10^{-8} to 10^{-9} sec, but no good evaluation of the exact value is available. In cloud chamber measurements the ratio of decays at rest to decays in flight cannot be well determined since decays at rest are difficult to detect. In emulsions just the opposite situation prevails and decays in flight are very likely to be missed. In single emulsions, decays in flight would most probably be interpreted as four prong stars since the direction of motion of the primary particle is then difficult to establish. In emulsion stacks, the decay of a τ-meson in flight lacks many of the identifying features of a decay at rest and certainly becomes more difficult to find and identify as the velocity of the τ-meson increases.

Thus although the total slowing down time for the 21 τ-meson decays observed in emulsion stacks and reported at the Padua Conference (AMALDI *et al.* [1954b]) was 4.2×10^{-9} sec, only a small amount of the track length involved was scanned for decays in flight and no exact conclusion about the lifetime is possible.

However, a mean life of 10^{-9} sec implies that in the plates from which the above 21 events were obtained $\sim$5 decays have occurred and escaped detection. For a mean life of 10^{-10} sec there must have been about 130 decays in flight. Since in the emulsion data only one example of a τ-meson which decayed in flight has been reported (CECCARELLI *et al.* [1954]), one concludes that, even though the bias against decays in flight is high, the mean life cannot be much

shorter than 10^{-9} sec. On the other hand τ^+-mesons which are observed to decay in flight in cloud chambers have each lived about 10^{-9} sec before decay. It is unlikely that the mean life is much longer or shorter than this value for then τ-mesons would constitute too great a fraction of the secondaries from nuclear interactions of moderate energy. The number of decays in flight is as yet too small to yield a significant mean life by comparing the actual lifetimes with the potential values (§ 4.1).

2, 3, 4, DECAY EVENTS PRODUCED BY K-MESONS AND CHARACTERIZED BY THE EMISSION OF A SINGLE CHARGED SECONDARY PARTICLE

2. Results concerning S-events; Observations with Photoemulsions

2.1 The alternate mode of decay of the τ-meson

Shortly after the discovery of the τ-meson it was pointed out that the alternate decay mode,

$$\tau^{\pm} \rightarrow \pi^{\pm} + 2\pi^0,$$

should exist (Pais [1952]). The frequency of this occurrence relative to that of the normal decay into three charged π-mesons has been calculated by (Dalitz [1953a and 1953c]). Assuming that the hypothesis of charge independence is valid, Dalitz found that the ratio of the alternate to the normal mode lies between the limits 0.25 to 1.00.

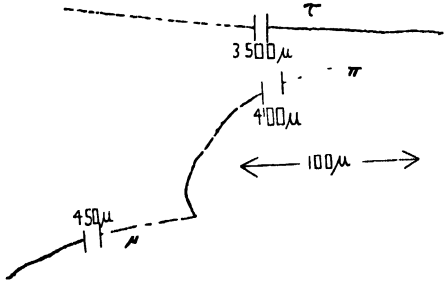

Fig. 1 – Schematic reproduction of the first event interpreted in terms of the alternate decay mode of the τ-meson, (Crussard *et al.* [1953]).

The first example of an S-event which could be interpreted in terms of this process was reported by the Rochester group (Crussard *et al.* [1953]). A schematic representation of the event is shown in Fig. 1. A K-meson came to rest in the emulsion and emitted a single low energy π^+-meson. The identification of

the secondary particle is certain because it stopped and gave rise to the characteristic π-μ-e decay.

It is always possible to interpret a single event of this nature as the nuclear absorption of a negative K-particle, (§ 6), although such an explanation appears very unlikely because of the absence of low energy fragments. For this reason Crussard *et al.* considered that their event probably represented an example of the decay process considered by Dalitz. Several other events similar to that of the Rochester group have been found and are listed in Table III. It is clear that the secondary particles are distributed in energy and thus the existence of a K-meson which decays into a charged π-meson and two or more neutral particles is established. Whether or not the events result from τ-mesons is not yet certain but appears very probable.

TABLE III

Examples observed in emulsions of stopped π-meson secondaries from K-*mesons*
These events can be interpreted in terms of the alternate decay of the τ-meson

Primary Particle		Secondary Particle		
Event	Mass m_e	Kinetic Energy MeV	$p\beta$ MeV/c	Behaviour on stopping
Cornell	—	4.3	8.4	π - μ - e
Genoa-Milan	—	41.5	73	π - μ - e
Padua	* 966 ± 100	6.0	11.8	π - μ - e
Paris	* 961 ± 51	22.3	41.5	π - μ - e
Rochester	* 951 ± 61	14.7 ± 0.3	28	π - μ - e
Rochester	* 1202 ± 58	15.2 ± 0.3	29	π - μ - e
Rome	* 1023 ± 56	38.5 ± 2.5	69	3-prong sigma star; could be K⁻-capture

* Weighted mean.

The frequency with which the alternate mode of decay has been observed in emulsions is about 0.1 to 0.2 times that of the normal mode. However, the detection probabilities for the two events are different. The normal mode of decay is more conspicuous because of the three coplanar π-mesons; in addition some of the events have been found by tracing back along tracks which produce π-μ decay or σ-stars. If the scanning is done in this manner the normal mode of decay is favoured because three charged secondaries instead of one are available for tracing.

Taking into account the experimental bias, the observed ratio of events is considered to be in agreement with the prediction of

Dalitz (DILWORTH *et al.* [1954a]). In any event the experimental evidence shows that the ratio cannot be much greater than unity.

2. 2 THE $\varkappa$-MESON

In 1951, O'CEALLAIGH observed two S-events which could not be interpreted in terms of the known decay processes of either π- or μ-mesons: In one event, Bristol K-2, a primary particle apparently decayed into a μ-meson whose range was about twice as great as that normally observed in the π-μ decay process. The identification of the secondary particle was certain because it stopped and decayed into an electron. The mass of the primary particle as determined from measurements of scattering versus range, and ionization versus range, was 1125 m_e.

In the other event, Bristol K-1, a particle whose measured mass was $\sim$1300 m_e stopped and produced a fast secondary particle which left the emulsion without coming to rest. Its $p\beta$ determined from the observed scattering was $\sim$250 MeV/c. The secondary particle could not be certainly identified but must have been a light meson or an electron. As the simplest explanation of these observations O'Ceallaigh assumed that the two events were examples of the same decay process in which a heavy meson of mass $\sim$1200 m_e decayed into a μ-meson. And, since the energies of the secondary particles were widely different in the two cases, he postulated a three-body decay scheme, *viz.*, $\varkappa \rightarrow \mu$ + neutral particles. The existence of this decay scheme has been firmly established by subsequent observations and data for 4 examples in which the μ-meson comes to rest in the emulsion are given in Table IVa. It is clear that the secondary μ-mesons are distributed in energy and that the decay is therefore not a two-body process.

The most important evidence concerning the $\varkappa$-meson is derived

TABLE IVa

Examples of stopped μ-meson secondaries from K-*mesons*

Event	Primary Mass m_e	Secondary		
		Kinetic Energy MeV	$p\beta$ MeV/c	Behaviour on stopping
Paris	* 1172 ± 56	33.3	58.6	μ - e
Rochester	980 ± 130	28	50.1	μ - e
Rome	* 942 ± 36	13.6 ± 0.3	25.6 ± .6	μ - e
Bristol	* 1125 ± 126	6	11.7	μ - e

* Weighted mean from several different methods of mass measurement.

TABLE IVb

Probable μ-meson secondaries identified by scattering and ionization

Event	Primary Mass m_e	Secondary $p\beta$ MeV/c	Secondary Mass m_e
Bristol K-5	* 1000 ± 180	66 ± 11	220 ± 20
Bristol K-24	* 1260 ± 80	119 ± 9	203 ± 8
Genoa-Milan K-12	750 ± 160	144 ± 12	222 ± 23
Padua K-8	* 1100 ± 120	149 ± 8	197 ± 25

* Weighted mean from several different methods of mass measurement.

from the events just considered in which the charged secondary particles have a low enough energy so that they come to rest in the emulsion. For, in these cases, the identification of the particle can be based on the characteristic behaviour of stopped μ- or π-mesons (decay or nuclear absorption), and is usually unambiguous. There are however many events in which the secondary particle leaves the emulsion without coming to rest, and then the particle identification depends on measurements of scattering and ionization. As the particle energy increases each of these quantities becomes insensitive to the mass, and as a result it is difficult to distinguish between π- and μ-mesons above a kinetic energy of about 100 MeV. Mu-mesons, π-mesons, and electrons have all been identified among the higher energy secondaries which leave the emulsion before stopping, but in most cases in which the secondary particle does not come to rest it cannot be identified. It is therefore difficult to know how many of these events result from κ-mesons.

Data for ~80 events in which the charged decay product does not stop in the emulsion are included in Table V. Although there are about a dozen cases in which the secondary particle appears to be a μ-meson rather than a π-meson or an electron, only a very few of these are surely identified. Events Bristol K-5, Bristol K-24, and Padua K-8 (with values of $p\beta$ equal to (66 ± 11), (119 ± 9), and (149 ± 8) MeV/c respectively) provide the best evidence for the existence of higher energy μ-meson secondaries. For convenience data concerning these last events are included in Table IVb.

We return to the questions of the energy distribution and the composition of the higher energy secondaries in a following section. From the results considered above it follows that the κ-meson is a particle of mass about 1000 m_e which decays into a μ-meson and two or more neutral particles whose nature is unknown.

TABLE V

K-mesons observed in emulsions

Data are given for those events in which significant measurements could be made on the charged secondary particle

	Primary Particle				Secondary Particle			
Reference	Event	Origin	Length mm	Mass m_e	Length mm	$p\beta c$ MeV	g^*	Mass m_e
Bombay (1, 2)	*K-1	20 + 5n	13.7	1130 ± 130[a] 955 ± 140[b] 950 ± 100[d]		226 ± 20		
(3)	*K-6	21 − 3p	5.0	1050 $^{+280}_{-200}$	25	240 ± 25	1.045 ± 0.02	
Bristol (4)	*K-1	—	4.10	1260 ± 260[a] 1380 ± 180[c]	2.2	235 ± 35	0.97 ± 0.04	
	K-2	—	5.67	1125 ± 230[a] 1125 ± 150[c]	1.1	11.8	—	$\mu \rightarrow e$
	K-3	—	0.53	1000 — 2000	5.9	144 ± 12	0.96 ± 0.26	170 ± 30
	K-5	—	1.54	1220 ± 400[a] 950 ± 200[c]	8.9	66 ± 11	1.705 ± 0.083	220 ± 20
	K-7	—	0.38	~1000	2.5	170 ± 29	1.090 ± 0.050	250 ± 50
	K-8	—	2.55	1460 ± 320[a] 900 ± 200[c]	7.65	187 ± 17	1.140 ± 0.025	330 ± 30
	K-9	—	0.63	~1000	19.5	162 ± 9	1.094 ± 0.016	265 ± 12
	K-14	—	3.44	925 ± 190[a]	0.5	120 ± 44	1.02 ± 0.10	
	K-15	—	9.56	1100 ± 170[a]	4.1	184 ± 30	1.028 ± 0.031	
	K-16	—	1.70	~1100	2.8	153 ± 24	1.030 ± 0.045	210 ± 35
	K-17	—	4.31	1200 ± 230[a]	6.5	172 ± 17	1.15 ± 0.03	295 ± 25
	K-18	—	1.85	~1500	4.0	315 ± 70	~1	
	K-19	—	1.02	1000 — 2000	0.8	125 ± 35	~1	
(5, 6)	K-21	—	0.35	1000 — 2000	18	205 ± 15	0.93 ± 0.02	
	*K-22	1 − 0p 1 + 0n	28.	780 ± 90[a]	6	170 ± 20	1.09 ± 0.04	280 ± 20
(5, 7)	*K-24	10 + 0p	8.56	1400 ± 200[a] 1380 ± 200[b] 1200 ± 100[d]	54	°119 ± 9	1.2 to 1.5	203 ± 8
(8)	*K-31	12 + 3n	19.09	900 + 200[f]		145 + 25		
(9)	*K-37	4 + 0n	8.7	800 ± 150[a] 720 ± 190[b] 1050 ± 100[e]	23	88.5 ± 6	1.01 ± 0.02	probable electron
(10)	*K-44	12 + 3p	11.49	1139 ± 100[d]	51.2	155 ± 10	0.98 ± 0.02	
(10, 11)	*K-46	19 + 6p	11.79	690 ± 160[a] 760 ± 110[b] 970 ± 100	25.6	49 ± 4 to 17 ± 2	1.00 ± 0.04	$e^{\pm}$
Brussels (5)	K-4	—	20.0	1100 ± 110[b]	5.0	200 ± 30	1.09	
Copenhagen (12, 13)	*K-1	—	1.4	1680 $^{+760}_{-530}$[b]	21.0	†190 ± 20	0.93 ± 0.02	
	*K-3	12 + 2p	3.0	1000 ± 300[b] 1110 ± 160[e]	52.	°220 ± 13	°0.95 ± 0.01	probable μ
	*K-5	11 + 12p	30.	850 ± 140[b] 996 ± 29 [c]	58.	°170 ± 8	°1.12 ± 0.01	π
(13)	*K-7	16 + 2n	44.	1290 ± 210[b] 998 ± 30 [c]	32.	°221 ± 16	°1.02 ± 0.02	probable π
	*K-12	17 + 2p	36.	740 ± 130[b] 969 ± 29 [c]	46.	°215 ± 13	°0.94 ± 0.01	probable μ
	*K-14	6 + 2p	22.	1200 ± 200[b]	52.	°233 ± 15	°0.97 ± 0.02	probable μ
	*K-20	3 + 3p	8.1	890 ± 140[b] 968 ± 59[c]	78.	°227 ± 10	°0.95 ± 0.01	probable μ
Cornell (14)	K-2	—	0.52		4.7	172 ± 26	1.07 ± 0.03	280 ± 50
	K-3	—	0.12		2.5	24.5 ± 2.5	2.75 ± 0.08	191 ± 30
	K-7	—	0.44		0.64	111 ± 35	1.1 ± 0.1	190 ± 60
	K-8	—	0.32				E_π = 4.3 MeV	$\pi \rightarrow \mu \rightarrow e$
Dublin (15)	*K-	10 + 4n	9.2	1010 $^{+190}_{-130}$ 970 ± 70	9.	81 ± 9	0.99 ± 0.03	$e^{\pm}$
Genoa-Milan (16)	K-1	—	2.0	1270 ± 290[b]	3.44	150 ± 27	0.094 ± 0.03	
	K-3	34 + 6p	1.88	1540 ± 380[b] 1170 ± 270	2.08	108 ± 18	1.14 ± 0.03	190 ± 32
	K-4	—	1.47	1360 ± 340[b]	2.5	200 ± 33	1.06 ± 0.04	300 ± 50
17, 18)	*K-9	7 + 0p	19.24	990 ± 200[b]	51.5	°174 ± 16	1.14 ± 0.014	278 ± 31
	*K-10	—	18.50	910 ± 220[b]	40.1	°216 ± 22	0.96 ± 0.017	assumed μ
	*K-11	14 + 2p	18.33	1030 ± 210[b]	53	°207 ± 18	0.97 ± 0.015	assumed μ
	*K-12	4 + 2p	15.85	750 ± 160[b]	46	°144 ± 12	1.25 ± 0.020	222 ± 23

(Continued)

TABLE V (*Continued*)

Reference	Primary Particle: Event	Origin	Length mm	Mass m_e	Secondary Particle: Length mm	$p\beta c$ MeV	g^*	Mass m_e
(18)	*K-15	31 + 9p	8.15	750 ± 190[b]	56.6	°216 ± 18	0.98 ± 0.013	assumed μ
	*K-19	22 + 7?	3	990 ± 390[b]	56.2	°217 ± 21	0.98 ± 0.016	assumed μ
	*K-21	18 + 5p	18.9	550 ± 200[b]	64.3	°195 ± 17	0.98 ± 0.015	assumed μ
	*K-22	17 + 7α	8.8	1690 ± 510[b]	18.3	°200 ± 27	0.96 ± 0.024	assumed μ
(19)	*K_π+-1	17 + 7p	7	§600 ± 160[b]	26		E_π = 41.5 MeV	$\pi \to \mu \to e$
Manchester								
(6, 20)	K-3	—	3.28	1030 ± 300[b]	9.1	124 ± 12	1.010 ± 0.05	
Oslo								
(21)	K-1	16 + 3p	14.0	970 ± 130[a] 1090 ± 180[b]	2.5	126 ± 21	1.05 ± 0.03	200 ± 20
Padua								
(22, 23)	*K-3	20 + 7n	42.5	964 ± 60 [d]	21.0	160 ± 9		278 ± 33
(22)	*K-4	15 + 1p	19.14	961 ± 122[f] 975 ± 200[d]	40.0	110 ± 15		
	*K-5	4 + 1p	19.31	920 ± 330[f] 1006 ± 100[d]	37.5	70 ± 16		
	*K-6	14 + 11p	17.24	865 ± 290[f] 850 ± 100[d]	44.4	52 ± 20		
(22, 23)	*K-7	5 + 1p	36.5	948 ± 100[f] 943 ± 60 [d]	24.0	159 ± 10		272 ± 30
	*K-8	15 + 7α	26.92	895 ± 225[f] 1180 ± 140[d]	44.4	149 ± 8		197 ± 25
(22)	*K-9	17 + 2p	12.02	1420 ± 360[f] 1060 ± 100[d]	21.0	153 ± 36		
	*K-10	10 + 5p	25.2	1100 ± 160	10.0	67 ± 15		
(22, 23)	*K-11			1132 ± 100[f]	44.8	172 ± 9		289 ± 28
(24)	*K_π+-1	8 + 3n	13.0	966 ± 100[f]	0.9		E_π = 6 MeV	$\pi \to \mu \to e$
Paris								
(25, 26, 28)	K-1	—	1.30	900 ± 300[b] 1150 ± 300[e]	20.0	197 ± 13	0.97 ± 0.030	216 ± 26
	K-6	—	1.40	810 ± 265[b] 970 ± 150[c] 960 ± 220[e]	3.40	290 ± 60	0.975 ± 0.050	
(27, 28)	*K-13		19.25	1390 ± 370[b] 960 ± 130[c] 870 ± 87 [d] 881 ± 80 [e]	22.00	°207 ± 33	°0.953 ± 0.033	233 ± 36
(27, 28, 29)	*K-14		13.2	895 ± 190[b] 1300 ± 175[c] 1115 ± 85 [d] 1240 ± 90 [e]	23.2		E_μ = 33.3 MeV	$\mu \to e$
(27, 28)	*K-17	3 + 6p	14.00	1000 ± 190[c] 1060 ± 145[d]	73.00	°216 ± 15	°0.918 ± 0.034	195 ± 14
	*K-22			995 ± 170[b] 920 ± 120[c] 983 ± 80 [e]	35.75	°205 ± 13	°0.939 ± 0.031	206 ± 24
	*K-23	7 + 0n	29.50	1210 ± 280[b] 1150 ± 190[c] 895 ± 90 [d] 855 ± 80 [e]	15.00	°166 ± 18	°1.087 ± 0.027	280 ± 21
(28, 30)	*K-32	21 + 1p	7.0	1280 ± 195[b] 930 ± 130[c] 920 ± 130[d] 947 ± 65 [e]	9.66		E_π = 22.3 MeV	$\pi \to \mu \to e$
Rochester								
(31)	*K-5		31.8	968 ± 200[h]		140 ± 10	1.19 ± 0.03	272 ± 25**
(31, 32)	*K-7	2 + 3p	20.2	982 ± 130[i]	16.63		E_μ = 28.0 MeV	$\mu \to e$
(31, 33)	*K-12	10 + 7n	22	940 ± 235[h] 912 ± 89 [i]	46	°261 ± 34	°0.96 ± 0.03	187 ± 30 $e^\pm$
(34)	*K_π+-1		16.	930 ± 170[a] 1070 ± 25 [b] 940 ± 100[c]	4.3		E_π = 14.7 ± 0.26 MeV	$\pi \to \mu \to e$
(31, 32, 35)	*K_π+-2	2 + 0p (2 + 1n)	13.8	1550 ± 100[h] 995 ± 100[i]	4.6		E_π = 15.2 ± 0.27 MeV	$\pi \to \mu \to e$
(33)	*K-20	5 + 0n	4.8	—	37.	°210 ± 40	°1 ± 0.06	$e^\pm$
	*K-21	16 + 9p	15.	1270 ± 290 840 ± 145	0.4	°20 ± 5	°1.06 ± 0.2	e^+
Rome								
(36, 37)	††*K-1	16 + 8n	12.1	1040 $^{+240}_{-180}$[b] 1020 ± 65 [d]	23.2		E_π = 38.5 ± 2.5 MeV	$\pi^- \to$ 3 prong σ-star

(*Continued*)

TABLE V (*Continued*)

	Primary Particle				Secondary Particle			
Reference	Event	Origin	Length mm	Mass m_e	Length mm	$p\beta c$ MeV	g*	Mass m_e
(37)	*K-2		24.6	935 ± 40 [d]	29		1.24 ± 0.07 at decay 1.36 ± 0.08 after 29 mm	
	*K-3	14 + 6n	20.2	$1020 \begin{smallmatrix}+150\\-120\end{smallmatrix}$ [b] 860 ± 35 [d] 980 ± 60 [c]	18.	230 ± 30	1.07 ± 0.06	
	*K-4	6 + 0p	35.7	$720 \begin{smallmatrix}+120\\-90\end{smallmatrix}$ [b] 950 ± 50 [d] 1000 ± 60 [c]	4.83		$E_\mu = 13.6 \pm 0.3$ MeV	$\mu \rightarrow e$
Turin (38)	K-1	27 + 9p	5.70	1020 ± 270[b] 1165 ± 130[c]	2.00	°104 ± 24	0.974 ± 0.033	

Primary mass determinations by the following methods:

a. multiple scattering vs. residual range; constant cell length.
b. multiple scattering vs. residual range; variable cell length.
c. gap length vs. residual range.
d. grain or blob density vs. residual range.
e. photometric determination of ionization vs. residual range.
f. average of determinations by methods a. and b.
g. multiple scattering vs. ionization.
h. multiple scattering vs. residual range, exact method not stated
i. ionization vs. residual range, exact method not stated.

* indicates stripped emulsion.
† $p\beta$ measurement considered unreliable.
§ systematic error unknown; steep track.
** Bristol calibration assumed.
†† can be interpreted as capture of K^--meson instead of decay.
° evaluated at the point of decay.

References to Table V

(1) LAL, D., Y. PAL and B. PETERS, 1953, Phys. Rev., **92**, 438.

(2) BISWAS, S., E. C. GEORGE and B. PETERS, 1953, Proc. Ind. Acad Sci., **38**, 418.

(3) DANIEL, R. R., A. KRISHNAN, S. MITRA and YASH PAL, 1954, Nuovo Cim., **12**, supplement no. 2, 231.

(4) MENON, M. G. K. and C. O'CEALLAIGH, 1954, Proc. Roy. Soc., A, **221**, 292.

(5) Bagnères Conference, 1953, report, 223.

(6) POWELL, C. F., 1954, Nuovo Cim., **11**, supplement no. 2, 192.

(7) RENARDIER, M., 1953, Bagnères Conference mimeographed report, 158.

(8) DILWORTH, C., G. P. S. OCCHIALINI and L. SCARSI, 1954, Annual Review of Nuclear Science, **4**, 296.

(9) FRIEDLANDER, M. W., D. KEEFE, M. G. K. MENON and L. VAN ROSSUM, 1954, Phil. Mag., **45**, 1043.

(10) DAHANAYAKE, C., P. E. FRANÇOIS, Y. FUJIMOTO, P. IREDALE, C. J. WADDINGTON and M. YASIN, 1955, Nuovo Cim., **1**, 888.

(11) DAHANAYAKE, C., P. E. FRANÇOIS, Y. FUJIMOTO, P. IREDALE, C. J. WADDINGTON and M. YASIN, 1954, Phil. Mag., **45**, 1219.

(12) BØGGILD, J. K., J. E. HOOPER and M. SCHARFF, 1954, Nuovo Cim., **12**, supplement no. 2, 224.

(13) BØGGILD, J. K., J. E. HOOPER, W. C. G. ORTEL and M. SCHARFF, 1955, Nuovo Cim., **1**, 1267; Dan. Mat. Fys. Medd., to be published.

(14) BARRETT, P., 1954, Phys. Rev., **94**, 1328.

(15) JOHNSTON, R. H. W. and C. O'CEALLAIGH, 1955, Phil. Mag., **46**, 393.

(16) BONETTI, A., R. LEVI SETTI, M. PANETTI and G. TOMASINI, 1954, Proc. Roy. Soc., A, **221**, 318.

(17) BONETTI, A., R. LEVI SETTI, B. LOCATELLI and G. TOMASINI, 1954, Nuovo Cim., **12**, supplement no. 2, 227.

(18) BONETTI, A., R. LEVI SETTI, B. LOCATELLI and G. TOMASINI, 1955, Nuovo Cim., **1**, 904.

(19) DICORATO, M., C. C. DILWORTH and L. SCARSI, 1954, Nuovo Cim., **12**, supplement no. 2, 202.

(20) BARKER, K. H., 1953, Duke Conference, report.

(21) ISACHSEN, N., P. VANGEN and S. O. SORENSEN, 1953, Phil. Mag., **44**, 224.

(22) BALDO, M., G. BELLIBONI, B. SECHI and G. T. ZORN, 1954, Nuovo Cim., **12**, supplement no. 2, 220.

(23) BALDO, M., G. BELLIBONI, M. CECCARELLI, M. GRILLI, B. VITALE and G. T. ZORN, 1954, private communication.

(24) BELLIBONI, G., B. SECHI and B. VITALE, 1954, Nuovo Cim., **12**, supplement no. 2, 195.

(25) CRUSSARD, J., L. LEPRINCE-RINGUET, D. MORELLET, A. ORKIN-LECOURTOIS and J. TREMBLEY, 1953, C. R. Acad. Sci. Paris, **236**, 872.

(26) CRUSSARD, J., L. LEPRINCE-RINGUET, D. MORELLET, A. ORKIN-LECOURTOIS and J. TREMBLEY, 1953, Phys. Rev., **90**, 1127.

(27) HOANG, T. F., L. JAUNEAU, G. KAYAS, A. ORKIN-LECOURTOIS, L. LE-

PRINCE-RINGUET, D. MORELLET, G. TARIEL and J. TREMBLEY, 1954, Nuovo Cim., **12**, supplement no. 2, 242.

(28) HOANG, T. F., L. JAUNEAU, J. JOUVIN, G. KAYAS, L. LEPRINCE-RINGUET, D. MORELLET, A. ORKIN-LECOURTOIS and J. TREMBLEY, 1954, private communication; see also, 1955, Nuovo Cim., **1**, supplement no. 3.

(29) HOANG, T. F., L. JAUNEAU, G. KAYAS, L. LEPRINCE-RINGUET, D. MORELLET, A. ORKIN-LECOURTOIS and J. TREMBLEY, 1954, C. R. Acad. Sci. Paris, **238**, 1633.

(30) HOANG, T. F., L. JAUNEAU, G. KAYAS, L. LEPRINCE-RINGUET, D. MORELLET, A. ORKIN-LECOURTOIS, G. TARIEL and J. TREMBLEY, 1954, Nuovo Cim., **12**, supplement no. 2, 208, 432.

(31) CRUSSARD, J., M. F. KAPLON, J. KLARMANN and J. H. Noon, 1954, private communication.

(32) CRUSSARD, J., M. F. KAPLON, J. KLARMANN and J. H. NOON, 1954, Phys. Rev., **95**, 584.

(33) KAPLON, M. F., J. KLARMANN and G. YEKUTIELLI, 1955, Phys. Rev., **99**, 1528.

(34) CRUSSARD, J., M. F. KAPLON, J. KLARMANN and J. H. NOON, 1954, Phys. Rev., **93**, 253.

(35) Report of the Committee on τ-mesons, Padua Conference, 1954, Nuovo Cim., **12**, supplement no. 2, 432.

(36) AMALDI, E., G. BARONI, C. CASTAGNOLI, G. CORTINI, C. FRANZINETTI and A. MANFREDINI, 1954, Nuovo Cim., **11**, 207.

(37) AMALDI, E., G. CORTINI and A. MANFREDINI, 1954, private communication; see also, 1954, Nuovo Cim., **12**, supplement no. 2, 210.

(38) DEBENEDETTI, A., C. M. GARELLI, L. TALLONE and M. VIGONE, 1954, Nuovo Cim., **12**, 374.

2. 3 THE MASS OF THE $\varkappa$-MESON

It will be noted from the data in Table IVa that the quoted mass values for the primary particles show a spread which is considerably greater than that expected from the statistical errors.

The weighted mean value of the primary mass for the Paris event is $(1172 \pm 56)\ m_e$ while that of the Rome event is $(942 \pm 36)\ m_e$. Since the different mass determinations for individual events are not strictly independent, the accuracy of the above values is probably overestimated. Nevertheless, the difference in the mass values is difficult to explain on statistical grounds.

This situation is at the moment characteristic of single events observed in emulsions; the measurements are subject to uncontrolled systematic errors considerably greater than those arising from the statistical nature of the energy loss or multiple scattering. Some of this difficulty apparently arises from the fact that the

functional relation between grain or blob density and the residual range of the particle depends on the particular emulsion batch, on the exact development procedure, and on other factors. Therefore a laborious calibration must be carried out for each series of plates and this has not always been done. The same comments apply, though to a lesser extent, to the value of the scattering constant which enters into the determination of mass by scattering and residual range.

In addition the validity of the scattering theory, as applied in emulsion work for particles of moderate and high velocities, has not yet been adequately verified. This is particularly true in respect to the shape and width of the $p\beta$ distribution, and in regard to mass values derived from measurements of scattering and ionization; at present the magnitude and frequency of the fluctuations in these measurements are unknown.

Because of these uncertainties no definite conclusion can be drawn from differences in mass values for individual events which are apparently statistically significant. Similarly, the systematic errors in the mass values derived for groups of K-mesons are largely unknown. For example the mean mass value for K-mesons obtained by scattering and range has been reported to be significantly higher than the value obtained using ionization and range (DILWORTH *et al.* [1954b]). On the other hand results of the Paris group (HOANG *et al.* [1955]) do not support such a conclusion; mass measurements by the above two methods show no significant differences. However the Paris photometric determination seems to give results which are systematically slightly lower than the other methods employed (grain density *vs.* range, gap density *vs.* range, and scattering *vs.* range).

The magnitude of the systematic errors can be evaluated by a series of measurements on known particles using different methods of mass determination. Several studies of this kind have been made by various workers who have usually used protons or π-mesons as reference tracks. However, no systematic study on a common sample of data has been made by the various groups whose results have been averaged to obtain K-meson masses. A calibration of this kind could be carried out using τ-mesons as a means of standardizing the different methods of mass determination. Since the mass and identification of the τ-meson depend on properties of the secondary particles and not on the measured

mass of the primary particle, the τ-meson is an ideal reference particle.

There is now in progress a very considerable experimental effort directed toward the solution of the problems just mentioned and in the near future one can expect individual measurements of K-particle masses with a precision of a few percent. Until more events and more precise measurements are available the value of the directly measured mass of the $\varkappa$-meson remains an open question. For the same reason nothing can be said concerning possible mass differences between the various K-mesons observed in emulsions.

2. 4 Evidence concerning the χ-meson

It was pointed out above that an unambiguous identification or separation of π- and μ-mesons by measurements of scattering and ionization becomes quite difficult above a kinetic energy of about 100 MeV. Nevertheless, the probable existence of monoenergetic π-meson secondaries in this energy region was reported by Menon and O'Ceallaigh in 1953 (Powell [1952]; Perkins [1952]; Menon and O'Ceallaigh [1953a, 1953b, 1954]).

A detailed analysis and discussion of the experimental evidence on which this hypothesis was based has been given by the authors in the last reference quoted. They noted that the distribution of mass values obtained for 10 fast K-particle secondaries was much broader than one would expect if the secondary particles were a homogeneous group of μ-mesons or π-mesons. To check the accuracy of the mass determinations they used the extensive calibrations carried out by Daniel and Perkins on π-mesons, and from these data they concluded that the width of the mass distribution obtained for the 10 K-particle secondaries could not be accounted for by statistical or systematic errors of measurement. From the individual mass values they were then able roughly to classify each secondary particle as a π-meson or a μ-meson. Those classified as π-mesons had very nearly the same energy while those classified as μ-mesons showed a distinct spread. Menon and O'Ceallaigh therefore assumed that the μ-mesons resulted from decays of $\varkappa$-mesons and they postulated that the π-mesons arose from a K-particle which decayed according to the two-body decay scheme $\chi^{\pm} \rightarrow \pi^{\pm} + \mathrm{N}^0$. The value of $p\beta$ obtained for the secondary particle was (180 ± 7) MeV/c. They considered that the evidence for

the $\varkappa$-decay was "decisive" and that the evidence for the χ-decay was "strong".

The validity of this last conclusion provoked considerable discussion mainly pertaining to the small size of the sample and to the errors which might possibly affect mass determinations in the higher energy region. Most of the calibration measurements were made on π-mesons in a region of $p\beta$ considerably lower than that of the decay products. In addition the majority of the tracks were of necessity short, and the statistical accuracy, particularly of the scattering measurements, was insufficient for good mass resolution. We will not consider these points in any detail since more recent measurements in emulsions and cloud chambers have confirmed the existence of the χ-meson. The evidence from cloud chambers is given in § 3.10. We now consider recent emulsion results concerning the χ-meson in some detail.

The introduction of large stacks of stripped emulsions has provided a significant increase in the statistical accuracy of the scattering measurements and in the case of "flat" tracks, has greatly improved the reliability of the mass determinations. The most recent evidence concerning the χ-meson has been obtained by the Padua group using these methods (Padua emulsion group, CECCARELLI [1954]). In examining two large stacks of stripped emulsions they obtained 13 K-particles which decayed with the emission of a single fast charged secondary particle. Measurements on the secondary particle were carried out if its path length per emulsion was 5 mm or greater and providing that its total length exceeded 2 cm. The first criterion ensures that the track is "flat" enough so that reliable scattering and ionization measurements can be made and the second determines the statistical accuracy. Four of the 13 events satisfied these criteria; the data concerning these are given in Table VI.

To determine the mass of the secondary particle it is necessary to establish experimentally the relationship between the ionization (blob or grain count) and the scattering for a known particle, preferably one whose mass is close to that of the unknown particle. The blob or grain count, I, is usually specified relative to the plateau value I_{pl}. The relative ionization, I/I_{pl}, in a given material is a function of the particle velocity and charge only, and, at constant velocity, $p\beta$ is directly proportional to mass. Therefore, given an experimental relation between I/I_{pl} and $p\beta$ for one particle,

TABLE VI

Data for selected K-*mesons observed by the Padua group*

Event	Primary Particle			Secondary Particle			
	Length mm	Length per plate	Mass (m_e)	Length mm	Length per plate	$p\beta$ (MeV/c)	Mass (m_e)
K - 3	42.6	4.5	964 ± 60	21.0	6.5	160 ± 9	278 ± 33
K - 7	36.5	7.0	945 ± 50	24.0	17.0	159 ± 10	272 ± 30
K - 11	4.9	1.6	1132 ± 100	44.8	10.0	172 ± 9	289 ± 28
Mean			976 ± 36			164 ± 5	
K - 8	27.0	1.7	1100 ± 135	44.4	16.4	149 ± 8	197 ± 25

calibration curves for other masses are obtained using the condition, that, at a particular value of I/I_{pl}, $(p\beta)_1/(p\beta)_2 = m_1/m_2$.

In this case π-mesons from nuclear disintegrations within the stack were selected for calibration particles using the same criteria applied to the K-particle secondaries. A set of such calibration tracks was chosen for each K-particle secondary and it was required that the calibration tracks be within 2 cm of the track to be measured. Scattering measurements were carried out for individual sections of the track about 5 mm in length and the values of $\bar{\alpha}_{100}$ so obtained were normalized to give the value of $p\beta$ at the point where the ionization was measured. The ionization measurement was made using determinations of the "blob" density based on about 1000 blobs and was normalized for the individual emulsions to the "plateau" value obtained from measurements of fast electron tracks. In this way four determinations of the relation between $p\beta$ and I/I_{pl} were obtained. It was found that the entire data were consistent with a unique curve part of which is reproduced in Fig. 2. Points for the four secondary tracks (given in Table VI) obtained by the procedure just outlined are indicated on the figure. The values of $p\beta$ indicated by the position of the crosses correspond to the point at which the ionization was measured and are not necessarily equal to the value of $p\beta$ at the point of decay. It should be remarked that the curve given in Fig. 2 is an expanded section from the calibration curve showing the region in which the K-secondaries occurred. The complete calibration extends over the region of $p\beta$ from 50–500 MeV/c corresponding to values of I/I_{pl} from 1.6–0.9. The points are very closely grouped about the line representing the best fit to the experimental points.

It is seen that three of the secondary particles are very probably π-mesons while the fourth is probably a μ-meson. Because of the limited amount of data these results are not in themselves conclusive. However the combined results from the Bristol and Padua groups provide convincing evidence for the existence of high energy π-meson secondaries in the photoplate events. For all events in which the π-meson is well identified the values of $p\beta$ obtained are consistent with a unique value of 170 MeV/c. (We exclude from consideration events discussed above, § 2.1, in which the value of $p\beta$ is less than 91 MeV/c. This is the maximum possible value for the charged π-meson produced in the alternate decay mode of the τ-meson.) The weighted mean value of $p\beta$ for the three Padua events is (164 ± 5) MeV/c. If one includes the Bristol data for tracks longer than 1 cm, this result is unchanged.

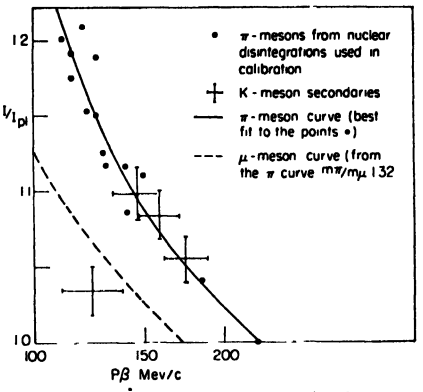

Fig. 2 – A portion of the ionization $-p\beta$ calibration curve obtained by the Padua group and used by them in their study of K-meson secondaries; I/I_{pl}, the blob count relative to the plateau value, is plotted against the $p\beta$ value determined from scattering measurements.

A single event has been reported by the Bombay group (APPA RAO and MITRA [1955]) in which the secondary particle from a K-meson is surely identified as a π-meson because it suffered a nuclear interaction after traversing 40.5 mm of emulsion and produced a star of the type 5 + 0p. The $p\beta$ at emission calculated from the observed scattering along the track and corrected for energy loss along the track using the Bombay range-energy relation (DANIEL *et al.* [1955]) was $(174.5\ ^{+16}_{-14})$ MeV/c. This event furnishes an additional piece of evidence in support of the decay process just discussed.

Further discussion of the χ-meson is postponed until § 3.8.

2. 5 The $p\beta$ distribution of the secondary particles

We now consider the overall data concerning the energy distribution of the secondary particles.

Table V contains data for 79 events produced by K-mesons in which significant measurements could be made on the secondary particle even though it did not stop in the emulsion. Unfortunately the more recent data cannot be easily compared with earlier measurements. We therefore consider the data available up to June 1954 separately.

These results are summarized in the $p\beta$ distributions shown in Figs. 3 and 4. The figures include events in which the statistical error is 20% or less and the effect of the errors on the histogram can be judged from Fig. 4. About half of the events were obtained using single emulsions and the remainder are early or preliminary results from stacks of stripped emulsions. The data is essentially that summarized at the Padua Conference, 1954. It is seen that the $p\beta$ distribution is peaked at about 170 MeV/c and that there are relatively few events above 210 MeV/c.

Mass determinations were carried out for about half of the events included in Fig. 3. Although these measurements are rarely precise enough to identify individual secondary particles with certainty the statistical separation of π- and μ-mesons should be satisfactory. For our purpose we therefore assume that those particles with mass values $< 240\ m_e$ are μ-mesons; those with mass values $> 240\ m_e$ are π-mesons. The $p\beta$ distributions which result from this classification of the secondary particles are shown in Fig. 5. It is apparent that *within the rather limited statistics* the μ-mesons have a broad continuous distribution in energy and that the π-mesons fall into two groups. The width of the distribution for the μ-mesons, omitting those events in which the secondary stopped, cannot be accounted for in terms of a line spectrum broadened by statistical fluctuations.

The $p\beta$ distributions shown in Figs. 3 and 5 can then be explained under the assumption that the secondary particles consist of μ- and π-mesons which result from the decay processes so far considered; the μ-mesons have a broad continuous energy distribution and arise from a single three-body decay process, that of the $\varkappa$-meson, while the π-mesons result from a mixture of the τ- and χ-decay processes discussed above.

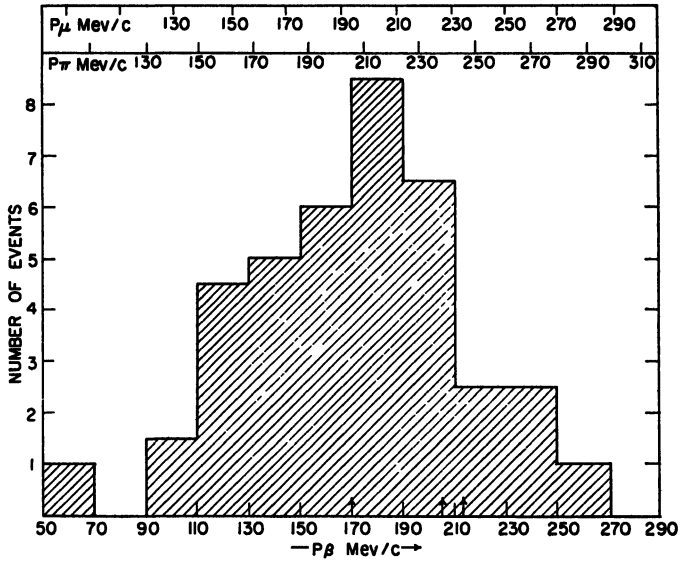

Fig. 3 – Histogram showing the number of K-meson secondaries with $p\beta$ in a 20 MeV/c increment as a function of $p\beta$. See text for the basis of selection of data.

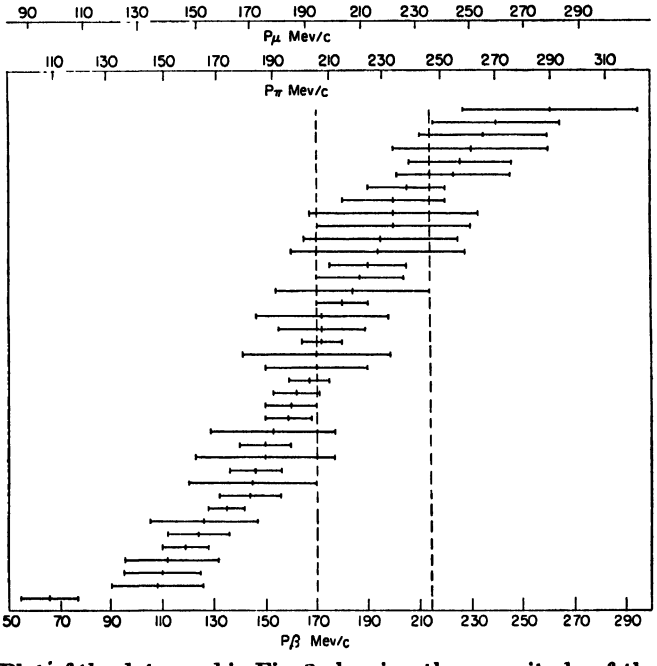

Fig. 4 – Plot of the data used in Fig. 3 showing the magnitude of the quoted individual errors.

This conclusion concerning the origin and energy distribution of the μ-mesons was extremely difficult to reconcile with cloud chamber results. On the one hand no evidence for low energy μ-mesons was found in experiments with multiplate cloud chambers; the results instead indicated a single group of monoenergetic high energy secondaries. Thus, to explain the absence of low energy

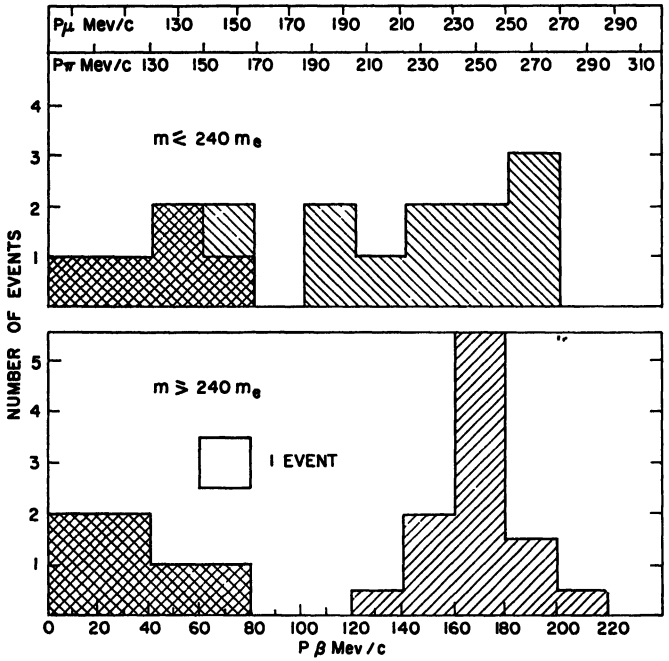

Fig. 5 – Histograms showing the frequency of K-meson secondaries against $p\beta$ for those events in which the mass of the secondary particle was determined. The double cross-hatching indicates that the secondary particle stopped in the emulsion and exhibited μ-e or π-μ-e decay. Single cross-hatching indicates events in which the secondary mass was determined from ionization and scattering.

μ-mesons observed in multiplate chambers and the relatively small number of high energy secondaries observed in emulsions, it seemed necessary to invoke a difference in the lifetime and production mechanism for the K-mesons observed using the two methods. On the other hand the data concerning charged V-particles (§ 4) included decay events in which μ-meson secondaries were produced and in some cases the μ-meson energy was certainly less than that expected from the K_μ-decay process. Thus the data concerning the charged V-particles supported the hypothesis that

most of the μ-mesons observed in emulsions resulted from $\varkappa$-mesons, and the data from multiplate chambers were in conflict with this view. However recent emulsion results show that the majority of the μ-mesons do have $p\beta$ values equal to or greater than 210 MeV/c; these secondaries unquestionably arise from the K_μ-decay process (§ 3.3, 4, 5, 6).

The $p\beta$ distribution, which is obtained largely from the final results from stacks of stripped emulsions flown in the Sardinia flights of 1954, is shown in Fig. 6. It is apparent that this distribution differs significantly from that of Fig. 3.

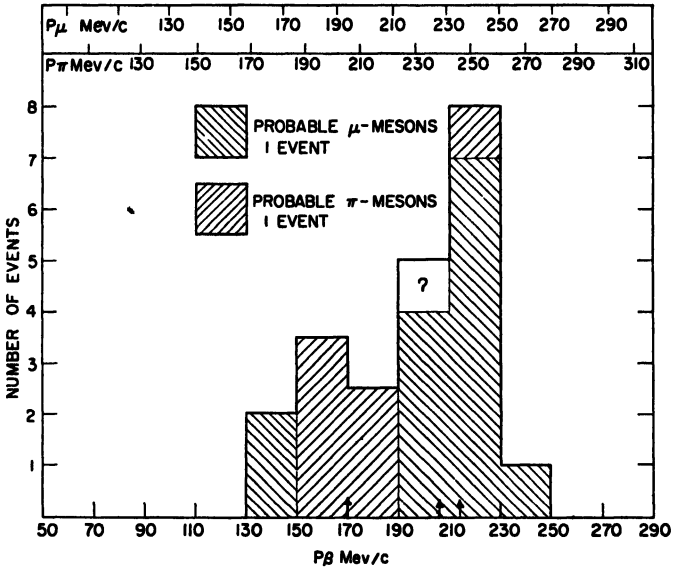

Fig. 6 – Histogram showing the frequency of K-meson secondaries as a function of $p\beta$. The data included is more recent than that used in Fig. 3.

There are at least two sources of systematic error in the $p\beta$ measurements which tend to lower the measured $p\beta$ values. Any distortion tends to increase the observed scattering and consequently lowers the observed value of $p\beta$; in the early measurements these distortion corrections, which may become particularly important in emulsion stacks, were not completely understood or applied. In addition many of the early measurements were not corrected for energy loss along the track; this becomes important for long tracks. It is thus clear that no conclusion concerning the high energy secondaries can be drawn from the histogram shown in Fig. 3 and

that the above effects account at least in part for the discrepancy between the two distributions.

The distribution of the $p\beta$ values shown in Fig. 6 is naturally explained in terms of two lines, one composed of π-mesons whose $p\beta$ is about 160 MeV/c and a second composed of μ-mesons whose $p\beta$ is about 215 MeV/c.

However if the probable identity of the secondaries as determined from ionization and scattering is taken into account one finds that there is one probable π-meson with $p\beta = (221 \pm 16)$ MeV/c and two μ-mesons with $p\beta = (144 \pm 12)$ and (149 ± 8) MeV/c respectively.

It should be noted again that the identification of μ-mesons becomes very difficult for values of $p\beta$ greater than $\sim$160 MeV/c and that the corresponding value for π-mesons is $\sim$205 MeV/c. Thus the identification of the π- and μ-mesons in the group of secondary particles centered at $\sim$160 MeV/c is good and the identification of the μ-mesons in the 215 MeV/c group is by elimination. Had these latter particles been π-mesons most should have been recognized as such, but the direct identification of μ-mesons in this region is not possible.

The single π-meson in the high $p\beta$ region can be explained either as a statistical fluctuation or as an example of K^--absorption in which a high energy π-meson was produced, (§ 6); unless there are larger unknown systematic errors the two μ-mesons which fall outside the high $p\beta$ region must be attributed to the decay of $\varkappa$-mesons.

It appears then, that the majority of the π-meson secondaries arise from the decay of τ- and χ-mesons and that only a few of the μ-mesons can be attributed to decay of $\varkappa$-mesons. Instead most μ-meson secondaries must result from the two-body decay process $K_\mu \rightarrow \mu + \nu$ which has been established by cloud chamber experiments, § 3.3.

The interpretation of the π-meson secondaries in terms of the τ- and χ-decay processes requires that the π-meson secondaries be distributed in $p\beta$ up to 91 MeV/c, the maximum possible value for the postulated alternate mode of the τ-meson, and that there be a line at $\sim$170 MeV/c corresponding to events which arise from the decay of the χ-meson. This interpretation depends critically on the existence of a gap in the $p\beta$ distribution between 91 and 170 MeV/c, and on the absence of π-mesons with values of $p\beta$ above $\sim$170 MeV/c. (The errors of measurement tend of course to narrow the

gap and must be taken into consideration.) Although the number of events is small, the existence of the gap seems rather well established, Fig. 5. It should be remembered that the identification of π-mesons in this $p\beta$ region is relatively easier than at higher values of $p\beta$ and that the scanning efficiency is better than that at higher energies. Therefore, it is difficult to understand how many events in the intermediate region could have been missed. The possible existence of π-mesons with $p\beta > 200$ MeV/c poses a much more difficult question and one must admit that, because of the small number of events and the difficulty in identifying the particles, there is no good evidence on this point.

The $p\beta$ distribution for the μ-mesons emitted in the decay of the $\varkappa$-mesons is at present almost completely unknown. Table IVb summarizes the available data for μ-mesons which cannot be attributed to the K_μ-meson.

2. 6 The electron secondaries

The usual procedure for mass determinations using an experimental relation between the grain density and $p\beta$ has been outlined above. As predicted by theory, (Sternheimer [1953]), it is found that the grain density, g, decreases with increasing $p\beta$, passes through a minimum at a value of $p\beta$ corresponding to a few times the rest energy, and, at high values of $p\beta$ corresponding to about ten times the rest energy, reaches a constant value denoted by g_0. For μ-mesons of $p\beta < 115$ MeV/c the value of $g^* = g/g_0$ is greater than ~ 1.10. For an electron however the minimum in the g^*-$p\beta$ relation occurs for very low values of $p\beta$ and g^* is essentially constant for values of $p\beta$ above about 7 MeV/c.

The statistical accuracy of the usual grain counts is more than sufficient to separate a g^* value of 1.00 from 1.10 and hence below $p\beta \sim 115$ MeV/c electrons can be distinguished from all known heavier particles through measurements of scattering and ionization.

An additional means of separating electrons from μ-mesons is provided by observations of the energy loss along the trajectory. In the case of electrons the predominate energy loss occurs through radiation; for μ-mesons this effect is negligible. Thus, depending on fluctuations in the radiation loss, a plot of the $p\beta$ values against distance from the point of decay can sometimes be used to establish the identity of an electron secondary.

The first probable electron secondary was reported by the Bristol group, (FRIEDLANDER *et al.* [1954]). These authors observed a K-meson which came to rest in the emulsion and decayed into a lightly ionizing secondary particle. The secondary particle traversed 2.3 cm of emulsion and then apparently suffered an inelastic scattering. After the scattering there was a large increase in the multiple scattering and grain density and the track had the typical appearance of a low energy electron. There was no recoil at the point where the scattering occurred. The secondary particle traversed 11 emulsions with a track length of about 2 mm per emulsion. Scattering and grain density measurements were made in each plate and no significant change in $p\beta$ or g^* was found along the track. The mean value of $p\beta$ was (88.5 $\pm$ 6) MeV/c and the mean value of g^* was (1.01 $\pm$ 0.02). From these values it is extremely improbable that the secondary particle was a π-meson but a μ-meson is not excluded. According to the g^*-$p\beta$ calibration, a g^* equal to 1.01 corresponds to $p\beta$ = 130 MeV/c for a π-meson and to $p\beta$ = 100 MeV/c for a μ-meson.

However the behaviour of the track at the point of scatter strongly suggests a bremsstrahlung process with large energy loss and is typical of the behaviour expected of an electron. The radiation length in emulsion is $\sim$2.9 cm and the secondary traversed 2.3 cm of emulsion up to the point of scatter . The most probable alternative interpretation is that the secondary particle was a μ-meson of $p\beta$ about 100 MeV/c which suffered $\mu \rightarrow$ e decay in flight. In view of the necessary error in the $p\beta$ measurements required by this explanation and of the apparent scarcity of μ-mesons in this energy region, such an explanation appears very unlikely. By considering the path length of all possible μ-meson secondaries observed in emulsions up to the time of the observation the authors estimate that, as an upper limit, 4×10^{-4} $\mu \rightarrow$ e decays in flight should have been observed.

A second example of electron decay in which both the comparison of ionization *vs.* scattering and the energy loss along the track are inconsistent with the expected behaviour of a μ-meson, has been reported from Bristol (DAHANAYAKE *et al.* [1954]). In this case a K-meson decayed into a lightly ionizing secondary particle which escaped from the emulsion stack after traversing 2.56 cm. The track was divided into 5 segments and it was found that the value of $p\beta$ varied from (49 $\pm$ 4) MeV/c in the segment nearest the point

of decay to (17 ± 2) MeV/c in the fifth segment. Because of the increasing steepness and the apparently large energy loss in the sections of track removed from the decay point, the identification of the secondary by scattering and ionization is based mainly on measurements in the first track segment. The value of $p\beta$ for this section is (49 ± 4) MeV/c and the normalized blob density, b^*, is (1.00 ± 0.04). A μ-meson of this $p\beta$ would have a value of $b^* \sim 2.0$, and a μ-meson whose $g^* = 1.00$ would have a $p\beta \sim 120$ MeV/c. Thus the probability that the secondary particle was a μ-meson is negligible. The apparent loss of energy along the track supports this conclusion.

Other examples of electron secondaries have been reported and this decay process is now well established. The available data are summarized in Table VII. It is seen that the electrons show a broad energy distribution and thus the decay mode must involve at least two neutral particles whose nature is at present completely unknown.

While the electron secondaries appear to be rare the frequency relative to other K-meson decay processes is unknown.

TABLE VII

Summary of data for K*-mesons with electron secondaries*

Event	Primary Mass, m_e	$p\beta c$ (MeV)	g^*	Probable identity
Bristol K - 37	*932 ± 76	88.5 ± 6	1.01 ± 0.02	$e^{\pm}$
K - 46	*842 ± 67	°49 ± 4 to 17 ± 2	1.00 ± 0.04	$e^{\pm}$
Dublin K -	*977 ± 64	°81 ± 9	0.99 ± 0.03	$e^{\pm}$
Rochester K - 12	*916 ± 83	°261 ± 34 to 150 ± 22	0.96 ± 0.03	$e^{\pm}$
K - 20	—	°210 ± 40 to 76 ± 15	1.00 ± 0.06	$e^{\pm}$
K - 21	*926 ± 130	°20 ± 5	1.06 ± 0.2	°°e^+

* Weighted mean.
° At point of decay.
°° Disappears in flight therefore probably annihilation of e^+.

3. Results concerning S-events; observations with Cloud Chambers

Introduction

The initial observations of S-events in multiplate cloud chambers were made by Bridge and Annis in 1951 and were followed very shortly by the discovery of similar events in emulsions (O'Ceallaigh [1951]). The measurements of ionization, scattering, and

range which can be made in a multiplate chamber are similar in principle to emulsion measurements but the accuracy of the ionization and scattering measurements does not approach that attained with emulsions. Nevertheless it was possible to show unambiguously by these methods that the S-events observed in the multiplate cloud chamber were K-mesons which decayed into fast L-mesons.

Some pertinent differences between S-events observed in emulsions and cloud chambers should be borne in mind. In photographic plates the more energetic secondary L-mesons from K-meson decays usually leave the emulsion before coming to rest, and their energies must be inferred from measurements of scattering and ionization. These measurements are impossible for individual events observed in multiplate chambers, but, because of the large amount of material in the metal plates, particles whose range is about 100 g cm^{-2} of lead ($\sim$20 cm of emulsion) can be brought to rest in the chamber. Significant information can thus be obtained from the observed ranges of the charged decay products.

The slowing down times of particles observed in emulsions are shorter, and the energies are generally considerably less than for corresponding particles observed in cloud chambers.

In single emulsions the length of track available is usually only a few millimeters; in emulsion stacks the track length may be several centimeters. The differences in energy and slowing down time between emulsions and cloud chambers are apparent from an inspection of Table VIII.

A decay at rest is probable only if the slowing down time is comparable to the mean life. Hence S-events which result from charged K-mesons with mean lives as short as 10^{-10} sec are recorded efficiently in emulsions whereas multiplate cloud chambers record similar events in which the mean life is roughly 10^{-9} sec.

A further contrast with observations in emulsions is in the relative probability of detecting possible neutral secondary particles, either photons or unstable particles whose mean life is greater than $\sim 10^{-10}$ sec. In the case of emulsions the materialization of a photon or the decay of a neutral particle associated with an S-event occurs in general so far from the point of stopping that the manifestation of the neutral particle is not easy to find. Even if it should be discovered, the large background of unrelated events makes the

TABLE VIII

Slowing down times for a K-*meson* (mc^2 = 493 MeV) *in emulsion and in a typical multiplate cloud chamber as a function of energy.*

Column 1 lists the kinetic energy of the K-meson in MeV, column 2 its approximate range in cm of emulsion, and column 3 gives the stopping time in the emulsion.

In column 4 the range of the K-meson is given in g cm^{-2} copper or emulsion, and the stopping time in the multiplate chamber is tabulated in column 5. In this example the average density of the emulsion and the cloud chamber are nearly the same, hence the stopping times are similar. The longer times characteristic of cloud chambers relative to emulsions arise mainly from the higher energies of particles observed in multiplate cloud chambers.

The values for emulsion were obtained from the tables of BARKAS and YOUNG [1954]; the cloud chamber values were computed from the range tables of ARON, HOFFMANN and WILLIAMS [1949]. In this latter calculation, it was assumed that the cloud chamber plates were of copper, 12 g cm^{-2} thick, spaced 2 cm apart, and that the K-meson came to rest after traversing 1/3 of the plate in which it stopped.

Kinetic Energy MeV	Range cm emulsion	Proper stopping time (10^{-10} sec)	Range g cm^{-2} Cu	Proper stopping time (10^{-10} sec)
5	.0266	0.09	0.102	
10	.0885	0.21	0.337	
25	.466	0.64	1.70	
50	1.50	1.5	5.72	
100	4.96	3.5	18.9	4.1
200	15.5	7.7	59.1	8.0
300	29.8	12	111	12
500	60.9	19	232	19
1000	149.5	32	570	33

fact of association difficult to establish. The observation of such events in the multiplate chamber is much easier and more probable than in emulsions.

Very little direct evidence concerning the masses of the primary particles can be obtained from the multiplate chamber alone. In an individual event measurements of ionization and residual range frequently suffice to distinguish between hyperons, K-mesons and L-mesons, but accurate mass measurements are not possible.

A direct determination of the mass *and sign* of the primary particle can be made by using an additional cloud chamber and associated magnetic field above the multiplate chamber. In this case the mass is specified by a measurement of momentum in the top chamber and residual range in the lower chamber.

A most elegent experimental arrangement of the type has been constructed by the physicists at the École Polytechnique and is shown schematically in Fig. 7 (6). The accuracy of a single mass

measurement obtained using this apparatus is between five and ten percent.

3. 1 The experimental results

The experiments carried out by the École Polytechnique group, EP, and by the Massachusetts Institute of Technology group, MIT, have been performed with rather similar experimental methods and one would hope to be able to supplement the data of one group with that of the other. At the present time there appears to be no disagreement between the two sets of data and we shall combine them where possible.

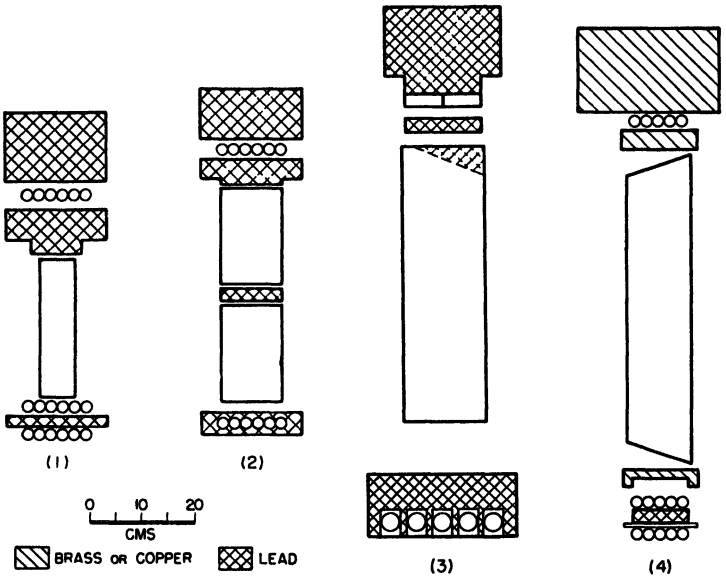

Fig. 7 – Schematic representation of the cloud chambers used by various groups in the study of unstable particles. All diagrams show side views of the experimental arrangement; illuminated volumes are shown, and the disposition of the counters and absorbers forming the detection system is indicated. Note the change in scale between (1, 2, 3, 4) and (5, 6, 7, 8).

(1) Cloud chamber with magnetic field originally used by Rochester and Butler, and subsequently used at the Pic du Midi (2870 m) by other members of the Manchester group (Barker *et al.* [1952]). The chamber is cylindrical in shape.

(2) Double cloud chamber arrangement with magnetic field used at Pasadena (220 m) by York *et al.* [1954]. The chambers are rectangular and are 30 cm in width.

(3) Chamber with magnetic field employed by Astbury, Newth and others of the Manchester group at the Jungfraujoch (3460 m); (Buchanan *et al.* [1954]). The chamber is 50 cm in width.

(4) Chamber with magnetic field employed by Thompson and his coworkers at Indiana (230 m), (Kim *et al.* [1954]). The chamber is 27 cm in width.

The experiments of both groups led to the conclusion that there is a monoenergetic group of μ-meson secondaries whose mean range is about 76 g cm^{-2} of copper. In addition the measurements of primary mass which are possible in the EP measurements showed that the mass of the K-meson responsible for these long range secondaries is at most equal to the τ-meson mass and established the two-body decay process: $K_\mu \rightarrow \mu + \nu$. The MIT results provided additional evidence for the K_μ-meson and established the existence of photons among the neutral decay products of K-mesons. It was shown that these photons were associated with secondary particles whose range is about 44 g cm^{-2} of copper. Together with the

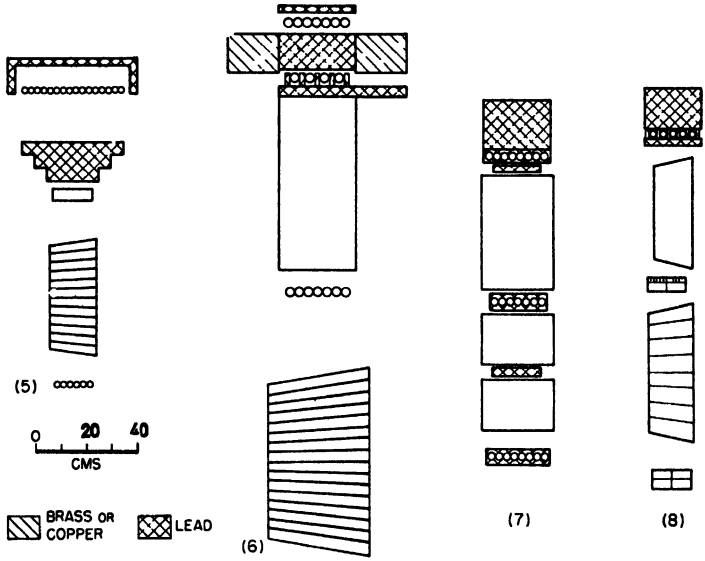

(5) Multiplate chamber used by the MIT group (Bridge *et al.* [1954]) at Echo Lake, Colo. (3230 m). The rectangular box above the chamber is a liquid scintillation counter. The width of the chamber is 48 cm.

(6) Double cloud chamber arrangement used on the Pic du Midi (2870 m) by the EP group (Gregory *et al.* [1954]). The top chamber uses a magnetic field, and the bottom chamber contains copper plates. The width of the chambers is 64 cm.

(7) Multiple chamber used by the CIT group at Pasadena (220 m). All of the chambers operate in a magnetic field, and the experimental arrangement can be varied to include a multiplate chamber if desired (Leighton [1954]). The chambers are 55 cm in width.

(8) Experimental arrangement used by the Princeton group at Echo Lake, Colo. (3230 m). The general arrangement is similar to that shown in (6). The rectangular boxes between and below the chambers are proportional counters (Hodson *et al.* [1954]). The upper and lower chambers are respectively 40 cm and 50 cm in width.

results of the Padua emulsion group (§ 2.4) this evidence established the decay scheme of the χ-meson as: $\chi \rightarrow \pi + \pi^{\circ}$.

From the MIT and EP results it is certain that the majority of the S-events observed in multiplate chambers arise from the decay of K_{μ}- or χ-mesons and we now consider the evidence leading to this conclusion.

3. 2 The range distribution of the secondary particles

The actual distribution of particle ranges is greatly modified by the cloud chamber. Since the amount of absorber in the chamber is limited, particles may leave the observation region without coming to rest; then only a lower limit to the range is available. If the particle does come to rest in the chamber, its exact point of stopping in the plate cannot be determined and hence the particle range is uncertain by about one plate thickness. The ranges therefore are usually specified by an upper and lower limit either of which may be modified by estimates of the specific ionization.

Results of measurements on 67 K-particle secondaries obtained by the MIT group using two different experimental arrangements are given in Table IX and are shown in Figs. 8a and 8b. Similar results from the EP group are given in Table X. For each event the histogram shows the potential range of the secondary particle in the illuminated region of the chamber. This quantity is defined as the amount of material traversed by the particle before it escaped from the chamber, or the amount of material which the particle would have traversed if it had not come to rest. In 10 cases the particle stopped before traversing this entire distance and its actual range could be determined. The boundaries of the solid regions indicate the upper and lower range limits for these events.

It is instructive to try to explain this distribution of ranges in terms of a single three-body decay process. If this hypothesis were tenable one might explain the majority of the cloud chamber events in terms of the $\varkappa$-meson. As a basis for this comparison we compute the number of secondary particles which would be expected to stop in the multiplate chamber and the momentum distribution of these stopped decay products. For this purpose one must know the theoretical momentum distribution for the charged secondary particle and the detection probability of the cloud chamber as a function of momentum.

Possible spectra for various three-body decay schemes which

involve either a photon or neutral π-meson have been calculated under various assumptions as to the interactions between the four particles involved in the decay (e.g. MICHEL [1950], MICHEL and STORA [1952], YORK [1952]). The shapes of the resulting distributions depend critically on the decay scheme and couplings assumed,

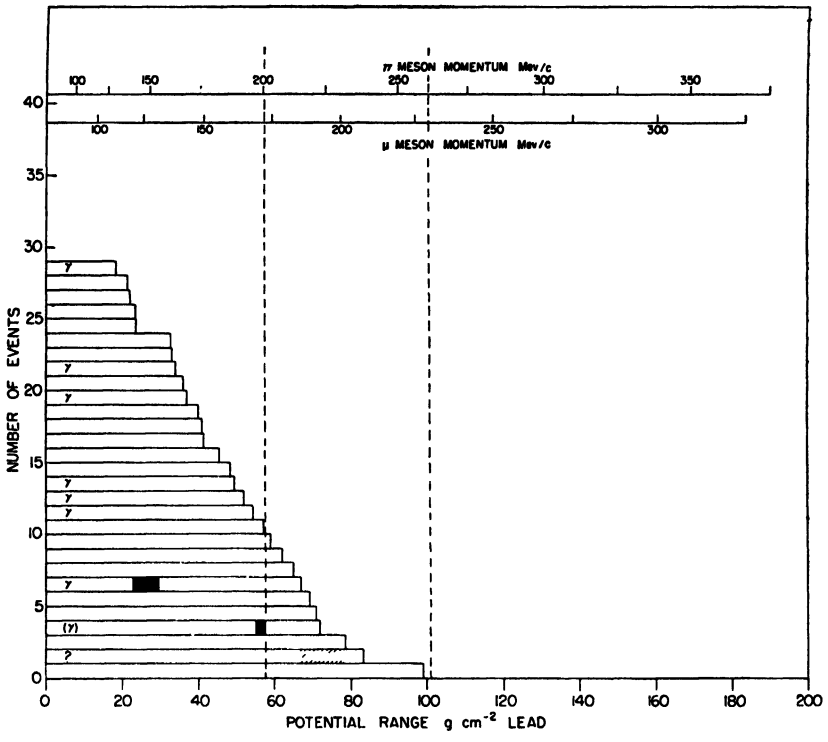

Fig. 8a – Histogram of S-particle ranges observed by the MIT group using lead plates in the cloud chamber. The plot shows the frequency of events with a potential secondary range greater than R. The solid regions indicate range limits for those secondary particles which stopped in the chamber. γ indicates an associated electron cascade. The dotted vertical lines are drawn at 57.4 and 102 g cm^{-2} lead.

and, since no unique choice is possible, we consider for simplicity the decay scheme

$$\varkappa \rightarrow \mu + \nu + \nu,$$

in which no photons are produced. The spectrum of the μ-meson is however peaked at the high momentum end, and the conclusions reached will apply to any spectrum of similar form.

The differential momentum distribution which is obtained for the above decay scheme is given by,

$$F(p)dp = A\{3(M^2c^4 + m^2c^4) - 6Mc^2(p^2c^2 + m^2c^4)^{1/2} + 2p^2c^2\}p^2c^2dp \tag{3.1}$$

where A is a constant of normalization, M is the mass of the primary particle, and m and p are respectively the mass and momen-

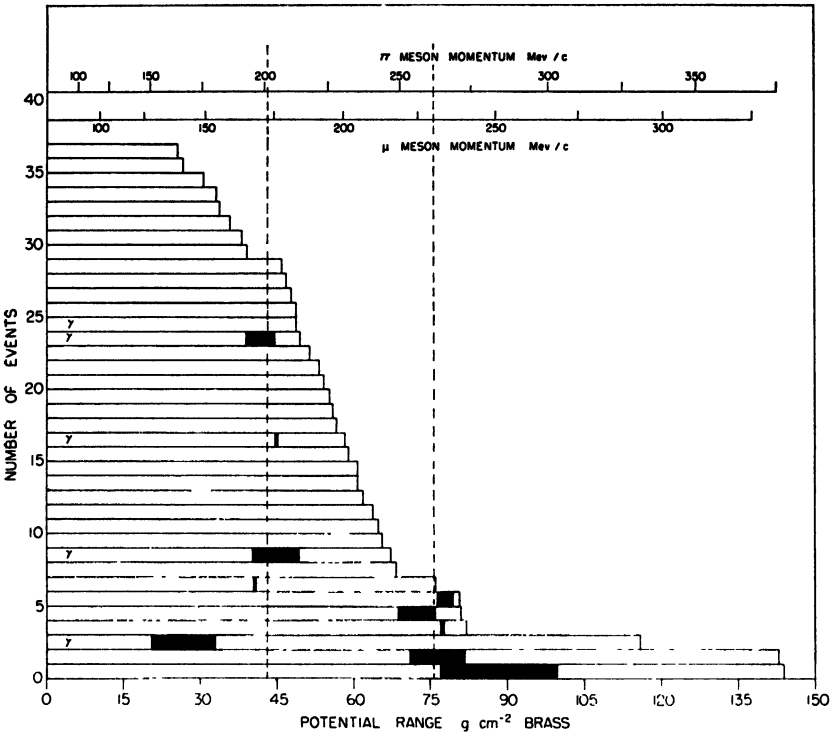

Fig. 8b – Histogram of S-particle ranges observed by the MIT group using brass plates in the cloud chamber. The dotted vertical lines are drawn at 43.1 and 76.5 g cm^{-2}.

tum of the charged secondary. The distribution is shown for a primary mass of 1120 m_e in Fig. 9. The momentum distribution of the secondary particles which would be observed in a multiplate chamber is however *not* given by this distribution but is modified by the detection probability of the instrument.

This detection probability depends on the particular experimental disposition and in general is strongly dependent on momentum. For a μ-meson in the MIT chamber the detection probability falls

Explanation of symbols in Tables IXa and IXb

The symbols in the various columns have the following significance: In the second column the origin of the S-particle is specified by (a), (b), or (c); (a) indicates that the origin of the S-particle was outside the chamber and undetermined, (b) in a nuclear interaction outside the chamber, and (c) in a nuclear interaction inside the chamber. In the columns referring to the charged secondary particle the letter (f) indicates that the secondary particle was emitted in the forward hemisphere w.r.t. the motion of the primary particle, and the letter (b) that it was emitted in the backward hemisphere. Ranges are given in g cm^{-2} of lead and the potential range is defined in the text. The sixth column indicates whether there was a non-ionizing link between the point of decay and the origin of the electron cascade; the seventh column gives the angle between the direction of motion of the charged decay product and the shower axis. Column eight lists the total number of visible electron tracks, N, and column nine gives the detection probability for a π^0-meson of 200 MeV/c momentum.

TABLE IXa

S-events observed by the MIT group using lead plates in the cloud chamber

Event	Origin of S	Charged Secondary			Photon Secondary			
		Direction	Pot. Range	Actual Range	n.i.l.	θ	N	π^0 det. prob.
			g cm^{-2} Lead					
H–1	a	f	67	23–29.5	yes	180°	3	.87
TR-2	a	b	99					.1
S-1	a	f	41					.63
S-2	a	f	33					.82
02877	b	b	50		yes	127°	3	.69
03246	b	f	18		no	147°	4	.38
12668 (S3)*	a	f	83	66.4–78.2				.38
25178	a	f	34		no	180°	5	.1
26049	a	f	52		no	157°	8–9	.48
26110 (S4)	?	b	72	55.2–57.5	yes	163°	2	.19
26653	b	b	79					.75
29428	c	f	59					.74
30122 (S5)	c	f	41					.29
30654	b	b	22					.67
32531	a	b	5		yes	180°	5	.52
39567	a	b	65					.0
42166 (S8)	a	f	48					.66
46796	a	b	36					.51
53688	a	b	57					.69
56409	a	b	62					.20
58070	a	b	24					.38
58649	a	b	71					.39
61641	c	f	33					.55
64228	a	f	22					.77
64700			37		no		2	.39
64888	a	f	54		yes	123°	4	.75
65479	c	f	69					.06
66672	a	b	46					.87
70557	a	b	40					.51
70589	a	b	24					

* stopping questionable.

TABLE IXb

S-events observed by the MIT group using brass plates in the cloud chamber

Ranges are given in g cm^{-2} brass, otherwise the data are quite comparable to those in Table IXa

Event	Origin of S	Charged Secondary			Photon Secondary			
		Direction	Pot. Range	Actual Range	n.i.l.	θ	N	π^0 det. prob.
			g cm^{-2} Brass					
76734	b	b	47					.62
77039	b	b	61					.79
77074	b	f	34					.60
77509	b	f	46					.58
78003	c	f	48					.53
78405	b	f	26					.66
78475	a	b	49					.62
80015	c	f	65					.73
81558	b	f	144	77.0–107.2				.02
82203	b	f	50	39.2–46.6	yes	170°	7*	.72
84965	a	f	56					.73
85380	a	b	143	70.9–81.7				.20
85415	a	f	68					.56
85494	c	f	27					.69
85751	b	f	53					.73
87415	b	b	61					.62
87981	c	f	67	40.2–49.2	yes	151°	3	.55
88405	c	f	55					.82
88515	a	b	62					.73
90713	b	b	57					.65
90912	a	b	116	20.5–33.0	no		4	.70
91256	c	f	54					.73
91829	b	b	39					.30
92136	c	f	76	40.7				.50
92329	c	f	81	76.4–79.4				.72
96787	c	f	81	68.6–75.9				.80
98367	c	f	64					.76
98529	a	b	59					.40
99319	b	f	38					.28
99705	b	b	51					.40
100846	a	f	49		no	112°	3	.72
102209	b	b	82	77.1–77.6				.56
102565	c	b	33					.82
105345	b	b	31					.68
105596	a	f	58	44.8	yes	166°	3	.69
105711	a	f	66					.40
106168	c	f	36					.66

* A second shower was apparently associated with this event.

TABLE X

S-events observed by the EP group using two cloud chambers, one above the other

The top chamber employed a magnetic field for the measurement of momentum, and the bottom chamber contained copper plates which afforded a measurement of residual range.

Group I consists of particles which were produced in the multiplate chamber and which lived $\sim 2 \times 10^{-9}$ sec.

Group II consists of particles which lived $\sim 5 \times 10^{-9}$ sec and which could be τ-mesons.

Group III consists of particles which lived $\sim 5 \times 10^{-9}$ sec and which could not be τ-mesons.

The next to the last column indicates the total visible number of electrons in those cascades which appeared to be associated with the decay, and the last column gives the angle, θ, between the charged secondary and the axis of the electron shower.

For the events in Group I the letter "c" in column 2 indicates that the S-particle originated in a visible nuclear interaction inside the cloud chamber; the letter "b" indicates that the nuclear interaction was outside the bottom cloud chamber. ϑ^* is the angle of the secondary track with respect to the primary track. R_1 and R_2 and the potential range are defined in the text (§ 3.5) and are given in g cm^{-2} of copper; $\triangle R_1$ is the statistical error in R_1.

Group I. Locally Produced Events

Event	Origin of S	Charged Secondary					Photon secondary
		ϑ^* degrees	R_1	$\triangle R_1$	R_2	Pot. Range	
			g cm^{-2} Copper				
17804	c	30	47.6	1.9	—	—	—
21073	b	150	61.5	2.5	71.6	100.7	—
21162	c	30	43.2	3.6	—	—	—
27924	c	30	53.7	2.2	—	—	—
28093	b	120	30.8	2.1	—	—	—
29321	c	90	41.4	2.5	—	—	—
38275	b	63	66.8	3.7	83.3	141.0	—
38797	b	120	64.6	4.2	84.2	84.2+	—
40359	c	135	27.6	1.3	—	—	—
40896	c	160	75.7	3.0	85.4	135.6	—
			94.7	3.5	105.6		
41676	c	50	41.1	2.0	—	—	—
43599	c	155	72.4	2.4	—	—	—
47066	c	45	73.3	3.1	85.2	108.2	—
47438	b	48	68.5	3.4	83.6	—	—

Group II. Positive Events Produced Above Top Chamber with $R_1 < 16$ g cm^{-2} Copper

Event	Primary Mass m_e	Charged Secondary					Photon secondary	
		ϑ* degrees	R_1	$\triangle R_1$	R_2	Pot. Range	N no. of electrons	θ degrees
			g cm^{-2} Copper					
16192	888 ± 57	95	8.66	1.9	41.4	41.4 + ε	—	
16307	979 ± 57	50	8.4	+1.5 −1.0	12.6	12.6 + ε	—	
16569	874 ± 57	—	—	—	—	—	—	
18805	928 ± 53	45	7.3	1.9	15.5	28.3	—	
23473	955 ± 56	—	0	—	—	—	6	
25679	970 ± 75	—	—	—	—	—	—	
28222	1052 ± 84	40	14.4	1.8	—	—	—	
30174	925 ± 59	60	12.6	1.7	37.8	112.8	Possible	
32232	888 ± 50	90	ε	—	—	—	—	
39306	—	150	8.7	1.1	20.6	56.6	12	~155

Group II. Negative Events Produced Above Top Chamber with $R_1 < 16$ g cm^{-2} Copper

26945	1240 ± 87	—	0	—	—	—	3	
41930	1050 ± 69	45	11.5	—	22.9	80.3	—	

Group III. Positive Events Produced Above Top Chamber with $R_1 > 16$ g cm^{-2} Copper

Event	Primary Mass m_e	Charged Secondary					PhotonSecondary	
		ϑ* degrees	R_1	$\triangle R_1$	R_2	Pot. Range	N no. of electrons	θ degrees
			g cm^{-2} Copper					
16197	916 ± 58	85	28	3	—	—	—	
18094	1040 ± 65	55	40	3.5	—	—	—	
19231	872 ± 76	45	50.6	2.3	—	—	—	
22964	902 ± 73	65	56.9	3.5	—	—	—	
25845	—	180	70.9	2.8	81.2	101	—	
26320	917 ± 58	25	59.8	—	—	—	—	
27170	933 ± 54	100	54.5	5	—	—	—	
30248	—	180	66.0	2.8	78.0	101.1	—	
30433	—	80	37.9	3.8	—	—	—	
32515	1045 ± 80	45	40.3	2.5	—	—	—	
40804	1096 ± 91	90	36.1	2.4	—	—	4	~180
40823	—	135	16.1	1.5	—	—	—	
42868	959 ± 87	180	46.9	3.1	—	—	—	
46348	971 ± 58	135	30.7	1.5	—	—	5	~110
47644	1016 ± 58	180	31.9	2.4	—	—	—	
48813	874 ± 57	80	48.5	3.4	76.5	131.5	—	

rapidly to zero below a momentum of about 100 MeV/c. Mu-mesons below this momentum which are produced in a plate may stop before they emerge; or they may emerge with an ionization greater than minimum and so be indistinguishable from the parent particle. Above this observational cut off at about 100 MeV/c, the detection probability depends on momentum because the cloud chamber is not infinite in extent. In evaluating this effect it is convenient to make use of the potential range defined above. To this "potential range" there corresponds a "potential momentum". Obviously only that portion of the momentum spectrum which lies below the "potential momentum" and above the cut off can be observed in any given event; thus the theoretical momentum distribution must be weighted by the "potential momentum" distribution and the low energy cut off. The resulting spectrum can be expressed as

$$W(p)dp = F(p)G(p)dp. \qquad (3.2)$$

Here F (p) is the distribution defined by Eq. 3.1, G(p) is the integral detection probability for a momentum of p or greater and $W(p)$ is the differential momentum distribution of the particles which are observed to stop in the chamber. The integral of the above expression over any particular momentum range gives the fractional number of particles which stop in the cloud chamber between the chosen momentum limits.

$G(p)$ should be purely a geometrical factor but it is difficult to evaluate analytically. However, it can be determined simply using the integral frequency distribution of potential ranges given in Figs. 8a and 8b.

On carrying out the above calculation for 35 of the events included in Fig. 8b, one finds that 15 particles should have stopped in the chamber and 20 should have left the illuminated region before coming to the end of their ranges. Instead only 8 particles stopped in the chamber. Furthermore the distribution of momentum for these 8 events does not agree with that predicted by Eq. (3.1). The expected distribution of the stopped particles is shown by the solid curve in Fig. 9. The histogram represents the experimental data. The area is normalized to the total number of stopped particles observed.

Thus one concludes that, in terms of the assumed distribution, not enough particles stop in the chamber, and those which do stop

are peaked at the higher end of the spectrum rather at the lower end as predicted. To obtain agreement with the experimental observations it is evident that $F(p)$ must have a very much sharper peak at the high momentum end than was assumed.

Using similar arguments, the EP group compare the observed

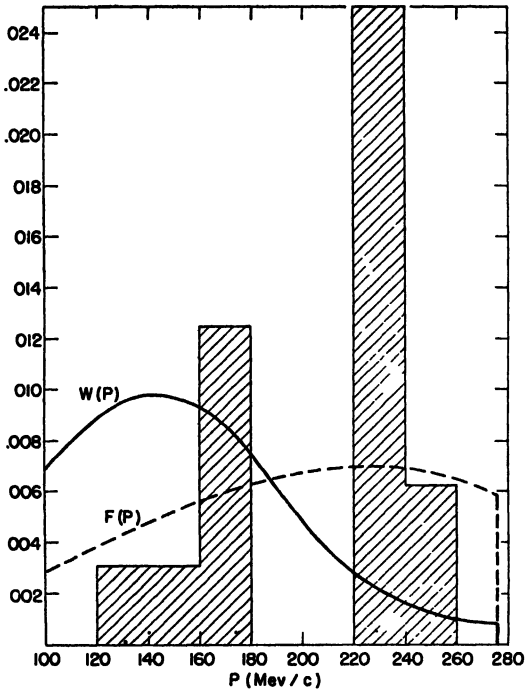

Fig. 9 – The differential momentum distribution obtained for stopped S-particle secondaries observed by the MIT group. $F(p)$ is a theoretical distribution for the decay process $K \rightarrow \mu + 2\nu$. $W(p)$ is obtained from $F(p)$ by taking into account the detection probability of the cloud chamber as a function of p. It represents the expected distribution which would be observed experimentally if the original charged decay products are distributed in momentum according to $F(p)$. The dots along the abscissa indicate momenta of individual stopped secondaries.

particle ranges with an assumed power low spectrum; they estimate that $F(p)$ must rise more sharply than $\sim p^{5\,5}$ between 130 and 240 MeV/c to explain the observed range distribution. From the photo plate evidence it seems impossible that the spectrum of the secondaries from $\varkappa$-decay is of this form and there is no possibility of explaining the cloud chamber data in terms of the $\varkappa$-meson.

A striking feature of the histograms shown in Figs. 8a and 8b is

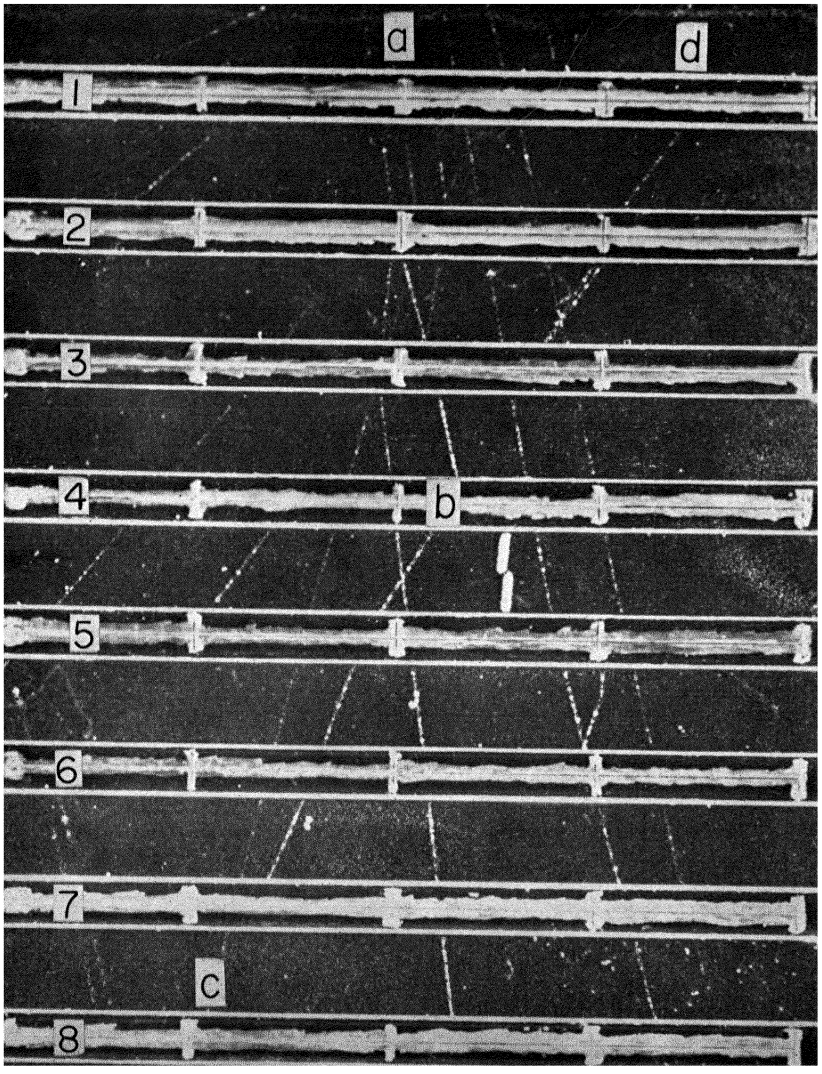

Plate II - An electron cascade associated with the decay of a K-meson (MIT event 87981 Table IXb). The K-meson enters the chamber at *a* and decays in plate 4 at *b*. The L-meson secondary stops at *c* after traversing ~ 45 g cm^{-2} of copper. The electron shower originates above the point at which the K-meson decayed. It starts in plate 3 and apparently stops (or escapes from the chamber) at *d*.

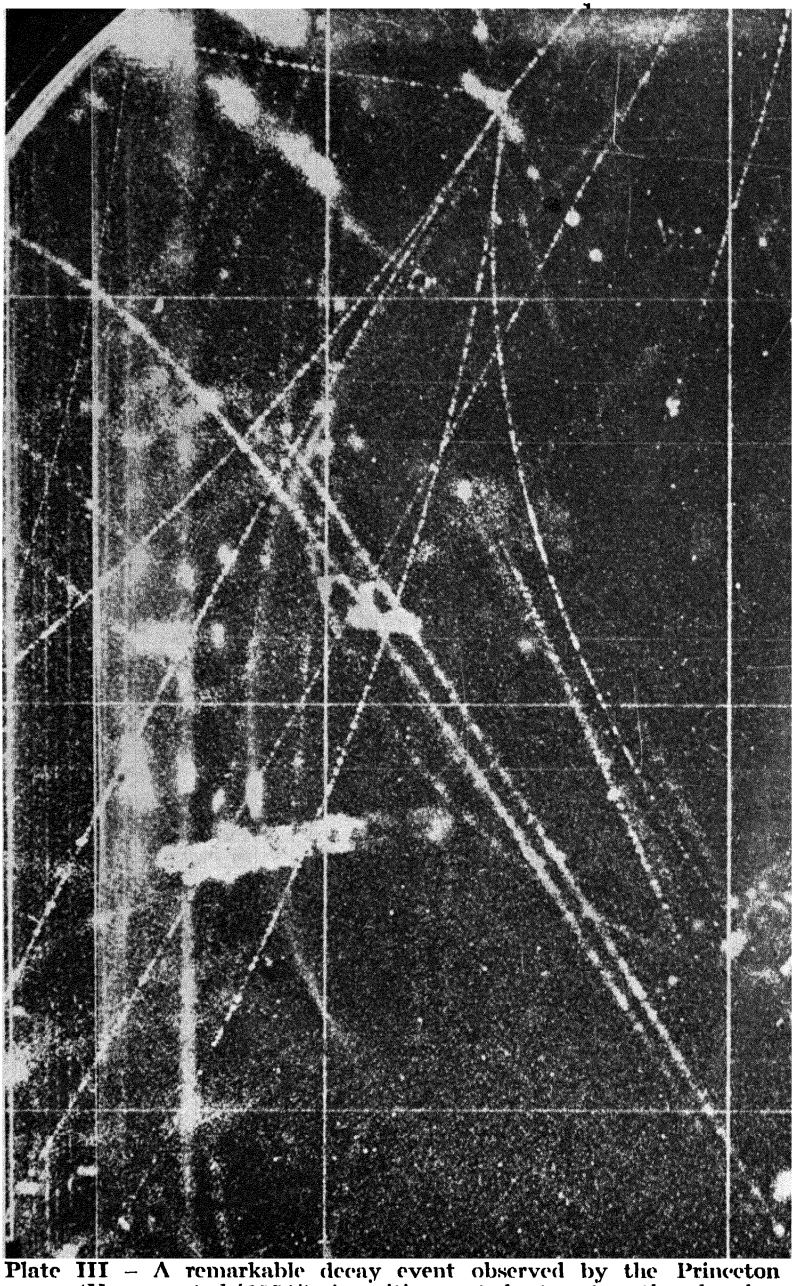

Plate III – A remarkable decay event observed by the Princeton group, (Hodson *et al.* [1954]). A positive particle, 1, enters the chamber and decays into five charged particles according to the process:

$$\chi^+ \rightarrow \pi^+ + \pi^0;\ \pi^0 \rightarrow e^+ + e^- + e^+ + e \ .$$

Particle 2 is interpreted as the π^+-meson; particles 3, 4, 5 and 6 as electrons. The event is discussed in the text.

the scarcity of events in which the actual secondary range is less than the potential value particularly for events in Fig. 8b. It is thus evident that the actual range of most secondaries exceeds the average potential range afforded by the chamber. This situation is improved in the second experimental arrangement and, as a result of the thicker plates, a larger fraction of the secondary particles are stopped. With two possible exceptions the stopped particles fall into two groups, one in which all ranges are about 45 g cm^{-2} of copper ($\sim$60 g cm^{-2} of lead), and another in which the ranges are about 75 g cm^{-2} of copper ($\sim$100 g cm^{-2} of lead). Five events fall into the first category and five into the second.

This grouping of the secondary ranges strongly suggests that the secondaries result from two different two-body decay processes; the arguments given above show that the fraction of the secondary particles which result from possible three-body decay processes must be small. The EP data, Table X, lead to similar conclusions concerning the grouping of the secondary ranges at $\sim$75 g cm^{-2} of copper. Out of 16 events, 6 stop with an observed range of $\sim$75 g cm^{-2} of copper and 1 stops with a range of about 45 g cm^{-2} of copper. The relatively larger number of stopped secondaries results from the greater potential range which is available in the EP chamber while the relatively smaller number of events at 45 g cm^{-2} of copper is presumably a statistical fluctuation.

Thus there is strong evidence from both the MIT and EP groups that the majority of the secondary particles have unique ranges close to 45 or 75 g cm^{-2} of copper.

From the MIT observations there is additional strong evidence for the existence of two distinct range groups which arise from different processes. These data show that the short range secondary particles are associated with photons whereas the long range group are not. We now consider the evidence concerning the K-mesons which are responsible for the S-events observed by the EP and MIT groups.

Evidence Concerning the K_μ-meson

3. 3 Discussion of experimental results

The identification of the K_μ mode of decay rests on the grouping of the secondary ranges just discussed and on the direct measurements of the mass of the primary particles which give rise to the secondaries of range $\sim$75 g cm^{-2} of copper.

A detailed report of the first results obtained by the EP group with the combined magnetic and multiplate chambers described above has been given by GREGORY *et al.* [1954]. The authors concluded that most S-events observed in multiplate chambers arise from a K-meson which is predominately positive, which probably undergoes two-body decay into a μ-meson and a massless neutral particle, and which has a mass that is probably less than that of the τ-meson. The present situation with regard to the experimental data of the EP and MIT groups (ARMENTEROS *et al.* [1955], BRIDGE *et al.* [1955]) reinforces all these points and we consider the above conclusions using the more recent data.

The S-events observed by the Paris group are listed in Table X and are divided into three groups. Group I includes all events in which the primary particle did not traverse the upper chamber; either it was produced in one of the plates or came from an undetermined origin. These events should be strictly comparable with those of the MIT group listed in Table IX. Groups II and III include all events in which the primary particle traversed the top chamber. In these events the sign of the primary particle can be determined and a measurement of its mass is usually possible.

For this reason S-events included in Groups II and III can be attributed to K-mesons even though the secondary track may be short or even absent. If the observed secondary path is less than $\sim 16\ g\ cm^{-2}$ of copper the event can be interpreted in terms of the alternate decay mode of the τ-meson (Table I). All events for which this interpretation is possible are listed separately in Group II and could be τ-mesons. This identification appears likely in a few cases but in the majority of the events there is very little information concerning the actual decay process. Thus most K-mesons in Group II should be regarded as unidentified.

In the following discussion the results listed in Groups I and III will be considered together. This procedure may not be completely valid because the primary K-mesons included in Group III were required to traverse the upper cloud chamber, whereas those included in Group I were not and were mostly produced in the multiplate chamber itself. Because of the greater distance traversed by the particles included in Group III these K-mesons must have lived at least $\sim 5 \times 10^{-9}$ sec while those observed in Group I lived at least $\sim 2 \times 10^{-9}$ sec . It is thus possible that the particles in Group I consist of a mixture in which the components have mean lives

greater than $\sim 10^{-9}$ sec while the particles in Group III are depleted of components with mean lives shorter than 5×10^{-9} sec. However secondary particles whose range exceeds 47 g cm^{-2} of copper appear both in Group I and in Group III and there is no evidence against, and strong evidence for, the assumption that the secondaries in both groups are identical.

3. 4 Direct measurement of the primary mass

From measurements of the momentum and residual range of the primary particles the EP group determined the masses of 22 K-mesons in Groups II and III. The weighted mean value for these events was

$$M_K = (928 \pm 13)m_e.$$

The group of K-mesons used in this measurement contains some τ-mesons and presumably some χ-mesons which can be eliminated by considering only those events in group III in which the secondary particle traversed more than 47 g cm^{-2} of copper (see Table I). There were 6 such events which yielded a weighted mean value of the mass equal to

$$M_K = (906 \pm 27)m_e.$$

These values of the primary mass differ from that of the τ-meson by more than two standard deviations, and the possible experimental errors must be carefully considered in assessing the significance of the result. The quoted statistical error arises from multiple scattering, errors in curvature measurement, and random distortions in the chamber. The effect of the multiple scattering was calculated in the usual way and the last two sources of error were evaluated from measurements on the tracks of 52 protons. The errors of the individual proton mass measurements are about 10% and the dispersion of the data is consistent with this value. From the width of the experimental distribution the combined statistical error which results from random distortions and errors in the measurements of track curvature can be estimated. This spurious curvature amounts to about 2000 m^{-1} and corresponds to a maximum detectable momentum of ~ 15 GeV/c for a track ~ 50 cm long.

Additional systematic errors could arise from the calibration of the magnetic field, systematic distortion in the cloud chamber, or uncertainty in the range energy relation. Since the mean value of

the proton mass obtained from the calibration measurements is $(1833 \pm 25)\ m_e$, it is unlikely that the systematic errors exceed 2%. However the difference between the measured mass of the K_μ-meson and the mass of the τ-meson is just of this order. We return to a discussion of the mass determination after considering the evidence derived from the ranges of the secondary particles.

3. 5 The long range group of secondary particles

There are 29 events in the MIT data and 18 events in the EP data in which the actual amount of material traversed by the secondary particle exceeds 45 g cm^{-2} of copper. Of these 47 particles 14 stop in the chamber and the distribution of their ranges is shown in Fig. 10. This distribution clearly suggests a line spectrum at about 76 g cm^{-2} of copper, and the arguments of § 3.2 show that in any event the spectrum must be very sharply peaked toward the higher ranges.

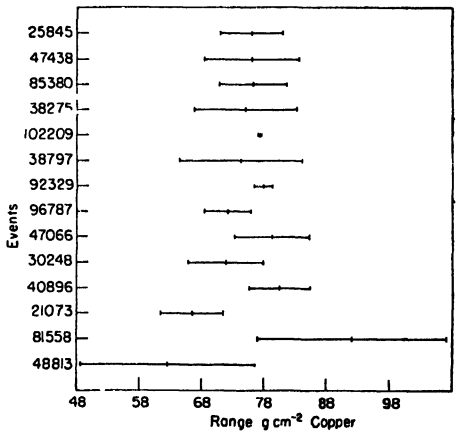

Fig. 10 – Distribution of range limits for stopped secondary particles from K-mesons observed by the EP and MIT groups.

The problem of determining the mean range of the secondaries is of obvious importance. At first sight it would appear that, in a cloud chamber, the accuracy of the range measurements is limited by the finite thickness of the plates. However the range straggling, which arises from fluctuations in the collision loss, introduces a statistical uncertainty of ~3% in a single measurement; thus even if the individual ranges can be measured very accurately, as in emulsions, a considerable number of determinations are required to establish the mean range.

A detailed study of this problem as applied to the multiplate chamber has been made by the EP group and we summarize the conclusions. Let R_1 be the path of the particle in the plates of the chamber up to the point at which it enters the last plate, and R_2 be the path up to the point at which the particle would have emerged (in the absence of scattering) had it not stopped in the

plate. $\triangle R_1$ is the statistical error in R_1 which results from range straggling, reconstruction errors and multiple coulomb scattering in the plates; it is usually about 3 g cm^{-2} of copper. In the absence of this statistical error the distribution of secondary ranges between R_1 and R_2 is flat. This follows from the experimental observation that the decay points of the S-events are uniformly distributed throughout the plate of decay and that the angular distribution of the secondary particles is isotropic.

The statistical error in R_1 is of course transferred unchanged to R_2 and hence the edges of the rectangular distribution at R_1 and R_2 are modified to correspond to the approximately gaussian distribution of $\triangle R_1$ and $\triangle R_2$. Then, depending on the actual plate thickness, the two sides of the resulting symmetrical curve may join smoothly to form a flat topped distribution function, meet smoothly at the center to give a final bell shaped curve, or may join at an angular point. The exact behaviour depends on the ratio of the error $\triangle R_1$ to the plate thickness, and, for the EP or MIT arrangement, the final distribution can be represented very well by a gaussian curve. This statement must be modified if the particle enters the final plate with an angle of incidence, Θ, greater than 45°. In this case scattering of the particle introduces an unsymmetrical fluctuation in the error $\triangle R_2$ and introduces a skewness into the resulting probability curve. The exact distribution function can be used if necessary, but for $\Theta < 45°$ it is sufficient to obtain the mean μ-meson range, $\langle R \rangle$, from the gaussian distribution defined by,

$$\langle R \rangle = \frac{R_1 + R_2}{2}, \qquad \Theta < 45°;$$

$$\langle (R - \langle R \rangle)^2 \rangle = \triangle R_1^2 + \frac{(\langle R \rangle - R_1)^2}{3} + (\langle R \rangle - R_1)^2 (0.022 \tan^2 \Theta).$$

The distribution of the individual ranges obtained by this method is shown in Fig. 11 which can be compared with Fig. 10. The final range distribution is perfectly consistent with that expected under the hypothesis that the secondary particles have all the same energy, and the results may be combined to give a weighted mean range for the secondary particle emitted in the K_μ-decay process. The result is $R = (75.8 \pm 1.2)$g cm^{-2} of copper. The range distributions shown in Figs. 10 and 11 and the absence of secondary particles which stop between 45 and 75 g cm^{-2} of copper (§ 3.2)

establish the existence of a two-body decay process in which the secondary particle has a range of ~ 76 g cm^{-2} of copper.

3. 6 The decay scheme of the K_μ-meson

From the discussion given in § 3.2, most secondary particles which traverse more than ~ 47 g cm^{-2} of copper must originate from the two-body decay process discussed in § 3.3 and have ranges of ~ 76 g cm^{-2} of copper. We recall that there were six particles in this group for which a direct measurement of the primary mass was possible and that the mean value of the mass was, $M_K = (906 \pm 27)m_e$. These two pieces of information lead to the conclusion that the charged secondary particle is a μ-meson and that the neutral particle is a neutrino. Suppose that, as a conservative upper limit, the mass of the primary particle is assumed equal to the mass of the τ-meson, 965 m_e, and that the lower limit for the range of the charged secondary particle is taken as 75 g cm^{-2} of copper. Then the maximum possible range of a π-meson emitted in the decay of a particle of mass 965 m_e is ~ 55 g cm^{-2} of copper. Thus, if the charged secondary is a known particle, it must be a μ-meson.

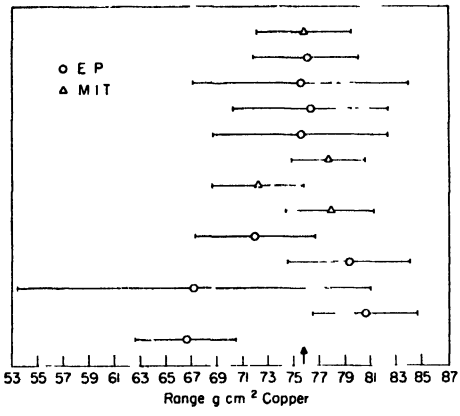

COMBINED DATA E P AND MIT FOR LONG RANGE SECONDARIES

Fig. 11 -- Distribution of mean ranges for stopped secondary particles observed by the EP and MIT groups. The determination of the mean range and its error is described in the text.

This conclusion is also reached independently when the MIT data is analyzed under the assumption that the majority of the secondary particles have a unique range of ~ 45 or ~ 76 g cm^{-2} of copper. The particles in the longer range group then traversed 16.5 geometric mean free paths of material without an interaction, whereas, using the known cross sections in the appropiate energy region, about 8 nuclear stoppings should have been detected had the secondary particles been π-mesons.

The mass of the neutral particle produced in the two-body decay

process can then be determined from the mass of the primary particle and the momentum of the μ-meson secondary as derived from its range. Using the above values of primary mass and secondary range the upper limit for the mass of the neutral particle is $\sim 50\ m_e$. Clearly the neutral particle must be a neutrino or a gamma ray. The latter possibility is eliminated because the gamma rays would be detected (by the observation of electron cascades) with very high efficiency. None have been seen. Thus the decay scheme originally proposed by the EP group,

$$K_\mu \rightarrow \mu + \nu,$$

is well established.

3. 7 The mass of the K_μ-meson

The "direct" mass of the K_μ-meson as determined from measurements on the primary particle is

$$(906 \pm 27)\ m_e.$$

The "indirect" mass determined from the decay scheme and the mean range of the secondary particles is*

$$(942 \pm 8)\ m_e.$$

Both values were computed using the range energy relation given by Aron, Hoffman and Williams [1949]. On this basis the secondary range of (75.8 ± 1.2) g cm^{-2} of copper corresponds to a momentum $p_\mu = (229 \pm 2)$ MeV/c.

The effect of a systematic error in the range energy relation on these two measurements can be seen from the following argument. Over a limited region the functional dependence of p, R and m can be written in the form of a power law,

$$\frac{p}{mc} = k\left(\frac{R}{mc^2}\right)^a,$$

where k and a are constants. The relative error in mass for the direct mass determination is then given by,

$$\left(\frac{\triangle M}{M}\right)_1 = \frac{1}{1-a}\left(\frac{\triangle p}{p}\right)_1 - \left(\frac{\triangle p}{p}\right)_2 = \frac{1}{1-a}\frac{\triangle B}{B} - \left(\frac{\triangle p}{p}\right)_2$$

* The mean range on which this mass value is based was obtained by combining the MIT and EP results. In the former case the ranges were determined in brass and in the latter, in copper. This procedure is justified since at 75 g cm^{-2} of copper the range of a μ-meson differs by less than 0.01 per cent in the two materials, (D. O. Caldwell [1955b]).

where $\left(\frac{\Delta p}{p}\right)_1$ is the error in momentum which results from the uncertainty in the magnetic field and $\left(\frac{\Delta p}{p}\right)_2$ is the error in momentum at constant range which results from the uncertainty in the range energy relation.

For the "indirect" mass measurement the relative error in mass is given by,

$$\left(\frac{\Delta M}{M}\right)_2 = \beta_1\beta_2 \left(\frac{\Delta p}{p}\right)_2,$$

where β_1 and β_2 are the velocities of emission of the charged and neutral secondary particle in the c.m.s., and p is the momentum of the charged secondary in the c.m.s.

Thus, at constant range, a change in the momentum produced by a change in the range-energy relation affects the direct and indirect mass measurements in an opposite sense.

Recent evidence (CALDWELL [1955a]) shows that the ionization potential for copper, I_{Cu}, is equal to about 377 eV and is constant for proton energies up to about 100 MeV. Thus all low energy data disagrees with the single high energy proton range measurement of MATHER and SEGRÉ [1951], which leads to an ionization potential of ~310 eV. It is nearly certain that the higher value is correct.

In their calculations ARON *et al.* used $I_{Cu} = 333$ eV. Calculations have also been made by ARON [1951], for $I_{Cu} = 309.9$ eV. From these two range-energy relations $\left(\frac{\Delta p}{\Delta I}\right)_R$ can be evaluated and used to calculate new values of the momentum for an ionization potential equal to 377 eV.* Based on $I_{Cu} = 377$ eV the corrected mass values then become (916 ± 27) m_e for the "direct" mass measurement and (934 ± 8) m_e for the "indirect" measurement.

These results appear to provide strong independent evidence for a mass lower than that of the τ-meson. However, although a lower mass is indicated, no positive conclusion can yet be drawn from the results. Assuming that the range-energy relation is correct, the direct mass measurement can still be affected by an error in the

* Caldwell concludes that for heavy elements $I \sim 13Z$. Correcting the range-energy relation for emulsion given by BARKAS [1954] (this is identical to the range-energy relation of Vigneron at proton energies below 220 MeV) for this fact one arrives at a corrected "best" range-energy relation for emulsion. A comparison of the published data for the ranges of π-meson secondaries emitted in the decay of the τ-meson leads to the conclusion that the Q-value (§ 1) is uncertain by about $\pm$ 3 MeV.

calibration of the magnetic field. A 2% error in this measurement is possible and changes the K_μ-mass by about the statistical error, 27 m_e. Thus the quoted value of the mass is certainly compatible with that of the τ-meson.

On the other hand the mean range of the secondary particle is derived from the application of a statistical treatment valid for large samples to 14 events, and a fluctuation affecting the entire data is possible. It is also possible that the sample is not homogeneous and that it contains some event wrongly classed as a K_μ-meson, or in which the K-meson decayed in flight. The effect of such an extraneous event can be estimated by eliminating from the data the two events with the highest and lowest range or, in case the alternate procedure gives a large effect, eliminating the event with the largest statistical weight. On eliminating the highest and lowest ranges from the 14 events discussed above, the best value of the "indirect" mass becomes

$$M_{K_\mu} = (934 \pm 9)\, m_e,$$

and the corresponding secondary momentum is

$$p_\mu = (229 \pm 2.5)\ \text{MeV/c}.$$

This mass value is about three standard errors, removed from the τ-meson mass. The total deviation corresponds to ~ 6 g cm^{-2} of copper or to a plate thickness of more than half a centimeter. While a gross error in range of this magnitude is practically out of the question, an unknown systematic error of 10 mass units could certainly be present. Allowing for an additional statistical fluctuation it is possible, though not probable, that the K_μ- and τ-meson masses are identical.

Evidence Concerning the χ-meson

The χ-meson has been the subject of intensive investigation ever since it was originally suggested by POWELL in 1952. Nevertheless no particular experiment has given decisive evidence for its existence and decay scheme; these questions have rather been answered slowly by a series of parallel measurements in emulsions and cloud chambers no one of which is in itself conclusive. The collective evidence however clearly establishes the decay mode $\chi \to \pi + \pi^0$.

The emulsion data have already been considered in § 2.4 and we now turn to the cloud chamber results. Finally, in § 3.11 we

consider some additional evidence concerning this mode of decay based on an unusual decay in flight observed by the Princeton group.

3. 8 The occurrence of photons among the decay products

The existence of photons as neutral decay products should result in electron cascades associated with the decay. Although these cascades were at first sought without success, their presence is now firmly established (Bridge *et al.* [1953]). About 14 of the 67 S-events observed by the MIT group, Table IX, show evidence for a photon.

The first nine of these events occurred in a sample of 33 S-events and have been rather completely analyzed (Courant [1954a, 1955]). We give a short summary of the conclusions:

(1) It is not possible to explain the association of electron cascades and S-events as chance coincidences. The probability for chance association between an unrelated electron cascade and an S-event can be evaluated rather easily and, although low energy electron showers occur frequently, the probability of a chance coincidence is only 0.0013. Hence the probability that each cascade is unrelated to its S-event is $(.0013)^9 = 10^{-26}$.

(2) The data cannot be explained by the decay of a K-meson into a charged meson and a photon. If such a two-body decay process were responsible for the events, the paths of the decay products would lie in the same line. Instead the line of flight of the photon is not always colinear with that of the charged decay product (Table IX).

(3) The neutral particle could be a π^0-meson emitted in a two-body decay process. In this case, since the decay occurs at rest, the line of flight of the π^0-meson is opposite to that of the charged decay product. The calculated angular distribution of the forward photon with respect to the line of flight of the π^0-meson (obtained by transforming the isotropic distribution in the rest system of the π^0-meson into the laboratory system) is shown in Fig. 12 for a π^0-meson of momentum 200 MeV/c. One sees that the distribution in the laboratory system is peaked at a relatively small angle to the line of flight, $\sim 20°$. The momentum at which the peak occurs depends, of course, on the momentum assumed for the π-meson, and it is found that the observed angular distribution of the photons is consistent with that expected from a π^0-meson of mo-

mentum between 200 and 400 MeV/c. If the photons arise from π^0-mesons, both photons should occasionally be detected. The detection probability for this second photon has been computed for all of the events given in Table IX for a π^0-meson of momentum 200 MeV/c and is essentially zero in most of these.

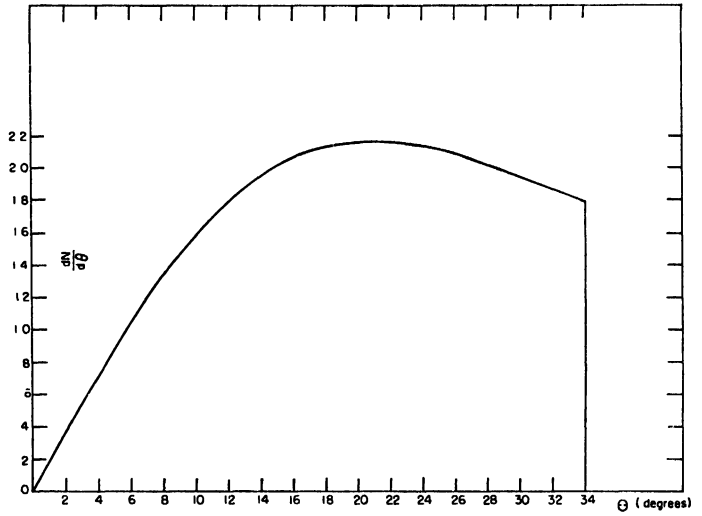

Fig. 12 – The differential frequency distribution of photons from the decay of the π^0-meson as a function of angle in the laboratory system. θ is the angle between the line of flight of the π^0-meson and the photon which is emitted in the forward hemisphere in the rest system. The figure is drawn for a π^0-momentum of 200 MeV/c.

(4) A two-body decay of the type $K \to \pi + \pi^0$ cannot account for all of the 33 S-events included in the sample of data. For, under this assumption, Courant found that 16 electron cascades should have been observed whereas only 9 were detected. Since the probability to observe 9 or fewer cascades was only 3×10^{-3}, the original hypothesis is quite unlikely.

3. 9 Discussion of the cloud chamber results

We now consider in detail the results concerning the secondary particles whose ranges are less than ~ 45 g cm^{-2} of copper. Define R' as the amount of material actually traversed by the secondary particle regardless of whether or not it was brought to rest. Then there are 38 events, Table IX, in which $R' < 45$ g cm^{-2} of copper and there are 29 events in which $R' > 45$ g cm^{-2} of copper. In none of the 29 events in which $R' > 45$ g cm^{-2} of copper is there

an associated electron shower, but in 14 of the 38 events in which $R' < 45$ g cm^{-2} of copper there is an associated electron cascade. Thus the photons are clearly associated with the group of events in which it is possible for the true range to be ~ 45 g cm^{-2} of copper. Of the 38 events in this class seven stop in the chamber; in five of these the range is close to 45 g cm^{-2} of copper, but in two events the range is appreciably less than this value. Four of the first five, and both of the second two events are associated with electron cascades.

It is then possible to explain the seven stopped particles in terms of a single three-body decay process in which one of the neutral particles is a π^0-meson or a γ-ray; or on the basis of the two-body decay process, $K \rightarrow \pi + \pi^0$. In the latter event the two short range secondaries can be accounted for by nuclear interactions and the charged particles must therefore be π-mesons rather than μ-mesons.

A detailed analysis of the 38 events in which $R' < 45$ g cm^{-2} of copper, under the assumption that all the events observed in the cloud chamber result either from the above two-body decay process or from the K_μ-meson, leads to the following conclusions. (a) From the average detection probability for the photons produced in the $\pi + \pi^0$ mode of decay, about 20 of the 67 events (or about 25 to 30 percent) included in Table IX must be attributed to this decay process while the rest arise from K_μ-mesons. (b) The mean range of the five secondary particles which have ranges close to 45 g cm^{-2} of copper is (44.2 $\pm$ 1.7) g cm^{-2} of copper.

Using the range energy relation of Aron, Hoffman and Williams and correcting to $I_{Cu} = 377$ eV as discussed in § 3.7 this value of the range corresponds to a secondary momentum

$$p_\pi = (202 \pm 4) \text{ MeV/c},$$

and to a primary mass of

$$M_K = (955 \pm 12)\, m_e.$$

For comparison we list again the corresponding values obtained by the Padua group (§ 2.4). From direct mass determinations on the tracks of the primary particles and scattering measurements on the secondary tracks they obtained

$$M = (976 \pm 36)\, m_e,$$

and

$$p_\pi = (200 \pm 6) \text{ MeV/c}.$$

3. 10 The decay scheme of the χ-meson; Discussion of the cloud chamber and emulsion results

The mass of the primary particle and momentum of the secondary particle obtained from the emulsion data were derived from independent measurements, and, under the assumption of two-body decay, they can be used to obtain the mass of the neutral secondary particle. Using the above values, the mass of the neutral particle is $(309 \pm 65)\ m_e$. To reduce this value to zero the mass of the primary particle would have to be reduced to $868\ m_e$ or about 1.7 standard deviations. The emulsion results thus indicate that the secondary particle is a π^0-meson.

The cloud chamber results concerning the photons have been discussed above and provide strong independent evidence to the same effect. If the decay process is a two-body one the angular distribution of the associated electron cascades can only be understood if the neutral particle is a π^0-meson. Moreover the good agreement between the values of the secondary momentum obtained in cloud chambers and emulsions depends on the assumption that the neutral particle has a mass about equal to that of the π-meson.

All of the above evidence supports the original hypothesis of a two-body decay scheme and confirms the assumption that the χ-meson observed in emulsions is identical with the K-meson which gives rise in cloud chambers to the shorter range group of secondary particles associated with photons. Either the emulsion or the cloud chamber data taken alone provide strong evidence for the decay scheme

$$\chi \rightarrow \pi + \pi^0 + 219\ \text{MeV};$$

taken together the evidence is conclusive.

3. 11 Other results concerning the χ-meson

Using a cloud chamber with associated magnetic field the Princeton group (Hodson *et al.* [1954]) have obtained the remarkable event shown in Plate III. A positive particle, 1, enters the cloud chamber and decays in flight into five charged particles, 2, 3, 4, 5 and 6. One of these, particle 2, is also positive and lighter than a K-meson. The remaining four particles are emitted as two pairs of positive and negative particles, and the angle included by either pair is small, of the order of one degree.

From ionization and momentum particle 6 must be an electron; particles 3 and 5 could be electrons or light mesons and particle 4 is less massive than a proton.

The momentum of the primary particle cannot be measured and therefore a complete momentum balance for the event is impossible. However the transverse momentum balance is very good and thus any neutral particle would have to have been emitted almost in the line of flight of the primary particle.

The authors have considered the various possible explanations for the event in detail and conclude that the most likely interpretation is in terms of the decay process

$$\chi \rightarrow \pi + \pi^0,$$

followed in $\sim 10^{-15}$ sec by the decay process

$$\pi^0 \rightarrow e^+ + e^- + e^+ + e^-.$$

Although the direct decay of the π^0-meson into four electrons had not been previously observed, it had been predicted theoretically, and the frequency of this occurrence relative to the normal decay $\pi^0 \rightarrow 2\,\gamma$ should be $\sim 4 \times 10^{-5}$, DALITZ [1954]. The assumption that a π^0-meson was actually responsible for the "electron" pairs is supported strongly by a dynamical analysis of the tracks in question. It turns out that they are equivalent to a particle of mass $(255\ ^{+15}_{-10})\ m_e$. There remains the question of the identity of particle 2 which from the experimental data could be either a π^+ or μ^+-meson. Under the assumption that the decay process is either $K^+ \rightarrow \mu^+ + \pi^0$ or $K^+ \rightarrow \pi^+ + \pi^0$, the calculated values of the mass of the primary particle are, respectively, $M = (876\ ^{+30}_{-20})\ m_e$, and $M = (954\ ^{+30}_{-20})\ m_e$. The second possibility obviously agrees well with the properties of the χ-meson whereas there is no evidence from other experiments which even suggests the existence of a K-meson of mass $\sim 900\ m_e$ which decays into a μ^+-meson and a π^0-meson. Thus the most probable explanation of the event is in terms of the χ-meson and it provides striking additional evidence that the neutral particle must be a π^0-meson.

The momentum, p^*, of the π^0-meson and π^+-meson in the c.m.s. is

$$p_\pi = (201\ ^{+9}_{-6})\ \text{MeV/c}.$$

The Charge Asymmetry of S-particles Observed in Cloud Chambers

3.12 Results of the EP group

Table X contains 22 positive and 2 negative events whose masses could be well determined. Thus in these cases the sign of the primary particle is unambiguous. From this result the EP group conclude that, in the energy and lifetime range determined by the experimental conditions, negative particles constitute less than 20% of the observed events. We return to this observation in the discussion concerning the charged V-particles.

4. Results Concerning Charged V-Particles Obtained with Cloud Chambers Using a Magnetic Field

4.1 Introduction

In comparison with emulsions or multiplate cloud chambers the usual experimental arrangement of cloud chamber with associated magnetic field contains a relatively small amount of stopping material. Therefore few particles are brought to rest and most decays take place in flight. In the case of a charged particle which decays into a single charged secondary particle (plus one or more neutral particles) the decay in flight is known as a charged V-particle. The experimental measurements which can be made on such an event consist of curvature determinations in the magnetic field and measurements of the relative specific ionization by droplet counting or photometric means. The magnetic curvature furnishes a measure of the particle sign and momentum and the ionization determines the velocity of the particle.

In practice the ionization is difficult to determine and it is only very recently that results of good precision have been obtained in experiments on unstable particles (Cowan [1954], Fretter and Friesen [1955]). In the usual experimental arrangements, however, measurements of momentum and estimates of ionization are often sufficient to specify the primary as a K-meson rather than a proton or hyperon.

In general the analysis of decays in flight is inherently more difficult and less complete than the analysis of decays at rest because the information concerning the primary and secondary particles is interdependent. One quantity which is usually used to

characterize the decay process is the momentum, p^*, of the secondary particle in the rest frame of its parent. For S-events p^* is obtained directly from measurements on the secondary particle alone; for a V-event, however, the transformation to the rest system requires a knowledge of the velocity of the primary particle as well as data concerning the secondary particle. The number of events which afford good measurements on both the primary and secondary particles is limited and the additional measurements increase the errors of individual determinations.

A further important quantity which characterizes any decay process is the mean lifetime of the parent particle. While decays at rest provide only a lower limit to the mean life, decays in flight afford, at least in principle, an exact determination.

Let the visible path of the particle up to the point of decay be defined as x, and let the total distance in which the decay process would have been identified as such, had the decay not taken place at x, be the potential path, x_0. These distances correspond to times in the rest system of the parent particle through the relation $t^* = Mx/P$, and $t_0^* = Mx_0/P$. Qualitatively, if the lifetime of the particle is long compared to t_0^* the decay points will be uniformly distributed throughout the chamber and $(t^*/t_0^*)_{Av} \approx \frac{1}{2}$. If the lifetime is short compared to t_0^*, the decay points will cluster closer to the producing material at the top of the chamber and $(t^*/t_0^*)_{Av} < \frac{1}{2}$. Considerable work has been carried out on statistical methods which are appropriate for treating the data (BARTLETT [1953a, 1953b], ALFORD and LEIGHTON [1953]) and on procedures which are necessary to avoid experimental bias (WILSON and BUTLER [1952], NEWTH [1954]). The same general methods have recently been applied to V-events observed in emulsions (AMALDI [1954c]). Several points deserve emphasis:

(a) The discussion just given implies a strong experimental bias in that events are selected on the basis of lifetime. The range of momentum over which precise measurements are possible is relatively small, therefore the vertical dimension of the chamber determines a proper time of flight, t_0^*, rather closely. Accordingly decay events are only observed with high probability if $\tau \approx t_0^*$. (b) The statistical information available per event depends on the length of time the particle can be observed relative to its mean life, i.e., on t_0^*/τ. If $t_0^* < \tau$ no useful information can be expected (BARTLETT [1953a]). (c) The methods of estimating τ assume a pure

sample of events and it is extremely difficult, using only statistical methods, to separate two mean lives which differ by a factor of ten or less (BARTLETT [1953a]). In this case it becomes necessary to identify the particles by some other feature of the decay process. While this is possible in case of the neutral V-events because of the great difference in the dynamics of the θ^0- and Λ^0-decay processes, it is much more difficult for the charged V-particles because the dynamics of different decay events are apparently very similar. Thus the unambiguous separation of events which arise from decays of K_μ- or χ-mesons requires very precise measurements on long tracks. The requirement that the primary and secondary track both be well measurable, and hence long, restricts the possible points of decay to a small region of the chamber and results in small values of x_0 and t_0. Then, according to (b), the measurement of τ becomes difficult.

4. 2 DYNAMICAL ANALYSIS OF V-EVENTS

In an analysis of decay events one of the more important pieces of information is the distribution of the secondary momenta in the rest frame of the parent particle. For a two-body decay process the secondary momentum has a unique value usually denoted by p^* while in the case of a three-body decay process the distribution of secondary momenta depends on specific assumptions concerning the decay products and the nature of the interactions between them.

In principle a two-body decay in flight is completely specified by five quantities (e.g., two momenta, two masses, and the angle between the line of flight of the primary particle and one of the secondary particles). Thus in order to compare events on an individual basis it is necessary to measure five experimental quantities for each. As indicated above the determination of velocity is difficult in cloud chamber measurements, and there are usually available measurements on only three quantities of the five. In the majority of events not even this much information is available. The experimental results have therefore usually been compared with an assumed decay scheme in a statistical way.

The simplest such treatment makes use of information concerning the charged secondary particle only. In a two-body decay process the differential distribution of the secondary transverse momentum, p_t, is given by (YORK [1952]):

$$dN = \frac{p_t}{p^{*2}(p^{*2} - p_t^2)}\, dp_t \qquad (4.1)$$

where $p_t = p \sin \Phi$, p is the secondary momentum in the laboratory frame of reference, and p^* is the momentum of the secondary in the frame of reference of the primary particle. Similarly Φ and Φ^* are the angles between the line of flight of the primary particle and that of the charged secondary particle in the two reference systems.

The effect of experimental errors on this distribution (York [1952]) modifies the shape considerably and makes it difficult to distinguish between the distributions predicted for two- and three-body decay processes. Furthermore, the experimental bias is certainly large and it is difficult to allow for this effect. One must be sure that, for each event accepted, it would have been possible to measure any value of p_t included in the experimental distribution, had this value occurred rather than the value actually observed (Lagarrigue and Peyrou [1951]). This bias greatly modifies the p_t distribution and has not been taken into account in any results published so far.

In addition to these experimental uncertainties there is a further difficulty in that a mixture of events from different decay processes can produce a p_t distribution of almost arbitrary shape. Therefore, since it is known that the charged V-events result from at least three decay processes, the significance of the results is questionable, and the p_t plot is only useful in comparing different sets of data. If, for example, the p_t distributions for positive and negative events show marked differences, then there must be some corresponding difference in the two classes of events. However the reason for such a result cannot be established from the p_t plots.

A good deal more information can be obtained from events in which a more complete dynamical analysis is possible. Consider a particle of mass M which decays into any number of secondary particles. In the rest frame of the primary the momentum, p_i^*, of a particular secondary particle can be written as:

$$p_i^{*2} = p_i^{*2} \cos^2 \Phi^* + p_i^{*2} \sin^2 \Phi^* = p_{il}^{*2} + p_{it}^{*2} \qquad (4.2)$$

where Φ^* is the angle between the lines of flight of the primary and secondary particles in the c.m.s. The terms on the right-hand side represent respectively the longitudinal and transverse components of the momentum of the secondary particle in the rest

system; the transverse component is invarient on transformation to the laboratory system. On transforming the longitudinal component one obtains an expression for p_t^* in terms of the measured quantities in the laboratory system:

$$p_t^{*2} = \left\{\frac{\beta Mc}{2}\left(\frac{2p_t \cos \Phi - P}{P} - \frac{2U_t^* - Mc^2}{Mc^2}\right)\right\}^2 + p_t^2 \sin^2 \Phi. \quad (4.3)$$

Here βM and P refer to the primary particle; βc is its velocity and M its mass. The momentum of the secondary particle in the laboratory system is p_t and its total energy in the c.m.s. is U_t^*. The term $(2p_t \cos \Phi - P)/P$ is commonly denoted by a_t. For the special case in which a particle of mass M decays into two secondary particles whose masses are m_1 and m_2, U_1^* is given by the relation

$$U_1^* = \frac{(M^2 + m_1^2 - m_2^2)c^2}{2M} = \frac{Mc^2}{2}(1 + \bar{a}), \quad (4.4)$$

where $\bar{a} = (m_1^2 - m_2^2)/M^2$ is the average value of a_1. It is apparent that $\bar{a}$ is a measure of the mass assymetry between the secondary particles, and varies between the limits ± 1 depending on the ratio of m_1/m_2 and the Q value of the decay. For the two-body decay process Eq. (4.3) may thus be written

$$p_1^{*2} = \left(\frac{\beta Mc}{2}\right)^2 (a_1 - \bar{a})^2 + p_1^2 \sin^2 \Phi, \quad (4.5)$$

where

$$p_1^{*2} = p_l^{*2} + p_t^{*2},$$

$$p_l = \frac{\beta Mc}{2}(a_1 - \bar{a})$$

$$p_t = p_1 \sin \Phi.$$

This relation is useful in the analysis of events in which the momenta of the primary and secondary particles can be measured. It is apparent from Eq. (4.2) that all events which result from the same two-body decay process can be plotted on a semicircle of radius p^*. Such a plot is simply a representation of the p^* vector in the centre of mass system; the length of the radius vector gives the value of p^* and the angle with the abscissa gives the angle, with respect to the line of flight of the primary particle, at which the secondary was emitted in the centre of mass system. Isotropy in the centre of mass system implies that one half of the events lie between $60° < \Phi^* < 150°$ and that one half lie outside this region.

In order to compare the experimental data with an assumed decay scheme, Eq. (4.5) and the parameters of the postulated decay process are used to compute p_t^* from the measured quantities P, p_1, and Φ. Values of p_t are obtained directly. The resulting values of p^* are plotted and compared with the expected semicircle.

The locus of points in the (p_l^*, p_t^*)-plane defined by Eqs. (4.2) and (4.5) provides a more sensitive test of an assumed two-body decay scheme than the constancy of the p^* values alone. Other dynamical treatments are possible in terms of a decay surface and perhaps, more advantageous than the one adopted here (THOMPSON [1953]; PODOLANSKI and ARMENTEROS [1954]). However for the charged V-events the surfaces which define a given decay scheme are very close together and no particular representation appears to be markedly superior to any other.

Some decay schemes already considered are very difficult to separate by such a treatment. In the case of the χ- and K_μ-decay processes the values of M, p^*, and $\bar{a}$ are nearly identical (Table I), and any dynamical analysis fails to distinguish between such events. Nevertheless, in view of the interpretation of decays at rest it is interesting to see whether or not the charged V-particles can be explained in terms of these two processes.

4. 3 DISCUSSION OF THE EXPERIMENTAL DATA: EVENTS WITH LOW VALUES OF P^*

Data for 38 positive and 22 negative charged V-events are presented in Figs. 13 and 14. For purposes of calculation we assume the decay scheme $K_\mu \rightarrow \mu + \nu$ with $M_K = 924\, m_e$ and $m_\mu = 207\, m_e$. These assumptions result in a value of $\bar{a} = 0{,}0504$, and the calculated points are expected to fall on a circle of radius $p^* = 224$ MeV/c. The positions of the experimental points are essentially unaltered if the decay scheme is instead $\chi \rightarrow \pi + \pi^0$ with $M_\chi = 966\, m_e$, but the expected circle is defined by $p^* = 205$ MeV/c.

From inspection of Figs. 13 and 14 it is evident that some points do not fall near the semicircle defined by the K_μ- or χ-decay and that it is impossible to explain this fact on the basis of the experimental errors. No unique interpretation of these results is possible. A single three-body decay process or a mixture of a two-body decay and a three-body decay could explain the results equally well.

Several arguments however show that the latter explanation

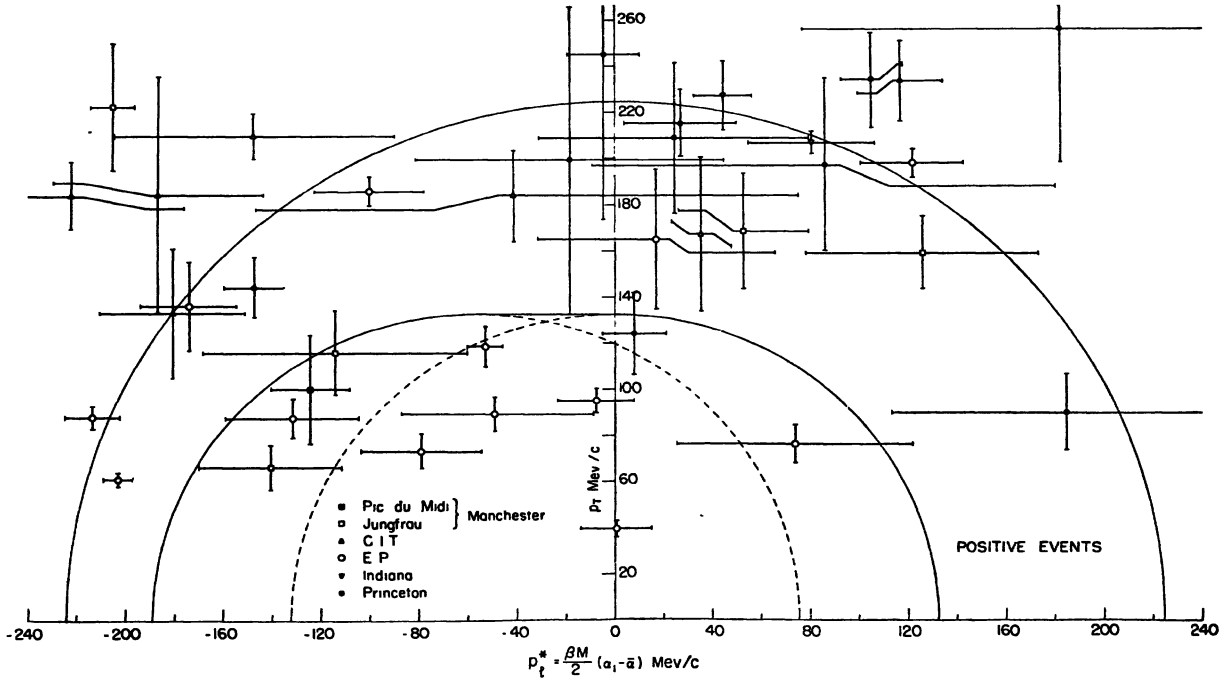

Fig. 13 – Experimental data for 38 positive charged V-particles. The ordinate represents the transverse momentum, p_t, of the charged secondary particle in MeV/c; the longitudinal momentum, p_l^*, of the secondary particle in the rest system of the primary is plotted on the abscissa. Thus a point on the plot specifies the momentum vector of the secondary particle in the rest frame. The length of the radius vector is equal to the momentum, p^*, with which the secondary particle was emitted, and its angle with the positive abscissa is equal to the angle, Φ^*, between the direction of motion of the primary particle and that of the charged secondary particle in the rest system. The significance of the displaced circle and the calculation p_l^* are discussed in the text.

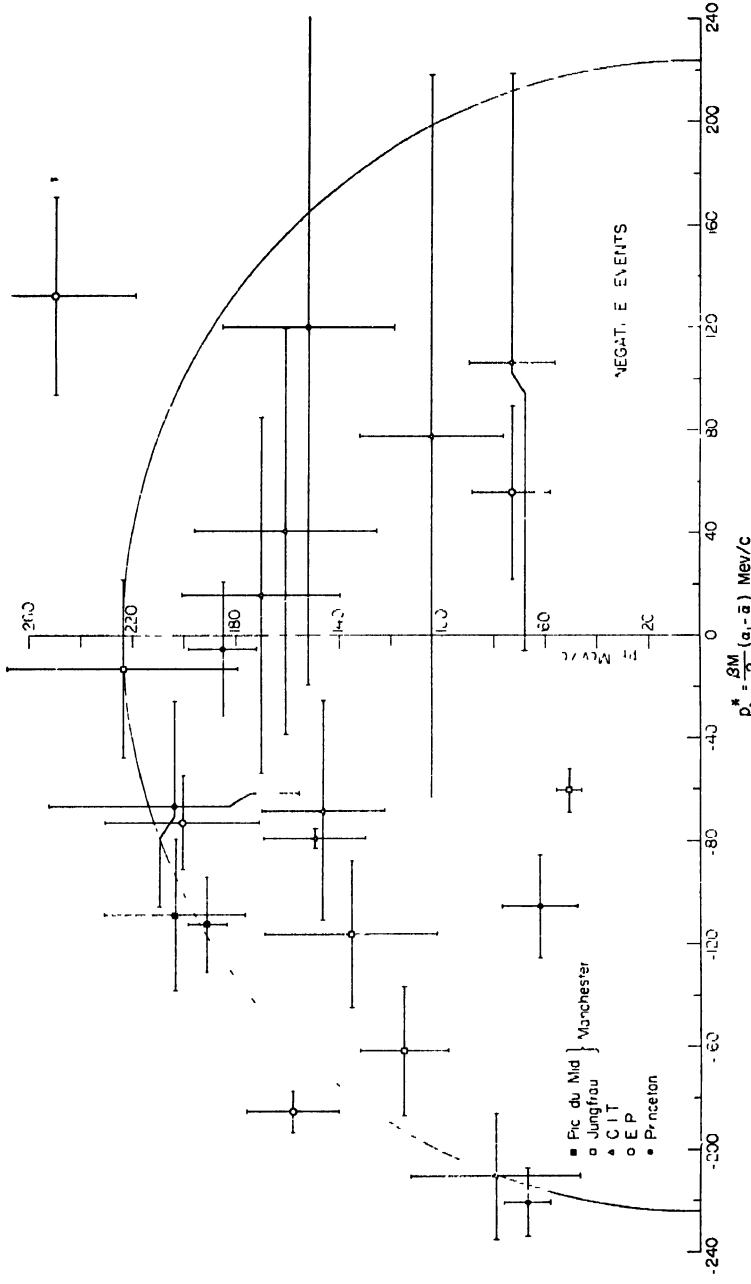

Fig. 14 – Experimental data for 22 negative charged V-particles. The plot has the same significance as Fig. 13.

cannot account for the majority of the data. Many of the slow primary particles which are responsible for the charged V-events shown in Figs. 13 and 14 lived for a time longer than 10^{-9} sec, and this value is about as long as the moderation time of a similar particle observed in a multiplate chamber (because of the larger average density the time for such a particle to come to rest in the usual multiplate chamber is $\sim 10^{-9}$ sec). Therefore many of the decays in flight observed in magnet chambers would have occurred at rest had the primary particles been observed in a multiplate chamber. The systems of counter control which have been used for magnet and multiplate chambers are similar; thus the selection of particles can only be on the basis of lifetime. For this reason it is certain that at least some V$^+$-events, observed in magnet cloud chambers are produced by the same K-mesons which are responsible for the S-events observed in multiplate cloud chambers. Thus some charged V-events must result from the decay of K_μ- or χ-mesons.

However not all charged V-events can be explained on this basis because of the spread in p^* values and because among the secondary particles there are several well identified μ-mesons whose momenta are considerably below that of the μ-meson produced in the K_μ-decay process. It thus seems reasonable to explain the observations of charged V-particles in terms of a mixture of two- and three-body decay processes. We therefore digress to consider how an actual three-body decay process, computed under the assumption of two-body decay, would appear in the representation used in Figs. 13 and 14.

Assume that the decay process involves three decay products, a charged particle of mass m_1 and two neutral particles of masses m_2 and m_3. U_1^* then varies from a minimum of m_1c^2 when the charged particle is produced at rest and $\bar{p}_2^* + \bar{p}_3^* = 0$, to a maximum of $\{[M^2 + m_1^2 - (m_2 + m_3)^2]c^2\}/2M$ when the neutral particles move with equal velocities in a direction opposite to that of the charged particle in the c.m.s. (ARMENTEROS *et al.* [1952]).

In the case of a three-body decay (or in the case of a two-body decay whose dynamics are unknown) it is convenient to write Eq. (4.3) in the form

$$p_1^{*2} = (\lambda - \lambda_0)^2 + p_t^2 \tag{4.6}$$

where $\lambda = \beta Mca/2$ and $\lambda_0 = \beta\,(2U_1^* - Mc^2)/2c$. This equation

defines a circle of radius p_1^* in the (λ, p_t) plane whose centre is at $\lambda = \lambda_0, p_t = 0$. Since p_1^* and λ_0 depend on U_1^*, each possible value of U_1^* ($U_{1\min}^* \leqslant U_1^* \leqslant U_{1\max}^*$) defines a different semicircle of radius $cp_1^* = (U_1^{*2} - m_1^2c^4)^{1/2}$ the centre of which is displaced along the λ axis by an amount $\beta\,(2U_1^* - Mc^2)/2c$.

In the limit of small β Eq. (4.6) reduces to Eq. (4.5) and the displacement becomes zero. In the general three-body decay the displacement λ_0 is a single valued function of U_1^* and varies between absolute limits of $\pm\ \beta\ Mc/2$, and, in a specific decay process, from a minimum value of $\beta c\ (m_1 - M/2)$ to a maximum of $\{\beta c\,[m_1^2 - (m_2 + m_3)^2]\}/2M$ corresponding respectively to minimum and maximum values of U_1^*. Note that values of p_1^* and λ_0 for any particular event cannot be determined, and the data for a three-body decay process must be treated in a statistical way.

For any particular value of β it can be shown that *all* points from a given three-body decay, i.e., points corresponding to *all* values of U_1^*, lie inside a semicircle of radius $cp_{1\max}^* = (U_{1\max}^{*2} - m_1^2c^4)^{1/2}$ whose centre is displaced from the origin by the amount $\beta(2U_{1\max}^* - Mc^2)/2c$. Therefore the area swept out by displacing this semicircle along the λ axis from an origin at $\lambda = 0$ to $\lambda = \{c\,[m_1^2 - (m_2 + m_3)^2]\}/2M$ (corresponding to $0 \leqslant \beta \leqslant 1$) defines the allowed area for the three-body decay.

The distribution of points in the semicircle allowed for a particular β is not uniform but strongly asymmetric because the average value of λ_0 is in general different from zero. If the distribution of U_1^* is known theoretically, the corresponding distribution of λ_0 can be computed; knowing these quantities the density of points inside the circle can be inferred. The allowed area for the alternate decay mode of the τ-meson is shown in Fig. 13. Fig. 15 shows the distribution of decay events in the (λ, p_t) plane for the decay process $K \to \mu + 2\nu$ and $\beta = 1$. The integral frequency distribution obtained from $F(p)$, Eq. (3.1), was used to obtain values of p_1^* corresponding to a given fraction of the total events. If $(p_1^*)_a$ denotes the momentum below which occur 50% of the events, then Eq. 4.6 defines a semicircle on which lie events with $p_1^* = (p_1^*)_a$ and inside of which lie all events with $p_1^* < (p_1^*)_a$. In Fig. 15 the semicircles are drawn so that each zone includes 20% of the decay events. If the angular distribution of the charged secondary is isotropic in the c.m.s., it can be shown that the hyperbola

$p_t^2 = \frac{1}{\beta^2}\left(\lambda + \frac{M\beta c}{2}\right)^2 - m_1^2 c^2$ divides the allowed area into two regions each of which contains half the events (ARNOLD [1954]).

We return now to the interpretation of the distributions of p^* values in Figs. 13 and 14. In most cases the values of p^* are not more than one or two standard deviations from the semicircles defined by the K_μ- or χ-decay scheme, and therefore the data can be explained under the *assumption* that most charged V-particles arise from one or the other of these processes.

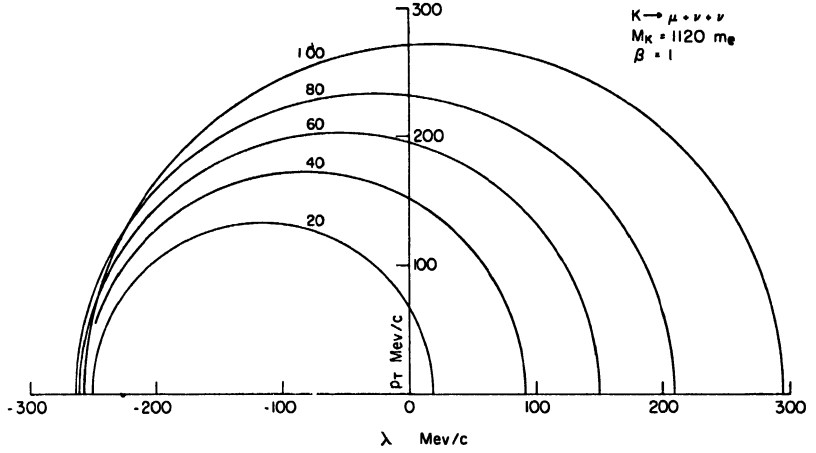

Fig. 15 – Distribution of decay events in the (λ, p_t) plane for the three-body decay process $K \to \mu + 2\nu$, and under the assumption that $\beta = 1$ for the primary particle. λ is the *apparent* longitudinal momentum in the rest system computed under the assumption of a two-body decay process with $\bar{\alpha} = 0$. The semicircles are drawn so that each zone in the figure contains 20% of the events. For a two-body decay all events fall on a single semicircle centered on the origin.

The points in the interior of the semicircle must then be interpreted as examples of some other decay process probably a three-body one. For the 38 positive events there are 10 cases which lie more than one standard deviation inside the semicircles defining the χ- or K_μ-decays and only one case which lies more than one standard deviation outside this region. Thus, if the discussion is restricted to decay processes already considered, events in the interior region must be explained in terms of the alternate decay mode of the τ-meson (§ 2.1) or in terms of the $\varkappa$-meson (§ 2.2). In all of the above 10 events the apparent value of p^* falls within the region allowed for the alternate decay mode of the τ-meson; accordingly, from the dynamics of the events, all can be interpreted

in this way. However the possibility that most of the events actually result from the decay process $\tau^+ \rightarrow \pi^+ + 2\pi^0$ can be ruled out on other grounds.

Six of the ten positive events with low values of p^* were observed by the EP group. In the same sample of data there were also six positive τ-mesons which decayed in flight and, in three of these p^* values could be determined. For each of these latter events all three of the secondary particles were measurable and thus, had they decayed via the alternate mode $\tau^+ \rightarrow \pi^+ + 2\pi^0$, the single charged secondary would have also been measurable. Within the limited statistics, the EP group should have observed as charged V-particles between 3/4 and 3 τ-meson decays *via* the alternate mode under the assumption that the ratio of the alternate to the normal mode is between 0.25 and 1.0. Since they observed instead six charged V-particles and since the above ratio seems to be less than 1.0, it is probable that not more than half of the low p^* values can arise from the alternate decay mode of the τ-meson. No lower limit to the number of events produced by τ-mesons can be set since no event has been reported in which the p^* value was low and the secondary particle was identified as a π-meson.

On the other hand the EP group observed one event with $p^* = (108 \pm 9)$MeV/c in which the mass of the secondary particle could be determined from measurements of momentum and range. The mass of the secondary particle was $(193 \pm 26)\ m_e$, and therefore μ-meson secondaries which cannot arise from the K_μ-meson occur among the V^+-particles. Presumably these arise from decays of the $\varkappa$-meson.

4. 4 Nature of the secondary particles associated with high P^* events

As we remarked above, K_μ- or χ-mesons could account for the events in Fig. 13 which are close to the region defined by $p^* = (200 - 230)$ MeV/c. Their negative counterparts, if they exist, could account for similar events in Fig. 14. In this case the secondary particles should be a mixture of μ- and π-mesons.

Although very few of the charged secondaries can be identified, that of the Princeton event discussed in sec 3.11 is inferred to be a π-meson of momentum $(201\ ^{+13}_{-9})$MeV/c. The Princeton group also observed an event in which the secondary particle produced

a star in the gas and it must therefore have been a π-meson (ARNOLD *et al.* [1955]). The value of p^* in this case was $(200\ ^{+75}_{-67})$MeV/c; thus one cannot rule out the alternate mode of decay of the τ-meson. Additional evidence for χ-mesons among the V^+-events comes from two events observed by the EP group. They assumed that each of their measurable high p^* events resulted from χ-decay and they calculated the expected position at which the photons from the π^0-meson should appear in the bottom multiplate chamber. Electron cascades of the correct energy were observed in the predicted position in two cases. The values of p^* in these events were (202 ± 10) and (222 ± 21) MeV/c respectively.

The EP group have also observed four V^+-events in which the secondary particle stops in the multiplate chamber and can be identified from the mass determination as a μ-meson. In two events the values of p^* were (214 ± 15)MeV/c and (108 ± 9)MeV/c respectively; in the other two cases p^* could not be determined but the values of the transverse momentum were $(195\ ^{+5}_{-2})$ and (221 ± 6)MeV/c respectively. It is thus probable that three events were produced by K_μ-mesons, and one by a $\varkappa$-meson.

From the above evidence high energy μ^+- and π^+-mesons occur among the secondary particles. Because of other experimental results it seems reasonable to attribute most of the former to the K_μ-meson, although some of the higher energy secondaries may be produced by the $\varkappa$-meson. The only known source for the high energy π^+-mesons is the χ-meson, and the V-events observed by the Princeton and EP groups provide supporting evidence for the π^0-meson emitted in this decay process.

4. 5 THE CHARGE ASYMMETRY

The ratio of positive to negative events in Figs. 13 and 14 is about 2/1, and becomes even higher, about 4/1, if it is required that the p^* values be determined to 15%. However, from about 300 cases, the overall ratio of positive to negative events is close to, or somewhat less than, 1.0 if no requirement as to measurability is imposed. This difference arises from the fact that the V^--particles have a considerably higher mean energy than the V^+-particles. Thus momentum measurements are on the average less favourable for the negative particles, and the p^* values are less precise or impossible to measure at all.

For the same reason the nature of the primary particles cannot

be determined for most of the negative V-particles. A mass estimate which distinguishes between K-mesons and hyperons is only possible for a primary momentum between about 200 and 800 MeV/c. The majority of the V^+-particles occur within this region and can be identified as K-mesons, however for a large fraction of the negative events the primary momentum is above 1 GeV/c and they could be hyperons or K-mesons. In this connection it is interesting to note that no hyperon has been found among the analyzable low energy V^--events (Fig. 14). However this argument cannot be invoked against the presence of negative hyperons because their lifetime is assumed to be $<10^{-10}$ sec and thus they could only be observed in cloud chambers if their energy is relatively great.

The Indiana and Princeton groups (Kim *et al.* [1954]; Arnold *et al.* [1955]) have reported that the distribution of transverse momentum and the distribution of cos Θ^* observed for their positive events is consistent with that expected if the decay process is isotropic in the c.m.s. On the other hand the distributions of the transverse momentum and of cos Θ^* for the negative events are quite different and are not consistent with two-body decay; too many negative events are found in the backward hemisphere.

However, just such an effect is expected from the difference in average energy between the positive and negative events. The laboratory energy of the secondary particle is lower when it is emitted backward in the rest system, and hence such events are easier to measure. Indeed at some particular primary energy it becomes possible to measure only events in which the secondary particle was emitted in the backward hemisphere in the c.m.s. It would appear therefore that the higher energy of the V^--particles could easily account for the differences mentioned above. In principle this bias can be avoided; we recall the remarks of Lagarrigue and Peyrou, § 4.1.

There are several pieces of evidence which indicate that the differences between the positive and negative events do not arise simply as a result of the higher average energy of the negative primaries but rather reflect a difference in composition. In the case of the positive particles a large fraction of secondaries appear to be μ^+-mesons while most of the negative secondaries are apparently π^--mesons.

The EP group observed 18 V^--events in which charged secondary

particles traversed the multiplate chamber. If these secondaries had all been π^--mesons, 12 nuclear interactions should have occurred; 11 were observed. Thus most fast V^--particles give rise to π^--meson secondaries. On the other hand among the V^+-events very few nuclear interactions have been produced by the secondaries and all positive secondaries which could be identified by measurements of momentum and range proved to be μ-mesons. Thus many of the V^+-particles decay to μ-mesons. It should be kept in mind that this result pertains to a rather small sample and that it may be influenced by the experimental arrangement.

A further asymmetry connected with the charge has been reported by the Indiana and CIT groups (KIM *et al.* [1954]; LEIGHTON [1954]). Both report that the decay points of the positive particles are distributed uniformly throughout the cloud chamber, but that the decay points of the negative particles are concentrated towards the top of the chamber. This result implies that the negative particles have a shorter lifetime than the positive particles. However no quantitive result has been published, and, in view of the generally conflicting evidence concerning the lifetime of the charged V-particles discussed in the following section, it is difficult to draw any conclusion from this result.

4.6 LIFETIME ESTIMATES

The first attempt to determine the mean life of the charged V-particles was that of BARKER *et al.* [1952]. The mean value of t^*/t_0^* was, within the experimental error, equal to 0.5. Under these conditions it is impossible to estimate the mean life but a lower limit to its value is given by the arithmetic mean value of t^* (PEIERLS [1935]). This limit was about 10^{-10} sec. The authors were also able to estimate an upper limit to the lifetime of $\sim 10^{-8}$ sec based on the number of charged V-particles observed relative to the total number of shower particles, on an assumed momentum spectrum for the shower particles, and on the assumption that not more than 10% of the particles produced in high energy nuclear interactions are heavy mesons which produce the charged V-events. The experimental apparatus is shown in Fig. 7 (1).

More recent measurements provide evidence for a component in the charged V-particles which has a lifetime greater than 10^{-9} sec (BUCHANAN *et al.* [1954]; YORK *et al.* [1954]; KIM and THOMPSON [1954]; LEIGHTON [1954]). However evidence for a short lived posi-

tive component and for a short lived negative component has also been adduced. The various data are summarized in Table XI. It is impossible to reconcile these results in terms of a single charged V-particle and it is difficult to explain them on the basis of a mixture of particles with different lifetimes. In view of the apparently conflicting results we give a brief discussion of some individual measurements.

The results of Buchanan *et al.* are based on measurements of 44 V-events (the apparatus used is shown in Fig. 7 (3)). The mean value of x/x_0 obtained was $0.55 \pm .04$, hence the value of $1/\tau$ is expected to be small and a statistical treatment of the data based on this assumption (BARTLETT [1953a]) leads to a value of $1/\tau = -(0.6 \pm 0.5)$ sec^{-1}. Under these circumstances an upper limit to the lifetime cannot be obtained; the time of observation is too short in comparison to the mean life. A lower limit of 2×10^{-9} sec is found by increasing $1/\tau$ by two standard deviations. This result applies to the entire sample of the data for which $N^+/N^- \sim 2$. In view of the results of other experiments the authors attempted to classify their events according to charge, velocity, and the p^* values. No finite upper limit for τ was obtained for any group; the lower limits were all less than the above value as one would expect from the reduced statistical information available.

York *et al.* used an experimental arrangement which consisted of two cloud chambers placed one above the other, Fig. 7 (2). Between the chambers there was placed a lead plate and, because of the construction, it was possible to observe particles very close to the plate. It was found that the charged V-particles produced above the chamber were predominately negative, $N^+/N^- = 11/17$ and that the values of x/x_0 associated with decays of this group were uniformly distributed throughout the top chamber. For 28 of of these events the mean value of x/x_0 was $(0.46 \pm .05)$ a result similar to that obtained by Buchanan *et al.*

On the other hand the unstable charged particles which originated in the plate between the two chambers were mostly positive, $N^+/N^- = \frac{2}{1}\frac{0}{0}$, and the average value of x/x_0 was found to be $(0.31 \pm .05)$, significantly less than 0.5. Assuming a uniform distribution of the decay points, the probability of a fluctuation in x/x_0 of at least this magnitude is $\sim 10^{-3}$.

The conversion of the measured values of x and x_0 was accomplished by a somewhat different procedure than that used by other

TABLE XI

Summary of lifetime measurements on charged V-particles

In column 2, N signifies the total number of events used in estimating other quantities in the same row. In columns 3 and 4 n^+ and n^- are the total number of positive and negative events, and $n^\pm$, column 5, indicates the number of events in which the sign was indeterminate. In the remaining columns, $(x/x_0)_{Av}$ is the mean value of the ratio of the distance, x, which the particle was observed to traverse before decay to the distance, x_0, it could have traversed before leaving the region of observation; $\bar{t}_0$* is the average proper time the particles lived before decay, and τ is the mean life.

References	N	n^+	n^-	$n^\pm$	n^+/n^-	$(x/x_0)_{Av}$	$\bar{t}_0$* 10^{-10} sec	τ 10^{-10} sec	$1/\tau$ 10^{10} sec^{-1}	Remarks
Barker *et al.* [1952]	18	7	9	2		$0.38 \pm .08$	2.6	>1.0		
York *et al.* [1954]	28				$0.65 \pm .37$	$0.46 \pm .10$*	<6.1 >2.9			Events with origin outside chamber.
	30	20	10	0		$0.31 \pm .09$*	<5.4	$<2.8\left(\begin{smallmatrix}+2.0\\-0.6\end{smallmatrix}\right)$†		Events with local origin.
							>2.4	$>1.5\left(\begin{smallmatrix}+1.3\\-0.3\end{smallmatrix}\right)$†		
Buchanan *et al.* [1954]	44	29	13	2			7.6		$-.06 \pm .05$	All particles.
	29	29	0	0			8.1		$-.06 \pm .06$	All positive particles.
	13	0	13	0			7.5		$-.05 \pm .11$	All negative particles
Kim *et al.* [1954]	13	13	0	0		≈ 0.5				Total of 31 events with p_t measurable to 5%.
	18	0	18	0		≈ 0.25				
Leighton [1954]	34	34	0	0		$0.57 \pm .06$				
	35	0	35	0		$0.37 \pm .06$				
Arnold *et al.* [1955]	9	9	0					$5.2\left(\begin{smallmatrix}+3.3\\-1.5\end{smallmatrix}\right)$†		Selected events which are interpreted as K_μ or χ-decays.
	6	0	6					$4.2\left(\begin{smallmatrix}+3.8\\-1.2\end{smallmatrix}\right)$†		

All errors are standard deviations unless otherwise noted. * 90% confidence limits. † 50% confidence limits.

experimenters: A lower limit to the value of P/Mc was found in each case from the estimated upper limit to the ionization of the primary particle; these values determine upper limits to the values of t^* and t_0^*. An upper limit to P/Mc was estimated from the lower limit of the ionization for those cases in which $I/I_{\min} > 1.5$. For the remainder of the data (~ 20 cases) in which the ionization could not be distinguished from minimum, upper limits to P/Mc were estimated assuming a primary mass of 1000 m_e. The upper momentum limit was determined from the available track length in each case using the known distortion limit of the chamber. This procedure implies that all the primary particles have momenta less than 3 GeV/c and assumes that there is no *systematic* gas distortion present. These upper limits to P/Mc determine lower limits for the corresponding times.

Upper and lower limits to the mean life were obtained from the corresponding sets of times using a maximum likelihood procedure. The values obtained were

$$\left[1.5\left(\begin{smallmatrix}+1.3\\-0.3\end{smallmatrix}\right) < \tau < 2.8\left(\begin{smallmatrix}+2.0\\-0.6\end{smallmatrix}\right)\right] \times 10^{-10} \text{ sec.}$$

The errors are 50% confidence limits obtained from the integral of the probability distribution over τ. Because of the method used to estimate upper limits for P/Mc the lower limit for τ may be too great, however the main significance of the results lies in the finite upper limit obtained for the mean life. The estimate of upper limits for the times is conservative and even taking account of the highly assymetric error in τ it is very difficult to interpret these results except in terms of a component whose mean life lies in the above range.

In two of the events in which the primary particle originated in the plate the mass of the secondary particle, as estimated from its ionization and momentum, is definitely greater than that of the π-meson and is consistent with the proton mass, (York *et al.* [1953] and [1954]). The authors suggested that the short-lived component might be composed of positive and negative hyperons which decay according to the schemes (§ 5):

$$\begin{aligned} Y^+ &\to n^0 + \pi^+ \quad (a) \\ &\to p^+ + \pi^0 \quad (b) \\ Y^- &\to n^0 + \pi^- . \quad (c) \end{aligned}$$

Not all of the events can be interpreted in this way since there are three positive events in which the upper limit of the primary mass as estimated from momentum and ionization is less than that of the proton.

Additional preliminary results of the CIT group obtained with a larger chamber, Fig. 7 (7), have been reported (LEIGHTON [1954]); 40 positive and 43 negative events were observed and the tentative conclusions are as follows: (a) The average momentum of the positive primaries is lower than that of the negatives and the majority of the slow primaries are positive. (b) Values of p^* could be computed for 18 positive events and for 6 negative events; this was done using an assumed primary mass of 1000 m_e. The values for the positive particles are consistent with a single value of $p_\mu^* = (232 \pm 12)$MeV/c although there is one event with $p_\mu^* = (142 \pm 16)$MeV/c. In this experiment it was not possible to observe particles close to the producing layer and no confirming evidence for the short-lived component described above was found. However for a lifetime $\sim 10^{-10}$ sec removing the producing layer to a position above the chamber decreases the decays which occur in the chamber by a very large factor, and it would seem that on this basis there is no contradiction between the short lifetime reported by York *et al.* and the results of other workers.

Recently the Indiana group (KIM and THOMPSON [1954]) have reported results of measurements on 14 positive and 19 negative events. They find that the x/x_0 values are uniformly distributed throughout the chamber for the positive events but that the negative particles all decay in the top half of the chamber. Furthermore the distributions of the p_t values for the positive and negative particles are markedly different. The p_t distributions are discussed in § 4.5.

No lifetime determination from these results has been published. They indicate however a value of τ^+ greater than about 5×10^{-9} sec and a value of τ^- equal to about 2×10^{-10} sec. Whether this last value is statistically significant, i.e. whether the upper limit to the lifetime is finite, cannot be determined from the published data.

4. 7 DISCUSSION OF THE RESULTS

The lack of agreement in the above results can be at least partially understood by recalling that the charged V-particles result from a mixture of primary particles; $\varkappa$-, K_π-, and χ-mesons are

certainly present as well as some hyperons. As we pointed out above lifetime determinations become very difficult if the experimental data include a mixture of different particles with different lifetimes. Furthermore, since it is now known that the sample of events is not pure, there is little further object in lifetime measurements on unidentified events. Rather the interest lies in determining the mean lives of the individual K-mesons and hyperons. This requires measurements on identified events, and the fact that a V-event can be measured with sufficient precision to establish its identity tends to seriously bias the lifetime measurement. In addition the separation of events is sometimes very difficult; in the case of the K_μ- and χ-meson very accurate measurements are required to identify individual examples with certainty and it is doubtful whether enough events to allow a significant determination of these two mean lives can be obtained from observations on decays in flight. We return to a discussion of the above results after considering some related and more conclusive evidence recently obtained from S-events.

4. 8 Delayed coincidence experiments on S-events

Two experiments have been reported recently in which the mean life of particles which decay at rest has been measured by using fast counter techniques to determine the difference in time between the observation of the S-particle and its decay product. We consider first the work of Hyams (Barker *et al.* [1955a], Barker *et al.* [1955b].

The measurements were carried out using a combination of counters and a multiplate cloud chamber. The counters above the chamber were arranged to select slow particles heavier than a π-meson which would stop in the multiplate chamber (Duerden and Hyams, [1952]). In the center of the cloud chamber there was a Čerenkov counter which was sensitive only to fast particles; thus it could be activated by a fast decay product but not by the slow unstable parent particle. The lifetime of an observed unstable particle can then be determined from the time difference between the signals from the counter system above the chamber and the internal Čerenkov counter.

With this arrangement 8 S-events were obtained which can be unambiguously identified as K-mesons. Their mean life was $\tau = (15.8\,^{+8.7}_{-4.0}) \times 10^{-9}$ sec. In addition 5 other events were obtained

in which the identification is not as certain. The authors estimate that at most one of these last could have been spurious. For the entire 13 events the mean life was $(11.0\ ^{+4}_{-2}\ ^{1}_{4}) \times 10^{-9}$ sec.

There is good reason to believe that the events observed by Barker *et al.* were produced by K_μ-mesons for the following reasons: (a) The experimental arrangement is similar to that used by the EP group in that the selection system requires a time of flight of about 5×10^{-9} sec. Under these conditions most of the S-events result from slow K_μ-mesons. (b) In three events the secondary penetrated more than 60 gcm^{-2} of lead ($\sim$45 gcm^{-2} of copper). Thus, in terms of known particles, these events must have been produced by K_μ-mesons. (c) The experimental arrangement favours the detection of γ-rays produced in the decay of the χ-meson but none were observed. (d) The lifetime of the τ-meson is presumably long enough so that these particles could be observed efficiently. However the abundance of the τ-meson appears to be much less than that of the K_μ-meson (e.g., from the results of the EP group under similar experimental conditions) and the normal mode of decay would not be detected since the fastest π-meson which can be emitted in this process cannot activate the internal Čerenkov counter. Other modes of decay of the τ-meson which involve a γ-ray directly or indirectly could be recorded through materialization but the efficiency is quite low.

Thus it seems certain that the majority of the events detected were K_μ-mesons and that the lifetime of this particle is about 10^{-8} sec. A further important conclusion drawn from this experiment is that the relative frequency of events with $\tau > 10^{-8}$ sec and which give rise to relativistic secondary particles must be small.

An experiment similar in principle to that just described but using only counters has been described by MEZZETTI and KEUFFEL ([1954a], [1954b]). The authors obtain a distribution of delayed counts which leads to a mean life of $(8.7 \pm 1.0) \times 10^{-9}$ sec. However there is some question about the significance of this result because the possibility of "after pulsing" in the photomultipliers is not completely ruled out.

4. 9 COMPARISON WITH THE CHARGED V-PARTICLE DATA

The lifetime obtained by Barker *et al.* for the K_μ-meson is in agreement with the general multiplate chamber results that the

K_μ-lifetime must exceed 10^{-9} sec and with the result of the EP group that most K_μ-mesons live longer than 5×10^{-9} sec.

Many of the slow positive charged V-particles appear to be K_μ-mesons and hence the long lifetime, $> 2 \times 10^{-9}$ sec, obtained in experiments which weight this type of event heavily is understandable.

On the other hand the mean lives of other particles present among the charged V-particles may be considerably shorter than 10^{-8} sec; it is known for example that the mean life of some charged hyperons is $\sim 10^{-10}$ sec. Then as higher energies are selected or as the experiments explore regions closer to the origin, shorter lifetimes may predominate. Thus the lack of agreement among the lifetime determinations for the charged V-particles is not surprising.

5. The Charged Hyperons

One of the major developments in the past two years has been the discovery of charged hyperons which apparently undergo the following modes of decay:

$$\begin{aligned} &\text{(a)} \quad \Sigma^+ \rightarrow \mathrm{p} + \pi^0 \\ &\text{(b)} \quad \Sigma^+ \rightarrow \mathrm{n} + \pi^+ \\ &\text{(c)} \quad \Sigma^- \rightarrow \mathrm{n} + \pi^- \\ &\text{(d)} \quad \Xi^- \rightarrow \Lambda^0 + \pi^- \end{aligned}$$

Most of the quantitative evidence for the first two decay processes comes from emulsion results. The evidence for (c) and (d) is derived mostly from cloud chamber results, although some decays in flight observed in emulsions, § 5.2 below, can best be interpreted in terms of (d). The evidence for (d) is discussed in detail in the following chapter by R. W. Thompson (p. 293).

5. 1 The decay process $\Sigma^+ \rightarrow \mathrm{p} + \pi^0$

The first emulsion results which gave evidence for the decay of a hyperon into a proton were presented in 1953 at the London and Bagnères Conferences (Bonetti *et al.* [1953a, 1953b, 1953c]). These authors observed an event, listed as Genoa-Milan Y-3 in Table XII, in which a particle whose measured mass was $(2330 \pm 800)\ m_e$ stopped and produced a single particle of range 1.67 mm which

was identified as a proton* (kinetic energy (18.7 ± 0.18) MeV).

They considered that the most likely interpretation of the event was that it represented a decay according to process (a) and they pointed out that the alternate decay mode (b) might be expected to exist. There are 7 similar events listed in Table XII in which the range of the secondary particle is very close to 1.68 mm. These events provide clear evidence for the existence of the two-body decay scheme (a); under the assumption that the kinetic energy of the proton is 18.80 MeV, the Q-value is 115.8 MeV and the mass of the primary particle is 2327 m_e. Because of the large difference in the Q-values the Σ^+-particle cannot be the charged counterpart of the Λ^0-particle.

A few S- and V-events which apparently give rise to proton secondaries cannot be explained according to decay scheme (a). In the Bristol S-event listed in Table XV the proton has an energy of ~100 MeV, and, in terms of (a), the Q-value is ~350 MeV. Since this is the only S-event in which the proton range is anomolous, the explanation as the nuclear absorption of a negative hyperon (§ 6.5) seems preferable to the introduction of another particle.

Table XII also lists five V-events in which a hyperon apparently decays into a proton. Three of the events are consistent with (a) and two, Bombay Y-3 and Y-4, are not. These latter two events can be easily accounted for since, in flight, the decay process $\Sigma^+ \rightarrow p + \pi^0$ is not always distinguishable from the inelastic scattering of a proton. In the case of a scattering the recoil may be absent or undetected, and mass measurements before and after the point of deflection are never precise enough to separate protons from hyperons. The only unambiguous criterion is a decrease in grain density after the point of deflection. In view of all of the above evidence the existence of the Σ^+-particle is well established.

Decay schemes (a), (b), and (c) were also suggested independently by the CIT group to explain some of the charged V-events observed in cloud chambers (Leighton [1953], York *et al.* [1953, 1954]. In two events the secondary particle from a V^+-event was identified as a proton and it was not possible to explain either event as the scattering of a proton in the gas or as the decay of a Λ^0-

* Direct mass measurements showed that the secondary particle had a mass near that of the proton and it came to rest without producing an interaction or undergoing decay.

TABLE XII

Hyperon events observed in emulsions

Data are given for those events in which significant information concerning the decay process could be obtained

Reference	Event	Type	Origin	Primary Particle: Length mm	Primary Particle: Mass	Primary Particle: β at decay	Primary Particle: θ lab degrees	Secondary: Length mm	Secondary: Range mm	Particle: $p\beta$ MeV/c	Particle: g^*	Particle: Mass	Particle: Kinetic Energy MeV	Q (MeV): $\Sigma^+ \to p + \pi^0$	Q (MeV): $\Sigma^+ \to n + \pi^+$	Q (MeV): $\Xi^- \to \Lambda^0 + \pi^-$	Remarks
Bombay																	
(1, 2)	Y-1	V	13+10α	19.3	2200^{+600}_{-400}[b] 2500 ± 380[d]			14.0		160 ± 13	$1.26 \pm .5$	330 ± 60	103 ± 9		135 ± 35		nearly at rest residual range at decay $3.5^{+2.5}_{-1.5}$ mm
(3)	Y-2	V	17+6p	8.0	2460 ± 500[g]			0.57			$1.25 \pm .10$				111 ± 25[v]		
(3)	Y-3	V	24+4p	5.40	2610^{+300}_{-250}[g]				12.45			1950^{+600}_{-400}[h]		129 ± 11			possible scatter
(3)	Y-4	V	17+12p	24.04	2775 ± 185[g]				0.824			(p)		225 ± 25			possible scatter
(3)	Y-5	V	1+2n	4.22	2470 ± 300[g]				0.116			(p)		212 ± 22			possible scatter
(25)	—	S				0			1.660			p		116.1 ± 1.2			
Bristol																	
(4)	Y-1	V	26+14p	4.72	2750 ± 500[g]	0.26	145.5	~13.		87 ± 3[v]	$1.34 \pm .02$	(π)			100 ± 6[v]		
(5, 6)	Y-3	V	12+7p	14.6	2200 ± 250[g]	$0.61 \pm .02$	42.4 ± 2	8.4			$1.15 \pm .05$	(π)	99 ± 14[v]		60 ± 11[v]		
(4, 9)	Y-4	V	9+8p	4.40	2500 ± 500[g]	$0.59 \pm .01$	26.2	23.73		227 ± 31	$0.97 \pm .04$	(π)			66 ± 28		
(7, 8, 9)	Y-5	V	19+3n	9.60	2350 ± 350[g]	$0.518 \pm .005$	46	13.3		>180	$1.02 \pm .04$	(π)			>85		
(8, 9)	Y-6	V	13+3p	17.5	1850 ± 250[g]	$0.548 \pm .005$	50	44.3		190 ± 10	$1.05 \pm .04$	(π)			116 ± 15		
(6)	Y-7	S	1+0n	2.01	2100 ± 300	0			1.675			p	$18.77 \pm .19$	115.8 ± 1			
(6)	Y-8	V	25+2p	13.86	2500^{+440}_{-320}[i]	$0.11 \pm .05$	112 ± 1	62.9				(π)	87.4 ± 3.5[v]		115 ± 7[v]		
(6)	Y-9	V	13+0p	8.79	$\geqslant m_p$[i]	$0.245 \pm .005$	54.7 ± 2	22.6				(π)	107.9 ± 10[w]		103 ± 10.5[w]		
(6)	Y-11	S	15+3n	3.60	~2000				1.602				$18.32 \pm .32$	113.5 ± 1.7			
(9)	Y-14	V	5+3p	10.2	2400 ± 300[g]	$0.55 \pm .01$	45.5	16.3			$0.95 \pm .04$	(π)			>80		
Cornell										90^{+18}_{-13}[v]							
(10)	Y-1	V			2500 ± 900[g]			0.9		108^{+32}_{-20}[w]	$1.70 \pm .15$	330^{+106}_{-63}			71^{+12}_{-8}[v]		
Genoa-Milan																	
(11, 12)	Y-3	S	—	0.9	1840^{+840}_{-590}[a] 2300 ± 800[b] 2700^{+1150}_{-900}[c]	0			$1.670 \pm .01$			2030^{+530}_{-480}[b] 1840 ± 670[c]	$18.7 \pm .2$	115 ± 3			
(13)	Y-6	V	K$^-$-star	0.6	2700 ± 1350[g]	$0.31 \pm .02$	32	28		204 ± 21	$1.07 \pm .02$	(π)	133		95 ± 21		
(13)	Y-7	V	7+1n	4.15	2700 ± 600[g]	$0.19 \pm .02$	38	27.5		166 ± 17	$1.1 \pm .02$	(π)	104		90 ± 20		
Göttingen																	
(14)		V	28+29p	1.6				23.1				271^{+195}_{-106}	112^{+14}_{-18}		135^{+15}_{-19}		
Padua																	
(15, 16)	Y-1	V	11+1n	3.25	2100 ± 400[g]	0.23	171	4.3				286 ± 30	70		131 ± 24		
(16)	Y-2	S	5+1n	.95	1840^{+900}_{-600}	0			$1.68 \pm .02$			2200^{+600}_{-400}	$18.5 \pm .3$	116.0 ± 2.0			
(16)	Y-3	V	11+3n	15.0	1900 ± 250[g]	$0.371 \pm .007$	$26.0 \pm .5$		$28.7 \pm .06$			p	97.7 ± 1.2	125 ± 30			cannot be scatter
(17)	Y-6	S			2100 ± 300				89.3 ± 3.0			$\pi^+ \to \mu^+ \to e^+$	90.2 ± 2.8		107.8 ± 3.5		
Rochester																	
(18)	Y-1	V	25+5n	1.8	2390 ± 500[g]	0.29	43.21			195 ± 30[v]	$1.015 \pm .05$	(π)	132 ± 30		116 ± 50[v]		

(Continued)

TABLE XI (*Continued*)

Reference	Event	Type	Origin	Primary Particle: Length mm	Primary Particle: Mass	Primary Particle: β at decay	Primary Particle: θ lab degrees	Secondary: Length mm	Secondary: Range mm	Particle: $p\beta$ MeV/c	Particle: g^*	Particle: Mass	Particle: Kinetic Energy MeV	Q (MeV): $\Sigma^+ \rightarrow p + \pi^0$	Q (MeV): $\Sigma^+ \rightarrow n + \pi^+$	Q (MeV): $\Xi^- \rightarrow \Lambda^0 + \pi^-$	Remarks
Rome (19)	Y-1	S	1+0n	4.3	1840 ± 500^b 3000 ± 500^c			12.0		>50	1	$<m_p$					secondary too steep for precise measurements
(19)	Y-2	V	>8	32.0	2100 ± 150^{bc}			7.2		170 ± 30	$1.25 \pm .08$						secondary too steep for precise measurements
(20)	Y-3	S	20+9p	1.25	$2800^{+1500}_{-900}{}^b$ 2670 ± 500^c				$1.675 \pm .03$		black	$>m_\pi$ (p)	$19.0 \pm .25$	117 ± 1.3			
Turin (21)	Y⁻-1	V	11+14α	0.93	$2300^{+270}_{-640}{}^g$		147.27±.25		16.59			$\pi^- \rightarrow \sigma$-star	$30.54 \pm .88^x$		107 ± 15		$p\beta$(pri.)=250±82 could be decay of K^-
Warsaw (22)		V	17+10p	2.9	1900^{+450}_{-300}	0.33	22	3.0		186 ± 30		2000^{+450}_{-300}	122	146 ± 40			$p\beta$(pri.)=120±20
Washington (23)		S		3.7	2860 ± 860			2.2		150 ± 35	$1.15 \pm .07$	330 ± 90			114 ± 32		
Wisconsin (24)		S			2300 ± 100				$1.78 \pm .03$			p	$19.5 \pm .2$	117 ± 2			Cosmotron exposure

Primary mass measurements by the following methods:

a. multiple scattering vs. residual range; constant cell length.
b. multiple scattering vs. residual range; variable cell length.
c. gap length vs. residual range.
d. grain or blob density vs. residual range.
e. photometric determination of ionization vs. residual range.
g. multiple scattering vs. ionization.

Average mass values obtained from more than one of the above methods are indicated by the appropriate combination of symbols.

Secondary energy determinations according to:

v. from ionization.
w. from scattering.
x. from range.

REFERENCES

(1) Lal, D., Yash Pal and B. Peters, 1953, Bagnères Conference, unpublished report, 146.

(2) Lal, D., Yash Pal and B. Peters, 1953, Phys. Rev., **92**, 438.

(3) Daniel, R. R., A. Krishnan, S. Mitra and Yash Pal, 1954, Nuovo Cim., **12**, supplement no. 2, 231.

(4) Friedlander, M. W., 1954, Phil. Mag., **45**, 418.

(5) Fowler, P. H. and D. H. Perkins, 1954, Nuovo Cim., **12**, supplement no. 2, 238, 450.

(6) Friedlander, M. W., D. Keefe and M. G. K. Menon, 1955, Nuovo Cim., **1**, 482.

(7) Dahanayake, C., P. E. François, Y. Fujimoto, P. Iredale, C. J. Waddington and M. Yasin, 1954, Nuovo Cim., **12**, supplement no. 2, 252, 450.

(8) Dahanayake, C., P. E. François, Y. Fujimoto, P. Iredale, C. J. Waddington and M. Yasin, 1954, Phil. Mag., **45**, 855.

(9) Dahanayake, C., P. E. François, Y. Fujimoto, P. Iredale, C. J. Waddington and M. Yasin, 1955, Nuovo Cim., **1**, 888.

(10) Barrett, P. H., 1954, Phys. Rev., **94**, 1328; (values quoted according to private communication Oct. 1954).

(11) Bonetti, A., R. Levi Setti, M. Panetti and G. Tomasini, 1953, Bagnères Conference, unpublished report, 182.

(12) Bonetti, A., R. Levi Setti, M. Panetti and G. Tomasini, 1953, Nuovo Cim., **10**, 1736.

(13) Bonetti, A., R. Levi Setti, B. Locatelli and G. Tomasini, 1954, Nuovo Cim., **12**, supplement no. 2, 292.

(14) Gottstein, K., 1955, Nuovo Cim., **1**, 284.

(15) CECCARELLI, M. and M. MERLIN, 1953, Bagnères Conference, unpublished report, 183.
(16) BALDO, M., G. BELLIBONI, M. CECCARELLI and B. VITALE, 1954, Nuovo Cim., **12**, supplement no. 2, 289.
(17) CECCARELLI, M., N. DALLAPORTA, M. GRILLI, M. MERLIN, G. SALANDIN and B. SECHI, preliminary report of "G-Stack Collaboration" circulated May 1955.
(18) KAPLON, M. F., 1954, (communicated at the Padua Conference), Nuovo Cim., **12**, supplement no. 2, 452.
(19) CASTAGNOLI, C., G. CORTINI and C. FRANZINETTI, 1954, Nuovo Cim., **12**, supplement no. 2, 297.
(20) CASTAGNOLI, C., G. CORTINI and A. MANFREDINI, 1954, Nuovo Cim., **12**, 464.
(21) DEBENEDETTI, A., C. M. GARELLI, L. TALLONE and M. VIGONE, 1954, Nuovo Cim., **12**, 952.
(22) DANYSZ, M., 1954, quoted by Castagnoli *et al.*, ref. 19, pp. 299, 452.
(23) KING, D. T., N. SEEMAN and MAURICE M. SHAPIRO, 1953, Phys. Rev., **92**, 838.
(24) FRY, W. F. and M. S. SWAMI, 1954, Phys. Rev., **96**, 235.
(25) PAI, YASH, 1955, preliminary results of the Bombay group reported at the Rochester Conference.

particle in which the π^--meson was emitted in the backward direction. The primary particles were heavily ionizing and their masses and momenta could not be determined (see discussion § 4.6).

5. 2 DECAY EVENTS IN WHICH THE CHARGED PRODUCT IS AN L-MESON

There are 19 V-events and one S-event listed in Table XII which can be interpreted as the decay of a hyperon into an L-meson, (BONETTI *et al.* [1953b, 1953d]; CECCARELLI and MERLIN [1953a, 1953b]). From the measured value of the primary mass and the measured energy of the L-meson secondary it is possible to conclude in several events that, if the decay process is a two-body one, the neutral secondary particle is heavier than a π-meson. It is natural to attempt an interpretation of these events in terms of decay schemes (b) and (c), and this suggestion was advanced by by several authors; YORK *et al.* [1953], BONETTI *et al.* [1953a, 1953b]. If this explanation is correct, the Q-value for process (b) is 114.5 MeV, and, under the assumption that the mass of the Σ^--particle is identical to that of the Σ^+-particle, the Q-value for the decay scheme (c) is 110.0 MeV.

Of the 19 V-events with L-meson secondaries mentioned above 10 have Q-values consistent with (b) or (c), three with (d), and two with (b), (c), or (d). In the other events the experimental data is insufficient for a good measurement of the Q-value. Thus, all the experimental data can be accounted for in terms of the postulated decay schemes. However the firm experimental evidence as to the exact details of (b) and (c) is scant. This situation arises from the imcompleteness of the experimental data for individual events, and from the difficulty in grouping the data for a statistical analysis.

No separation of the decay processes (b) and (c) is possible using the sign of the secondary particle or the observed Q-values. In the majority of the V-events the secondary particle escapes from the emulsion before coming to rest; therefore no determination of its sign can be made, and grouping the particles in this way is impossible. A similar difficulty arises in the case of the Q-values.

The Q-values for (b) and (c) are derived from V-events and are inherently much less accurate than those obtained for S-events of type (a), (see discussion of V-events § 4). Thus a separation of events in classes (b) and (c) cannot be made on the basis of the Q- or p^*-values.

For these reasons no grouping and subsequent statistical treatment of the data is possible. The ratio Σ^+/Σ^- is unknown and the mass of the Σ^--particle is not necessarily equal to that of the Σ^+-particle.

5. 3 Experimental evidence for the decay processes $\Sigma^+ \to \pi^+ + \mathrm{n}$ and $\Sigma^- \to \pi^- + \mathrm{n}$

A single Σ^+-event has been observed in which the Σ-particle comes to rest and decays into a π^+-meson; the π^+-meson stops in the emulsion and undergoes $\mu \to \mathrm{e}$ decay, (Ceccarelli *et al.* [1955]); details of the event, Padua Y-6, are given in Table XII. The preliminary Q-value obtained was (107.8 $\pm$ 3.5)MeV. This observation is the only certain experimental result on the decay process $\Sigma^+ \to \mathrm{n} + \pi^+$ and provides very strong evidence that decay process (b) is responsible for some of the hyperon decays in flight and that process (b) is indeed an alternate of process (a).

There are a few individual events from emulsions and cloud chambers which provide direct evidence for decay process (c). In emulsions a single V-event has been observed in which the decay

product, a π^--meson, came to rest and produced a σ-star (DEBENEDETTI *et al.* [1954]). Details of the event, Turin Y-1, are given in Table XII. Although the analysis of the event supports decay scheme (c), the results are not conclusive. The primary mass measurements are not precise enough to eliminate the possibility that the decay was produced by a K^--meson, nor is this explanation ruled out from the dynamics of the event. Using the experimental data and considering three possible decay schemes: $\Sigma^- \rightarrow n + \pi^- + 110$ MeV; $\chi^- \rightarrow \pi^- + \pi^0 + 218.5$ MeV, and $\Xi^- \rightarrow \Lambda^0 + \pi^- + 66$ MeV, one obtains the following corresponding values of $p\beta$ for the primary particle: 270 MeV/c; 154 MeV/c, and 88 MeV/c. The experimental value of $p\beta$ obtained for the primary particle was 250 ± 82 MeV/c. Thus, although the Σ^--particle is more probable, a K^--meson is not ruled out as the parent particle; the Ξ^--particle appears to be excluded.

Shutt and his coworkers have observed two negative V-events in a hydrogen filled diffusion cloud chamber which are most easily interpreted in terms of process (c), (FOWLER *et al.* [1954]). In the first event a Y^--particle and a K^+-meson are probably produced in the reaction $\pi^- + p \rightarrow Y^- + K^+$. The presumed Y^--particle then decays into an identified L-meson. The momentum of the L-meson is somewhat uncertain; under the assumption $Y^- \rightarrow n + \pi^- + Q$, the Q-value is $\geqslant 50$ MeV. An alternate possible, but very unlikely, explanation is that the entire event resulted from the scattering and subsequent decay of a K^--meson.

In the second example a V^--particle originated in the chamber wall and decayed into an identified π^--meson. An analysis of the event according to the various known, or assumed, decay processes given in Table I leads to the conclusion that it is only consistent with $\Sigma^- \rightarrow n + \pi^-$. For this case the calculated value of Q is $(130\ ^{+25}_{-15})$MeV.

There is no direct experimental evidence for the π^0-meson secondary in (a) or for the neutron in (b) and (c). Although the neutral particle emitted in (b) can be shown in several events to be heavier than a π-meson, it could equally well be a Λ^0 or heavier unstable neutral particle rather than a neutron. The evidence for a symmetrical decay scheme involving positive and negative primary particles of the same mass rests on the apparent close identity of the p^* values observed for the protons, scheme (a), and the π^+-mesons, scheme (b); see Table I.

5. 4 Other modes of decay

Some evidence exists for a heavy hyperon which decays into a K-meson, (Eisenberg [1954]; Fry *et al.* [1955]). No definite conclusions can be drawn from the two events so far published.

6. Nuclear Absorption of Heavy Mesons and Hyperons

6. 1 Possible absorption processes of K-mesons

When a negative unstable particle comes to rest in matter its behaviour will depend on the nature and strength of the interaction between the particle and nucleons. Since there appear to be several K-mesons and hyperons whose properties are not well known, no definite predictions can be made concerning the modes of capture. The following possibilities, among others, have been considered:

(i) The K^--meson is a boson and, by analogy to the π^--capture process, it interacts strongly with pairs of nucleons;

$$K^- + p + p \rightarrow p + n + \sim 500 \text{ MeV}$$
$$K^- + p + n \rightarrow n + n + \sim 500 \text{ MeV}.$$

A large fraction of the kinetic energy imparted to the nucleons will in general be transferred to the nucleus and an evaporation star of medium energy is the expected result. The total energy involved is sufficient so that a maximum of three π-mesons can be produced in the secondary nucleon-nucleon collisions following the capture of the K^--meson. The number of π-mesons is, of course, reduced by reabsorption in the nucleus. Exact predictions concerning the kinds of particles emitted and their energy distribution have not yet been possible particularly in light nuclei. However, approximate calculations have been carried out for heavy nuclei and it is reasonable to expect that a large fraction of the capture stars will contain one or two low energy π-mesons and that the capture star would be visible in practically all cases.

(ii) The K^--meson interacts very weakly with nuclei. In this case the K^--meson is captured into a bound orbit where it remains until it decays. In light elements the orbit is outside the nucleus and when decay occurs interaction between the decay products and the nucleus is unlikely. The nucleus however takes up an arbitrary amount of momentum and acquires an inappreciable kinetic

energy. The spatial relationships among the decay products which are the characteristic features of a decay at rest are therefore destroyed; in the case of three-body decay, e.g., the τ-meson, the decay products are in general no longer coplanar, and in the case of two-body decay they are not colinear.

If capture takes place in a heavy element, the orbit is inside the nucleus, and when decay occurs, the decay products must traverse the nucleus. If they are π-mesons the probability that they interact before escaping from the nucleus is high, and a small star results; if they are non-interacting particles the decay is similar to the case for the light elements just discussed.

(iii) The K^--meson is a fermion and interacts with nuclei in a manner similar to the μ-meson;

$$K^- + p \rightarrow n + \nu.$$

The ratio of the particles which are captured by the nucleus to those which decay depends on the strength of the interaction in the above reaction. Under the assumption that this is equal to the Fermi interaction constant for the corresponding μ-meson process the ratio of captures to decays in either light or heavy elements turns out to be 0.1, and most of the captures result in a small star (DALLAPORTA and LANZA, [1954]). While the calculations are instructive for order of magnitude considerations it should be borne in mind that the ratio of capture to decay depends sensitively on the coupling constant which may be different from that assumed. Furthermore, the neutrino may not be the neutral fermion which enters into the charge exchange reaction. Thus if the neutral particle were a μ^0- or a K^0-meson, the available energy for star production would be decreased.

(iv) A fourth possibility is (GOLDHABER, [1953], TOUSCHEK, [1954]):

$$K^- + n \rightarrow \Lambda^0 + \pi^-$$
$$K^- + n \rightarrow Y^- + \pi^0$$
$$K^- + p \rightarrow \Lambda^0 + \pi^0.$$

These processes represent the inverse of the production process observed at Brookhaven by Shutt's group (FOWLER, *et al.* [1954]).

6. 2 OBSERVATIONS WITH PHOTOEMULSIONS

The earliest example of K^--capture is that reported by LEPRINCE-RINGUET, *et al.* [1948, 1949]. In this event a stopping particle

produced a σ-star in which the energy release was greater than 350 MeV. The particle which produced the star was therefore not a π^--meson. Since only a single event was found, and since at the time the evidence for K-mesons also consisted of a single event no definite conclusion was possible. The authors however considered that the event was most probably caused by "a negative meson whose mass is at least $700m_e$ and which interacts with nuclei".

Confirmation for this view was some time in coming. As soon as K-meson decays in emulsions were well established the fate of the negative particles, which were known to exist from cloud chamber observations (§ 4), engaged a great deal of attention. However the capture stars produced in the emulsion by K^--mesons cannot be readily distinguished from the large background of similar stars which result from π-mesons and low energy neutrons. Nor is the behaviour of the stopping K-meson always sufficient to positively identify a K^--capture star. In single G-5 emulsions most of the tracks are necessarily short and the direction of the K-meson is difficult to determine from scattering and ionization. For these reasons, and also because the rate of K^--capture stars seems to be low compared to the rate of decay events, no capture stars produced by heavy mesons were found in the first systematic search (FRIEDLANDER *et al.* [1953, 1954]).

However, in 1952 an additional event was reported by Fry and Lord, and in 1953 Peters reported conclusive evidence for K^--capture (LAL *et al.* [1953a, 1953b, 1953c]). In the course of scanning a large block of emulsions four σ-stars were observed which could not have been produced by π^--mesons. In two of the events the mass of the σ-meson was determined within 10% and the initiating particles were certainly K-mesons.

About 30 events which can be interpreted in terms of the absorption of a negative K-meson are listed in Table XIII, and data for six additional events which presumably result from the nuclear absorption of negative hyperons are given in Table XV. If we consider only those cases in which the star was produced by a K-meson, the capture stars may be classified as follows:

(a) Evaporation stars with no π-mesons: 14 cases.

(b) Stars in which a π-meson or a lightly ionizing particle which could be a π-meson is produced with or without evaporation prongs: 12 cases.

(c) Stars in which a hyperon is produced: 2 cases.

TABLE XIII

Examples of the nuclear absorbtion of negative K-mesons observed in emulsions

The interpretation of events is often not unique, and some could be regarded as arising from negative hyperons (see Table XV)

		Primary Particle			Star Particles			
Reference	Event	Origin	Length mm	Mass m_e	Identity	Energy MeV	Total Visible Energy MeV	Remarks
	Bombay							
(1, 2)	K⁻-1	14 + 2n	0.31	$1000 \pm \begin{matrix}720\\400\end{matrix}$[a]	(p)	1.0	30	Could be Y⁻
					(p)	0.5		
					π	28.1 ± 0.8		
(1, 2)	K⁻-2	25 + 5n	0.09	$>m_\pi$	(p)	7.8	42	Could be Y⁻ or excited fragment.
					(p)	0.5		
					(p)	4.2		
					π^-	29.2 ± 0.9		
(1, 2)	K⁻-3	4 + 6n	25.00	1015 ± 120[a]	(p)	7.8	211	
				975 ± 100[d]	(p)	2.1		
					(p)	4.1		
					(p, d)	17.		
					p	180.		
(1, 2)	K⁻-4	—	29.26	890 ± 95 [a]	(p)	8.1	17	
				1020 ± 100[d]	(p)	9.0		
(1, 2)	K⁻-5	—	1.20	$540 \pm \begin{matrix}290\\170\end{matrix}$[a]	(p)	6.5	127	
					(p)	>120		
(3)	K⁻-	7 + 8p	2.9		π^-	44.4	119	π^- and p could result from decay of Λ^0.
					p recoil	74.3		
	Bristol							
(4)	K⁻-1	3 + 0n	12.23	750 ± 120[a]	p	71.5	~110	
				590 ± 130[b]	(p)			
				840 ± 100[d]	?			
(4)	K⁻-2	12 + 0p	0.56	$630 \pm \begin{matrix}160\\120\end{matrix}$[c]	p		~59	
					(d, t)			
					(p, d)			
					?			
	Brookhaven							
(5)	K⁻-1	2.2 GeV p on Be target	43.	1200 ± 300[a]	?g* < 1.5			*PC* of K⁻ between 310 and 380 MeV
				1050 ± 150[c]	(t, α)			
				1080 ± 220[j]				
	Chicago							
(6)	K⁻-1			~1000[c]	(π)	~130	151	
					(π)	~ 15		
					(p, d)	5.5		
	Copenhagen							
(7)	K-4	11 + 4p	21.0	880 ± 250[a]	2?short black			
					?g* ⩽ 1.2			
	Cornell							
(8)	K-2	1 + 0 (Y, K)	21.9	940 ± 200[b]	p	1.0	69	See footnote*
					p	5.5		
					p	0.5		
					α	29		
					L-meson	33 ± 4		
	Dublin							
(4)	K⁻-1			780 ± 100[b]	3 ?low			
				950 ± 60 [c]	energy			
				1100 ± 100[c]	prongs			
	Genoa-Milan							
(9)	K⁻-1	10 + 2n	10.64	1170 ± 230[b]	(d, p, π)	~1	~60	
					Y	~60		
(9)	K⁻-2	7 + 4p	41	970 ± 90[b]	p	6.7	25	
					p	18.3		
					slow e			
	Lund							
(10, 11)	K-1	—	3.45	905 ± 70 [e]	0			See footnote**
(10, 11)	K-2	5 + 0n	3.30	960 ± 70 [e]	0			
(10, 11)	K-3	—	5.70	890 ± 90 [e]	0			
				1100 ± 185[a]				
(10)	K⁻-4	2 + 1n	1.8	985 ± 70 [e]	p	22	22	
					(π)			
					? short			
	Manchester							
(12)	K⁻-1	—	1.62	1900 ± 500[ae]	(π)	54	69	
				1000 ± 150[c]	(p)	15		
(12)	K⁻-2	—	1.56	1260 ± 400[a]	(p)	>1	10	
					(p)	>1		
					(p)	>7.5		

(Continued)

TABLE XIII (*Continued*)

Reference	Event	Primary Particle: Origin	Primary Particle: Length mm	Primary Particle: Mass m_e	Star Particles: Identity	Star Particles: Energy MeV	Star Particles: Total Visible Energy MeV	Remarks
	Minneapolis							
(13)	K⁻-	—	16.35	1010 ± 200	p	30 ± 7	84	See footnote ***
					(p, d)	4.9 ± .1		
					(p, d)	1.10 ± .05		
					(He_2^4**)	14.1 ± .2		
	Padua							
(14)	K⁻-1	6 + 1p	11.14	1070 ± 160[d]	p	42	96	
					p	17		
					π	37		
					recoil			
(14)	K⁻-2	9 + 1n	47.0	985 ± 150[d]	p	13	24	
					p	11		
(14)	K⁻-3	5 + 1n	75.10	987 ± 120[d]	p	7	149	
					α	7		
					p	90		
					p	45		
	Paris (Ecole Polytechnique)							
(15, 16)	K-				5 prongs			
					π^-			
(17)	K-		2.30	530 ± 200[a]	p	130 ± 20	130	
				580 ± 150[ce]				
(18)	K⁻-1	large star	25.35	1036 ± 46[bcde]	(p)			
					(p)			
					short black recoil			
	Rome							
(19)	K-1	16 + 8n	12.1	1020 ± 65[bd]	π^-	38.5 ± 2.5	39	Probable K⁻-absorption; could be K⁻-decay.
	Tel Aviv							
(20)	K-	4 + 4α	34	1310 ± 245[g]	5 + 0K			

Primary mass determinations by the following methods:

a. multiple scattering vs. residual range; constant cell length.
b. multiple scattering vs. residual range; variable cell length.
c. gap length vs. residual range.
d. grain or blob density vs. residual range.
e. photometric determination of ionization vs. residual range.
g. multiple scattering vs. ionization.
j. momentum (magnetic analysis of K⁻-beam) vs. range.

Average mass values obtained from more than one of the above methods are indicated by the appropriate combination of symbols.

* The negative K-meson is believed to originate in the decay of a hyperon heavier than the Σ- or Ξ-particles discussed in § 6.
** In these three events the K-mesons stop without producing a visible interaction. The possibility that these events result from "faded" proton tracks cannot be excluded, see ref. 11.
*** The excited fragment undergoes mesonic decay probably according to the reaction: $He^4_2{}^* \rightarrow \pi + p + He^3_2 + 34.2 \pm 0.9$ MeV. The kinetic energy of the decay products. 34.2 MeV., is included in the total visible kinetic energy given above.

For references see next page.

References to Table XIII

(1) Lal, D. Yash Pal and B. Peters, 1953, Proc. Ind. Acad. Sci., **38**, 398.
(2) Lal, D. Yash Pal and B. Peters, 1953, Phys. Rev., **92**, 438.
(3) Pal, Yash, 1955. Preliminary results of the Bombay group reported at the Rochester Conference.
(4) Friedlander, M. W., D. Keefe, M. G. K. Menon, R. H. W. Johnston, C. O'Ceallaigh and A. Kerman, 1955, Phil. Mag., **46**, 144.
(5) Hornbostel, J. and E. O. Salant, 1954, Phys. Rev., **93**, 902.
(6) Fry, W. F. and J. J. Lord, 1952, Phys. Rev., **87**, 533.
(7) Bøggild, J. K., J. E. Hooper and M. Scharff, 1954, Nuovo Cim., **12**, supplement no. 2, 223.
(8) Eisenberg, Y., 1954, Phys. Rev., **96**, 541.
(9) Di Corato, M., B. Locatelli, G. Mignone and G. Tomasini, 1954, Nuovo Cim., **12**, supplement no. 2, 270.
(10) von Friesen, S., 1954, Nuovo Cim., **12**, supplement no. 2, 273.
(11) von Friesen, Sten, 1955, Ark. f. Fysik, **8**, 305.
(12) Macpherson, I., J. V. Major, Om Parkash, G. D. Rochester and A. M. Short, 1954, Nuovo Cim., **12**, supplement no. 2, 275.
(13) Freier, P. S., G. W. Anderson and J. E. Naugle, 1954, Phys. Rev., **94**, 677.
(14) Baldo, M., M. Ceccarelli, M. Grilli and G. T. Zorn, 1954, Nuovo Cim., **12**, supplement no. 2, 257.
(15) Leprince-Ringuet, L., Hoang Tchang-Fong, L. Jauneau and D. Morellet, 1948, C. R. Acad. Sci. Paris, **226**, 1897.
(16) Leprince-Ringuet, L., Rev. Mod. Phys., **21**, 42.
(17) Crussard, J., 1953, Bagnères Conference, unpublished report, 169.
(18) Hoang, T. F., L. Jauneau, J. Jouvin, G. Kayas, L. Leprince-Ringuet, D. Morellet, A. Orkin-Lecourtois and J. Trembley, 1955, Nuovo Cim., **1**, supplement no. 3, 184.
(19) Amaldi, E., G. Baroni, C. Castagnoli, G. Cortini, C. Franzinetti and A. Manfredini, 1954, Nuovo Cim., **11**, 207.
(20) Rosendorff, S., R. Stahl and G. Yekutieli, 1954, Phys. Rev., **93**, 901.

6. 3 Observations with cloud chambers

In 1953 the Manchester group reported an event observed in a magnetic chamber which could be interpreted according to the process $K^- + p \rightarrow \Lambda^0 + ?$, (Barker, [1953a, 1953b]). Λ negative particle of mass (1000–2000) m_e stopped in a plate and apparently produced a Λ^0-particle.

The MIT group has observed three events in a multiplate chamber which can be interpreted in a similar manner (DeStaebler [1954]). Two of the events, 81882 and 93242, are similar to that described by Barker; a V^0-particle appears to originate from a

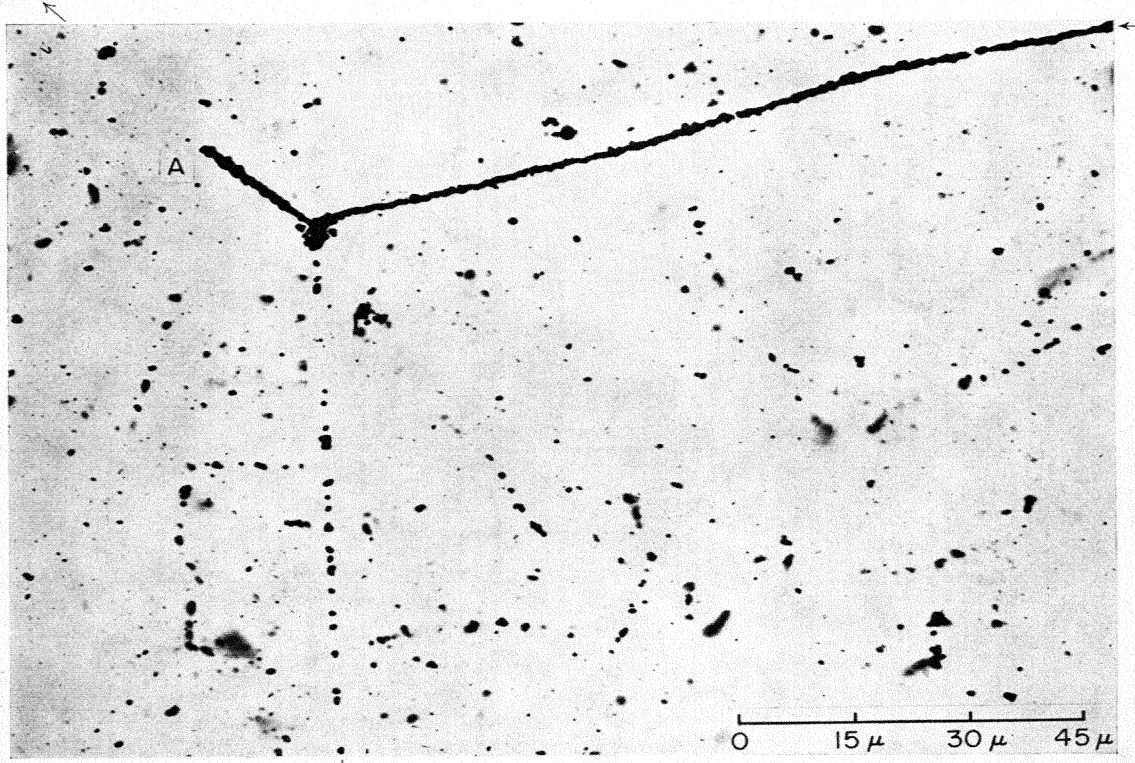

Plate IV

Plate IV – The absorption of a negative K-meson in emulsion. This example, observed by Salant and his co-workers at the Brookhaven Laboratory, is one of the first events in which a negative K-meson was produced by artificially accelerated particles (HILL *et al.* [1954]). The particle which leaves the emulsion at A could equally well be interpreted as a Σ^+-particle rather than a proton.

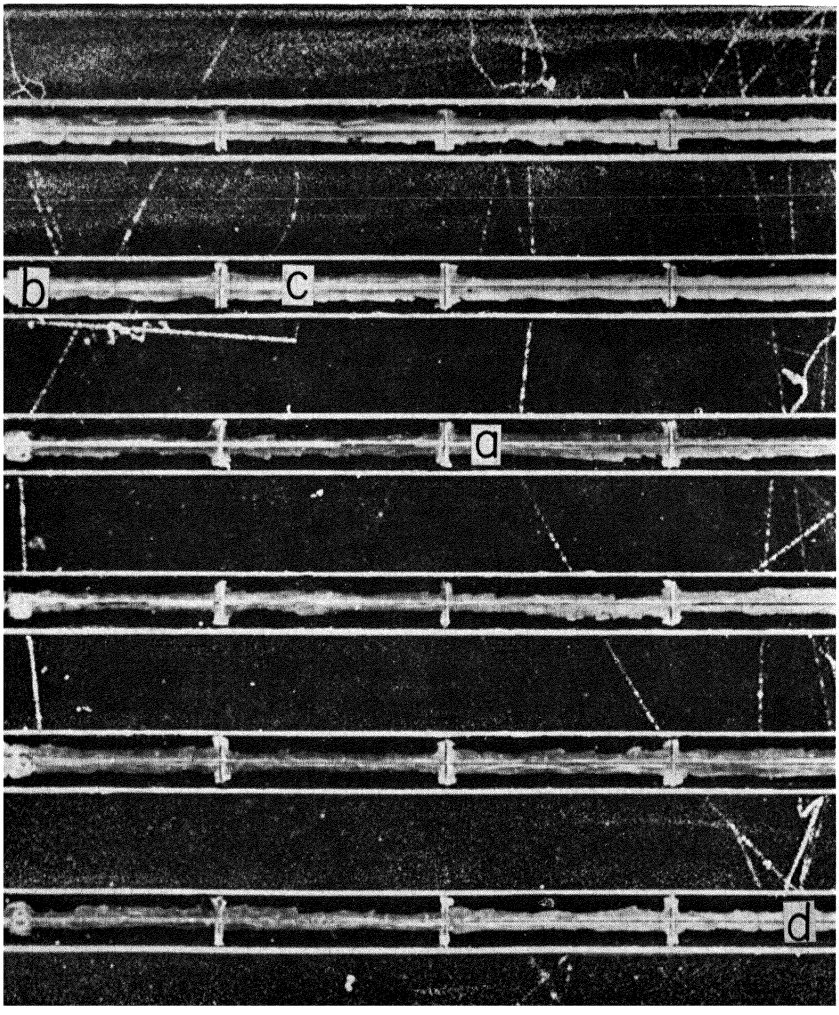

Plate V – Absorption of a negative K-meson observed by DESTAEBLER [1954], in a multiplate cloud chamber. The K-meson stops at *a*, and gives rise to an L-meson which stops at *d*, and a Λ^0-particle whose decay products enter a plate at *b* and *c*.

stopped K-meson, i.e., the plane of the V^0-particle intersects the last track segment of the K-meson inside of a plate. In event 86407 a V^0-particle and an L-meson originate from the point of stopping of a heavy particle. All of the V^0-particles are probably normal Λ^0-particles and cannot be interpreted as θ^0-mesons.

Details of the events are given in Table XIV; column 3 gives the kinetic energy of the V^0-particle computed under the assumption that it is a Λ^0-particle.

TABLE XIV

Summary of data for negative K-mesons observed in a multiplate cloud chamber by DE STAEBLER [1954]

Columns two and three list values of Q and kinetic energy for the Λ^0-particle and column four gives the kinetic energy of the π-meson.

Event	Q-value* for Λ^0-particle	Kinetic Energy of Λ^0-particle MeV	Kinetic Energy of π-meson MeV
86407	34 ± 3 — 43 ± 1	31 ± 3	$(81 - 106) \pm 3.5$
91882	32 ± 4 — 60 ± 8	30 ± 8	—
93242	33 ± 14 — 41 ± 5	59 ± 15	—

* The Q-values are computed under the assumption that the V^0-particles are Λ^0-particles. None of the V^0-particles could be interpreted as θ^0-mesons.

6. 4 INTERPRETATION

The cloud chamber results show the presence of a hyperon among the interaction products and this result is supported by some events observed in emulsions. The events which show hyperons can then be interpreted in terms of the process

$$\text{K}^-\text{-meson} + \text{nucleon} \rightarrow \text{hyperon} + \pi\text{-meson}$$

discussed in § 6.1 (iv). Specifically, if one assumes

$$\tau^- + \text{n} \rightarrow \Lambda^0 + \pi^-,$$

the Q-value of the reaction is

$$Q = (m_\tau + m_\text{n} - m_\pi - m_{\Lambda_0})c^2 = 179 \text{ MeV}.$$

The kinetic energy of the π-meson is 151 MeV and of the Λ^0-particle 28 MeV. These values of the energy will be modified because of the internal motion of the nucleons within the nucleus; for example 200 MeV/c Fermi momentum will produce Λ^0-particles

with energies up to 65 MeV. The π-meson energies will be similarly smeared out by the internal motion and, in addition, in heavy nuclei the interaction of the π-meson with the nucleus would usually produce a small star.

The events observed in emulsions seem to be predominately rather small stars in which only a small fraction of the K-particle rest mass appears as visible energy. A π-meson of about 30 MeV energy is frequently emitted but high energy π-mesons appear to be rare. Because of the rather moderate energy released in most events process (i) appears to be rare. Absorption by the mechanism (ii) may be present but would be difficult to observe except in the case of the τ^--meson. Process (iii) should not be important since the majority of K-mesons are certainly bosons.

None of the emulsion or cloud chamber events are clearly inconsistent with absorption process (iv) and it is possible that all can be explained in this way. On this basis the small number of Λ^0-particles observed in emulsion events is understandable since they can only be observed with appreciable probability when emitted in an unstable fragment. However there is as yet no conclusive evidence as to the nature of the absorption process; it is nearly certain that several types of K^--mesons exist and it is possible that these different particles interact with nuclei in different ways.

6. 5 The absorption of negative hyperons

The available data are summarized in Table XV. All of the absorptions appear to result in a small evaporation star with a visible energy of the order 20–100 MeV. Because of the conservation of heavy fermions the maximum energy released on the capture of a Σ^--particle cannot exceed about 250 MeV.

Although no definite conclusions can be drawn concerning the absorption process, all of the events listed in Table XV can be explained in terms of process § 6.1 (ii); under this assumption the hyperon is captured by the nucleus and subsequently decays. The nuclear disintegration results from interaction of the π-meson produced in the decay with the nucleus or from the energy released in the decay itself.

TABLE XV

Examples of the nuclear absorption of hyperons

Some of these events could be interpreted as negative K-mesons, see Table XIII

		Primary Particle			Star Particles			
Reference	Event	Origin	Length mm	Mass m_e	Identity	Energy MeV	Total Visible Energy MeV	Remarks
	Bristol							
(1)	Y-2	31 + 3n	4.64	2680 ± 350^b 2200 ± 350^c	p	100 ± 15	100	Could be decay of Y^+.
(2)	Y-12	18 + 4p	0.096	—	π^- 1-short black	29 ~1	30	Could be K^--absorption
	Dublin							
(3)		~31 + ?	7.35	$2280 \begin{smallmatrix}+700\\-480\end{smallmatrix}$	p	~1	~21	
				$2100 \begin{smallmatrix}+600\\-800\end{smallmatrix}^c$	p	~20		
(4)		23 + 1p	7	$2950 \begin{smallmatrix}+530\\-420\end{smallmatrix}^b$ $2580 \begin{smallmatrix}+530\\-400\end{smallmatrix}^b$ 2400 ± 250^c	6-black (p)	~22	~22	
	Padua	27 + 2p	9.43	2150 ± 300	(p) recoil 1-short black	~60	~60	
	Paris (Ecole Normale)							
(6)		—	16.15	1745 ± 100^d	e $?g^* \leqslant 1.5$ π^+	~2 27	29	Possibly K^--absorption

REFERENCES

(1) FRIEDLANDER, M. W., 1954, Phil. Mag., **45**, 418.
(2) FRIEDLANDER, M. W., D. KEEFE and M. G. K. MENON, 1955, Nuovo Cim., **1**, 482.
(3) JOHNSTON, R. H. W. and C. O'CEALLAIGH, 1954, Phil. Mag., **45**, 424.
(4) JOHNSTON, R. H. W. and C. O'CEALLAIGH, 1955, Nuovo Cim., **1**, 468.
(5) BALDO, M., G. BELLIBONI, M. CECCARELLI and B. VITALE, 1954, Nuovo Cim., **12**, supplement no. 2, 289.
(6) MORAND, M. and TSAI-CHÜ, 1954, Nuovo Cim., **12**, supplement no. 2, 280.

ACKNOWLEDGEMENTS

In the preparation of this article much material of the École Polytechnique cloud chamber workers and of the Padua emulsion group was very generously made available prior to final publication. I would like to express particular thanks to Drs. B. P. Gregory and R. Armenteros (École Polytechnique); to Drs. M. Ceccarelli and G. T. Zorn (Padua), and to Prof. G. T. Reynolds, Dr. A. L. Hodson and Dr. J. Ballam (Princeton).

In addition the material provided by Dr. R. H. Dalitz, Prof. M. F. Kaplon, Dr. Y. B. Kim, Prof. R. B. Leighton, Prof. L. Leprince-Ringuet, Dr. J. A. Newth, Prof. A. Rostagni and Prof. R. W. Thompson has been most useful.

REFERENCES

ALFORD, W. L. and R. B. LEIGHTON, 1953, Phys. Rev., **90**, 622.

AMALDI, E., C. D. ANDERSON, P. M. S. BLACKETT, W. B. FRETTER, L. LEPRINCE-RINGUET, B. PETERS, C. F. POWELL, G. D. ROCHESTER, B. ROSSI and R. W. THOMPSON, 1954a, Nuovo Cim., **11**, 213; Nature, Lond., **173**, 123. (This proposal was originally made by the authors at the Bagnères Conference 1953).

AMALDI, E., E. FABRI, F. T. HOANG, W. O. LOCK, L. SCARSI, B. TOUSCHEK and B. VITALE, 1954b, Nuovo Cim., **12**, supplement no. 2, 419.

AMALDI, E., C. CASTAGNOLI, G. CORTINI and C. FRANZINETTI, 1954c, Nuovo Cim., **12**, 668.

ARMENTEROS, R., K. H. BARKER, C. C. BUTLER, A. CACHON and C. M. YORK, 1952, Phil. Mag., **43**, 597.

ARMENTEROS, R., B. GREGORY, A. HENDEL, A. LAGARRIGUE, L. LEPRINCE-RINGUET, F. MÜLLER and C. PEYROU, 1955, Nuovo Cim., **1**, 915.

ARNOLD, W., 1954, private communication.

ARNOLD, W. H., J. BALLAM and GEO. T. REYNOLDS, 1955, Phys. Rev., **100**, 295.

APPA RAO, M. V. K. and S. MITRA, 1955, Proc. Ind. Acad. Sci., **41**, 30.

ARON, W. A., B. G. HOFFMAN and F. C. WILLIAMS, 1949, unpublished; U. S. Atomic Energy Commission Report AECU-663.

BARKAS, WALTER H. and D. M. YOUNG, 1954, UCRL–2579 Rev. unpublished.

BARKER, K. H., C. C. BUTLER, M. G. SOWERBY and C. M. YORK, 1952, Phil. Mag., **43**, 1201.

BARKER, K. H., 1953, Proceedings of the Duke Conference, II–20.

BARKER, P. R., D. M. BINNIE, B. D. HYAMS and R. J. ROUT, 1955a, Phil. Mag., **46**, 300.

BARKER, P. R., D. M. BINNIE, B. D. HYAMS, R. J. ROUT and J. SHEPHERD, 1955b, Phil. Mag., **46**, 307.

BARTLETT, M. S., 1953a, Phil. Mag., **44**, 249.

BARTLETT, M. S., 1953b, Phil. Mag., **44**, 1407.

BELLIBONI, G., B. SECHI and B. VITALE, 1954, Nuovo Cim., **12**, supplement 195.

BONETTI, A., R. LEVI SETTI, M. PANETTI and G. TOMASINI, 1953a, London Conference, (unpublished).

BONETTI, A., R. LEVI SETTI, M. PANETTI and G. TOMASINI, 1953b, Proc. Bagnères Conference, 182.

BONETTI, A., R. LEVI SETTI, M. PANETTI and G. TOMASINI, 1953c, Nuovo Cim., **10**, 1736.

BONETTI, A., R. LEVI SETTI, M. PANETTI and G. TOMASINI, 1953d, Nuovo Cim., **10**, 345.

BRIDGE, H. S. and M. ANNIS, 1951, Phys. Rev., **82**, 445.

BRIDGE, H., H. COURANT, H. DESTAEBLER, Jr. and B. ROSSI, 1953, Phys. Rev., **91**, 1024.

BRIDGE, H., H. COURANT, B. DAYTON, H. C. DESTAEBLER, Jr., B. ROSSI, R. STAFFORD and D. WILLARD, 1954, Nuovo Cim., **12**, 81.

BRIDGE, H. S., H. DESTAEBLER, Jr., B. ROSSI and B. V. SREEKANTAN, 1955, Nuovo Cim., **1**, 874.

BROWN, R., U. CAMERINI, P. H. FOWLER, H. MUIRHEAD, C. F. POWELL and D. M. RITSON, 1949, Nature, Lond., **163**, 82.

BUCHANAN, J. S., W. A. COOPER, D. D. MILLAR and J. A. NEWTH, 1954, Phil. Mag., **45**, 1025.

CALDWELL, DAVID O., 1955a, Nuovo Cim., **2**, 183; see also Phys. Rev., **100**, 291.

CALDWELL, DAVID O., 1955b, private communication.

CECCARELLI, M. and M. MERLIN, 1953a, Proc. Bagnères Conference, 183.

CECCARELLI, M. and M. MERLIN, 1953b, Nuovo Cim., **10**, 1207.

CECCARELLI, M., 1954, private communication for the Padua group (M. BALDO, G. BELLIBONI, M. CECCARELLI, M. GRILLI, B. SECHI, B. VITALE and G. T. ZORN).

CECCARELLI, M., N. DALLAPORTA, M. MERLIN, G. QUARENI and G. T. ZORN, 1954, Proc. Roy. Soc., A, **221**, 386.

CECCARELLI, M., N. DALLAPORTA, M. GRILLI, M. MERLIN, G. SALANDIN and B. SECHI, preliminary report of "G-Stack Collaboration", circulated May 1955.

COURANT, H., 1954, Thesis, Massachusetts Institute of Technology.

COURANT, H., 1955, Phys. Rev., **99**, 282.

COWAN, E. W., 1954, Phys. Rev., **94**, 161.

CRUSSARD, J., M. F. KAPLON, J. KLARMANN and J. H. NOON, 1954, Phys. Rev., **93**, 253.

DAHANAYAKE, C., P. E. FRANÇOIS, Y. FUJIMOTO, P. IREDALE, C. J. WADDINGTON and M. YASIN, 1954, Phil. Mag., **45**, 1219.

DALITZ, R. H., 1953a, Proc. Bagnères Conference, pp. 236–238.

DALITZ, R. H., 1953b, Phil. Mag., **44**, 1068.

DALITZ, R. H., 1953c, Proc. Phys. Soc., Lond., A, **66**, 710.

DALITZ, R. H., 1954, Private communication to the Princeton group (see Hodson *et al.* 1954).

DALITZ, R. H., 1955, private communication.

DALLAPORTA, N. and G. LANZA, 1954, Nuovo Cim., **12**, supplement no. 2, 260.

DANIEL, R. R. and YASH PAL, 1954, Proc. Ind. Acad. Sci., A, **40**, 114.

DANIEL, R. R., E. C. GEORGE and B. PETERS, 1955, Proc. Ind. Acad. Sci., A, **41**, 45.

DEBENEDETTI, A., C. M. GARELLI, L. TALLONE and M. VIGONE, 1954, Nuovo Cim., **12**, 952.

DESTAEBLER, HERBERT, Jr., 1954, Phys. Rev., **95**, 1110.

DILWORTH, C., G. P. S. OCCHIALINI and L. SCARSI, 1954a, Annual Review of Nuclear Science, vol. **4**, 282.

DILWORTH, C. C., A. MANFREDINI, G. D. ROCHESTER, J. WADDINGTON and G. T. ZORN, 1954b, Nuovo Cim., **12**, supplement no. 2, 435–441.

DUERDEN, T. and B. D. HYAMS, 1952, Phil Mag., **40**, 717.

EISENBERG, Y., 1954, Phys. Rev., **96**, 541.

FABRI, E., 1954, Nuovo Cim., **11**, 479.

FOWLER, W. B., R. P. SHUTT, A. M. THORNDIKE and W. L. WHITTEMORE, 1954, Phys. Rev., **93**, 861. Private communication A. M. THORNDIKE.

FRETTER, W. B. and E. W. FRIESEN, 1955, Rev. Sci. Inst., **26**, 703.

FRIEDLANDER, M. W., D. KEEFE, M. G. K. MENON and L. VAN ROSSUM, 1954, Phil. Mag., **45**, 1043.

FRY, W. F. and J. J. LORD, 1952, Phys. Rev., **87**, 533; see also SCHEIN, M. and D. HASKIN, Proc. Bagnères Conference, 168.

FRY, W. F., J. SCHNEPS and M. S. SWAMI, 1955, Phys. Rev., **97**, 1189.

GELL-MANN, M., 1953, Phys. Rev., **92**, 833.

GELL-MANN, M. and A. PAIS, 1954, Proceedings of the 1954 Glasgow Conference on Nuclear and Meson Physics, (London and New York; Pergamon Press, 1955), 342.

GOLDHABER, M., 1953, Phys. Rev., **92**, 1279.

GREGORY, B., A. LAGARRIGUE, L. LEPRINCE-RINGUET, F. MÜLLER and CH. PEYROU, 1954, Nuovo Cim., **11**, 292.

HILL, R. D., E. O. SALANT and M. WIDGOFF, 1954, Phys. Rev., **95**, 1699.

HOANG, T. F., L. JAUNEAU, J. JOUVIN, G. KAYAS, L. LEPRINCE-RINGUET, D. MORELLET, A. ORKIN-LECOURTOIS and J. TREMBLEY, 1955, Nuovo Cim., **1**, supplement no. 3, 169.

HODSON, A. L., J. BALLAM, W. H. ARNOLD, D. R. HARRIS, R. RONALD RAU, GEO. T. REYNOLDS and S. B. TRIEMAN, 1954, Phys. Rev., **96**, 1089.

KIM, Y. B., J. R. BURWELL, R. W. HUGGETT and R. W. THOMPSON, 1954, Phys. Rev., **96**, 229.

LAGARRIGUE, A. and C. PEYROU, 1951, J. Phys. Radium, **12**, 848.

LAL, D., YASH PAL and B. PETERS, 1953a, Proc. Bagnères Conference, 141.

LAL, D., YASH PAL and B. PETERS, 1953b, Phys. Rev. **92**, 438.

LAL, D., YASH PAL and B. PETERS, 1953c, Proc. Ind. Acad. Sci., **38**, 398.

LEIGHTON, R. B., 1953, Proc. Bagnères Conference, 98, 254.

LEIGHTON, R. B., 1954, Loeb Lectures, Harvard University, unpublished; (private communication).

LEPRINCE-RINGUET, L., HOANG TCHANG-FONG, L. JAUNEAU and D. MORELLET, 1948, C. R. Acad. Sci. Paris, **226**, 1897.

LEPRINCE-RINGUET, L., 1949, Rev. Mod. Phys., **21**, 42.

MENON, M. G. K. and C. O'CEALLAIGH, 1953a, Proc. Bagnères Conference

MENON, M. G. K. and C. O'CEALLAIGH, 1954, Proc. Roy. Soc., A, **221**, 292.

MEZZETTI, L. and J. W. KEUFFEL, 1954, Nuovo Cim., **12**, supplement no. 2, 245.

MEZZETTI, L. and J. W. KEUFFEL, 1954, Phys. Rev., **95**, 858.

MICHEL, L., 1950, Proc. Phys. Soc. A, **63**, 514.

MICHEL, L. and R. STORA, 1952, C. R. Acad. Sci. Paris, **234**, 1257.

NEWTH, J. A., 1954, Nuovo Cim., **11**, supplement no. 2, 290.

O'CEALLAIGH, C., 1951, Phil Mag., **42**, 1032.

Padua Conference, 1954, reported in Nuovo Cim., **12**, supplement no. 2 (1954).
PAIS, A., 1952, Phys. Rev., **86**, 663.
PAIS, A., 1953, Physica, **19**, 869.
PEIERLS, R., 1935, Proc. Roy. Soc., A, **149**, 467.
PERKINS, D. H., 1953, Report of Rochester Conference.
PODOLANSKI, J. and R. ARMENTEROS, 1954, Phil. Mag., **45**, 13.
POWELL, C. F., 1952, Report of Copenhagen Conference, 29.

STERNHEIMER, R., 1953, Phys. Rev., **91**, 256.

THOMPSON, R.W., 1953, Proc. Bagnères Conf. 30.
TOUSCHEK, B., 1954, Nuovo Cim., **12**, supplement no. 2, 281.

WILSON, J. G. and C. C. BUTLER, 1952, Phil. Mag., **45**, 993.

YORK, C. M., 1952, Phil. Mag., **43**, 985.
YORK, C. M., R. B. LEIGHTON and E. K. BJORNERUD, 1953, Phys. Rev., **90**, 167.
YORK, C. M., Jr., R. B. LEIGHTON and E. K. BJORNERUD, 1954, Phys. Rev. **95**, 159.

CHAPTER III

DECAY PROCESSES OF HEAVY UNSTABLE NEUTRAL PARTICLES

BY

R. W. THOMPSON

University of Indiana

INTRODUCTION. 255

1. EARLY WORK ON V°-PARTICLES 256

2. EXPERIMENTAL AND ANALYTICAL TECHNIQUES 259

3. THE Λ°-PARTICLE. 280

4. THE θ°-PARTICLE 297

5. THE ANOMALOUS V°-DECAYS 310

6. THE PRODUCTION OF V°-PARTICLES 321

7. SUMMARY 331

ACKNOWLEDGEMENTS 333

REFERENCES. 334

INTRODUCTION

Since the existence of neutral heavy unstable particles was established by ROCHESTER & BUTLER [1947] and SERIFF *et al.* [1950], considerable effort has been devoted to the study of these particles in many different laboratories. Progress, however, has been relatively slow, since from the experimental point of view the area is an inherently difficult one. The phenomenon has turned out to be surprisingly complex with respect to the number and types of particles and the variety of their decay schemes. While greatly stimulating interest in the area, this complexity has made the experimental problem formidable, since relevant observations must be sufficiently detailed and quantitative to identify the type, or at least the class, of particles to which they refer.

The earlier V°-particle work was done almost exclusively with the magnetic cloud chamber. More recent investigations have also utilized a number of other instruments, with the resultant data being, in many cases, advantageously complementary. The multiplate chamber has proved to be a very effective tool, both alone and in conjunction with a magnetic chamber. The nuclear emulsion, particularly in the form of stacks of stripped emulsions, has now been successfully applied to the V°-particle problem. One of the major accomplishments of the last year has been the artificial production of V°-particles in the pressurized hydrogen diffusion chamber at the Brookhaven Cosmotron.

The two most common types of V°-particle, the Λ° and θ°, now appear to be well identified. Interest is therefore shifting to the so-called anomalous types. There is preliminary evidence for several decay processes distinct from those of the normal Λ° and θ°. Some of this evidence may lead to the discovery of more new particles, some of it may turn out to be explicable in terms of alternate decay modes of particles already identified, and some of it may not be confirmed by further work. The anomalous events amount to only 5 to 10% of all V°-particles observed; hence they must be studied against a large background of normal Λ° and θ° decays. Experimentally, the first and most necessary step in the interpretation of data is to establish that the few unusual

examples are genuinely anomalous, rather than the result of larger than average errors. Work in the last year has therefore been characterized by increased emphasis on reliability of measurements and reduction of data.

Since the present article is apparently the first experimental review devoted exclusively to the neutral heavy unstable particles, it is appropriate to begin, in the first section, with a brief account of the basic earlier work. In the second section, the observational techniques are discussed, with particular emphasis on developments of the last year. The third and fourth sections are devoted to the present status of work on the two best established V°-particles, the Λ° and θ°, respectively. The fifth section discusses the so-called anomalous events, and the final section, the production and nuclear interactions of V°-particles.

1. Early Work on V°-Particles

In this section, the basic earlier work, which lead to the discovery of V°-particles and later to the realization of the complexity of the problem, is discussed.

1. 1 Discovery of V°-particles

The first suggestion of the existence of heavy neutral unstable particles was made by Rochester & Butler [1947] in the course of a cloud chamber investigation of cosmic ray induced penetrating showers under lead with the original electromagnet of Blackett [1936]. Among some fifty penetrating shower photographs, these authors noted a most striking event, comprising the apparently copunctual origin in the gas of a pair of oppositely charged particles of considerable rigidity. [1] Both tracks of the fork were at minimum ionization and no visible evidence for a recoil fragment was found in the vicinity of the apex. The angle between the tracks was 67°, about 1000 times larger than expected for a positron-electron pair of the observed energy. It was further argued that if the event were due to a collision process in the gas, several hundred times as many similar processes should have been seen in the 3-cm. lead plate across the center of the chamber,

[1] The original photographs of Rochester and Butler are beautifully reproduced in the compilation of Rochester & Wilson [1952], hereinafter referred to as the Atlas.

whereas very few of such were observed. Thereupon, Rochester and Butler pointed out that the event could be explained in terms of the spontaneous decay of a new type of heavy neutral unstable particle. A second fork in the same observations was similarly interpreted to represent the decay of a charged particle.

The observations of Rochester and Butler were confirmed and their arguments put on firm statistical ground by SERIFF *et al.* [1950] [1], who observed 34 examples of the forked tracks associated with penetrating showers under lead at sea level and at 3200 m. Of the 34 examples, 30 were of the first, or neutral, type and 4 were of the second, or charged, type. In addition to confirmation of the existence of such particles, these observers obtained a variety of results on the properties of the particles:

1. The incidence of the particles under lead was shown to increase markedly with altitude.
2. The number of neutral unstable particles produced in penetrating showers was estimated to be about 3% of the total number of ionizing particles.
3. The decay fragments were shown to be heavier than electrons from the absence of radiative collisions in a 2 cm. lead plate across the center of the chamber.
4. Some of the fragments were shown to have strong nuclear interactions.
5. Some of the fragments were shown to be mesons (π or μ) from ionization and curvature.
6. The mean rest lifetime of the neutral particles was estimated to be of the order of $(3 \pm 2) \times 10^{-10}$ sec. from the distribution of decay points in the chamber.
7. Subsequent use of the coplanarity test for a third neutral fragment was anticipated, but the authors did not consider the accuracy of their coplanarity measurements in this early paper to be definitive.

All of these conclusions have been well-confirmed by subsequent work and have become a part of our general knowledge of the properties of the new unstable particles.

At the suggestion of Blackett and Anderson, the generic term "V-particle" was adopted to refer to the unstable parent particles which on decay were responsible for the forked tracks.

[1] ATLAS, pp. 104–107.

1. 2 Early evidence for the complexity of V°-particles

The first examples of identified protons among the decay fragments of V°-particles came from further work of the Manchester group [1, 2] with the Blackett electromagnet installed on the Pic-du-Midi at an altitude of 2867 m. Among 36 examples of V°-particle decay, four heavily ionizing positive decay fragments were found whose estimated ionizations were in good agreement with that calculated for protons of the appropriate momenta. In all four events the track of the negative fragment was at or near minimum ionization. Since the measured momenta ranged from 1 to $5 \cdot 10^8$ eV/c, it was inferred that the negative fragment in these cases was a meson (π^- or μ^-). Assuming a 2-body decay, these authors thus proposed the scheme

$$V^\circ \rightarrow p + \pi^- \qquad (1)$$

and gave calculated values of the V°-mass ranging from 2180 to 2400 m_e. The division of momentum between the charged fragments (in favour of the positive fragment) suggested that a substantial fraction of other examples might also be of this type.

However, in the same set of data, there were two or possibly three V°-decays in which the upper limit for the mass of the positive fragment, from ionization and momentum, was found to be distinctly less than the proton mass and in the most favorable case only slightly more than the pion mass. Unfortunately, the track of the negative fragment in all three photographs was at minimum ionization and either too short or too straight for identification or measurement.

Contemporaneously with the work of the Manchester group, the Indiana group [3, 4] had independently reached similar conclusions. Among nine examples of V°-decay obtained at sea level with a 12 in. diameter magnetic chamber, there were three cases in which the positive fragment, from ionization and momentum, was found to have a mass near that of the proton. In two of the three cases, the negative fragment could be shown to be light and therefore was inferred to be a π (or μ) meson. The use of the Q-value was introduced; for the decay scheme $V^\circ \rightarrow p + \pi + Q$,

[1] Armenteros *et al.* [1951a].
[2] Atlas, pp. 108–109.
[3] Thompson *et al.* [1951].
[4] Atlas, pp. 112–113.

the two cases gave Q-values of (31 ± 5) MeV and (34 ± 10) MeV [1].

In the same set of observations, there was also a V°-decay (film ⫶ 50) in which the positive fragment could not be much heavier than a π-meson. The negative fragment, at minimum ionization, had a measured momentum in the neighbourhood of 1.3 GeV/c; thus the upper mass limit was too high to be informative and the negative fragment was not identified. This event is further discussed in section 4.

2. Experimental and Analytical Techniques

In this section, a few of the recent advances in technique which have been applied to the investigation of V°-particles are briefly discussed. The first part is concerned with experimental technique, the second part, the analysis of V°-particle data.

2. 1 Experimental techniques

Although very valuable V°-data is now coming from the nuclear emulsion, the main source of information is still the cloud chamber. In the interest of brevity, therefore, we will treat cloud chamber techniques only. The status of stripped emulsion technique has been discussed by a number of authors, including Powell [1953], Lal *et al.* [1953a], and Stiller *et al.* [1954].

2. 1a *Distortions in the Magnetic Chamber*

The main source of error in the measurement of momentum with the magnetic cloud chamber is usually the so-called chamber distortion [2]. Unfortunately, in many of the earlier V°-particle investigations, the exemplary work of Blackett & Brode [1936] has not been taken into account. As a result, it is not evident from the literature to what extent the various groups have established that their curvatures are significant.

Because of work done during the last year or so, the situation has tightened considerably with respect both to the reduction of the distortions themselves and to the realistic assessment of their contribution to the uncertainty of the result. The line of attack on this problem has been different in every laboratory; the most

[1] The published Q-value for film ⫶ 55 should read 34 MeV instead of 28 MeV, as may be verified from the basic data given.

[2] The subject of chamber distortions has been treated at length by Wilson [1951]. For examples, see Atlas, pp. 9, 105, 107.

concerted effort has probably been that of the Indiana group [1].

The new large magnetic chamber at Indiana University was designed from the beginning with the express object of reduction and control of track distortion. In order to prevent temperature differences which can result in track distortions, the chamber is completely surrounded by a heavy copper thermal jacket with dead air space between. To the jacket are soldered several hundred feet of flattened copper tubing through which distilled water, thermostated to $\pm$ 0.02° C, is pumped at the rate of 30 gal./min. At the sides of the jacket opposite the flash lamp housings, a storm porch arrangement is used to compensate for the poor thermal conductivity of the side glass windows. The hollow pole of the magnet is constructed in two parts; the inner one, a wedge-shaped iron shell, is an integral part of the thermal jacket, thermally insulated from the main pole.

No-field tracks are taken with the pancakes of the magnet coils connected in opposing pairs to insure that thermal conditions are identical to those existing when the apparatus is recording data [2]. The chamber is of the rubber diaphragm type, with exhaust valves located outside the iron yoke to the rear of the solid pole. Thus, there is no question of a difference of conditions due to the absence of eddy-current forces on, for example, a light metal piston. The "test tracks" are those of μ-mesons, sufficiently fast (range $\geqq$ 42 in. of lead) to ensure that multiple scattering in the gas (argon) of the chamber does not obscure the results.

Fig. 1 shows representative examples of the comparator plots of three no-field tracks exhibiting various amounts of distortion, from one of the worst to one which is considerably better than average. In Fig. 2 is shown a representative distribution of such no-field tracks. It should be noted that the mean value of curvature does not occur at zero, indicating a small tendency toward systematic distortions. The spread about the mean corresponds to a maximum detectable momentum of about $5 \cdot 10^{10}$ eV/c.

The data of Fig. 1 and Fig. 2 refer to tracks which traverse essentially the full illuminated height of the chamber (22 in.). For

[1] Proceedings of the Bagnères Congress, 1953, p. 4.

[2] CARTER & STREET [1954] report an elegant method of determining the distortion in an individual track in the presence of a magnetic field. The technique is based on the use of a narrow ribbon of soft x-rays, pulsed in synchronization with the Geiger counter triggering signal.

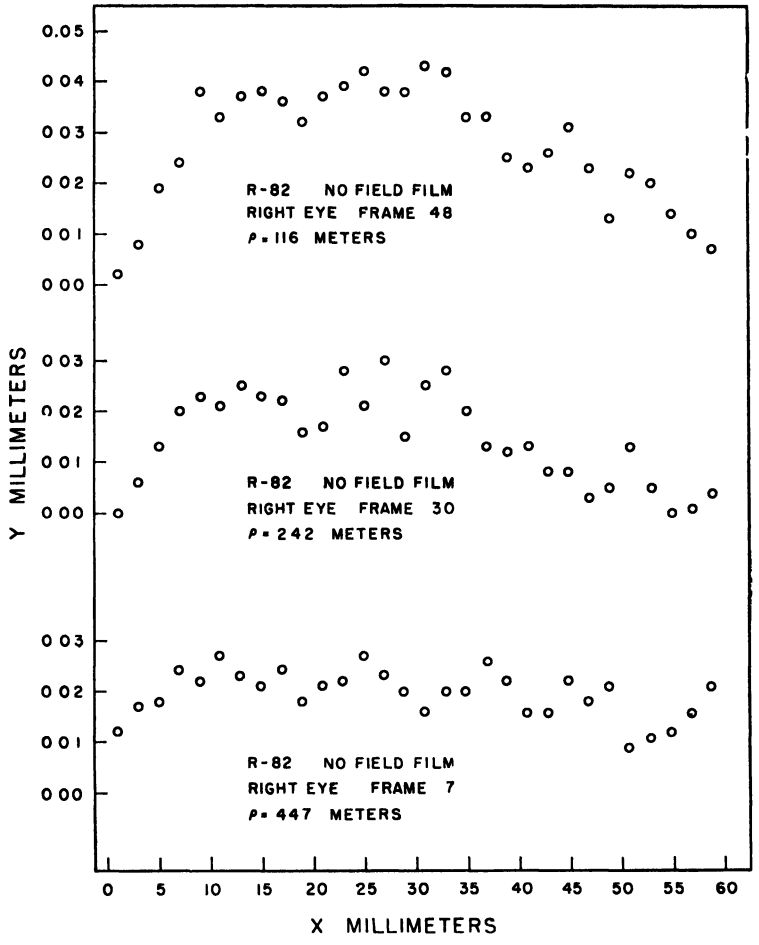

Fig. 1 – Representative comparator plots of 3 no-field tracks from the large Indiana magnet chamber. The ordinate scale is greatly expanded. All curvatures are reduced by the new least squares method developed for the large Indiana chamber (THOMPSON *et al*, Proceedings of the Bagnères Congress, p. 4).

shorter tracks, the probable error is taken inversely as the length of track, a procedure which has been recently confirmed in a study by FRETTER & FRIESEN [1954a].

2. 1b *Reduction of Curvature and Angle Data*

There were some difficulties in comparison of the earlier results from various laboratories since it has appeared that some curvature and angle data were incompletely or improperly reduced. The

situation has greatly improved during the last year or so. However, since the particular methods which are used to reduce the data vary considerably from group to group, it would be desirable if all laboratories reporting data with magnetic chamber would carry out a *direct* test of their particular methods of reduction to insure that systematic errors have not been overlooked. [1]

In order to illustrate the method, the results of such tests, as

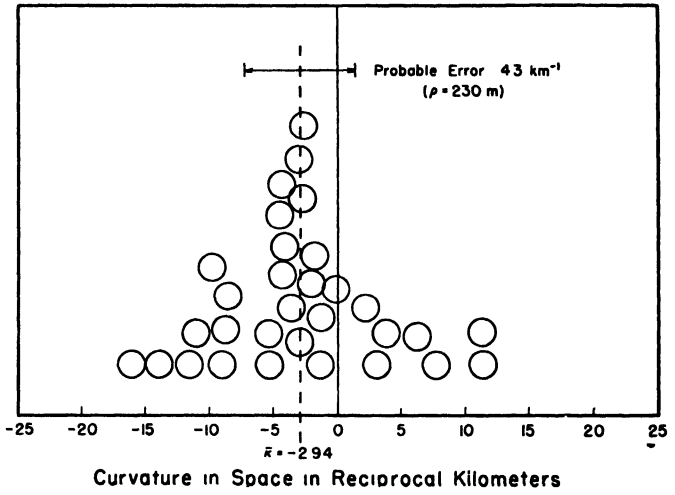

Fig. 2 – Representative distribution of no-field tracks from the large Indiana magnet chamber.

carried out by the Indiana group [2], are given. Table I illustrates the results of a curvature test. In this test, a dummy track [3] was photographed behind a duplicate front glass plate with one of the two stereoscopic cameras which are alternately used to photograph

[1] We are indebted to Dr. V. A. J. van Lint for pointing out one very subtle source of error, which illustrates the importance of checking the procedures. It was found, in preliminary work with the new 48 in. chamber at C.I.T., that the determinations of the angle between Λ^0-decay fragments were in substantial error in those cases in which the decay plane was inclined to that of the chamber. Careful study revealed that the cause of difficulty was the use of the reprojection lenses at full aperture, for reasons of intensity.

[2] Proceedings of the Fourth Annual Rochester Conference on High Energy Physics, 1954, p. 78.

[3] The dummy track used was one constructed with B. Gregory in the summer of 1948 for a similar test. The dummy was remeasured for the present test and a very slight change in curvature was found, which was attributed to warping of the sheet of plastic on which the track was engraved.

the chamber. The films were developed and the radius of curvature of the image on each film measured with the standardized comparator procedures. The results are given in column 2. The films were then replaced in the original camera and reprojected to determine the space orientation of the track. Column 3 gives the measured magnification, column 4 gives the quotient of column 2 by column 3, and column 5 gives the space radius of curvature after projective corrections. Note that the radii in column 4 exhibit considerable variation both with respect to each other and with respect to the true value. However, the corrections leading from column 4 to column 5 remove this variation and bring the results from the three views into close agreement with the actual value.

TABLE I

Curvature Reduction Test

Stereoscopic view	ϱ_f mm (on film)	m = magnification at track centre	ϱ_f/m cm (in space)	ϱ_s cm (in space)
Right	66.31	0.1096	60.52	75.2
Central	60.95	0.1099	55.48	76.4
Left	56.17	0.1067	52.62	76.2
			mean	75.9
			actual value	75.6

TABLE II

Angle Reduction Test

Stereoscopic view	θ_f angle on film	θ_s angle in space
Right	21.98°	24.62°
Central	19.68°	24.53°
Left	16.78°	24.51°
		mean θ_s 24.55°
		actual value 24.54°

Similarly, Table II illustrates the results of an angle reduction test. Column 2 gives the angle θ_f of the image on the film, as determined by the standardized comparator procedures. Column 3

gives the angle θ_s in space as computed from θ_f and from the track orientation in space determined from reprojection. Again, the final result is in close agreement with the known value of the dummy angle.

2. 1c *Determination of Ionization*

In the majority of V°-particle investigations with the magnetic cloud chamber, the momentum-ionization compromise [1] has been made in favour of momentum with no concession to drop counting. The determination of ionization has therefore been a rough visual estimate best made through the use of comparison tracks. The resulting mass determinations have given very valuable qualitative information. However, the importance of obtaining accurate momentum *and* ionization measurements on the same track has been generally recognized. One approach to this problem has been reported by COHN *et al.* [1953].

COWAN [1954] and FRETTER & FRIESEN [1954a] have developed techniques which represent a substantial advance in this direction. The relevant technical data are summarized in Table III.

The drop count is made on the original negatives with the aid of a stereoscopic viewer, as a result of which the background correction is neglible. The track is divided into N equal cells, each of length approximately equal to the track width, by means of a transparent reticule placed over the film. The number of drops per cell n is recorded, with the exception that cells containing more than 25 drops are rejected [2]. The relative ionization [3] of the track is then given by $\bar{n}$, and the standard deviation in $\bar{n}$ is calculated from the observed distribution of n from the formula [4]

$$\sigma_{\bar{n}} = \frac{\sigma_n}{\sqrt{N}} \tag{2}$$

From the central limit theorem, the distribution of $\bar{n}$ is approximately Gaussian; Cowan's errors are given in terms of the probable

[1] WILSON [1951].

[2] For tracks of 1.5 times minimum ionization, the number of cells so rejected in only 1.5%.

[3] In order to make the drop count independent of the condensation efficiency (NIELSEN [1942]), each expansion is individually calibrated by means of electron tracks of known momenta.

[4] Eq. (2) presumes that n is an uncorrelated random variable. This assumption may not be entirely correct; however, the resultant effect on the error so calculated is probably small.

error $\varrho = 0.6745\,\sigma$. A numerical example, referring to a track of about 1.5 times minimum ionization and total number of drops $N\bar{n} = 1482$ is given in Table IV. The probable errors determined in this way turn out to be about 1.7 times larger than those calculated assuming the total number of drops is Poisson distributed. This result corresponds to $\frac{1}{2} \cdot (1.7)^2$ ion pairs per primary ionizing event, which is not far from the observed values.

TABLE III

Data on Momentum-Ionization Compromise

	Cowan	Fretter and Friesen
Photographed area	48 × 48 cm	40 × 50 cm
Gas	2 He, 1 A	He
Vapor	2/3 ethyl alcohol 1/3 water	2/3 ethyl alcohol 1/3 water
Compressed pressure	100 cm Hg	100 cm Hg
Light flash delay	125 msec	125 msec
Magnification	1/8.4	1/12.5
Focal length	125 mm	50 mm
Aperture	*f*/19	*f*/16
Track width in space	1.5 mm	1.25 mm
Track width on film	~ 177 μ*	~ 100 μ
Drop image size on film	~ 26 μ*	~ 10 μ
Maximum detectable space radius of curvature	100 m	180 m
Magnetic field	4200 gauss	8000 gauss
Maximum detectable momentum	1.3×10^{10} eV/c	4×10^{10} eV/c

* Measured by the present author and Dr. Friesen on a negative supplied by Dr. Cowan. We are indebted to Dr. Cowan for permission to quote these figures.

TABLE IV

Estimation of Statistical Errors in Cowan's Drop Count

Number of cells: N	=	164
Average drops per cell: $\bar{n}$	=	9.03
Standard deviation in n: σ_n	=	4.73
Standard deviation in $\bar{n}$: $\sigma_{\bar{n}}$	=	0.370
Probable error in $\bar{n}$: ϱ	=	0.249
% probable error in $\bar{n}$: $\frac{100\varrho}{\bar{n}}$	=	2.8%

In addition to the statistical error estimated as described above, Cowan includes a flat 10% "counting error".

2. 2 Analysis and representation of V°-particle data

There are two characteristic features of the V°-particle problem which make the analysis of data more complicated than in the case of the charged unstable particles. First, V°-particles have so far been detected only by their decay into charged fragments [1]. Thus, the properties of the neutral parent particle must be indirectly inferred from study of the decay fragments. Second, V°-particles are electrically neutral and hence do not lose energy by ionization. Their decay must therefore be studied in flight. In contrast, the decay of the charged particles is most advantageously observed at the end of the range where the velocity of the parent particle is not only known, but is zero.

As a result of these two factors, a variety of special methods for the analysis of V°-particle data have been introduced. Some of these are also of interest in the analysis of the decay of charged particles.

In view of the comprehensive article of Podolanski & Armenteros [1954], the problem of summarizing the analysis of data is greatly simplified. Accordingly, much of the material in the present section is expository in nature.

2. 2a *Properties of Q and α*

The Q-Value. The parameter most frequently used to characterize V°-decay is the Q-value, defined by the equation

$$Q \equiv \sqrt{(E_+ + E_-)^2 - |\vec{p}_+ + \vec{p}_-|^2} - (m_+ + m_-)\,, \qquad (3)$$

where E_+, E_-, $\vec{p}_+$, $\vec{p}_-$, m_+ and m_- are the energies, momenta, and masses of the fragments. The Q-value so defined for given input data clearly depends on the values assigned to m_+ and m_-; this dependence may be explicitly displayed by indicating the nature of the fragments in parenthesis, with the positive fragment written first. Thus for the decay $\Lambda^\circ \to \mathrm{p} + \pi^-$, $Q(\mathrm{p}, \pi^-) = 37$ MeV.

In the special case of 2-body decay in which m_+ and m_- are correctly assigned, Eq. (3) represents the sum of the kinetic

[1] Cases A and B of the Brookhaven group (cf. section 6), in which recoil effects indicate the production of K°-particles, provide exceptions to this statement.

energies of the decay fragments in the center of mass system, or, what is the same thing, the mass decrement in the decay process. In other cases, the Q-value is used as a parameter, and as such has a number of useful properties. For example, it is a convenient test of compatibility with a given decay scheme. Conversely, given a set of decay data, the Q-values for various schemes may be computed and the resulting histograms examined for peaks. However, it should be emphasized that the Q-value is not an adequate substitute for basic data.

The use of the Q-value as a decay parameter, in preference to the computed V°-mass, was originally introduced because it tends, under certain conditions, to be relatively insensitive to the assumed fragment masses and thus is more closely related to the experimental measurements. This fact is illustrated by differentiation of Eq. (3)

$$\frac{\partial Q}{\partial m_+} = \frac{\gamma}{\gamma_+} - 1$$

where γ and γ_+ refer to the V°-particle and the positive fragment, respectively. On applying the Lorentz transformation, we find

$$\frac{\partial Q}{\partial m_+} = \frac{1}{\gamma_+'(1 + \beta\beta_+' \cos\theta_+')} - 1$$

where γ_+' and β_+' refer to the positive fragment in the centre of mass system, θ_+' is the angle of emission of the positive fragment in the centre of mass system, and β refers to the V°-particle. It is seen that $\beta_+' \leqslant 1$ is a sufficient condition to insure that Q is insensitive to m_+.

The errors in Q quoted in the literature are invariably those resulting from uncertainties in the measured momenta and angles alone and do not reflect uncertainties in the masses of the assumed fragments. Although the fragment masses may be well determined in very fortuitous individual cases, this information is used for identification of the fragments only; the best available masses for the identified fragments then are used in the computation of Q.

If the errors in p_+, p_-, and θ are assumed to be small, the corresponding errors in Q may be calculated from the first derivatives:

$$\frac{\partial p_\pm}{\partial Q} = \gamma(\beta_\pm - \beta\cos\theta_\pm)\ ;\ \cos\theta_\pm = \left(\frac{p_\pm + p_\mp\cos\theta}{P}\right)$$

$$\frac{\partial\theta}{\partial Q} = \gamma\beta p_\nu\ ;\quad p_\nu = \frac{P}{p_+ p_- \sin\theta}$$

where $\vec{P} = \vec{p}_+ + \vec{p}_-$, θ_+ is the angle which $\vec{p}_+$ makes with P, p_y is the component of $\vec{p}_+$ normal to $\vec{P}$, and θ is the angle between $\vec{p}_+$ and $\vec{p}_-$. If the errors δp_+, δp_-, and $\delta\theta$ are assumed to be independent, their respective contributions to the error in Q are combined geometrically. The relative contribution of $\delta\theta$ is usually negligible with reasonable track length.

In practice, however, it is often the case that neither assumption

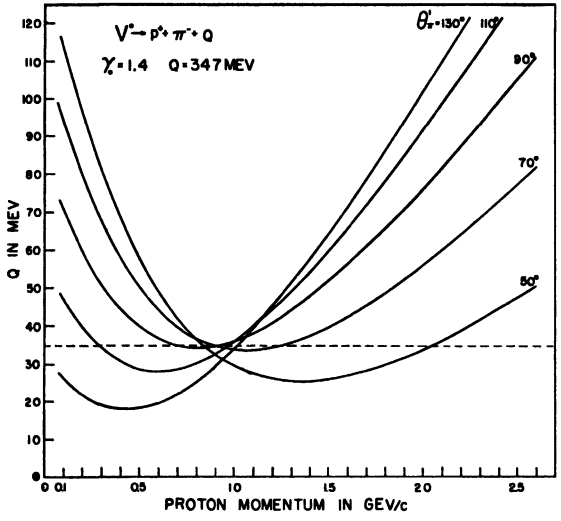

Fig. 3 – The dependence of Q(p, π) on the measured momentum of the proton for $\gamma = 1.4$ and various angles of emission of the pion in the center of mass system. These curves were calculated in 1951 on the basis of a slightly lower value of Q than is indicated at present.

is correct. Linear estimation of the errors may not be justified if the errors are large. This is well illustrated in Fig. 3 in which the dependence of Q(p, π), for Λ^0-decay, on the measured momentum of the proton is shown for $\gamma = 1.4$ and various angles of emission of the pion in the centre of mass system. The curves show a minimum; for 90° emission in the centre of mass system, the minimum Q is close to the true value. It is clear that large errors in the proton momentum will produce an asymmetric Q(p, π) distribution [1].

[1] The curves illustrated in Fig. 3 were explained dynamically and offered as an explanation of the high energy tail of Q(p, π)-values reported in some of the earlier work (Thompson, R. W., C. J. Karzmark and H. O. Cohn, 1952, Phys. Rev., 87, 182).

The errors in the measured quantities are often strongly dependent rather than independent. This fact may result in underestimation or overestimation of the errors in Q, depending on the nature of the dependence and on the dynamics of the particular V°-event. It happens that the two most important types of dependence are very easily described with the aid of the Q-curve diagram, and therefore will be discussed in paragraph 2. 2b.

One of the most important applications of the Q-value is in connection with the problem of 3-body decay. If a third neutral fragment is produced in the decay, the quantity calculated from Eq. (3), based on the two (observed) charged fragments only, does not represent the true energy release in the process. The Q-value calculated by Eq. (3) in these circumstances is called the "apparent Q-value" and denoted by Q^*.

The problem of the distribution of Q^* for 3-body decay has been treated by LEIGHTON *et al.* [1951] and more completely by BRUECKNER & THOMPSON [1952]. The latter authors obtain the equation

$$Q^* = \frac{2(m_+ + m_-) + Q}{2(m_+ + m_-) + Q^*}\left(1 - \frac{T_0'}{T_0'(max)}\right)Q, \qquad (4)$$

where Q is the true energy release in the decay, T_0' is the kinetic energy of the neutral fragment in the true centre of mass system, and $T_0'(max)$ is the maximum value of T_0'. It is clear from Eq. (4) that Q^* ranges from 0 to Q as T_0' ranges from $T_0'(max)$ to 0, respectively. The physical significance of the limiting values of Q^* is readily understood if it is noted that Eq. (3) gives the sum of the kinetic energies of the two charged fragments in that frame of reference in which the sum of their momenta is zero. For $T_0' = 0$, that condition is satisfied by the true centre of mass system of the V°-particle, and the sum of the kinetic energies of the charged fragments in that coordinate system is evidently the true Q-value. For $T_0' = T_0'(max)$, the two charged fragments are emitted with the same velocity and direction, the latter being opposite to that of $\vec{p}_0'$. The frame of reference in which the sum of their momenta is zero is the frame of reference in which they are at rest, and therefore $Q^* = 0$. In the laboratory frame the angle θ between the two charged fragments is zero for $Q^* = 0$.

Eq. (4) provides the relationship between the distribution of Q^* and the distribution of T_0'. Let $F(Q^*)$ and $f(T_0')$ be the differential distributions of Q^* and T_0', respectively. Then we obtain

$$f(T_0') = \frac{M}{(m_+ + m_-) + Q^*} F(Q^*), \tag{5}$$

where M is the true mass of the V°-particle. It is apparent from Eq. (5) that knowledge of one distribution is equivalent to knowledge of the other, and that the relationship between the two distributions is independent of the V°-particle velocity, the orientation of the decay plane in the centre of mass system, etc. The application of Eq. (5) will be illustrated in sections 3, 4, and 5.

The Manchester Parameter a. The first attempt to classify V°-decay schemes by purely dynamic methods was made by ARMENTEROS *et al.* [1951b]. The method used by these authors was essentially dependent on the fact that asymmetries in the masses of V°-decay fragments are reflected statistically, in the laboratory frame, in asymmetries in the longitudinal components of the fragment momenta. As a measure of the latter, these authors used the dimensionless parameter

$$a \equiv \frac{(p_+)_x - (p_-)_x}{P}.$$

The motive for use of this particular function of the longitudinal components of momentum rather than the longitutinal components themselves derives from the properties of the transformation equations.

Consider the decay in flight, as in Fig. 4, of a particle of mass M and velocity β into two fragments of masses m_+ and m_- and momentum $\vec{p}'$ in the centre of mass system. Resolve $\vec{p}'$ into components p_x' and p_y' along the x' and y' axes, where x' corresponds to the direction of motion β. Consider the x-component of momentum of one of the decay fragments in the laboratory frame:

$$p_x = \gamma (p' \cos \theta' + \beta E'). \tag{6}$$

For a given value of β and isotropic emision in the centre of mass system, p_x is uniformly distributed over a range $2\gamma p'$ which is centered about the mean value $\gamma\beta E'$. Thus, the width and mean of the distribution are measures of the center of mass momentum p' and energy E' of the fragment, respectively. However, since the V°-particle velocity is not known in practice, and varies over a considerable range, it is desirable to eliminate the dependence of the distribution on β, insofar as possible. Considerable improve-

ment results if we consider the distribution of Eq. (6) after division by the V°-particle momentum $P = \gamma\beta M$:

$$\frac{p_x}{P} = \frac{p' \cos\theta'}{\beta M} + \frac{E'}{M}.$$

The ratio p_x/P is also uniformly distributed for given β. The velocity dependence of the mean is removed, however, and that of the width is reduced. The distribution of any linear function of the ratio p_x/P has the same properties. The parameter

$$a = \frac{2\,(p_T)_x}{P} - 1 = \frac{2\,p' \cos\theta'}{\beta M} + \frac{E_+' - E_-'}{M} \tag{7}$$

is a convenient choice since it is antisymmetric with respect to the fragments.

It is readily verified that a may be expressed in terms of the masses:

$$a = \frac{E_+' - E_-'}{M} = \frac{m_+^2 - m_-^2}{M^2},$$

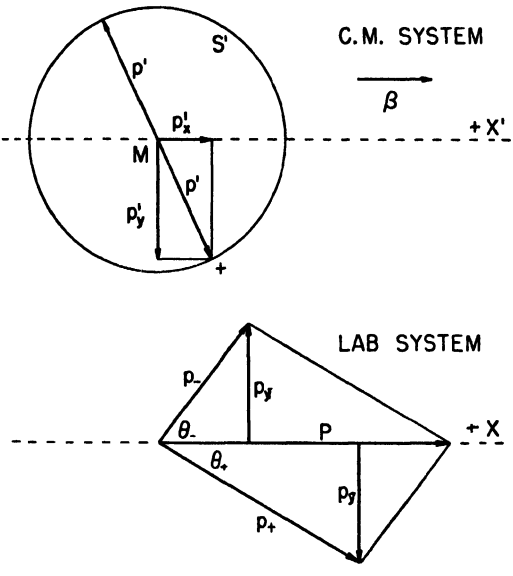

Fig. 4 – Vector diagram of a V°-decay into two charged fragments.

and that a itself may be expressed in terms of the resultant momenta or in terms of the angles

$$a = \frac{p_+^2 - p_-^2}{P^2} = \frac{\sin^2\theta_- - \sin^2\theta_+}{\sin^2\theta}.$$

The latter form is applicable in cases where the momenta are not determined, providing the V° line of flight is known.

2. 2b *The Q-Surface Representation*

The majority of V°-particles produced by cosmic radiation are so energetic that the observable fragments are near minimum ionization and very little can be said about their masses, although much valuable qualitative information has come from those cases in which the masses of one or both fragments can be estimated

from ionization and momentum in the magnetic chamber, or one or both fragments can be stopped in a multiple plate chamber. However, the question of the nature of the relativistic disintegrations of charged and neutral particles remains and will undoubtedly attract increasing attention in the future. Hence it is of some interest to discuss methods of representation of decay data which are applicable in the complete absence of *a priori* knowledge of the primary or secondary masses.

The general idea of a dynamic representation for 2-body decay is seen immediately from the energy equation [1]

$$\sqrt{P^2 + M^2} - \sqrt{p_+^2 + m_+^2} - \sqrt{p_-^2 + m_-^2} = 0\,, \qquad (8)$$

where P is given by

$$P = \sqrt{p_+^2 + p_-^2 + 2\,p_+ p_- \cos\theta}\,.$$

Eq. (8) is of the form

$$h(M, m_+, m_-; p_+, p_-, \theta) = 0\,, \qquad (9)$$

where the masses M, m_-, and m_+ characterize the decay process; and p_+, p_-, and θ are the variables directly observed in the laboratory system with the magnetic chamber. Eq. (9) may be regarded as the equation of a family of surfaces in a (p_+, p_-, θ) — space, the parameters of the family being M, m_+, and m_-. Each observed disintegration yields a (p_+, p_-, θ) triad and may be represented by a point in the space. All points representative of a given decay scheme form a surface which characterizes the decay and permits evaluation of the parameters M, m_+, and m_-. Since, for two given fragments m_+ and m_- the locus of representative points of constant Q is a member of the family, the name Q-surface has been suggested.

It is evident that the observable triad need not be restricted to the variables p_+, p_-, and θ. In the decay of charged particles, the momenta of the primary and charged secondary and angle may be used; or in the multiple plate chamber, angles, ranges, average scattering angles, etc. may be used. The essential point is that coordinates in the disintegration space must be a triad of quantities which are functions of three direct observables only, and thus do not depend on assumed masses or other basic parameters of the decay.

The general idea of a Q-surface is in itself of little practical use.

[1] THOMPSON *et al.* [1953c].

The question is whether a space can be constructed such that the Q-surfaces are geometrically simple and have evident physical significance. Such a space is readily found as follows: Consider a 2-body decay in flight as in Fig. 4. In the equation

$$p_x'^2 + p_y'^2 = p'^2 , \tag{10}$$

transform p_x' and p_y' to the laboratory frame. The y'-component of momentum is invariant and equal to the transverse component of momentum p_y in the laboratory frame

$$p_y' = p_y = \frac{p_+ p_- \sin\theta}{p} .$$

The x'-component of momentum may be expressed in terms of p_x by means of Eq. (6). The dependence of the result on the V°-particle velocity β will be less, however, if p_x' is expressed in terms of α by Eq. (7). Thus we have

$$p_x' = \frac{(\alpha - \bar{\alpha})}{(\bar{2}/\bar{\beta}\bar{M})} = \frac{(\alpha - \bar{\alpha})}{2\sqrt{\frac{1}{M^2} + \frac{1}{P^2}}} ,$$

and Eq. (10) becomes

$$\frac{(\alpha - \bar{\alpha})^2}{4p'^2\left(\frac{1}{M^2} + \frac{1}{P^2}\right)} + \frac{p_y^2}{p'^2} = 1 . \tag{11}$$

Eq. (11) is of the form:

$$H\left(\bar{\alpha}, p', M;\ \alpha, p_y, \frac{1}{P}\right) = 0 \tag{12}$$

in which $\bar{\alpha}$, p', and M characterize the decay process and α, p_y, and $1/P$ are functions of quantities observed in the laboratory frame only. Thus Eq. (12) defines a family of Q-surfaces in $(\alpha, p_y, 1/P)$-space; $\bar{\alpha}$, p', and M are parameters of the family. A drawing of the Q-surface for $\Lambda^\circ \to \mathrm{p} + \pi + 37$ MeV is shown in Fig. 5.

The cross-sections of the Q-surfaces parallel to the (α, p_y)-plane are vertical ellipses, with centers in the $(\alpha, 1/P)$-plane on the line $\alpha = \bar{\alpha}$, p_y semi axis equal to p', and α semi axis equal to

$$2p'(1/M^2 + 1/P^2)^{\frac{1}{2}} .$$

These ellipses have very simple physical significance, for if their dimensions parallel to the α-axis are divided by the factor $2(1/M^2 + 1/P^2)^{\frac{1}{2}}$, the centre remaining at $\alpha = \bar{\alpha}$, the circle of radius p' which results corresponds precisely to the circle on which

lie the terminal points of $\vec{p}'$ in the centre of mass system. The initial points of $\vec{p}'$ are at $\alpha = \bar{\alpha}$, and the direction of motion $\vec{\beta}$ lies along the $+\alpha$-direction. Thus the cross-section of the Q-surface gives a slightly distorted picture of the vector diagram in the centre of mass system, and a number of questions may be answered by inspection.

As $1/P \to 0$, the cross section approaches a limiting shape with

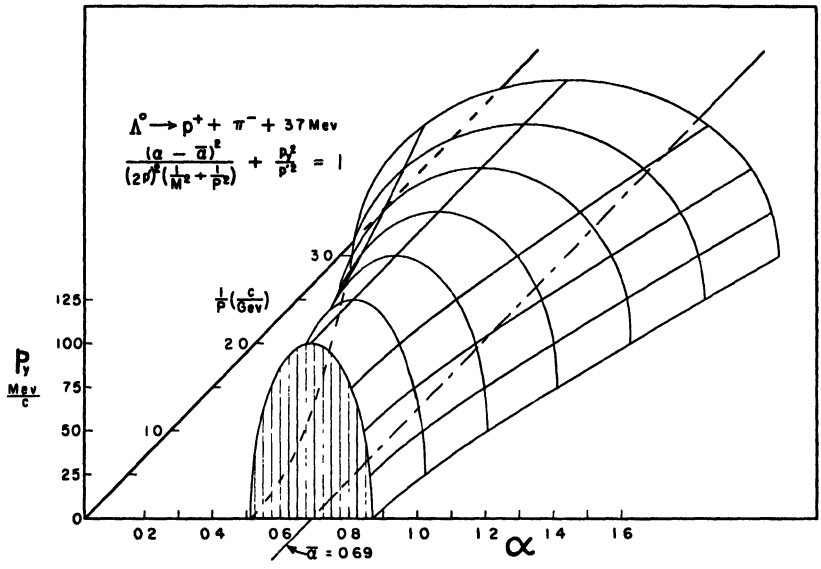

Fig. 5 – Isometric drawing of the Q-surface for Λ°-decay in (α, p_y, $1/P$)-space. The limiting form of the cross-section as $1/P \to 0$ is vertically cross-hatched.

α semi axis equal to $2p'/M$. Thus for $P^2 \gg M^2$, the velocity of the centre of mass is completely separated and a two dimensional representation of the motion in the centre of mass (Q-curve plot) is possible. For relativistic decays, $|\alpha| \leq 1$; the condition that the α-intercept of the Q-curve is ± 1 is that $m_\mp = 0$.

Fig. 6 shows the Q-curves for the decay $\Lambda^\circ \to p + \pi + Q$ with various values of Q.

One of the most useful properties of the Q-curve plot is that the propagation of errors may be described by a few simple rules which cover a number of situations. Given an observed triad $(p_+ \pm \delta p_+, p_- \pm \delta p_-, \theta \pm \delta\theta)$, where the errors are, for the present, assumed to be independent, the independent effects of δp_+, δp_-, and $\delta\theta$ on the coordinates (α, p_y) of the representative point in the

Q-curve plot may be represented by error segments of the appropriate length and slope. The combined effect corresponds to an ellipse of uncertainty.

ADAMS [1953] has shown that for relativistic decays, the p_+- and p_--segments radiate from the points (0, —1) and (0, +1), respectively [1]. The result is illustrated in Fig. 7, where the solid Q-curve

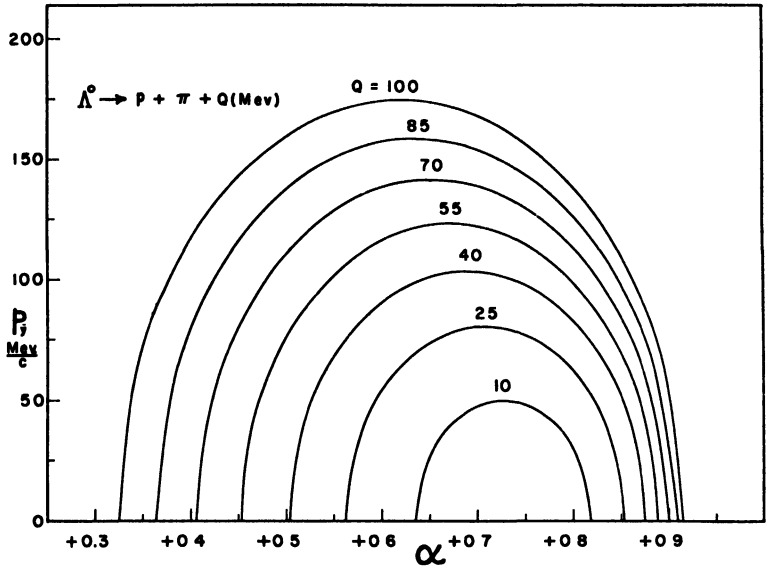

Fig. 6 – Q-curves for Λ°-decay with various values for Q from 10 to 100 MeV. The curves form a nested set. The slow decrease of $\bar{\alpha}$ with increasing Q results from the increase in Λ° mass.

is drawn for the decay $0^\circ \to \pi^+ + \pi^- + 214$ MeV. The p_+-segments radiate from F_1; the p_--segments from F_-. All error segments shown are drawn for 10% error in the momenta. Consider a decay for which P is the representative point. The p_--segment, in the direction PF_-, is almost tangent to the Q-curve. Since for given fragment masses, the Q-curve is the locus of points of constant Q, it is clear that δp_- will contribute relatively little error to the calculated $Q(\pi, \pi)$-value. On the other hand, the p_+-segment is almost normal to the Q-curve, hence the calculated $Q(\pi, \pi)$-value will be sensitive to δp_+. The situation is just reversed with regard to determination of the angle of emission θ' in the centre of mass system. Most of the uncertainty in θ' derives from δp_-.

[1] Adams' result holds for finite increments in the momenta.

For relativistic decays, the θ-segments are very nearly vertical. However, for reasonable track length, the errors in θ are relatively small and may be neglected.

The assumption that δp_+ and δp^- are independent is not at all appropriate in many situations. Let us examine the opposite case, in which they are dependent according to a relation

$$g(\delta p_+, \delta p_-) = 0 . \tag{13}$$

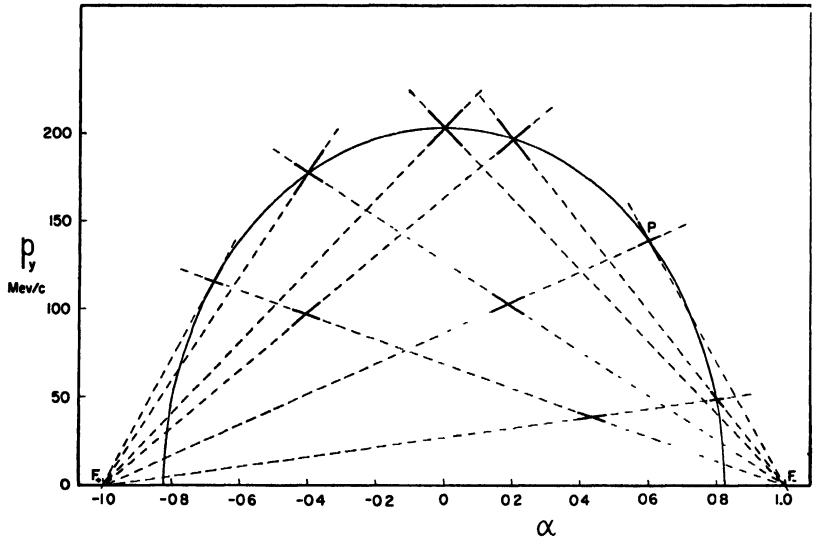

Fig. 7 – Representation of error segments in the Q-curve plot for relativistic decays.

In this case, the ellipse of uncertainty [1] degenerates to a segment whose slope we now determine for two important particular forms of Eq. (13).

In the magnetic chamber, distortions are usually the main source of large errors, particularly for fast V°-particles. The tracks of the decay fragments, for fast V°-particles, are in relatively close proximity since θ is small. Hence it may be assumed that whatever distortions are present affect both tracks in the same way; i.e. $\delta K_+ = \delta K_-$. In terms of the momenta, Eq. (13) becomes

$$\frac{\delta p_+}{p_+^2} + \frac{\delta p_-}{p_-^2} = 0 . \tag{14}$$

Optical distortions, film distortions, and some other types, will

[1] We assume $\delta\theta$ to be negligible.

also be described by Eq. (14), under the assumption that the tracks are in close proximity. For Eq. (14), it is readily verified that the resultant error segment is very nearly horizontal, and of magnitude

$$\delta a \cong (1 - a)\frac{\delta p_+}{p_+}.$$

It is evident that this effect is to the advantage of the experimenter in the determination of Q-values, since for isotropic decay, the representative points cluster near the top of the Q-curve, where the slope is zero.

A second important case arises when Eq. (13) has the form

$$\frac{\delta p_+}{p_+} - \frac{\delta p_-}{p_-} = 0. \tag{15}$$

Eq. (15) applies, for example, when the momentum of one fragment is determined from p_y-balance. Errors due to field calibration, magnification, and film shrinkage may also be included. For Eq. (15), the resultant error segment is very nearly vertical, and of magnitude

$$\frac{\delta p_y}{p_y} - \frac{\delta p_+}{p_+}.$$

Three-Body Decay. If, in addition to the two charged fragments, a neutral particle is produced in the decay, it can be shown that the representative points in (a, p_y, $1/P$)-space scatter, but all lie within the Q-surface which corresponds to zero kinetic energy for the neutral fragment in the true centre of mass system.

2. 2c *The Podolanski-Armenteros Parameter* ε

Podolanski & Armenteros [1954] have developed a very interesting and useful representation which differs from that described above in that the dimensionless parameter

$$\varepsilon = \frac{2p_y}{P}$$

is used instead of p_y itself. The equation of the Q-surfaces in (a, ε, $1/P$)-space becomes

$$\frac{(a - \bar{a})^2}{\varepsilon^{*2}[1 + (M/P)^2]} + \frac{\varepsilon^2}{\varepsilon^{*2}(M/P)^2} = 1, \tag{16}$$

where $\varepsilon^* \equiv 2p'/M$. In Eq. (16), $\bar{a}$, ε^*, and M are constants characteristic of the decay; a, ε, and $1/P$ are decay parameters which are functions of the measured quantities only. Fig. 8 shows a

drawing of the Q-surface for the decay $\Lambda^\circ \to p + \pi + 37$ MeV. The salient difference between Fig. 5 and Fig. 8 is that in the latter, the cross-section perpendicular to the $1/P$-axis does not approach a limiting shape, but rather degenerates into a line on the α-axis as P becomes large in comparison with p'.

Very useful features of the Podolanski-Armenteros representation are found in the (α, ε)-projection, and are related to the fact that ε is dimensionless. Thus, the coordinates of a V°-event

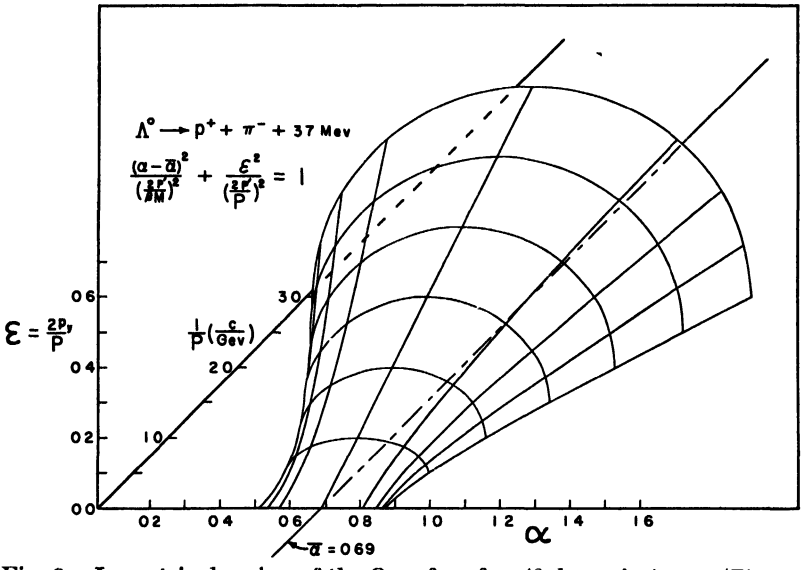

Fig. 8 – Isometric drawing of the Q-surface for Λ°-decay in $(\alpha, \varepsilon, 1/P)$-space. The cross-section degenerates to a line on the α-axis as P becomes large, as a result of the velocity dependence of the Podolanski-Armenteros parameter ε.

in that projection depend on the angles θ_+ and θ_- only, providing the signs of the fragments can be determined. Hence

$$\left.\begin{aligned} \varepsilon &= \frac{2 \sin \theta_+ \sin \theta_-}{\sin \theta}, \\ \alpha &= \frac{\sin (\theta_- - \theta_+)}{\sin \theta}. \end{aligned}\right\} \tag{17}$$

Fig. 9 shows the (α, ε)-diagram, with curves of constant P for $\Lambda^\circ \to p + \pi + 37$ MeV and $0^\circ \to \pi_+ + \pi^- + 214$ MeV. The curves, given by Eq. (16), are confocal ellipses with foci F_1 and F_2 on the α-axis at $(\bar{\alpha}—\varepsilon^*)$ and $(\bar{\alpha} + \varepsilon^*)$, respectively. The loci of constant θ' and constant p_y are confocal hyperbolae with the same foci as the ellipses.

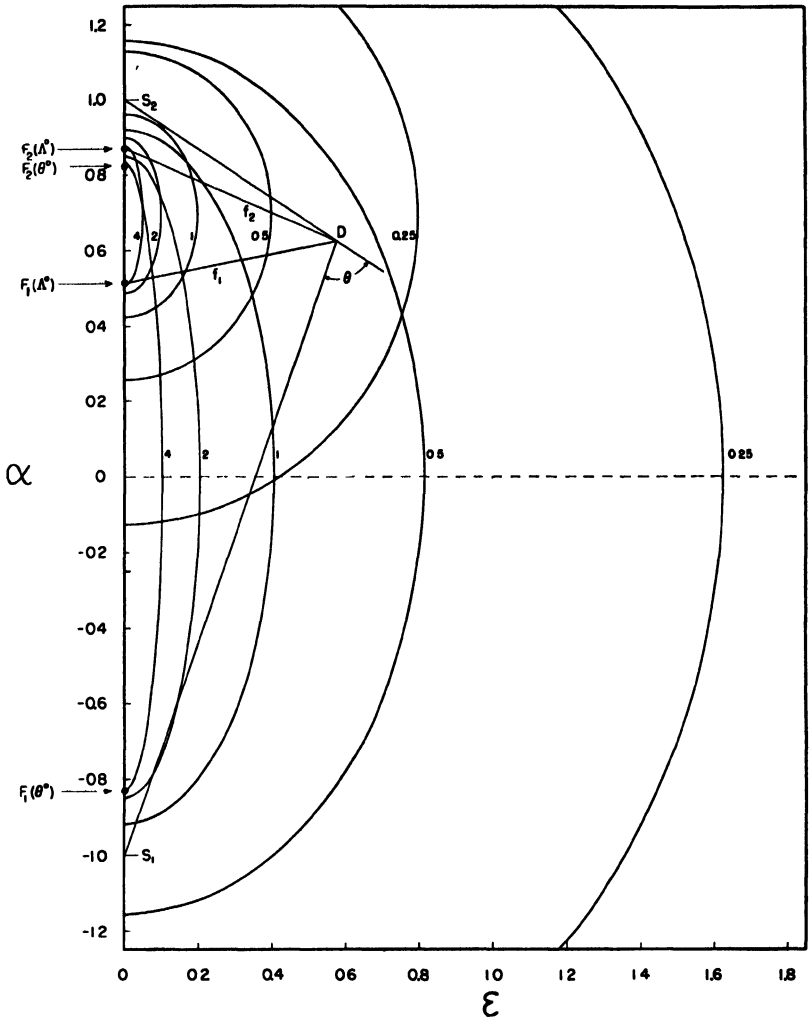

Fig. 9 – The (α, ε)-diagram of Podolanski and Armenteros. The curves drawn refer to $\theta°$—($\bar{\alpha} = 0$) and $\Lambda°$—($\bar{\alpha} = +0.69$) decay with $P = 0.25, 0.5, 1, 2, 4$ GeV/c. Triangle DS_1S_2 is the vector triangle of the decay as seen in the laboratory frame, where $\overrightarrow{DS_1} \sim \vec{p}_+$, $\overrightarrow{S_2D} \sim \vec{p}_-$, and $\overrightarrow{S_2S_1} \sim \vec{P}$.

Let D represent an observed V°-event with coordinates given by Eq. (17). It is readily verified that angles DS_1S_2 and DS_2S_1 are θ_+ and θ_-, respectively. Thus the loci of constant θ_+, θ_-, and θ are lines through S_1, lines through S_2, and circles through S_1 and S_2, respectively.

If the nature of the decay represented by D is known *a priori*,

various quantities of interest may be evaluated graphically from the diagram. For example, if D is a Λ°, the momentum P, by interpolation between the curves, is about 340 MeV/c. The center of mass velocity β and angle of emission θ' can be calculated from the relations

$$\frac{1}{\beta} = \frac{f_1 + f_2}{2\varepsilon^*}$$

$$\cos \theta' = \frac{f_1 - f_2}{2\varepsilon^*}$$

where f_1 and f_2 are the distances from D to the foci F_1 and F_2, respectively.

An excellent example of the utility of the Podolanski-Armenteros method is found in the work of GAYTHER [1954].

3. The Λ°-Particle

During the last year, considerable confirming evidence for the decay scheme $\Lambda^\circ \rightarrow p + \pi^- + 37$ MeV has become available, as a result of which the existence and decay scheme of the Λ°-particle are generally considered to be well-established. There is a variety of detailed evidence that the decay fragments are indeed an ordinary proton and a negative pion and that the decay is a 2-body process. All observers are now agreed that all, or practically all, decays of this type occur with an energy release near 37 MeV. There is still some evidence, principally from the Pasadena group, for lower and higher Q-values. The recent, more accurate, work of that group with the new 48 in. magnet indicates that the number of these anomalous case, however, is only a few percent and thus is much less than was previously reported.

In the first four parts of this section, the detailed evidence for the Λ°-decay scheme, the determination of Q and the lifetime are discussed. The fifth part summarizes the emulsion work, the last part the cascade decay process.

3.1 NATURE OF THE CHARGED FRAGMENTS

As discussed in § 1.2, the first evidence that protons were among the decay fragments of V°-particles was based on mass determinations from ionization and momentum in the magnetic chamber. Additional evidence of this type has been reported by LEIGHTON *et al.* [1951], ARMENTEROS *et al.* [1951b], THOMPSON *et al.* [1952a], ARMENTEROS *et al.* [1953], FRETTER & FRIESEN

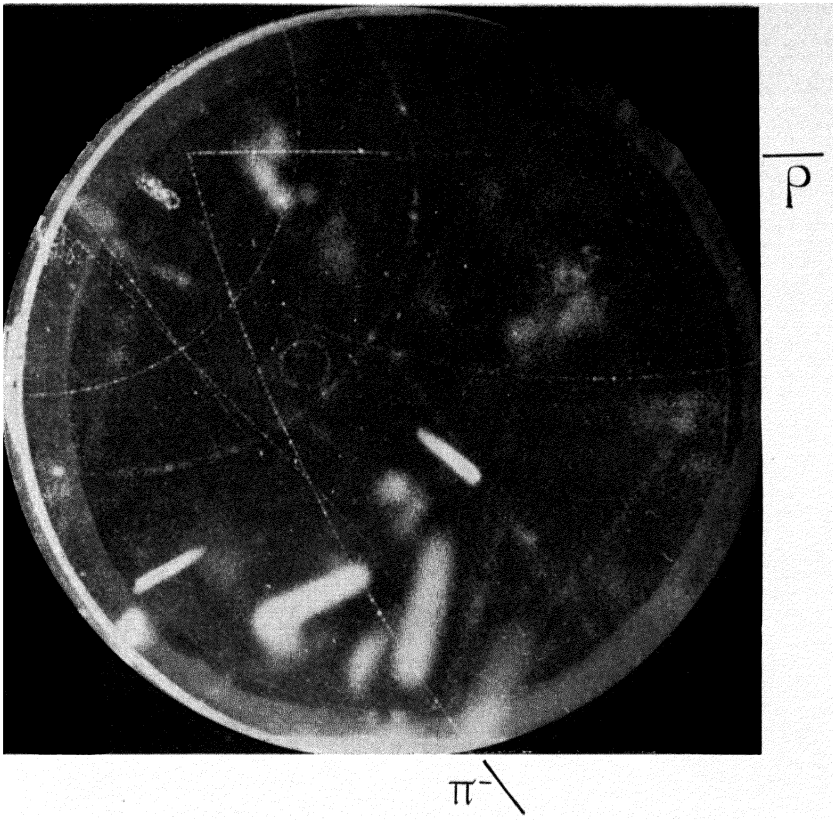

Plate I - Example of a V^0-decay with identified proton fragment from ARMENTEROS *et al.* [1951b]. The positive fragment has a momentum of (350 ± 35)MeV/c and an estimated ionization of 4—6 I_0, which corresponds to a mass range of 1450 – 2300 m_e. The negative fragment has a momentum of (142 ± 10)MeV/c and is near minimum ionization. The angle between the tracks is 87.5° and the $Q(p, \pi)$-value is (58 ± 5)MeV.

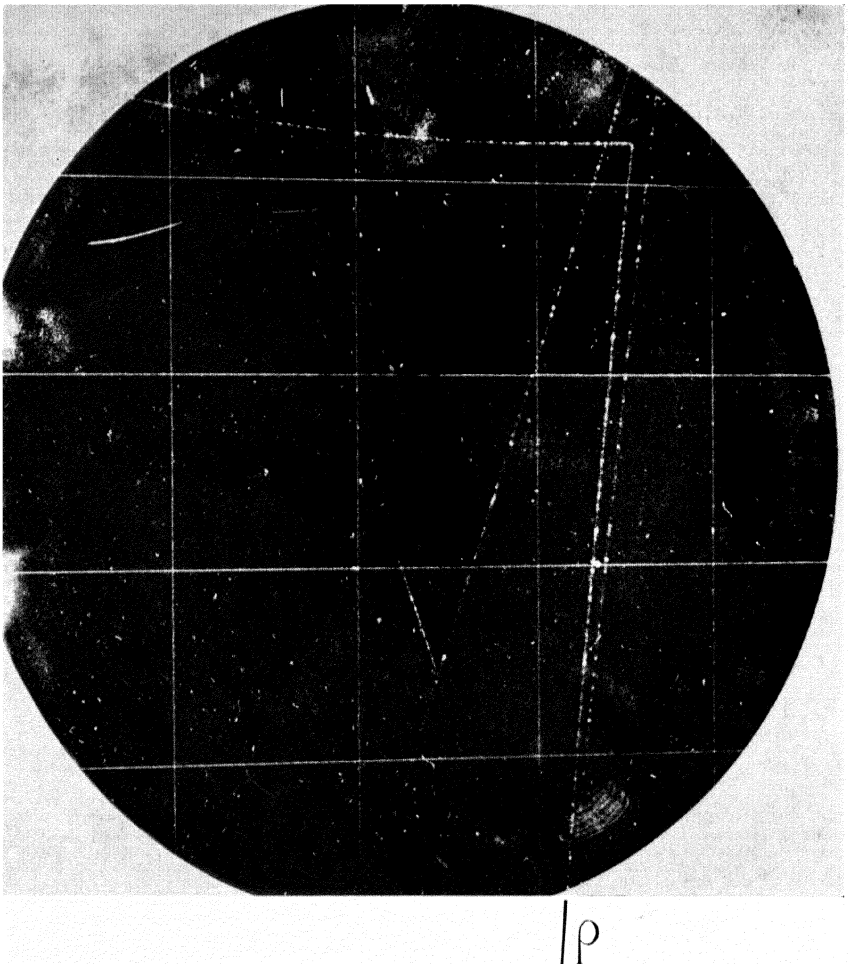

Plate II – Example of a V°-decay with identified proton fragment from THOMPSON *et al.* [1952a]. The positive fragment has a momentum of (660 ± 130)MeV/c and an estimated ionization of 2 – 3 I_0, which corresponds to a mass range of 1640 – 2180 m_e. The negative fragment has a momentum of (65 ± 3)MeV/c and an estimated ionization of 3– 4 I_0, which corresponds to a mass range of 210 –265 m_e. The angle between the tracks is (84.5 ± 0.5)° and the $Q(p, \pi)$-value is 36 ± 10 MeV.

[1953], LEIGHTON *et al.* [1953a], MILLAR & PAGE [1953], and COWAN & GUESS [1954]. The nature of this type of evidence is illustrated in Plates I and II. Although the individual mass estimates are rough, with the exception of the recent work of FRETTER & FRIESEN [1953] and COWAN & GUESS [1954], the combined data indicate that the commonly occurring heavy positive fragment from V°-decay has mass equal to that of the proton, within 200 m_e or less.

If the proton-like fragment were a new type of positive particle (meson or hyperon) with mass only slightly different from that of the proton, it would be expected to be unstable and occasionally to decay in flight in the chamber. No example of such decay has been recorded. Further evidence for stability has come from the multiplate chamber work of FRETTER *et al.* [1953a] and BRIDGE *et al.* [1953a] in which many of the proton-like fragments were observed to stop in the plates with no evidence for instability. MILLAR & PAGE [1953] report an unusual example in which the proton-like fragment stops in the gas (argon) of a magnetic chamber, again with no indication of instability.

The early mass-determinations by ionization and momentum clearly indicated that the negative fragment is a π-or μ-meson. Distinction between the two possibilities was provided by observations of ARMENTEROS *et al.* [1951b], LEIGHTON *et al.* [1953a] and BRIDGE *et al.* [1953a] in which a number of nuclear interactions and π-μ-decays were found.

The Q-curve plot of THOMPSON *et al.* [1953a] provided evidence of a purely dynamic nature that the earlier mass measurements of the Λ^0-fragments were indeed correct, and extended those measurements to relativistic Λ^0-particles.

Courant [1] has measured the interaction mean free path of V°-secondaries for a group of V°-particles containing a large proportion of Λ^0-particles and reports a value of (163 ± 40) gm.cm^{-2} of lead, which corresponds very nearly to the geometric cross section for lead. This result indicates that both decay fragments have strong nuclear interactions, which is to be expected if they are a proton and pion.

Finally, very convincing confirmation of the nature of the Λ^0-decay fragments has come from the recent stripped emulsion work, e.g. that of FRIEDLANDER *et al.* [1954]. The discussion of

[1] As reported by BRIDGE *et al.* [1953a].

this work will be deferred until § 3.5, since the approach is somewhat inverse to that followed in the cloud chamber work.

By way of summary, there is detailed evidence that the majority of Λ°-decays yield an ordinary proton and a negative pion. However, none of the evidence excludes the possibility that a small fraction, say 5%, of the V°-events with heavy positive fragment are of a different type. LEIGHTON *et al.* [1953a], in fact, report evidence for such, to be discussed in § 3. 3 and section 5.

3. 2 TWO-BODY DECAY

A third neutral decay fragment cannot be directly observed in the cloud chamber or emulsion, but would be expected to produce detectable recoil effects on the charged fragments. At present, all attempts to detect such effects have been uniformly negative. Some neutral particles (e.g. γ, π°, n) would, if present, produce recognizable effects in metal plates placed in the chamber. ARMENTEROS *et al.* [1951b], DEUTSCHMANN [1952], FRETTER *et al.* [1953a] and BRIDGE *et al.* [1953a] have looked for such effects, but none has been found. Thus, there is good evidence that the Λ°-decay is a 2-body process.

The dynamic tests which have been used to search for effects of a third neutral fragment are: (*a*) coplanarity and transverse momentum balance, and (*b*) uniqueness of the Q-value. The two tests of the first type are closely related and detect apparent lack of momentum balance in the decay process. Knowledge of the V°-particle origin is required. The Q test depends on the fact, discussed in § 2. 2a, that a third neutral fragment would be expected to take up variable amounts of kinetic energy in the true centre of mass system, as a result of which the apparent Q-values in the laboratory frame are distributed over a spectrum. The Q test is independent of assumption as to the V°-particle origin.

3. 2a *Coplanarity and Transverse Momentum Balance*

If a third neutral fragment is produced in the decay process, its recoil would be expected to cause a discrepancy between the direction of the Λ° trajectory and that of the resultant momentum $(\vec{p}_+ + \vec{p}_-)$ of the two charged fragments. In practice, the hypothetical recoil momentum to be detected has been resolved into components perpendicular to and parallel to the plane of the charged fragments, and the two components have been treated

separately. The perpendicular component produces a deviation from coplanarity; the parallel component a discrepancy in transverse momentum balance. It turns out that the two tests are closely related. Of the two, the coplanarity test has been more widely used, since it does not require knowledge of the charged fragment momenta and therefore can be applied in multiplate chamber work or in magnetic chamber work in which momentum measurements are not reliable.

BRUECKNER & THOMPSON [1952] have given an approximate

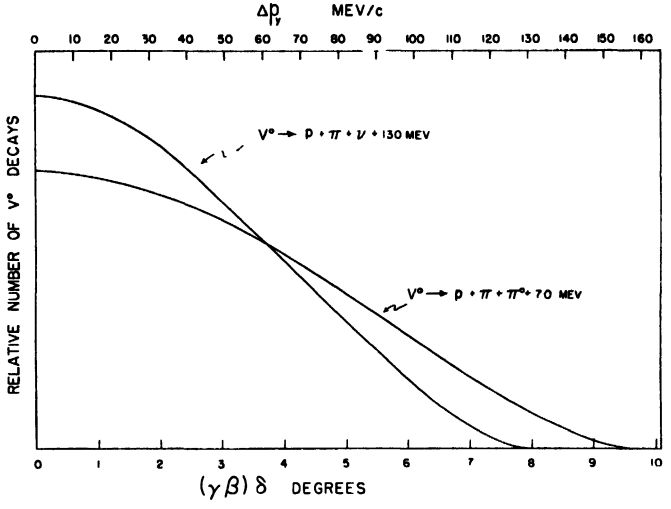

Fig. 10 – Theoretical distributions in deviation from coplanarity δ and residual transverse momentum Δp_y.

calculation of the expected distributions in deviation from coplanarity and transverse momentum balance for the hypothetical decay schemes:

$$\left.\begin{aligned} \Lambda^\circ &\to \mathrm{p} + \pi^- + \pi^\circ + 70\ \mathrm{MeV}\,. \\ \Lambda^\circ &\to \mathrm{p} + \pi^- + \nu + 130\ \mathrm{MeV}\,. \end{aligned}\right\} \qquad (18)$$

The true Q-values in Eq. (18) were determined from the condition that the most probable apparent Q-value coincide with experiment. The results are shown in Fig. 10, where, on the lower abscissa, δ is the angle between the Λ° trajectory and the plane of the charged fragments, and $\gamma\beta$ is the reduced Λ° momentum. Unfortunately, from the point of view of comparison with experiment, the curves have the same general form as the error function, with

maximum at zero. In other words, even if a light neutral fragment is produced in the decay, the most probable situation is that the event is "coplanar". Clearly, for both tests, the most definitive results will be obtained for slow Λ°-particles. For the coplanarity test, the width of the theoretical δ-distribution varies inversely as the Λ° momentum. For the transverse momentum balance, the distribution of residual transverse momentum is independent of the Λ° momentum; however, the error in the determination of residual transverse momentum will be less for slow Λ°-particles.

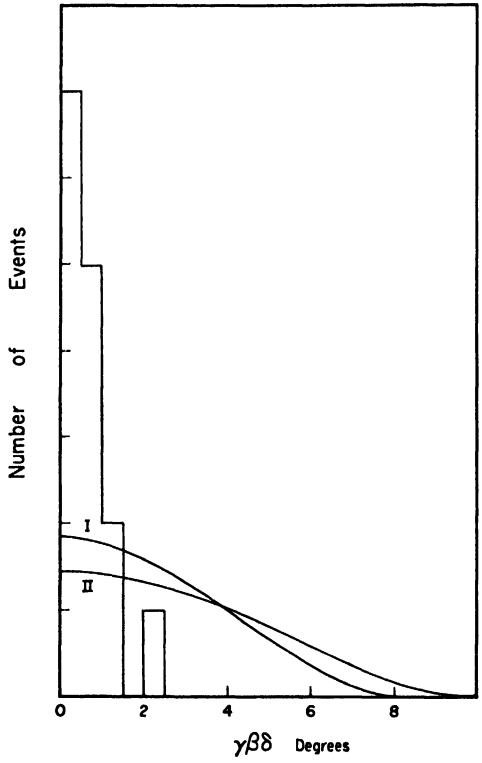

Fig. 11 – Comparison between the distribution of observed uncoplanarity angles of BRIDGE *et al.* [1953a] and the Brueckner-Thompson distributions for 3-body decay. Curve I refers to $V^\circ \rightarrow p + \pi + \nu$ + 130 MeV; curve II to $V^\circ \rightarrow p + \pi +$ π° + 70 MeV.

Experimental coplanarity distributions have been reported by LEIGHTON *et al.* [1953a], FRETTER *et al.* [1953a], and BRIDGE *et al.* [1953a]. The results of BRIDGE *et al.* [1953a] are the most significant, since they are based on a set of very low momentum Λ°-decays. The experimental histogram, based on 16 Λ°-decays with average $\gamma\beta$ of about 0.4, is compared with the theoretical curves in Fig. 11. It is apparent that the observed distribution of $\gamma\beta\delta$ is much narrower than that expected if a light neutral fragment is produced in Λ°-decay.

LEIGHTON *et al.* [1953a] report measurements of residual transverse momentum for 28 cases of Λ°-decay. The experimental histogram is compared with the theoretical curves in Fig. 12. The distributions are seen to be of comparable width; however, the entire width of the experimental histogram can be accounted for

by the experimental errors, and the results are therefore considered to be compatible with 2-body decay.

3. 2b *Uniqueness of the Q-Value*

BRUECKNER & THOMPSON [1952] have given an approximate calculation of the distribution in apparent Q-value for the hypothetical 3-body decay schemes of Eq. (18). The energy spectrum

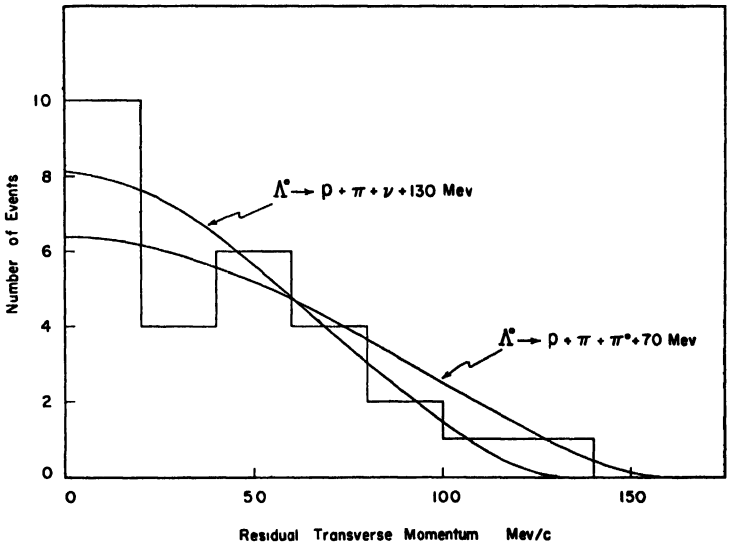

Fig. 12 – Comparison of the observed distribution of residual transverse momentum of LEIGHTON *et al.* [1953a] with the calculated distributions of of Brueckner and Thompson. The width of the experimental distribution could be due entirely to errors of measurement; thus the results are entirely compatible with 2-body decay.

of the neutral fragment used in Eq. (5) was that given by the statistical factor, with the approximation that the proton is heavy. It should be pointed out that the shape of the Q^* distribution so obtained is sensitive to the assumed distribution of T_0' [1]. The results are shown in Fig. 13 where the end points are adjusted so that the maxima coincide with the majority of experimental values.

Cloud chamber determinations of the Q(p, π)-value for Λ^0-decay have been reported by THOMPSON *et al.* [1951], LEIGHTON *et al.*

[1] The theoretical δ-distributions given in Fig. 10 are relatively insensitive since they depend on an integral of the p'_0 spectrum.

[1951], ARMENTEROS *et al.* [1951b], THOMPSON *et al.* [1952a], LEIGHTON *et al.* [1953a], THOMPSON *et al.* [1953a], BRIDGE *et al.* [1953a], ARMENTEROS *et al.* [1953], VAN LINT *et al.* [1954a], and COWAN and GUESS [1954]. The emulsion work will be discussed in § 3.5.

The status of cloud chamber work in various laboratories is shown in the histograms of Fig. 14. The data represented are those of:

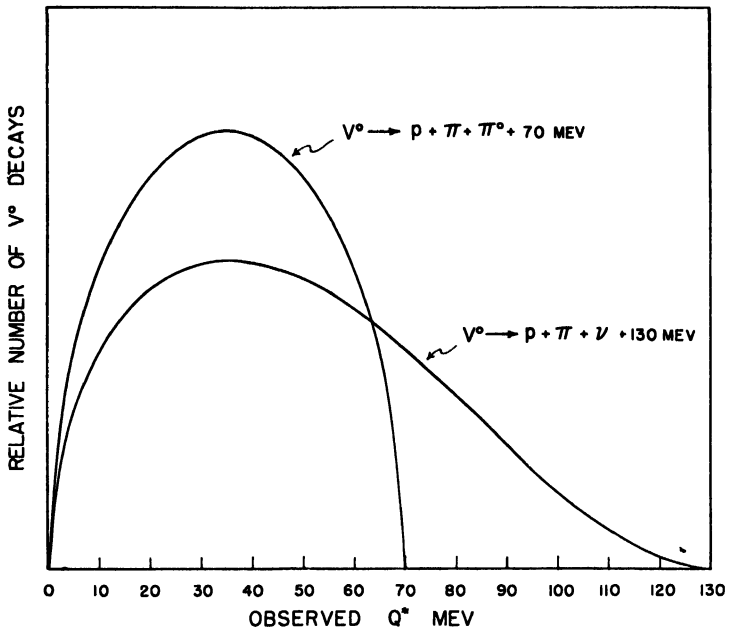

Fig. 13 – Theoretical distributions of apparent Q(p, π)-values calculated by BRUECKNER and THOMPSON (1952].

i. Manchester. The data shown are the 22 events reported by ARMENTEROS *et al.* [1953] and obtained with the Blackett electromagnet operated on the Pic-du-Midi. The events were selected because they have heavily ionizing proton-like fragments, and have tracks long enough for accurate measurements to be made. The spread is considered to be compatible with the estimated errors. The most probable Q(p, π) is (42^{+3}_{-2}) MeV.

ii. Indiana. The data shown comprise 15 events obtained with the 22 in. magnet at sea level. Half of these data were reported at the Bagnères Congress; the remainder have

been obtained more recently. The events were selected on the basis of measurability and of the criterion $\delta Q \leqq 7$ MeV. Only 3 of the events have heavily ionizing positive fragments. The events designated by triangles have $p_\nu > 90$ MeV/c and, following the discussion in § 2.2*b*, are probably the most accurate. The weighted mean is (37 ± 1) MeV, the same as published earlier by THOMPSON *et al.* [1953a]. The event with $Q(\mathrm{p}, \pi) = 50.6$ MeV is R-65B.

iii. C. I. T. 48 in. The data shown are the 19 selected events of VAN LINT *et al.* [1954a] plus two $Q(\mathrm{p}, \pi)$-values, (50 ± 8) and (85 ± 15) MeV, privately communicated by R. B. Leighton. The data were obtained with the new 48 in. magnet operated at Pasadena. The events all have a heavily ionizing proton-like fragment and were selected by the criterion $\delta Q \leqq 5$ MeV. A few anomalously low $Q(\mathrm{p}, \pi)$-values have also been observed with this magnet. The best $Q(\mathrm{p}, \pi)$-value for the main group is (34.7 ± 1) MeV.

iv. C. I. T. 22 in. The data shown are 16 events obtained by COWAN & GUESS [1954] with the 22 in. magnet at sea level. The events are low momentum cases in which the proton fragment is identified by droplet count. The data include two or three deviant cases with $Q(\mathrm{p}, \pi) = (20 \pm 5), (25 \pm 5)$, and (80 ± 30) MeV. The mean $Q(\mathrm{p}, \pi)$-value for the main group is (35.9 ± 1) MeV.

v. M. I. T The data shown are the 22 events reported by BRIDGE *et al.* [1953a] and obtained with a multiplate chamber at Echo Lake. The selection criteria were: (*a*) an event must have an identifiable origin in the chamber, (*b*) one (or both) decay fragment must stop in the plates, and (*c*) the observed ionizations must be compatible with the proton and pion masses. The uncertainty in the Q-values given in the diagram is that corresponding to the finite thickness of the plates. The errors in the limits due to range straggling, uncertainty in the range-energy relation, and other factors, are not included. The asterisk refers to Frame No. 43065, which is analyzed by two different methods. The results are consistent with a unique $Q(\mathrm{p}, \pi)$-value of 37 MeV.

It is apparent from comparison of Fig. 14 with Fig. 13 that the observed distributions of $Q(\mathrm{p}, \pi)$-values for Λ^0-decay are very

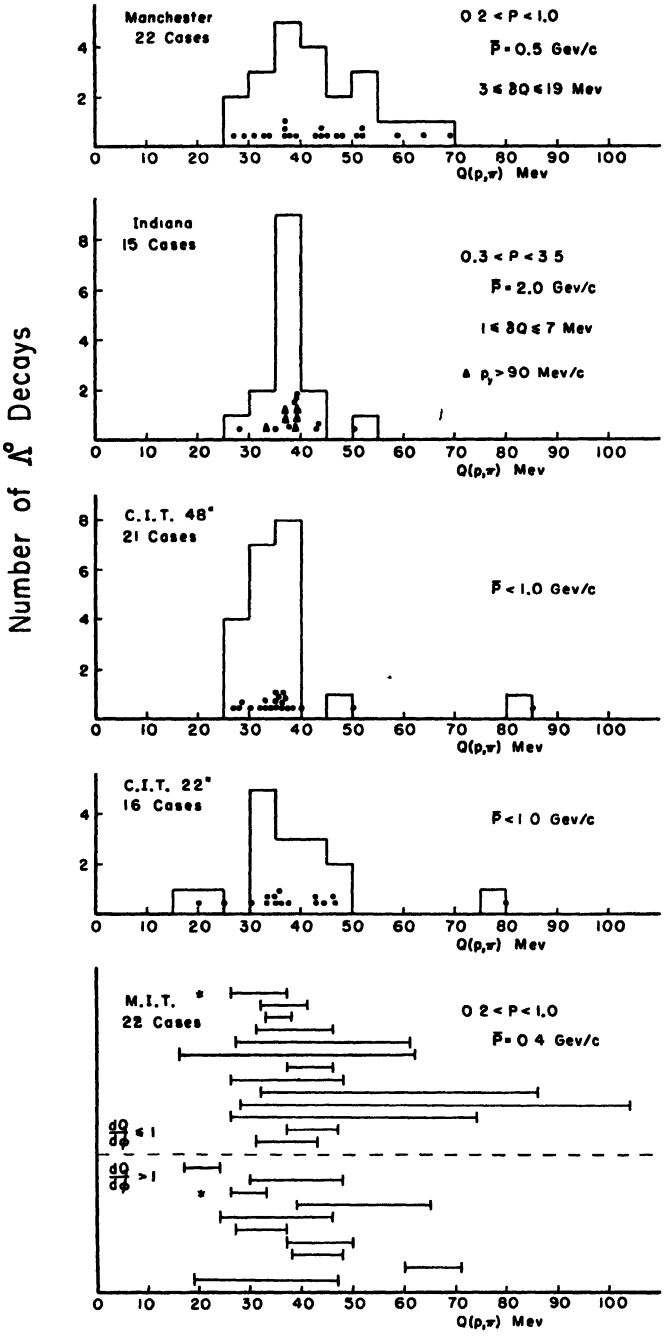

Fig. 14 – Cloud chamber determinations of $Q(p, \pi)$-values from various laboratories. The histograms give the number of events per 5 MeV interval. The diagram of the M.I.T. results is that used by BRIDGE *et al.* [1953a].

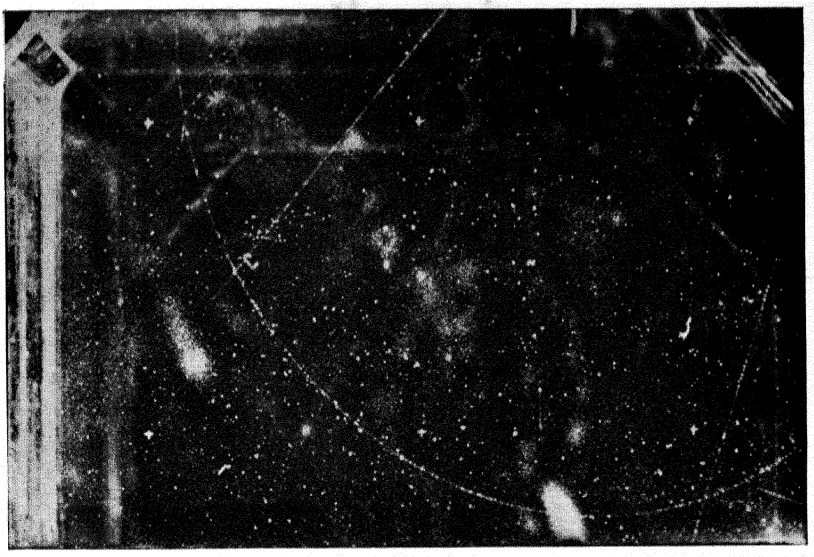

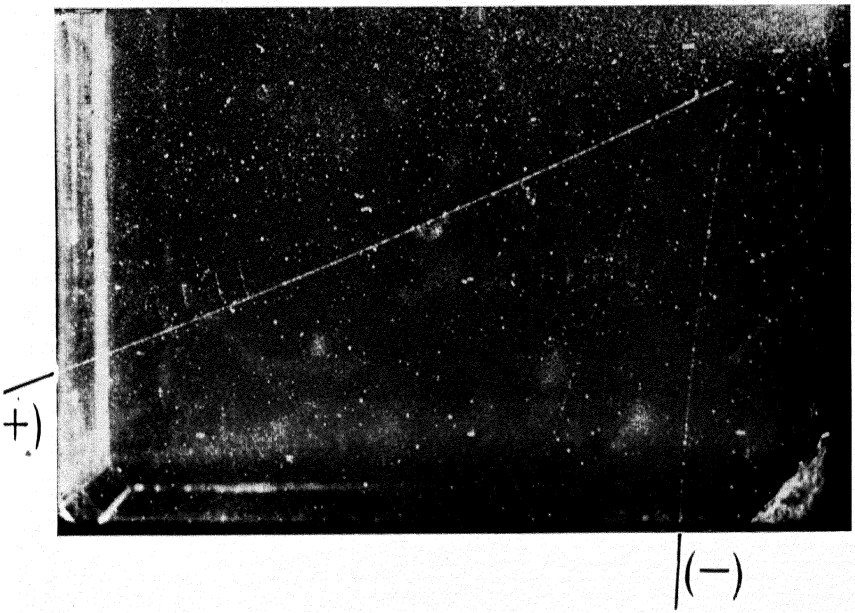

Plate III Example of a V°-event with abnormally high $Q(p, \pi)$-value by LEIGHTON [1954]. The positive track has a momentum of (320 ± 15)MeV/c and an estimated ionization of 3.5 − 7 I_0, which corresponds to a mass range of 1100—1950 m_e. The negative track has a momentum of (225 ± 15)MeV/c and the estimated ionization is stated to be less than 1.5 I_0 which corresponds to an upper mass limit of 800 m_e. The angle between the tracks is 61° and the $Q(p, \pi)$-value is (85 ± 15)MeV.

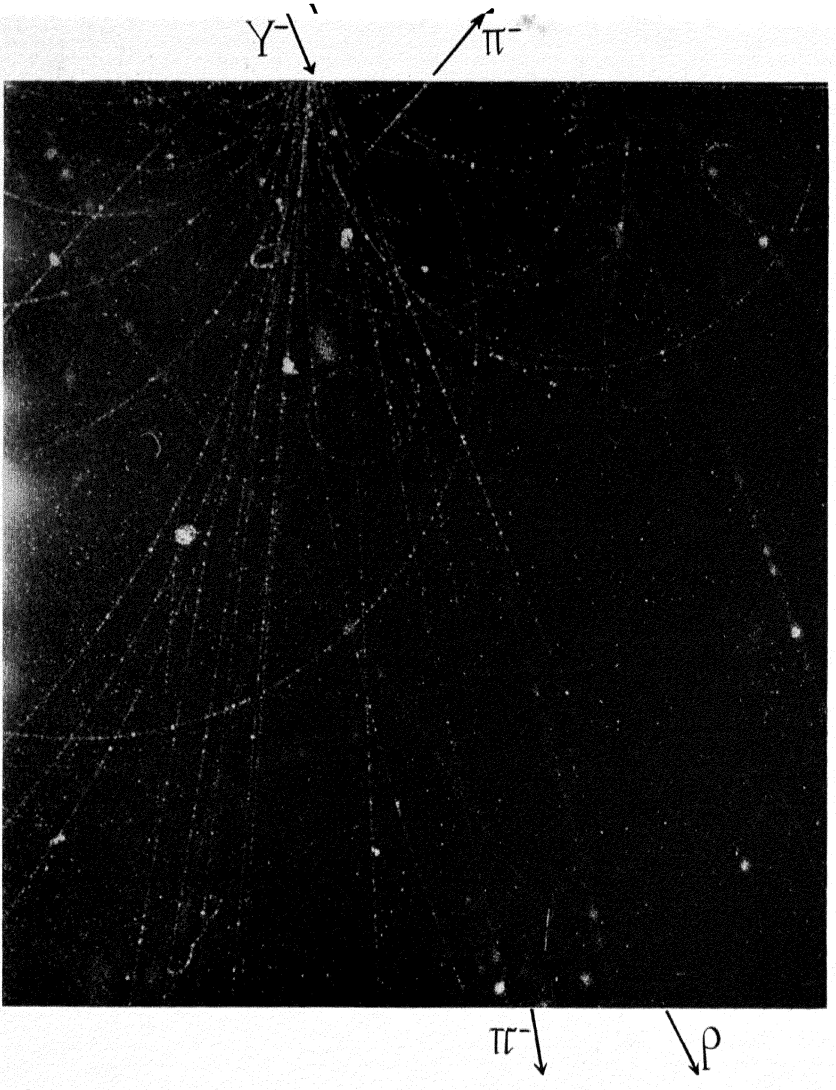

Plate IV – Cascade decay photograph of Cowan [1954] in which the V°-decay is identified to be a Λ^0.

much narrower than that expected if a light neutral fragment were produced in the decay. However, none of the observations excludes the possibility of other types of V°-events in a few percent of cases. The C. I. T. data, in fact, provide evidence for such, to be discussed in § 3.3.

3. 3 The abnormal Q(p, π)-values

The Pasadena group has consistently reported Q(p, π)-values which are both lower and higher than 37 MeV [1].

The recent, more accurate work of Van Lint *et al.* [1954a] with the new 48 in. magnet indicates that the number of abnormal cases is certainly much smaller than was previously reported; thus the discrepancy with work of other groups is removed. However, a few of the original examples and a few new examples, both with the 48 in. and 22 in. magnets at Pasadena, are not easily explained in terms of errors of measurement or interpretation. Some of these abnormal cases are represented in the histograms of Fig. 14. The example from the 48 in. magnet with $Q(\mathrm{p}, \pi) = -(85 \pm 15)$ MeV is reproduced in Plate III.

Leighton [1954] suggests that these abnormal cases can all be interpreted in terms of an alternate mode of decay, in which a muon and a neutrino appear in place of the pion fragment:

$$\Lambda^0 \rightarrow \mathrm{p} + \mu^- + \nu\,. \tag{19}$$

The true Q for Eq. (19) would than be $37 + (m_\pi - m_\mu) = 71$ MeV, and the apparent Q-values should range from 71 MeV down to zero.

Primakoff & Cheston [1954] suggest that some of the abnormal $Q(p, \pi)$-values may be due to the decay of "V-dineutrons" according to the scheme

$$[\Lambda^0 + \mathrm{n}] \rightarrow \mathrm{p} + \pi^- + \mathrm{n}$$

In this case, the apparent Q(p, π^-)-values would be distributed over a spectrum with an upper limit in the neigborhood of 125 MeV.

3. 4 Lifetime of the Λ^0-particle

A considerable number of determinations of the mean lifetime τ of the Λ^0-particle have been made, as a result of which that

[1] Leighton *et al.* [1951], Leighton *et al.* [1953a], Leighton [1954], Cowan & Guess [1954].

parameter appears to be relatively well-determined. The general character of the problem has been discussed by WILSON & BUTLER [1952]. The most complete discussions of the statistical problem of estimation are those of BARTLETT [1953a, b]. The subject has been recently reviewed by PAGE & NEWTH [1954].

The various determinations are listed in Table V. The weighted mean of all the published results is given by PAGE [1954] to be

$$\tau = \left(3.7^{+\ 0.6}_{-\ 0.5}\right) \times 10^{-10} \text{ sec.}$$

TABLE V

Determination of the Λ° Mean Lifetime

Authors		Type of Chamber	Number of Events	$\tau \times 10^{10}$ sec
ALFORD & LEIGHTON 1953	"High Q(p, π)" $50 \leqq Q \leqq 150$	Magnetic, with Central Plate	20	1.3 ± 0.5
	"Low Q(p, π)" $Q \leqq 50$	,,	37	2.9 ± 0.8
BRIDGE *et al.* 1953		Multiplate	22	3.5 ± 1.2
DEUTSCHMANN 1953b		Multiplate	22	$4.8^{+\ 2.6}_{-\ 1.3}$
PAGE & NEWTH 1954		Magnetic	26	$3.7^{+\ 3.9}_{-\ 1.3}$
GAYTHER 1954		Multiplate	21	$4.0^{+\ 3.7}_{-\ 1.2}$
PAGE 1954		Magnetic	23	$3.6^{+\ 1.1}_{-\ 0.7}$

3. 5 THE EMULSION WORK

Observation of Λ°-decays in the nuclear emulsion is greatly complicated by the presence of a large background of 2-pronged stars which simulate V°-events. In addition, the origin of a decay cannot be (or at least has not so far been) located. Nevertheless, a considerable amount of work on this problem has been done by the emulsion groups in the last year with substantial success. It has been possible to resolve the Λ°-decay from the background of 2 + On events yielding a proton and a negative pion on the basis of an observed sharp concentration of Q(p, π)-values in the

neighbourhood of 37 MeV. The possibility that a nuclear interaction would simulate such a "line" is very remote. It therefore seems certain that a large number of Λ^0-decays have been observed in the emulsions, although positive identification cannot be made in an isolated case.

The available data were tabulated at the Padua Conference and include contributions of HOPPER & BISWAS [1950], DANYSZ [1953], YASIN [1954], BONETTI *et al.* [1953], TEUCHER [1953], PETERS [1953], AMALDI *et al.* [1953], FRIEDLANDER *et al.* [1954], CECCARELLI *et al.* [1954], and KAPLON *et al.* [1954]. Altogether, there are 50 (p, π^-) events reported, of which 34 have been observed in stripped emulsions. The Q(p, π)-values, calculated under the assumption that the event represents a 2-body decay, are shown in the histogram of Fig. 15. There is a sharp line at 35–40 MeV superimposed on a diffuse background; the latter, as yet, does not give any indication of subsidiary lines at 10 MeV or 75 MeV.

The most extensive individual work is that of the Bristol group (FRIEDLANDER *et al.* [1954]). In an emulsion stack exposed at 85,000 ft., these authors find 20 events of type 2 + On in each of which the outgoing particles are identified to be a negative pion and a proton. In all cases, the negative pion stopped in the emulsion and was identified to be a σ-meson. (19 of the 20 events were found by tracing back σ-mesons.) The pion energy was therefore determined from range. In 11 cases, the proton stopped in the stack and its energy was deduced from the range. In the remaining 9 cases, the proton went out of the stack and the energy was deduced from grain density or scattering.

The calculated Q(p, π)-values range from 0.5 to 85.0 MeV. However, ten of the values are concentrated in the narrow interval 35.5–38.5 MeV, and are distributed as shown in the histogram of Fig. 16. Of these, nine are of high quality, in which both particles come to rest, and give a weighted mean $Q(\mathrm{p}, \pi) = = (36.92 \pm 0.22)$ MeV. The error given is the standard deviation of the mean, and thus does not include estimates of systematic error. The principal source of systematic error, as these authors point out, derives from uncertainty in the range-energy relationship, and probably does not exceed 1%.

The work of Friedlander *et al.* provides excellent confirmation of the mean value Q(p, π) = 37 MeV given by the Indiana group

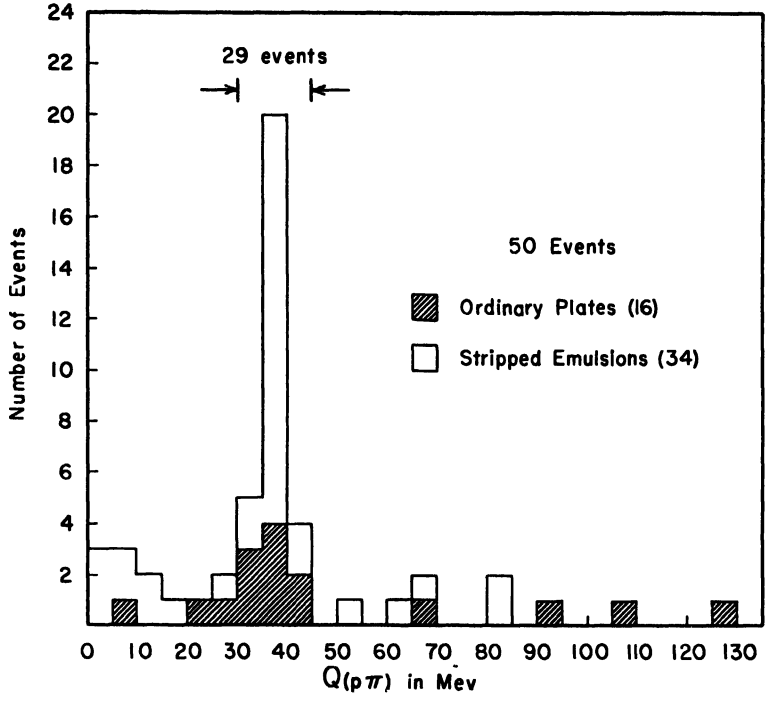

Fig. 15 – Histogram of Q(p, π)-values for 2 + 0n events observed by various groups in nuclear emulsions. The histogram gives the number of events per 5 MeV interval. The peak at 35—40 MeV is identified as Λ^0-decay and the diffuse background is attributed to 2-prong stars.

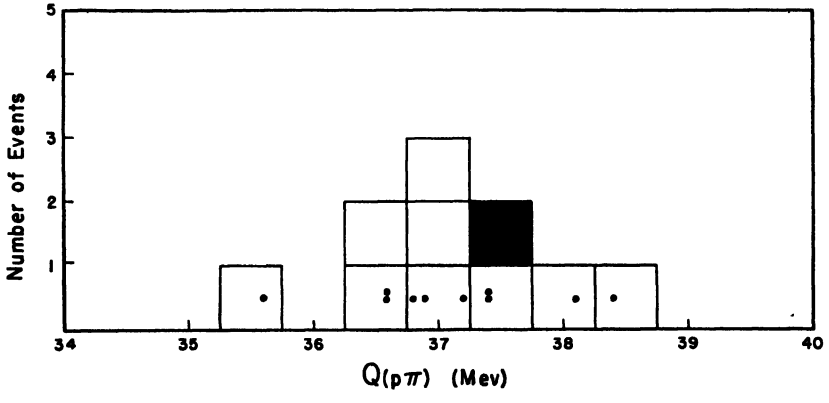

Fig. 16. – Histogram of the Q(p, π)-values of FRIEDLANDER *et al.* [1954] for the interval 34—40 MeV. The histogram gives the number of events per 0.5 MeV interval. The solid square represents event No. 10, in which the proton prong did not stop in the stack.

(THOMPSON *et al.* (1953a]) and the estimate of 37 MeV by the M. I. T. group (BRIDGE *et al.* [1953a]).

Fig. 17 shows the Q-curve plot of the data of Friedlander *et al.* It is apparent that in the majority of cases found, the proton was emitted strongly in the forward direction. On comparison with the cloud chamber data which indicate isotropy, within the available statistics (see the corresponding plot of THOMPSON *et al.* [1953a]), it seems likely that this apparent strong anisotropy is a

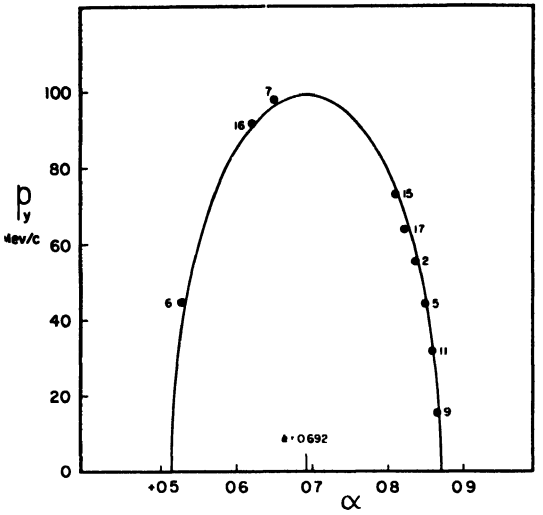

Fig. 17 – Q-curve plot of the data of FRIEDLANDER *et al.* [1954] from Fig. 16. Event No. 10 is omitted. The use of the Q-curve plot in this instance requires assumption as to the nature of the V°-particle since $\beta \ll 1$ for these events. The values of a plotted are therefore calculated by means of eq. (21).

result of scanning for σ-stars. Since the forward directions observed correspond to a small fraction of the total solid angle, it is likely that the actual number of Λ^0-decays which took place within the emulsion stack is greater than indicated by this sample.

3. 6 THE CASCADE DECAY

The first evidence for the cascade decay process was obtained by the Manchester group on the Pic-du-Midi (ARMENTEROS *et al.* [1952]). Front and side view orthogonal projections of the event are shown in Fig. 18. An energetic V^--particle AB, produced above the chamber, penetrates the 2 cm. lead plate and decays at D, giving rise to the negative decay fragment DE. The apex

F of a V°-decay occurs 1.25 cm. below D and the orientation of the decay tracks FG and FH is such that it strongly suggests that the V°-particle was produced in the V⁻-decay at D, according to the scheme:

$$V^- \rightarrow V^\circ + L^-$$

A second incident particle JK interacts at 0, resulting in two charged particles below the plate. The authors are careful to point out that the photograph admits an alternate interpretation, *viz.* that the V°-particle was produced in the interaction 0 rather than in the V⁻-decay D.

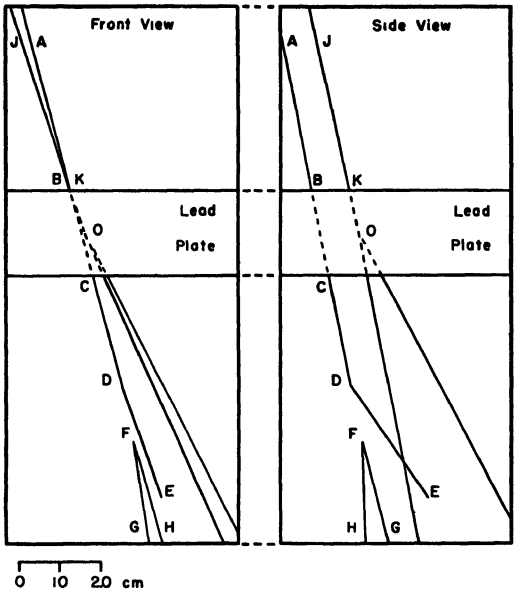

Fig. 18 – Front and side view orthogonal projections of the original Manchester cascade decay photograph.

Striking confirmation of the Manchester observation has been given by LEIGHTON *et al.* [1953b], ANDERSON *et al.* [1953], COWAN [1954], and FRETTER and FRIESEN [1954b]. The examples reported by Cowan and more recently by Fretter and Friesen provide the most detailed evidence since these were obtained under conditions which permit a droplet count. Cowan's example is shown in Plate IV. Schematic drawings of Cowan's example and that of Fretter and Friesen are shown in Fig. 19 and Fig. 20, respectively. These two events, and those referred to above, provide strong evidence that the phenomenon is correctly interpreted as decay in cascade. In addition, the V°-particle and the V⁻-decay fragment DE are identified to be a Λ° and π^-, respectively.

In Cowan's example, Fig. 19, the momentum and drop count can be determined for both V°-decay fragments, FL and FR. The resulting mass of the positive fragment FR is $(2050 \pm 350)m_e$, which is easily compatible with the protonic mass. The momentum

and ionization of the negative fragment FL establish a low upper limit for the mass. The $Q(p, \pi)$-value is (40 ± 13) MeV, in good agreement with the accepted value of 37 MeV for the normal Λ^0.

Since the Λ^0 is known to undergo 2-body decay, its direction of flight is given by the vector sum of $\overrightarrow{FL}$ and $\overrightarrow{FR}$. The direction of this resultant, $\overrightarrow{FG}$, is found to pass through the apex D of the V^--decay within the experimental errors [1].

The most troublesome alternative interpretation of this and similar photographs is that the V^- and Λ^0 are produced in the same origin above the chamber, with strong angular correlation. If the lifetime of the V^- were then shorter than that of the Λ^0, the observations would tend to simulate a cascade decay [2]. Cowan's example is apparently unique in that the extended resultant FG is at a distinct distance from possible origins of the V^--particle. The double production interpretation can thus be ruled out.

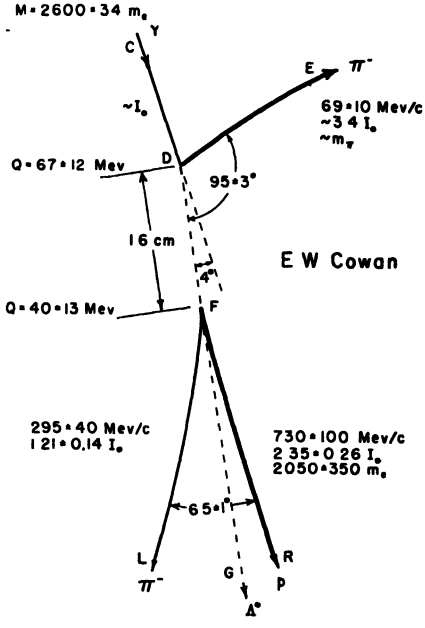

Fig. 19 – Schematic drawing of Cowan's cascade decay photograph. The angles and curvatures are not drawn to scale.

In the event observed by Fretter and Friesen, the fragments FL and FR unfortunately pass out of the illuminated region and are too short for curvature measurement. The identification of the Λ^0 is therefore indirect but nonetheless convincing. Since the apex D is coplanar with plane LFR and the direction DFH lies between FL and FR, it is probable that DF represents the direction of motion of the V^0. The measured angles LFH and HFR and the ionization of FL and FR are then used to identify the V^0. For Λ^0-decay, the observed angles require that track

[1] In Cowan's paper, this fact is expressed in terms of *a*) the coplanarity of apex D with LFR, and *b*) transverse momentum balance of FL and FR with respect to the direction DF.

[2] R. B. Leighton has, in fact, found photographs containing a V^- and a V^0 which are approximately collimated but in which the V^0-decay takes place above the V^--decay. [Private communication].

FR be that of a proton of 590 MeV/c momentum and 2.65 I_0 ionization. The latter is in excellent agreement with the observed drop count of 2.5 I_0. For $\theta°$-decay, track FR would have to be that of a pion of 1.6 GeV/c momentum and only 1.1 0_0 ionization.

In both examples cited, momentum and ionization measurements favor the pion rather than the muon mass for the charged fragment DE of the V⁻-decay. In Cowan's example, the calculated ionizations based on the measured momentum of (69 ± 10) MeV/c are 3.7 and 2.6 I_0 for pion and muon respectively, to be compared with the observed ionization of ≧ 3.4 I_0. In that of Fretter and Friesen, the mass of DE is determined to be (254 + 18)m_e. The pion mass is just within the stated (probable) error; the muon mass is 2.6 errors below.

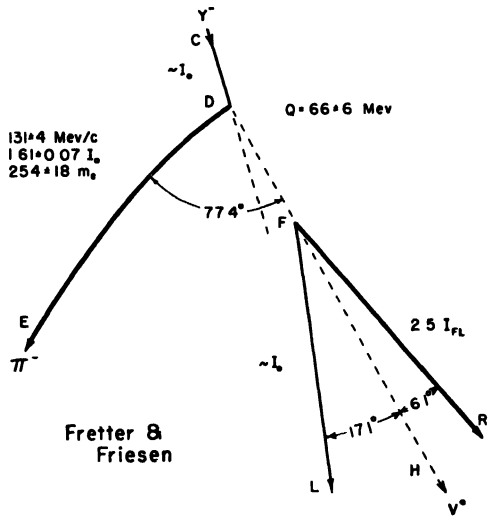

Fig. 20 – Schematic drawing of the cascade decay photograph obtained by Fretter and Friesen. The angles and curvatures are not drawn to scale.

In both events, the $\Lambda°$-decay apex F is coplanar with CDE, a necessary condition that the Y⁻-decay be a 2-body process. In Cowan's example, there is also approximate transverse momentum balance of the $\Lambda°$ and the negative pion DE with respect to the Y⁻-line of flight CD. However, as Cowan points out, neither coplanarity nor transverse momentum is measurable with sufficient accuracy to definitely establish that the Y⁻-decay is a 2-body process [1].

The $Q(\Lambda°, \pi^-)$-values for the two events, (67 ± 12) and (66 ± 6) MeV, are in excellent agreement, a fact which is consistent with 2-body decay. Under the assumption of 2-body decay, we thus have

[1] The difficulty is due to the short distance between the decay points D and F and to the small angle (4°) between the Y⁻ and $\Lambda°$ lines of flight. The same difficulties are undoubtedly present in the example of Fretter and Friesen.

$$Y^- \rightarrow \Lambda^0 + \pi^- + (66 \pm 6)\,\text{MeV}.$$

The corresponding mass of the negative hyperon is $(2583 \pm 12)m_e$, based on $m_{\Lambda^0} = 2181\, m_e$ (FRIEDLANDER *et al.* [1954]) and $m_\pi = 273\, m_e$ (SMITH *et al.* [1953]).

In conclusion, the reality of the cascade decay phenomenon appears to be well established. The V°-decay fragment is very probably a normal Λ^0, which in itself implies the parent particle is a hyperon. The charged decay fragment is probably a pion. There is no indication so far for the presence of a third neutral decay fragment, although further work will be necessary to establish definitely the 2-body character of the decay.

4. The θ^0-Particle

Although the magnetic chamber work in early 1951 clearly demonstrated that in some instances of V°-decay the positive fragment was appreciably less massive than a proton, the corresponding negative fragment was not identified. From the standpoint of simplicity, the hypothesis that the negative fragment was a well-known particle, namely π or μ, was very attractive. ARMENTEROS *et al.* [1951b] discussed the implications of this possibility with respect to the α-distribution and presented data which were consistent with this hypothesis, although not specifically supporting it in preference to others. Also, the measurements on which this work was based were later withdrawn and revised. On the other hand, LEIGHTON *et al.* [1953a] reported an α-distribution, and in addition some direct mass estimates, which indicated the presence of positive and negative fragments of intermediate mass. Both papers, and the work of FRETTER *et al.* [1953a] have been reviewed by WILSON [1954].

As the result of work done during the last year, all laboratories are now in substantial agreement to the effect that the non-protonic or "V^0_2" group is itself complex. It appears to be reasonably well-established that the main constituent is the θ^0-meson; but in addition there is convincing evidence for the so-called anomalous V°-events, and preliminary indications for at least one or two other types. In this section, the present status of work on the θ^0-meson is reviewed; in the following section (§ 5), the evidence for the various other types will be examined.

4. 1 The Q-surface representation of the data

The first firm evidence for the existence of the θ°-meson in the V_2° group came from the work of the Indiana group (Thompson *et al.* [1952b], [1953a, b]; see Plate V), based primarily on dynamic arguments. The present status of that work may be quickly grasped in terms of the Q-surface representation which is illustrated by stereoscopic photographs of a 3-dimensional model in Fig. 21. The 28 points shown are selected from approximately 250 V°-events on the basis of measurability [1]. An approximately equal number of measurable events which determine the Λ°-surface for $Q = 37$ MeV have also been observed among the 250 events, but are omitted in the interest of clarity in stereoscopic viewing of the photographs. It is seen that, with the exception of four clearly deviant cases, the main group delineates a Q-surface. The vertical semi-axis indicates. a centre of mass momentum of the fragments near 200 MeV/c; $\bar{\alpha}$ is near zero, indicating equal, or nearly equal, masses for the fragments; and the eccentricity of the limiting ($1/P \to 0$) cross-section indicates a parent mass near 1000 m_e. The position of the theoretical Q-surface given by Eq. (11) for the decay

$$\theta^\circ \to \pi^+ + \pi^- + 214 \text{ MeV} \tag{20}$$

is indicated by smooth curves for $P = 1$, 2, 3 and ∞ GeV/c.

The increase in the α semi axis of the cross-section for increasing $1/P$ is seen to be inappreciable for all but the 2 or 3 slowest events. The individual θ° momenta range from 0.7 to 9.0 GeV/c, with a mean of 3.0 GeV/c. This mean momentum corresponds to a θ° velocity $\beta = 0.987$, hence it is clear that the majority of cases may be accurately represented on the 2-dimensional or Q-curve plot ($\beta = 1$). Fig. 22 shows the Q-curve plot of the data together with the theoretical Q-curve for Eq. (20). The several events for which β is appreciably less than unity are represented in this plot, after identification with the appropriate Q-surface in Fig. 21, by the coordinates (α', p_y), where α' is given by [2]:

$$\alpha' - \bar{\alpha} = \beta(\alpha - \bar{\alpha}) . \tag{21}$$

[1] The criterion of acceptance is that the space sagittae of both tracks be of the order of 0.6 mm or greater.

[2] The resulting position of the representative point in the Q-curve plot is precisely that arrived at after the representative point in the Q-surface plot of Fig. 21 is slid along the surface of appropriate $Q(\pi, \pi)$-value, at constant height p_y above the (α, $1/P$)-plane, until it reaches the limiting plane $1/P = 0$.

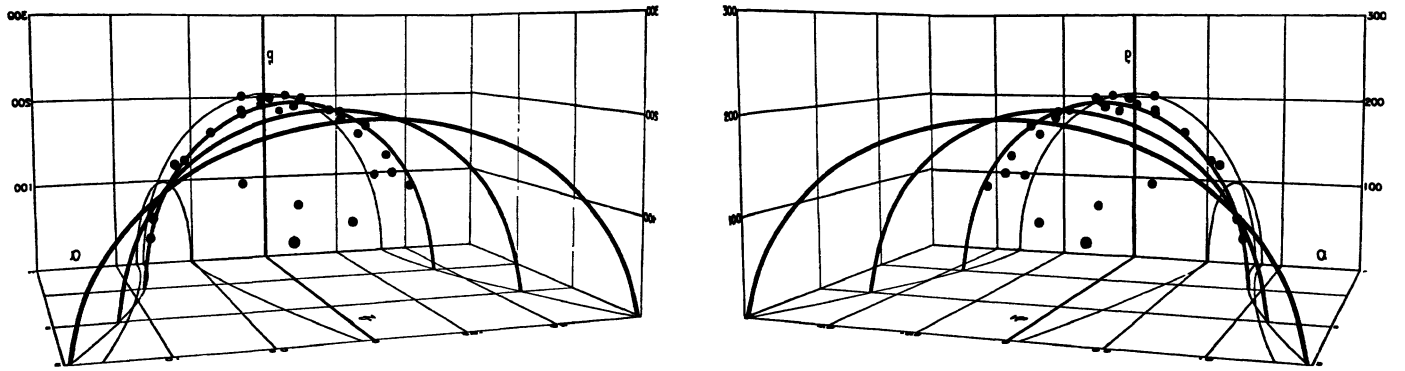

Fig. 21 – Stereoscopic drawing of the Q-surface representation of the Indiana data. The figure should be viewed stereoscopically, at the normal viewing distance of about 10 in., with the aid of a good plane mirror (preferably front surface quality) held normal to the page between the views. It is a pleasure to acknowledge the skilled work of Messrs. Kenneth Skirvin and Harvey Frye of the Indiana University Audio Visual Laboratory in the preparation of this figure.

The 4 anomalous cases are projected normally on to the plane $1/P = 0$.

The 4 anomalous cases are discussed in section 5. The interpretation of the main group is summarized in the following itemized remarks:

i. The scatter of the main group is quite compatible with

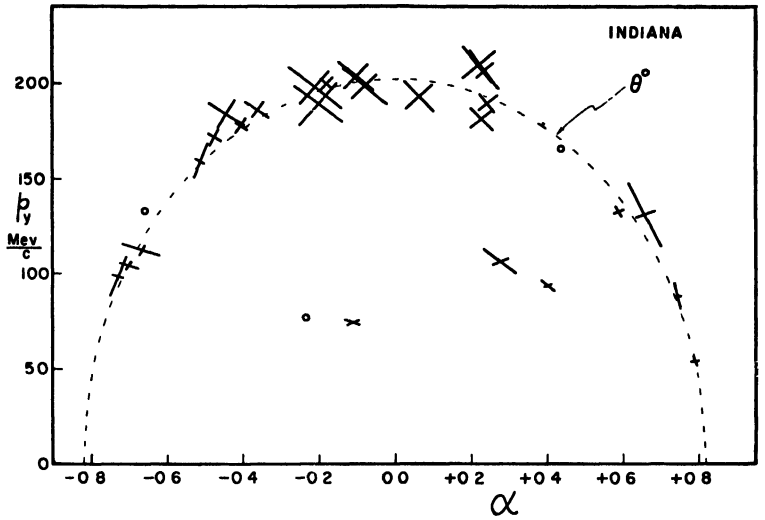

Fig. 22 – Q-curve plot of the Indiana data. The three points plotted as circles are events observed with the 12 in. chamber described by THOMPSON *et al.* [1951]. Of these, the point near the $0°$-curve with negative a is ∓ 50, discussed in § 1.2. The remaining 25 points were obtained with the 22 in. rectangular chamber described by THOMPSON *et al.* [1953a]. The errors shown are those corresponding to independent errors in p_+ and p_-. The principal source of error is usually distortion, hence in many cases the errors are dependent as described by eq. (14).

that to be expected from the internally estimated errors shown. Thus, the data indicate, in a natural way, the presence of a 2-body decay plus 4 anomalous points.

ii. The distribution of points along the curve indicates isotropic or nearly isotropic emission in the centre of mass system. For example, there are 10 points on the right branch [1] ($a > 0$) and 14 points on the left branch ($a < 0$), indicating, within the statistics, equal emission of the

[1] The presence of the $\Lambda°$ curve at $\bar{a} = 0.69$ results in discrimination against $\theta°$-decays with $a > 0$. It is quite possible that one or two of the events classified as $\Lambda°$ in Fig. 14 are actually $\theta°$.

positive fragment in the forward and backward directions, respectively.

iii. The dynamic method of analysis provides means for the absolute determination of parent and fragment masses. In the case of θ^0-decay, the dynamic distinction between pion and muon fragments is difficult since those fragments are quite relativistic in the centre of mass system [1]. However, a straightforward fitting procedure indicates that, to 99% confidence level, both fragments are pions. Conversely, under the assumption that both fragments are of equal mass, the most probable value of that mass is 285 m_0. The error in this result is difficult to evaluate; however, it is certainly small enough to exclude the possibility that both fragments are muons.

iv. It follows from *iii*, *a fortiori*, that the Indiana data do not lend any support to the scheme

$$V^0_3 \rightarrow K^{\pm} + \pi^{\mp}$$

reported by LEIGHTON *et al.* [1953a] and BARKER [1954], although one or two cases might be of this type [2].

The Manchester group, operating on the Pic-du-Midi, has obtained a total of 14 non-protonic V°-events. [3] The circular form of the Q-curve plot of the data is shown in Fig. 23, where the errors given are the uncertainties in p_ν only. It is suggested, in view of the approximate coplanarity of 7 cases, that the apparent scatter in Fig. 23 results from an admixture of different 2-body decay schemes. Comparison is made with the work of THOMPSON *et al.* [1952b] and LEIGHTON *et al.* [1953a], and these authors conclude the data are compatible with a mixture of θ^0- and V^0_3-particles in the approximate ratio 10 : 4.

4. 2 IDENTIFICATION OF THE FRAGMENTS

The dynamic evidence that the θ^0-decay fragments are both L-mesons is supported by individual mass-estimates from ion-

[1] Q-curves for the decay $\theta^0 \rightarrow \pi^{\pm} + \mu^{\mp}$ have been reproduced in the Proceedings of the Bagnères Congress, p. 34, and in the Proceedings of the Duke Conference, p. II–37.

[2] The Q-curve for $V^0_3 \rightarrow K^- + \pi^+$ is reproduced in the Proceedings of the Bagnères Congress, p. 34, and in the Proceedings of the Duke Conference, p. II–37.

[3] BARKER [1954].

ization and momentum in a few cases. As to the distinction between π and μ, there is good evidence, however again only in a few cases, that at least one of the fragments is a pion from observations of nuclear interactions and π-μ-decay.

Mass-Determination by Ionization and Momentum. Since the center of mass momentum, p'. of the $0°$-decay fragments is near

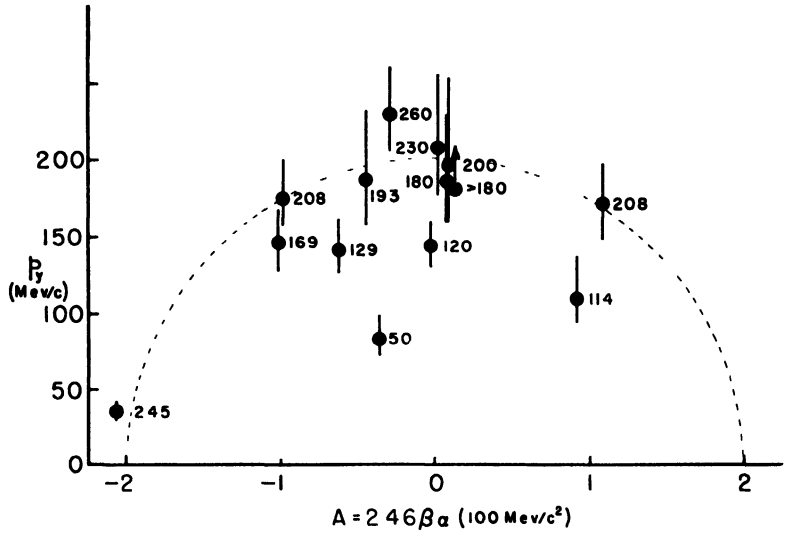

Fig. 23 – Circular form of the Q-curve plot of the Manchester V° data, exclusive of $\Lambda°$-decay. The numbers adjacent to the respective points are the $Q(\pi, \pi)$-values. The vertical segments are the errors in p_y only. The event at the extreme left of the diagram with $Q(\pi, \pi) = 245$ MeV might appear to be the most accurate single example, whereas, in fact, it is the least accurate, the error in Q being $^{+\,140}_{-\,\ \ 70}$ MeV.

200 MeV/c, it is apparent that both fragments are near minimum ionization in the centre of mass frame. It follows that at most one of the fragments can be heavily ionizing in the laboratory frame and that situation is relatively improbable since it is associated with ejection in a small cone in the backward direction in the centre of mass system. The earlier difficulties in identification of the negative fragment from non-protonic V°-decays are now readily understood since the majority of those decays were undoubtedly $\theta°$, unrecognized at the time. The criterion that the event be non-protonic, namely that the upper mass limit on the positive fragment be low, necessarily tended to restrict the obser-

vations to examples in which the upper mass limit on the negative fragment was high and therefore relatively uninformative. The two instances in which a direct mass identification is possible in the Indiana data are given in Table VI. The remarks above on the condition for observing a heavily ionizing θ^0-fragment are illustrated by the inverse correlation between the charge of the identified fragment and the sign of a.

TABLE VI

Identification of θ^0-secondaries by Ionization and Momentum

Film	a	P MeV/c	Sign of Fragment	p MeV/c	Estimated I/I_0	Calculated I/I_0 for π	Mass Range (m_e)
R—118	+0.914	690.	negative	94. ± 8.	2—3	2.5	220—310
R—267	+0.871	1100.	negative	89. ± 4.	2—4	2.7	210—360

Recently, several similar examples have been obtained by COWAN and KADYK [1954] and by FRETTER and FRIESEN [1954a] under conditions which permit a droplet count.

Nuclear Interactions of the Fragments. There are a number of examples of non-protonic decay in the literature in which one (or both) fragment undergoes a nuclear interaction. Unfortunately, there are only a few cases in which the data are sufficiently detailed or accurate that definite identification of the θ^0 can be made. The Paris group (GREGORY [1953]) reports two examples of θ^0-decay giving Q-values of 187 and 200 MeV and a third case with $p_T > 160$ MeV/c which is probably a θ^0. Four of the decay fragments traverse a multiplate chamber (GREGORY *et al.* [1954]) and 3 nuclear interactions are produced, an occurrence which is 4 times more probable if both fragments are pions than if one is a pion and the other a muon.

BARKER [1954] records an event (Plate XXXVIII, ARMENTEROS *et al.* [1951b]) in which the transverse momentum is greater than 160 MeV/c and which probably can be classified as a θ^0. The positive fragment was observed to undergo a scattering of 15° in a 2 cm. lead plate.

(π-μ)-decay. There is one example with negative a in the Indiana data in which the positive fragment undergoes (π-μ)-decay.

Production of θ^0-particles. In § 6, the evidence for the reaction

$$\pi^- + p \rightarrow \Lambda^0 + \theta^0$$

is discussed. THOMPSON *et al.* [1954b] point out that this reaction implies the θ^0-particle is a boson, in which case it cannot decay into a pion and muon.

4. 3 THE $Q(\pi, \pi)$-VALUES

Histograms of the $Q(\pi, \pi)$-values obtained by various groups are shown in Fig. 24. The data represented are those of:

i. Indiana. The data shown are 25 cases obtained with the 22 in. magnet plus the first anomalous example, #328 (THOMPSON *et al.* [1953a]), obtained with the 12 in. chamber. Two earlier θ^0-decays observed with the 12 in. magnet are omitted {#50, $Q(\pi, \pi) = (231 \pm 49)$; and #516, $Q(\pi, \pi) = (203 \pm 49)$.} The weighted mean of the main group is

$$Q(\pi, \pi) = (214 \pm 5)\ \text{MeV}\,,$$

which corresponds to a θ^0-mass

$$\mathrm{m}(\pi, \pi) = (966 \pm 10)\ \mathrm{m_e}\,.$$

The 4 anomalous cases will be discussed in § 5.

ii. MANCHESTER. The data shown are those reported by BARKER [1954] and obtained with the Blackett electromagnet operated on the Pic-du-Midi. An additional case with $Q(\pi, \pi) > 180$ MeV is not shown. The Manchester data also show a concentration of values in the neighborhood of 200 MeV, plus some other values.

iii. C. I. T. 48 in. The data shown are the 13 cases reported by VAN LINT [1953] and obtained with the new 48 in. magnet operated at Pasadena. Eleven of these give a distribution centered about 200 MeV, the with of the distribution again being consistent with the errors of measurement. However, 2 cases in this set of data are too low to be consistent with the group around 200 MeV.

In addition, $Q(\pi, \pi)$-values have been reported by a number of other groups:

COWAN & KADYK [1954], working with the 22 in. magnet [1], report 16 examples, of which 12 are compatible with $Q = 214$ MeV. The 3 best cases give $Q = (206 \pm 17)$, (200 ± 20) and (223 ± 16) MeV. However, there are 4 cases which are not compatible and give Q-values in the range from 79 to 125 MeV.

[1] COWAN [1954].

is discussed. THOMPSON *et al.* [1954b] point out that this reaction implies the θ^0-particle is a boson, in which case it cannot decay into a pion and muon.

4. 3 THE $Q(\pi, \pi)$-VALUES

Histograms of the $Q(\pi, \pi)$-values obtained by various groups are shown in Fig. 24. The data represented are those of:

i. Indiana. The data shown are 25 cases obtained with the 22 in. magnet plus the first anomalous example, #328 (THOMPSON *et al.* [1953a]), obtained with the 12 in. chamber. Two earlier θ^0-decays observed with the 12 in. magnet are omitted {#50, $Q(\pi, \pi) = (231 \pm 49)$; and #516, $Q(\pi, \pi) = -(203 \pm 49)$.} The weighted mean of the main group is

$$Q(\pi, \pi) = (214 \pm 5)\ \text{MeV},$$

which corresponds to a θ^0-mass

$$m(\pi, \pi) = (966 \pm 10)\ m_e .$$

The 4 anomalous cases will be discussed in § 5.

ii. MANCHESTER. The data shown are those reported by BARKER [1954] and obtained with the Blackett electromagnet operated on the Pic-du-Midi. An additional case with $Q(\pi, \pi) > 180$ MeV is not shown. The Manchester data also show a concentration of values in the neighborhood of 200 MeV, plus some other values.

iii. C. I. T. 48 in. The data shown are the 13 cases reported by VAN LINT [1953] and obtained with the new 48 in. magnet operated at Pasadena. Eleven of these give a distribution centered about 200 MeV, the with of the distribution again being consistent with the errors of measurement. However, 2 cases in this set of data are too low to be consistent with the group around 200 MeV.

In addition, $Q(\pi, \pi)$-values have been reported by a number of other groups:

COWAN & KADYK [1954], working with the 22 in. magnet [1], report 16 examples, of which 12 are compatible with $Q = 214$ MeV. The 3 best cases give $Q = (206 \pm 17)$, (200 ± 20) and (223 ± 16) MeV. However, there are 4 cases which are not compatible and give Q-values in the range from 79 to 125 MeV.

[1] COWAN [1954].

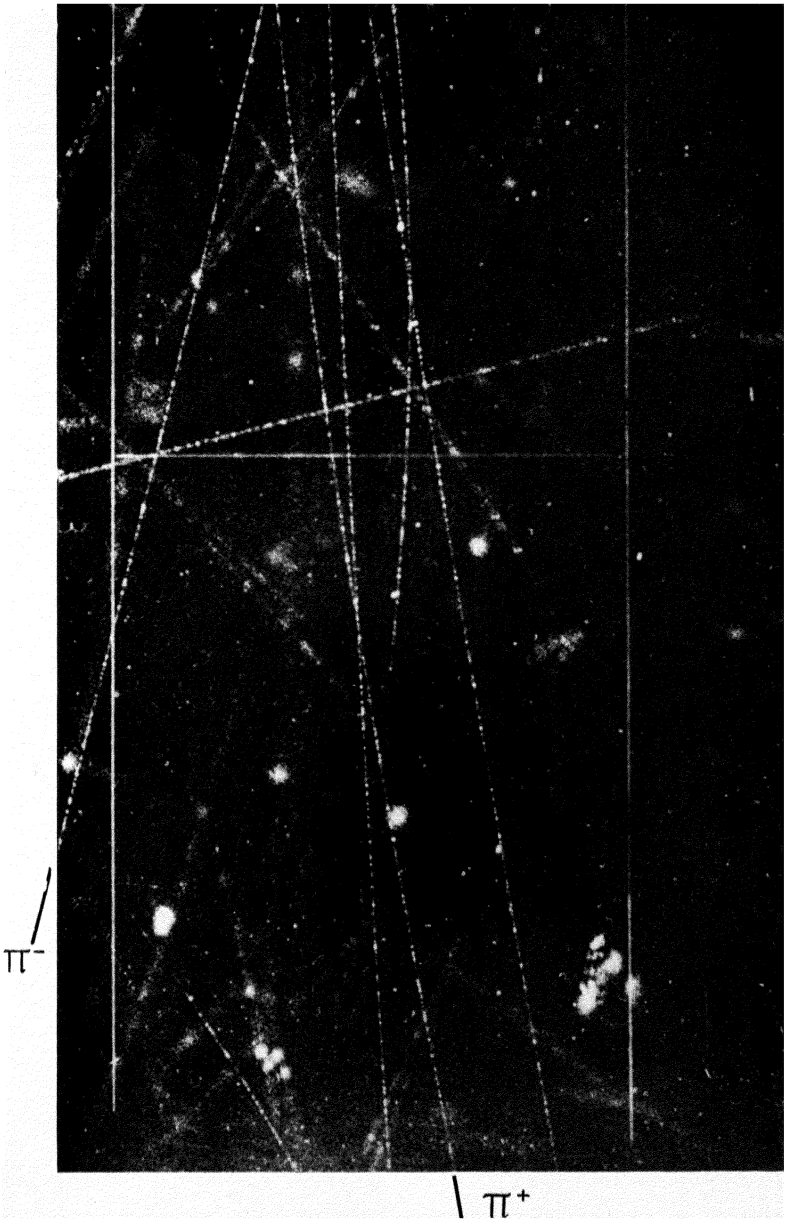

Plate V – Example of θ^0-decay (film #R-151) by THOMPSON *et al.* [1953b]. The momenta of the positive and negative fragments are (0.90 ± 0.02) and (1.9 ± 0.1)GeV/c, respectively. Both tracks are at minimum ionization. The angle between the tracks is (17.5 ± 0.1)° and the $Q(\pi, \pi)$-value is (219 ± 12) MeV.

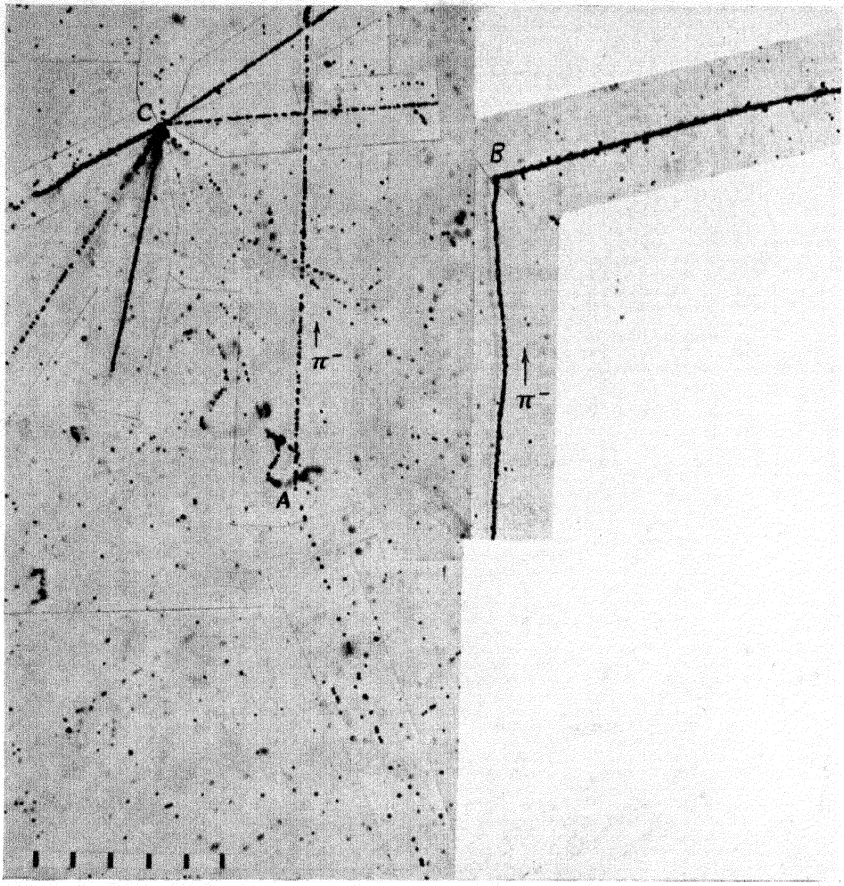

Plate VI – Probable θ°-decay (at A) observed by YASIN [1954] in nuclear emulsion. The π^- fragment stopped in the emulsion and produced a 1-prong σ-star at B. The calculated θ° line of flight passes through C (10 + 7p) within the errors of measurement.

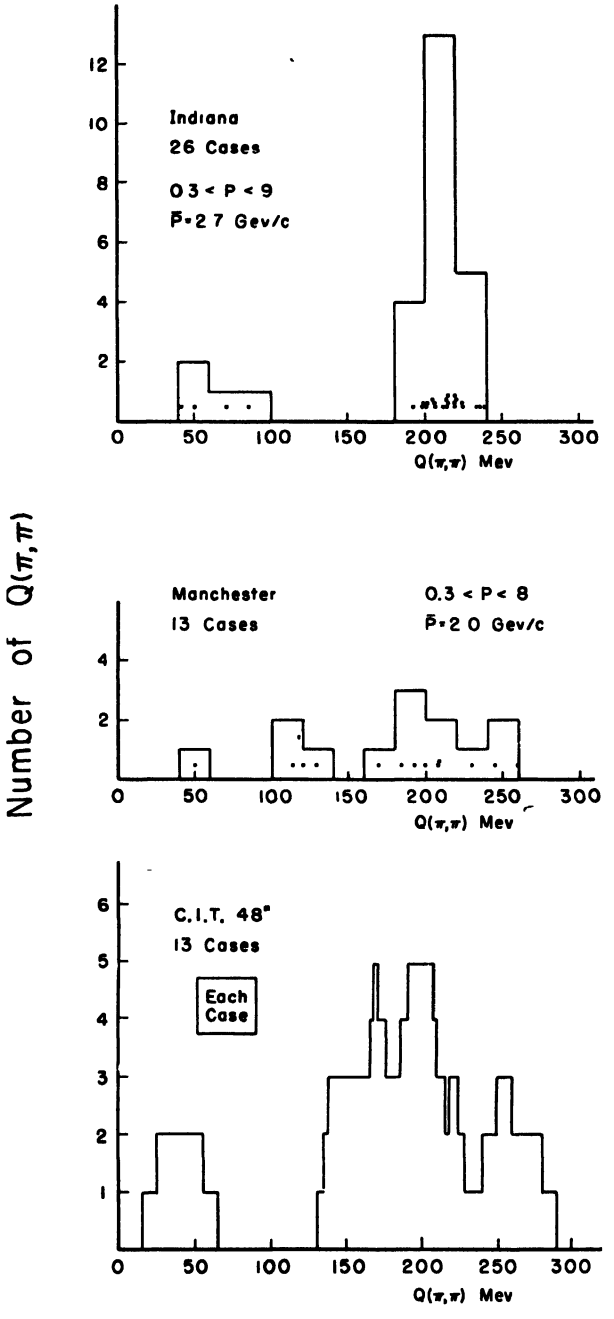

Fig. 24 – Cloud chamber determinations of $Q(\pi, \pi)$-values from various laboratories. The histograms give the number of events per 20 MeV interval. The diagram of the C.I.T. results is of a different type and is reproduced from VAN LINT [1953].

FRETTER & FRIESEN [1954a] report 5 examples giving

$$Q = (230 \pm 15),\ (251 \pm 20),\ (225 \pm 12) \text{ and } (225 + 7);$$

the last case being of unusual quality. One example, however, gives $Q = (295 \pm 25)$.

BRIDGE *et al.* [1953a] report 4 events in the M. I. T. multiplate chamber which are compatible with (π, π) decay and give Q-values in the range from 115 to 185 MeV. DAYTON & WILLARD [1953] report an unusual example with $Q = (173\text{–}198) + 11$ MeV. According to BRIDGE [1953] none of the upper limits is actually inconsistent with $Q = 214$ MeV.

Thus, the work of all groups indicates, or at least is consistent with, a strong concentration of Q-values in the neighborhood of 214 MeV. The evidence for a unique Q-value appears to rest primarily on the work of the Indiana group, although the data of that group also contain a substantial number of accurate anomalous cases. In the combined data of all groups, about 20% of the events give lower Q-values and one case (that of Fretter and Friesen) may be higher.

Uniqueness of the θ^0 Q-Value. The fact that different $Q(\pi, \pi)$-values are observed brings up the question of 3-body decay, since the presence of a third neutral fragment would reveal itself in a continuous distribution of apparent Q-values. It is therefore necessary to compare the data with the theoretically expected distribution of apparent or Q^*-values for a 3-body decay. Fig. 25 compares the histogram of the Indiana $Q(\pi, \pi)$-values with the theoretical Q^* distribution, normalized to equal area. The theoretical distribution is computed from Eq. (5) for the hypothetical decay scheme

$$0^\circ \to \pi^+ + \pi^- + \nu + 516 \text{ MeV}.$$

The energy spectrum of the neutrino is taken to be that given by the statistical factor, and the end point $Q^* = 516$ MeV is adjusted so that the maximum of the distribution occurs near $Q^* = 214$ MeV, to agree with experiment. It would appear difficult to reconcile the observations by a 3-body decay process of the general sort deduced by statistical considerations.

4. 4 EMULSION WORK ON THE 0°-MESON

For studies of the 0°-meson, the difficulties with emulsion work on V°-events discussed in § 3.5 are augmented by the imprac-

ticability of stopping both fragments with emulsion blocks of convenient size. If the events are located by tracing back σ-mesons or $(\pi$-$\mu)$-decays, therefore, the observations will be biased heavily toward decays with $|\alpha| \gg 0$, in which one fragment momentum is high and is therefore measured by scattering rather than range. Since the Q-value depends primarily on the higher momentum in such cases (cf. Fig. 7), very little benefit is derived from precise knowledge of the other fragment through range.

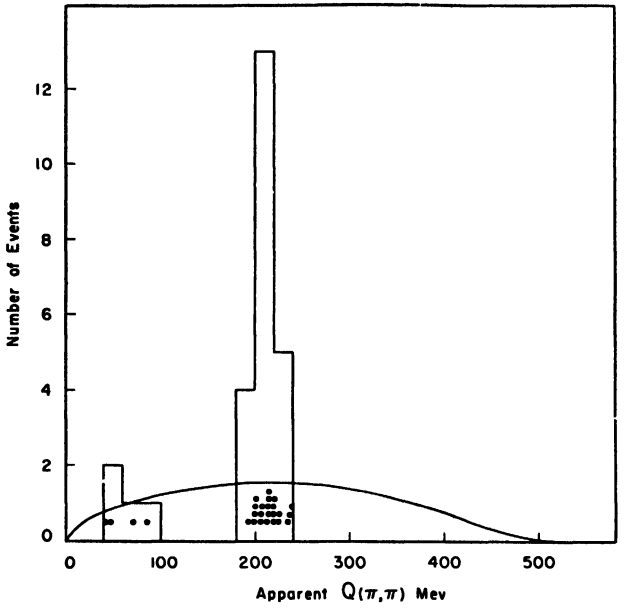

Fig. 25 – Comparison of the observed $Q(\pi, \pi)$ distribution of the Indiana group with the theoretical Q^* distribution given by the statistical factor. The end point of the theoretical distribution is adjusted to place the maximum in the neighborhood of 214 MeV.

Precision comparable to that of the emulsion work on Λ^0 has not yet been obtained.

Thus far, 4 examples of 2 + 0n events in which one fragment is an identified π and the other is probably an L-meson have been reported. The data are contained in Table VII and show very clearly the effects of the bias just discussed. In the event of Lal *et al.*, the π^+ is brought to rest and identified by $(\pi$-$\mu)$-decay. In the remaining 3 events, the π^- is brought to rest and is identified to be a σ-meson. The statistics are very meager in comparison

TABLE VII

Emulsion Data on $\theta°$.

Authors	π^+			π^-			θ	$Q(\pi, \pi)$ MeV
	Range μ	T MeV	p MeV/c	Range μ	T MeV	p MeV/c		
Lal *et al.* [1953b]	2640	11	—	—	—	450 ± 70	69.°	132 ± 17
Yasin [1954]	—	—	412 ± 21	3128	12.2 ± 0.2	—	$146.7 \pm 0.5°$	202 ± 11
Di Corato *et al.* [1954]	—	—	$960 \begin{matrix} + 180 \\ - 140 \end{matrix}$	1836	8.7	—	23.°	210 ± 35
Hirschberg [1954]	—	—	1130 ± 230	13.675	27.2	—	31.4°	216 ± 45

with the Λ^0 material. The most probable interpretation of the last three events, however, is that they do indeed represent θ^0-decay. The example of YASIN [1954] is shown in Plate VI.

4.5 LIFETIME OF THE θ^0-PARTICLE

Several groups have reported determinations of the θ^0 lifetime, the most recent being that of GAYTHER [1954], who reviews the previous work. The available data, as compiled by Gayther, are given in Table VIII. The weighted mean lifetime, from these observations, is:

$$\tau = \left(1.7 \begin{smallmatrix} +0.6 \\ -0.35 \end{smallmatrix}\right) \times 10^{-10} \text{ sec.}$$

TABLE VIII

Determinations of the θ^0 Mean Lifetime

Authors	Type of Chamber	Number of Events	$\tau \times 10^{10}$ sec.
ASTBURY [1953]*	Magnetic	11	$1.6 \begin{smallmatrix} +2.2 \\ -0.6 \end{smallmatrix}$
DEUTSCHMANN [1953]*	Multiplate	9	$2.3 \begin{smallmatrix} +2.1 \\ -0.7 \end{smallmatrix}$
BRIDGE [1953]*	Multiplate	6	$0.9 \begin{smallmatrix} +1.6 \\ -0.3 \end{smallmatrix}$
GAYTHER [1954]	Multiplate	8	$1.2 \begin{smallmatrix} +0.8 \\ -0.3 \end{smallmatrix}$

* As reported by GAYTHER [1954].

4.6 RELATIONSHIP OF THE θ^0-MESON TO THE K-PARTICLES

The fact that the masses of the θ^0-meson, $(966 \pm 10)m_e$, and of the $\tau^\pm$-meson, $(965.5 \pm 0.7)m_e$, are almost identical suggests a close relationship between these particles, i.e. $\theta^0 \equiv \tau^0$. Preliminary evidence against this identification is found in the analysis of τ- decay data by DALITZ [1954]. The theoretical dependence of the distribution of decay configurations on the τ-meson spin j and parity w is calculated and compared with the experimental results with the aid of a very convenient 2-dimensional plot. The available data are insufficient to permit a definite conclusion but rather suggest even j and odd w for the $\tau^\pm$-meson.

On the other hand, the fact that the θ^0-meson very probably undergoes 2π decay requires $w = (-1)^j$, which is incompatible with even j and odd w if $\theta^0 \equiv \tau^0$. Thus there is preliminary evidence that the θ^0-meson and the $\tau^\pm$-meson represent different K-particle families with almost identical masses.

It is possible, but by no means certain, that some of the so-called anomalous V°-events, to be discussed in section 5, represent the decay of a neutral τ-meson, according to the decay scheme $\tau^\circ \rightarrow \pi^+ + \pi^- + \pi^\circ + 80$ MeV. On the other hand, HODSON *et al.* [1954] report a remarkable photograph which provides strong evidence for a charged counterpart of the θ°-meson, decaying according to the scheme $\theta^+ \rightarrow \pi^+ + \pi^\circ + (213^{+15}_{-10})$ MeV. The π° is identified by the possible but very improbable mode of decay $\pi^\circ \rightarrow 4e$ (see p. 205).

5. The Anomalous V°-Decays

It was concluded in the previous section that the majority of non-protonic V°-events are decays of the θ° type. A substantial number, however, appear to be incompatible with the θ° scheme. In the present section, these so-called anomalous events are considered in more detail, although the present available data do not appear to admit many definite conclusions.

5. 1 THE BASIC DATA

In the list of anomalous events given by ASTBURY [1954], the examples relating to Λ°-decay with high or low $Q(p, \pi)$-values have been discussed in section 3. The cases of non-protonic events in that list in which the authors of the data do not themselves consider the abnormality to be beyond the experimental error are omitted. There remain 2 examples of THOMPSON *et al.* [1953a], [1954a] and 2 examples of BALLAM *et al.* [1953]. Fig. 16 of LEIGHTON *et al.* [1953a] will be discussed in § 5.3. Since Astbury's list was prepared, a number of additional examples have become available. The basic data on the new examples, together with the residual examples from Astbury's list, are given in Table IX.

Reality of the phenomenon. It is evident from the data in Table IX that a substantial number of cases cannot be interpreted in terms of gross errors of measurement, assuming that the only V°-particles are the Λ° and θ°. For example, consider event #3, which is shown in Plate VII. For this event to be of the Λ° type, the upper mass limit on the positive fragment would have to be in error by a factor 3. Assuming that the ionization is correctly estimated to be less than twice minimum, the momentum would have to be increased by a factor of 3, whereas the estimated proba-

ble error is about 2%, the major part of which is due to multiple scattering. Assuming that the momentum measurement is firm, we find that a proton of this momentum would be heavily ionizing by a factor of about 10, which would not easily escape observation. The possibility that the event represents a distorted θ° is also remote, as may be judged from the $Q(\pi, \pi)$-value of (71 ± 2) MeV. The positive momentum would have to be increased by a factor of 2.8 or the negative momentum by a factor of 3.8 to bring the $Q(\pi, \pi)$-value up to 214 MeV. The possibility that the event represents a $V^{\pm}$-event can be excluded on energetic grounds.

Masses of the Charged Fragments. Only two of the fragments in Table IX are heavily ionizing; viz. the negative fragments in #5 and #10, which give masses in the ranges 220–420 m_e and 160–300 m_e, respectively. In #8, the authors indicate that in view of uncertainty in the minimum level of ionization, the masses given are not incompatible with the π mass. In 6 cases, #1, 3, 6, 7, 8, and 10, both fragments are probably less massive than the τ-meson.

5. 2 The Q-surface representation of the data

Stereoscopic drawings of the Q-surface plot of the data in Table IX are shown in Fig. 26. The theoretical surface for the normal $0^\circ \to \pi^+ + \pi^- + 214$ MeV is indicated as in Fig. 21. The normal Λ° surface is represented by its intercepts with the (α, p_v)- and $(\alpha, 1/P)$-planes. The interpretation of the plot is summarized in the following remarks:

i. It is evident from the figure that the points are quite uniformly dispersed. There does not appear to be any indication of a surface or surfaces. Therefore, it does not appear feasible to try to interpret the available data in terms of a single type of 2-body decay process. The possibility that the sample is heterogeneous cannot be excluded; however, if it is homogeneous or almost homogeneous, a 3-body decay is probably indicated.

ii. Within the statistics, the points are symmetrically distributed with respect to the plane $\alpha = 0$, 8 events having $\alpha > 0$ and 8 having $\alpha < 0$ [1]. The mean value of α is $+0.063$.

[1] Astbury [1954] points out that discrimination against Λ°-decay should result in a negative value of $\bar{\alpha}$ even if both fragments have equal mass. Such discrimination is undoubtedly present and must be taken into consideration when better statistics are available.

TABLE IX

Basic Data on the Anomalous V°-Events

	Author	Event	Sign	p GeV/c	I/I_{min}	Mass (m_e)	θ	α	p_y MeV/c	$1/P$ c/GeV	$Q(\pi, \pi)$ MeV
1	Thompson *et al.* [1953a]	328	+ —	0.25 ± 0.06 0.39 ± 0.08	< 2 < 2	< 620 < 970	29.6 ± 0.5°	—0.233	77.7	1.61	47 ± 14
2	Thompson *et al.* [1954a]	R–439	+ —	0.86 ± 0.04 0.49 ± 0.05	< 2 < 2	< 2100 < 1210	19.65 ± 0.05°	+0.277	106.9	0.749	86 ± 6
3	Indiana (unpublished)	R–553	+ —	0.253 ± 0.005 0.138 ± 0.006	< 2 < 2	< 630 < 340	65.0 ± 0.2°	+0.399	94.3	2.98	71 ± 2
4		R–561D	+ —	0.77 ± 0.03 0.96 ± 0.03	< 2 < 2	< 1900 < 2400	10.2 ± 0.1°	—0.112	75.9	0.580	41 ± 2
5	Van Lint *et al.* [1954b]	8796 (18 in.)	+ —	0.57 ± 0.13 0.120 ± 0.005	≤ 1.7 1.5—3	< 1200 220—420	44°	+0.709	71.8	1.51	116 ± 30
6		56337 (18 in.)	+ —	0.24 ± 0.065 0.39 ± 0.03	≤ 1.7 < 1.7	< 600 < 830	63°	—0.321	153.6	1.84	148 ± 30
7		59824 (18 in.)	+ —	0.124 ± 0.01 0.365 ± 0.055	≤ 2 < 1.7	< 310 < 780	61°	—0.612	90.2	2.28	96 ± 16
8		12590 (22 in.)	+ —	0.493 ± 0.033 0.249 ± 0.012	1.4 ± 0.2 1.3 ± 0.2	840 ± 150 385 ± 130	34°	+0.356	96.3	1.40	79 ± 10
9		15329 (48 in.)	+ —	0.94 ± 0.1 1.42 ± 0.3	≤ 1.7 ≤ 2	< 2000 < 3500	8°	—0.204	78.9	0.425	45^{+25}_{-10}
10		19143B (48 in.)	+ —	0.26 ± 0.02 0.087 ± 0.0045	≤ 2 1.5—3	< 640 160—300	40°	+0.547	43.9	3.02	41 ± 5
11	Cowan & Kadyk [1954]	10475 (22 in.)	+ —	0.59 ± 0.02 1.09 ± 0.2			15.7°	—0.298	104.8	0.600	87 ± 21
12		15559 (22 in.)	+ —	0.22 ± 0.03 0.91 ± 0.09			27.9°	—0.638	83.1	0.909	125 ± 15
13		12424 (22 in.)	+ —	0.81 ± 0.1 0.20 ± 0.01			31.6°	+0.640	85.1	1.013	125 ± 21
14	Ballam *et al.* [1953]	79—166	+ —	0.37 ± 0.1 0.087 ± 0.015	< 2 < 3	< 1200 < 400	36.5 ± 1°	+0.661	43.3	2.25	66 ± 24
15		80–206	+ —	0.33 ± 0.1 0.26 ± 0.04	< 2.5 < 2	< 1400 < 800	32.5 ±1°	+0.120	80.8	1.78	45 ± 17
16	Fretter & Friesen [1954a]		+ —	0.57 ± 0.05 0.97 ± 0.08			38.5 ± 0.5°	—0.291	238.4	0.684	295 ± 25

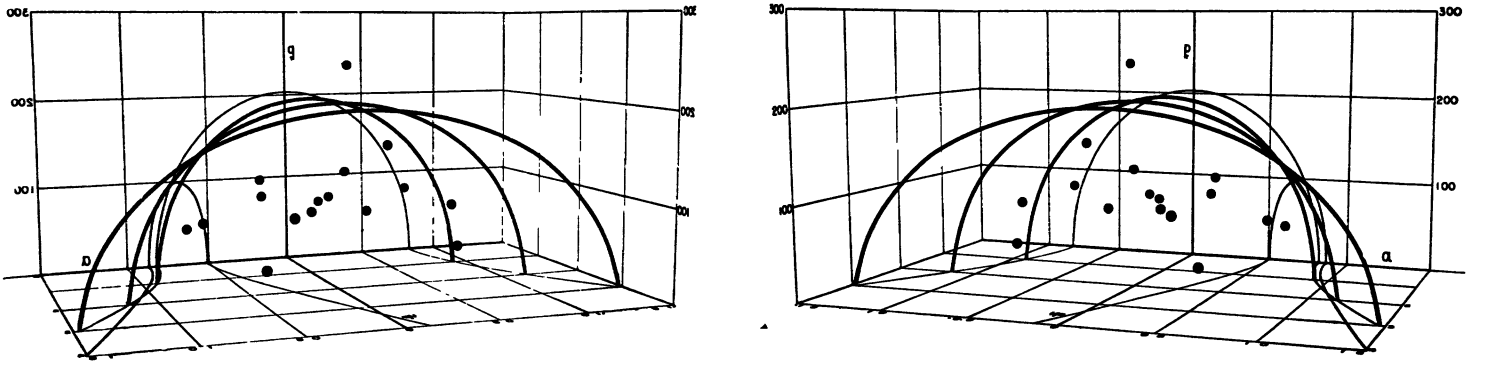

Fig. 26 – Stereoscopic drawings of the Q-surface representation of the anomalous V°-events from various laboratories as in Table IX. (Directions for viewing are given in the caption to Fig. 21). It is a pleasure to acknowledge the skilled work of Messrs. Kenneth Skirvin and Harvey Frye of the Indiana University Audio Visual Laboratory in the preparation of this figure.

There is as yet no apparent correlation of p_ν or $1/P$ with the sign of a, with the possible exception of one or two events (#6 and #16. See footnotes). Thus on the average, the momentum appears to be symmetrically divided between the positive and negative fragments, which suggests they are of approximately equal mass. An important exception would be a decay in which the charged fragments, although of different mass, have equal likelihood of being positive or negative. However, in six of the slowest cases, both fragments are apparently light from ionization. Therefore it is reasonable to conjecture that both charged fragments are light in a number of the faster examples, although the possibility that a few fragments are as heavy as 1000 m_e cannot be excluded.

iii. If the events represent a single 3-body decay process, the representative points should lie within a limiting Q-surface which corresponds to zero kinetic energy of the neutral fragment in the true C.M. system. Clearly, the available data are insufficient to delineate a limiting surface, particularly since, from statistical considerations, the density of points near the limiting surface is expected to approach zero. However, it should be noted that with the exception of one event [1], the representative points all lie within the normal θ° surface. In fact, with the exception of one other event [2], they lie well within it, although this fact may be a result of selection bias. For example, if the correct decay scheme were an alternate decay mode of the θ°-particle

$$\theta^\circ \rightarrow \pi + \mu + \nu \qquad (22)$$

or any dynamically similar process, the limiting surface would be very similar to that for normal θ°-decay. By

[1] #16 in Table IX. Two remarks about this event should be made. First, the $Q(\pi, \pi)$-values obtained by Fretter and Friesen for normal θ°-decay (cf. section 4) give a weighted mean of 230 MeV and thus may be running a little higher than 214 MeV. The discrepancy between #16 and Q = 230 MeV is only 2.6 times the stated probable error. Second, the disposition of this particular event is such that full benefit from the technique of these authors is not derived. The track of the negative fragment is of intermediate length and the curvature plot shows a slight irregularity.

[2] #6 in Table IX. $Q(\pi, \pi) = (148 \pm 30)$ MeV is only 2.2 errors from 214 MeV.

definition, events are considered to be anomalous when they are markedly dissimilar to the well-established types. Thus, in view of the experimental errors, the process of selection of events similar to Eq. (22) would be expected to produce a strong bias in favor of events which lie well within the normal θ°-surface.

iv. Conversely, if the two charged fragments are assumed to be L-mesons, the set of all possible limiting surfaces form a nested family of one parameter, that parameter being the true Q-value of the decay [1]. Thus the smallest limiting surface which encloses the available data is the surface corresponding to the largest Q(L, L)-value. The distribution of apparent Q-values is simply related to the disposition of representative points; the events with apparent Q-value between Q^* and $Q^* + dQ^*$ lie, in Fig. 26, in the thin shell between the corresponding Q-surfaces. In the following paragraph, the Q-values are discussed.

5. 3 The Q(π, π)-values, and discussion

In the absence of more specific information, the Q-values for anomalous V°-events given in the literature are invariably $Q(\pi, \pi)$-values. Fig. 27 shows the histogram of the $Q(\pi, \pi)$-values of the 16 events in Table IX. Again, the spread of the distribution suggests that the available data cannot be interpreted in terms of a single 2-body decay process. There are 5 events with $Q(\pi, \pi)$ in the range 41–47 MeV, but the statistics are insufficient to determine whether this grouping is a fluctuation or the beginning of a "line".

Several possible explanations of the anomalous V°-events have been discussed, although these do not, by any means, include all the possibilities.

i. Radiative decay of the θ°-particle. Treiman [1954] has estimated the radiative effects to be expected from the charge acceleration in θ°-decay

$$\theta^\circ \rightarrow \pi^+ + \pi^- + \gamma$$

and points out that, although large effects should be quite infrequent, some of the anomalous events may be so interpreted. The probability that θ°-decay is accompanied by a

[1] Cf. Fig. 6

photon with energy in $d\omega$ is approximately of the form

$$f(\omega)d\omega \sim \frac{d\omega}{\omega},$$

whence, from Eq. (5), the distribution of apparent Q-values is approximately

$$F(Q^*)dQ^* \sim \frac{dQ^*}{Q - Q^*}, \tag{23}$$

where $Q = 214$ MeV. Eq. (23) exhibits the familiar infra-

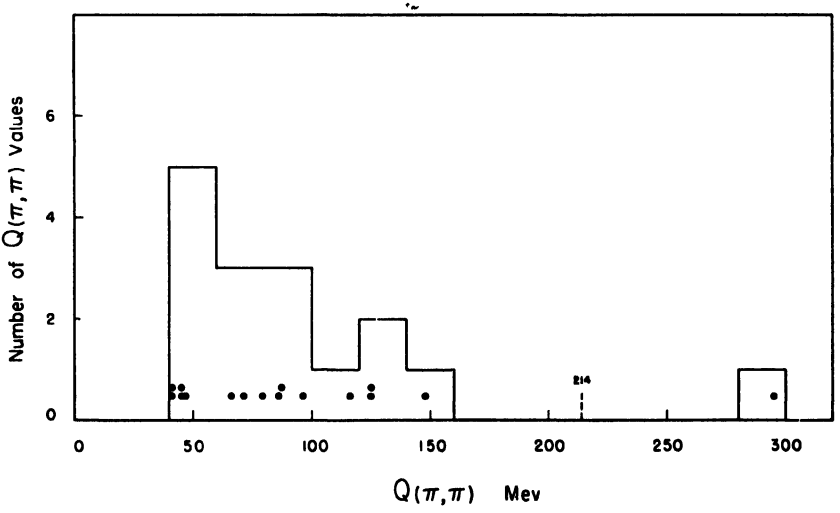

Fig. 27 – Cloud chamber determinations of $Q(\pi, \pi)$-values of the anomalous V°-events from various laboratories as in Table IX. The histogram gives the number of events per 20 MeV interval.

red divergence; thus the probability of large radiative depression of the Q-value is small. The integral of Eq. (23) from 0 to 194 MeV. is 0.7%, and most of this probability is concentrated near the upper end of the interval. Consequently, as pointed out by Treiman, the observed anomalous $Q(\pi, \pi)$-values would appear to be too low and too numerous all to be explained in this way.

ii. Neutral τ-decay. By analogy with the well known decay scheme of the charged τ-meson, a neutral τ would be expected to decay according to the scheme:

$$\tau^\circ \to \pi^+ + \pi^- + \pi^\circ + 80 \text{ MeV}. \tag{24}$$

Decays of this hypothetical type would appear in the cloud

chamber as anomalous V°-events with apparent $Q(\pi, \pi)$-values distributed from 0 to 80 MeV. The limiting Q-surface for Eq. (24) is easily visualized in Fig. 26 since it is concentrically located within the $\theta°$-surface and about half as large ($\bar{\alpha} = 0$, $p' = 110$ MeV/c, $2p'/m = 0.63$). Under the assumption that the energy spectrum of the $\pi°$ is given by the statistical factor [1], the theoretical distribution of

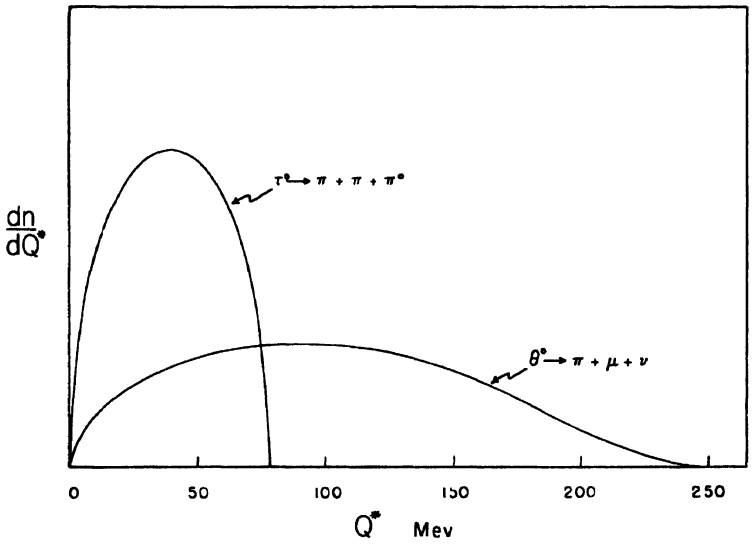

Fig. 28 – Theoretical Q^* distributions given by the statistical factor for the hypothetical decay schemes

$$\tau^\circ \rightarrow \pi^+ + \pi^- + \pi^\circ + 80 \text{ MeV and}$$
$$\theta^\circ \rightarrow \pi + \mu + \nu + 248 \text{ MeV}.$$

apparent Q-values, from Eq. (5), is found to be elliptical as shown in Fig. 28.

It appears that many of the observed $Q(\pi, \pi)$-values in Fig. 27, principally those of the Pasadena group, are too high to be compatible with Eq. (24), although a few may be of this type. It should be noted that the grouping in the range 41—47 MeV occurs very near the expected maximum; the statistics are obviously insufficient to permit conclusions, however.

iii. Decay of the type $K^\circ \rightarrow L^+ + L^- + (\gamma$ *or* $\nu)$. As the dynamic

[1] The preliminary analysis of DALITZ [1954] indicates that this assumption is at least not inconsistent with the available data on $\tau\pm$-decay.

prototype of this class of decay processes, we may take the hypothetical alternate decay mode of the θ°:

$$\theta^\circ \rightarrow \pi^\pm + \mu^\mp + \nu + 248\ \text{MeV}\,, \qquad (25)$$

in which a muon and a neutrino appear in place of one of the pion fragments. The limiting Q-surfaces for Eq. (25) are similar to, but slightly larger than, that for normal θ°-decay in Fig. 26. Under assumption that the energy spectrum of the neutrino is given by the statistical factor, the theoretical distribution of apparent $Q(\pi, \mu)$-values, from Eq. (5), is shown in Fig. 28. The theoretical spectrum has a broad maximum in the neighborhood of $Q^* = 95$ MeV.

Approximate comparison may be made with the observed histogram in Fig. 27 since the differences between the computed $(Q(\pi^\pm, \mu^\mp)$-values and the $Q(\pi, \pi)$-values for the data in Table IX are of the order of the stated errors in $Q(\pi, \pi)$ in all cases except #2, 3, 4 and 10. Again the statistics are obviously insufficient; however, it should be noted that the absence of observed values in the upper third of the Q^* range is to be expected, since the data in Table IX have been selected on the basis of incompatibility with the θ° scheme.

VAN LINT *et al.* [1954b] have pointed out that the decay scheme of Eq. (25) is compatible with the available data and does not require the assumption of a new type of particle.

iv. Decay of type $V^\circ_3 \rightarrow K^\pm + L^\mp$. LEIGHTON *et al.* [1953a] have reported evidence, based mainly on a single photograph (Fig. 16 of the reference cited), for the decay scheme

$$V^\circ_3 \rightarrow K^\pm + L^\mp + 60\ \text{MeV}\,. \qquad (26)$$

Confirming evidence for Eq. (26) has not been forthcoming, although BARKER [1954] reports several examples which are consistent with this decay scheme. More recently, LEIGHTON [1954] has concluded that the one Pasadena example may be explained as a charged V-event.

5. 4 THE COWAN PHOTOGRAPH

COWAN [1954] has published a most unusual photograph which provides evidence for a V°-decay into a positive pion and a heavy negative fragment. The photograph is reproduced in Plate VIII,

and Fig. 29 shows a schematic drawing of the event. A V°-particle produced in an interaction in lead above the chamber, decays at 0, giving rise to two oppositely charged fragments OA and OB.

The positive fragment OB is very probably a pion since it undergoes characteristic decay in flight at B. The directly measured momentum of OB is about 135 MeV/c; since the track is short, however, the value given in Fig. 29 is derived from the momentum of the muon fragment BC and the angle OBC, assuming the well-known dynamics of (π-μ)-decay. The observed ionizations of OB and BC are compatible with this interpretation.

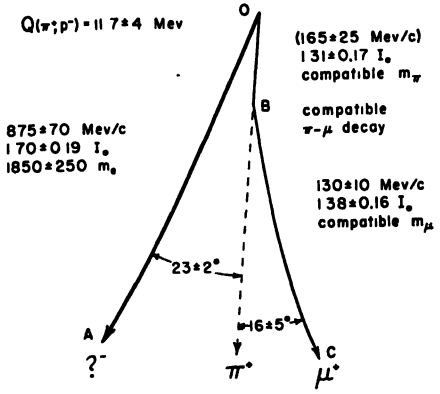

Fig. 29 – Schematic drawing of the Cowan photograph. The angles and curvatures are not drawn to scale.

The unusual thing about the photograph is the negative fragment, which appears to be heavily ionizing, (1.70 ± 0.19) I_0, although the momentum is high, (875 ± 70) MeV/c, and well-measured. The calculated mass is $(1850 \pm 250)m_e$, which is lower than that of the negative hyperon of cascade decay ($\sim 2600\ m_e$) and higher than that of the K⁻-particle group ($\sim 1000\ m_e$).

The vector resultant of OA and OB intersects an origin in the lead above the chamber. Thus there is no indication for the presence of a third neutral decay fragment. The $Q(\pi^+, p^-)$-value is (11.7 ± 4) MeV, which is appreciably lower than $Q(p^+, \pi^-) = 37$ MeV, so that the event is probably not a counterpart of normal Λ^0-decay.

As Cowan points out, an alternate interpretation is possible since the determination of mass by ionization and momentum is double valued, because of the relativistic increase in ionization above the minimum. The observed ionization of the negative fragment is consistent with that of an electron of the observed momentum. The possibility that the event is an electron pair is remote, however, in view of the angle, $(23 \pm 2)°$, and the abrupt angular deflection at B. The $Q(\pi^+, e^-)$-value is (225 ± 20) MeV. The β-decay of a V°-particle would, of course, be of considerable interest.

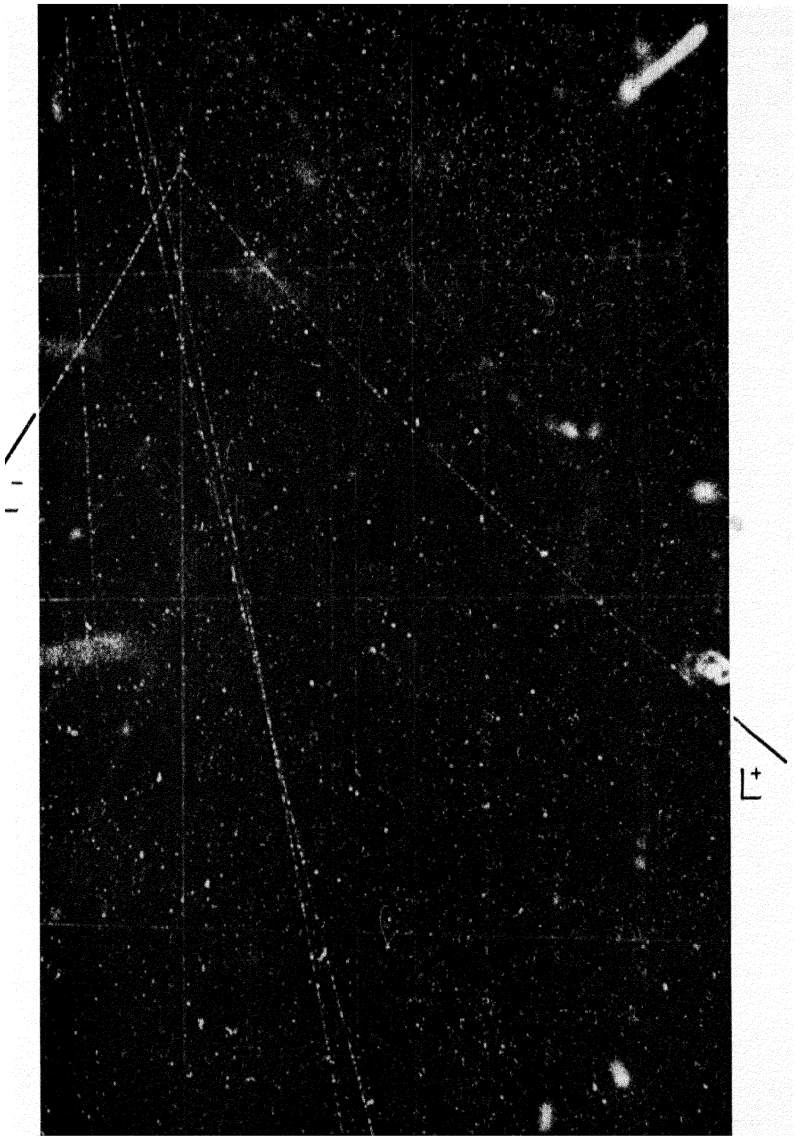

Plate VII – Example of anomalous V°-event by the Indiana group, unpublished (#3 in Table IX).

Plate VIII – The unusual photograph of COWAN [1954] with the heavily ionizing negative track. The abrupt angular deflection in the positive track, attributed to $\pi - \mu$ decay, is from front to back and thus is just barely discernable in this print.

Since the publication of this photograph, a further alternative is suggested by the preliminary report of a K-particle of 1400 m_e (FOWLER & PERKINS [1953]). A decrease of the momentum and of the ionization, by about the stated error in each, brings the calculated mass down to 1400 m_e.

The crucial question in the interpretation of this photograph is the reliability of the droplet count and the estimate of error therein, since the momentum of the negative fragment is very probably well-measured. The probable error given is only 3.5 times less than the difference between the observed ionization and the minimum value, which corresponds to a probability of 1%. It should be noted, however, that the main contribution to the stated error is the so-called counting error which is arbitrarily taken to be 10%. This estimate is conservative and is in the nature of a limit of error. The statistical part of the estimated error is only 5%. However, it would be desirable to see the shape of a mass-spectrum based on a large number of measurements of, for example, heavily ionizing protons. The $Q(\pi, \pi)$-value is (116 $\pm$ 15) MeV, so that the event does not resemble normal $0°$-decay from the dynamic point of view.

6. The Production of V°-Particles

Although the production and nuclear interactions of V°-particles is still a subject about which very little is known, there have been a number of new results during the last year or so:

1. There is additional information about the production of V°-particles at cosmic ray energies, but in view of the experimental difficulties of the problem, the work is still in a very qualitative stage.
2. An outstanding development has been the artificial production at the Brookhaven Cosmotron by Shutt and his collaborators. These authors have found several examples indicating the simultaneous production of a Y°-particle and a K°-particle in an elementary (π^-, p)-collision. Since the dynamics are such that the available energy is insufficient to create the rest mass of the neutral hyperon, the implication is that it is formed, in some sense, out of the target proton. Independent evidence for these conclusions has been obtained from cosmic ray observations by the Paris group and the Indiana group.

3. There is preliminary evidence from BARKER [1953] and from DE STAEBLER [1954] for the emission of V°-particles consequent to the nuclear absorption of K⁻-particles. These phenomena are reviewed by H. S. Bridge in the companion article in the present volume.
4. A substantial number of unstable nuclear fragments have now been observed in the nuclear emulsion. These are all consistent with the hypothesis suggested by DANYSZ & PNIEWSKI [1953] that a neutron in the fragment is replaced by a Λ°. The available data are tabulated in the Proceeding of the Padua Conference.

6. 1 PRODUCTION OF V°-PARTICLES AT COSMIC RAY ENERGIES

A number of cloud chamber studies of V° production by cosmic rays are available at present. In some, principally those of FRETTER *et al.* [1953a] and DEUTSCHMANN [1953a], the observations relate to production by the primaries of locally produced penetrating showers which are predominately protons and neutrons. Others, for example those of LEIGHTON *et al.* [1953a], BRIDGE *et al.* [1953a], and REYNOLDS [1953], are concerned with the production by the secondaries of locally produced penetrating showers which are a mixture of nucleons and mesons, the latter predominating. Thus, in discussing the two types of observations, we must bear in mind the differences in energy and nature of the producing particles.

6. 1a *Production by Primaries of Locally Produced Penetrating Showers*

FRETTER *et al.* [1953a] and DEUTSCHMANN [1953a] have used large multiple plate chambers, without absorber above, in order to study the occurrence of V°-particles in penetrating showers produced in the plates of the chamber.

Both groups report that the relative rate of occurrence of V°-particles in penetrating showers varies slowly with the energy of the shower. For example, Fretter *et al.* find that the average multiplicity of all showers is (4.4 ± 1.0), whereas for showers containing a V°-particle, it is (4.9 ± 1.2). Showers with multiplicities greater than or equal to 8 constitute 14% of all showers as against 16% for showers containing a V°-particle. Deutschmann, estimating the energy of the shower from the π° component, finds

that the production rate per shower increases at most a factor 3 for shower energies from 5 GeV to 100 GeV.

Deutschmann reports that the charged to neutral primary ratio is the same for showers containing a V°-particle as for all showers.

Among 75 V° photographs, Fretter *et al.* report only 3 pairs. This observation therefore does not provide support for the hypothesis that all V°-particles are produced in pairs; however, as these authors point out, this evidence would be invalidated if one V°-particle of the pair had, on the average, a $\beta\gamma$ which is 5 to 10 times as large as the other [1].

6. 1b *Production by Secondaries of Locally Produced Penetrating Showers*

LEIGHTON *et al.* [1953a] and REYNOLDS [1953] have studied production by secondaries of locally produced penetrating showers with magnetic cloud chambers. In both of the experimental arrangements, there is a thick absorber above and a metal plate across the centre of the chamber. The data relate to production in the central plate by secondaries of penetrating showers produced in the absorber above.

BRIDGE *et al.* [1953a] have also studied production by secondaries but with a large multiple plate chamber triggered by a penetrating shower detector with lead placed entirely above the chamber [2].

All three groups report that charged secondaries are appreciably more effective in producing V°-particles than neutral secondaries. The majority of the latter are probably neutrons, whereas the charged secondaries are a mixture of protons and mesons. With the assumption that the number of protons and neutrons is equal, it is inferred that mesons can produce V°-particles and, in fact, are probably more effective than the nucleons which occur as secondaries. This conclusion may be dependent on a difference in the energy spectrum of the meson and nucleon secondaries.

As to the energy dependence of V° production, REYNOLDS

[1] cf. remarks at the end of § 6.1b.

[2] The experimental dispositions used by the three groups are substantially different; e. g., the Princeton group uses Geiger counters ($\geqq 1$) above the chamber and proportional counters ($I \geqq 3I_0$) below. The original references should be consulted; the experimental arrangement used by the M. I. T. group is described by BRIDGE *et al.* [1953b].

[1953] reports that the rate of V° production relative to the number of showers increases by a factor 7 from 2 GeV to 20 GeV. BRIDGE *et al.* [1953a] find that the probability of V° production increases with the observed multiplicity of the shower, but point out this correlation may be partly due to an increase of the degree of plurality with energy.

LEIGHTON *et al.* conclude that the majority of V°-particles are not produced in pairs. With a mean rest lifetime of 3×10^{-10} sec. and $\gamma \leqq 5$, these authors estimate a detection probability $\geqq 0.2$. Thus among 37 V°-particles produced in the central plate, at least 7 pairs should have been found, whereas only one such case (V°, V^+) was observed. This conclusion would not hold if one particle of the pair had a lifetime much longer or much shorter than 3×10^{-10} sec. This conclusion would also be weakened if a substantial fraction of V°-particles were to decay into neutral fragments.

6. 2 PRODUCTION OF V°-PARTICLES AT LOW ENERGIES

One of the major accomplishments during the last year has been the artifical production of V°-particles at the Brookhaven Cosmotron by Shutt and his collaborators [1, 2]. The apparatus comprises a 16 in. diameter diffusion cloud chamber with a sensitive depth of 2 to $2\frac{1}{2}$ in. The filling is 20 atmospheres of hydrogen and the vapor is methyl alcohol which diffuses from top (at 10° C) to bottom (at dry ice temperature). The chamber is situated between the poles of an electromagnet which is pulsed to produce a field of 10,500 gauss. Stereoscopic photographs are taken every 7 to 8 seconds through a conical hole in the top plate of the magnet.

The chamber was exposed to a collimated, magnetically analyzed π^- beam of 1.37 ± 0.1 GeV [3] kinetic energy produced in a carbon target by the 2.2 GeV circulating proton beam of the Cosmotron.

With this experimental arrangement, Shutt and his collaborators have found four examples indicating, directly or indirectly, the simultaneous production of a Y°-particle and a K°-particle in an

[1] FOWLER *et al.* [1953].

[2] FOWLER *et al.* [1954].

[3] The π^- beam energy was given by FOWLER *et al.* [1953] and FOWLER *et al.* [1954] to be 1.56 GeV. It has since been remeasured and the value 1.37 given here is quoted by THORNDIKE [1954]. Masses and Q-values given in the text are accordingly revised insofar as they are affected.

elementary (π^-, p)-collision. In case D [1], shown in Plate IX, the entire process, including the decay of both neutral particles, is seen in the hydrogen gas of the chamber. In cases A and B, the (π^-, p)-collision and the Y°-particle decay are seen, and the simultaneous production of a K° is inferred by application of the conservation laws. In case C, a Y°-decay and a K°-decay are seen in the same photograph, and their simultaneous production in the bottom wall of the chamber is strongly suggested.

The argument that one of the products is a neutral hyperon is based on mass determination of the positive decay fragment which is distinctly heavily ionizing in all four cases. The mass values derived from momentum and ionization estimates are consistent with the proton mass. Furthermore, the Q(p, π)-values, when they can be directly determined from measured momenta (cases A and C give Q-values of 51 and (54 $\pm$ 20) MeV, respectively), are compatible with the cosmic ray mean value of 37 MeV for the normal Λ°. Thus, one of the reaction products is very probably a Y°-particle. More specifically, it is probably a normal Λ°, although the quoted errors do not entirely exclude the types reported by LEIGHTON *et al.* [1953a].

The K°-meson is not clearly identified. In cases A and B, in which the K°-decay is not observed, the best estimate of the K°-mass is indirectly obtained from the known π^- beam energy and from the angular orientation of the Y°-fragments, with the assumptions that the Y° is a normal Λ° and that the K° and the Λ° are the only particles produced in the process. The resulting masses in the two cases are (1280 $\pm$ 70)m_e and (1190 $\pm$ 80)m_e, respectively. Both are somewhat higher than, although perhaps not entirely incompatible with, the 0° mass of (966 $\pm$ 10)m_e. As these authors are careful to point out, however, it is possible in both events to balance energies and momenta if it is assumed that two neutral particles (one of which may be a π°) are produced in addition to the Λ°.

In case C, low upper limits for the masses of both K°-decay fragments can be set. The directly determined $Q(\pi, \pi)$-value is (271 $\pm$ 30) MeV. This is again somewhat higher than the cosmic ray value of (214 $\pm$ 5) MeV, although much lower than the

[1] The notation used is that of the original papers. Cases A and B are described by FOWLER *et al.* [1953]; cases C and D by FOWLER *et al.* [1954].

results for cases A and B, which correspond to $Q(\pi, \pi)$-values of (375 $\pm$ 35) MeV and (330 $\pm$ 40) MeV, respectively [1].

Unfortunately, none of the tracks in case D permits good direct measurement, so the momenta are indirectly derived from the π^- beam energy and the angles, under the assumptions that the only products of the reaction are the two V°-particles which are observed to decay and that both V°-particles undergo 2-body decay. The observed coplanarities are consistent with these assumptions. The directions of flight of the incident pion and of the two V°-particles are coplanar within the errors. The decay planes of the two V°-particles contain the endpoint of the incident pion track. The result is $Q(\mathrm{p}, \pi) = (24 \pm 11)$ MeV for the Y° and $Q(\pi, \pi) =$ $= (233 \pm 41)$ MeV for the K°. The $Q(\pi, \pi)$ is a little high, and in this case, the $Q(\mathrm{p}, \pi)$ is a little low. In view of the quoted errors, however, both are entirely compatible with the cosmic ray results for the Λ° and θ°.

Independent evidence for the process $\pi^- + \mathrm{p} \rightarrow \mathrm{Y}^\circ + \mathrm{K}^\circ$ has been obtained from a cosmic ray photograph by the Indiana group [2]. The photograph is reproduced in Plate X and the basic data on the two V°-particles is given in Table X. The ionization of tracks 3 and 4 together with the $Q(\mathrm{p}, \pi)$-value of (37 $\pm$ 4) MeV identify the Y°-particle to be a normal Λ° and the Q is limited to a sufficiently narrow interval to exclude anomalous values of 10 or 75 MeV. Tracks 1 and 2 are at minimum ionization and the upper

TABLE X

Basic Data on the Two V°-Events

Track	Event (1, 2)		Event (3, 4)	
	1	2	3	4
Charge	+	—	+	—
Momentum (GeV/c)	0.35 $\pm$ .01	0.94 $\pm$ .04	0.30 $\pm$ .02	0.106 $\pm$ .008
Angle between tracks	40.4 $\pm$ 0.2°		88.1 $\pm$ 0.2°	
V°-momentum (GeV/c)	1.23 $\pm$ .05		0.32 $\pm$ .02	
a	—0.512		+0.758	
p_y (GeV/c)	0.172		0.099	
Q-value (MeV)	$Q(\pi, \pi) = (223 \pm 10)$		$Q(\mathrm{p}, \pi) = (37 \pm 4)$	
V°-identity	θ°		Λ°	

[1] These $Q(\pi, \pi)$-values were computed from the revised K°-masses given by THORNDIKE [1954], assuming $m_\pi c^2 = 139.7$ MeV.

[2] THOMPSON *et al.* [1954b].

mass limits are too high to be informative. Identification of the decay must therefore be based on dynamics alone. The $Q(\pi, \pi)$-value is (223 $\pm$ 10) MeV, very near the mean value of (214 $\pm$ 5) MeV for the normal θ°.

The relative orientation of the two V°-decays suggests that the Λ° and the θ° were produced in the same interaction. A copunctuality test may be applied here since all four decay fragment momenta are directly measured. The result is that the lines of flight of the θ° (as deduced from the vector sum $\vec{P}_\theta = \vec{P}_1 + \vec{P}_2$) and of the Λ° (as deduced from the vector sum $\vec{P}_\Lambda = \vec{P}_3 + \vec{P}_4$) pass within 0.2 mm of each other and thus very probably intersect. The intersection falls at the inside surface of the top wall (brass) of the chamber, with an uncertainty of a few mm. Thus the interaction may have occurred just within the brass wall or in the gas (argon) itself. In either case, the absence in the chamber of ionizing tracks from the same origin suggests that the interaction may have been a relatively simple one, involving a single peripheral nucleon.

Under the assumption that the target particle was a single nucleon and that the Λ° and θ° were the only particles produced, the mass of the incident particle may be computed, although it is clear that the value so obtained will be rough since the incident particle is quite relativistic. The result is $mc^2 = (0.27 \pm 0.13)$ GeV [1], which is easily compatible with the pion rest energy.

By way of summary, the Brookhaven examples, particularly case D, provide convincing evidence for the process $\pi^- + p \rightarrow Y^\circ + K^\circ$. The Y°-particle is probably a Λ°. However, as these authors point out, the K°-masses tend to come out higher than that of the normal θ°, and in cases A and B, they are substantially higher. In the Indiana example, the V°-products are relatively well identified to be a normal Λ° and θ°. The nature of the incident particle and the elementary character of the interaction are less well established than in the Brookhaven work, however. Although there is no indication for a third neutral product, e. g. a π°, neither group can exclude that possibility.

Table XI gives (a), the angle Φ between the decay plane of the

[1] The motion of the target nucleon in the nucleus (brass or argon) introduces additional uncertainty in the value of mc^2 so derived, although the most likely situation is that the nucleon is moving at right angles to the incident pion, in which case the effect is inappreciable.

V°-particle and its production plane, and (b), the angle of emission θ' of the Λ° in the center of mass system. Two very interesting facts are evident from the table. First, there is a marked tendency for the Λ°-decay to be polarized in the production plane. Second, in the center of mass system, the Λ° is emitted very preferentially in the backward direction, and therefore has very low kinetic energy in the laboratory frame. This fact may provide a basis for explanation of the report of BALLAM *et al.* [1953] that an anomalously large number of cosmic ray produced Λ°-particles have very low kinetic energies (REYNOLDS & TREIMAN [1954]).

TABLE XI

Angular Relationships for the Reaction

$\pi^- + p \rightarrow \Lambda^\circ + \theta^\circ$

Angle	Brookhaven				Indiana
	A	B	C	D	
$\Phi(\Lambda^\circ)$	$5 \pm 5^\circ$	$30 \pm 20^\circ$	$18 \pm 7^\circ$	$27 \pm 10^\circ$	26.5°
$\Phi(\theta^\circ)$	—	—	$60 \pm 6^\circ$	$70 \pm 5^\circ$	10.6°
θ'	141°	125°	177°	174°	168°

One of the most important results of the Brookhaven work is that the Λ°-particle can be produced below the threshold corresponding to its rest energy. For a pion beam of 1.37 GeV kinetic energy, the centre of mass kinetic energy of pion and proton is only 0.86 GeV/c, to be compared with the Λ° rest energy of 1.11 GeV and the θ° rest energy of 0.50 GeV. The implication is that the Λ°-particle is, in some sense, made out of the target proton.

The Brookhaven group find a cross section of the order of 10^{-27} cm^2 for V-particle production by 1.37 GeV negative pions on hydrogen [1].

Additional evidence that the Λ°-particle can be produced below the threshold corresponding to its rest energy has been reported by FRETTER *et al.* [1953b] using the double chamber described by GREGORY *et al.* [1954]. A drawing of the event is given in Fig. 30. A negative primary AO, whose momentum is measured in the upper chamber, interacts at O, giving an evaporation proton OH, a V°-particle EDF, and two electronic showers OM and ON.

[1] This cross section is based on cases A, B, D, and E, the last being interpreted as an example of Y^- production.

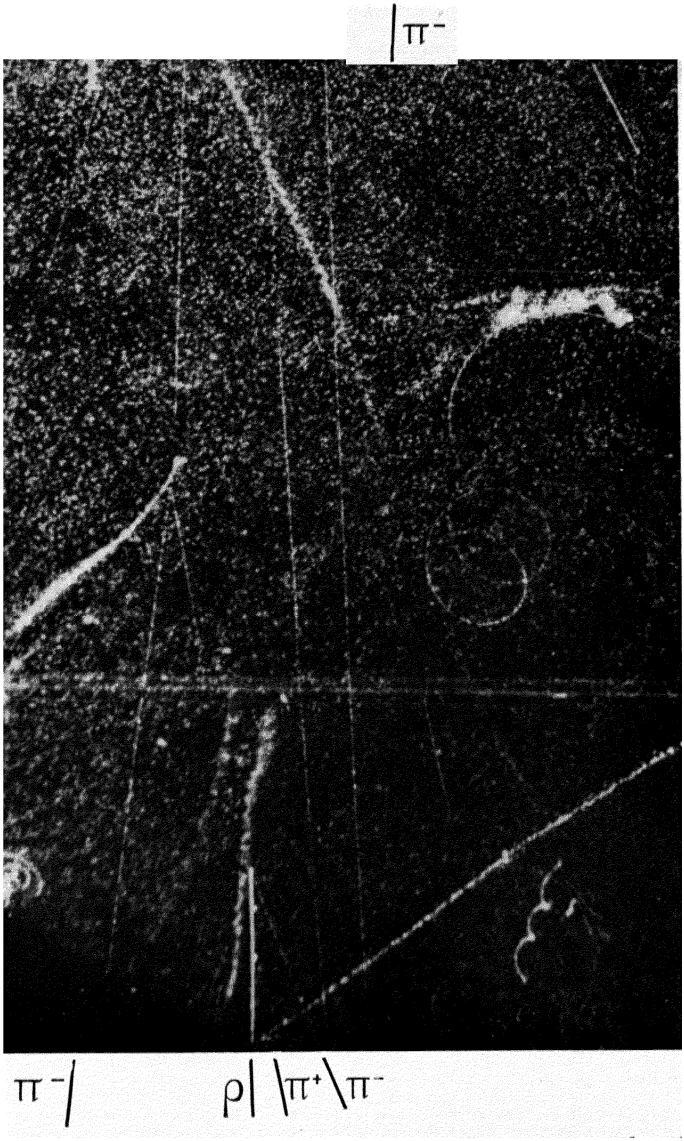

Plate IX – Simultaneous production of a Λ^0 and a θ^0 by a Cosmotron-produced 1.37 GeV π^- in a hydrogen-filled diffusion cloud chamber by FOWLER *et al.* [1954]. The collision takes place where the incident π^--track disappears abruptly. The decay products of the θ^0 are visible a short distance away (π^-, π^+). Further down, the decay products of the Λ^0 (p, π^-) can be seen. ($\pi^- + p \rightarrow \Lambda^0 + \theta^0$; $\Lambda^0 \rightarrow p + \pi^- + Q_{\Lambda^0}$; $\theta^0 \rightarrow \pi^+ + \pi^- + Q_{\theta^0}$).

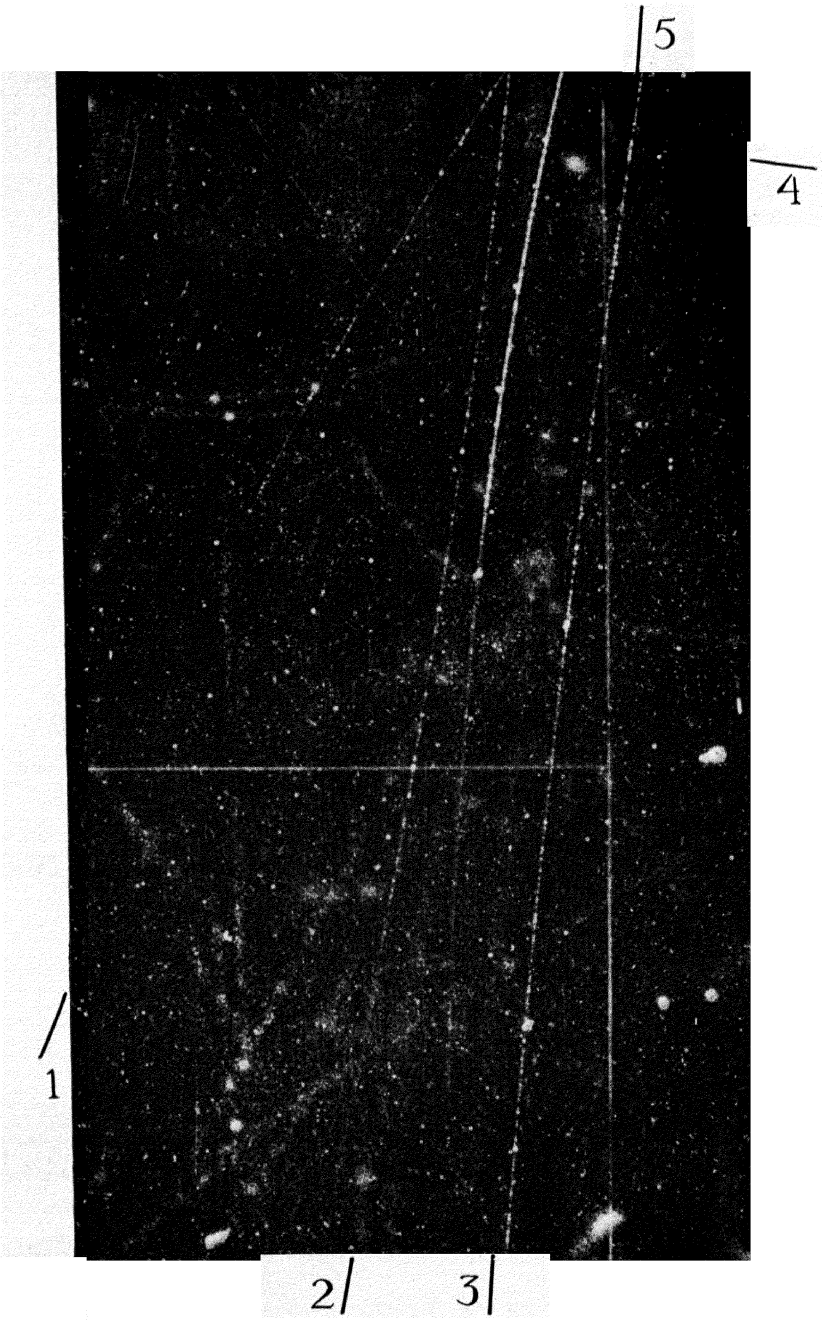

Plate X – Example (film #R-530) of the process $\pi^- + p \rightarrow \Lambda^0 + \theta^0$ observed in cosmic radiation by THOMPSON *et al.* [1954b].

The V°-particle is well identified to be a Λ° since both proton fragment DE and pion fragment DF stop in the plates, the latter appearing to produce a σ-star of which FG is a prong. The $Q(p, \pi)$-value lies between 34 and 40 MeV. The decay plane EDF contains the origin O within 2 degrees, and the transverse momenta of the

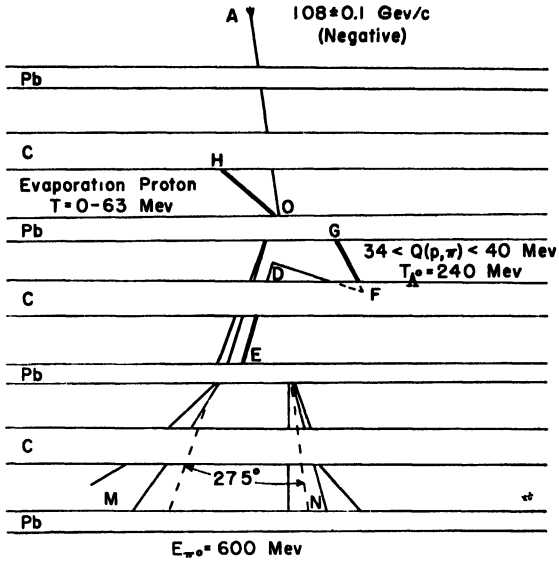

Fig. 30 – Schematic drawing of the Paris event showing cosmic ray production of Λ° by a negative primary of 1.08 GeV/c.

decay fragments balance with respect to the V°-particle line of flight OD.

The electronic showers OM and ON are attributed to the decay of a π° whose energy is determined from the angle between the γ-rays.

Thus, the tentative interpretation of the process is

$$(\pi^- \text{ or } K^-) + p \rightarrow \Lambda^\circ + \pi^\circ$$

The possibility that the π° was the decay product of a second Λ° ($\rightarrow \pi^\circ + n$) produced at O can be excluded on energetic grounds, even if the primary were a K^-. It is just possible that the π° came from a $0^\circ(\rightarrow 2\,\pi^\circ)$; however, this interpretation requires an improbable angle of emission in the C.M. system of the 0°.

There have been a variety of attempts to produce particles with energies in the range 200–500 MeV. The results are tabulated in Table XII and are seen to be uniformly negative, with the possible

TABLE XII

Production of Λ^0-Particles in the Energy Range 200–500 MeV.

Reference	Reaction	Energy MeV	Detection	Result	Cross-Section per Nucleus
Cocconi & Silverman [1951]	$\gamma + C$	$\leqq 310$	$\Lambda^0 \to p + \pi^-$ Counters	Negative	$\left(\frac{d\sigma}{d\Omega}\right)_{90°} < 5 \times 10^{-32}$ cm²/sterad.
Hildebrand & Leith [1953]	$p + C$	345	—	Negative	$\left(\frac{d\sigma}{d\Omega}\right)_{30°} < 1.4 \times 10^{-28}$ cm²/sterad.
Garwin [1953]	$p + C$	450	$\Lambda^0 \to \pi^0 + n$ Counters $\searrow 2\gamma$	Negative	$\sigma < 10^{-31}$ cm²
Rosenfeld & Treiman [1953]	$p + CH_2$	430	$\Lambda^0 \to p + \pi^-$ Emulsion	Negative	$\sigma \leqq 3.5 \times 10^{-28}$ cm²
Bernadini & Segre [1954]	$\gamma + Al$	$\leqq 330$	$\Lambda^0 \to p + \pi^-$ Emulsion	Negative	$\sigma \leqq 2 \times 10^{-4}$
Schein *et al.* [1952]	$\pi^- + C$	227	$\Lambda^0 \to p + \pi^-$ Emulsion	Positive*	—
Schein *et al.* [1953]	$\pi^- + C$	227	$\Lambda^0 \to p + \pi^-$ Emulsion	Positive*	—

* Cf. discussion in text.

exception of the work reported by SCHEIN *et al.* [1952], [1953]. These observers report 5 events of the type 2 + 0n which give Q(p, π)-values ranging from 30 to 49 MeV with a mean of (35 $\pm$ 3) MeV. A control exposure indicated that production of 2-prong stars simulating Λ^0-decay by the neutron flux could be neglected. A survey of 200 1-prong stars induced by 40 MeV (approximately the kinetic energy of the fragment from Λ^0-decay) π^--mesons indicated that the few percent which do not have an associated recoil give widely scattered Q(p, π)-values. Thus it appears unlikely that the phenomenon can be attributed to π^--mesons which are back-scattered from the apparatus. However, it is felt [1] that further work must be done before a definite statement can be made.

7. Summary

The Λ^0-Particle. In view of a considerable variety of detailed evidence, the decay scheme

$$\Lambda^0 \rightarrow \mathrm{p} + \pi + Q$$

appears to be relatively well-established. The specific identity of the decay fragments has been determined in a number of different ways. The 2-body character of the decay is indicated by the uniqueness of the Q-value and by coplanarity. The best available value of Q is 36.9 MeV with an uncertainty which probably does not exceed 1%. The corresponding parent mass is (2181 $\pm$ 1)m_e. The best value of the mean life is $(3.7\ ^{+0.6}_{-0.5}) \times 10^{-10}$ sec.

There is good evidence, both from artificial production at the Cosmotron and from cosmic ray observations, that the Λ^0-particles can be produced at energies below the threshold corresponding to their rest mass, the implication being that they can be formed or excited, in some sense, from an existing proton.

Further indication for a close relationship between the Λ^0-particle and the nucleon is provided by the unstable nuclear fragments which are consistent with the hypothesis that a neutron in the fragment is replaced by a Λ^0.

A number of new examples of the cascade decay process have been observed. The V° fragment is very probably a normal Λ^0 and the charged fragment is probably a pion. The observations

[1] SCHEIN, M., private communication, [1954].

rather suggest, or at least are entirely compatible with, 2-body decay. Thus we have

$$Y^- \rightarrow \Lambda^\circ + \pi^- + Q$$

where $Q = (66 \pm 6)$ MeV and the corresponding mass of the Y^- is $(2583 \pm 12)m_e$. If the Λ° is, in some sense, an excited nucleon, the Y^- would then correspond to a higher level of excitation.

There is evidence from the Pasadena group that, in a few percent of the cases, a decay process (or processes) occurs which is similar to Λ°-decay but has abnormally high and low $Q(p, \pi)$-values.

The 0°-Particle. As a result of work done during the last year, there is reasonably firm evidence for the decay scheme

$$0^\circ \rightarrow \pi^+ + \pi^- + (214 \pm 5)\ \text{MeV}.$$

One of the fragments is certainly a pion; the other is very probably a pion. The 2-body character of the decay is very probably indicated by the uniqueness of the Q-value. The best values of the mass and lifetime are $(966 \pm 10)m_e$ and $\left(1.7^{+0.6}_{-0.35}\right) \times 10^{-10}$ sec., respectively.

Although the masses are almost identical, there is preliminary indication, based on the analysis of τ-decay data by Dalitz, that the 0° is not the neutral counterpart of the τ-meson, but rather represents a different family of K-particles. Striking evidence for the existence of a positively charged counterpart of the 0° has been reported by the Princeton group.

The Anomalous V°-Events. Although the existence of the phenomenon appears quite probable, very little can be said as yet about the decay scheme (or schemes) and the parent particle (or particles). If the group is homogeneous or almost homogeneous, a 3-body decay is probably indicated. In a substantial number of cases, both charged fragments are probably light. The $Q(\pi, \pi)$-values range from 40 to at least 125 MeV. Some events, but not all, can be interpreted as $\tau^\circ \rightarrow \pi^+ + \pi^- + \pi^\circ + 80$ MeV; however, there is no specific evidence in favor of this particular scheme. All of the events can be interpreted as an alternate 0°-decay mode $0^\circ \rightarrow \pi + \mu + \nu + 248$ MeV; but again there is no specific evidence for this particular scheme.

Cowan has reported a photograph which suggests a V°-decay in which the negative fragment is near either nucleonic or electronic mass. The positive fragment is identified to be a pion from π-μ-decay.

Production of V°-Particles. There is good evidence, both from artificial production at the Cosmotron and from cosmic ray observations, that V°-particles are sometimes doubly produced by the reaction

$$\pi^- + \mathrm{p} \rightarrow \Lambda^\circ + \theta^\circ$$

The specific identification of the V° products is very probable in one or two cases; the presence of an additional neutral product cannot be excluded, however. There appears to be a strong angular correlation between the Λ°-decay plane and the reaction plane which suggests that the Λ° may have a large spin. In the centre of mass system, the Λ° appears to be preferentially emitted in the backward direction.

There is preliminary evidence for the emission of V°-particles consequent to the nuclear absorption of K^--particles.

ACKNOWLEDGEMENTS

It is a pleasure to acknowledge the considerable help of Mr. J. R. Burwell, Mr. R. W. Huggett and Dr. C. J. Karzmark in the preparation of various parts of the manuscript. The 3-dimensional models, on which Fig. 21 and Fig. 26 are based were constructed by Mr. Burwell and Mr. Huggett, respectively.

We should like to thank the many authors who sent us data or prepublication copies of manuscripts.

The work of the Indiana group is assisted by the U. S. Office of Ordnance Research and by grant of the Frederick Gardner Cottrell Fund of the Research Corporation.

REFERENCES

ADAMS, R. V., 1953. Private communication from R. B. Leighton.

ALFORD, W. L., and R. B. LEIGHTON, 1953, Phys. Rev., **90**, 622.

AMALDI, E., C. CASTAGNOLI, G. CORTINI and A. MANFREDINI, 1953, Nuovo Cim., **10**, 1351.

ANDERSON, C. D., E. W. COWAN, R. B. LEIGHTON and V. A. J. VAN LINT, 1953, Phys. Rev., **92**, 1089.

ARMENTEROS, R., K. H. BARKER, C. C. BUTLER, A. CACHON and A. H. CHAPMAN, 1951a, Nature, **167**, 501.

ARMENTEROS, R., K. H. BARKER, C. C. BUTLER and A. CACHON, 1951b, Phil. Mag., **42**, 1113.

ARMENTEROS, R., K. H. BARKER, C. C. BUTLER, A. CACHON and C. M. YORK, 1952, Phil. Mag., **43**, 597.

ARMENTEROS, R., K. H. BARKER, C. C. BUTLER, M. S. COATES and M. G. SOWERBY, 1953, Phil. Mag., **44**, 861.

ASTBURY, J. P., J. S. BUCHANAN, G. D. JAMES, D. D. MILLAR, J. A. NEWTH, D. I. PAGE, A. B. SAHIAR and A. RYTZ, 1953, Phil. Mag., **44**, 352.

ASTBURY, J. P., 1954, Proceedings of the Padua Conference.

BALLAM, J., D. R. HARRIS, A. L. HODSON, R. R. RAU, G. T. REYNOLDS, S. B. TREIMAN and M. VIDALE, 1953, Phys. Rev., **91**, 1019.

BARKER, K. H., 1953, Proceedings of the Duke Conference, II–18.

BARKER, K. H., 1954, Proc. Roy. Soc., **A221**, 328.

BARTLETT, M. S., 1953a, Phil. Mag., **44**, 249.

BARTLETT, M. S., 1953*b*, Phil. Mag., **44**, 1407.

BERNARDINI, G., and E. SEGRE, 1954, Proc. Roy. Soc., **A221**, 413.

BLACKETT, P. M. S., 1936, Proc. Roy. Soc., **A154**, 564.

BLACKETT, P. M. S., and R. B. BRODE, 1936, Proc. Roy. Soc., **A154**, 573.

BONETTI, A., R. LEVI-SETTI and B. LOCATELLI, 1953, Proceedings of the Bagnères Congress, 171.

BRIDGE, H. S., H. COURANT and B. ROSSI, 1952, Phys. Rev., **85**, 159.

BRIDGE, H. S., 1953, Proceedings of the Bagnères Congress, 244.

BRIDGE, H. S., C. PEYROU, B. ROSSI and R. SAFFORD, 1953a, Phys. Rev., **91**, 362.

BRIDGE, H. S., C. PEYROU, B. ROSSI and R. SAFFORD, 1953b, Phys. Rev., **90**, 921.

BRUECKNER, K. A. and R. W. THOMPSON, 1952, Phys. Rev., **87**, 390.

CARTER, R. S. and J. C. STREET, 1954, Rev. Sci. Inst., **25**, 627.

CECCARELLI, M., M. GRILLI and B. VITALE, 1954, Proceedings of the Padua Conference.

CHESTON, W. and H. PRIMAKOPF, 1953, Phys. Rev., **92**, 1537.

COCCONI, C. and A. SILVERMAN, 1951, Phys. Rev., **84**, 1062.

COHN, H. O., L. R. ETTER and R. W. THOMPSON, 1953, Phys. Rev., **91**, 445.

COWAN, E. W., 1954, Phys. Rev., **94**, 161.

COWAN, E. W. and A. GUESS, 1954. Private communication.
COWAN, E. W. and J. KADYK, 1954. Private communication.
DALITZ, R. H., 1953, Phil. Mag., **44**, 1068.
DALITZ, R. H., 1954, Phys. Rev., **94**, 1064.
DANYSZ, M. and J. PNIEWSKI, 1953, Phil. Mag., **44**, 348.
DANYSZ, M., 1953, Bulletin de L'Academie Polonaise des Sciences, **1**, 177.
DAYTON, B. and D. WILLARD, 1953, Phys. Rev., **91**, 348.
DE STAEBLER, H., 1954, Phys. Rev., **95**, 1110.
DEUTSCHMANN, M., 1952, Z. Naturforsch., **7a**, 142.
DEUTSCHMANN, M., 1953a, Proceedings of the Bagnères Congress, 48.
DEUTSCHMANN, M., 1953b, as reported by PAGE and NEWTH [1954].
DI CORATO, M., C. DILWORTH and L. SCARSI, 1954, Proceedings of the Padua Conference.
FOWLER, P. H., and D. H. PERKINS, 1953, Proceedings of the Duke Conference,
FOWLER, W. B., R. P. SHUTT, A. M. THORNDIKE and W. L. WHITTEMORE. 1953, Phys. Rev., **91**, 1287.
FOWLER, W. B., R. P. SHUTT, A. M. THORNDIKE and W. L. WHITTEMORE, 1954, Phys. Rev., **93**, 861.
FRETTER, W. B., 1951, Phys. Rev., **82**, 133.
FRETTER, W. B., 1951, Phys. Rev., **83**, 1053.
FRETTER, W. B., M. M. MAY and M. P. NAKADA, 1953a, Phys. Rev., **89**, 168.
FRETTER, W. B. and E. W. FRIESEN, 1953, Phys. Rev., **92**, 1089.
FRETTER, W. B., B. P. GREGORY, R. JOHNSTON, A. LAGARRIGUE, H. MEYER, F. MULLER and C. PEYROU, 1953b, Proceedings of the Bagnères Congress, 26.
FRETTER, W. B. and E. W. FRIESEN, 1954a. Private communication.
FRETTER, W. B. and E. W. FRIESEN, 1954b, Bulletin of the American Physical Society, vol. 29, Number 6, p. 18.
FRIEDLANDER, M. W., D. KEEFE, M. G. K. MENON and M. MERLIN, 1954, Phil. Mag., **45**, 533.
GARWIN, R. L., 1953, Phys. Rev., **90**, 274.
GAYTHER, D. B., 1954, Phil. Mag., **45**, 570.
GREGORY, B., 1953, Proceedings of the Bagnères Congress, 35.
GREGORY, B., A. LAGARRIGUE, L. LEPRINCE-RINGUET, F. MULLER and C. PEYROU, 1954, Nuovo Cim., **11**, 292.
HILDEBRAND, R. H. and C. E. LEITH, 1953, as quoted by ROSENFELD and TREIMAN [1953].
HIRSCHBERG, D., 1954. Private communication.
HODSON, A. L., J. BALLAM, W. H. ARNOLD, D. R. HARRIS, R. R. RAU, G. T. REYNOLDS and S. B. TREIMAN, 1954, Phys. Rev., **96**, 1089.
HOPPER, V. D. and S. BISWAS, 1950, Phys. Rev., **80**, 1099.
KAPLON, M. F., 1954, Report of the Padua Conference.
LAL, D., YASH PAL and B. PETERS, 1953a, Proc. Ind. Acad. Sci., **38**, 277.
LAL, D., YASH PAL and B. PETERS, 1953b, Phys. Rev., **92**, 438.
LEIGHTON, R. B., S. D. WANLASS and W. L. ALFORD, 1951, Phys. Rev., **83**, 843.
LEIGHTON, R. B., S. D. WANLASS and C. D. ANDERSON, 1953a, Phys. Rev., **89**, 148.

LEIGHTON, R. B., E. W. COWAN and V. A. J. VAN LINT, 1953b, Proceedings of the Bagnères Congress, 97.
LEIGHTON, R. B., 1953c, Proceedings of the Bagnères Congress, 250.
LEIGHTON, R. B., 1954. Private communication.
MILLAR, D. D. and D. I. PAGE, 1953, Phil. Mag., **44**, 1049.
NEWTH, J. A., 1953, Proceedings of the Bagnères Congress, 57.
NIELSEN, C. E., 1942, Phys. Rev., **61**, 202.
PAGE, D. I. and J. A. NEWTH, 1954, Phil. Mag., **45**, 38.
PAGE, D. I., 1954, Phil. Mag., **45**, 863.
PETERS, B., 1953, Proceedings of the Bagnères Congress.
PODOLANSKI, J. and R. ARMENTEROS, 1954, Phil. Mag., **45**, 13.
POWELL, C. F., 1953, Phil. Mag., **44**, 219.
POWELL, C. F., 1954, Nature, **173**, 469.
PRIMAKOPF, H. and W. CHESTON, 1954, Phys. Rev., **93**, 908.
REYNOLDS, G. T., 1953, Proceedings of the Bagnères Congress, 42.
REYNOLDS, G. T. and S. B. TREIMAN, 1954, Phys. Rev., **94**, 207.
ROCHESTER, G. D. and C. C. BUTLER, 1947, Nature, Lond., **160**, 855.
ROCHESTER, G. D. and J. G. WILSON, 1952, Cloud Chamber Photographs of the Cosmic Radiation, (London; Pergamon Press Ltd.).
ROSENFELD, A. H. and S. B. TREIMAN, 1953, Phys. Rev., **92**, 727.
SCHEIN, M., J. FAINBERG, K. BROWN and R. GLASSER, 1952, Proceedings of the Third Annual Rochester Conference on High Energy Nuclear Physics, (New York; Interscience Publishers, 1953), 95.
SCHEIN, M., D. HASKIN, R. GLASSER, J. FAINBERG and K. BROWN, 1953, Proceedings of the Bagnères Congress, 166.
SCHEIN, M., 1954. Private communication.
SERIFF, A. J., R. B. LEIGHTON, C. HSIAO, E. W. COWAN and C. D. ANDERSON, 1950, Phys. Rev., **78**, 290.
SMITH, F. M., W. BIRNBAUM and W. H. BARKAS, 1953, Phys. Rev., **91**, 765.
STILLER, B., M. M. SHAPIRO and F. W. O'DELL, 1954, Rev. Sci. Inst., **25**, 340.
TEUCHER, M., 1953, Proceedings of the Bagnères Congress, 172.
THOMPSON, R. W., H. O. COHN and R. S. FLUM, 1951, Phys. Rev., **83**, 175.
THOMPSON, R. W., 1952a, Proceedings of the Second Rochester Conference on High Energy Nuclear Physics, 73.
THOMPSON, R. W., A. V. BUSKIRK, L. R. ETTER, C. J. KARZMARK and R. H. REDIKER, 1952b, Proceedings of the Third Rochester Conference on High Energy Nuclear Physics, (New York; Interscience Publishers, 1953), 39.
THOMPSON, R. W., A. V. BUSKIRK, L. R. ETTER, C. J. KARZMARK and R. H. REDIKER, 1953a, Phys. Rev., **90**, 329.
THOMPSON, R. W., A. V. BUSKIRK, L. R. ETTER, C. J. KARZMARK and R. H. REDIKER, 1953b, Phys. Rev., **90**, 1122.
THOMPSON, R. W., A. V. BUSKIRK, H. O. COHN, C. J. KARZMARK and R. H. REDIKER, 1953c, Proceedings of the Bagnères Congress, 30.
THOMPSON, R. W., J. R. BURWELL, H. O. COHN, R. W. HUGGETT, C. J. KARZMARK and Y. B. KIM, 1954a, Proceedings of the Fourth Rochester Conference of High Energy Nuclear Physics.

THOMPSON, R. W., J. R. BURWELL, R. W. HUGGETT and C. J. KARZMARK, 1954b, Phys. Rev., **95**, 1576.

THORNDIKE, A. M., 1954. Private communication.

TREIMAN, S. B., 1954, Phys. Rev., **95**, 1360.

VAN LINT, V. A. J., 1953, Proceedings of the Duke Conference, II–42.

VAN LINT, V. A. J., G. H. TRILLING, R. B. LEIGHTON and C. D. ANDERSON, 1954a, Phys. Rev., **95**, 295.

VAN LINT, V. A. J., C. D. ANDERSON, E. W. COWAN, R. B. LEIGHTON and C. M. YORK, JR., 1954b, Phys. Rev., **94**, 1732.

WILSON, J. G., 1951, The Principles of Cloud Chamber Technique (London; Cambridge University Press).

WILSON, J. G. and C. C. BUTLER, 1952, Phil. Mag., **43**, 993.

WILSON, J. G., 1954, Progress in Cosmic Ray Physics, Vol. II (Amsterdam; North-Holland Publishing Co.), Ch. 2.

YASIN, M., 1954, Phil. Mag. **45**, 413.

CHAPTER IV

THE ENERGY BALANCE OF COSMIC RADIATION

BY

G. PUPPI
University of Bologna

INTRODUCTION. 341

1. THE MESONIC COMPONENT AT 50° GEOMAGNETIC LATITUDE 345

2. THE ELECTRON-PHOTON COMPONENT AT 50°. . 369

3. THE NUCLEONIC COMPONENT AT 50° 378

4. CONCLUSION 385

ACKNOWLEDGEMENT 386

REFERENCES. 387

INTRODUCTION

The scope of the present paper is a discussion in detail of the way in which knowledge of an energy balance for cosmic radiation at a given latitude is acquired, and in this sense the present study links up with attemps made by Rossi [1948], Puppi & Dallaporta [1952] and Puppi [1953]. For the definition of the balance terms, it has been tried, where possible, to follow several methods of approach, in order to obtain results which might be internally consistent. The scope of this study is also practical, in the sense of suggesting opportune experiments to be carried out in order to reach a more complete knowledge of the phenomenology. Since we believe that we possess a fair overall description of the phenomena, this further research study is valuable insofar as it is guided by the knowledge of the experimental results that could effectively improve the situation. What is above all important is the knowledge, for every experimental result, of its accuracy and what internal verifications it should satisfy. It must be recognized that it is now necessary, if we wish to advance in the study of cosmic ray phenomenology in the atmosphere, to institute a true and proper metrology. To do so we may take as standard the data in a vertical direction at a certain latitude, making all the measurements relatively. In this paper the reference latitude is 50° North, since almost all the available data refer to stations located between 45° and 55°; it must be noted that the said data are not effectively those of the latitude examined, but a mean of data within this latitude interval.

The actual balance sets, perhaps, more problems than it answers, but as has been mentioned above it is hoped that it may be of use for precisely this reason.

In the construction of an energy balance, three substantial elements are present:

(1) Knowledge of the primary radiation, both as regards its composition and its intensity. This knowledge is summarized in the construction of energy spectra of the various components. For the purposes of the present balance, the knowledge of the said spectra in a vertical direction at 50°, to be derived from what

we already know (PETERS [1952], NEHER [1952]), is sufficient. This permits the calculation of the energy flux at its entry into the atmosphere, to be compared with the energy dissipated in the atmosphere and underground by the various components. The knowledge of the primary spectra is, moreover, a useful guide also in the discussion of the secondary components.

(2) Knowledge of the nature and intensity, throughout the atmosphere and at sea level, of the various secondary components which are excited by the primary radiation, in order to be able to construct on them the overall dissipation of the primary radiation in its absorption processes in the atmosphere.

(3) Knowledge of the exact modality of the various processes in which, on the one hand, the primary radiation generates the secondary components, and, on the other, these components transform themselves one into another or are gradually absorbed.

It is evident that this last element serves as a guide in distinguishing and following up the various components, and in defining them quantitatively; equally, since the first two elements are of an experimental nature, their exact definition would permit us to understand them, if the description which we actually have of the various elementary phenomena be correct, complete and adequate.

It is thus first necessary to specify the phenomenological scheme on which the balance itself is based, which reflects what is the actual state of our information on the processes undergone by the elementary particles. Such a scheme naturally contains both deficiencies and inaccuracies, so much the more as notable extrapolations are often made from "laboratory physics" in order to formulate it; a satisfactory balance could offer some confirmation of the scheme itself. We shall see unfortunately that, with the experimental panorama at our disposition, we are still far from this situation.

We assume that the primary component can be thought of as constituted of protons and helions, omitting any treatment of the heavy nuclei which form only a very small fraction. We shall take as energy spectra at 50° in a vertical direction those most recently elaborated, due to Singer, which are summarized in the following table.

We do not consider there to be any sensible contribution to the primary flux either by electrons or by neutral particles with strong nuclear interaction.

TABLE I

Lat.	55°	41°	0°	
$\frac{pc}{Z}$(GeV)	1.6	4.8	15	$\gg 15$
Proton flux (cm^{-2} sec^{-1} $sterad^{-1}$)	0.190	0.058	0.018	power law with exponent between —1.6 and —1.7
α—flux (cm^{-2} sec^{-1} $sterad^{-1}$)	0.030	0.011	0.002	

We moreover assume that the origin of the secondary components can always directly or indirectly be connected with the inelastic collisions of the primaries with air nuclei, in which there will in general be produced:

(*a*) Nucleons and nuclear fragments of various types which are capable of giving new inelastic collisions of the same kind.

(*b*) Low-energy nucleons, which are capable of exciting nuclei, but not of creating particles.

(*c*) Positive and negative pions with a mean life at rest equal to 2.55×10^{-8} sec. and with a rest mass equal to 273 electron masses. These particles disintegrate into the μ-particle and neutrino. The μ-particle has a rest mass equal to 207 electron masses, and disintegrates with a mean life of 2.2×10^{-6} sec. into an electron and two neutrinos.

(*d*) Neutral pions with a rest mass equal to 264 electron masses, a mean life of about 10^{-14} sec. and disintegrating into two gamma rays.

(*e*) Heavy mesons and hyperons. No detailed calculation in the present balance involves these particles in a quantitative manner, but a hint is given as to the possible effects which they may have.

The chain of generative processes is illustrated by the following plan (p. 344).

The collision path for the inelastic collisions with air nuclei is small with respect to the atmosphere, and primary energy degradation after every collision rather marked, so that the chain of inelastic events consists, on an average, of only a few collisions and develops almost entirely in the high atmosphere. This naturally complicates the study of the phenomena, and often obliges us to reason on these events by way of the information which is brought by the secondary components into the middle and low

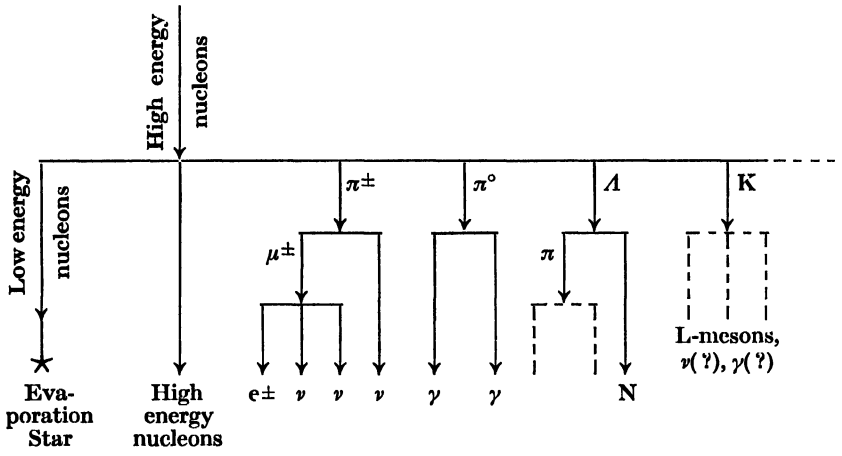

atmosphere. The chain of relatively modest energy phenomena, in which the secondary components are progressively diminished in energy and absorbed, is, on the contrary, long and quite different.

Because of their very short mean life, neither the pions (charged or uncharged) nor any type of heavy meson or hyperon can constitute a component of marked intensity anywhere in the atmosphere, for which reason when we speak of secondary components we mean to refer principally to (*a*) μ-particles, (*b*) electrons and photons and (*c*) nucleons. As the basis of the balance there will be, therefore, the information on the behaviour of these components with altitude, and our first task will be that of distinguishing these components in the vertical beam of cosmic rays in the atmosphere; of distinguishing, for example, muons from electrons and protons among the charged particles; of photons from neutrons in the uncharged ones. This has been understood for some time (Rossi [1948]), and we do not intend to repeat the criteria which lead to the separation of the physical components. Let us assume in Fig. 1 the result of such a separation for the ionizing particles. In tracing the height intensity curves we have taken into account the most recent experimental results (see Dymond [1954]). Other data will be introduced as necessary throughout the text. In Table II we have derived, the total track length of the various ionizing components, defined by

$$T_1 = \int_0^{t_0} I_1(t)dt$$

which will be found useful for what is to follow.

TABLE II

Component	Ionizing Total	Mesonic	Electronic	Protons + Alpha
Total track (g. cm^{-4} sec,$^{-1}$ sterad^{-1})	155	28	99	28

1. The Mesonic Component

1.1 The μ-spectrum at sea level

For an understanding of the mesonic component and its behaviour in the atmosphere it is essential to have an energy spectrum, at some depth, which should be as accurate as possible. The knowledge of this spectrum, and of the behaviour of the component with depth, then permits the definition of a generation spectrum, which is of prime importance for the energy balance.

The efforts of workers have for many years been concentrated on this problem, and the muon spectrum at sea level has always been the best-known datum in the phenomenology of cosmic rays. In recent years new experimental results have been added to the already existing ones, and we shall try in this paper to construct what we consider to be the most reliable muon spectrum at sea level. It should be remembered that this spectrum is based on two series of experimental data, i.e. integral and differential.

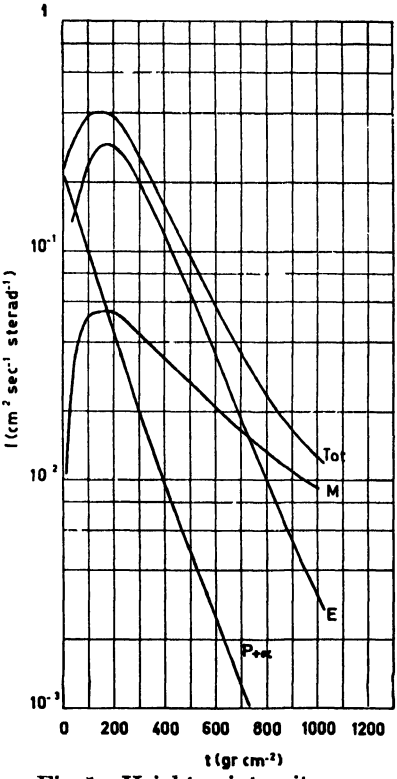

Fig. 1 – Height — intensity curves for the various components at 50° North.

Integral data consist of absolute measurements of the flux of muons of a range greater than a certain value R: such data are the measurements obtained at sea level with counter telescopes surmounted by absorbers of condensed matter, or the measurements

of the underground intensity. The measurement has a precise meaning in that the range of a muon is a well-defined quantity which, in all homogeneous condensed materials, depends only on muon energy. This fact also permits the transformation of a *range* spectrum into one in *energy* or *momentum*. As a point of reference we may take the measurement of the vertical intensity below 15 cm of lead, at sea level in normal conditions and at 50° N., which has already been discussed in previous papers (ROSSI [1948], PUPPI & DALLAPORTA [1952]), as

$$I_v = 0.83 \times 10^{-2}\ \mathrm{cm^{-2}\ sec^{-1}\ sterad^{-1}}\ .$$

The measurements of the underground flux at various depths have been collected and discussed by GEORGE [1952], and this analysis leads to the tracing of an intensity-depth function which, if we assume that there is no sensible generation underground of penetrating particles and that the nuclear interaction of muons may be overlooked, can also be considered as an integral range spectrum of muons at sea level. From this spectrum we can deduce a differential range spectrum, which appears as a continuously decreasing function of the range, at least for ranges greater than some metres of water. It is true that the method of deducing a differential spectrum from an integral one is not very sensitive, owing to the dispersion of the individual measurements, and it is not to be expected that this method will give anything beyond the general behaviour of the spectrum. Local peculiarities of the spectrum, in particular, may not be shown, and therefore direct inspection is required. Certain measurements, in particular, GLASER *et al.* [1950], have shown, even though never completely outside the experimental errors, indications of some pecularities in the differential spectra in the muon energy range around 3 GeV. An accurate experiment on the behaviour of the differential range spectrum carried out with iron absorbers (BRINI *et al.* [1952]) has shown that in the energy interval between 1 GeV and 3.5 GeV there does not exist, at least insofar as the range spectrum of the ionizing particles is concerned, (which we consider in such conditions to be the range spectrum of the muons), any fine structure of an amplitude greater than a small percentage of the local mean intensity. The measurements on the differential momentum spectrum dealt with below, also seem to corroborate this conclusion. More complicated, and not yet resolved from an

experimental point of view, is the problem of the absolute value of the differential range spectrum for very small ranges, i.e. from zero to one or two metres of water. As is known and as has been discussed elsewhere (ROSSI [1948], PUPPI & DALLAPORTA [1952]), the measurements in this interval are made by a method of delayed coincidence and anticoincidence, but the corrections which must be adopted to isolate the effective contribution of the muons vary from one experiment to another and from device to device, and are considerable, so that an estimation of the absolute intensity is always uncertain. The problem has also been amply discussed in various papers (DEL ROSARIO & DAVILA-APONTE [1952], YORK [1952], LICHTENSTEIN [1954]), and we shall adopt the solution proposed by Lichtenstein of a flat spectrum in this region. This solution provides a differential range spectrum which never increases with energy, and which fits well with the spectrum in range transformed from the momentum measurements.

Passing to the direct measurements of the differential spectrum, we note the magnetic spectrograph measurements of the Melbourne and Manchester groups, which are the completest up to date and cover a large range of momenta. Reference is made for the first group of measurements in GEORGE'S paper [1952]; the behaviour of the differential spectrum agrees well with that transformed by the range measurements. The new Manchester measurements (OWEN & WILSON [1955]) cover a range of momenta between 0.5 GeV/c and 20 GeV/c, the uncertainty at every point being of the order of 2%. These values have been normalized for our present purpose in the manner described below.

The agreement between the behaviour of the spectrum defined by these measurements, (Melbourne group), and the one transformed by the range measurements is very good, and there remains only the problem of the normalization of the magnetic measurements, and in general the problem of the absolute value. With such a purpose in view we may take as a reference point the value of the vertical intensity below 15 cm of lead, which we may also consider as the value of the vertical intensity for total energies of muons greater than 400 MeV. It is now necessary to construct a differential spectrum; in order to do this let us take:

(a) between mc^2 and 0.5 GeV, the transformed value of the flat range spectrum;

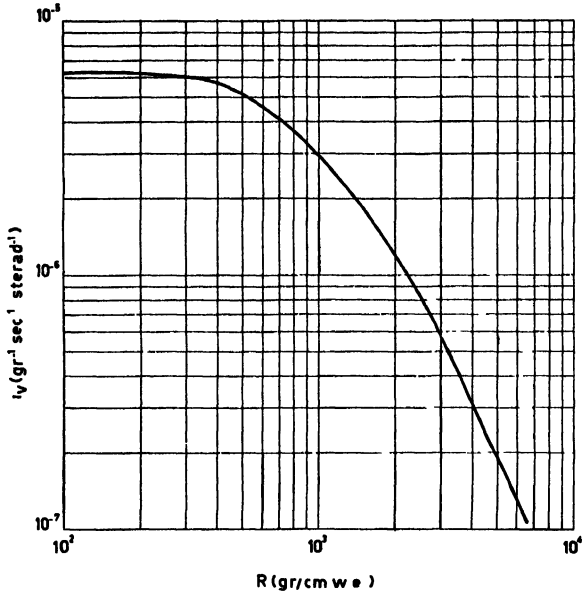

Fig. 2a – Differential range spectrum of muons at sea level and 50°N.

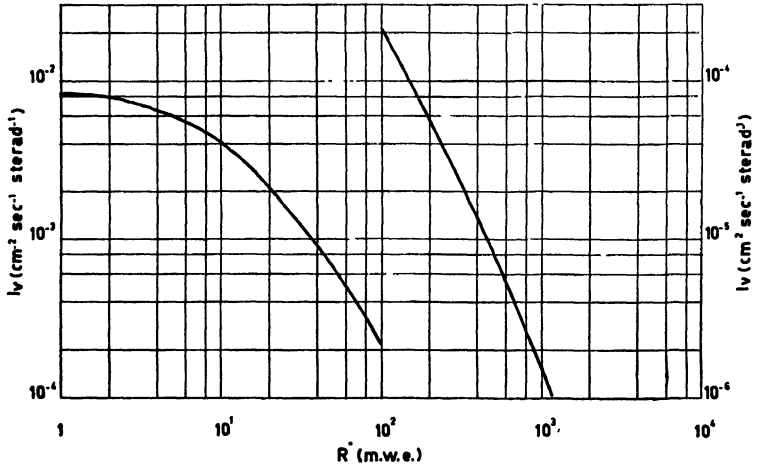

Fig. 2b – Differential range spectrum of muons at sea level and 50°N.

(b) between 0.5 GeV and 20 GeV, the values deduced from the magnetic measurements;

(c) beyond 20 GeV, the Melbourne magnetic measurements and the integral range spectrum.

The result of these operations is represented by the spectra

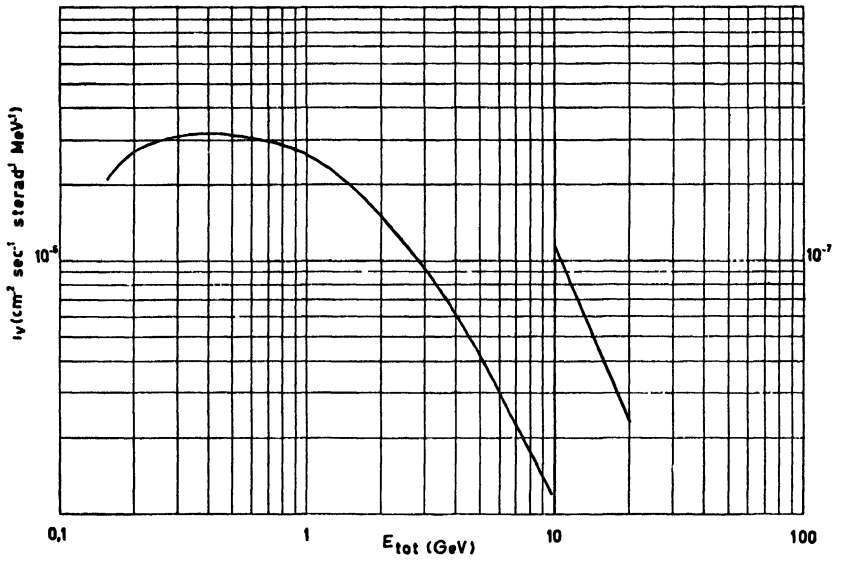

Fig. 3a – Differential energy spectrum of muons at sea level and 50°N.

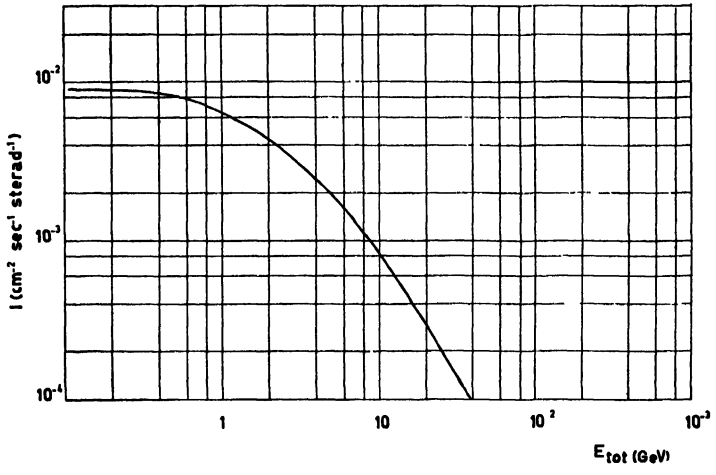

Fig. 3b – Integral energy spectrum of muons at sea level and 50°N.

reported in Figures 2(a and b) and 3(a and b), differential and integral, as a function of the range in water, and of the total energy of the muon. If we compare these spectra with those given by Rossi [1948], it can be seen that, in addition to a difference of behaviour in the low energies, to which it is not possible to ascribe great importance, (uncertainties still existing in this region), there

exists a definite difference towards the very high energies, a difference which is considerable beyond 10 GeV. In the interval between 1 and 10 GeV, on the other hand, the new spectrum follows faithfully that one traced by Rossi, but the absolute value is approximately greater by 5%.

The value of the total flux for the muons of any energy can be shown thus —

$$0.89 \times 10^{-2}\ \text{cm}^{-2}\ \text{sec}^{-1}\ \text{sterad}^{-1},$$

and the total energy contained in the spectrum (kinetic energy together with rest energy of the muons) may be represented as

$$38\ \text{MeV. cm}^{-2}\ \text{sec}^{-1}\ \text{sterad}^{-1}.$$

1. 2 Construction of the generation spectrum of muons in the atmosphere

The spectrum of the muons at sea level, and the growth of the μ-component with altitude allow the construction of a generation spectrum.

We describe the construction of this function for latitude 50° N., and mention thereafter how it is possible to proceed for other latitudes.

The method lies in assuming that the muons originate from the disintegration of pions in flight, and that these pi-mesons are produced by a primary nucleonic component absorbed exponentially, or, to be more exact, that the production function of the π-mesons in the atmosphere can be formulized thus:

$$g_\pi(E, t) = g_\pi(E) \frac{1}{L} \exp(-t/L).$$

With the experimental data to hand it is not possible, or indeed justifiable, to make wider hypotheses by introducing a dependence of the energy spectra on depth; this is not to say, however, that such a dependence does not exist, as is shown by the fact that the primary spectrum which generates the pions certainly varies considerably through the atmosphere; what is actually constructed is to be considered as a mean production spectrum, diluted in the atmosphere in an exponential manner. Only a knowledge of the differential spectra at various depths could permit the construction of the effective production function of the π-mesons, namely $g_\pi(E, t)$.

We first consider the high energy part of the spectrum, i.e., those pions which at sea level give muons of energy greater than

1 GeV. In order to establish the relation between π-mesons and μ-mesons in this region of energy, recourse can be made (PUPPI & DALLAPORTA [1952]) to the diffusion equations which describe their behaviour in the atmosphere. Let us call

$$\mu(\varepsilon, t)d\varepsilon \qquad\qquad \pi(E, t)dE$$

the differential energy spectra (total energy) respectively of the two kinds of particles, and let us indicate by the function β the energy losses by ionization, with b and B standing for the two well-known quantities:

$$b = \frac{m_\mu c}{\tau_\mu} H_0 \qquad\qquad B = \frac{m_\pi c}{\tau_\pi} H_0 .$$

Let g_π represent the generation function of the π-mesons and L_π their production length, λ_π their collision length for inelastic events, and lastly let ε and E stand for the total energy of the muons and pions respectively. Then the differential equations which describe the propagation of the two components in a unidimensional approximation are:

$$\begin{cases} \dfrac{\partial \mu}{\partial t} = \dfrac{\partial}{\partial \varepsilon}(\beta_\mu \mu) - \dfrac{b}{t\varepsilon}\mu + \dfrac{B}{tkc}\pi(k\varepsilon, t) \\ \dfrac{\partial \pi}{\partial t} = \dfrac{\partial}{\partial E}(\beta_\pi \pi) - \left(\dfrac{1}{\lambda_\pi} + \dfrac{B}{tE}\right)\pi + \dfrac{1}{L_\pi}\exp(-t/L_\pi) g_\pi(E) . \end{cases}$$

The quantity k is the ratio between the total pion and muon energy in the laboratory system, which, on an average, has the same value in the centre of the mass system, and which from recent data (SMITH *et al.* [1953]) appears to be 1.27. As regards energy losses through electromagnetic interaction, these can be represented for mu-mesons of energy greater than 1 GeV in air by means of the formula —

$$\beta_\mu = (0.256 \ln \varepsilon + 2) \text{ MeV. g}^{-1} \text{ cm}^2 .$$

and for π-mesons the following relation can be adopted, taking into account that, at equal velocities, the total energies are proportional to the masses

$$\beta_\pi = (0.256 \ln \frac{E}{1.32} + 2) \text{ MeV. g}^{-1} \text{ cm}^2 .$$

The equations with variable energy losses are rather complicated to solve, and are also beyond the limits of our purpose; an approximate solution can, however, be attempted for high energies ($\gg$ 1 GeV), where the losses can be assumed to be constant. If we

consider, for example, a muon which reaches sea level with 10 GeV, it is immediately apparent that in the atmosphere the maximum loss variation amounts to 2%. Assuming for any particular meson a mean constant loss equal to that relative to 11 GeV, the error committed is very small. In other words, the diffusion equations concern only a limited range of energies, between that at the limit of the atmosphere and that at sea level; such a condition allows the losses to approach the constant losses. The difference in the function of loss between the mu-mesons and pi-mesons can also be overcome; it is sufficient to remember that at high energies those mesons which are genetically related have energies which are approximately proportional to the relative masses at rest.

In these conditions and with the hypothesis that the pion production spectrum can be represented in a limited range of energies with a power spectrum of the form

$$g_\pi(E) = \frac{\gamma A}{E^{\gamma+1}}, \qquad \text{and} \qquad \lambda_\pi \approx L_\pi,$$

the equations offer approximately a solution:

$$\mu \approx \frac{\gamma A}{K\gamma}\left[\frac{L_\pi(\eta - \beta_0 t)}{\eta \beta_0 t}\right]^{b/\eta} \cdot \frac{B}{B + K\eta} \cdot \frac{1}{\eta^{\gamma+1}},$$

and a comparison with the spectrum at sea level allows us to define the parameters A and γ. We have thus arrived at the point of considering that, for energies much greater than 1 GeV, the pi-meson production spectrum in the atmosphere is given by

$$g_\pi(E) = \frac{0.23}{E^{2.75}} (\text{GeV})^{-1}\ \text{cm}^{-2}\ \text{sec}^{-1}\ \text{sterad}^{-1}.$$

[It must be noticed that the slope of this spectrum is intermediate between that of the spectrum of the primary nucleonic component and that of the spectrum of the secondary muons].

Use of the diffusion equations is, however advisable only for energies which are sufficiently high (see also MESSEL [1954], HABER-SCHAIM & YEKUTIELI [1954]). For low energies the problem has been attacked in a direct manner (OLBERT [1954]), by first constructing the so-called generation function of the muons, a step already taken by SANDS [1950], and then passing to the production function of the pi-mesons.

The use of the range spectrum is more convenient in this region, and we shall indicate by

$$\mu(R, t)dR \qquad\qquad \pi(R, t)dR$$

the differential range spectra of the μ-mesons and π-mesons at the depth t. If in this case also we assume exponential production of muons in the atmosphere, as was assumed for the pi-mesons at high energies, the relation between the mu-differential spectrum at a certain altitude and the generation function G of the same μ-mesons appears to be of the type

$$\mu(R, t) = \int_0^t G(R + t - \tau) \exp(-\tau/L)\, w(R, t, \tau) d\tau ,$$

where the function

$$w(R, t, \tau)$$

indicates the probability that a muon with residual range $R + t - \tau$ produced at depth τ may reach the depth t without disintegration. Such a survival probability depends on atmospheric density at the various levels and on the mean life of the muon, and can be calculated starting from these data.

In the actual calculation, the sea level mu-spectrum, the 4,500 m. mu-spectrum (KRAUSHAAR [1949]) and the variation of the slow mesons with altitude (CONVERSI [1950]) were used as experimental data. This calculation has permitted the construction of the generation function of the mesons at 50° N. for energies which are not too high; this function can be joined smoothly, as can also the absolute values, with the calculation deduced for high energies through the diffusion equations. The result of the two methods is given in Fig. 4 as a differential energy spectrum at production, integrated over the whole atmosphere. This production spectrum will constitute one of the fundamental elements of the energy balance; it refers to the vertical direction and a well-defined latitude, and its meaning requires some comment. As regards the high energy part, it can, apart from the approximations inherent in the calculation, effectively represent the π-meson spectrum, if all the μ-mesons originate in effect from the pions and only from these. But at low energies the question is a little more complicated. It is necessary to remember that the function which is actually reached is the μ-meson generation function; from this one passes to that of the π-mesons, substituting for every mu-meson at a certain energy, and in a certain direction, a pi-meson in the same direction and with a total energy equal to 1.27 times the total mu energy. The entire treatment implies

unidirectionality of trajectory development. It can be effectively shown (OLBERT [1954]) that both deviations due to scattering and those due to angulation in the process of pi → mu disintegration are contained, for energies which are not very small,

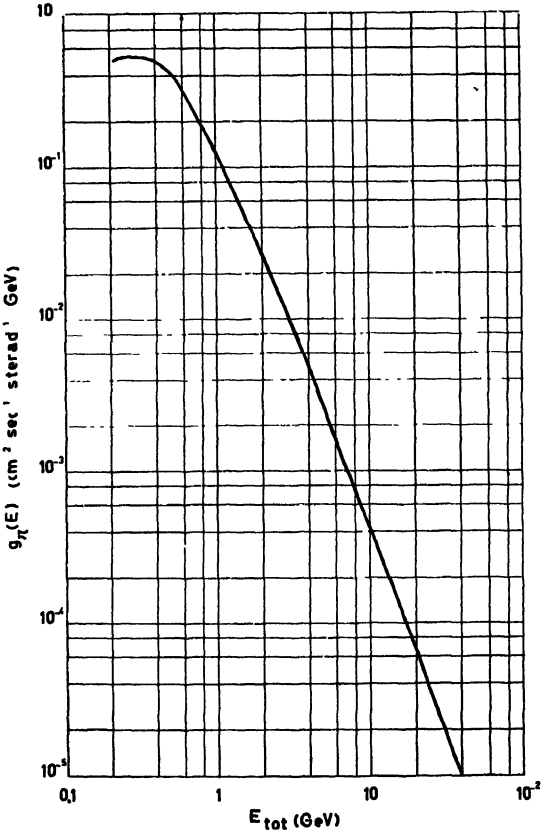

Fig. 4 – Generation spectrum of charged pions in the atmosphere at 50°N.

i.e. for $R > 100$ g. cm^{-2} residual range, within limits such that a unidimensional treatment can be considered satisfactory. The problem of angular coherence between the nucleonic component and the mesonic one is more complicated, but this will be dealt with in relation to the balance. In conclusion it can be said that a unidimensional treatment of the diffusion of the mesonic components in the atmosphere is probably a good approach to the effective state of things, and that in each case the production spectrum obtained is to be considered as a lower limit, since every

deviation from unidimensionality necessarily causes an increase in the generation function in order that the same condition in the secondary spectrum at sea level may be reached. Continuing to approach the matter from a unidimensional point of view, one can easily estimated what effect would be expected if part of the μ-mesons with the same spectrum in total energy originated from K-mesons instead of from π-mesons. At high energies, if we assume, just to emphasize the ideas, a two-body decay for the K-meson, into a μ-meson and a neutrino, the decisive factor is the ratio between the total energies of K- and μ-. Representing the production spectrum in the following manner

$$g = g_\pi + g_K = \frac{\gamma(A_\pi + A_K)}{E^{\gamma+1}}$$

the mu spectrum is given by the approximate expression

$$\mu \approx \gamma \left[\frac{L(\eta - \beta_0 t)}{\eta \beta_0 t}\right]^{b/\eta} \frac{1}{\eta^{\gamma+1}} \left\{\frac{A_\pi}{K_\pi^\gamma} \frac{B_\pi}{B_\pi + K_\pi \eta} + \frac{A_K}{K_K^\gamma} \frac{B_K}{B_K + K_K \eta}\right\}$$

The problem is of interest for the energy balance and will be taken up again in that connexion. Given the extremely qualitative character of these last considerations, we do not consider it opportune to advance more complicated hypotheses, since the available information has itself an essentially qualitative character.

Returning to the hypothesis that the π-mesons are alone responsible for the mu-mesons, the total energy contained in the production spectrum represented in Fig. 4 amounts to

$$366 \text{ MeV. cm}^{-2} \text{ sec}^{-1} \text{ sterad}^{-1}.$$

1. 3 Development of the mesonic component in the atmosphere

The study of the development of the mesonic component in the atmosphere and, in particular, the calculation of energy losses by ionization was a basic element in the old balances for reaching the energy transported by the mu-particles. Let us summarize briefly the features of the procedure. We may still consider that the mu-mesons in the atmosphere originate from the generation function $G(\varepsilon, \lambda)$, without worrying ourselves for the moment with the pions which produce them. Let us go back to the diffusion equation, which we may rewrite:

$$\frac{\partial \mu}{\partial t} = \frac{\partial}{\partial \varepsilon}(\beta \mu) + \frac{b}{tp}\mu + \frac{1}{L}\exp(-t/L)\, G(\varepsilon)$$

In the term describing mu-disintegration, it is to be noted that we have now written p in the denominator instead of ε, because we are not always at high energies, and identification of total energy and momentum is not permitted.

Multiplying now every term of the equation by ε and integrating over all the energies and the whole atmosphere, we obtain the expression:

$$\int_{m_\mu c^2}^{\infty} \varepsilon G(\varepsilon) d\varepsilon = \int_{m_\mu c^2}^{\infty} \varepsilon \mu(\varepsilon, t_0) d\varepsilon + \int_0^{t_0} dt \int_{m_\mu c^2}^{\infty} \beta(\varepsilon) \mu(\varepsilon, t) d\varepsilon + \int_0^{t_0} dt \int_{m_\mu c^2}^{\infty} \frac{b}{t} \frac{\varepsilon}{p} \mu(\varepsilon, t) d\varepsilon$$

$$+ \int_0^{t_0} m_\mu c^2 \beta(m_\mu c^2) \mu(m_\mu c^2, t) dt .$$

Here, the left hand side represents the total energy contained in the generation spectrum, i.e. the global energy *transferred* to the mu-mesons; the various terms on the right hand side represent the manner in which this energy is dissipated in the atmosphere, the first representing the energy residue at sea level, the second the energy lost in ionization and, in general, in electromagnetic interaction, the third the energy which disappears with the μ-mesons which disintegrate in flight, and the fourth the energy which disappears with the mu-mesons which disintegrate at rest. It is to be noted that the energy contained in the two latter terms is in part recuperated; the disintegration process being a ternary process in three light particles a third of the energy which disappears at the act of disintegration is recovered in the electro-photonic component.

If we succeed in measuring the four terms on the right hand side, we have the possibility of being in a position to measure the energy transported by the μ-mesons. Since the process is not independent of what leads to the construction of the generation function described in the preceding paragraphs, it is opportune to follow it up, to prove the coherence of the treatment which we are developing.

As regards the first term, i.e. the total energy contained in the mu spectrum at sea level, this has already been discussed in connexion with the construction of this spectrum, and we get:

$$38 \text{ MeV. cm}^{-2} \text{ sec}^{-1} \text{ sterad}^{-1} .$$

For the calculation of the second term, i.e. of the energy dissipated

in electromagnetic interactions, it is necessary to know the differential spectra at various altitudes, or to measure a mean β, (i.e. a mean loss over all the energies of the spectrum) and, by transforming the integral into

$$\int \bar{\beta}(t) I_v(t) dt$$

make use, as a direct datum, of the global variation of the mesonic component I_v.

Let us begin then by calculating a $\bar{\beta}$ at sea level where the spectrum is well known, then in the middle of the atmosphere and thereafter at the limit, adopting the generation function, since for $t \to 0$ the form of the μ-spectrum tends to the expression

$$\mu(\varepsilon, 0) = \frac{G(\varepsilon)}{1 + b/p}\left(\frac{t}{L}\right)$$

The result of these calculations is that $\bar{\beta}$ appears as a very slowly-varying function of altitude. The knowledge of it now permits us, taking $I_v(t)$ as a basis, to calculate the second term. We get:

$$59 \text{ MeV. cm}^{-2} \text{ sec}^{-1} \text{ sterad}^{-1}.$$

It must be said that the fundamental element of this calculation, I_v, is affected by a notable uncertainty. As we know, it is obtained initially from the vertical intensity of the so-called hard component of cosmic radiation, i.e. by radiation filtered through a block of lead, the thickness of which, according to experiments made, varies from about 10 to 20 cms. In the low atmosphere it is presumed that, below such an absorber thickness, only the μ-particles are registered by counter telescopes, since the electro-photonic component is rapidly absorbed and the nucleons reduced to a small percentage. There it only remains to add the contribution of the slow muons, i.e. of those cut out by the aforesaid lead block for reasons of minimum range; the measurement of this contribution is carried out on the basis of the absolute intensity of slow muons. In the high atmosphere, however, the problem is much more complicated, since the nucleonic component grows rapidly, until at the limit of the atmosphere it becomes the totality of cosmic radiation, or practically so, because of the slight contribution of non-nucleonic radiation to the primary albedo.

In the high atmosphere, then, the knowledge of the vertical mu-meson intensity depends on a subtraction operation, in which

the nucleonic contribution is subtracted from the penetrating component, and this operation is not without uncertainty. If we remember that the high atmosphere is, for all its components, much more important than the low, and therefore in particular the mesonic component grows rapidly with altitude, it is clear that the errors which may be made can be large. The same situation also appears in connexion with the other terms, when the sea level residue has been removed, and it is thus easy to understand how, in all balances made in this manner, one must at the end put large limits of uncertainty.

Passing to the third term, i.e. to the energy which disappears with the disintegration of muons in flight, it is apparent that the knowledge of differential spectra at the various altitudes would also be useful here. But let us proceed here too as in the preceding case by introducing an auxiliary function a which is slowly variable with altitude and depends on the relation existing in the spectrum at the various altitudes between the low energy mesons, for which $\varepsilon \neq p$, and the high energy ones for which $\varepsilon = p$. Having written, then

$$a(t) = \int_{m_\mu c^2}^{\infty} \frac{\varepsilon - p}{p} \mu(\varepsilon, t) d\varepsilon / I_v(t) ,$$

the integral in question appears as

$$\int_0^{t_0} \frac{b}{t} [1 + a(t)] I_v(t) dt .$$

The computation of the integral gives us for this term

$$187 \text{ MeV. cm}^{-2} \text{ sec}^{-1} \text{ sterad}^{-1}.$$

The fourth term is very small, arising from those mesons which stop in the air and disintegrate at rest. It depends essentially on the growth with height of slow mesons, and can be calculated:

$$5 \text{ MeV. cm}^{-2} \text{ sec}^{-1} \text{ sterad}^{-1}.$$

Summing up the various terms, we reach a total energy contained in the muon generation spectrum:

$$289 \text{ MeV. cm}^{-2} \text{ sec}^{-1} \text{ sterad}^{-1}.$$

When we pass from the muons to the pions, in the usual way, we get for the total energy contained in the pion spectrum:

367 MeV. cm^{-2} sec^{-1} $sterad^{-1}$

as given by the generation function.

Insofar as the two procedures use many common elements we repeat that the agreement which has now been found should be considered simply as a proof of the internal consistency of the calculations which we are carrying out, and not as a confirmation of the generation function. It is necessary also to point out immediately that the figures obtained, when the various losses have been added up, cannot yet serve as a basis for the balance, since the problem of the angular corrections to be applied to the one-dimensional treatment has not yet been discussed. In constructing the muon vertical intensity in the atmosphere, we have given particular importance, as regards muon separation from the protons in the high atmosphere, to CLARK's experiment [1952], which agrees with many other authors, (see DYMOND [1954]) on the other hand, as regards the growth of the penetrating component. The agreement reached in the computation on the basis of energy losses shows the coherence between the various data on the mesonic component, namely between the spectra at sea level and 4,500 metres, the growth of the slow mesons and the global growth of the μ-mesons.

1. 4 ANGULAR CORRECTION ON THE VERTICAL BEAM

In the preceding paragraphs we have discussed the structure of the vertical beam of μ-mesons at 50° N., both as to shape of the spectrum and as to behaviour with height. We have seen that everything can be derived from a μ-meson generation function, from which a pion generation function can be deduced. In the hypothesis that all the μ-mesons come from pions, this generation function permits us to calculate the energy dissipated in the production of pions by the primary radiation, and then to define one of the principal terms of the balance. But at this point our calculations require an important correction, one which takes into account the particular manner in which the generation function has been constructed. This function was constructed initially from the secondary mu-mesons, which were observed in a vertical direction, making a μ-meson originating in the same direction correspond to every μ-meson observed in a vertical direction at a certain level, with an energy increased by an amount equal to

the losses in the passage from the μ-meson point of origin to that of observation. This implies naturally that the μ-meson trajectory from the point of origin to the one of observation can be supposed straight, or, in other words, that from the point of origin to that of observation, the density per unit solid angle of μ-meson tracks is conserved. This is true only if we completely overlook the multiple Coulomb scattering undergone by μ-mesons in the collisions with the air nuclei; this approximation will, therefore, be so much the better as the μ-meson energy is greater. To get an idea of the angular spread caused by multiple scattering, it is necessary to calculate the mean square angle of scattering for a μ-meson as a function of the initial level, that of observation and the relative energies. Assuming the product of the energy loss and velocity to be constant and limiting our considerations to μ-mesons which have energy that is not very small, we get from the standard theory of Coulomb scattering

$$< \theta^2 > = 4.9 \left(\frac{1}{p_0} - \frac{1}{p} \right)$$

For a μ-meson produced at the 100 mb level and reaching sea level with a residual momentum of 300 MeV/c, this mean square angle of scattering measures 7.3°, while for a μ-meson produced in the middle of the atmosphere and reaching sea level with the same residual momentum the figure is 6.4°. On the other hand, a μ-meson which, produced at the 100 mb level, traverses the atmosphere at an angle of 30° and also reaches sea level with residual momentum 300 MeV/c, we have a figure of 7.4°.

From these examples it can be concluded that, owing to the exponential production in the atmosphere, angular spread is essentially a function of μ-meson energy at the point of observation, the μ-mesons of very low energy being as usual excluded. For this problem then we can go back to our schematizing where all the mesons originate from the 100 mb level and try to discover by how much it is necessary to increase the density of tracks at the origin in a vertical direction in respect to those arriving, in order to take multiple scattering into account. If the angular distribution around the vertical is representable with a function of the type $\sin^m$, it is immediately apparent that the relation between the vertical intensity in the absence of scattering, I°, and that effectively measured is given approximately by

$$I_v \approx I_v^\circ \left(1 - \frac{m}{2} < \theta^2 >\right)$$

$< \theta^2 >$ being in every case of the order of 10^{-2}, we can at once see that this correction, which amounts at most to a small percentage, does not have a sensible effect on the balance and can be overlooked. It, however, would behave in the sense of increasing the muon generation function at very low energies. To be more exact, for a muon of residual momentum of 300 MeV/c, the correction at the vertical intensity and, therefore, at the generation function, would amount to 2%; it would not, on the other hand, be of any use to extend these considerations to muons of momentum inferior to such a limit, in that in the construction of the generation function, muons of momentum inferior to 300 MeV/c, which corresponds approximately to a residual range of 100 g. cm^{-2} of air, have never entered.

We can in consequence conclude by saying that in the limits of approximation in which the muon generation function has been constructed, the variation in density of vertical tracks between the points of origin and observation is maintained within limits so small (2%) as justify the procedure by which the muons tracks in the atmosphere were considered straight.

We can now definitely pass on to considering how the pion generation function can be corrected, and, to begin with, let us explain how we pass from muons to pions. At high energies the passage from the muon generation spectrum to that of the pions implies in substance the substitution of a μ-meson with a total energy ε with a pion of a total energy $E = \varepsilon k$, which moves in the same direction as the μ-meson. This means that the density of the tracks in a vertical direction is maintained in the passage from the μ-meson generation spectrum to that of the pions. This procedure is certainly coherent in that for great energies the maximum emission angle is very small in respect to the direction of the pions, and the passage from a power spectrum for pions to one for μ-mesons can be made with a good approximation through the mean energies. Referring to the formula which gives the maximum muon emission angle in the laboratory system:

$$\tan \alpha_{\max} = \frac{p_0 m_\pi c^2}{\sqrt{p_\pi^2 \varepsilon_0^2 - E_\pi^2 p_0^2}}$$

and to that which gives the passage from a pion spectrum $S(E_\pi)dE_\pi$

to a muon spectrum $g(\varepsilon)d\varepsilon$:

$$g(\varepsilon)d\varepsilon = \frac{m_\pi c^2}{2p_0}\, d\varepsilon \int_{E_{\min}}^{E_{\max}} \frac{1}{p_\pi}\, S(E_\pi)dE_\pi ,$$

it is immediately apparent that, for energies greater than 1 GeV, the maximum angle of emission is always less than 2° and the passage formula between the two spectra

$$g(\varepsilon)d\varepsilon = S(k\varepsilon)d(k\varepsilon) ,$$

where we use $k = \frac{m_\pi c^2}{\varepsilon_0}$, is correct for the power spectrum in question to about 2%.

As for the passage on the other hand between the spectra at lower energies, this does not offer any difficulty as far as regards energy dependence, since the transformation formulae above were in fact used for this purpose (OLBERT [1954]), and it only remains, therefore, to discuss the question of angular spread.

Let us consider as usual as a limiting case, that of a muon of momentum equal to 300 MeV; we may examine the maximum and minimum energies of the originating pions, which measure respectively 550 and 330 MeV of total energy. At such total pion energies, 4.3° and 7.6° are respectively the maximum emission angles for μ-mesons. Considering the higher limit, it represents an angular diffusion comparable to that of multiple scattering, for which the error introduced into the vertical beam intensity is still only of the order of 2%. In concluding this first analysis we can therefore affirm that neither the multiple Coulomb scattering nor the angulation in the disintegration process $\pi \to \mu$ represents an important correction, since it reaches a maximum of 4% for the pions with a total energy of 330 MeV.

There remains the third correction, the most important to the balance effects, that relative to the angular distribution of pions at the act of generation. We are at this moment interested in a balance on the vertical cosmic ray beam, and it is necessary to know what relation exists in the infinitesimal vertical solid angle between the density of primary nucleons and that of secondary pions. We consider two limiting cases, that of a secondary which is in complete angular coherence with its primary, and that of a secondary which is part of an isotropic distribution. In the first case we can compare directly the vertical fluxes per unit of solid angle of primaries and secondaries, both as a number of particles in order

to express the number of pions which are produced on an average per primary nucleon, and as a power in order to express what fraction of the power transported by the primary is expended in the generation of charged mesons.

In the second case, if there is a primary absorbed in a directional manner and a secondary produced isotropically, the parameters to be in related are at every level respectively for the pions and nucleons:

$$4\pi I_v(t) \qquad\qquad 2\pi \int_0^{\pi/2} J(t, \theta) \sin \theta d\theta .$$

If we put α for the mean number of collimated mesons and β for the number of isotropic mesons produced per primary nucleon, (considering the mean values over whole atmosphere, given the demonstrative character of the relation), we have the two following relations, where M indicates the intensity of the pions produced per unit length and J the intensity of the nucleons:

$$M(t) = \alpha \frac{J(t)}{L} \qquad\qquad M(t) = \frac{\beta}{2L} \int_0^{\pi/2} J(t, \theta) \sin \theta d\theta .$$

It is easy to see that, as regards the isotropic mesons, if we want to make a directional balance, it is necessary to introduce a corrective factor which is 2 for pions produced at the limit of the atmosphere and 10 for pions produced in the mid-atmosphere. This obviously means that, even taking into account the compensation due to the inclined primaries (which at these latitudes we consider to be distributed uniformly on entry over the whole hemisphere), only a fraction of the isotropic mesons is counted in the vertical beam. This correction can by no means be overlooked, and we must therefore try to measure it. We begin by integrating the loss factor as a function of atmospheric depth, in order to decide what is the maximum correction to be adopted in the case of mesons produced isotropically. The calculation cannot be made in a very detailed manner, because we have no precise information on the production length of pions in the high atmosphere, and it would be necessary also to take into account the deformation of the primary spectrum due to absorption in the atmosphere. It is not possible then to make other than a rough estimate which furnishes four as a corrective factor. As was to be

expected, it is a question of a big and, therefore, rather important factor for the balance. We must now decide as to the manner of applying this corrective factor, since in reality these two limiting cases do not exist, there is rather a gradual passage from one to the other which is a function of pion energy. Let us see when we may expect the pions to be produced isotropically. It is important to note that what is of interest is that they may emerge from the air nuclei with an isotropic distribution, and not that they are generated with an isotropic distribution in the nucleon-nucleon collision. In determining an isotropic distribution, or at least one which is not collimated in a forward direction, both the generation process in the nucleon-nucleon collision itself, (when the primary and secondary energies are not high), and the successive diffusion of the pions among the nucleons of the same air nucleus in which they were produced, can contribute. There exists a large energy interval for the pions, which extends approximately between 300 and 400 MeV of total energy where the pions (FERMI [1954]) present a very high cross section for diffusion in which large diffusion angles are favoured; the composition of the angular distribution in the generation process and the successive one due to scattering can well simulate nearly isotropic distribution, and in any case a distribution which is not collimated in a forward direction. The back-scattered mesons in such collisions emerge with a mean total energy of 350 MeV, and it is to such mesons that we must apply the correction.

We may remark that the differential cross section for pions in the energy range considered gives, on an average, a greater number of pions diffused backward for energies lower than 150 MeV, and, on the contrary, a greater number of pions diffused forward for energies greater than 350 MeV.

Whatever the distribution form, even should it be strongly collimated at 0° and 180°, the corrective factor for those mesons which have undergone scattering can never be less than two. On the other hand, the probability of subsequent scattering in the air nucleus in which the meson has been formed varies, in the energy range which we have considered, between 60% and 90%; it accordingly seems reasonable, on the basis of the preceding considerations, to assume a corrective factor of two. With the increase of pion energy this factor will be rapidly reduced to one. Correcting the pion generation spectrum with these criteria and

computing the global energy contained in the spectrum, we obtain

$$409 \text{ MeV. cm}^{-2} \text{ sec}^{-1} \text{ sterad}^{-1} .$$

The applied correction is not far from the correction which was made in the previous balance, and so the global balance of this component does not differ in substance from the old balances; this depends essentially, however, on the fact that in the two balances very similar height curves were used. We consider that only a very substantial change on muon vertical intensity, especially at very high altitudes, can appreciably modify the present conclusion.

1. 5 Positive excess for the vertical muon beam

As is well known the muon beam which forms the vertical component present a positive charge excess, in the sense of the number of positive muons being in general, if the very low energies are excluded, greater than the negative muons for each energy. The problem of the presence of this excess has already been discussed in a previous paper (Puppi & Dallaporta [1952]); we only want here to touch on the most recent results and their link with the incoming primary spectrum.

We can be said to-day to have a very exact knowledge of the behaviour of the charge excess for the muon spectrum at sea level in the energies between 1 and 20 GeV, thanks to two groups of experiments, which were carried out in completely different ways but are in perfect agreement one with the other. The first relates to measurements made at 55° North at sea level by the Manchester group (Owen & Wilson [1951]) with the magnetic spectrograph, in which mu-particles of a given momentum and of both signs were magnetically separated and purified of the small proton percentage through observation of interaction properties. The second relates to measurements made at 45° North underground by the Padua group (Beretta [1953], Filosofo [1954]), in which the muons of a certain energy band were detected in a device containing a magnetized iron core, which distinguished them by the sign of the charge. The energy band which enters the device is always the same, but is picked up at various depths underground, and is thus relative to diverse energies at sea level. Fig. 5 shows the results of the two groups of measurements; as regards the low energies (< 1 GeV), we do not intend here to repeat the report

which has recently been made in this connexion (MORFWITZ & SHAMOS [1953]). A study of the figure will show clearly that this charge excess is a very slowly-varying function of muon energy at sea level, and therefore also of pion energy, from which the muons are derived. Now the pion charge excess is derived from the charge excess transported by the primary beam; since this is predominantly made up of protons, it possesses, in respect to the normal state of the electric charge per nucleon existing in the air nuclei (1/2), a positive charge excess. Let us consider for an instant the primary beam to be constituted of protons alone, and let us take a collison between a primary proton and a nucleon in an air nucleus with production of charged mesons. Since after the collision the primary proton can emerge either as a proton or as a neutron, we can understand how a certain fraction of the charge is transmitted on average to the charged mesons, bestowing on them a positive excess. In order to make quantitative estimates it is of course necessary to go back to a production theory, i.e. to make some hypotheses on the number and energy of the mesons produced in the elementary collision.

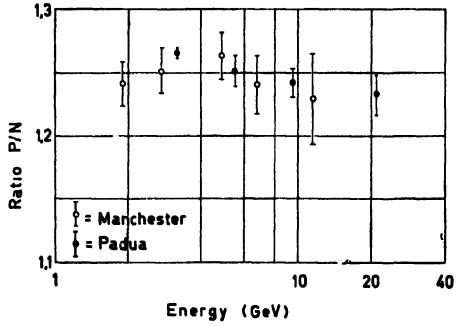

Fig. 5 – Ratio of positive to negative muons at sea level.

The result which may be expected is that the value of the positive excess is dependent on the multiplicity with which the pions are produced. Without having recourse to a particular, theory, we can, however, single out the factors which will enter in the aforesaid relation, by recalling the quantity

$$\partial = 2\frac{n_+ - n_-}{n_+ + n_-}$$

which is defined as positive excess.

Let us refer to the first collision of a primary proton with an air nucleus, generating $n = n_+ + n_-$ mesons; then $n_+ - n_-$ will, on average, be zero should the collision take place against a neutron, and unity if it takes place against a proton. We may put $n_+ - n_- = \frac{\sigma_{PP}}{\sigma_{PP} + \sigma_{PN}}$ where the various σ indicate the cross sections for

generation of the said number n of charged mesons in the collision under examination. Not all the primaries are protons, for there is a fraction of alpha particles and heavy nuclei which does not contribute to the positive excess of the mesons generated; we must bear this in mind by introducing a factor Φ which represents the fraction of mesons of a given energy generated by protonic primaries; this factor is determined by a study of the efficiency of α-particles and protons of the same energy in producing mesons.

The actual state of things is difficult to determine. It depends on the model which we take for the alpha particle in its interaction with a nucleon, and we can construct two extreme models, between which the true one will be included. We can think that the alpha particle, whose dimensions are given by the range of the nuclear forces, is a very compact system; in this case what will regulate the inelastic collision process will be the total energy in the centre of mass of the alpha particle and the nucleon which has suffered the collision. We can, on the other hand, imagine the alpha particle as a rather loose system, a system whose dimensions are considerably greater than the range of the nuclear forces, and in this case interaction will take place between the nucleon which has suffered collision and one of the alpha particle nucleons. In this second case the phenomenon depends on the relative energy which exists in the centre of mass system of the nucleon which has suffered collision and one of the alpha nucleons. In the laboratory system, in the first case, the number of mesons produced will depend on alpha energy, and in the second on the energy per nucleon. The effective situation will probably be an intermediate one between the two, since the alpha particle is ascribed dimensions which are bigger, but not very much so, than the range of the nuclear forces. Principally on the basis of the second model, whose essential value is of bringing the problem back to that of a nucleon-nucleon collision, calculations have been carried out (HABER-SCHAIM and YEKUTIELI [1954]) in order to forecast pion behaviour in the atmosphere. In these cases it can be assumed that, on average, only a fraction of the alpha nucleons produce mesons as if they were free, and this fraction is about one half. In order to calculate the alpha contribution to meson production we shall have then to about double the initial alpha spectrum expressed in energy per nucleon.

From known data we can in consequence see that the factor Φ will be of the order of 0.8.

What we measure is the positive excess at sea level, which is not only the result of the first collision in the atmosphere, but of the successive ones too. Since these successive collisions are caused on average by primaries with normal charge, i.e. made up of protons and neutrons in comparable numbers, this will merely dilute the primary excess, and the dilution factor will approximately, (if we overlook the finer effects originating from the spectrum differences between protons and neutrons at sufficiently-high energies), be equal to the ratio between the absorption length and the collision length of the generating component. Putting the various factors together, we find that the link between the positive excess of the μ-mesons with an energy ε and the generation multiplicity of pions with an energy $E = k(\varepsilon + \beta t_0)$ will be:

$$\mathrm{n}(E) = \frac{2\Phi}{\partial(\varepsilon)} \frac{\sigma_{PP}}{\sigma_{PP} + \sigma_{PN}} \left(\frac{\Lambda}{R}\right)$$

where we have as usual indicated with βt_0 energy losses through ionization in order to reach sea level, and where $k = m_\pi c^2/\varepsilon_0$.

This multiplicity refers to the first collision; if we limit ourselves to a consideration of an average global multiplicity in the various collisions in the atmosphere, it is sufficient to cancel the factor Λ/R. Assuming $\sigma_{PP} \simeq \sigma_{PN}$, we see that for charged pions with an energy at generation between 4 and 30 GeV, the average production multiplicity is around 4. This multiplicity, more precisely, can be represented with a function of the type:

$$n(E) = 3.5\, E^{0.1}$$

which is very slowly variable with pion energy. Unfortunately the datum which has now been obtained, is expressed as a function of the energy of the pions produced, and the link with the generating component is not so immediate, and involves a knowledge of the pion energy spectra, the primary and, above all, the inelasticity function, about which it is at present not possible to say very much. Without going into further details we can only point out the circumstance that the positive excess distribution is a datum on the pion generation spectrum independent, from an experimental point of view, of the behaviour of the spectrum, and that it reflects a peculiarity of the generating primary radiation; if at least another unknown term of the problem, for example the

primary spectrum, could be determined, we should have sufficient elements to set out the problem of the production model.

2. The Electron-Photon Component

2. 1 Origin of the electron-photon component

We can see at once from the phenomenological picture traced at the beginning of this paper, that the origin of the electron-photon component is, as for the meson component, wholly in the atmosphere; it originates from three principal sources:

(1) from muon, pion and proton knock-on and bremsstrahlung processes,

(2) from muon disintegration, in flight or at rest, into an electron and neutrinos, and

(3) from neutral pion disintegration in flight into two photons. From these three processes either electrons or photons are produced, which, by multiplication in cascade form the electron-photon component.

The cascade multiplication produces a progressive degradation of the mean energy of the electrons and photons because of the increase in their number; it is the dominating phenomenon for energies which are much greater than the critical energy, which in air is about 84 MeV. Such an energy having been reached, the multiplication begins to exhaust itself, and the shower enters a phase in which the most important phenomenon is absorption, due substantially to energy losses through ionization. Such losses through ionization are the principal source of shower energy dissipation, if we exclude a small contribution due to nuclear processes initiated by the photons, which depending on the photon energy may be either pion production processes, or excitations of nuclei in different forms. We are not going to devote ourselves to these secondary processes, because, albeit they are of great interest as regards a detailed phenomenological knowledge, their contribution to the global balance is not very sensible, since, if they lead to π-meson formation, their contribution has been computed and included in the generation function of charged pions, and will be in that of neutral mesons; should they lead in the last instance, on the contrary, to the production of either neutrons, protons or low-energy alpha particles, they are included in the nucleonic component. On the other hand, the drive for a very detailed

analysis requires us to take other secondary contributions into account; for example, the contribution to the soft component by high-energy charged pions, which, interacting with nuclei in the atmosphere, generate neutral mesons which then produce photons. Our knowledge of the phenomenology of cosmic rays in the atmosphere is unfortunately incapable of furnishing elements for such an analysis, and we must continue to be satisfied with a global analysis, in which we state how many charged and uncharged pions are generated in the atmosphere, whose secondary products we can recognize, be they muons or photons, without being able to distinguish if they are generated by the nucleonic component directly or at secondhand, i.e. as a product of secondary products. An analysis which claimed to be complete, should take these secondary effects into account, by using a more complicated phenomenological scheme than the one which we have put at the basis of the present balance. In our scheme we can, however, say that the whole electron-photon shower energy must reappear as ionization, and consequently that the basis of our balance on this component will be (Rossi [1948]) the total electronic track-length, i.e. the total development of tracks of all the electrons in the atmosphere. The expression to be calculated would generally be of the form:

$$\int_{mc^2}^{\infty} \int_{0}^{t_0} \beta(E) f(E, t)\, dE\, dt$$

where $f(E, t)$ indicates the differential energy spectrum of the electrons at the level t; but since at this point our information is completely insufficient, we must have recourse to the approximate calculation already given, which connects the total track of electrons of energy greater than a certain limit (which, in our present case, is usually 10 MeV) with the global energy of the primaries which have generated the cascade. The connexion between the two quantities has been calculated by various authors (Rossi, Ch. 5, [1952]), and, according to Rossi and Klapman, for electrons with an energy greater than 10 MeV, it measures

$$E_0 = 3.27\, T_e$$

2. 2 Division of the integral electron track length

With the measurement which we obtained for the electronic integral track, it is be possible to reach an estimate of 324 MeV.

cm^{-2} sec^{-1} $sterad^{-1}$. It should, however, be remembered that the electron-photon component is obtained by means of a difference between the height intensity curves of the total ionizing component and the mesonic component, and that the differences in the experimental results of various authors, especially as regards the total component, are considerable, so that the figure for the track length which we have obtained can very well have a 10%, and perhaps even a 20%, error, as can easily be seen by taking extreme cases. Continuing, however, in our component analysis, we note that part of the electrons come from electromagnetic interactions of muons, and part from muon decay, and represent, in consequence, energy terms, which we have already taken into account in the mesonic component. The "knock-on" electron contribution, which is small, is easily calculated by supposing a condition of equilibrium throughout the atmosphere with the mesonic component, by evaluating what fraction of the total electron track must be attributed to the secondary electrons of the muon knock-on processes, and by neglecting the contributions of the bremsstrahlung of muons, and the proton knock-on processes. It is only necessary then to know what fraction of the hard component produces knock-on electrons, which are in equilibrium with it in the low atmosphere. The calculation supplies this datum as about 7%, and, in consequence, we can see that the small contribution will be about 6 MeV. cm^{-2} sec^{-1} $sterad^{-1}$. We have still to isolate the contribution which comes from the μ-disintegration electrons taking into account the three-body decay of muons into an electron and two neutrinos, and the form of the spectrum (MICHEL [1952]). Taking for this contribution one third of the decay losses of muons, i.e. 62 MeV. cm^{-2} sec^{-1} $sterad^{-1}$, there remains

$$256 \text{ MeV. cm}^{-2} \text{ sec}^{-1} \text{ sterad}^{-1}$$

for the third source of the electron-photon component, i.e. for the neutral mesons.

2. 3 SPECTRA OF ELECTRONS AND PHOTONS

The above-mentioned figure has been obtained by considerations of the electron-photon component based on the difference method, and without any information as to the shape of the spectrum of this component and its variation with depth. The information which we possess to-day is not very great and is, in

any case, not such as to provide the basis for any procedure of analysis, so we will only hint at it briefly. We can say that, once in possession of the differential spectra of photons and electrons at various altitudes and of the zenithal dependence, we shall have an effective knowledge of the electron-photon component. Some indications have been obtained in the last few years both as regards the electron spectrum and the photon spectrum. PALMATIER [1952], by accurately analyzing the soft component of various ranges at altitudes of 275 m and 3,240 m, both for intensity and zenithal distribution, has succeeded in giving us indications on the integral electron spectrum at these two levels, and in isolating the contribution which is not secondary to the muon component, which in the present scheme we are attributing to the neutral pions. In the low atmosphere such a contribution is expressed as the directional intensity of the electrons with an energy greater than 30.8 MeV through the formula:

$$I(\theta, t) = 0.70 \exp. \{-t/(160 \cos \theta)\} \text{ cm}^{-2} \text{ sec}^{-1} \text{ sterad}^{-1} .$$

A direct attempt (BARONI [1953]) was also made at 2,860 m altitude with photographic plates; this was carried out by examining the isolated tracks of relativistic particles and identifying the electrons directly up to energies of 70 MeV through multiple-scattering, and by evaluating the contribution for energies greater than 70 MeV by difference, assuming the muon intensity to be known. With the data obtained and by means of the angular distribution determined by Palmatier for the various energy bands, an integral spectrum which is in good agreement with Palmatier's can be constructed. As regards photon spectra, we must remember two direct determinations with photographic plates, one at 2,860 m found in the above-mentioned work (BARONI [1953]), and the other at an altitude of 20 km (CARLSON *et al.* [1950]). In both these experiments what is observed are the pairs of electrons generated in the photographic plate by photon materialization. From the energy and angular distribution of the materialized photons, on the basis of the knowledge of the cross sections for materialization at the various energies, and on the basis of the geometry of the experiment, it was possible to go back to the spectra of the photons entering the plates. The results of these various experiments have been gathered in Fig. 6, and can be supplemented, as regards the highest energies, with the following information. For very high

energies it is possible to obtain some indications on the differential electron and photon spectra by observing the showers produced in condensed matter; the analysis of the development of an electron-photon shower, for example in a cloud chamber, can permit an estimation of the energy of the primary. Recent experiments of this kind (LOVATI [1954]) state that the differential spectrum, whether of photons or electrons with an energy greater

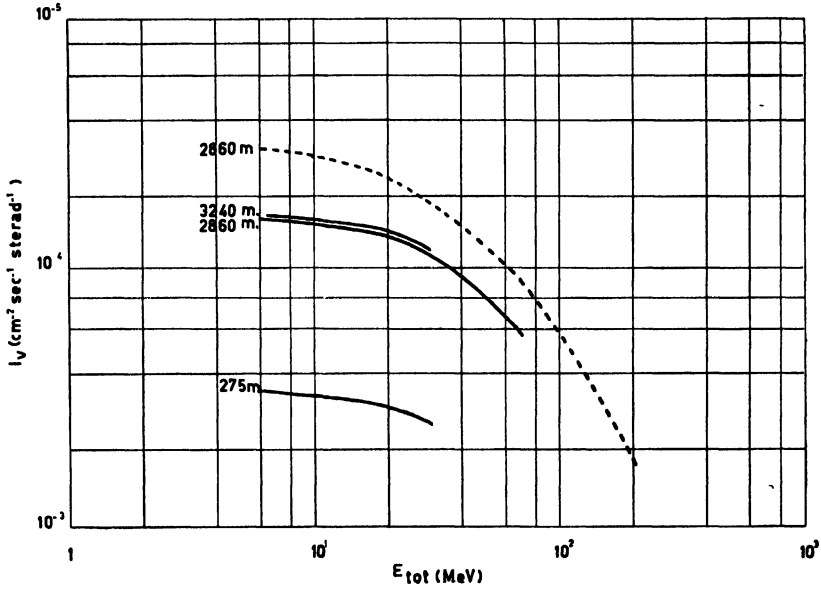

Fig. 6. – Integral energy spectrum of electrons and photons in the low atmosphere ———— (electrons) – – – – (photons).

than 300 MeV, can be represented at 3,500 m with a power law of exponent 2.5. Previous results (HAZEN [1944]) in a cloud chamber at 3,240 m, BRIDGE & ROSSI [1947]), using ionization chambers), indicated an exponent between 2.6 and 3 for energies greater than 1 GeV. Both the results obtained with plates and those with cloud chambers in the mountains show high-energy photons to be more numerous than electrons, which fact confirms the photonic origin of this main component, as would be the case should it originate from neutral pion disintegration.

Another group of experiments in this direction, i.e. experiments intended to emphasize the behaviour of the differential spectrum of the photon component, relates to the frequency of the showers under lead. From a comparison between the previsions of the

cascade theory and the experimental results, something can be said on the behaviour of the photon spectrum; for example, if we assume a power law for the said spectrum, we can try to measure the exponent. Let us give some recent results at sea level; for example, in the photon spectrum for a given energy band, centred at moderate energies (1 GeV), CERNIGOI & POIANI [1954] have found a 2.1 exponent for the differential spectrum. These estimations are not in disagreement with various older ones of 2.5 reached by CLAY [1949] and JANOSSY & ROSSI [1940]. The problem of obtaining absolute values for the frequencies from these experiments is, on the contrary, most uncertain, and we do not intend to pursue the matter further.

We draw attention to another experiment, which is understood to emphasize the behaviour of the said spectra (CHOU [1953]), and which was carried out practically at sea level (60 m). Here we again go back from the dimensions of the electron-photon shower which emerges from a certain thickness of condensed matter to the primary energy which has generated it; we are dealing, therefore, with experiments which are analagous to those made with ionization chambers or in cloud chambers; in this experiment scintillation counters are used for the detection of the shower. The results obtained both for the photon primary and the electron primary refer to an energy band between about 80 MeV and 2,000 MeV, and show that, in an energy interval between 300 MeV and 2,000 MeV, the differential spectra of the photons and electrons which initiate the showers, can be well represented with a power law with exponents of -2.71 and -2.81 respectively; they show, moreover, that the frequencies of the showers initiated by photon and electrons in the abovementioned energy interval are practically the same. If we assemble all the information which we have gathered up to the present, we can arrive at the following conclusions in regard to the low-atmosphere electron-photon component:

(*a*) The integral spectra of photons and electrons in a vertical direction can be represented with functions of the form

$$\left(\frac{A}{1+E/B}\right)^{\gamma}$$

with γ lying between 1.7 and 1.8 and B between 50 and 150 MeV. Before reaching more detailed conclusions, it would be opportune for new data to make their contributions, especially to the

problem of absolute intensity; in this connexion, it would be useful if, in all research studies of this type, people would try to give absolute intensity measurements, by referring to the absolute value of the hard component.

(*b*) The photon-electron ratio never seems to be less than unity, or, to state the matter more clearly, a ratio of about unity at sea level already leads back at the 3,000—3,500 m altitude to a ratio of about two. This fact, should it not be contradicted by future experiments, might constitute a proof that the origin of the bulk of the electron-photon component is to be found in the decay photons of neutral pions. In fact, at mountain altitudes where the electron-photon component is practically wholly of nuclear origin, the ratio is in favour of the photons, while at sea level it is lower, because the muon secondary contribution is relatively more important, and this contribution originates substantially through decay electrons and "knock-on", with the bremsstrahlung contribution being negligible. In conclusion, it is suggested that an experiment which is carried out to determine both the electron-photon ratio and the behaviour of the spectra, by means of the same device, underground, at sea level and at high altitudes, could confidently allow us to prove the descriptive scheme which, at present, we consider valid for the electron-photon component, and, with it, the nuclear origin of part of the component itself through the neutral pions. At the present time this origin is indicated by the photon spectrum at a high altitude, by generation experiments in condensed matter in cloud chambers, and by what we have learned in cosmic rays and in the physics of accelerating machines on nuclear inelastic collisions.

The knowledge of the spectra at various levels would also permit a direct calculation of the global energy dissipated in the electrophotonic component, and would thus allow us to control the worth of the subtraction method, on which to-date all estimations have been based.

2. 4 The total contributions arising from neutral and charged pions

Turning to the balance, let us observe that to the global energy which enters the electron-photonic component through the neutral pions, it would be necessary as usual to apply an angular correction of the same kind as that discussed in connexion with the

charged mesonic component. The two major corrections affect (*a*) angular diffusion of the low-energy electrons due to multiplicative processes during the development of the electron-photon cascade, and to multiple Coulomb scattering, essentially below the critical energy; (*b*) angular correlation in the generation processes in air nuclei between the generating nucleonic component and the neutral pion component which is produced. For the purposes of the present balance, we do not consider it opportune to enter into details about these corrections, because to do so would be to go back to the uncertainties which actually exist, and which we have already mentioned, on the entity of the electron-photon component. We prefer for this reason, then, not to correct the energy figure obtained above and to keep the measurement of

$$256 \text{ MeV. cm}^{-2} \text{ sec}^{-1} \text{ sterad}^{-1}$$

for neutral pion energy.

The comparison between this figure and that given by the total energy dissipated in the production of charged mesons, can be of use in determining the relation between charged and neutral pions, if some hypotheses on the behaviour of the relative production spectra were made. If it is assumed, as the most reasonable hypothesis, given the actual state of things, that the two spectra are alike, we obtain

$$\pi^0/\pi^{\pm} = 0.63$$

as a figure for this relation.

This value is slightly higher than might have been expected on the basis of our knowledge of the elementary generation processes at low energies, and is also greater than what is normally found in cloud chambers in direct experiments (DULLER & WALKER [1954]), the difference is not such as to demand any essential novelties in the generative processes.

2. 5 COMMENTS ON SECONDARY GENERATION PROCESSES

In conclusion, we return for an instant to the secondary generation processes, in order to appraise their importance; we shall consider two typical cases, i.e. the production of neutral mesons from charged ones, and the production of charged mesons from photons. With regard to the first contribution, this is determined by those charged mesons which, instead of disintegrating into muons and neutrinos, undergo nuclear interaction with an air

nucleus which is different from that in which they were generated. If we recall that, for energies which are sufficiently high, the pion generation global spectrum can be represented by the function

$$\gamma^A / E^{\gamma+1}$$

we can at once calculate that the pion spectrum which interacts with air nuclei is given approximately by

$$\frac{\gamma^A}{E^{\gamma+1}} \left(\frac{E}{E + B} \right)$$

A numerical calculation shows that the fraction of the interacting pions is of the order of 1% of their total number, and that the energy which can be reconverted into neutral pions is of the order of 2% of the total energy which goes into charged pions; from this figure it can be understood how the situation cannot be much modified in this way. The situation is, however, different should we think of those secondary processes which can take place within the same air nucleus and which can alter the results of the elementary nucleon-nucleon collision, but this is beyond the limits of our analysis, since what we purpose to establish is the proportion of charged and discharged mesons which escape per air nucleus.

In order to calculate the second contribution, i.e. the fraction of charged mesons which are produced by the photons, we must know the mean cross-section of production, per air nucleus, above the production threshold, which is of the order of $\bar{\sigma} \approx \frac{1}{2} mb$. Then, T_γ being the integral photon track for energies above the threshold, the number of mesons produced is given by:

$$n_\gamma = \int_0^{t_0} dt \int_{W_{\text{th}}}^{\infty} \left(\frac{N}{\varrho} \right) \sigma_\gamma(w)\, \gamma\,(w, t)\, dw \approx \frac{\bar{\sigma}}{A m_H} \cdot T_\gamma .$$

A numerical estimation shows immediately that this number only represents a very small percentage of the total number of pions produced by the nucleonic component.

We may conclude, therefore, that neither of the second-hand generation processes which we have taken into consideration can modify our balance in a substantial manner, and that the phenomenological scheme which we assumed represents the wide generality of the phenomena.

3. The Nucleonic Component

3. 1 Collision losses and star formation

We have now to discuss the contribution of the nucleonic component to the balance. To be more exact, what is left to consider is the nature of the energy dissipated throughout the atmosphere by this component in processes other than the generation of charged or neutral pions. As usual in our current considerations we shall leave out the production of heavy mesons and hyperons. The nucleonic component is fundamentally composed of protons, neutrons and alpha particles, and the energy dissipation to be discussed will consist partly of energy losses through ionization of the protons and alpha-particles and partly of energy losses through nuclear excitation. As regards the first, the quantities to be calculated are

$$\int_{m_P c^2}^{\infty} \int_0^{t_0} \beta_P(E) f_P(E,t)\, dE\, dt \qquad \int_{m_a c^2}^{\infty} \int_0^{t_0} \beta_a(E) f_a(E,t)\, dE\, dt$$

where β_P and β_a indicate energy losses through ionization of the two components, $f_P(E, t)$ and $f_a(E,t)$ representing the relative differential spectra.

We can, however, as usual leave the exact knowledge of the spectra out of consideration, and assume average losses, so that the problem is reduced to a knowledge of the resulting tracks which are respectively

$$T_P = \int_0^{t_0} I_P(t)\, dt \qquad T_a = \int_0^{t_0} I_a(t)\, dt$$

We are thus in a position to estimate the figure of

$$70 \text{ MeV cm}^{-2} \text{ sec}^{-1} \text{ sterad}^{-1}$$

for the said contribution.

The problem of the analysis of the losses by nuclear excitation, being more complicated, deserves some comment. Consider a nucleon which collides with an air nucleus; inside the nucleus one or two elementary collisions against the nucleons will take place, and in these collisions pions will sometimes be created. In consequence of these collisions, and the successive phase of rearrangement, the nucleus can be completely broken-down into its component nucleons, which will escape with different energies, or the

break-down may be partial into one or more residual groups and some nucleons. In order to effect this partial or total break-down, a certain quantity of energy is, of course, necessary, and this is one of the terms to be estimated, to which we have given the name of nuclear "binding energy". If the breakdown were always complete, an estimation would not be difficult, because we know that in such a case the mean energy required would be, in round figures, 10^8 eV per breakdown. In reality the breakdown is often only partial, as is shown by the fact that for such light elements (BARBOUR [1954]) the frequency N of nuclear disintegration as a function of the number n of the ionizing prongs emitted can be represented at balloon and mountain altitudes respectively with the expressions

$$N(>n) = N_0 \exp(-0.4\, n) \qquad N(>n) = N_0 \exp(-0.55\, n)$$

To be able to estimate the effective value, we must know the nature of the ionizing prongs emitted from the stars, and in particular the ratio α/p, because of the high binding energy of the alpha particle GRILLI *et al.* [1954]. We do not possess sufficient data for a calculation of this quantity. Bearing in mind, however, that the average number of prongs per star at mountain altitude (BROWN [1954]) is around 3 for N, it does not seem likely that the figure will go below one half. This binding energy is in practice not recovered, since the low-energy protons stop through ionization and the slow neutrons are captured mainly according to reaction N (n, p) C; it would be interesting to be able to calculate it correctly, since it is above all important for the omnidirectional balances founded on ionization chamber data. In our balance, which is founded fundamentally on counter data, and for the nucleonic component on the frequency of the nuclear disintegrations, there are other energy terms which we must bear in mind. Normally, the frequency of nuclear disintegration throughout the atmosphere is judged on the basis of the frequency of the disintegration processes themselves which take place in a nuclear plate, where the necessary energy for producing a star with at least three ionizing prongs is of the order of 100 MeV; this means that, if we take the data given by the photographic plates as the basis for our calculations, we shall exclude the nucleonic component with an energy less than this limit from our measurements. An improvement in the situation can be made by carrying out the

measurements in the gas of a cloud chamber (BROWN [1954]), because then the above-mentioned cut-off is considerably lowered, to an energy of the order of 20 MeV, since all nuclear interactions, in which a global energy greater than 8 MeV is dissipated within the chamber are registered. Measurements analogous to these are obtained by measuring ionization bursts in a fast ion-chamber with a low cut-off (BRIDGE & ROSSI [1947]). In a previous summary (PUPPI & DALLAPORTA [1952]), we traced a height curve for these nuclear disintegrations, which, for what concerned absolute intensity, was based on the frequency of disintegrations registered in photographic plates, but which was also in agreement, as regards the law of growth with height, with the disintegrations measured in other ways. We said there that the attenuation of production of emulsion stars with at least three prongs could be represented in the atmosphere by a law of the type:

$$N_{em} = 2500 \exp(-t/140) \text{ cm}^{-3} \text{ day}^{-1} .$$

Reducing this to stars in air on the basis of the ratio between the geometrical cross-sections, i.e. by means of the formula

$$N_{air} (\text{g}^{-1} \text{ sec}^{-1}) = 4.8 \times 10^{-6} N_{em} (\text{cm}^{-3} \text{ day}^{-1})$$

we find the equivalent of these disintegrations in air. The datum is not very significant, both because the reduction with the geometrical cross sections certainly represents an overestimate, and, above all, because the behaviour of the disintegrations in the air and in emulsion is fundamentally different; the datum on the disintegration in a cloud chamber seems more significant. Numerical estimates for both cases (BROWN [1954]) show how the frequency in the cloud chamber is higher than that calculated on the basis of the plate data. But these data too represent only one part of nuclear disintegrations, because they lack those with emission of neutrons alone, and those in which the energy dissipated by ionizing sprongs is lower than the cut-off. We cannot estimate such a contribution, but we consider that it is important, a point of view which is further strengthened from the analysis of the slow neutrons.

Let us take as a basis the absolute frequencies for stars as a function of N, and, using the height curve already mentioned, integrate this frequency over the whole atmosphere: we obtain a global number of disintegrations in a small atmospheric column of unit section per second equal to about

$3\ \text{cm}^{-2}\ \text{sec}^{-1}$.

If we knew how to increase this figure in order to take the undetected disintegrations into account, and if we knew the mean energy for each disintegration which is not recovered, because it is either a matter of nuclear binding energy, or of kinetic energy of low-energy particles, we should be in a position to define this term of the balance. For each of the nuclear disintegrations now examined, we must not, of course, bear in mind only the ionizing particles, because we know that neutrons are also emitted, together with the ionizing particles. On the contrary, it is known that at mountain altitudes (ORTEL [1954]) for every nuclear disintegration with N ionizing particles, there are about $1.5\,N$ neutrons, which would lead to $4.5\ \text{cm}^{-2}\ \text{sec}^{-1}$ as a total production of neutrons in the unit atmospheric column. Of course this figure does not take into account disintegrations in which neutrons only are produced, or of those which are excluded by the selection device for ionizing particles. We therefore need to control these figures in another way, and, in order to do so, we turn to the slow neutrons.

3. 2 SLOW NEUTRON DATA

We recall how during recent years our knowledge on the behaviour of slow neutrons in the atmosphere has increased in a remarkable manner. Many experiments have been carried out to determine the behaviour with height and absolute intensity, variations with latitude, and variations with time (SIMPSON [1949]). As a result we are well informed for the latitude in question on the frequency of the captures in air of slow neutrons produced by cosmic radiation, and on the variation of this frequency with height. The origin of these slow neutrons in the atmosphere must be sought in the nuclear collisions produced by primary and secondary nucleonic radiation with the nuclei in the atmosphere. More precisely, these slow neutrons originate principally from the low-energy stars, where they are emitted with modest energies of the order of some MeV; through various collisions with air nuclei, they are slowed down until they reach thermal energy; in these conditions they are captured by N in the reaction $N^{14}(n, p)C^{14}$.

We measure the number of thermal neutrons captured per gram of air at various levels, what is of interest for the balance is, on the contrary, the number of neutrons produced in nuclear inter-

actions, because they do not all reach the thermal condition. There is a fraction of them which escapes from the atmosphere (albedo) measurable as about 10%, and a very marked part which does not reach thermal energies having first undergone nuclear interactions. The theoretical problem has been treated by many authors from 1940 onwards (BETHE *et al.* [1940]); according to such an analysis, in order to justify the number of captures in air per atmospheric unit column per second, which measures

$$3.5 \text{ cm}^{-2} \text{ sec}^{-1},$$

(KOUTS & YUAN [1952]), it is necessary to suppose that the number of neutrons produced is much greater. If we assume for the sake of simplicity, that the neutrons are generated in nuclear disintegrations with kinetic energy of 4 MeV, we find that the number (GALLI [1953] of neutrons produced must be

$$(22 \pm 4)\text{cm}^{-2} \text{ sec}^{-1}.$$

Continuing this hypothesis, it is possible to interprete the variation with height in the atmosphere of the neutron capture frequency by admitting a generation function for neutrons at 4 MeV of the type:

$$0{,}218 \left[\exp\left(-t/157\right) - 0.8 \exp\left(-t/70\right)\right] \text{ g}^{-1} \text{ sec}^{-1}.$$

This expression, as we can see, shows a very marked transition effect. Since we are at northern latitudes, this means that the slow neutrons are essentially produced in low-energy nuclear disintegrations, for this transition effect emphasizes the contribution of nucleons of energy below the magnetic cut-off to the generation function for slow neutrons. Figure 7 shows the growth of captures of slow neutrons and the behaviour of the generation function at 4 MeV.

From the above-mentioned results we can at once proceed to a calculation of the binding energy which must be supplied for the production of neutrons alone, taking as a basis the binding energy of the last nucleon in N and O, which appears as $\sim$11.5 MeV.

We think it more opportune to apply ourselves to the binding energy of the last nucleon, instead of to the mean binding energy per nucleon, since we consider the production of alpha particles in the disintegration air nuclei to be likely, and reject the possibility of there being always a complete breakdown; moreover, the localization of production in low-energy events is coherent with this assumption.

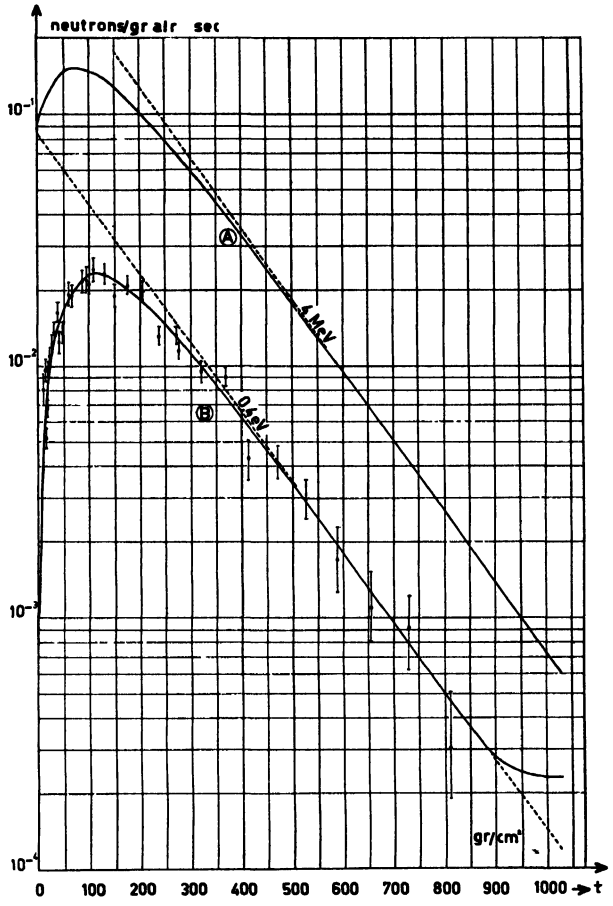

Fig. 7 – Slow neutron capture, (B), and neutron generation function, (A), in the atmosphere.

3. 3 Comparison between the stars and neutron captures

If we compare the results obtained in the two preceding paragraphs, we at once see that the results do not agree. What happens is that, while, from the frequency of the disintegrations with ionizing particles, we should have expected to find a neutron production frequency in the usual air column of 4.5 per sec., with the thermal neutron captures in the air as a basis, we reach a figure which is five times greater. If we consider this estimate reliable, we must conclude that the major source of the slow neutrons is not to be found in nuclear disintegrations with ionizing particles, but probably takes place in events in which only a

neutron is emitted, and, therefore, principally in processes of the type (p, n) and (n, 2n) or in processes in which the energy found in ionizing particles is extremely small. It is true that the result also depends on the energy with which we imagine the neutrons to be produced, but it seems rather improbable that a much lower production energy could be adopted. It is easy to see that the (γ, n) processes can be overlooked; in fact only γ-rays with an energy near the giant resonance, i.e. those with an energy included between 19 and 26 MeV, could in practice contribute; but the cross section is too small even in this region (8mb per air nucleus) to make an effective contribution (FERGUSON *et al.* [1954]). We must then conclude that it is a matter of disintegrations which are produced by the low-energy nucleonic component. On the basis of the results quoted, we ought to conclude that only 1/5 of the slow neutrons come from those disintegrations which contain ionizing particles, while 4/5 escape our control. For this part there is a contribution of at least 270 MeV cm^{-2} sec^{-1} to the energy. Adding a global estimation of 150 MeV cm^{-2} sec^{-1} in the disintegrations with ionizing particles for the energy dissipated in low-energy particles which is not recoverable into the present balance, we have a total:

$$720 \text{ MeV. cm}^{-2} \text{ sec}^{-1}$$

The fraction of this energy to be attributed to the vertical beam, on which we are making the balance, is, as we know, $\sim I/\pi$, whence we obtain for this contribution

$$230 \text{ MeV. cm}^{-2} \text{ sec}^{-1} \text{ sterad}^{-1}.$$

We would point out that the figure proposed for those neutrons which do not originate from visible disintegrations is a minimum one, since, in order to extract it, we merely added the energy of 4 MeV at production to the mean binding energy of the last nucleon (11.5 MeV for each neutron). We are not thus taking into account the inelastic losses of neutrons generated with energies greater than 4 MeV; we have, moreover, not considered the eventual low-energy particles (protons, alpha and deuterons) which are generated together with these neutrons.

As regards the visible disintegrations, we do not think that we have gone too far in our estimate of the disintegration energy, at least as it effects of the present balance. In fact, the average number of ionizing particles emitted per disintegration (BROWN

[1954]) is about 3, and the particles produced are to be considered as lost to the effects of the present balance should their energy be not considerably greater than 100 MeV for reasons of energy loss through ionization.

The figures presented are of course very uncertain, and the whole problem of the low-energy nucleonic component would merit a more profound examination in order that the situation might be improved.

4. Conclusion

As a conclusion of our analysis on the vertical beam of cosmic rays at 50° North, let us summarize and tabulate the various contributions to the balance.

Energy dissipated through production of charged pions	409 MeV. cm^{-2} sec^{-1} $sterad^{-1}$	
Energy dissipated through production of neutral pions	256	,,
Energy dissipated by the nucleonic component	300	,,
Total	965	,,

The figure obtained will always remain below that estimated for the incoming energy transported by the primary component, which, is around 1400 MeV. cm^{-2} sec^{-1} $sterad^{-1}$. Owing to the uncertainties which are still to be found in the balance, especially as regards the low-energy nucleonic component and the contribution to the nucleonic cascade of particles other than those considered in the present balance, we do not consider it yet possible to affirm that there is a real conflict of results.

It would be very interesting to construct balances of a kind similar to the one presented here at other latitudes; an attempt made in such a sense at the equator (BENZI [1954]) has brought to our notice that there exists, even at that latitude, a difference between the incoming power flux and the power flux dissipated in the atmosphere.

A further improvement might consist in passing from the vertical balance to the omnidirectional one, by taking advantage of the zenithal dependencies of the various components at the different levels. Moreover, the uncertainties on the data in the high atmosphere being what they are, a very interesting type of

control could be that of carrying out a balance between two levels within the atmosphere.

All this concerns directional balances, which are essentially founded on data obtained from counters, and in which an attempt is made at distinguishing the physical components. There exists, however, another way of attacking the problem, which has been known for some time and which consists in measuring the total ionization induced by cosmic rays through the whole atmosphere.

It is evident that experimental results of this kind must be coherent with directional experiments, and that therefore the total ionization measured in a unit column of atmosphere must coincide with what can be calculated on the basis of directional balances.

From our results we can in particular derive an indication for a comparison of such a type by subdividing the total energy in the following way

Energy which goes in ionization	615	MeV cm^{-2} sec^{-1} $sterad^{-1}$
,, ,, ,, ,, neutrinos	232	,,
,, set against the binding of nuclei	80	,,
Residual energy at sea level	38	,,
	965	,,

The figure relative to the energy dissipated through ionization is obtained here by difference. It agrees with what can be extracted from direct measurements (NEHER [1952]).

ACKNOWLEDGEMENTS

The author wishes to thank Professors B. Rossi, M. Schein, S. F. Singer, J. G. Wilson and Dr. Galli for stimulating discussions and help given in preparing this article.

REFERENCES

BARBOUR, I. G., 1954, Phys. Rev., **93**, 535.

BARONI, G., G. CORTINI, A. MILONE, L. SCARSI and G. VANDERHAEGHE, 1952, Nuovo Cim., **9**, 867.

BENZI, V., 1954, Nuovo Cim., **11**, 686.

BERETTA, E., I. FILOSOFO, B. SOMMACAL and G. PUPPI, 1953, Nuovo Cim., **10**, 1354.

BETHE, H., C. KORFF and G. PLACZEK, 1940, Phys. Rev., **57**, 573.

BRIDGE, H. and B. ROSSI, 1947, Phys. Rev., **71**, 379.

BRINI, D., O. RIMONDI and I. FILOSOFO, 1952, Nuovo Cim., **9**, 505.

BROWN, W. W., 1954, Phys. Rev., **93**, 528.

CARLSON, A., J. E. HOOPER and D. T. KING, 1950, Phil. Mag., **41**, 701.

CERNIGOI, G. and G. POIANI, 1954, Nuovo Cim., **11**, 41.

CHOU, C. N., 1953, Phys. Rev., **90**, 473.

CLARK, M. A., 1952, Phys. Rev., **87**, 87.

CLAY, J., 1949, Physica, **14**, 569.

CONVERSI, M., 1950, Phys. Rev., **79**, 749.

DEL ROSARIO, L. and J. DAVILA-APONTE, 1952, Phys. Rev., **88**, 998.

DULLER, N. M. and W. D. WALKER, 1954, Phys. Rev., **93**, 215.

DYMOND, E. G., 1954, Progress in Cosmic Ray Physics, Vol. II (Amsterdam; North Holland Publishing Co.), Ch. III.

FERGUSON, G. A., J. HALPERN, R. NATHANS and P. F. YERGIN, 1954, Phys. Rev., **95**, 776.

FERMI, E., 1954, Lectures at the Varenna School.

FILOSOFO, I., E. POHL and J. POHL-RULING, 1954, Nuovo Cim., **12**, 809.

GALLI, M., 1953, Nuovo Cim., **10**, 1187.

GEORGE, E. P., 1952, Progress in Cosmic Ray Physics, Vol. I (Amsterdam; North Holland Publishing Co.), Ch. VII.

GLASER, D. A., B. HAMERMESH and G. SAFONOV, 1950, Phys. Rev., **80**, 625.

GRILLI, M., P. E. HODGSON, M. LADU and B. VITALE, 1954, Nuovo Cim., **12**, 889.

HABER-SCHAIM, U. and G. YEKUTIELI, 1954, Nuovo Cim., **11**, 172, 683.

HAZEN, W. E., 1944, Phys. Rev., **65**, 67.

JANOSSY, L. and B. ROSSI, 1940, Proc. Roy. Soc., **A175**, 88.

KOUTS, H. J. and L. C. L. YUAN, 1952, Phys. Rev., **86**, 128.

KRAUSHAAR, W. L., 1949, Phys. Rev., **76**, 1045.

LICHTENSTEIN, P. G., 1954, Phys. Rev., **93**, 858.

MESSEL, H., 1954, Progress in Cosmic Ray Physics, Vol. II (Amsterdam; North Holland Publishing Co.), Ch. IV.

MICHEL, L., 1952, Progress in Cosmic Ray Physics, Vol. I (Amsterdam; North Holland Publishing Co.), Ch. III.

MOREWITZ, H. A. and M. H. SHAMOS, 1953, Phys. Rev., **92**, 134.

NEHER, H. V., 1952, Progress in Cosmic Ray Physics, Vol. I (Amsterdam; North Holland Publishing Co.), Ch. V.

OLBERT, S., 1954, Phys. Rev., **96**, 1400.
ORTEL, W. G. C., 1954, Phys. Rev., **93**, 561.
OWEN, B. G. and J. G. WILSON, 1951, Proc. Phys. Soc., **A64**, 417.
OWEN, B. G. and J. G. WILSON, 1955, Proc. Phys. Soc., **A68**, 409.
PALMATIER, E. D., 1952, Phys. Rev., **88**, 761.
PETERS, B., 1952, Progress in Cosmic Ray Physics, Vol. I (Amsterdam; North Holland Publishing Co.), Ch. IV.
PUPPI, G. and N. DALLAPORTA, 1952, Progress in Cosmic Ray Physics, Vol. I (Amsterdam; North Holland Publishing Co.), Ch. VI.
PUPPI, G., 1953, Supplemente Nuovo Cim., **10**, 115.
ROSSI, B., 1948, Rev. Mod. Phys., **20**, 537.
ROSSI, B., 1952, High Energy Particles (New York; Prentice Hall Inc.).
SANDS, M., 1950, Phys. Rev., **77**, 180.
SIMPSON, J. A., 1949, Phys. Rev., **76**, 1750.
SMITH, F. M., W. BIRNBAUM and W. H. BARKAS, 1953, Phys. Rev., **91**, 765.
YORK, C. M., 1952, Phys. Rev., **85**, 998.

AUTHOR INDEX

ADAMOVITCH, M. I.
see L. K. Eidus.

ADAMS, R. V.
1949: ———, C. D. Anderson and E. W. Cowan, Rev. Mod. Phys., **21**, 72. *77, 78.*

ALFORD, W. L.
1953: ——— and R. B. Leighton, Phys. Rev., **90**, 622. *208.*
see R. B. Leighton.

AMALDI, E.
1953: ———, L. Mezzetti and G. Stoppini, Nuovo Cim., **10**, 803, *117.*
1953: ———, C. Castagnoli, G. Cortini and A. Manfredini, Nuovo Cim., **10**, 1351. *291.*
1954a: ——, C. D. Anderson, P. M. S. Blackett, W. B. Fretter, L. Leprince-Ringuet, B. Peters, C. F. Powell, G. D. Rochester, B. Rossi and R. W. Thompson, Nuovo Cim., **11**, 213; Nature, Lond., **173**, 123. *146.*
1954b: ——, E. Fabri, F. T. Hoang, W. O. Lock, L. Scarsi, B. Touschek and B. Vitale, Nuovo Cim., **12**, suppl., 419. *151, 152, 155.*
1954c: ——, C. Castagnoli, G. Cortini and C. Franzinetti, Nuovo Cim., **12**, 668. *208.*
——————— *166, 211*

ANDERSON, C. D.
1953: ———, E. W. Cowan, R. B. Leighton and V. A. J. van Lint, Phys. Rev., **92**, 1089. *294.*
see R. V. Adams, E. Amaldi, R. B. Leighton, V. A. J. van Lint, A. J. Seriff.

ANISHENKO, U. V.
1952: ———, G. T. Zatsepin, I. L. Rosental and L. I. Saritcheva, J. Exp. Theor. Phys., **22**, 143. *86, 107.*

ANNIS, M.
see H. S. Bridge.

APPA RAO, M. V. K.
1955: ——— and S. Mitra, Proc. Ind. Acad. Sci., **41**, 30. *171.*

ARLEY, N.
1938: ——, Proc. Roy. Soc., **A168**, 519. *22.*

ARMENTEROS, R.
1951a: ——, K. H. Barker, C. C. Butler, A. Cachon and A. H. Chapman, Nature, Lond., **167**, 501. *258.*
1951b: ——, K. H. Barker, C. C. Butler and A. Cachon, Phil. Mag., **42**, 1113. *270, 280, 281, 282, 286, 297, 303.*
1952: ———, K. H. Barker, C. C. Butler, A. Cachon and C. M. York, Phil. Mag., **43**, 597. *215, 293.*

1953: ———, K. H. Barker, C. C. Butler, M. S. Coates and M. G. Sowerby, Phil. Mag., **44**, 861. *280, 286.*
1955: ———, B. Gregory, A. Hendel, A. Lagarrigue, L. Leprince-Ringuet, F. Muller and C. Peyrou, Nuovo Cim., **1**, 915. *194.*
see J. Podolanski.
ARNOLD, W. H.
1955: ———, J. Ballam and G. T. Reynolds, Phys. Rev., **100**, 295. *223.*
see A. L. Hodson.
ASTBURY, J. P.
1953: ———, J. S. Buchanan, G. D. James, D. D. Millar, J. A. Newth, D. I. Page, A. B. Sahiar and A. Rytz, Phil. Mag., **44**, 352. *309.*
1954: ———, Proc. Padua Conference. *310.*
AUGER, P.
1938: ———, R. Maze and T. Grivet-Meyer, C. R. Acad. Sci. Paris, **206**, 1721. *3.*
1938: ———, and R. Maze, C. R. Acad. Sci. Paris, **207**, 228.
1939: ———, R. Maze, P. Ehrenfest and A. Freon, J. Phys. Radium, **10**, 39. *3.*
1939: ———, R. Maze and J. Robley, C. R. Acad. Sci. Paris, **208**, 1641. *3.*
1939: ———, P. Ehrenfest, R. Maze, J. Daudin, J. Robley and A. Freon, Rev. Mod. Phys., **11**, 288. *3.*
1942: ——— and J. Daudin, Phys. Rev., **61**, 91. *73.*
1945: ——— and J. Daudin, J. Phys. Radium, **6**, 233. *57.*
BALLAM, J.
1953: ———, D. R. Harris, A. L. Hodson, R. R. Rau, G. T. Reynolds, S. B. Treiman and M. Vidale, Phys. Rev., **91**, 1019. *310, 312, 328.*
see A. L. Hodson, W. H. Arnold.
BARBOUR, I. G.
1954: ———, Phys. Rev., **93**, 535. *379.*
BARKAS, W. H.
see F. M. Smith.
BARKER, K. H.
1952: ———, C. C. Butler, M. G. Sowerby and C. M. York, Phil. Mag., **43**, 1201. *182, 221, 223.*
1953: ———, Proc. Duke Univ. Conference, II–18, 20. *165, 244, 322.*
1954: ———, Proc. Roy. Soc., **A221**, 328. *301, 303, 304.*
see R. Armenteros.
BARKER, P. R.
1955a: ——, D. M. Binnie, B. D. Hyams and R. J. Rout, Phil. Mag., **46**, 300. *226.*
1955b: ——, D. M. Binnie, B. D. Hyams, R. J. Rout and J. Shepherd, Phil. Mag., **46**, 307. *226.*
BARONI, G.
1952: ———, G. Cortini, A. Milone, L. Scarsi and G. Vanderhaeghe, Nuovo Cim., **9**, 867. *372.*

BARRETT, P. H.
1952: ———, L. M. Bollinger, G. Cocconi, Y. Eisenberg and K. Greisen, Rev. Mod. Phys., **24**, 133. *42, 48, 69, 114, 128, 135.*
1954: ———, G. Cocconi, Y. Eisenberg and K. Greisen, Phys. Rev., **95**, 1571. *124.*
——————— *165, 233.*
BARTLETT, M. S.
1953: ———, Phil. Mag., **44**, 249, 1407. *208, 209, 222, 290.*
BASSI, P.
1952: ———, A. M. Bianchi, C. Cadorin and C. Manduchi, Nuovo Cim., **9**, 1037. *78.*
1953: ———, G. Clark and B. Rossi, Phys. Rev., **92**, 441. *77, 79.*
BELENKY, S. Z.
1941: ———, C. R. Acad. Sci. USSR, **30**, 608. *12, 17.*
1944: ———, J. Phys. USSR, **8**, 9. *12, 20.*
see I. Tamm.
BELLIBONI, G.
1954: ———, B. Sechi and B. Vitale, Nuovo Cim.,**12**, suppl., 195, *165*
——————— *149.*
BENZI, V.
1954: ———, Nuovo Cim., **11**, 686. *385.*
BERETTA, E.
1953: ———, I. Filosofo, B. Sommacal and G. Puppi, Nuovo Cim., **10**, 1354. *365.*
BERNARDINI, G.
1954: ——— and E. Segre, Proc. Roy. Soc., **A221**, 413. *330.*
BERNSTEIN, I. B.
1950: ———, Phys. Rev., **80**, 995. *11.*
BETHE, H.
1940: ———, C. Korff and G. Placzek, Phys. Rev., **57**, 573. *382.*
BHABHA, H. J.
1935: ———, Proc. Roy. Soc., **A152**, 559. *11.*
1948: ——— and S. K. Chakrabarty, Phys. Rev., **74**, 1352, *12, 16.*
1950: ——— and A. Ramakrishnan, Proc. Ind. Acad. Sci., **32**, 141, *19.*
1953: ———, Proc. Roy. Soc., **A219**, 293. *52, 93.*
BIANCHI, A. M.
see P. Bassi.
BIEHL, A. T.
1951: ——— and H. V. Neher, Phys. Rev., **83**, 1169. *62, 64, 74, 81.*
BIERMANN, L.
1953a: ——, Ann. Rev. Nuclear Sci., **2**, 335. *118.*
1953b: ——, Vorträge über Kosmische Strahlung (ed. Heisenberg, Berlin, Springer) *118.*
BINNIE, D. M.
see P. R. Barker.
BIRNBAUM, W.
see F. M. Smith.

Biswas, S.
see V. D. Hopper.
———— *165*
Bjornerud, E. K.
see C. M. York.
Blackett, P. M. S.
1936: ———, Proc. Roy. Soc. **A154**, 564. *256.*
1936: ——— and R. B. Brode, Proc. Roy. Soc., **A154**, 573. *259.*
see E. Amaldi.
Blatt, J. M.
1949: ———, Phys. Rev., **75**, 1584. *45, 69.*
Block, M. M.
1954: ———, D. T. King and W. W. Wada, Phys. Rev., **96**, 1627. *10.*
Bollinger, L. M.
see P. H. Barrett.
Bonetti, A.
1953: ———, R. LeviSetti and B. Locatelli, Proc. Bagnères Conf., 171. *291.*
1953a: ——, R. LeviSetti, M. Panetti and G. Tomasini, Proc. Bagnères Conf., 182. *228, 233, 234.*
1953b: ——, R. LeviSetti, M. Panetti and G. Tomasini, Nuovo Cim., **10**, 1736. *228, 233, 234.*
1953c: ——, R. LeviSetti, M. Panetti and G. Tomasini, Nuovo Cim., **10**, 345. *228.*
———— *165, 233*
Borsellino, A.
1950: ———, Nuovo Cim., **7**, 323, 638, 700. *20, 29, 32.*
Bothe, W.
1937: ——— —, W. Gentner, H. Maier-Leibnitz, W. Maurer, E. Wilhelmy and K. Schmeiser, Physik. Zeits., **38**, 964. *3.*
see K. Schmeiser
Bradt, H. L.
see M. F. Kaplon.
Branch, G. M.
1951: ———, Phys. Rev., **84**, 147. *85, 96.*
1951: ——— and G. Cocconi, Phys. Rev., **84**, 146. *105.*
Bridge, H. S.
1947: ——— and B. Rossi. Phys. Rev., **71**, 379. *373, 380.*
1951: ——— and M. Annis, Phys. Rev., **82**, 445.
1952: ———, H. Courant and B. Rossi, Phys. Rev., **85**, 159.
1953: ——— —, Proc. Bagnères Conf., 244, *306, 309.*
1953: ———, H. Courant, H. DeStaebler and B. Rossi, Phys. Rev., **91**, 1024. *202.*
1953a: ——, C. Peyrou, B. Rossi and R. Safford, Phys. Rev., **91**, 362 *281, 282, 284, 286, 287, 288, 293, 306, 322, 323, 324.*
1953b: ——, C. Peyrou, B. Rossi and R. Safford, Phys. Rev., **90**, 921.
1954: ———, H. Courant, B. Dayton, H. DeStaebler, B. Rossi, R. Safford and D. Willard, Nuovo Cim., **12**, 81. *183.*

1955: ———, H. DeStaebler, B. Rossi and B. V. Sreekantan, Nuovo Cim., **1**, 874. *194.*

BRINI, D.

1952: ———, O. Rimondi and I. Filosofo, Nuovo Cim., **9**, 505. *346.*

BROADBENT, D.

1947: ——— and L. Janossy, Proc. Roy. Soc., **A191**, 557. *110.*

1950: ———, E. W. Kellermann and M. A. Hakeem, Proc. Phys. Soc. **A63**, 864. *56, 58.*

BRODE, R. B.

see P. M. S. Blackett.

BROWN, K.

see M. Schein.

BROWN, R.

1949: ———, U. Camerini, P. H. Fowler, H. Muirhead, C. F. Powell and D. Ritson, Nature, Lond., **163**, 82. *149.*

BROWN, W. W.

1949: ——— and A. S. McKay, Phys. Rev., **76**, 1034, *76, 78, 85, 86, 94, 96, 107.*

1950: ——— and A. S. McKay, Phys. Rev., **77**, 342. *105.*

1954: ———, Phys. Rev., **93**, 528. *379, 380, 384.*

BRUECKNER, K. A.

1952: ——— and R. W. Thompson, Phys. Rev., **87**, 390. *269, 283, 285.*

BUCHANAN J. S.

1954: ———, W. A. Cooper, D. D. Millar and J. A. Newth, Phil. Mag., **45**, 1025, *182, 221, 223.*

see J. P. Astbury.

BUDINI, P.

1951: ———, Nuovo Cim., **8**, 446. *74, 84, 86.*

1953: ——— and G. Molière, Vorträge über Kosmische Strahlung (ed. Heisenberg, Berlin, Springer) *117.*

BURWELL, J. R.

see R. W. Thompson, Y. B. Kim.

BUSKIRK, A. V.

see R. W. Thompson.

BUTLER, C. C.

see R. Armenteros, K. H. Barker, G. D. Rochester, J. G. Wilson.

CACHON, A.

see R. Armenteros.

CADORIN, C.

see P. Bassi.

CALDWELL, D. O.

1955: ———, Nuovo Cim., **2**, 183; see also Phys. Rev., **100**, 291. *199, 200.*

CAMAC, M.

1952: ———, Phys. Rev., **88**, 745. 10.

CAMERINI, U.

see R. Brown.

CAMPBELL, I. D.

1952: ——— and J. R. Prescott, Proc. Phys. Soc., **A65**, 258, *44, 45.*

CARLSON, A.
1950: ———, J. E. Hooper and D. T. King, Phil. Mag., **41**, 701. *372.*
CARTER, R.S.
1954: ——— and J. C. Street, Rev. Sci. Instr., **25**, 627. *260.*
CASTAGNOLI, C.
1950: ———, A. Gigli and S. Sciuti, Nuovo Cim., **7**, 307. *73.*
see E. Amaldi.
——————— *234*
CECCARELLI, M.
1953: ——— and M. Merlin, Proc. Bagnères Conf., 183. *234.*
1953: ———, Nuovo Cim., **10**, 1207.
1954: ———, M. Grilli and B. Vitale, Proc. Padua Conf. *150, 291.*
1954: ———, N. Dallaporta, M. Merlin, G. Quareni and G. T. Zorn, Proc. Roy. Soc., **A221**, 386. *155, 169.*
——————— *234*
CERNIGOI, G.
1954: ——— and G.Poiani, Nuovo Cim., **11**, 41. *374.*
CHALOUPKA, P.
1954: ———, Phys. Rev., **96**, 1709. *36.*
CHAKRABARTY, S.
see H. J. Bhabha.
CHANDRASEKHAR, S.
1953: ——— and E. Fermi, Astrophys, J., **118**, 113. *120.*
CHAPMAN, A. H.
see R. Armenteros.
CHESTON, W.
1953: ——— and H. Primakoff, Phys. Rev., **92**, 1537.
see H. Primakoff.
CHOU, C. N.
1953: ———, Phys. Rev., **90**, 473. *374.*
CHOWDHURI, B.
1948: ———, Nature, Lond., **161**, 680. *57, 98.*
1950: ———, Proc. Phys. Soc., **A63**, 165. *95.*
1952: ———, R. C. Saxena and A. Subramanian. Proc. Ind. Acad. Sci., **A36**, 457. *96, 103.*
CITRON, A.
1952: ———, Z. Naturforsch., **7a**, 712. *72, 73, 84, 123, 124.*
CLARK, G.
see P. Bassi.
CLARK, M. A.
1952: ———, Phys. Rev., **87**, 87. *359.*
CLAY, J.
1949: ———, Physica, **14**, 569. *374.*
CLEMENTEL, E.
1948: ——— and L. Fabbrichesi, Nuovo Cim., **5**, 78. *15.*
1949: ——— and L. Fabbrichesi, Nuovo Cim., **6**, 399. *15, 27, 33.*
see N. Dallaporta.

COATES, M. S.
see R. Armenteros.
COCCONI, G.
1943: ———, A. Loverdo and V. Tongiorgi, Nuovo Cim., **1**, 314. *54.*
1944: ———, A. Loverdo and V. Tongiorgi, Nuovo Cim., **2**, 14. *54.*
1947: ———, Phys. Rev., **72**, 964. *84.*
1949: ——— and V. C. Tongiorgi, Phys. Rev., **75**, 1058. *56, 58, 59, 71.*
1949a: ———, V. C. Tongiorgi and K. Greisen, Phys. Rev., **75**, 1063. *60, 94, 98, 100, 113, 115.*
1949b: ———, V. C. Tongiorgi and K. Greisen, Phys. Rev., **76**, 1020. *37, 38, 39, 95, 98, 135.*
1950: ——— and V. C. Tongiorgi, Phys. Rev., **79**, 730. *86, 105, 107.*
1951: ——— and A. Silverman, Phys. Rev., **84**, 1062. *330.*
1954a: ———, Phys. Rev., **93**, 1107. *53, 86, 87.*
1954b: ———, Phys. Rev., **93**, 646 and **95**, 1705. *35.*
see P. H. Barrett, G. M. Branch.
COHN, H. O.
1953: ———, L. R. Etter and R. W. Thompson, Phys. Rev., **91**, 445. *264.*
see R. W. Thompson.
CONVERSI, M.
1950: ———, Phys. Rev., **79**, 749. *353.*
COOL, R. L.
1951: ——— and O. Piccioni, Phys. Rev., **82**, 306. *107, 109.*
see O. Piccioni.
COOPER, W. A.
see J. S. Buchanan.
CORTINI, G.
see E. Amaldi, G. Baroni.
COURANT, H.
1955: ———, Phys. Rev., **99**, 282. *202.*
see H. S. Bridge.
COWAN, E. W.
1954: ———, Phys. Rev., **94**, 161. *207, 264, 294, 319.*
see R. V. Adams, C. D. Anderson, R. B. Leighton, V. A. van Lint, A. J. Seriff.
CRANSHAW, T. E.
1954: ——— and W. Galbraith, Phil. Mag., **45**, 1109. *124.*
CRESTI, M.
1953: ———, A. Loria and G. Zago, Nuovo Cim., **10**, 779. *57, 78.*
CRUSSARD, J.
1954: ———, M. F. Kaplon, J. Klarmann and J. H. Noon, Phys. Rev., **93**, 253. *156, 166.*
——— ——— *165, 166, 244*
DAHANAYAKE, C.
1954: ———, C. P. François, Y. Fujimoto, P. Iredale, C. J. Waddington and M. Yasin, Phil. Mag., **45**, 1219. *165, 178.*
——— ——— *165, 232*

DALITZ, R. H.
1953a: ——, Proc. Bagnères Conf., 236. *153*, *156*.
1953b: ——, Phil. Mag., **44**, 1068. *153*, *154*.
1953c: ——, Proc. Phys. Soc., **A66**, 710. *156*.
DALLAPORTA, N.
1946: —— and E. Clementel, Nuovo Cim., **3**, 235. *15*.
1947: —— and G. Poiani, Nuovo Cim., **4**, 1, *15*.
1954: —— and G. Lanza, Nuovo Cim., **12**, suppl., 260. *238*.
see M. Ceccarelli, G. Puppi.
DANIEL, R. R.
1954: —— and Yash Pal, Proc. Ind. Acad. Sci., **A40**, 114. *151*.
1955: ——, E. C. George and B. Peters, Proc. Ind. Acad. Sci., **A41**, 45. *165*, *171*, *232*.
DANYSZ, M.
1953: —— and J. Pniewski, Phil. Mag., **44**, 348. *322*.
1953: ——, Bull. Acad. Polonaise Sci., **1**, 177. *291*.
DAUDIN, A.
1949: —— and J. Daudin, J. Phys. Radium, **10**, 394. *73*.
1953: —— and J. Daudin, J. Atmos. Terr. Phys., **3**, 245; J. Phys. Radium, **14**, 169; Proc. Bagnères Conf. *59*, *72*, *73*, *84*, *123*, *124*, *126*, *127*.
1954: ——, Thesis, Paris.
DAUDIN, J.
1943: ——, C. R. Acad. Sci. Paris, **216**, 483. *54*.
1944a: ——, C. R. Acad. Sci. Paris, **218**, 830.
1944b: ——, C. R. Acad. Sci. Paris, **218**, 882. *54*.
1945: ——, J. Phys. Radium, **6**, 302. *76*, *78*.
see P. Auger, A. Daudin, A. Loverdo.
DAVILA-APONTE, J.
see L. del Rosario.
DAVIS, L.
1951: ——, Phys. Rev., **81**, 890. *119*.
1951: —— and J. L. Greenstein, Astrophys. J., **114**, 206. *119*.
1954: ——, Phys. Rev., **96**, 743. *120*, *121*.
DAVIS, W. P.
1954: ——, W. E. Hazen and R. E. Heineman, Nuovo Cim., **12**, 233. *48*.
DAYTON, B.
1953: —— and D. Willard, Phys. Rev., **91**, 348. *306*.
see H. S. Bridge.
DEBENEDETTI, A.
1954: ——, G. M. Garelli, L. Tallone and M. Vigone, Nuovo Cim., **12**, 952. *234*, *236*.
—— *166*
DEL ROSARIO, L.
1952: —— and J. Davila-Aponte, Phys. Rev., **88**, 998. *347*.
DESTAEBLER, H. C.
1954: ——, Phys. Rev., **95**, 1110. *244*, *245*, *322*.
see H. S. Bridge.

DEUTSCHMANN, M.
1947: ———, Z. Naturforsch., 2a, 61. *78.*
1952: ———, Z. Naturforsch., 7a, 142. *282.*
1953: ———, Proc. Bagnères Conf., 48. *309, 322.*
DICORATO, M.
1954: ———, C. C. Dilworth and L. Scarsi, Proc. Padua Conf. *165, 244, 308.*
DILWORTH, C. C.
1954; ———, G. P. S. Occhialini and L. Scarsi, Ann Rev. Nuclear Sci., 4, 282. *158, 165.*
1954: ———, A. Manfredini, G. D. Rochester, J. Waddington and G. T. Zorn, Nuovo Cim., 12, suppl., 435. *167.*
see M. DiCorato.
DUERDEN, T.
1952: ——— and B. D. Hyams, Phil. Mag., 40, 717. *226.*
DULLER, N. M.
1954: ——— and W. D. Walker, Phys. Rev., 93, 215. *376.*
DYMOND, E. G.
1954: ———, Progress in Cosmic Ray Physics Vol. II, Ch. 3. *341, 359.*
EHRENFEST, P.
see P. Auger.
EIDUS, L. K.
1952: ———, M. I. Adamovitch, I. A. Ivanovskaya, V. S. Nikolaev and M. S. Tulyankina, J. Exp. Theor. Phys., 22, 440. *96, 135.*
see G. T. Zatsepin.
EISENBERG, Y.
1954: ———, Phys. Rev., 96, 541. *237, 244.*
see P. H. Barrett.
ELLIOT, H.
1952: ———, Progress in Cosmic Ray Physics Vol. I, Ch. 8. *118.*
1953: ———, Proc. Bagnères Conf. *124.*
EL-MOFTY, O.
1953: ———, Phys. Rev., 92, 461. *48.*
ETTER, L. R.
see H. O. Cohn, R. W. Thompson.
EULER, H.
1940: ——— and H. Wergeland, Astrophys. Norwegica, 3, 615. *20.*
EYGES, L.
1948: ———, Phys. Rev., 74, 1801. *20, 23, 27, 28.*
1951: ——— and S. Fernbach, Phys. Rev., 82, 23, 287. *20, 28, 30, 31.*
FABBRICHESI, L.
see E. Clementel.
FABRI, E.
1954: ———, Nuovo Cim., 11, 479. *153, 154.*
see E. Amaldi.
FAHY, E. H.
1951: ———, Phys. Rev., 83, 413. *85.*

FAINBERG, J.
see J. J. Lord, M. Schein.
FARLEY, F. J. M.
1954: ——— and J. R. Storey, Nature, Lond., **173**, 445. *124*, *127*.
FERGUSON, G. A.
1954: ———, J. Halpern, R. Nathans and P. F. Yergin, Phys. Rev., **95**, 776. *384*.
FERMI, E.
1949: ———, Phys. Rev., **75**, 1169. *118*.
1951: ———, Progr. Theor. Phys., **5**, 570; Phys. Rev., **81**, 683. *51*, *92*.
1954: ———, Astrophys. J., **119**, 1. *120*, *364*.
see S. Chandrasekhar.
FERNBACH, S.
1951: ———, Phys. Rev., **82**, 288. *20*, *28*.
see L. Eyges.
FILOSOFO, I.
1954: ———, E. Pohl and J. Pohl-Rüling, Nuovo Cim., **12**, 809. *365*.
see E. Beretta, D. Brini.
FLUM, R. S.
see R. W. Thompson.
FORNACA, G.
1953: ——— and G. Martelli, Proc. Bagnères Conf. *124*.
FOWLER, P. H.
1953: ——— and D. H. Perkins, Proc. Duke Univ. Conf. *321*.
see R. Brown.
——————— *232*
FOWLER, W. B.
1953: ———, R. P. Shutt, A. M. Thorndyke and W. L. Whittemore, Phys. Rev., **91**, 1287, *324*, *325*.
1954: ———, R. P. Shutt, A. M. Thorndyke and W. L. Whittemore, Phys. Rev., **93**, 861. *236*, *238*, *324*, *325*.
FRANÇOIS, P. E.
see C. Dahanayake.
FREIER, P.
1953: ——— and J. Naugle, Proc. Duke Univ. Conf. *10*.
see J. Naugle.
———————*244*
FRÉON, A.
see P. Auger, R. Maze.
FRETTER, W. B.
1949: ———, Phys. Rev., **76**, 511. *96*, *101*, *104*, *110*, *112*.
1951: ———, Phys. Rev., **82**, 137.
1951: ———, Phys. Rev., **83**, 1053.
1953: ——— and E. W. Friesen, Phys. Rev., **92**, 1089. *280*.
1953a: ——, M. M. May and M. P. Nakada, Phys. Rev., **89**, 168. *281*, *282*, *284*, *297*.
1953b: ——, B. P. Gregory, R. Johnston, A. Lagarrigue, H. Meyer, F. Müller and C. Peyrou, Proc. Bagnères Conf., 26.

1954: ——— and E. W. Friesen, Bull. Amer. Phys. Soc., **29**, no. 6. *294.*
1955: ——— and E. W. Friesen, Rev. Sci. Instr., **26**, 703. *207.*
see E. Amaldi, J. Ise, Jr..
FRIEDLANDER, M. W.
1954: ———, D. Keefe, M. G. K. Menon and M. Merlin, Phil. Mag., **45**, 533. *281, 291, 292, 293, 297.*
1954: ———, D. Keefe, M. G. K. Menon and L. van Rossum, Phil. Mag., **45**, 1043. *165, 178, 239.*
——————— *232, 244, 248.*
FRIESEN, E. W.
see W. B. Fretter.
——————— *244.*
FRY, W. F.
1952: ——— and J. J. Lord, Phys. Rev., **87**, 533. *244.*
1955: ———, J. Schneps and M. S. Swami, Phys. Rev., **97**, 1189. *231, 237.*
FUJIOKA, G.
1953: ———, International Conf. (Japan). *10, 41, 95, 98. 102.*
FUJIMOTO, Y.
see C. Dahanayake.
GALBRAITH, W.
see T. E. Cranshaw.
GALLI, M.
1953: ———, Nuovo Cim., **10**, 1187. *382.*
GARELLI, C. M.
see A. DeBenedetti.
GARWIN, R. L.
1953: ———, Phys. Rev., **90**, 274. *330.*
GAYTHER, D. B.
1954: ———, Phil. Mag., **45**, 570. *280, 309.*
GELL-MANN, M.
1953: ———, Phys. Rev., **92**, 833.
1954: ——— and A. Pais, Proc. Glasgow Conf., 342. *149.*
GENTNER, W.
see W. Bothe.
GEORGE, E. C.
see R. R. Daniel.
GEORGE, E. P.
1950: ——— and A. C. Jason, Proc. Phys. Soc., **A63**, 1081. *110, 112.*
1952: ———, Progress in Cosmic Ray Physics Vol. I, Ch. 7. *346, 347.*
1953: ———, J. W. MacAnuff and J. W. Sturgess, Proc. Phys. Soc., **A66**, 345. *114.*
GIGLI, A.
see C. Castagnoli.
GLASER, D. A.
1950: ———, B. Hamermesh and G. Safonov, Phys. Rev., **80**, 625. *346.*
GLASSER, R.
see M. Schein.

GOAD, W.
1953: ———, Thesis, Duke University. *51*, *86*, *92*.
GOLDHABER, M.
1953: ———, Phys. Rev., **92**, 1279. *149*, *238*.
GOTTLIEB, M. B.
1951: ———, Phys. Rev., **82**, 349. *85*.
GREEN, H. S.
1952: ——— and H. Messel, Phys. Rev., **88**, 331. *20*, *21*, *23*, *34*.
GREENSTEIN, J. L.
see L. Davis.
GREGORY, B.
1953: ———, Proc. Bagnères Conf., 35. *303*.
1954: ———, A. Lagarrigue, L. Leprince-Ringuet, F. Müller and C. Peyrou, Nuovo Cim., **11**, 292. *183*, *194*.
see W. B. Fretter, R. Armenteros.
GREISEN, K.
1949: ———, Phys. Rev., **75**, 1071. *94*.
1950: ———, W. D. Walker and S. P. Walker, Phys. Rev., **80**, 535. *85*, *86*, *95*, *98*, *105*, *107*, *108*.
1953: ——— and W. D. Walker, Phys. Rev., **90**, 915. *85*, *105*, *108*.
see P. H. Barrett, G. Cocconi, B. Rossi, J. E. Treat.
GRILLI, M.
1954: ———, P. E. Hodgson, M. Ladu and B. Vitale, Nuovo Cim., **12**, 889. *379*.
see M. Ceccarelli.
GRIVET-MEYER, T.
see P. Auger.
HABER-SCHAIM, U.
1954: ——— and G. Yekutieli, Nuovo Cim., **11**, 172, 683. *352*, *367*.
HADDARA, S. R.
1953: ——— and D. Jakeman, Proc. Phys. Soc., **A66**, 549. *40*, *41*.
HAKEEM, M. A.
see D. Broadbent.
HALPERN, J.
see G. A. Ferguson.
HAMERMESH, B.
see D. A. Glaser.
HARRIS, D. R.
see J. Ballam, A. L. Hodson.
HASKIN, D.
see M. Schein.
HAZEN, W. E.
1944: ———, Phys. Rev., **65**, 67. *373*.
1952: ———, Phys. Rev., **85**, 455. *44*, *48*.
1952: ———, R. E. Heineman and E. S. Lennox, Phys. Rev., **86**, 198. *92*.
1954: ———, R. W. Williams and C. A. Randall Jr., Phys. Rev., **93**, 578. *46*, *48*, *76*, *78*, *84*.

1954: ———, Nuovo Cim., **11**, 393. *49.*
see W. P. Davis, R. E. Heineman.
HEINEMAN, R. E.
1953: ——— and W. E. Hazen, Phys. Rev., **90**, 496. *48.*
1954: ———, Phys. Rev., **96**, 161. *48.*
see W. P. Davis, W. E. Hazen.
HEISENBERG, W.
1953: ———, Vorträge über Kosmische Strahlung (Springer, Berlin), 148. *52.*
HENDEL, A.
see R. Armenteros.
HILBERRY, N.
1941: —— , Phys. Rev., **60**, 1. *70, 71.*
HILDEBRAND, R. H.
1953: ——— and C. E. Leith, see Rosenfeld and Treiman [1953]. *330.*
HILL, R. D.
1954: ———, E. O. Salant and M. Widgoff, Phys. Rev., **95**, 1699. *150.*
HILTNER, W. A.
1951: ———, Astrophys. J., **114**, 241. *119.*
HOANG, T. F.
1955: ———, L. Jauneau, J. Jouvin, G. Kayas, L. Leprince-Ringuet, D. Morellet, A. Orkin-Lecourtois and J. Trembley, Nuovo Cim., **1**, suppl., 169. *166, 167, 244.*
see E. Amaldi, L. Leprince-Ringuet.
——————— *165, 166.*
HODGSON, P. E.
see M. Grilli.
HODSON, A. L.
1951: ———, Proc. Phys. Soc., **A64**, 1061. *124, 126.*
1952: ———, Proc. Phys. Soc., **A65**, 702. *103, 111, 112.*
1953a: ———, Proc. Phys. Soc., **A66**, 49. *58, 63, 64, 71, 73.*
1953b: ———, Proc. Phys. Soc., **A66**, 65. *103, 111, 112.*
1954: ———, J. Ballam, W. H. Arnold, D. R. Harris, R. R. Rau, G. T. Reynolds and S. B. Treiman, Phys. Rev., **96**, 1089. *183, 205, 310.*
see J. Ballam.
HOOPER, J. E.
1952: ———, D. T. King and A. H. Morrish, Phil. Mag., **43**, 853. *10.*
see A. Carlson.
HOPPER, V. D.
1950: ——— and S. Biswas, Phys. Rev., **80**, 1099. *291.*
HSIAO, C.
see A. J. Seriff.
HUDSON, D. E.
1950: ———, Thesis, Cornell University. *59.*
1952: ———, Phys. Rev., **86**, 453. *59.*
HUGGETT, R. W.
see R. W. Thompson, Y. B. Kim.

HYAMS, B. D.
see P. R. Barker, T. Duerden.
IREDALE, P.
see C. Dahanayake.
ISE, J. Jr.
1949: ——— and W. B. Fretter, Phys. Rev., **76**, 933. *55, 56, 59, 94, 96, 104, 115.*
IVANOVSKAYA, I. A.
see L. K. Eidus.
JAKEMAN, D.
see S. R. Haddara.
JAMES, G. D.
see J. P. Astbury.
JANOSSY, L.
1938: ——— and A. C. B. Lovell, Nature, Lond., **142**, 716. *3.*
1940: ——— and B. Rossi, Proc. Roy. Soc., **A175**, 88. *374.*
1942: ———, Proc. Roy. Soc., **A179**, 361. *95.*
1948: ———, Cosmic Rays (London, Oxford Univ. Press). *20, 24, 35.*
1950: ———, Proc. Phys. Soc., **A63**, 1009. *20, 32.*
1950: ——— and H. Messel, Proc. Phys. Soc., **A63**, 1101. *18.*
see D. Broadbent.
JASON, A. C.
see E. P. George.
JAUNEAU, L.
see T. F. Hoang, L. Leprince-Ringuet.
JOHNSTON, R.
see W. B. Fretter.
JOUVIN, J.
see T. F. Hoang.
KAMATA, K.
see J. Nishimura.
KAPLON, M. F.
1949: ———, B. Peters and H. L. Bradt, Phys. Rev., **76**, 1735; Helv. Phys. Acta, **23**, 24. *53, 86.*
1952a: ——— and D. M. Ritson, Phys. Rev., **85**, 932. *53, 86.*
1952b: ——— and D. M. Ritson, Phys. Rev., **88**, 386. *53, 86, 109.*
1954: ———, W. D. Walker and M. Koshiba, Phys. Rev., **93**. 1424. *109.*
1954: ———, Report of Padua Conf. *234, 291.*
see J. Crussard.
KARZMARK, C. J.
see R. W. Thompson.
KASNITZ, H. L.
1954: ——— and K. Sitte, Phys. Rev., **94**, 977. *45, 85, 96, 98, 106, 107, 108.*
KAYAS, G.
see T. F. Hoang.
KECK, J. C.
1949: ——— and K. Greisen, Proc. Echo Lake Conf. *58, 59.*

KEEFE, D.
see M. W. Friedlander.
KELLERMANN, E. W.
see D. Broadbent.
KEUFFEL, J. W.
see L. Mezzetti.
KHRISTIANSEN, G. B.
see G. T. Zatsepin.
KIM, Y. B.
1954: ———, J. Burwell, R. W. Huggett and R. W. Thompson, Phys. Rev., **96**, 229. *182, 220, 221, 223.*
see R. W. Thompson.
KING, D. T.
see M. M. Block, J. E. Hooper, A. Carlson.
—— ———— *234.*
KLARMANN, J.
see J. Crussard.
KOFSKY, I. L.
see K. Sitte.
KOLHORSTER, W.
1938: —— —, I. Matthes and E. Weber, Naturwiss., **26**, 576. *3.*
KORFF, C.
see H. Bethe.
KOSHIBA, M.
1955: ——— and M. F. Kaplon, Phys. Rev., **97**, 193. *10.*
see M. F. Kaplon.
KOUTS, H. J.
1952: —— — and L. C. L. Yuan, Phys. Rev., **86**, 128. *382.*
KRAUSHAAR, W. L.
1949: ——, Phys. Rev., **76**, 1045. *353.*
1954: ——— and L. J. Marks, Phys. Rev., **93**, 326. *52, 93.*
KRAYBILL, H. L.
1949: —— —, Phys. Rev., **76**, 1092. *58, 59, 62, 63, 64, 71, 81, 127.*
1954: ——, Phys. Rev., **93**, 1362. *63, 64, 74, 78.*
LADU, M.
see M. Grilli.
LAGARRIGUE, A.
1951: — —— and C. Peyrou, J. Phys. Radium, **12**, 848. *210.*
see R. Armenteros, W. B. Fretter, B. Gregory.
LAL, D.
1952: — —, Y. Pal, B. Peters and M. S. Swami, Proc. Ind. Acad. Sci., **A36**, 75; Phys. Rev., **87**, 545. *53, 86.*
1953a: ——, Y. Pal and B. Peters. Proc. Ind. Acad. Sci., **A38**, 277, 398. *239, 244, 259.*
1953b: ——, Y. Pal and B. Peters, Phys. Rev., **92**, 438. *165, 232, 239, 244, 308.*
1953c: ——, Y. Pal and B. Peters, Proc. Bagnères Conf., 141. *232, 239.*

LANDAU, L.
1940: ———, J. Phys. USSR, **3**, 237. *20.*
1953: ———, Izv. Akad. Nauk. SSSR, Ser. Fiz. **17**, n. 1. *52, 93.*
LANZA, G.
see N. Dallaporta.
LAPP, R. E.
1943: ———, Phys. Rev., **64**, 129. *58.*
1946: ———, Phys. Rev., **69**, 321. *58.*
LEIGHTON, R. B.
1951: ———, S. D. Wanlass and W. L. Alford, Phys. Rev., **83**, 843. *269, 280, 286, 289.*
1953a: ——, S. D. Wanlass and C. D. Anderson, Phys. Rev., **89**, 148. *281, 282, 284, 286, 289, 297, 301, 310, 319, 322, 323, 324, 325.*
1953b: ——, E. W. Cowan and V. A. J. van Lint. Proc. Bagnères Conf., 97. *294.*
1953c: ——, Proc. Bagnères Conf., 250, 254. *229.*
see W. L. Alford, C. D. Anderson, V. A. J. van Lint, A. J. Seriff, C. M. York.
—— ——— *295.*
LEITH, C. E.
see R. H. Hildebrand.
LENNOX, E. S.
see W. E. Hazen.
LEPRINCE-RINGUET, L.
1948: ———, T. F. Hoang, L. Jauneau and D. Morellet, C. R. Acad. Sci. Paris, **226**, 1897. *238, 241.*
1949: ———, Rev. Mod. Phys., **21**, 42. *238, 244.*
see E. Amaldi, R. Armenteros. B. Gregory, T. F. Hoang.
——————— *165.*
LEVINGER, J.
1949: ———, Phys. Rev., **75**, 1540. *95, 103.*
LEVI-SETTI, R.
see A. Bonetti.
LEWIS. H. W.
1948: ———, Phys. Rev., **73**, 1341. *86.*
LICHTENSTEIN, P. G.
1954: ———, Phys. Rev., **93**, 858. *347.*
LOCATELLI, B.
see A. Bonetti.
LOCK, W. O.
see E. Amaldi.
LORD, J. J.
1950: ———, J. Fainberg and M. Schein, Phys. Rev., **80**, 970; Nuovo Cim., **7**, 774. *53, 86.*
see W. F. Fry.
LORIA, A.
see M. Cresti.

LOVATI, A.
1951: ———, A. Mura, C. Succi and D. Tagliaferri, Nuovo Cim., **8**, 271. *105.*
LOVELL, A. C. B.
see L. Janossy.
LOVERDO, A.
1948: ——— and J. Daudin, J. Phys. Radium, **9**, 134. *59.*
see G. Cocconi.
MACANUFF, J. W.
see E. P. George.
MAIER-LEIBNITZ, H.
see W. Bothe.
MANDUCHI, C.
see P. Bassi.
MANFREDINI, A.
see E. Amaldi, C. C. Dilworth.
MARKS, L. J.
see W. L. Kraushaar.
MARSHAK, R. A.
1952: ———, Meson Physics (New York, McGraw-Hill Book Co.) *53, 86.*
MARTELLI, G.
see G. Fornaca.
MATHEWS, P. M.
see A. Ramakrishnan.
MAURER, W.
see W. Bothe.
MAY, M. M.
see W. B. Fretter.
MAZE, R.
1949: — — and A. Fréon, J. Phys. Radium, **10**, 85. *62.*
see P. Auger.
MCCUSKER, C. B. A.
1950: — ——, Proc. Phys. Soc., **A63**, 1240. *85, 95, 102.*
1951: — - - and D. D. Millar, Proc. Phys. Soc., **A64**, 915. *98, 99, 115.*
MCKAY, A. S.
see W. W. Brown.
MENON, M. G. K.
1954: ——— and C. O'Ceallaigh, Proc. Roy. Soc., **A221**, 292. *165, 168.*
see M. W. Friedlander.
MERLIN, M.
see M. Ceccarelli, M. W. Friedlander.
MESSEL, H.
1953: ——— and R. B. Potts, Nuovo Cim., **10**, 754. *117.*
1954: ———, Progress in Cosmic Ray Physics, Vol. II, Ch. 4. *117, 352.*
see H. S. Green, L. Janossy.
MEYER, H.
see W. B. Fretter.

MEZZETTI, L.
1954: ——— and J. W. Keuffel, Nuovo Cim., 11, suppl. 245. *227.*
1954: ——— and J. W. Keuffel, Phys. Rev., 95, 858. *227.*
see E. Amaldi.
MICHEL, L.
1950: ———, Proc. Phys. Soc., A63, 574, *185.*
1952: ———, Progress in Cosmic Ray Physics, Vol. I, Ch. 3. *153, 371.*
1952: ——— and R. Stora, C. R. Acad. Sci. Paris, 234, 1257. *185.*
MIGDAL, A.
1945: ———, J. Phys. USSR. 9, 183. *25.*
MILLAR, D. D.
1951: ———, Proc. Roy. Irish Acad., 54, 115. *73.*
1953: ——— and D. I. Page, Phil. Mag., 44, 1049. *281.*
see J. P. Astbury, J. S. Buchanan, C. B. A. McCusker.
MILLER, V. V.
see G. T. Zatsepin.
MILLS, M. M.
1948: ———, Phys. Rev., 74, 1555; Thesis, Calif. Inst. Tech. *86.*
MILONE, C.
1951: ———, Nuovo Cim., 8, 643. *98, 99.*
1952a: ———, Nuovo Cim., 9, 549. *58.*
1952b: ———, Nuovo Cim., 9, 637. *101.*
see G. Baroni.
MITRA, S.
see M. V. K. Appa-Rao.
MOLIÈRE, G.
1942: ———, Naturwiss., 30, 87. *20, 22.*
1946: ———, Cosmic Radiation (ed. W. Heisenberg, New York Dover Publ.) *20, 22.*
1953: ———, Vorträge uber Kosmische Strahlung (ed. W. Heisenberg Berlin, Springer), 446. *20, 22.*
1954: ———, Phys. Rev., 93, 636.
see P. Budini.
MONTGOMERY, C. G.
see J. Wei.
MORELLET, D.
see T. F. Hoang, L. Leprince-Ringuet.
MOREWITZ, H. A.
1953: ——— and M. H. Shamos, Phys. Rev., 92, 134. *366.*
MORRISH, A. H.
see J. E. Hooper.
MORRISON, P.
1954: ———, S. Olbert and B. Rossi. Phys. Rev., 94, 440. *118.*
MUIRHEAD, H.
see R. Brown.
MÜLLER, F.
see R. Armenteros, W. B. Fretter, B. Gregory.

MURA, A.
see A. Lovati.
NAKADA, M. P.
see W. B. Fretter.
NATHANS, R.
see G. A. Ferguson.
NAUGLE, J. E.
1953: ——— and P. S. Freier, Phys. Rev., **92**, 1086. *10.*
see P. S. Freier.
NEHER, H. V.
1952: ——— —, Progress in Cosmic Ray Physics, Vol. I, Ch. 5. *342, 386.*
see A. T. Biehl.
NEWTH, J. A.
1953: ———, Proc. Bagnères Conf., 57.
1954: ———, Nuovo Cim., **11**, suppl., 290. *208.*
see J. P. Astbury, J. S. Buchanan.
NIELSEN, C. E.
1942: ——— —, Phys. Rev., **61**, 202. *264.*
NIKOLAEV, V. S.
see L. K. Eidus.
NISHIMURA, J.
1950: ——— and K. Kamata, Progr. Theor. Phys., **5**, 899. *20, 22, 24, 25.*
1951: ——— and K. Kamata, Progr. Theor. Phys., **6**, 628, *20, 22, 23, 24.*
1952: ——— and K. Kamata, Progr. Theor. Phys., **7**, 185. *20, 22, 24.*
NOON, J. H.
see J. Crussard.
NORDHEIM, L. W.
see J. A. Richards, J. Roberg.
OCCHIALINI, G. P. S.
see C. C. Dilworth.
O'CEALLAIGH, C.
1951: ———, Phil. Mag., **42**, 1032. *158, 179.*
see M. G. K. Menon.
——————— *248.*
O'DELL, F. W.
see B. Stiller.
OLBERT, S.
1954: ———, Phys. Rev., **96**, 1400. *352, 362.*
see P. Morrison.
ORKIN-LECOURTOIS, A.
see T. F. Hoang.
ORTEL, W. G. C.
1954: ———, Phys. Rev., **93**, 561. *381.*
OWEN, B. G.
1951: ——— and J. G. Wilson, Proc. Phys. Soc., **A64**, 417. *365.*
1955: ——— and J. G. Wilson, Proc. Phys. Soc., **A68**, 409. *347.*

PAGE, D. I.
1954: ——— and J. A. Newth, Phil. Mag., **45**, 38. *290.*
1954: ———, Phil. Mag., **45**, 863. *290.*
see J. P. Astbury, D. D. Millar.
PAIS, A.
1952: ———, Phys. Rev., **86**, 663. *156.*
1953: ———, Physica, **19**, 869. *149.*
see M. Gell-Mann.
PAL, Y.
see R. R. Daniel, D. Lal.
——————— *234.*
PALMATIER, E. D.
1952: ———, Phys. Rev., **88**, 761. *61, 372.*
PANETTI, M.
see A. Bonetti.
PEIERLS, R.
1935: ———, Proc. Roy. Soc., **A149**, 467. *221.*
PERKINS, D. H.
see P. H. Fowler.
PETERS, B.
1952: ———, Progress in Cosmic Ray Physics, Vol. I, Ch. 4. *342.*
1953: ———, Proc. Bagnères Conf. *291.*
see E. Amaldi, R. R. Daniel, M. F. Kaplon, D. Lal.
PEYROU, C.
see R. Armenteros, H. S. Bridge, W. B. Fretter, B. Gregory, A. Lagarrigue.
PICCIONI, O.
1953: ——— and R. L. Cool, Phys. Rev., **91**, 433. *111, 112.*
see R. L. Cool.
PICKUP, E.
1951: ——— and L. Voyvodic, Phys. Rev., **84**, 1190. *53, 86.*
PLACZEK, G.
see H. A. Bethe.
PNIEWSKI, J.
see M. Danysz.
PODOLANSKI, J.
1954: ——— and R. Armenteros, Phil. Mag., **45**, 13. *212, 266, 277.*
POHL, E.
see I. Filosofo.
POHL-RULING, J.
see I. Filosofo.
POIANI, G.
1952a: ——— and C. Villi, Nuovo Cim., **9**, 825. *20, 27.*
1952b: ——— and C. Villi, Nuovo Cim., **9**, 1109. *20, 33.*
see G. Cernigoi, N. Dallaporta.
POMERANCHUK, I.
1944: ———, J. Phys. USSR., **8**, 17. *25.*
POTTS, R. B.
see H. Messel.

POWELL, C. F.
1952: ———, Report Copenhagen Conf., 29. *168*, *201*.
1953: – ——, Phil. Mag., **44**, 219. *259*.
1954: ———, Nature, Lond., **173**, 469.
see E. Amaldi, R. Brown.
———— *165*
PRESCOTT, J. R.
see I. D. Campbell.
PRIMAKOFF, H.
1954: ——— and W. Cheston, Phys. Rev., **93**, 908. *289*.
see W. Cheston.
PUPPI, G.
1952: ——— and N. Dallaporta, Progress in Cosmic Ray Physics, Vol. I, Ch. 6. *341*, *346*, *347*, *351*, *365*, *380*.
1953: ———, Nuovo Cim., **10**, suppl., 115. *341*.
see E. Beretta.
QUARENI, G.
see M. Ceccarelli.
RACAH, G.
1937: ———, Nuovo Cim., **14**, 93. *11*.
RAMAKRISHNAN, A.
1953: ——— and P. M. Mathews, Progr. Theor. Phys., **9**, 679. *19*.
see H. J. Bhabha.
RANDALL, C. A. Jr.
see W. E. Hazen.
RAU, R. R.
see J. Ballam, A. L. Hodson.
RAVENHALL, D. G.
1950: ———, Proc. Phys. Soc., **A63**, 1177. *11*.
REDIKER, R. H.
see R. W. Thompson.
RELF, K. E.
1955: ———, Phys. Rev., **97**, 172. *44*, *48*.
REYNOLDS, G. T.
1953: ———, Proc. Bagnères Conf., 42. *322*, *323*.
1954: ——— and S. B. Treiman, Phys. Rev., **94**, 207. *328*.
see W. H. Arnold, J. Ballam, A. L. Hodson.
RICHARDS, J. A. Jr.
1948: ——— and L. W. Nordheim, Phys. Rev., **74**, 1106. *11*, *14*, *16*.
RIMONDI, O.
see D. Brini.
RITSON, D. M.
see R. Brown, M. F. Kaplon.
ROBERG, J.
1949: ——— and L. W. Nordheim, Phys. Rev., **75**, 444, *20*, *33*.
ROBLEY, J.
see P. Auger.

ROCHESTER, G. D.
1947: ——— and C. C. Butler, Nature, Lond., **160**, 855. *255, 256.*
1952: ——— and J. G. Wilson, Cloud Chamber Photographs of the Cosmic Radiation (London, Pergamon Press). *256.*
see E. Amaldi, C. C. Dilworth.
ROSENFELD, A. H.
1953: ——— and S. B. Treiman, Phys. Rev., **92**, 727. *330.*
ROSENTAL, I. L.
1952: ———, J. Exp. Theor. Phys., **23**, 440. *117.*
see U. V. Anishenko, G. T. Zatsepin.
ROSSI, B.
1941: ——— and K. Greisen, Rev. Mod. Phys., **13**, 240. *12, 14, 20, 24.*
1948: ———, Rev. Mod. Phys., **20**, 537. *311, 313, 346, 347, 349, 370.*
1952: ———, High Energy Particles (Prentice-Hall, New York). *10, 12, 370.*
see E. Amaldi, P. Bassi, H. S. Bridge, L. Janossy, P. Morrison.
ROUT, R. J.
see P. R. Barker.
RYTZ, A.
see J. P. Astbury.
SAFFORD, R.
see H. S. Bridge.
SAFONOV, G.
see D. A. Glaser.
SAHIAR, A. B.
see J. P. Astbury.
SALANT, E. O.
see R. D. Hill.
SALVINI, G.
1949: ——— and G. Tagliaferri, Nuovo Cim., **6**, 108. *95, 98.*
SANDS, M.
1950: ———, Phys. Rev., **77**, 180. *352.*
SARITCHEVA, L. I.
see U. V. Anishenko, G. T. Zatsepin.
SAXENA, R. C.
see B. Chowdhuri.
SCARSI, L.
see E. Amaldi, G. Baroni, M. di Corato, C. C. Dilworth.
SCHEIN, M.
1952: ———, J. Fainberg, K. Brown and R. Glasser, Proc. 3rd Rochester Conf. (Interscience, New York), 95. *330, 331.*
1953: ———, D. Haskin, R. Glasser, J. Fainberg and K. Brown, Proc. Bagnères Conf., 166. *330, 331.*
see J. J. Lord.
SCHMEISER, K.
1938: ——— and W. Bothe, Ann. Phys., Lpz., **32**, 161. *3.*
see W. Bothe.

SCHNEPS, J.
see W. F. Fry.
SCIUTI, S.
see G. Castagnoli.
SECHI, B.
see G. Belliboni.
SEGRE, E.
see G. Bernardini.
SERBER, R.
1938: ———, Phys. Rev., **54**, 317. *12.*
SERIFF, A. J.
1950: ———, R. B. Leighton, C. Hsiao, E. W. Cowan and C. D. Anderson, Phys. Rev., **78**, 290. *255, 257.*
SHAMOS, M. H.
see H. A. Morewitz.
SHAPIRO, M. M.
see B. Stiller.
SHEPHERD, J.
see P. R. Barker.
SHERMAN, N.
1953: ———, Phys. Rev., **89**, 25. *124.*
SHUTT, R. P.
see W. B. Fowler.
SILVERMAN, A.
see G. Cocconi.
SIMPSON, J. A.
1949: ———, Phys. Rev., **76**, 1750. *381.*
SINGER, S. F.
1951: ———, Phys. Rev., **81**, 579. *55, 58.*
SITTE, K.
1950: ———, Phys. Rev., **78**, 721. *85, 95, 113.*
1952: ———, Phys. Rev., **87**, 351. *85, 95, 98, 106.*
1954: ———, D. L. Stierwalt and I. L. Kofsky, Phys. Rev., **94**, 988. *45, 48.*
see H. L. K. Kasnitz.
SMITH, F. M.
1953: ———, W. Birnbaum and W. H. Barkas, Phys. Rev., **91**, 765. *297, 351.*
SNYDER, H. S.
1938: ———, Phys. Rev., **53**, 960. *12.*
1949: ———, Phys. Rev., **76**, 1563. *12, 13, 14, 15, 24.*
SOMMACAL, B.
see E. Beretta.
SOWERBY, M. G.
see R. Armenteros, K. H. Barker.
SREEKANTAN, B. V.
see H. S. Bridge.

STAFFORD, R.
see H. S. Bridge.
STERNHEIMER, R.
1953: ———, Phys. Rev., **91**, 256. *177.*
STIERWALT, D. L.
see K. Sitte.
STILLER, B.
1954: ———, M. M. Shapiro and F. W. O'Dell, Rev. Sci. Inst., **25**, 340. *259*
STINCHCOMB, T. G.
1951: ———, Phys. Rev., **83**, 422. *85.*
STOPPINI, G.
see E. Amaldi.
STOREY, J. R.
see F. J. M. Farley.
STRANAHAN, G.
1954: ———, Astrophys. J., **119**, 465. *119.*
STREET, J. C.
see R. S. Carter.
STORA, R.
see L. Michel.
STURGESS, J. W.
see E. P. George.
SUBRAMANIAN, A.
see B. Chowdhuri.
SUCCI, C.
see A. Lovati.
SWAMI, M. S.
see W. F. Fry, D. Lal.
TAGLIAFERRI, G.
see A. Lovati, G. Salvini.
TALLONE, L.
see A. DeBenedetti.
TAMM, I.
1946: ——— and S. Belenky, Phys. Rev., **70**, 660. *12, 17.*
TEUCHER, M.
1953: ———, Proc. Bagnères Conf., 172. *291.*
THOMPSON, R. W.
1951: ———, H. O. Cohn and R. S. Flum, Phys. Rev., **83**, 175. *258, 285, 300.*
1952a: ———, Proc. Second Rochester Conf., 73. *280, 286.*
1952b: ———, A. V. Buskirk, L. R. Etter, C. J. Karzmark and R. H. Rediker, Proc. Third Rochester Conf. (Interscience, New York), 39. *298, 301.*
1953a: ———, A. V. Buskirk, L. R. Etter, C. J. Karzmark and R. H. Rediker, Phys. Rev., **90**, 329. *281, 286, 287, 293, 298, 300, 304, 310, 312.*
1953b: ———, A. V. Buskirk, L. R. Etter, C. J. Karzmark and R. H. Rediker, Phys. Rev., **90**, 1122. *298.*

1953c: ——, A. V. Buskirk, H. O. Cohn, C. J. Karzmark and R. H. Rediker, Proc. Bagnères Conf., 30. *212, 272.*
1954a: ——, J. R. Burwell, H. O. Cohn, R. W. Huggett, C. J. Karzmark and Y. B. Kim, Proc. Fourth Rochester Conf. *312.*
1954b: ——, J. R. Burwell, R. W. Huggett and C. J. Karzmark, Phys. Rev., **95**, 1576. *304, 326.*
see E. Amaldi, K. A. Brueckner, H. O. Cohn, Y. B. Kim.
——————— *268.*

TICHO, H. K.
1952: ——— , Phys. Rev., **88**, 236. *85.*

THORNDIKE, A. M.
see W. B. Fowler.

TOMASINI, G.
see A. Bonetti.

TONGIORGI, V.
1948a: ——, Phys. Rev., **73**, 923. *95, 103.*
1948b: — , Phys. Rev., **74**, 226. *95, 103.*
1949: ——— , Phys. Rev., **75**, 1532. *95, 103.*
see G. Cocconi.

TOUSCHEK, B.
1954: ———, Nuovo Cim., **12**, suppl., 281. *238.*
see E. Amaldi.

TREAT, J. E.
1948: - - --- and K. Greisen, Phys. Rev., **74**, 414. *56, 59, 62.*

TREIMAN, S. B.
1954: ———, Phys. Rev., **95**, 1360. *316.*
see J. Ballam, A. L. Hodson, G. T. Reynolds, A. H. Rosenfeld.

TREMBLEY, J.
see T. F. Hoang.

TRILLING, G. H.
see V. A. J. van Lint.

TULYANKINA, M. S.
see L. K. Eidus.

VANDERHAEGHE, G.
see G. Baroni.

VAN LINT, V. A. J.
1953: -- ---, Proc. Duke University Conf., II-42. *304, 305.*
1954a: ——, G. H. Trilling, R. B. Leighton and C. D. Anderson, Phys. Rev., **95**, 295. *286, 287, 289.*
1954b: ——, C. D. Anderson, E. W. Cowan, R. B. Leighton and C. M. York Jr., Phys. Rev., **94**, 1732. *312, 319.*
see C. D. Anderson, R. B. Leighton.

VAN ROSSUM, L.
see M. W. Friedlander.

VIDALE, M.
see J. Ballam, M. Ceccarelli.

VIGONE, M.
see A. DeBenedetti.

VILLI, C.
see G. Poiani.
VITALE, B.
see E. Amaldi, G. Belliboni, M. Grilli.
VOYVODIC, L.
see E. Pickup.
WADA, W. W.
see M. M. Block.
WADDINGTON, C. J.
see C. Dahanayake, C. C. Dilworth.
WALKER, S. P.
see K. Greisen.
WALKER, W. D.
see K. Greisen, M. F. Kaplon, N. M. Duller.
WANLASS, S. D.
see R. B. Leighton.
WEI, J.
1949: ——— and C. G. Montgomery, Phys. Rev., **76**, 1488. *81.*
WERGELAND, H.
see H. Euler.
WHITTEMORE, W. L.
see W. B. Fowler.
WIDGOFF, M.
see R. D. Hill.
WILHELMY, E.
see W. Bothe.
WILLARD, D.
see H. S. Bridge, B. Dayton.
WILLIAMS, R. W.
1948: ———, Phys. Rev., **74**, 1689. *26, 45, 46, 48, 59, 78, 135.*
see W. E. Hazen.
WILSON, J. G.
1951: ———, The Principles of Cloud Chamber Technique (London, Cambridge Univ. Press). *259, 264.*
1952: ——— and C. C. Butler, Phil. Mag., **43**, 993. *208, 290.*
1954: ———, Progress in Cosmic Ray Physics, Vol. II. Ch. 2. *297.*
see G. D. Rochester, B. G. Owen.
WILSON, R. R.
1952: ———, Phys. Rev., **86**, 261. *19.*
YASIN, M.
1954: ———, Phil. Mag., **45**, 413. *291, 308, 309.*
see C. Dahanayake.
YEKUTIELI, G.
see W. Haber-Schaim.
YERGIN, P. F.
see G. A. Ferguson.
YORK, C. M. Jr.
1952: ———, Phil. Mag., **43**, 985. *185, 209. 210.*

1952: ———, Phys. Rev., **85**, 998. *347.*
1953: ———, R. B. Leighton and E. K. Bjornerud, Phys. Rev., **90**, 107. *224, 229.*
1954: ———, R. B. Leighton, and E. K. Bjornerud, Phys. Rev., **95**, 159. *182, 221, 223, 224, 229.*
see R. Armenteros, K. H. Barker, V. A. J. van Lint.
YUAN, L. C. L.
see H. J. Kouts.
ZAGO, G.
see M. Cresti.
ZATSEPIN, G. T.
1947: ———, V. V. Miller, I. L. Rosental and L. K. Eidus, J. Exp Theor. Phys., **17**, 1125. *58, 59, 64.*
1953: ———, Izv. Akad. Nauk, SSSR. Ser. Fiz., **17**, 39. *43, 58, 59, 64 96, 135.*
see U. V. Anishenko.
ZORN, G. T.
see M. Ceccarelli, C. C. Dilworth.

SUBJECT INDEX

Age parameter "s" of EAS 14, 23, 24, 39, 41, 47.
"α", dynamical constant of two-body decay 270.
altitude variation of EAS 70.
altitude variation of N-component in EAS 109.
atmosphere, constant density approximation 22.
— effect of density variation 34.
— isothermal 34.
— magnetic deflection of EAS secondaries in 35.
— time variations affecting EAS 123.
attenuation coefficient of EAS 80.
axial region of showers 46, 47.
barometric effect for EAS 3, 72.
bursts identified with EAS 44, 45, 46.
cascade V-events 293—.
Čerenkov counter 226.
charge asymmetry of S-particles 207.
charged hyperons 228.
charged V-particles 207—.
χ-meson 168, 201, 205.
cloud chamber arrangements 182.
cloud chamber technique 259—.
Compton effect 11, 12, 15, 16.
core selectors 37, 40, 98.
Cosmotron 324.
decay schemes of K-mesons and hyperons 147, 148.
diffusion equation (electron cascades) 20.
delayed coincidence measurements on S-events 226.
density gradient in EAS, effects of 56—.
density spectrum of EAS 53—.
distortions in cloud chamber 259.
dynamical analysis of V-events 209.
earth's magnetic field 35.
extensive air showers (EAS), altitude variation 80.
— attenuation coefficient 80.
— axial regions of 46, 47.
— barometer effect for 3, 72.
— core selectors 37, 40, 98.
— density spectrum of 53—.
— electrons as primaries 5.
— energy of primaries 4, 129, 135.
— energy spectrum of electrons and photons 84.
— growth at high altitude 86.
— μ-mesons in 95, 96, 101, 113.

— nucleons in 3, 85, 93.
— number spectrum 65.
— penetrating component 3, 93—.
— time variations 117.
— upper limit of primary energy 5.
electron cascades, age parameter "s" 14, 23, 24, 39, 41, 47.
— approximate lateral structure expressions 26.
— approximations A and B 10.
— critical energy 10, 15.
— diffusion equations 20.
— fluctuations in 18
— Molière structure function 21, 22.
— moments of lateral and angular distributions 20.
— Monte Carlo calculations 19.
— Nishimura-Kamata structure functions 22, 23.
— total track length 12.
— trident formation 10.
— effect of variation of atmospheric density 34.
electron-photon component of cosmic radiation 369.
electron secondaries from K-mesons 177, 179.
electron primaries 5.
emulsion block technique 145.
energy spectrum of EAS primaries 129, 135.
energy spectra of electrons and photons, in EAS 84.
— in general cosmic ray beam 371.
errors in mass determination (in emulsions) 166, 167.
Fermi collision model 51, 52.
flux of μ-mesons at sea level 350.
galactic magnetic fields 118.
"γ", index of density spectrum of EAS 57-
Gell-Mann, Pais selection rules 147.
generation spectrum of μ-mesons 300.
Gross transformation 71, 74, 111.
hydrogen diffusion chamber 324.
hyperons, charged 228, 237.
— absorption of negative charged 246.
ionization measurements (cloud chamber) 264.
isotropy of early collisions in EAS 50.
Janossy "P-set" 95, 103, 110.
$\varkappa$-meson 158.
— mass of 166.
K-meson 146—, 160, 177, 180, 195, 237.
— electron secondaries from 177, 179.
— nuclear absorption of 237, 240.
— $p\beta$ distribution of secondaries 172.
— photons in decay products 202.
— slowing down time for 181.
K^0-meson 318.

— production with Y-particle 324
K_μ-meson 174, 198.
— mass of 199.
— range of secondaries 193.
knock-on electrons 11.
Λ°-particle 255, 280—, 331.
— abnormal Q-values 289.
— lifetime 289.
— nature of secondaries 280.
Landau diffusion equations 20, 21, 22.
lateral structure of showers 20—.
lateral structure of N-component in EAS 107.
latitude effect of EAS 127.
L-meson 146.
— from hyperon decay 235
magnetic fields, galactic 118.
— of earth 35.
magneto-hydrodynamic waves in galactic arms 119.
masses of K-mesons 195.
mass of K_μ-meson 199.
maximum primary energy of EAS 135.
Molière structure function 21, 22, 99.
moments of lateral structure of showers 20,21.
Monte Carlo calculations of electron showers 19.
multiple shower cores 48.
multiplicity at early collisions of EAS 88.
μ-mesons, in EAS 95, 101, 113.
— generation spectrum of 350.
— lateral distribution in EAS 96.
— positive excess 365.
— spectrum at sea level 345.
negative hyperons, absorption of 246.
neutrons in EAS 94.
Nishimura-Kamata structure functions 22, 23.
nuclear absorption of K-mesons and hyperons 237.
nuclear cascade (calculations) 117.
nuclear interaction of θ°-secondaries 303.
nucleonic component (N-component) of EAS 85, 93, 102—.
number spectrum of EAS 65—.
"particle", use of term 147.
penetrating particles in EAS 3, 93—, 96, 100—.
(π^-, p) interaction 325.
π°-mesons, lifetime 80.
Podolanski-Armenteros parameter (ε) 277.
positive excess of sea level μ-mesons 365.
potential path 208.
primary cosmic radiation 4.
primary energy of EAS 4, 129, 135.

primary particles, energy cut-off 119.
Princeton event (π + 4e) 205.
"P-set" of Janossy 95, 103, 110.
protons from V°-decay 258
Q-surface representation 271.
Q-value 266.
— abnormal (p, π) values 289.
— precision of determinations 267, 268.
Q*-value 269.
radiation length 10.
range distribution for K-meson secondaries 184.
range relations for K-mesons 181.
range spectrum of μ-mesons, in EAS 113.
— at sea level 348.
range, straggling in 196.
Rossi transition curve 3.
"s", age parameter of EAS 14, 23, 24, 39, 41, 47.
Sardinia expedition 145, 175.
S-events 146.
— charge asymmetry 207.
— in cloud chamber 179.
— in photoemulsions 156.
— momentum distribution of secondaries 192.
— ranges of secondaries 184.
Σ-particles 228.
sidereal time variations of EAS 122.
single scattering in EAS 27.
slowing down times for K-mesons 181.
slow neutrons in general cosmic ray flux 381.
solar time variations of EAS 123.
star formation 378.
τ-meson 149—.
— alternate mode of decay 151, 156.
— constants of 150—.
— charge of 152.
— lifetime of 155.
— spin and parity of 153.
τ°-meson 317.
temperature effects on EAS intensity 126, 127.
θ°-particle 297—, 332.
— decay products 301, 303.
— production of 303.
— Q-values 304
— relationship to K-particles 309.
time variations of EAS 117—.
track density, photometric method 167.
track length distribution 14.
track length integral 130, 370.

trapping of cosmic ray primaries 5, 118—.
trident formation 10.
"tunnelling" collisions 87.
underground observations on EAS 114—.
upper limit of primary spectrum 5, 135.
V-events 146.
— dynamical analysis of 209.
— in cascade 293.
V-particles, charged 207—.
— lifetime of 221, 223.
V^c-particles 255.
— anomalous events 310—, 312.
— production of 321—.
V_3^0-events 319.
Y-particles 146.
— production with K-particles 324.
zenith angle variations of EAS 74, 76, 79.
— measurement of 78.